Evolution of Bone Histological Characters in Amniotes, and the Implications for the Evolution of Growth and Metabolism

By

Sarah Anne Werning

A dissertation submitted in partial satisfaction of the

requirements for the degree of

Doctor of Philosophy

in

Integrative Biology

in the

Graduate Division

of the

University of California, Berkeley

Committee in charge:

Professor Kevin Padian, Chair
Professor Marvalee H. Wake
Professor Charles R. Marshall
Professor Sabrina C. Agarwal

Fall 2013

Evolution of Bone Histological Characters in Amniotes, and the Implications for the Evolution of Growth and Metabolism

Abstract

Evolution of Bone Histological Characters in Amniotes, and the Implications for the Evolution of Growth and Metabolism

by

Sarah Anne Werning

Doctor of Philosophy in Integrative Biology

University of California, Berkeley

Professor Kevin Padian, Chair

Histological studies have established relationships between the microstructural features of bone, the growth rates of primary cortical bone, and whole-body growth rates of the animal. For animals of a given body size, the density and connectivity of vascular canals and the disorganization of collagen fibers increase with the rate of bone deposition, and osteocyte density is positively correlated with metabolic rate.

I first review and refine several methods to improve the quantification of growth-related patterns in fossil bone tissue, focusing on specific microstructural characters known to correlate with growth and metabolic rates in living tetrapods. The most critical histological indicator of growth, the rate of bone deposition, is rarely reported in fossil studies. However, zonal area and average zonal width directly measure annual deposition, and can be used to bracket daily deposition rates. Estimating bone tissue growth based on vascularization pattern ("Amprino's Rule") likely confounds three separate vascular signals: density, connectivity, and orientation/patterning. I discuss ways to measure these separately, using qualitative and quantitative means. Collagen fiber orientation, a sensitive indicator of bone deposition rate that may resolve seasonal shifts, is sometimes obscured in fossils by diagenetic alteration. Patterns of osteocyte organization and orientation, more than cell shape, are highly associated with fiber orientation and may be more appropriate proxies. Osteocyte and canal density, not typically reported in paleohistological studies, are easily measured using digital boxplots along radial transects through the cortex. These measures suggest the possibility of more useful quantification of osteohistological indicators as proxies for growth and metabolic rates in extinct and extant vertebrates.

I next investigate the origins of avian growth rates. Birds grow much faster than other extant reptiles, a trait that is reflected in the appearance of their bone microstructure. However, some of these traits are shared by their dinosaurian ancestors, and it is not known when this condition first evolved. I expand the histological database of archosaurs and their ancestors to include early archosauromorphs, pseudosuchians, and dinosauromorphs. By sampling through deep time and in taxa whose character states are not represented among living animals, I show

that the avian histological features associated with faster growth and higher metabolic rates evolved not among birds or dinosaurs, but earlier than the common ancestor of birds and crocodylians. Most of these character changes accumulated in a short segment of the archosauriform tree before the end of the Triassic.

Finally, I examine histological patterns of growth in marsupial mammals. Among extant mammals, the bone tissue of placentals has been fairly well characterized, and is known to vary with size and ecology. Comparative data on marsupials, however, are lacking. I sampled the mid-diaphyseal femora of more than 50 extant and extinct marsupial species, as well as some afrotherian, xenarthran, and laurasiatherian placentals. My marsupial sample encompasses all extant orders, spans a 10 g-2500 kg size range, and comprises mainly wild-caught animals. The main factors influencing marsupial bone microstructure are life history and body size. The histological differences resulting from body size are subtle, occur gradually, and hold across six of the seven extant orders. The uniformity of marsupial bone histology reflects uniformity of their life history, especially related to the ontogeny of growth rates. Across all body sizes, marsupials share a common ontogeny: they are extremely altricial, experience their time of fastest growth at or just prior to weaning, and then continue to grow at lower rates for an extended period relative to their lifespan. Among placental mammals, histological variability likely reflects greater diversity in the ontogeny of growth rates. It is likely that sampling biases have obscured both size and phylogenetic signals in the distribution of mammalian bone growth patterns.

By incorporating natural history and life history, the fossil record and the modern record, the study of bone microstructure can facilitate a much richer understanding of growth at the organismal level, and the evolution of growth strategies at higher levels.

For my peeps.

TABLE OF CONTENTS

Front Matter

Main Text

ACKNOWLEDGMENTS

I owe so much to my adviser and mentor, Kevin Padian. Kevin, it has been a joy and a privilege to work in your lab for the past seven years; I cannot thank you enough for the excellent opportunities and all the support you have given me. I'm grateful for the many hours we've spent geeking out over bone histology and the Triassic, your helpful advice on navigating the academic jungle, and the patience and encouragement you've always shown me as I transitioned from student to colleague. The lab dinners, kick-ass music, and heated philosophical debates (especially the important topics like football, comic books, and lamb) are just a few of the many things I will miss when I leave Berkeley.

The rest of my committee (Sabrina Agarwal, Charles Marshall, and Marvalee Wake) provided balance, support, and a helpful kick in the butt when I needed it the most. Marvalee, you are the type of biologist I strive to be: one who considers the organism from every aspect, integrating development, life history, natural history, and phylogeny. You always keep me on my toes; our meetings are always intellectually stimulating and I leave more excited about biology than when I came in. Charles and Sabrina, it was wonderful to hear your perspectives on evolution and bone, and you both provided such clear and helpful career advice.

I was fortunate to have a shadow committee of unofficial advisers, who were every bit as critical to my academic survival as my actual committee. Berkeley would have been much rougher without these colleagues and mentors, who I also am proud to call my friends: Pat Holroyd, Jim McGuire, and Chris Nasrallah. All of you were there with a sympathetic ear, candid advice, and the occasional game of pool or poker whenever I needed it. Thank you so, so much.

My labmates have been excellent sounding boards, spirited debaters, and great friends. Jackie, Matt, Drew, Randy, Katie, Brian, Jessie, Liz, Mariska, and Ash: thank you all for being enjoyable, considerate, and generally excellent people. My extended labmates, Dan, Skip, Stubbs, and Sarah: your friendship and nonpaleo perspective mean so much to me. I can't think of better herping partners or roadtrip companions. Randy, I cannot thank you enough for bringing me to Ghost Ranch my first summer here, for always being up to watch movies, sports, and concerts, and for the many hours of stimulating conversation. Liz, I'm so happy to have shared four years here with you; your complete lack of pretension, sarcastic humor, and direct demeanor are just three reasons you're one of my favorite people in Berkeley. Ash and Skip, it's been great rooming and working with you; there are not many people who I could tolerate seeing at home and the office (or who would afford me the same tolerance). Thank you so much for your patience, especially over the last year. I'm going to miss you both so much. To all of you, I look forward to many more years of collaboration and friendship.

I was also privileged to mentor some wonderful students during my time at Berkeley. Among these, Zach Morris, Sarah Tulga, and Dominique Bertrand spent countless hours making slides, counting osteocytes, and studying lizard skulls. It was a joy to work with all of you, and to see you begin your own careers in science.

Anyone would be lucky to work in the UCMP or the MVZ. I can't believe I was fortunate enough to work and have a home in both museums. Not only are both collections incredible (I'm going to go through specimen withdrawal!), but my two museum families

were so welcoming and so supportive. There are few places where natural history and organismal biology are embraced so enthusiastically and considered so rigorously.

Most important, this dissertation could not have been completed without the love and support of my family and friends. Who could have predicted, back in 1993, that I'd meet two ladies and a group of guys whose friendship I'd still cherish twenty years later? Well, a lot of cliché high school nostalgia movies, but still. Greta, Renee, Dan, Matt, Saunders, and Brian: thanks for everything, from cross-country visits to midnight calls. The group chats helped me feel normal and at home when I was going dissertation-stir-crazy. I hope we're still hanging out in twenty more years (or longer). Eva and Chris, I doubt I could have survived Berkeley without you. You helped me through rough emotional waters and have shown me incredible love and kindness. There have been so many times over the last year I wished you both were still here; I can't wait to be in the same time zone again. Matt, you're my oldest friend in academics, but we would have been friends if we met in a bar or army surplus store, too. I think you might have been the first person to believe I could do this, and you've never wavered in that belief. Thanks again for the hundreds of hours of high quality conversation, and for introducing me to SCOTS.

To my parents I owe my love of learning and work ethic, and to my sisters and brother I owe my sense of humor. These have always been the most critical components of my success and happiness. Mom and Dad, thanks for understanding when I couldn't make holidays or visit as often as I wanted to. Theresa, Pat, Liz, Brian, Emily, Davey, Becca, and John: I love you all so much. I was blessed to be born into a family of smart, hilarious people. You keep me grounded and keep me sane. To my adopted family, Mom and Dad Purcell, Greta, Chris, and Renee: thank you for your love and for your confidence in me, and for countless wonderful memories filled with laughter and music. Brian, mi tesoro, you are my rock; I care so much for you. You made my last two years in Berkeley wonderful.

Finally, to my nephews and niece, who give me hope for the future, two pieces of advice: First and foremost, be kind to other people. Don't be assholes. Second, find something that makes you happy and make it a big part of your life, even if it takes a lot of work. Most of the best things in life require hard work to obtain and to maintain, so the road getting there can be rough. But if you're good to people, you will not be alone on that journey. The people you meet along the way will be there to help you when you stumble, and they'll be there to celebrate when you triumph, but mostly, they will be a great reward in and of themselves. May the people you meet on your paths to greatness be as wonderful as the people I have known en route to my goals.

CHAPTER ONE

The utility of some bone microstructural characters in assessing growth and metabolic rates

ABSTRACT

Histological studies have established relationships among the microstructural features of bone, the growth rates of primary cortical bone, and whole-body growth rates of the animal. For animals of a given body size, the density and connectivity of vascular canals and the disorganization of collagen fibers increase with the rate of bone deposition, and osteocyte density is positively correlated with metabolic rate. Although these relationships are quantifiable, paleohistological studies generally use a tissue-level approach to describe and compare bone growth, except when reconstructing growth curves. In this chapter, I review and refine several methods to improve the quantification of growth-related patterns in fossil bone tissue, focusing on specific microstructural characters known to correlate with growth and metabolic rates in living tetrapods. The most critical histological indicator of growth, the rate of bone deposition, is rarely reported in fossil studies. Occasionally, it has been estimated using values associated with specific vascular patterns in extant birds, a relationship that is not constant across tetrapods. Zonal area and average zonal width directly measure annual deposition, and can be used to bracket daily deposition rates. Estimating bone tissue growth based only on vascularization pattern ("Amprino's Rule") likely confounds three separate vascular signals: density, connectivity, and orientation/patterning. I discuss ways to measure these separately, using qualitative and quantitative means. Collagen fiber orientation, a sensitive indicator of bone deposition rate that may resolve seasonal shifts, is sometimes obscured in fossils by diagenetic alteration. Patterns of osteocyte organization and orientation, more than cell shape, are highly associated with fiber orientation and may be more appropriate proxies. Osteocyte and canal density, not typically reported in paleohistological studies, are easily measured using digital boxplots along radial transects through the cortex. These measures suggest the possibility of more useful quantification of osteohistological indicators as proxies for growth and metabolic rates in extinct and extant vertebrates.

INTRODUCTION

Bone tissue is a useful tool for studying vertebrate growth and life history because as it is deposited, it leaves a record of its own formation and growth (Enlow and Brown 1956; Peabody 1961; Enlow 1969; Castanet et al. 1993; de Ricqlès et al. 2004). Unless primary bone tissues are subsequently obscured by resorption or secondary remodeling, a significant portion of a bone's growth record is retained throughout an individual's lifespan. If conditions are suitable for skeletal preservation after death, this record may remain largely intact even after an animal's death; many aspects of bone tissue can be directly observed (e.g., collagen

fiber orientation, compact vs. cancellous bone) or inferred (e.g., osteocyte position and orientation based on the position and orientation of the lacunae they occupied in life) in dead bone. These characteristics can be examined in recently dead as well as fossilized individuals, using identical methods of preparation, observation, and analysis. This facilitates the study of histological variation and evolution within and among lineages, and through Deep Time.

In extant vertebrates, whole-organism growth rate is reflected in the appearance of bone tissue (Amprino 1947; Peabody 1961; de Ricqlès 1975; de Ricqlès et al. 1991; Castanet et al. 2000; de Margerie et al. 2002, 2004; Montes et al. 2007, 2010; Cubo et al. 2008, 2012) and many histological characteristics are known to vary with whole-organism growth rate. These include the density, arrangement, and organization of blood vessels (Amprino 1947; de Margerie et al. 2002, 2004; Montes et al. 2007, 2010; Cubo et al. 2012), the density, arrangement, and organization of osteocyte lacunae (Francillon-Vieillot et al. 1990; de Ricqlès et al. 1991; Cubo et al. 2012); the organization of collagen fibers (de Ricqlès 1975; Francillon-Vieillot et al. 1990; de Ricqlès et al. 1991; de Margerie et al. 2004), the number of annual growth lines (Peabody 1961; de Ricqlès 1975; de Ricqlès et al. 1991), and rates of yearly bone deposition (Peabody 1961; Montes et al. 2007; Cubo et al. 2008, 2012).

Whole-organism growth rate is correlated with metabolic rate in living animals (Case 1978a, 1978b; Montes et al. 2007; Cubo et al. 2008), so if whole-organism growth rates can be assessed using bone histology, then bone tissues may potentially serve as a proxy for metabolic rate as well. This hypothesis is supported by recent evidence that osteocyte density strongly correlates with basal metabolic rate (BMR) in extant amniotes (Mullender et al. 1996; Bromage et al. 2009, 2012; Cubo et al. 2012).

The potential to reconstruct or estimate growth and metabolic rates for fossil taxa therefore seems high. Such efforts are necessary in order to examine the evolutionary history of growth and metabolism directly in the fossil record, rather than relying solely on living taxa and their extant outgroups. Furthermore, this initial groundwork must be laid in order to identify factors that could have influenced (or at least have been correlated with) evolutionary changes in growth or metabolism (e.g., shifts in body size, morphology, or ecology, or major events in Earth history).

The purpose of this introductory chapter is to review the microstructural characteristics that have been used to correlate the appearance of bone tissue with differences in growth and metabolic rates. I outline the characters I will describe in the remainder of this dissertation, discuss their utility, and offer insights into how they can be improved.

LEVELS OF ORGANIZATION IN BONE

Petersen (1930) classified bone tissues into four hierarchical levels of organization: (1) anatomical, (2) histological, (3) cytological, and (4) molecular, which correspond to different scales of observation. The scale at which one observes bone tissue dictates which growth-related features one can comment on. Petersen's (1930) first (anatomical) level corresponded to observations not only of the external morphology of bone, but also whether bone was compact or spongy, and the orientation of large vascular canals within the bone. Basically, this order includes the aspects of bone and its tissues that one can see with the naked eye

(Petersen 1930; Francillon-Vieillot et al. 1990), but one can observe some of these traits using an optical microscope. The second (histological) level overlaps in scale with the first somewhat, but always requires an optical microscope for detailed observations and measurements. Second level observations relate to the number, size, and orientation of trabeculae and vascular canals, and the overall structure of the extracellular matrix (Petersen 1930). The third (cytological) level similarly overlaps the second; at this level, one observes the number, size, organization and arrangement of osteocytes, and the finer details of the extracellular matrix. Third level observations can be made using an optical or electron microscope (Francillon-Vieillot et al. 1990). The fourth (molecular) level concerns the chemical, subcellular, and (presumably) genetic properties of the cells and the extracellular matrix (Petersen 1930).

Ideally, a thorough description of bone growth would integrate all four levels. However, this is not usually done. From a practical standpoint, to some extent the first three level can all be analyzed using the same piece of equipment (an optical microscope), and so they are most commonly included when growth analyses involve bone microstructure. Histological examinations of Recent bone at all levels are directly comparable (at least in some aspects) to those made on fossil bone. However, characteristics of the fourth level are most subject to taphonomic alteration during fossilization. For my dissertation research, I have not made any fourth level observations. Therefore, I restrict subsequent comments to the first three levels.

BONE MICROSTRUCTURE AND GROWTH RATE

Categorical approaches

The relationship between bone microstructure and growth rate was established broadly by Amprino (1947), who noted connections between bone growth rate and the overall structure and organization of periosteally deposited cortical bone tissues. For animals of a given body size, cortical vascular density, vascular connectivity, osteocyte density, and collagen fiber disorganization all increased with bone deposition rates. These general relationships that Amprino established were not contested despite more extensive taxonomic sampling among living vertebrates over the course of the next three decades by Enlow and Brown (1956, 1957, 1958; Enlow 1963, 1969), Peabody (1961), and de Ricqlès (1968, 1969, 1972, 1974a, 1974b, 1975, 1976, 1977a, 1977b, 1978a, 1978b, 1976, 1981). The concept that bone structure usually and mainly reflects bone growth rate gradually came to be known as "Amprino's rule".

Between 1968 and 1981, Armand de Ricqlès published a series of eleven papers in *Annales de Paléontologie (Vertébrés)*, largely based on his dissertation work. Parts I through VI (de Ricqlès 1968, 1969, 1972,1974a, 1974b, 1981) described the bone microstructure of various Paleozoic and Mesozoic vertebrate groups - early amphibians, dinosaurs and other reptiles, and mammalian ancestors. Part VII (published in five parts; de Ricqlès 1975, 1976, 1977, 1978a, 1978b) is a synthetic work that examined the dual influences of evolution and function on the appearance and formation of bone tissue. Part VII also proposed a

classification system that, for the first time, incorporated developmental and depositional criteria as well as several types of constituent characters (e.g., collagen fibers, vascular arrangement, and osteocyte arrangement, rather than focusing on any one of those) into its diagnoses (de Ricqlès 1975). de Ricqlès' classification acknowledged that aspects of each of the previous diagnostic schemas (based on single processes or types of characters) were biologically relevant. It represented a significant turning point in how people viewed bone, not only because it was integrative, but also because it clarified the extent of bone tissue diversity and provided a "framework for interpreting the overall functional significance of bone tissues" (Francillon-Vieillot et al. 1990).

In Part VII, de Ricqlès (1975) described and classified six main types of primary cortical bone tissue. This classification scheme was expanded and clarified in a 1990 paper by Francillon-Vieillot and colleagues:

- lamellar-zonal bone [term follows Gross (1934)]:
    - avascular lamellar or parallel-fibered (pseudo-lamellar) bone
    - lamellar or parallel-fibered bone with simple canals
    - lamellar or parallel-fibered bone with primary osteons
- woven-fibered bone:
    - avascular woven-fibered bone
    - woven-fibered bone with simple canals
    - fibro-lamellar bone = woven-fibered bone with primary osteons

Note that in the above list, there are three types of lamellar-zonal bone, each of which may be composed of either lamellar or parallel-fibered bone (or both), and that fibro-lamellar bone is just one type of woven bone. Additionally, each of the terms that describe categories (woven bone, simple canals, etc.) has a specific definition. Importantly, although these definitions contain information for several characteristics of the appearance of bone tissue at one or more of Petersen's (1930) observational levels, they do not contain information about every characteristic at every level. The categories themselves and their constituent terms' definitions are often specific at one order but flexible at another (e.g., woven-fibered bone "*may* reach a high degree of mineralization" and "*can* be associated with a dense vascularization" [Francillon-Vieillot et al. 1990: p.502; my emphasis added]), acknowledge great variation but not fully describe it ("The volume, shape, abundance and canalicular development of osteocytes can vary greatly from one bone tissue to another." [Francillon-Vieillot et al. 1990: p.508]), or silent altogether on some observable characteristics of the bone tissue (e.g., the orientation and arrangement of osteocytes within laminar bone, described below).

Here and in other works, de Ricqlès and his colleagues (e.g., de Margerie et al. 2002) referred to their categorical classification of bone tissue types as "typological." This is a common translation of the French *typologie*, but it has a different meaning in English: "typological" carries the negative connotation of "non-evolutionary" or "essentialist". This stems largely from the work of Ernst Mayr (e.g., Mayr 1982), who contrasted his view of "populational thinking" with approaches that emphasized "typical" characterizations of species and did not sufficiently take into account the importance of population-level variation. In French, however, the term *typologie* is better translated as the more neutral concepts

"categorization," "system," or "taxonomy" (in a non-biological sense), and I will use these terms here.

In that same paper, de Ricqlès also expanded on Amprino's (1947) observations relating vascular complexity (the number and directions of connections between vascular canals) to bone deposition rates and whole animal growth rate. Using new/standardized terminology, de Ricqlès erected this hierarchy for vascular patterning in fibro-lamellar bone tissue (vascular patterns are listed in order of increasing deposition/growth rate):

- lamellar-zonal bone
    - avascular lamellar/parallel-fibered bone
    - lamellar/parallel-fibered bone with longitudinal primary osteons (randomly and sparsely distributed)
    - lamellar/parallel-fibered bone with longitudinal primary osteons in bundles
    - lamellar/parallel-fibered bone with longitudinal and circular primary osteons
    - lamellar/parallel-fibered bone with longitudinal and circular primary osteons anastomosing with short radial simple primary canals
    - lamellar/parallel-fibered bone with longitudinal primary osteons anastomosing with short reticular simple primary canals
    - lamellar/parallel-fibered bone with longitudinal primary osteons and long radial simple primary canals (anastomosing or not; radial is the dominant orientation/canal type)
- fibro-lamellar bone
    - woven bone with longitudinal primary osteons (randomly and sparsely distributed)
    - woven bone with longitudinal primary osteons in radial or circular rows
    - woven bone with laminar pattern (anastomosing circular and longitudinal primary osteons)
    - woven bone with plexiform pattern (laminar pattern anastomosing with radial primary osteons)
    - woven bone with radiating (radial) pattern (similar to plexiform, but with radial primary osteons as the dominant orientation/canal type)
    - woven bone with reticular pattern of primary osteons

de Ricqlès (1975) and Francillon-Vieillot et al. (1990) noted that parallel-fibered bone is deposited more rapidly than lamellar bone, but did not describe how the various combinations of fiber type and vascular pattern intercalate in this schema.

In 1990, Francillon-Vieillot and colleagues published a longer explanation of these bone tissue types, which included a discussion of histological variation at each of Petersen's (1930) orders and further discussion of variation in vascular patterning within fibro-lamellar bone. Their additional observations support the conclusions of de Ricqlès (1975) and Amprino (1947). Basically, these can be summed up this way: all else being equal, highly-organized lamellar tissues with simpler vascular patterns are more likely to be found in slower-growing bone tissue and animals, and the more disorganized, woven tissues with more complex vascular patterns are found in faster-growing bone tissue and animals.

Since the publication by Francillon-Vieillot et al. (1990), this general relationship has been generally accepted by the paleohistological community (e.g., Castanet et al. 1996; Chinsamy-Turan 2005; Erickson 2005; Chinsamy-Turan 2011; Huttenlocker et al. 2013; but see Starck and Chinsamy 2002 for some specific criticisms, which I also discuss below). It is important to note that this relationship is a *relative* one. The categories hold true when certain factors (such as age, skeletal element, phylogeny, and especially body size) are controlled (Castanet et al. 1996; Erickson et al. 2009), but the relationships are less clear when they are not (Starck and Chinsamy 2002).

de Ricqlès' system did much to advance our understanding of bone tissue appearance as it relates to growth rate. However, there are some potential problems with this categorical approach. The first is shoehorning. Each category within the Amprino/de Ricqlès hierarchy describes a specific suite of characters that together span Petersen's (1930) first three levels. However, the categories do not include all known combinations of the component characters, and lump others together despite known differences in growth rate (parallel-fibered and lamellar bone, for example). The original intention of this system (explicitly!) was not to make an exhaustive list of character combinations, but rather to discuss the relative growth rates of some commonly observed character combinations (de Ricqlès 1975; Francillon-Vieillot et al. 1990). A problem may arise when attempting to interpret taxa that do not exhibit one of the common suites of characters defined by the pre-existing categories. Here, the researcher may choose to exclude the specimen from comparative analysis, or assign it to a category despite a mismatch in one or more component characters. In either situation, basic descriptive information is lost.

The most extreme version of the above problem occurs when a false dichotomy is erected that places all bone in one of two categories: fibro-lamellar bone or lamellar-zonal bone. Although de Ricqlès (1975) and Francillon-Vieillot et al. (1990) were clear that these categories are just small parts of a large continuum of bone variability, some authors have persisted in presenting bone in such a reductionist manner. This view is not uncommon in the literature arguing against dinosaur endothermy (e.g., Reid 1987; Ruben et al. 2003).

Another potential problem is that reliance on categorical descriptors can obscure data from or variation within component characters. This is an inevitable result of shoehorning, but also occurs when dealing with variable characters and characters not discussed in the category's definition. Thus, if any of the component characters are more strongly correlated with growth rate than others, it may be difficult to parse out the true signal.

In summary, although there are clear advantages to a categorical approach when describing bone tissues, there is also a potential for a reduced, obscured, or confounded signal when attempting to correlate growth rates with bone tissue appearance. This makes it difficult to discuss growth rates with confidence for taxa for which the bone microstructure has only been described categorically. Instead, researchers should separately and systematically discuss the histological characters known to correlate more specifically with growth and metabolism.

Character-based approaches

Many studies have attempted to relate bone and organismal growth rates to specific histological characteristics rather than character suites. This body of work has occurred

mainly outside the paleohistological literature; such papers are more common in the medical, archaeological, and zoological literature. Broadly, these can be grouped into several categories based on the type of character they describe; for example, bone deposition rates, growth lines, vascularity, collagen fibers, osteocytes, and bone turnover. Microstructural characters may be analyzed independently, or as part of a suite of characters to determine covariation. For example, Cubo et al. (2012) measured bone deposition rate, vascular canal density, vascular canal orientation, osteocyte size, and osteocyte density to derive a model that could predict bone deposition rate based on the other characters.

Unlike categorical approaches, which are always qualitative, character-based analyses may be qualitative or quantitative. However, because the characters are analyzed separately, the methods of diagnosis and analysis are generally defined more explicitly. This has several potential benefits: first, explicit means of character assessment reduce the possibility that different researchers (or the same researcher at different times) may diagnose tissues differently. This increases comparability among studies. Second, the quantification of growth indicators allows changes to be tracked separately and at a finer scale, and to be correlated with other biological variables, such as body mass or metabolic rate. Finally, defining characters in more discrete terms allows them to be incorporated into phylogenetic analyses.

I have taken a character-based approach in my dissertation. Below, I have mostly limited my discussion to the characters I examined in Chapters 2 and 3. One character (bone deposition rate) was not examined for my dissertation projects, but will be incorporated into future studies. All characters are those that have been proposed to correlate with growth rate, metabolic rate, or growth senescence, based on observations in living animals.

ASSESSMENT OF MICROSTRUCTURAL CHARACTERS

For each character discussed below, I first describe the history of its use in histological studies, and the different methods that have been used in its assessment. I then provide a summary of how I assessed (or would assess) the character in Chapters 2 and 3. This summary includes a list of possible character states, a brief description of the character, the means of diagnosis, a summary of its relevance to growth or metabolism, and a discussion of its utility in fossil taxa. The summaries are intended for future use in analyses of the phylogenetic distribution of histological characters. It is important to note that many other characters relating to the chemistry of Recent bone may be analyzed (e.g., ash content, isotope ratios), but I restrict my discussion to those characters that can be observed in Recent and fossil bone.

Bone deposition rates

These studies directly measure bone deposition over a given amount of time. Typically, bones are labeled by feeding or injecting an animal with a substance that is taken up into the mineral phase of the bone and remains there. At a later time, the animal is dissected and the amount of new bone deposited external to the label is measured. This value is divided by the length of time since labeling to determine bone deposition rates. The amount of bone deposition is commonly measured linearly and reported as μm/[unit time] (most often

μm/day, but sometimes μm/year). When such studies are performed on long bones, bone deposition rate as the rate of expansion of the diaphysis (either elongation or girth; Cubo et al. 2008).

This line of experimentation dates back to at least the eighteenth century (Duhamel 1739, 1742; Hunter 1798), when researchers fed domestic animals madder (plants in the genus *Rubia*) for several weeks in order to stain their bones red. Madder extract had been used to stain samples of dead bone for scientific examination since at least 1562 (Cameron 1930). When the bones were sectioned, the red color did not penetrate deeply into the cortex. Animals allowed to live for some time after eating madder also had a red ring, but it did not touch the periosteal surface, and new bone had been deposited outside the ring (Duhamel 1739, Hunter 1798). Other early labeling approaches included fitting silver rings around the bone shafts of growing animals and waiting for bone to grow around it (Duhamel 1742).

Today, bone deposition rates are most often assessed using fluorochrome labels. These fluorescent dyes bind to calcium as new bone is deposited, thereby marking the calcification front at the time of injection. Common labels include tetracyclines (Milch et al. 1958), calcein (Suzuki and Mathews 1966), alizarin (initially derived from madder; Puchtler et al. 1969), and xylenol orange (Rahn and Perren 1971). Often, a series of differently colored labels is used at known intervals to track bone deposition and/or bone remodeling (e.g., Cubo et al. 2012). For obvious reasons, fluorochrome labeling of bone can only be performed on living animals. Another way to assess bone deposition rates is to measure the width of the zones that lie between lines of arrested growth (LAGs) and divide it by a unit of time, typically the known duration of growth (e.g., Castanet 1985, 1986-1987; Castanet et al. 1988) or a bracket of estimates for this value (Botha-Brink and Smith 2011). This result is similarly reported as μm/day. Lee and O'Connor (2013) estimated average bone deposition rates from growth curves estimated in turn from measurements of LAG circumferences; rates of circumferential increase were converted to radial rates of bone deposition in μm/day. Deposition estimates were reported as a range: low estimates assumed a growth duration of one Maastrichtian year, and high estimates assumed a Maastrichtian half-year. Their method could easily be modified to estimate maximum bone deposition rate, or ontogenetic trajectories in bone deposition rate.

Once the rate is known, the histology of the tissues that lie between labels or LAGs may be studied in order to obtain estimates of bone deposition rate for certain types of bone. Variations on this approach were used by Castanet et al. 2000, Montes et al. 2007, Cubo et al. 2012, and Legendre et al. (in press) to estimate bone deposition rates in extinct vertebrates. Periosteal bone growth rate was measured using *in vivo* fluorochrome labeling, and afterwards various histological parameters (such as vascular density, vascular pattern, and/or osteocyte size, shape, and density) were estimated. Regression analyses that incorporated phylogeny were used to construct models of bone growth that could predict bone deposition rate using the histological parameters described above. These predictive models were subjected to cross-validation tests and ultimately, bone deposition rates estimated for fossil taxa using histological parameters. One benefit to this method is that it does not require the use of fluorochrome labels, some of which are toxic to vertebrates. Additionally, the method produces directly comparable results for both Recent and fossil specimens. However, the initial sample set used to make these models is small (18 species; Cubo et al. 2012, Legendre et al. in press), and cannot be validated for fossil taxa. The sample does incorporate a phylogenetically broad range of taxa, but not a broad range of body sizes or ecologies. If these

relationships do not hold at larger/smaller masses, or for physiologies and ecologies not represented among sampled taxa, the model would not be suitable.

Variation in bone deposition rates complicates such extrapolations. Within a single element, bone is not always deposited at uniform rates throughout the year, or for the entire year (Caetano and Castanet 1993, Köhler et al. 2012). Additionally, within individuals, the rate of bone deposition has been shown to vary within a single element (Castanet et al. 2000, Starck and Chinsamy 2002, Köhler et al. 2012), among elements (Castanet et al. 1996, 2000; Starck and Chinsamy 2002), and ontogenetically (Castanet et al. 1996, Castanet et al. 2000). There is also variability among individuals of the same species (Chidlow et al. 2007), with food availability (Starck and Chinsamy 2002), seasonally (Castanet et al. 2004, Köhler et al. 2012), and in wild-caught vs. captive specimens (Chidlow et al. 2007). Bone deposition rates have also been shown to reflect biological differences at larger scales; for example, there are strong differences between ectotherms and endotherms (Montes et al. 2007, 2010). This likely reflects a positive correlation between bone growth rate and resting/standard metabolic rate; both within individuals (Pacheco et al. 2010, Köhler et al. 2012) and among species (Montes et al. 2007, 2010; Köhler et al. 2012). Finally, there is also a phylogenetic signal in bone deposition rates (Castanet et al. 2000, Montes et al. 2007, 2010; Cubo et al. 2008). When complicating factors can be controlled, evidence from bone deposition rates can be used to support hypotheses about growth and metabolic physiology in fossil animals.

Bone deposition rate: Character summary and diagnosis

Character states: Continuous character

Description: This character estimates the average amount of radial bone deposition at the mid-diaphysis in a single day, or a minimum estimate of yearly bone growth. It is specific to the element described. This character is expressed in estimated μm/day or estimated μm/year.

Diagnosis: The width of each zone between adjacent LAGs is measured moving from the geometric centroid of the bone along the major and minor axes. These four measurements are averaged for each zone, or across all zones during the active phase of growth (i.e., not in the external fundamental system). When yearly growth duration (days/months of growth per year) is known, it is divided by this amount to estimate deposition in μm/day. When growth duration is unknown, the mean obtained for the zone or active phase can be reported in μm/year, or bracketed with the μm/year representing a minimum estimate of growth rate.

Relevance: Bone deposition rate is a direct measure of bone growth rate. It has been shown to be positively correlated with basal metabolic rate (Montes et al. 2007, 2010, Köhler et al. 2012) and to vary significantly between endotherms and ectotherms (Montes et al. 2007, 2010). It has been shown to carry a phylogenetic signal (Castanet et al. 2000, Montes et al. 2007, 2010; Cubo et al. 2008) and to covary with other histological attributes such as collagen fiber orientation and vascular patterning (de Margerie et al. 2002, Montes et al. 2010). This character measures bone growth directly in Recent and fossil bone, and in a comparable way.

Utility and Discussion: In my diagnosis above, I describe a method in which zonal widths are measured and then averaged by zone (or across the entire active phase of growth). Previous studies have estimated daily bone deposition rates in a similar manner, but only using one radial "transect" through the cortex (e.g., Castanet 1985, Castanet and Naulleau 1985, Castanet et al. 1988). In some cases, fluorochrome injections were timed with LAG

deposition (Castanet 1985, Castanet and Naulleau 1985). These studies established that LAGs were annual and that new bone was deposited only during times of activity (i.e., when they were not hibernating). In the third, bone remained unlabeled and zonal width between LAGs was used as an estimate of growth (Castanet et al. 1988). In each of these studies, the inter-label or zonal width was divided by a 7-month estimate of non-hibernation time to achieve a bone deposition rate, reported in μm/day, even though the exact times between labels were known in two studies.

Montes et al. (2007) stated that bone deposition rate (bone growth rate or BoneGR in that paper) cannot be measured for fossil species, but that the relationship between deposition rate and tissue type can be used to estimate it for fossil species. I agree that bone labeling methods are impossible for fossils, but it is not necessary to make such an indirect (and somewhat circular) inference of this value. My diagnosis suggests one way to deal with the uncertainty of growth duration in dead or fossil taxa, which would be to report growth rate differently depending on whether or not annual growth duration is known. When growth duration is known or can be reasonably estimated, bone deposition is reported in μm/day as is typical for fluorochrome labeling studies (the method of Castanet et al. 1988). When growth duration is unknown, as it will certainly be for nearly all fossil taxa, the estimate is given in μm/year. I suggest that this is a more reasonable measure for two reasons.

First, it is difficult to determine the absolute time of yearly growth duration without direct observation, although recent work linking cyclical growth patterns in lamellar bone and tooth enamel (Bromage et al. 2009, 2012) may lead to new methods to do so. The exact duration of bone growth each year cannot be determined precisely in fossil taxa, but it can be constrained. Assuming annual LAG deposition, there is an upper bound of approximately one year for the duration required to deposit each zone. Based on observations of growth in living taxa, this will overestimate growth duration in nearly all cases. Therefore, dividing each zonal width by a year provides a minimum estimate of growth rate. Assuming that a year's worth of growth was completed in a single day is also unlikely, given what is known about growth in extant species. However, this can be used to estimate a maximum possible growth rate. Thus, growth rate can be reasonably bracketed for fossil taxa.

Second, whereas the time the Earth takes to orbit the sun (a sidereal year) has likely remained constant through its history, the number of days per year has decreased through time as the speed of Earth's rotation has slowed (Wells 1963). Therefore, any estimate of daily growth rate must be calibrated for the number of days at the time the animal was alive, as noted by researchers estimating growth rates based on age-mass curves (e.g., Erickson et al. 2001). This may be difficult to estimate precisely for fossils for which no geologic age is known. If the duration of a year has remained constant through time, it may be more reasonable to report deposition rates in $year^{-1}$ rather than day^{-1}, even if this is not how the results of labeling studies are reported (although Wells [1963] estimated a difference of only 14 days/year between the end-Carboniferous and the end-Cretaceous, so perhaps precision dating would not affect estimates drastically).

My method of averaging radial bone growth based on measurements along the major and minor axes also accounts for differences in growth rate around the circumference of the bone, a problem noted by Starck and Chinsamy (2002). Werning et al. (2008) described a similar method that measured along 36 transects radiating from the geometric centroid of the bone (starting at a major or minor axis), but this method took considerably longer to complete,

requires several additional steps during image preparation, and must be done digitally. Another method that would remove the effects of differential deposition around the bone circumference entirely would be to report zonal area rather than a linear estimate of bone growth. However, the results would not be directly comparable to the current body of literature without subsequent conversion to a linear measure, and would need to be reported as $year^{-1}$ rather than day^{-1}. The method I describe above does not necessarily require digitization of slides, is methodologically consistent with previous studies, and does not necessarily require a complete cross-section.

Note: I did not examine this character in Chapters 2 and 3, but I have estimated annual deposition rates in the dinosaurs *Allosaurus* and *Tenontosaurus* (Werning et al. 2008). The focus of that study was to show the effect of sampling location when estimating bone growth parameters, such as zonal width or number of LAGs. Average measurements incorporating data from around the entire circumference of the section were compared to estimates of growth based only on one region of the bone.

Growth Marks

Growth rates are not uniform throughout the life of an organism. For example, each individual experiences changes in growth rate through ontogeny (Amprino 1947; de Ricqlès 1975; Hall 2005), and many exhibit seasonal changes in growth rate as resource availability, activity levels, and other biological pressures (e.g., climate, reproduction, migration) cause shifts in the energy that can be devoted to growth (Caetano et al. 1985; Klevezal 1996; Chinsamy-Turan 2005; Köhler et al. 2012). As noted above, changes in growth rate are reflected in the appearance of bone tissue. Animals that grow for more than one year experience cycles of growth, and so their bone tissues reflect both annual and ontogenetic shifts in growth rate.

One commonly used indicator of changes in growth rates is the presence of annual growth marks. These present either as annuli or as LAGs, which indicate a temporary slowing or a complete cessation of growth, respectively (de Ricqlès 1975; Francillon-Vieillot et al. 1990; Klevezal 1996). Annual growth marks are known to occur in all major vertebrate groups and are plesiomorphic for tetrapods (de Ricqlès 1975, 1976). They occur in fast and slow growers, in endotherms and ectotherms, and are visible in Recent and fossil bone (Peabody 1961; Enlow 1969; de Ricqlès 1975, 1976; Castanet et al. 1993). Although similar lines can form during times of physiological stress (such as hibernation, birth, or weaning; Castanet et al. 2004; García-Martínez et al. 2011), experimental studies have shown that the annual lines reflect endogenous rhythms (Klevezal 1996; Castanet et al. 2004; Bromage et al. 2009; Marangoni et al. 2009).

The annual periodicity of LAGs was first suggested by Mattox (1935), who observed concentric rings in the long bones of turtles, and noticed that more were present in the bones of larger individuals. As Castanet (1985) noted, these lines had been observed by previous authors, including Seitz (1907) and Gross (1934), but their annual periodicity had not been appreciated. For the next fifty years, the meaning and utility of growth marks were either ignored (e.g., Amprino and Godina 1947; Enlow and Brown 1956, 1957, 1958) or debated in the literature. Although some authors argued that they were likely annual (e.g., Peabody 1961;

de Ricqlès 1975), other authors (most notably Enlow 1969) found the experimental evidence lacking. This debate was largely put to rest as a result of the work of Castanet (1985, 1986-1987; Castanet and Naulleau 1985), who used tetracycline labeling to establish that growth marks in reptiles were annual. Castanet's (1986-1987) study also included a thorough discussion outlining the reasons why the number of LAGs might be higher or lower than an individual's actual age, even though they occurred annually (see below for brief summary).

Since Castanet's landmark studies, the question of whether or not amniotes produce LAGs on an annual basis has not been in dispute, at least for ectotherms. However, their annual periodicity in endotherms was questioned (Reid 1981; 1984; 1985; 1987; 1990; Ruben et al. 2003), based on the incorrect perception that they were not present in endotherms except as a result of extreme physiological stress. Since that time, many studies have confirmed that growth marks are annual in mammals (Castanet et al. 2004; García-Martínez et al. 2011; Köhler et al. 2012) and even in some birds (Turvey et al. 2005; Bourdon et al. 2009) that take more than a year to reach asymptotic mass or linear size.

Because they have a periodicity of known duration, annual growth marks have been used to assess vertebrate growth in a number of ways. Perhaps most important, the number of growth marks is an estimate of absolute age at the time of death (Castanet 1986-1987; Castanet et al. 1993; Horner et al. 1999; Woodward et al. 2013). Growth marks form at the depositional front at the periosteal surface. Because long bone circumference is a function of mass (Anderson et al. 1985), growth mark circumference also may be used as a proxy for body size at the time of their deposition (Cooper et al. 2008; Lee and O'Connor 2013). Thus, the number and the circumference of growth marks may be used to construct age-size growth curves for vertebrates, whether extant or extinct (e.g., Erickson and Tumanova 2000, Erickson et al. 2001, 2004; Horner et al. 2004; Lee et al. 2013).

Because annual growth marks demarcate zones of yearly growth, they are key for assessing the distribution of growth rates within a single growth cycle, or comparing changes in annual growth through ontogeny (e.g., Horner et al. 2000; Werning 2012). Other types of growth marks are also helpful in this regard, even though they are not annual. For example, some individuals show more than one line at the end of a growth cycle (double LAGs, triple LAGs, or LAG packets). The spaces between these LAGs do not represent a year of growth; rather, these LAG packets reflect an animal's capacity to turn growth "on and off" within a single year. This capacity is known to vary ecologically in some taxa. For example, Caetano et al. (1985) showed that individuals of *Triturus marmoratus* (although not an amniote) from low-elevation populations only exhibited single LAGs, but the percentage of individuals exhibiting double/twin LAGs increased dramatically with elevation. The difference was one of ecology: high elevation populations tended to estivate for a short time between their aquatic phase and their winter hibernation, but low-elevation populations did not. The space between twin LAGs corresponded to growth between estivation and hibernation. The capacity to turn growth on and off also varies ontogenetically: Köhler et al. (2012) showed that bovids only produced single LAGs as juveniles, but double LAGs were present in adults.

Growth marks may also be used as indicators of skeletal senescence. An external fundamental system (EFS; Cormack 1987) is a series of very closely spaced growth deposited in a zone of avascular and acellular bone tissue at the periosteal surface. It is found in individuals that have finished the active phase of skeletal growth and reflects minor amounts of appositional growth late in life. The EFS was first recognized in mammals (Cormack 1987;

Klevezal 1996), but has since been discovered in a variety of birds (Chinsamy 2002; she used the term "outer circumferential layer"), dinosaurs and pterosaurs (Horner et al. 1999, 2000; Werning 2012), and pseudosuchian archosaurs (de Ricqlès et al. 2003, Woodward et al. 2011).

Castanet (1986-1987), Klevezal (1996), Horner et al. (1999), and Woodward et al. (2013) review other, noncyclical life history events that may result in the appearance of similar, but non-annual, annuli or LAGs; these include hatching/birth, weaning, starvation, and differences in growth rates and resorption around the circumference of the bone. Recently, Griebeler et al. (2013) recommended the use of modulations in other microstructural features (e.g., vascular density, vascular patterns, and collagen fiber organization) to the annual periodicity of growth marks.

Growth marks: Character summaries and diagnoses

Growth marks: presence

Character states: Growth marks are either present (0) or absent (1)

Character polarity: The presence of growth marks is plesiomorphic for tetrapods (de Ricqlès 1975).

Description: The presence or absence of growth marks (annuli or LAGs) in primary cortical bone tissue.

Growth marks: type

Character states: Categorical; annulus or LAG. These may transition into each other regionally and may co-occur within a growth cycle.

Description: The type of growth mark observed in primary cortical bone tissue.

Growth marks: number

Character states: Descriptive; continuous character

Description: The number of observed growth marks (annuli or LAGs) in primary cortical bone tissue. This character differs from "reconstructed growth marks", which are estimates of the growth marks lost to secondary remodeling or medullary cavity expansion.

Growth marks: external fundamental system (EFS)

Character states: Present or absent

Description: The presence or absence of an EFS (a series of closely spaced LAGs at the periosteal surface of the bone), representing low rates of appositional mid-diaphyseal growth after of the active phase of skeletal growth has finished.

Diagnosis (for all four characters listed above): Growth marks vary in appearance, but share several features in common. They are relatively thin bands that travel around part or all of the bone circumferentially, and differ in appearance from the flanking zones in a way that reflects slower or temporarily stopped growth (see character descriptions of fibrillar organization and vascularity, below).

I diagnose annuli following the criteria of Francillon-Vieillot et al. (1990): a thin band of parallel-fibered or lamellar bone tissue, generally avascular or poorly vascularized

compared to the flanking zones. Annuli are often distinct in regular transmitted light, because they are associated with changes in vascularity and osteocyte organization, and in some cases the border between lamellae are visible. Wherever possible, I confirmed the presence of a histological transition to lamellar or parallel-fibered bone under crossed plane polarized light or elliptically polarized light. The differences between parallel-fibered and lamellar bone are sometimes difficult to observe in regular transmitted light when the annuli are very thin, or the region is partially obscured by secondary osteons.

Following Francillon-Vieillot et al. (1990), I diagnose a growth mark as a LAG when I observe a cement line. This discontinuity must present as a clear break in bone tissue, visible at several magnifications. This is determined by focusing through the plane of section at the point of the hypothesized LAGs. Two or more LAGs running parallel to each other in extremely close succession are diagnosed as double LAGs, triple LAGs, or LAG packets. The individual LAGs in these LAG packets share very subtle changes in morphology not found in the previous or subsequent years' LAGs (Castanet et al. [1993] refer to them as "twin lines"). They are not separated by larger, annual zones of deposition, and the regions of bone between them are avascular. Within a LAG packet, one line is often more distinct than the others. In these cases, I measured circumference along this line. When all LAGs were equally distinct, I measured to the outermost line.

LAGs often lie within an annulus (Francillon-Vieillot et al. 1990) or at their inner or outer periphery (personal observation). I note their position relative to the annulus when they co-occur. Additionally, a growth mark may appear as an annulus in one region of the bone and as a LAG in another region. I describe these marks based on whichever state is more common around most of the circumference, but always note that they locally grade into the other state.

An EFS is a series of closely spaced LAGs separated by very narrow zones of avascular, lamellar bone, and occurring in the outermost portion of the bone cortex (at the periosteal surface). An EFS may be distinguished from distinct lamellae by the presence of a cement line (break in tissue). An EFS may be distinguished from a LAG packet in several ways: first, the lines within an EFS are usually separated only by 1-2 lamellae (they may be more widely spaced in a LAG packet). Second, the lines within an EFS do not necessarily share subtle changes in morphology, a defining criterion of a LAG packet. Finally, no additional bone lies between an EFS and the periosteal surface, whereas this is expected if an animal died during a time of zonal growth after depositing a LAG packet.

In all cases, I number growth marks from the internalmost to the externalmost. I count each LAG packet as marking the end of one growth cycle (i.e., I do not count each line as a separate growth mark). Within the EFS, I count each line separately, although I note that each line may not correspond to a year's worth of appositional growth.

Relevance (for all four growth mark characters listed above): Growth marks in bone often reflect endogenous, cyclical rhythms (Klevezal 1996; Castanet et al. 2004; Bromage et al. 2009; Marangoni et al. 2009). When these cycles are annual, growth marks allow an estimation of absolute age (Castanet 1985, 1986-1987; Francillon-Vieillot et al. 1990; Castanet et al. 1993; Klevezal 1996). The circumference of annual growth marks reflects the circumference of the bone at the time it was deposited, which corresponds to mass (Cooper et al. 2008; Lee and O'Connor 2013); therefore, the number and circumference of growth marks

may be used to construct age-size growth curves (Erickson and Tumanova 2000, Erickson et al. 2001, 2004; Horner and Padian 2004; Lee et al. 2013). By delimiting annual segments, growth marks allow the distribution of growth rates within a single growth cycle or during ontogeny to be compared (e.g., Horner et al. 2000; Werning 2012).

The type of growth mark visible indicates whether growth temporarily stopped (LAG) or merely slowed (annulus). Depending on the details of their morphology and cortical location, a series of closely spaced LAGs or annuli may represent an organism's ability to start and stop growth within a year (LAG packet; Caetano et al. 1985; Köhler et al. 2012) or serve as a marker of skeletal senescence (EFS; Cormack 1987; Klevezal 1996; Horner et al. 1999).

When growth marks are not annual, they may result from major life history events or times of great physiological stress, such as birth, weaning, or starvation (Castanet 1986-1987; Klevezal 1996), or they may reflect differential growth around the circumference of the bone (Woodward et al. 2013). Annual and non-annual growth marks may be distinguished from each other by the presence of other microstructural indicators of growth cyclicity (Griebeler et al. 2013), or with knowledge of an animal's natural and life histories (García-Martínez et al. 2011).

Utility and Discussion: Growth marks have long been known from fossil bone (Peabody 1961). They are quite important because they provide the only means of estimating age at death for a fossil specimen. As for Recent bone, the interpretation of fossilized growth marks requires the observer to assess whether or not they are annual. Interpretation may be somewhat more difficult for extinct taxa, because independent means of assessing life history (e.g., direct observation of the timing of weaning or senescence), are only rarely available. This problem is complicated by the lack of replicates in fossil data sets; often, only one or two specimens are available for analysis. Higher confidence in growth mark assessment can be achieved in fossil specimens when more than one element or individual is examined, especially when the individuals form an ontogenetic series.

Collagen fibers

A relationship between the rate of cortical bone deposition and the disorganization of collagen fibers has long been hypothesized (Amprino 1947; Pritchard 1956; Enlow 1969, de Ricqlès 1975). In general, collagen fibers are less organized in tissues that are deposited faster (i.e., woven-fibered and fibrolamellar bone) and more organized in tissues that are deposited at slower rates (i.e., parallel-fibered and lamellar bone). Newell and Sirianni (1982) provided the first evidence for this; using fluorescent bone labeling techniques, they showed that bone depositional rates were higher in woven-fibered cortical bone of fetal macaques than in the parallel-fibered bone tissue they deposited after birth. Using the same method, de Buffrénil and Pascal (1984) determined that bone deposition rates in *Mustela vison* were higher for woven-fibered bone than for fibrolamellar bone, which in turn was deposited faster than parallel-fibered bone. Subsequent studies have confirmed this relationship between bone deposition rate and fibrillar organization (Castanet et al. 2000; de Margerie et al. 2002). Bone deposition rates for the same type of fibrillar organization are different when comparing

periosteally-derived and endosteally-derived tissues, which tend to be deposited at higher rates (Newell and Sirianni 1982; de Buffrénil and Pascal 1984; Francillon-Vieillot et al. 1990).

Different methods have used been to diagnose fibrillar organization. Francillon-Vieillot et al. (1990) outline a number of methods, including examination under polarized light and staining. The latter method may not be useful for studies of fossil bone, which undergo chemical changes in the mineralized component of the matrix during fossilization, so I do not consider it here. Polarized light is commonly used to examine fossil bone; collagen is often preserved in fossils (Wyckoff et al. 1963; Pawlicki et al. 1966; Bocherens et al. 2003) or may be replaced in situ by secondary apatite, which is also birefringent (albeit with the opposite optical sign of collagen; Lee and O'Connor 2013).

Under crossed plane polarized light, Francillon-Vieillot et al. (1990) report that woven-fibered bone should reveal general optical isotropy; that is, it should remain optically extinct (dark) regardless of the orientation and rotation of the polarizers. Conversely, parallel-fibered bone should be optically anisotropic, changing from light to dark as the polarizers are rotated. Lamellar bone will appear differently under polarized light, depending on how the fibrillar orientation changes from layer to layer. When all layers share a common fibrillar orientation (either longitudinal or circumferential/transverse), all layers will be anisotropic, and change colors from light to dark simultaneously as the polarizers are rotated (Bromage et al. 2003). When lamellae alternate in fibrillar orientation from layer to layer, the layers should exhibit alternating anisotropy (Francillon-Vieillot et al. 1990; Bromage et al. 2003). Thus, rotation of plane polarizers is necessary to distinguish among the tissue types (Bromage et al. 2003).

This means of diagnosis is problematic for several reasons. First, static images taken under crossed plane polarized light cannot necessarily be used to verify fibrillar organization, because different fibrillar organizations will appear light or dark depending on the orientation of the sample and the rotation of the polarizers (Bromage et al. 2003, note Figure 1, p. 159; Stein and Prondvai 2013). There are many ways to solve this; for example, several images or video could be taken of the specimen as the polarizers were rotated. Stein and Prondvai (2013) recommended producing and examining specimens in both longitudinal and cross section as a way to confirm orientation of fibers. It is also possible to use circularly polarized light, which transmits maximum light intensity regardless of the rotation of the polarizers (i.e., the pattern of birefringence is the same regardless of polarizer orientation; Bromage et al. 2003). The second problem with the diagnosis of Francillon-Vieillot et al. (1990), as Warshaw (2008), Woodward et al. (2013), Lee and O'Connor (2013) note, is that woven-fibered bone should not appear completely dark under polarized light, but rather as a mosaic of relatively light and dark areas (or multicolored in elliptically polarized light). This reflects the disorganization of the tissue, with fibers and fiber bundles showing not preferred orientation.

Other ways to diagnose fibrillar organization use the shape, orientation, and arrangement of osteocyte lacunae. Based on a large sample of extant and extinct vertebrates, de Ricqlès (1974, 1975, 1976, 1980) and Francillon-Vieillot et al. (1990) noted that osteocytes in woven-fibered bone tended to be globular or round in cross section, whereas osteocytes in lamellar and parallel-fibered bone tended to appear flattened in cross section, suggesting that osteocyte shape might also predict fibrillar organization. This was confirmed by Remaggi et

al. (1998) and Ferretti et al. (1999), who performed histomorphometric analyses on osteocytes from five mammals, a chicken, and a frog. In all species examined, osteocyte cell bodies approximated a triaxial ellipsoid in lamellar and parallel-fibered bone, whereas in woven bone they were more spherical or lenticular. In lamellar bone, the osteocytes were flatter than in parallel-fibered bone.

Fibrillar orientation is also reflected in the orientation of osteocyte lacunae, although most of the work establishing this correlation has been done using mammals. Remaggi et al. (1998) established that osteocytes in parallel-fibered bone were always aligned with their major axis parallel to the orientation of the collagen fibers, and Ferretti et al. (1999) found that the osteocytes of lamellar bone were regularly spaced and aligned in rows along lamellae. Using mouse, horse, and sheep models, Hirose et al. (2007) and Kerschnitzki et al. (2011) found that osteocytes in woven-fibered bone showed no preferred orientation relative to the long axis of the bone and no preferred orientation or arrangement relative to each other. They also confirmed the results of Remaggi et al. (1998) and Ferretti et al. (1999) regarding the orientation and spacing of osteocytes in parallel-fibered and lamellar bone.

In a study of primate microstructure, Warshaw (2008) further subdivided this character from the standard woven-parallel-lamellar trichotomy. She examined woven bone, fast fibrolamellar bone, slow fibrolamellar bone, parallel-fibered bone, hybrid parallel-fibered and lamellar bone, and lamellar bone. Her study is notable not only because of the level of specificity in the organization type, but also because it is one of the most explicit in terms of its diagnostic criteria. Woven-fibered bone was identified based on a combination of characters: osteocyte shape (stellate or round), random distribution of the osteocyte lacunae, and multidirectional fibrillar organization in circularly polarized light. The two categories of fibrolamellar bone were distinguished based on vascular density, not fibrillar differences. She identified parallel-fibered bone based on the appearance in circularly polarized light, in which she observed bulk birefringence with less than 25% of the tissue showing lamellae. Warshaw (2008) also noted that osteocyte lacunar shape and distribution were somewhat variable in parallel-fibered bone. Lamellar bone was similarly birefringent as parallel-fibered bone, but had more than 25% of the tissue had lamellae. In lamellar bone, the osteocytes differed somewhat in shape, but in general were flattened, and aligned parallel to each other and to the lamella. Additionally, lamellar borders were distinct under regular and polarized light.

Collagen fiber orientation: Character summary and diagnosis

Character states: lamellar, parallel-fibered, or woven-fibered. These characters are often treated as categorical characters, but parallel-fibered and woven-fibered bone may together comprise a continuous character.

Description: The type of collagen fiber orientation/organization in the primary cortical tissue. This character may be modified to describe the dominant fibrillar organization throughout the section, rather than applied specifically to one region. It also may be useful to note the fibrillar organization associated with the fastest bone deposition rates in the section, in addition to the dominant organization, as an estimate of the fastest potential bone deposition rates.

Diagnosis: This character may be diagnosed using circularly polarized, crossed plane polarized or elliptically polarized light. For my observations in Chapters 2 and 3, I examined the specimens in regular transmitted light, crossed plane polarized light, and elliptically

polarized light. In specimens that preserved collagen or secondary apatite replacement of collagen, I diagnosed lamellar bone and parallel-fibered bone in a manner similar to that of Warshaw (2008) and Francillon-Vieillot et al. (1990). Both tissues required an observation of bulk anisotropy, but a diagnosis of lamellar bone required an additional observation of lamellar borders. I diagnosed bone tissue as lamellar only if lamellae were visible across 2/3 or more of the observed region (by eye), and parallel-fibered bone if no lamellae were visible across 2/3 of more of the region (by eye). I referred to bone tissue as "mixed parallel-fibered and lamellar" when bulk refringence was present but lamellae were present in intermediate amounts. For woven-fibered bone, I followed the diagnoses of Warshaw (2008) and Lee and O'Connor (2013) in that I required an observation of a mosaic or woven-textured mix of fibers.

This character may also be diagnosed using osteocyte orientation in primary cortical bone. In the materials examined for Chapters 2 and 3, I observed variation in osteocyte shape, but noted that orientation was always correlated with fibrillar organization. The lacunae in woven-fibered bone show no preferred orientation to the long axis of the bone, and no preferred orientation, arrangement, or alignment relative to each other. The lacunae in parallel-fibered bone are generally oriented perpendicular to the long axis of the bone, but some (no more than 1/3) may be slightly oblique. The lacunae show a general circumferential orientation, but are not spaced evenly. In lamellar bone, lacunae are oriented in the same direction as the lamella with which they are associated (in most cases, perpendicular to the long axis of the bone). These align circumferentially along lamellae, and show fairly regular spacing.

Relevance: The organization of collagen fibers is correlated with bone deposition rate (Newell and Sirianni 1982; de Buffrénil and Pascal 1984), with more organized tissues deposited at slower rates. However, the deposition rate for each fibrillar organization may be taxon specific (de Buffrénil and Pascal 1984).

Utility and Discussion: Slide thickness affects the observation of collagen fibers in fossil bone. Although collagen may be retained in fossils, it can be present in lower levels compared to Recent bone. Because the replacement minerals in fossil bone are often darker than the original bone, fossil bone is generally ground to optical clarity, which occurs at different thicknesses in different specimens (Lamm 2013; Woodward and Horner 2013). In the process of grinding to optical clarity, the resulting specimen may be so thin that the remaining collagen will not produce a strong pattern of birefringence (Woodward and Horner 2013; personal observation). This means that polarized light will not always be sufficient to verify fibrillar organization.

Based on my observations (Chapters 2 and 3), patterns of osteocyte organization and orientation, more than cell shape, are highly correlated with fiber orientation. This relationship is consistent in marsupial and placental mammals and a broad taxonomic sample of extant and extinct archosauromorph reptiles. I also found osteocyte orientation to be a better predictor of fibrillar organization than canal type, canal density or vascular patterning.

My results confirm those of earlier studies (Remaggi et al. 1998; Ferretti et al. 1999; Hirose et al. 2007; Kerschnitzki et al. 2011) and establish that osteocyte orientation is a useful proxy for fibrillar organization across a wide range of vertebrates. This method may be used as a secondary diagnosis in specimens that retain an adequate signal of collagen birefringence

(e.g., Warshaw 2008). In fossils that do not preserve collagen or that show only a weak signal, this method may be used to infer fibrillar organization.

It is worth noting that most paleohistological studies do not report the method used to diagnose collagen fiber orientation. The classic reference most often cited for diagnostic terminology (Francillon-Vieillot et al. 1990) provides fairly general guidelines for distinguishing among the main tissues types, but they are not explicit at and one of them (isotropy of woven-fibered bone) is incorrect (Stein and Prondvai 2013), or at the very least insufficient (Bromage et al. 2003). Whether specific patterns of birefringence, osteocyte orientation, or a combination of both are used, the method of diagnosis should be reported.

Vascularity

Amprino (1947; Amprino and Godina 1947) noted that animals with faster growth rates were better vascularized than animals that grow slowly, citing differences in the number of canals, the extent to which they anastomosed with other canals, and the complexity of the patterns that these anastomoses formed. de Ricqlès (1975) confirmed these observations in a broader taxonomic sample, focusing especially on the differences in canal patterning. He described the different canal patterns more explicitly, and determined the sequence of canal patterns associated with increasing bone deposition rate. These classifications were described in more detail by Francillon-Vieillot et al. (1990), who noted that the range of canal patterns was not limited to a specific tissue type, although the most complex patterns tended to occur in more disorganized tissue.

This hypothesis, since termed "Amprino's Rule", received support from two studies by Castanet et al. (1996, 2000). These studies used fluorescent labeling techniques to determine bone deposition rates, and compared the vascular patterns in regions of bone where bone was deposited faster. The authors observed that certain patterns (radial, laminar, subplexiform, plexiform) were more common in tissues with higher deposition rates than other patterns (longitudinal). Though the relative order of canal patterns was similar across different elements, the absolute rate of bone deposition associated with each canal pattern was different. Importantly, Castanet et al. (1996) did not report the range of variation in deposition rates associated each canal pattern. The ranges of deposition rates for each pattern were reported by Castanet et al. (2000), and showed some degree of overlap between some canal patterns (e.g., laminar and reticular). Furthermore, although the authors note that tissues deposited at hatching were woven and tissue deposited later were fibrolamellar (i.e., having both lamellar and woven components), they did not take this into account.

de Margerie et al. (2002, 2004) also attempted to correlate bone deposition with vascularity in the Mallard. The results of this study are difficult to interpret because the authors did not report whether the data from all six elements sampled (all major long bones) and all 17 individuals were pooled or analyzed separately. The graphs presented separate results by bone type, but this refers to the histology, not the element. With this caveat, the results of this study were mixed. de Margerie et al. (2002) found statistically significant differences in bone deposition rate associated with four different types of vascularization: primary osteons in woven-fibered bone (= fibrolamellar bone; FLC; acronym as in de Margerie et al. 2002), primary osteons in parallel-fibered/lamellar bone (LPO), simple

vascular canals in parallel-fibered/lamellar bone (LSV), and avascular parallel-fibered/lamellar bone (LNV). The greatest differences were between FLC and the other types; LPO was also statistically different from LSV and LNV. The latter two bone types showed no difference in associated depositional rates. However, note that this analysis conflates two aspects of microstructure; fibrillar organization and canal type. Fibrillar organization is also known to correlate with deposition rate, with woven-fibered bone deposited more rapidly than parallel-fibered or lamellar bone (Newell and Sirianni 1982; de Buffrénil and Pascal 1984). That FLC is deposited faster than LPO, LSV, and LNV could reflect differences in fibrillar organization rather than canal type. In the same study, de Margerie et al. (2002) found no difference in bone deposition rate based on the pattern of primary osteons in fibrolamellar bone (longitudinal, laminar, and reticular). However, they did note a strong positive correlation between canal diameter and bone deposition rate.

In a fluorescent labeling study of growth in the King Penguin, de Margerie et al. (2004) examined the relationship between bone deposition rate and canal pattern, this time controlling for skeletal element, age of the individual sampled, and tissue type (only fibrolamellar bone was observed). Once these factors were controlled, statistical differences in bone deposition rate were found among four canal patterns, an order that held for most long bones examined. However, within and among elements, the range of deposition rate associated with each canal pattern overlapped with that of other patterns. de Margerie et al. (2004) concluded that their results generally supported Amprino's rule, but warned against inferring deposition rates based solely on canal pattern, as the rates were likely age- and element-specific.

It is worth noting that the order of canal patterns based on increasing bone deposition rates varies among studies. Castanet et al. (1996) found this order in the Mallard: longitudinal, reticular, plexiform, laminar/subplexiform. Castanet et al. (2000) found this order in the Ostrich: longitudinal/subreticular, laminar, reticular. In the emu, they found that although longitudinal/subreticular canals were always associated with the lowest bone deposition rates, the position of laminar and reticular switched or were equivocal, depending on the element observed. de Margerie et al. (2004) found this order in the King Penguin: laminar, longitudinal, reticular, and radial. Of these, only the results for the ostrich roughly match the order de Ricqlès (1975) and Francillon-Vieillot et al. (1990) predicted: longitudinal, longitudinal canals aligned in radial rows, longitudinal canals aligned in circumferential rows, laminar, plexiform, radial, reticular.

The evidence to date does not support a straightforward link between vascular pattern and bone deposition rate. It may be that vascular canal pattern does not show a consistent order because there is no general pattern, or that patterns exist but are species-specific. However, another possibility is that the concept of vascular pattern *sensu* de Ricqlès (1975) and Francillon-Vieillot et al. (1990) confounds three separate vascularization signals: vascular density (the relative amount of space devoted to the vascular and nonvascular component of bone), vascular connectivity (the extent of anastomosis among longitudinal canals), and vascular pattern (i.e. the dominant orientation of anastomoses). It is possible that only some of these correlate with bone growth rate, and that the reason that vascular pattern produces such a messy signal is that the orientation of anastomoses is not the component that actually correlates with bone growth. Increased vascular density and vascular connectivity both would result in more space devoted to vasculature; however, the orientation of those canals and their

anastomoses may reflect other influences, for example space (i.e., there may be only so many ways to pack blood vessels into a small space) or biomechanics. The latter hypothesis is supported by evidence from studies relating vascular canal pattern to function. For example, de Margerie (2002, 2006) observed that laminar canals were most common in the bones and taxa that experienced the highest levels of torsion during flight. Additionally, Simons and O'Connor (2012) found that laminarity index (the ratio of laminar to plexiform canals) was significantly different in birds who exhibited different flight modes (flapping, static soaring, dynamic soaring).

Unlike vascular pattern, there is evidence that the vascular density *sensu lato* (i.e., some ratio of the vascular and nonvascular components of bone) is associated with bone growth rates. As noted above, de Margerie et al. (2002) found a strong positive correlation between canal diameter and bone deposition rate in the Mallard. Montes et al. (2010) also found that "vascularity" (estimated by calculating the ratio of canal space to mineralized bone space) was positively correlated with bone growth rate in a variety of amniotes, even when controlled for body size, phylogeny, and metabolic rate. This same relationship was recovered by Cubo et al. (2012) and Legendre et al. (in press) when vascular density (number of canals/mm^2) was used, rather than the vascularity measurements of Montes et al. (2010).

Comparative studies of amniote bone growth most often report estimates of vascular density using qualitative terms (e.g., 'very dense', 'moderately dense', 'nearly avascular') or relative terms (e.g., 'decreases periosteally'). Unfortunately, these terms are rarely defined and may be inconsistent among authors. One exception is Warshaw (2008), who examined various histological parameters in the primary cortical bone of living primates. Warshaw defined three categories of vascular density based on the distance between canals relative to their diameter. For example, the category "intense vascularization" meant canals were "separated from each other by less than the diameter of two canals" (Warshaw 2008: 404. It is this approach I adopt in Chapters 2 and 3; see character diagnosis below).

In the paleontological literature, vascular density has been quantified it in several ways. One method to quantify vascular density is to estimate the area occupied by primary vascular canals as a percentage of cortical area, sometimes called bone porosity (although the term is used slightly differently in the archaeological/forensic literature, where it may include secondary osteons, erosion rooms, or the interstices between trabeculae). This method was described by Chinsamy (1993), who compared vascularization in the femora of five species of extinct and extant archosaurs. In this study, Chinsamy used sampling techniques to determine how density varied along the bone wall radius and standardized estimates based on bone wall thickness. Subsequent studies have varied in method somewhat. For example, Horner et al. (2001) compared porosity across the entire section (no subsampling) in ten additional archosaurs, but did not standardize based on bone wall thickness. Cubo et al. (2005) described vascularity in the femora of 35 extant sauropsids, but restricted their study to primary cortical bone and accounted for phylogeny in their regression analysis. In a similar study, de Buffrénil et al. (2008) compared porosity (termed vascular density index) with canal orientation and obliquity in a number of varanid lizard species, and incorporated mass, growth stage, and phylogeny in their analysis. Notably, porosity methods cannot distinguish between higher levels of vascularization achieved by increasing vascular density (canals/unit bone) and canal connectivity (number of anastomoses).

Another way to estimate vascular density is to measure the number of canals per unit of primary bone. This method is essentially identical to those used in the medical, forensic, and zooarchaeological literature to determine osteonal density in mammals that remodel the cortex extensively (e.g., Zedda et al. 2008), except that it describes primary and not secondary/Haversian/remodeled bone. Studies that have used this method include Singh et al. (1974) compared the rib, femur, and/or tibia of 24 species of extant mammals and reported the number of primary longitudinal canals per microscopic field. Cubo et al. (2012) measured the number of canals/mm^2 in 52 individuals from 16 amniote species. In the paper, they did not explain their methods of counting canals, other than to state that sections showing a single vascular canal were considered avascular. However, I spoke with Jorge Cubo (personal communication, June 2013), and he reported that only longitudinal canals were counted (i.e., no anastomoses were counted). Legendre et al. (in press) expanded the Cubo (2005) dataset to include eight specimens of two additional bird species, using methods similar to those of Cubo et al. (2012).

Higher levels of canal density are often, but not necessarily, associated with high levels of anastomosis. For example, neonatal archosaurs often exhibit high canal density and low levels of anastomosis (e.g., Horner et al. 2001; Lee 2004). For this reason, I discuss these characters separately. To date, no studies have examined the relationship between vascular connectivity and bone growth rate specifically, but I describe a potential means of doing so below.

Vascular density may also correlate with metabolic rate. Montes et al. (2010) also found that porosity was positively correlated with resting metabolic rate across Amniota, even when body size, phylogenetic relatedness, and bone deposition rate were controlled statistically. Additionally, blood flow to the long bones is higher in animals with higher active metabolic rates (Seymour et al. 2011).

Secondary osteons are used to assess age in extant mammals, especially humans (e.g., archaeological remains). The number of generations of secondary osteons (determined by the number of overlapping canals) is known to increase with age (e.g., Kerley 1965; Alquist and Damsten 1969), but the absolute values vary taxonomically and by element, and must be determined by observation in animals of known age (Stover et al. 1992, Mulhern and Ubelaker 2003). This relationship has also been described for ranid frogs (LeClair 1990). A general relationship between the extent of secondary remodeling (secondary osteons plus erosion rooms) and size/age has been noted in extinct taxa (e.g., Horner et al. 1999, 2000; Klein and Sander 2008; Werning 2012), but has not been quantified. The presence of secondary osteons is most likely a function of age, biomechanics, and the development of the element examined, and does not reflect bone deposition rate (Enlow and Brown 1958; Schaffler and Burr 1984; Paine and Godfrey 1997; McFarlin et al. 2008).

Vascularity: Character summaries and diagnoses

Primary vascular canal type

Character states: Categorical; simple primary canal, primary Haversian cavity, primary osteon, secondary osteon

Description: This character describes the type of primary vascular canal present in a region of bone. This character may be modified to describe the predominant primary canal

type across a larger region (e.g., the inner cortex), a specific type of bone tissue (e.g., primary woven-fibered bone), or the whole section.

Diagnosis: I used the diagnostic criteria of de Ricqlès (1975) and Francillon-Vieillot et al. (1990), briefly summarized here: Simple primary canals are vascular canal spaces that are enclosed in matrix, but are not lined by lamellar bone. Primary osteons are vascular canal spaces lined with concentric lamellae (though generally not more than one or two in most mammals), and show no signs of previous resorption at the lamellar border. Primary Haversian spaces are precursors to primary osteons; the original scaffolding has begun compacting toward the canal, but the lamellar lining has not yet been deposited (i.e., the canal is "unfinished"). These canal spaces are most common early in ontogeny and are larger than simple primary canals.

Relevance: Basic description of the appearance of bone microstructure. Simple canals and primary osteons both occur in association with lamellar, parallel-fibered, and woven-fibered bone tissue (de Ricqlès 1975; Francillon-Vieillot et al. 1990). However, simple canals are thought to be more common in bone tissues that are deposited slowly (de Ricqlès 1975; Francillon-Vieillot et al. 1990). Primary osteons are the most common type of vascular canal in fibrolamellar bone, a tissue associated with relatively high bone deposition rates (de Ricqlès 1975; Francillon-Vieillot et al. 1990; de Buffrénil and Pascal 1984).

Utility and discussion: These terms are used consistently throughout Chapters 2 and 3, based on the diagnostic criteria described above. However, I have some reservations about this way of diagnosing vascular canals. Based on a broad taxonomic sample of archosaur bone tissues (Chapter 2), I noted that different canal morphologies could result from similar processes, and that similar canal morphologies could result from different processes. For example, in fast-growing tissues, an initial woven scaffold is deposited, which then compacts towards the canal and eventually may be finished, often with lamellar bone. However, if the canal is finished with parallel-fibered bone, it would not meet the diagnostic criteria of a primary osteon, even though it formed by the same process of scaffolding, compaction, and finishing. Simple primary canals form in lamellar bone when the vessel is enclosed by new appositional bone, but they can form in woven fibered bone when a scaffold is built and then compacted. I am not advocating that the current structural diagnosis be abandoned in favor of developmental criteria, but perhaps a second set of terms should be erected to discuss the aspect of development.

Secondary vascular canal (space) type

Character states: Descriptive; secondary osteon, erosion room

Description: This character describes the type of secondary vascular canal present in a region of bone. This character may be modified to describe the predominant vascular canal type across a larger region (e.g., the inner cortex), or the whole section.

Diagnosis: Following de Ricqlès (1975) and Francillon-Vieillot et al. (1990), secondary bone is deposited where bone was previously deposited and resorbed. The external border of secondary vascular spaces is marked by a distinct cement line or a scalloped resorption surface. Secondary osteons are ringed by concentric lamellae, of which there are often many. The number of lamellae and the diameter of the central canal vary with age (younger secondary osteons have fewer lamellae and larger canal spaces).

Erosion rooms (erosion bays in Francillon-Vieillot et al. 1990), form by the same process, but are usually much larger, restricted to the inner cortex, and do not compact as extensively (i.e., they are thin walled relative to their diameter).

Utility and discussion: Secondary bone deposition is not related to bone deposition rate, which record deposition of primary bone. Secondary bone may be deposited at faster rates than primary bone (Newell and Sirianni 1982; de Buffrénil and Pascal 1984).

The number of generations of secondary osteons is useful in assessing relative age in living and fossil vertebrates (e.g., using the methods of Kerley 1965 and Alquist and Damsten 1969). In living animals, older animals have more generations of secondary osteons, but the interpretation of absolute requires knowledge of the relationship for a particular element in a particular species, and must be determined by observation in animals of known age (Stover et al. 1992, Mulhern and Ubelaker 2003). This technique may be applicable to extinct taxa, in which a general relationship between the extent of secondary remodeling and size/age has been noted (e.g., Horner et al. 1999, 2000; Klein and Sander 2008; Werning 2012). Therefore, if such relationships are quantified in a fossil specimen, the absolute values should not be extrapolated to other taxa or elements. Also, secondarily remodeling may occur as a response to biomechanical stress (Frost 1987), so observers must avoid conflating biomechanical and ontogenetic signal. This can be done by sampling regions away from muscle attachment regions, which are expected to have higher remodeling rates (Frost 1987).

Vascular canal orientation

Character states: Descriptive; longitudinal, circumferential, radial, oblique

Description: This character describes the orientation of primary vascular canals relative to the long axis of the bone and the plane of section, and assumes the sample is in cross section (transverse section). They may be assessed regionally or be describing the dominant orientation throughout the cross section. These terms apply to canals and their anastomoses, to simple primary canals and primary osteons.

Diagnosis: I follow the diagnostic criteria of Francillon-Vieillot et al. (1990), briefly summarized here: Longitudinal canals are oriented parallel to the long axis of the bone; they appear circular or slightly oval in cross section. Circumferential canals or anastomoses are oriented perpendicular to the long axis of the bone and appear as arcs running around the circumference of the bone in cross section. Radial canals or anastomoses are oriented perpendicular to the long axis of the bone and appear as straight lines running in the periosteal-endosteal direction. Oblique canals are oriented perpendicular to the long axis of the bone and run at an angle intermediate to radial and circumferential canals.

Relevance: Basic description of the appearance of bone microstructure. Additionally, canal orientation may be influenced by biomechanical pressures (de Margerie 2002, 2006; Simons and O'Connor 2012).

Vascular canal density

Character states: This may be assessed as a continuous character, as the number of primary longitudinal canals divided by cortical area (vascular density). It also may be assessed as a continuous character, the ratio of vascular area to total cortical area (porosity). It may also be assessed as a categorical character. In this dissertation, I use the categorical

method and these states: very well vascularized, well vascularized, moderately vascularized, poorly vascularized, avascular.

Description: This character describes the density of vascularization in the primary cortical bone tissue.

Diagnosis: Porosity may be diagnosed by dividing the area occupied by vascular spaces by cortical area. It is reported as a percentage. Vascular density may be diagnosed by counting the number of canals in a given area and dividing it by cortical area. In previous studies (Cubo et al. 2012; Legendre et al. in press), only longitudinal canals were counted to avoid conflation of vascular density and vascular connectivity. It is reported as canals/unit bone (e.g., *n* canals/mm^2). Both methods may be assessed across the whole section (e.g., Horner et al. 2001) or using representative regions (Chinsamy 1993), as is common in the archaeological and primate literature (e.g., Iwaniec et al. 1998; Zedda et al. 2008; see comments below).

The proportion of primary cortical bone tissue occupied by simple or primary vascular canals also may be described qualitatively. The same method is used regardless of canal orientation. I define the categories above using a method similar to that of Warshaw (2008):

- *Very well vascularized*: vascular canals are separated from surrounding canals by a distance less than three times the average canal diameter
- *Well vascularized*: vascular canals are separated from surrounding canals by a distance three to five times the average canal diameter
- *Moderately vascularized*: vascular canals are separated from their surrounding canals by a distance six to seven times the average canal diameter six to seven to eight
- *Poorly vascularized*: vascular canals are separated by a distance eight or more times the average canal diameter
- *Avascular*: vascular canals absent

Relevance: Vascular density is positively correlated with bone growth rate (Montes et al. 2010; Cubo et al. 2012; Legendre et al. in press). Vascular density is also positively correlated with resting metabolic rate (Montes et al. 2010). Blood flow to the long bones is higher in animals with higher active metabolic rates (Seymour et al. 2011).

Utility and Discussion: This character can be assessed in several ways, but each method carries its own assumptions and limitations. All three methods described above can be used on both living and fossil taxa. Qualitative assessments may be subjective and are rarely defined explicitly, so terms like “highly vascularized” or “moderately vascularized” may vary among studies, making comparisons difficult. As noted by Chinsamy (1993) and Starck and Chinsamy (2002), porosity methods always overestimate the area actually devoted to blood vessels. In life, vascular canals contain not only blood vessels, but also lymphatic vessels, nerves, and connective tissue. If the relative space devoted to blood vessels varied (as it might, phylogenetically or with body size), the amount of overestimate would be hard to determine, especially for fossil taxa. Starck and Chinsamy (2002) also noted that this is complicated by canal ontogeny; older canals (those deposited earlier) appear smaller because more time has elapsed in which they could finish compaction. Additionally, porosity methods conflate vascular density and vascular connectivity. Density methods assume that canal number and vessel number are tightly correlated; they underestimate vessel number when canals contain more than one blood vessel, as observed in some canals in Japanese quails

(Starck and Chinsamy 2002). Additionally, density methods must explicitly acknowledge whether or not anastomoses are counted as separate canals or not. Cubo et al. (2012) and Legendre et al. (in press) counted longitudinal canals and did not count anastomoses; the former are generally present in vascularized tissue, regardless of the level of anastomosis, and thus comparisons are made among similar structures.

Canal density and porosity may be measured across the whole section or estimated using subsampling techniques (Chinsamy 1993; Iwaniec et al. 1998). Subsampling methods seek to minimize the space analyzed (and time of analysis) without compromising the accuracy of the estimation. Iwaniec et al. 1998 assessed various subsampling methods (radial transects, circumferential or radial series of boxplots) and found that all produced reasonable estimates of vascular density across the section. However, to ensure comparability, sampling methods, skeletal element, and sampled region must be similar across all samples. I outline some possible sampling methods for fossil bone in Figure 1.1. For statistical reasons, canals that cross the border of the sample plot should not be counted.

Canal counts are easily verified when digital images are used rather than observations under a microscope. For example, a region of bone can be photographed, and sampling regions of uniform size (transects or squares, as in Figure 1.1) can be overlaid digitally in image analysis software such as Photoshop (Adobe Systems Inc., San Jose, CA). For example, when counting osteocytes (see below), I used a sampling method similar to the one depicted in Figure 1.1 (bottom image). I created and numbered boxes of uniform size as a separate layer in Photoshop CS5, then used the Count Tool to count the number of cell bodies in each box. Because the numbered position of each counted object is saved in the file as metadata and can be recalled at a later time, this method also facilitates quick verification of counts.

Vascular connectivity

Character states: Continuous character; either the number of primary longitudinal canals that do not anastomose with other canals, or the number that do anastomose with other canals, relative to the total number of primary longitudinal canals, and is expressed as a percentage.

Description: This character describes the relative proportion of canals that connect with other canals, or the average number of canals linked by anastomoses.

Diagnosis: For the whole section or a subsample, the number of primary longitudinal canals that anastomose (or do not anastomose) with at least one other canal is divided by the total number of longitudinal canals in the same area.

Relevance, Utility, and Discussion: No studies have explicitly examined the relationship between vascular connectivity and growth rate. Because anastomoses increase the amount of space devoted to vascular canals, it is plausible that this character would track bone deposition rate, as with vascular density (Montes et al. 2010; Cubo et al. 2012; Legendre et al. in press).

Vascular pattern

Character states: Descriptive; includes the four basic canal/anastomosis orientations (longitudinal, circumferential, radial, oblique), as well as their combinations: longitudinal canals in radial rows, laminar, plexiform, reticular.

Description: This character describes the pattern of primary vascular canals within the primary cortical bone tissue. It applies both to simple primary canals and primary osteons. As in the description of vascular canal orientation, my diagnosis below is relative to the long axis of the bone, assuming the bone is examined in cross section.

Diagnosis: I follow the diagnosis used by de Ricqlès (1975) and Francillon-Vieillot et al. (1990), and illustrated in the latter work (Figure 14: p. 509). A laminar pattern results when most canals are oriented or anastomose circumferentially, forming circular rows. The plexiform pattern is similar to the laminar pattern, except that radial anastomoses link adjacent circular rows. I use the term subplexiform to indicate a plexiform pattern in which radial canals are present but infrequent. The laminar, subplexiform, and plexiform patterns all have a strong circumferential signal. Canals that form reticular patterns anastomose in all directions (circumferential, oblique, radial), none of which is dominant.

Relevance: Basic description of the appearance of bone microstructure. The complexity of the pattern may relate to bone deposition rate (Amprino 1947; de Ricqlès 1975; Francillon-Vieillot et al. 1990; Castanet et al. 1996, 2000; de Margerie et al. 2002, 2006). I question this relationship (see discussion above).

Utility and Discussion: Vascular pattern is consistently described among authors of paleohistological and histological studies. However, some conflate vascular canal pattern with tissue type, assuming that complex vascular patterns (laminar, plexiform, reticular) occur only in fibrolamellar bone. However, as I show in Chapter 2, these patterns may occur in parallel-fibered or woven bone, and may involve simple primary canals or primary osteons. Indeed, both de Ricqlès (1975) and Francillon-Vieillot et al. (1990) made this same observation, and stressed that although these patterns were most common in fibrolamellar bone, they did not occur in that tissue type exclusively. Tissue type cannot be inferred automatically from canal pattern in the absence of other evidence, even if there is a frequent association.

Osteocytes

The relationship between osteocytes and other aspects of vertebrate biology has long been a question of interest. The earliest comparative studies of vertebrate bone microstructure put much focus on osteocyte canalicular organization and the orientation of lacunae relative to vascular canals (Quekett 1849a, 1949b,1855; Foote 1916; Amprino 1947; Amprino and Godina 1947). de Ricqlès (1975) described more general patterns of osteocyte shape, orientation, and density relative to other aspects of bone microstructure. For example he (and later Francillon-Vieillot et al. 1990) noted that osteocytes in woven-fibered bone tended to be globular or stellate in cross section, whereas osteocytes in lamellar and parallel-fibered bone tended to appear flattened or oval in cross section. Additionally, they tended to occur in higher densities in woven-fibered bone, and were often oriented perpendicular to the long axis of the bone in parallel-fibered and lamellar tissues.

Studies of osteocyte shape have recovered general shape differences between the osteocytes in woven-fibered bone and those in parallel-fibered/lamellar bone, but note much shape variation within groups and a good deal of overlap between groups (Warshaw 2008).

More recent evidence supporting a relationship between osteocyte orientation and collagen fiber orientation comes from studies of how bone formation during static and

dynamic osteogenesis (Remaggi et al. 1998; Ferretti et al. 1999) and a large number of direct observations in living and fossil amniotes (e.g., Hirose et al. 2007; Warshaw 2008; Kerschnitzki et al. 2011; Chapter 2 of this dissertation). This relationship is discussed in more detail above in the discussion of collagen fiber organization, and in the Discussion section of Chapter 2. Because osteocyte orientation is strongly correlated with fibrillar organization, and because collagen fiber organization reflects bone deposition rate, osteocyte orientation also correlates with bone deposition rate, albeit indirectly.

Osteocyte density has been proposed to reflect metabolic rates. This relationship was initially hypothesized based on the observation that osteocyte density in trabecular was inversely correlated with body mass in mammals (Mullender et al. 1996; Bromage et al. 2009). Subsequent studies (e.g., Skedros et al. 2005) have failed to find correlations between osteocyte density and either bone mineral content or the level or type of strain experienced in a particular region of cortical bone, although such relationships were found for porosity and collagen fiber orientation. Rather, osteocyte densities were fairly uniform around the circumference of a given element.

Other studies (Remaggi et al. 1998; Feretti et al. 1999) of osteocyte density failed to recover an inverse correlation between cortical osteocyte density and body size in samples that included a frog, chick, and several mammals. Based on this, they suggested that body size and metabolic rate were not related to osteocyte density. However, this is not necessarily a correct inference; they did not actually compare osteocyte density to mass-specific metabolic rate (or any measure of metabolic rate), and did not correct for the influence of phylogeny. When body size, element, and phylogeny were statistically controlled, Cubo et al. (2012) did recover a positive correlation between osteocyte density and basal metabolic rate. A positive correlation between basal metabolic rate and osteocyte density was also shown across a sample of 29 primate species (Bromage et al. 2012). Within a relatively large group of closely-related taxa, osteocyte density is a good predictor of basal metabolic rate (Bromage et al. 2012); however, it is not yet known how sensitive an indicator it is within other clades.

Osteocytes: Character summaries and diagnoses

Osteocyte shape

Character states: Categorical: flattened, oval, globular/round

Description: The shape of osteocytes in cross section

Diagnosis: Osteocytes are diagnosed as flattened when they appear as a thin line in cross section, globular/round when they appear circular or circular/stellate in cross section, and elongate when they appear oval.

Relevance: Basic description of the appearance of bone microstructure. Correlates somewhat with fibrillar organization (de Ricqlès 1975; Francillon-Vieillot et al. 1990; Ferretti et al. 2002; Palumbo et al. 2004; Marotti 2010; although note observations by Warshaw 2008, and my observations in Chapter 2).

Utility and Discussion: de Ricqlès (1975) and Francillon-Vieillot et al. (1990) noted that osteocytes in woven-fibered bone tended to be globular/round in cross section, whereas osteocytes in lamellar and parallel-fibered bone tended to appear flattened or oval in cross section. This relates somewhat to differences in how woven-fibered, parallel-fibered, and lamellar bone tissue form at the mid-diaphysis (Ferretti et al. 2002; Palumbo et al. 2004;

Marotti 2010; see extended discussion in Chapter 2). However, Warshaw (2008) noted that that the relationship was not especially strong, and that the cells in woven-fibered and parallel-fibered bone were quite variable in shape.

Osteocyte orientation

Character states: Categorical: perpendicular, parallel, oblique, no preferred orientation. Perpendicular osteocytes may be additionally described as by their arrangement within the cross section: circumferential, radial, no preferred arrangement.

Description: The orientation of the major axes of osteocyte lacunae in primary bone, relative to the long axis of the bone. May be assessed for osteocytes occurring near the canals, as well as those in the interstices between canals.

Diagnosis: Osteocyte orientation was assessed by focusing through the plane of section under the microscope. Most cross-sections show more than one type in at least a few localized areas; however, the overall pattern of dominance across the entire section is considered. In sections where there is a mixture of parallel, perpendicular, and oblique osteocytes, no preferred orientation is occurred,

Relevance: Basic description of the appearance of bone microstructure. As noted above, osteocyte orientation may be used to support a diagnosis of collagen fiber orientation; see that section for relevance, utility and discussion.

Osteocyte density

Character states: Continuous

Description: The number of osteocyte lacunae per mm^2

Diagnosis: The number of osteocyte lacunae in primary bone tissue (primary osteons and the interstices between them) are counted and divided by the area of bone examined.

Relevance: Osteocyte density is thought to correlate with basal metabolic rate in several living vertebrates (Mullender et al. 1996; Skedros et al. 2005; Bromage et al. 2009, 2012; Stein 2010).

Utility and Discussion: The method I used can be applied to Recent and fossil bone. I digitally photographed radial transects from the endosteal margin to the periosteal surface along the major and minor axes of each element. Following the methods of Remaggi et al. (1998) and Ferretti et al. (1999), these photographs were taken in reflected light (rather than regular transmitted light) so that only the cells in one plane (the plane of reflection) were in focus. In Photoshop CS5, I created boxes (square outlines, generally 250 μm x 250 μm) and placed these in a numbered row in a separate layer on top of the transect image (see Figures 1.1, bottom image; 1.2; 1.3). The number of osteocytes in each box were counted (except boundary crossers) using Count Tool (Photoshop) and recorded. As noted above, the numbered position of each lacuna is saved as metadata and can be recalled at a later time, so this method facilitates quick verification of counts by a second observer. When 100 μm x 100 μm boxes were used, osteocyte was slightly overestimated compared to other box sizes (250x250, 400x400, 500x500), which all gave similar estimates. Therefore, I recommend the use of 250 μm x 250 μm boxes unless the bone is too small to accommodate boxes of that size.

DISCUSSION AND CONCLUSIONS

This chapter reviews the evidence linking various aspects of bone microstructure to bone deposition rate, bone growth rate, and metabolic rate. In experimental and descriptive studies of living bone, bone deposition rate is the standard measure of bone growth. It is the only direct measure of bone growth used to test whether other aspects of bone microstructure correlate with bone growth. Despite this, estimates of bone deposition rate are rarely reported in paleohistological studies. Some authors have constructed elaborate models that use a combination of microstructural features to estimate bone deposition rates for fossil bone samples. For example, Cubo et al. (2012) and Legendre et al. (in press) use a model that incorporates vascular canal orientation, vascular canal density, osteocyte density, osteocyte size, and an element-specific constant to estimate these values. These models assume a constancy of rates based on a small sample of extant amniotes raised in laboratory conditions, and cannot be experimentally tested in extinct taxa. In taxa that produce annual growth marks, measurements of zonal widths can be used to bracket bone deposition rates, and present no issues of circularity when comparing microstructure to deposition rate.

Few microstructural features have been shown to correlate explicitly with bone deposition rate; these are currently limited to collagen fiber orientation, vascular density, porosity, and vascular canal diameter. Fibrillar organization seems most useful as a relative indicator of bone deposition rate; when ranked by associated bone deposition rate, the relative order of organization types is always the same in primary bone tissue. However, the absolute rates of bone deposition vary with age, element, body size, and phylogeny, and thus, the ability to extrapolate rates for extinct taxa is limited. All of the vascular characters shown to correlate with growth rate are measures of the amount of cortical space devoted to vascularity. Studies linking vascular pattern to bone growth do not show consistent results. Amprino (1947), de Ricqlès (1975), and Francillon-Vieillot et al. (1990) predicted that the complexity of vascular pattern would increase with bone deposition rate; this prediction was not supported by later studies (Castanet et al. 1996, 2000; de Margerie et al. 2002, 2006). Within an element, a given vascular pattern tended to occur within a specific range of deposition rates, but the ranges between vascular patterns showed strong overlap. Furthermore, when ranked by deposition rate, a different sequence was obtained for each taxon, and only one of these roughly matched the predictions of Amprino, de Ricqlès, and Francillon-Vieillot et al. These results suggest that vascular pattern is not an especially good indicator of bone deposition rate, because the range of deposition rates associated with each overlap within and among elements. Also, if a sequence of patterns exists, it is probably taxon-specific, and therefore vascular pattern should not be used to estimate rates in extinct taxa. “Amprino’s Rule”, the concept that bone microstructure changes with increasing growth rate, likely holds with regards to some aspects of vascularization, but probably not with regard to vascular pattern.

Osteocyte orientation is useful as an indicator of collagen fiber orientation and osteocyte density shows promise as an indicator of metabolic rate. The evidence supporting a relationship between osteocyte orientation and collagen fiber orientation comes from studies of bone formation (Remaggi et al. 1998; Ferretti et al. 1999) and a large sample of living and fossil amniotes (Hirose et al. 2007; Kerschnitzki et al. 2011; Chapter 2 of this dissertation). This relationship will be especially helpful for inferring fibrillar organization in fossil

specimens that show weak or no birefringence. The relationship between osteocyte density and metabolic rate has been established among a small but taxonomically broad group of extant amniotes (Mullender et al. 1996; Bromage et al. 2009, 2012; Cubo et al. 2012), my estimates of osteocyte density for extant taxa are also broadly consistent with this hypothesis (Ch 2). However, future studies will be key to establishing how sensitive an indicator of metabolism osteocyte density is.

ACKNOWLEDGMENTS

My understanding of bone has benefitted greatly from discussions with Sabrina Agarwal, Tim Bromage, Matt Brown, Armand de Ricqlès, Mark Goodwin, Pat Holroyd, Jack Horner, Leslea Hlusko, Randy Irmis, Ellen Lamm, Drew Lee, Zach Morris, Kevin Padian, Marvalee Wake, Vicki Wedel, and Holly Woodward. Ellen is slidemaking genius, goddess, and guru; I am so grateful to have trained with her a decade ago, and for every phone consult since then. Kevin and Marvalee have been especially wonderful sounding boards as my ideas about the evolution, ontogeny, and histology of bone developed.

I grateful to the following institutions for funding and financial support during my dissertation: Geological Society of America (Graduate Student Research Grant); Jurassic Foundation; Museum of Vertebrate Zoology (Louise Kellogg research award); Paleontological Society (N. Gary Lane Award), University of California, Berkeley (Graduate Division Summer Fellowship); University of California Department of Integrative Biology (Gray Research Award, Resetko Summer Research Scholarship); University of California Museum of Paleontology (Annie M. Alexander Fellowship; Doris O. and Samuel P. Welles Fund; Peabody Fellowship).

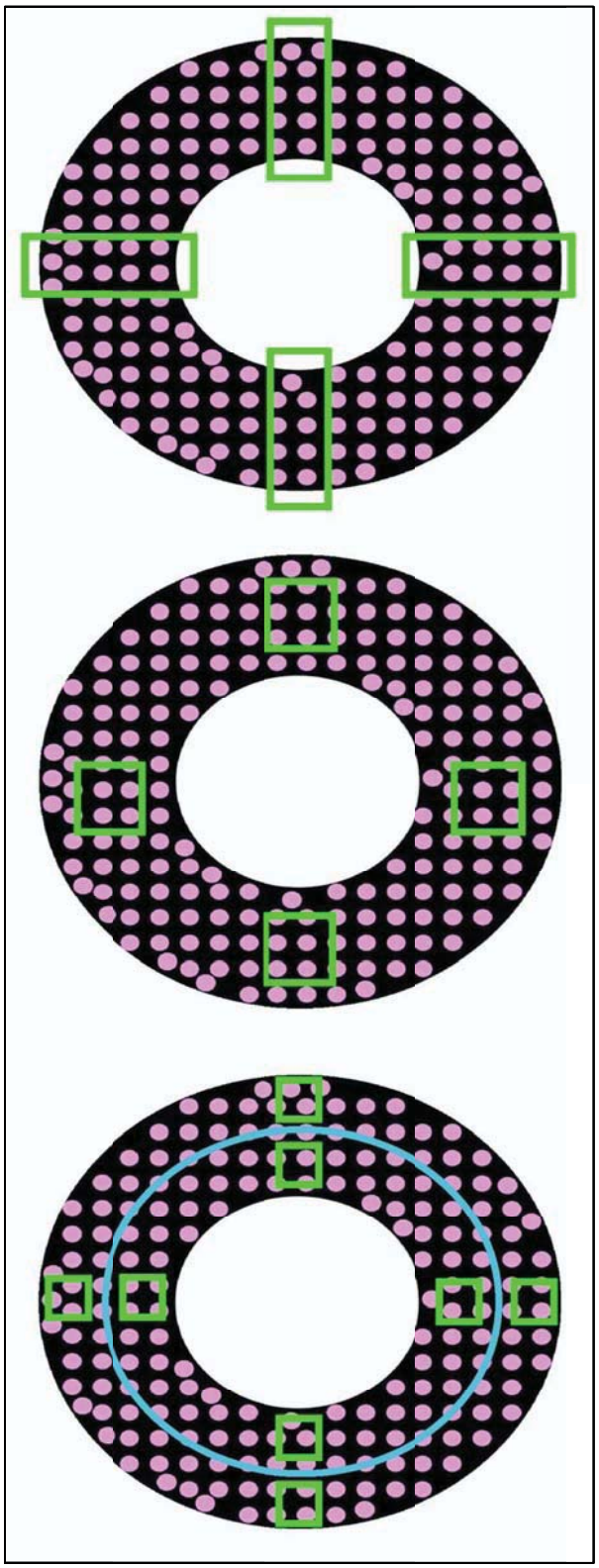

Figure 1.1 Potential sampling strategies for analyzing porosity, vascular density, and osteocyte density. In this image, the major axis is horizontal, the minor axis is vertical, green boxes represent sampling locations, pink circles represent vascular canals (or osteocytes, depending on the analysis), and black represents the nonvascular/noncellular component of primary cortical bone. Porosity is the proportion of vascular space relative to total cortical area (pink / [black + pink]). It may be assessed across the entire section or by subsampling. Vascular/osteocyte density is the number of canals/lacunae divided by the area of the region analyzed.

Different sampling methods are employed to estimate these values. The top image shows a transect approach, in which these values are assessed for a radial strip extending from the endosteal margin to the periosteal surface along the major and minor axes. The middle image shows a box plot approach, in which the midcortex is sampled. The results from both approaches yield time-averaged results, though the effect of averaging is stronger in the top image.

The bottom image shows the approach used in this dissertation, in which series of box plots extend along a radial transect. This minimizes the effect of time averaging, and allows changes in vascular/osteocyte density to be tracked through ontogeny. General trends may be noted, or boxes may be placed relative to age-related landmarks, such as LAGs or annuli (blue circle in bottom image). Figure 1.2 illustrates an example of such a transect.

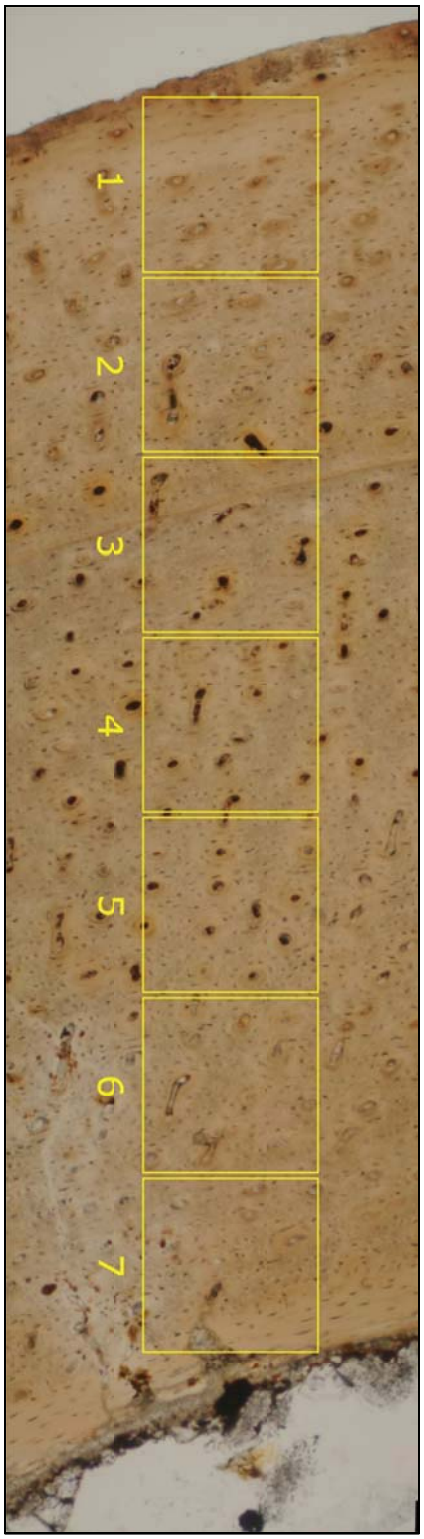

Figure 1.2 Example transect for estimating osteocyte density in the tibia of the dinosauromorph *Dromomeron romeri* (GR 253). A radial transect is digitally photographed in reflected light, to ensure that all osteocytes in focus occur in the same plane. A series of numbered 250 μm x 250 μm boxes is placed over the digital transect in Photoshop CS5 (Adobe Systems, Inc.). For all transects created for this dissertation except one, Box 1 is closest to the periosteal margin (see Appendix A for counts). Osteocyte lacunae (excluding those that cross the box plot borders) are then counted using the Count Tool in Photoshop (see Figure 1.3).

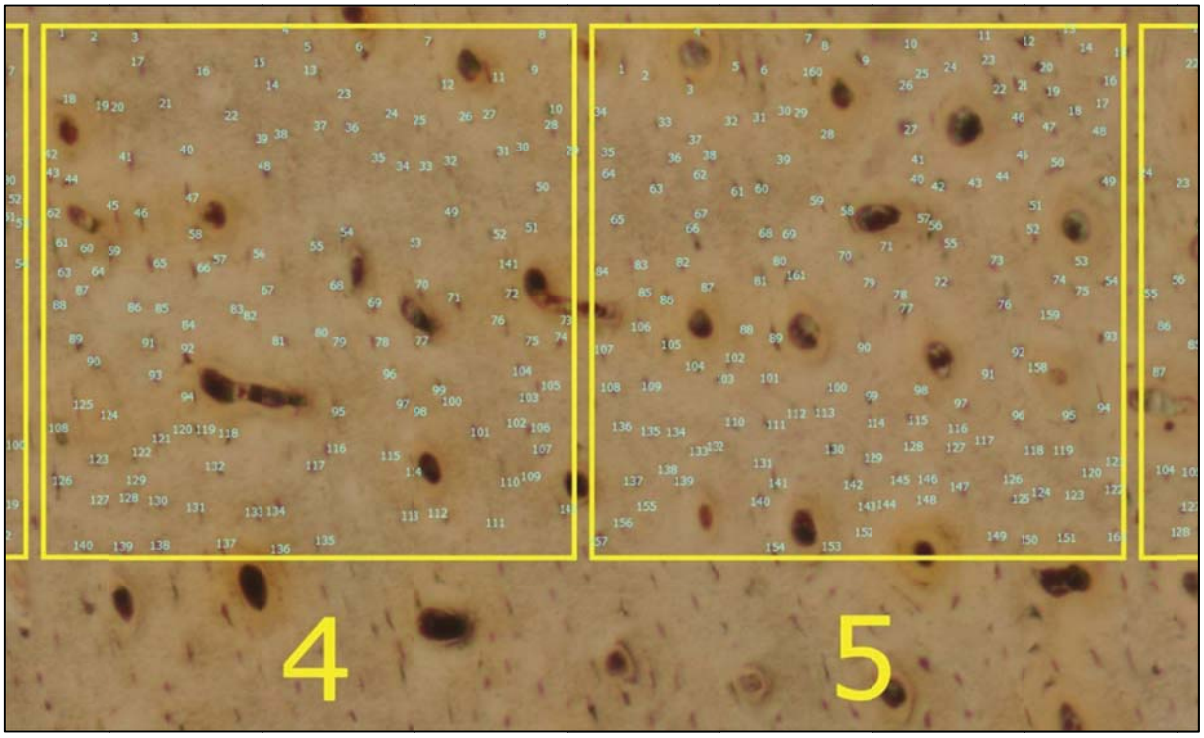

Figure 1.3 Example lacunar counts during estimation of osteocyte density in the tibia of the dinosauromorph *Dromomeron romeri* (GR 253). A radial transect is digitally photographed in reflected light, to ensure that all osteocytes in focus occur in the same plane (see Figure 1.2). A series of numbered 250 µm x 250 µm boxes is then placed over the digital transect in Photoshop CS5 (Adobe Systems, Inc.). Osteocyte lacunae (excluding those that cross the box plot borders) are then counted using the Count Tool in Photoshop (see Figure 1.3). Because the numbers and positions of the counted lacunae (small blue numbers) are saved as metadata in Photoshop, counts are quickly verified by a second observer. The Count Tool also allows counted osteocytes to be added or deleted at a later time. For this dissertation project, this flexibility enabled a large number of osteocytes to be counted by undergraduate research assistants.

CHAPTER TWO

Osteohistological variation in archosauromorph reptiles

ABSTRACT

Birds exhibit much higher growth and metabolic rates compared to other extant reptiles, which is reflected in the appearance of their bone microstructure. Building on these relationships between bone tissue appearance, growth rate, and metabolic rate, previous studies examining the bone histology of dinosaurs and pterosaurs have established that they also grew at elevated rates. However, it remains uncertain when these features first evolved, temporally or phylogenetically. In this chapter, I describe the bone microstructure of 37 archosauromorph reptiles and four outgroup taxa in detail. My study expands the histological database of archosaurs and their ancestors to include early archosauromorphs, pseudosuchians, and dinosauromorphs. This differs from previous works not only in its phylogenetic breadth and level of taxonomic sampling, but also in its standardization of histological characters and sampling locations.

Incorporating the fossil record of bone tissue provides a much richer understanding of the evolution of growth and life history than can be obtained by examining living animals and their extant outgroups alone. By sampling through deep time and in taxa whose character states are not represented among living animals, I show that the avian histological features associated with faster growth and higher metabolic rates evolved not among birds or dinosaurs, but earlier than the common ancestor of birds and crocodylians. Most of these character changes accumulated in a short segment of the archosauriform tree before the end of the Triassic.

INTRODUCTION

As discussed in Chapter 1, numerous bone microstructural characters have been used to establish correlative relationships among bone growth, whole-animal growth rate, and metabolic rate. Because most of these characters can be directly observed in fossil bone, it is possible to reconstruct or estimate growth and metabolic rates for fossil taxa. This allows the evolutionary history of growth and metabolic rates to be examined directly in the fossil record, rather than relying solely on living taxa and their extant outgroups. By doing so, changes in growth and metabolism can be tracked along a much greater portion of a given vertebrate lineage. Sampling fossil taxa allows more proximate outgroups to be used, and a greater diversity of sampled taxa to be included. This diversity includes not only taxonomic and phylogenetic breadth, but also diversity in body size, ecology, and other life history characteristics.

This approach can be used to address questions about the origins of novel growth and metabolic strategies in vertebrates. For example, among living tetrapods, birds and mammals exhibit relatively fast growth and high metabolic rates compared to amphibians, turtles,

crocodylians, and lepidosaurs (Ricklefs 1973, Case 1978a, 1978b, Arendt 1997, Starck and Ricklefs 1998a), and the ancestral condition for all tetrapods is assumed to be one of relatively slow growth and low metabolic rates. Given our understanding of their phylogenetic relationships, it is uncontested that fast growth and higher metabolic rates evolved independently in birds and mammals, and both lineages offer an opportunity to explore their evolution using osteohistological measures.

In this chapter, I illustrate how the inclusion of extinct species in growth studies can reveal information about the evolution of growth rates that cannot be obtained from examining the living record only. My study describes bone microstructural variation among archosauromorph reptiles, the clade that includes all reptiles more closely related to living birds and crocodylians than to lepidosaurs. I chose this group for several reasons. First, as noted above, Archosauromorpha contains at least one clade (Aves) with derived, elevated growth and metabolic rates; both ends of the growth, metabolic, and histological continua are represented within the broader lineage. Second, relationships among archosauromorph reptiles have been revised and clarified in recent years, especially among bird-line archosaurs (= Ornithodira; see Langer et al. 2009; Nesbitt et al. 2009a, 2010; Brusatte et al. 2010a, 2010b for discussion), early crocodile-line archosaurs (= Pseudosuchia; see Brusatte et al. 2010a, Nesbitt 2011), and taxa outside the crown (Nesbitt 2011). Synapomorphies identified in these studies permit higher confidence in our taxonomic assignments, allowing us to place the results in broader phylogenetic context. Additionally, the osteohistology of some clades nested within Archosauromorpha are well-studied at the tissue level, especially among dinosaurs (e.g., Currey 1962; Pawlicki 1975; de Ricqlès 1980, 2000; Reid 1981, 1984, 1985, 1987, 1990, 1996; Barreto 1997; Horner et al. 1999, 2001, 2009; Sander 1999, 2000; Erickson and Tumanova 2000; Erickson et al. 2001, 2009a; Padian et al. 2001, 2004; Starck and Chinsamy 2002; Sander and Klein 2005; Sander et al. 2006) and pterosaurs (e.g., de Ricqlès et al. 2000, Jenkins et al. 2001; Sayão 2003; Steel 2003; Padian et al. 2004; Chinsamy et al. 2008, 2009; Prondvai et al. 2012), so histological sections taken at standardized locations are already available for some taxa.

Despite these advances, a review of the current literature and especially the primary histological data is necessary. For some taxa, the bone microstructure has only been described typologically, rather than separately and systematically discussing the histological characters known to correlate more specifically with growth and metabolism. Furthermore, the microstructure of many archosauromorphs has been described using two terms, “fibrolamellar bone” and “lamellar-zonal bone”, even when finer-scale histological characteristics directly contradict these assessments (see Chapter 1 for further explanation). Another problem is that histological assessments often have been made for taxa as a whole, without consideration of ontogenetic changes in bone tissue deposition, even when these changes are visible within a single thin section. Finally, additional taxonomic sampling is necessary to address some significant phylogenetic gaps in our understanding of archosauromorphan growth and metabolic evolution. These include dinosauromorphans outside Dinosauria, archosauromorphans outside Archosauria, and pseudosuchians outside crown Crocodylia.

MATERIALS AND METHODS

Institutional Abbreviations—AMNH FARB, American Museum of Natural History, Collections of Fossil Amphibians, Reptiles and Birds, New York City, NY, USA; **BPI**, Bernard Price Institute for Palaeontological Research, University of the Witwatersrand, Johannesburg, South Africa; **CM**, Carnegie Museum of Natural History, Pittsburgh, PA, USA; **CMC**, Foote Collection, Creighton Medical Center, Omaha, NE, USA; **FMNH**, The Field Museum, Chicago, IL, USA; **GR**, Ruth Hall Museum of Paleontology at Ghost Ranch, Abiquiu, NM, USA; **JC**, Personal collection of Jacques Castanet, Paris, France; **LACM**, Natural History Museum of Los Angeles County, Los Angeles, CA, USA; **MCZ**, Museum of Comparative Zoology, Harvard University, Cambridge, MA, USA; **MGUH**, Geological Museum, University of Copenhagen, Denmark; **MOR**, Museum of the Rockies, Montana State University, Bozeman, MT, USA; **MWC**, Museum of Western Colorado, Grand Junction, CO; **MVZ**, Museum of Vertebrate Zoology, University of California, Berkeley, CA, USA; **NGMC**, Geological Museum of China, Beijing, China; **NHMUK**, Natural History Museum, London, UK; **NM** Nasionale Museum, Bloemfontein, South Africa; **NMB**, Naturhistorisches Museum Basel, Switzerland; **NMT**, National Museum of Tanzania, Dar es Salaam, Tanzania; **NMZB**, Natural History Museum of Zimbabwe, Bulawayo, Zimbabwe; **PEFO**, Petrified Forest National Park, AZ; **PIN**, The Paleontological Institute, Russian Academy of Sciences, Moscow, Russia; **PU**, former collections of the Princeton Natural History Museum, Princeton University, Princeton, NJ, USA; **SAM-PK**, Iziko South African Museum, Cape Town, South Africa; **SMNS**, Staatliches Museum für Naturkunde Stuttgart, Stuttgart, Germany; **TMM**, Texas Memorial Museum Vertebrate Paleontology Collection, University of Texas, Austin, TX, USA; **UCMP**, University of California Museum of Paleontology, Berkeley, CA, USA; **UF**, Florida Museum of Natural History, University of Florida, Gainesville, FL, USA; **UMMP**, University of Michigan Museum of Paleontology, Ann Arbor, MI, USA; **UMNH**, Natural History Museum of Utah, University of Utah, Salt Lake City, UT, USA; **UWBM**, Burke Museum, University of Washington, Seattle, WA, USA; **USNM**, National Museum of Natural History (Smithsonian), Washington, DC, USA; **YPM**, Yale Peabody Museum, Yale University, New Haven, CT, USA; **VdB**, Personal collection of Vivian de Buffrénil, Paris, France; **ZPAL**, Instytut Paleobiologii PAN, Warszawa, Poland.

Materials—I examined histological thin sections made from the mid-diaphysis of 94 humeri, femora, and (or) tibiae from 64 specimens representing 37 taxa of Recent and fossil archosauromorph reptiles, as well as three extant lepidosaurs and a captorhinid for comparison. Taxa, specimen numbers, and elements sampled are listed in Table 2.1. These elements were selected for two reasons: (1) they are weight-bearing bones whose growth is known to correlate with body size and whole-body growth in living terrestrial vertebrates (Cubo et al. 2008, 2012) and (2) these elements are among the most commonly sampled elements in studies of recent and especially fossil vertebrates, facilitating comparisons with an even broader dataset outside the scope of my current study. I sampled the mid-diaphysis because cortical compact bone is thickest in this region, and because it preserves the longest portion of the growth record compared to other parts of the diaphysis (Sander 2000; Stein and Sander 2009).

Mechanical Preparation—All Ghost Ranch (GR) specimens, as well as *Trilophosaurus*, *Revueltosaurus*, and the MCZ proterochampsian, required additional mechanical preparation before histological sampling could occur. These specimens were rough-prepared (i.e., consolidated and the majority of matrix removed) before I received them.

The *Trilophosaurus* specimens required the most preparation. Before removing matrix, exposed bone surfaces were first coated with clear Acryloid B-72 ethyl methacrylate copolymer (Rohm and Haas Company, Philadelphia, PA) dissolved in acetone. This was allowed to dry for several hours before the elements were immersed overnight in a 1-gallon plastic bag containing 3% hydrogen peroxide (Walgreen Co., Deerfield, IL). This dissolved much of the red mudstone matrix without damaging the bone surfaces. Elements were then rinsed in tap water and allowed to dry completely. For all specimens (including *Trilophosaurus*), the remaining rock matrix was removed from the bone surface by hand, first using a toothbrush wet with tap water or acetone and then using a sharpened carbide stylus in a pin vise. Stubborn matrix was removed with a HW10 pneumatic airscribe (Hardy Winkler, Germany). All mechanical preparation was completed under magnification using a Wild M5 stereomicroscope (Wild Heerbrugg, Heerbrugg, Switzerland).

Prior to histological sampling, the prepared elements were measured, sketched, and photographed. Each element was molded using GT-5092 condensation cure silicone rubber base catalyzed with CA-5275 Fast Catalyst silicone curing agent (GT Products, Inc., Grapevine, TX); no mold-release was used. After whole-element molding, the Acryloid B-72 in the cracks surrounding the mid-diaphysis was dissolved with acetone, and the mid-diaphysis was removed along those natural breaks. The mid-diaphysis preserves a greater ontogenetic span of the cortex than other areas of the bone and is subject to less remodeling than other parts of the diaphysis (Stein and Sander 2009). I cast each whole element and mid-diaphyseal segment using TC-891 A/B rigid polyurethane casting resin pigmented neutral grey with a mix of black (6836) and white (6834) liquid pigments (BJB Enterprises, Inc., Tustin, CA). Whole-element casts of each sectioned GR element will be reposited in the following museum collections: AMNH, FMNH, GR, TMM, UCMP, UMNH. *Trilophosaurus* casts will be reposited at TMM, UCMP, and UMNH. Proterochampsian casts will be reposited at MCZ and UCMP. *Revueltosaurus* casts will be reposited at PEFO and UCMP.

Histological Preparation—My slide preparations were completed using the same equipment and methods described in Nesbitt et al. (2013) and Werning (2012). I produced histological thin-sections of fossil specimens using standard fossil histological techniques (e.g., Chinsamy and Raath 1992, Wilson 1994, Lamm 2013), with the following chemical and equipment modifications. After molding and casting the removed portion, I embedded it in Silmar-41 clear polyester casting resin (Interplastic Corporation, Saint Paul, MN) catalyzed with methyl ethyl ketone peroxide (Norac, Inc., Helena, AK) at 1% by mass and allowed it to cure for 72 hours before sectioning. I then cut several sections (1-1.5 mm thick) from each embedded mid-diaphyseal portion using a diamond-tipped wafering blade on a low-speed Isomet lapidary saw (Buehler, Inc., Lake Bluff, IL). I manually wet-ground the mounting-side of these sections using 600/P1200-grit CarbiMet abrasive papers and an EcoMet 3 grinder/polisher (Buehler, Inc.). I mounted the resulting samples to glass slides using water clear 2-ton epoxy (Devcon, Danvers, MA) and allowed them to cure for at least 24 hours. I then wet-ground the slides using CarbiMet abrasive papers of increasing grit size (120/P120,

180/P180, 320/P400, 400/P800, 600/P1200) and an EcoMet 3 grinder/polisher (Buehler, Inc.) at 80-110RPM to optical clarity (~30-50 microns). Opaque areas of the slide were further hand-ground using 600/P1200 CarbiMet papers before polishing the slides using 5.0 micron aluminum oxide abrasive powder and a MicroCloth synthetic polishing cloth (Buehler, Inc.). Some slides were further polished with 1 micron MicroPolish II deagglomerated alumina powder (Buehler, Inc.).

Histological Imaging—Histological imaging was completed using the same equipment and methods described in Nesbitt et al. (2013) and Werning (2012). For all specimens, I examined slides using a Nikon Optiphot-2 Pol light transmission microscope under regular transmitted light, under crossed plane-polarizing filters, and under crossed plane-polarizing filters with full wave plate retarder (= red tint plate; $\lambda = 530$ nm). The tint plate and polarizers were used to enhance birefringence. Histological descriptions were made from direct observations of slides under the microscope.

For specimens smaller than 6 cm in diameter, I took digital photomicrographs both with and without the above filters using a Nikon D300 DSLR camera (Nikon Inc., Melville, NY) mounted to a Nikon Optiphot-2 Pol light transmission microscope (Nikon Inc.). Images were taken at multiple magnifications (5x, 10x, 25x, and 100x total magnification). All digital photomicrographs were taken as 8-bit jpgs (quality = fine, compression = optimal quality, image size = large/4288x2848 pxl). My interface program (e.g., for focusing, white balance) was Camera Control Pro 2 (Nikon Inc.) running on a Windows 7 (64-bit; Microsoft, Redmond, CA) computer (HP, Palo Alto, CA). I took overlapping digital photographs (overlap 50% by eye in X and Y directions) across the entire section at 5x total magnification, radial "transects" across the major and minor axes of the section (from the endosteal to periosteal surface) at 25x total magnification, as well as representative images at 10x and 100x total magnification. Specimens were often kept wet with water during photography to increase transparency and image clarity.

I assembled photomontages of full and partial cross sections and the radial "transects" using Autopano Giga 2.0 64Bit (Kolor, Challes-les-Eaux, France), with the following settings: Detection settings: detection quality = high, layout = free; Optimization settings: strong (for partial cross section and radial "transects") and gigapixel (for full cross section), optimizer stages: local approach, strong algorithm, first optimization, clean up control points or links, keep only control points below the error RMS = 2.0, final optimization, advanced distortion; Panorama settings: preferred projection = automatic, preferred extend = clamp to panorama content, initial type of anchor = mono transfer function; Render settings: size = 100%, algorithms: interpolating = bicubic, blending = smartblend, format = jpg, depth = 8 bits, layers = none, DPI = 72. At full resolution, the scale conversions for all images are as follows: 5x (including montages): 925 pxl = 1.0000 mm, 10x: 1850 pxl = 1.0000 mm, 25x (including montages): 4625 pxl = 1.0000 mm, 100x: 1850 pxl = .1000 mm.

For histological cross sections larger than 6 cm in diameter (excluding *Effigia*), specimens were imaged using a DS-Fi1 digital sight camera (Nikon, Inc.) mounted to a Optiphot-Pol light transmission microscope (Nikon, Inc.). Images were taken at 4x total magnification,1280 x 960 resolution, and at uniform contrast. Images were taken across the entire sample at 15% overlap (both X and Y directions using the automated stage) and assembled using NIS-Elements Basic Research 3.0 (Nikon, Inc.). At full resolution, the scale conversions for these images are 625 pxl = 1.0000 mm.

Further processing of all digital photomontages was completed using Photoshop CS5 Extended (Adobe Systems Inc., San Jose, CA). Adjustments were limited; to all full and partial cross sections, I cropped the images, added a black background, text, and scale bar. I used the Brightness/Contrast and Levels tools to adjust brightness and contrast across the images.

For some specimens that had been crushed taphonomically, I additionally reconstructed the original shape of the cross section using Photoshop CS5 Extended. de Ricqlès et al. (2003a) used a similar method to reconstruct sections of *Confuciusornis*, but did not provide details of their method. I digitally extracted each segment using the Pen Tool and placed them into their own layers. I used the morphology of the lines of arrested growth and annuli and the arrangement and orientation of the vascular canals, osteocytes and microcracks in the bone to realign each segment. In this way, the original shape of the bone was estimated as closely as possible. This method assumes no movement of the individual segments in the Z-axis relative to the cross sectional plane, but it is the closest approximation one can make, and allows a reasonable estimate of some parameters (periosteal circumference, major and minor axis length, medullary cavity and cortical shape) that are not obtainable from a crushed specimen. These images are marked "reconstructed" to prevent confusion.

All images produced for this study have been uploaded to the digital image repository MorphoBank (http://www.morphobank.org) under several projects. The projects and MorphoBank accession numbers are listed in Table 2.1. To keep file sizes reasonable for uploading/downloading, the MorphoBank .jpgs were downscaled (maintaining the original aspect ratio) from the original .psd files after scale bars, labels, and backgrounds were added. All images (more than 700) will be published on MorphoBank upon publication of my dissertation; images for published projects are already available. In this chapter, I provide images only for previously undescribed taxa, or specimens for which my interpretation differs from previous studies.

Measurements—The following measurements are reported for sectioned elements in Table 2.2: mid-diaphyseal circumference, mid-diaphyseal diameter, medullary cavity diameter, average cortical thickness, number of growth marks (lines of arrested growth or annuli) preserved, relative bone wall thickness, and osteocyte density.

To measure circumference at mid-diaphysis, I traced the perimeter of the periosteal surface on the raw photomontage or reconstructed cross section using the Pen Tool in Photoshop, and then measured circumference using the Record Measurements feature. For specimens in which the periosteal surface was obviously missing a small portion, I visually estimated the path of the original circumference. For specimens in which too much of the periosteum was missing to be estimated reasonably or only a partial cross section was preserved, I do not report it.

I measured the mid-diaphyseal diameter of the cortex and medullary cavity along their major and minor axes using the Ruler Tool in Photoshop. These values are reported in the format "major axis x minor axis." I measured the thickness of the cortex along the major and minor axes of the shaft and provide an average of these four measurements in most cases (average cortical thickness). To measure cortical thickness, I measured from the periosteum to the outermost erosion room (see Chapter 1 for discussion of characters) or to the endosteal lamellae. For specimens in which much of the periosteum was missing or only a partial cross section was preserved, I measured the areas with an intact periosteum and averaged these

measurements (these are noted in Table 2.2). Relative bone wall thickness describes the average cortical thickness as a percentage of the diameter of the bone; it is a way to describe the hollowness of the element. I calculated relative bone wall thickness using a modified version of the method described by Botha and Chinsamy (2004), using the measure of average cortical thickness as described above. This affects measurements of cortical width only in specimens showing significant resorption of the internal cortex.

I identified and counted annuli and lines of arrested growth under the microscope and then confirmed their number and positions on the digital photomontages of cross sections. To measure the circumference of or distance between annuli and (or) LAGs, I used the following guidelines: In cases where annuli were present but not LAGs, I measured to the center of the annulus. In cases where a series of LAGs (LAG "packets") were present, I measured to the externalmost LAG. All other histological measurements were made on the digital cross sections or digital transects in Photoshop CS 5 Extended (Adobe).

To estimate average osteocyte densities, I drew a series of square box plots onto the radial transect photomontages in Photoshop. For each box, I used the Count Tool to count the number of osteocyte cell bodies lying in the plane of focus. The advantage of this method is that the positions of counted osteocytes can be saved in the metadata and later checked for consensus, without requiring laborious recounting. I converted the counts to cells/mm^2 and averaged the tallies by element to estimate the average osteocyte density (cells/mm^2) for each element. The raw osteocyte count data are reported in Appendix A.

Histological Abbreviations—ACT, average cortical thickness; **EL**, endosteal lamellae; **ICL**, inner circumferential layer; **OCL**, outer circumferential layer; **RBT**, relative bone wall thickness; **EFS**, external fundamental system; **HR**, hematoxylinophilic ring; **LAGs**, preserved lines of arrested growth; **MA**, major axis; **ma**, minor axis; **MSC**, midshaft circumference; **MCD**, medullary cavity diameter; **MSD**, midshaft diameter; **OD**, osteocyte density.

Histological Descriptions—Histological descriptions are based on direct observation of each histological thin section made through an Optiphot2-Pol light transmission microscope (Nikon Inc., Melville, New York) under regular transmitted light, and using compensators to enhance birefringence [both crossed plane-polarizing filters and a red tint plate (full wave retarder), λ =530 nm)]. My histological terminology follows that of Francillon-Vieillot et al. (1990), with clarifications to diagnosis as described in Werning (2012). I describe each character in detail, as well as how I diagnosed them, in Chapter 1 of this dissertation.

HISTOLOGICAL DESCRIPTIONS

Here, I describe the histological characteristics of 37 archosauromorph taxa. Additionally, I characterize the bone microstructure of three lepidosaurs and a captorhinid as outgroup comparisons. In this section, I discuss taxa phylogenetically, moving crownward towards crocodylians and birds following the phylogenetic tree presented in Figure 2.1. Within taxa, I discuss elements in this order: humeri, femora, tibiae; and when elements vary ontogenetically, I proceed from smallest/histologically youngest to largest/histologically

oldest. For all specimens, histological measurements are listed in Table 2.2. I describe the overall (first order) characteristics of the section first. I then describe the second and third order bone microstructure beginning with the internalmost tissues, and moving outward to the periosteal surface. Where I disagree with previous assessments, I also include a short discussion section. To keep this chapter of somewhat reasonable size and length, I figure only those elements whose bone microstructure is described for the first time here, or elements in which I contradict previous assessments.

It is important to note that these histological descriptions represent only a sample of the histological variability for each taxon. Because I am investigating phylogenetic variation, my samples were selected to control for age, skeletal element, and sampling location. I also avoided obviously pathological sections, and for most taxa was only able to sample one element, individual, or locality. In doing so, the apparent natural variation resulting from ontogenetic, positional, intra-elemental, biomechanical, environmental, and (or) individual variation is minimized (see Horner et al. 1999, 2000, and the Discussion section below for a longer discussion of these influences). Where I have sampled several elements, age classes, or individuals from different localities (see, for example, *Trilophosaurus*, *Vancleavea*, *Alligator*, or Coelophysoidea), differences in vascularity, osteocyte density, and even collagen orientation may occur. This is not to suggest that such efforts are futile, just that focusing on one thing that may influence histological variability necessarily obscures variation that results from other influences.

Most important, it should always be kept in mind that any description of the histology of any region within any bone tissue represents merely an instantaneous stage of growth and remodeling. Divorced from an assessment of the stage of ontogeny (and, where possible, of absolute chronological age), it is not possible to characterize any particular tissue sample as typical of the growth trajectory of the taxon.

EUREPTILIA

All taxa in this study are part of the clade Eureptilia.

Captorhinus aguti

Specimen number and element: UCMP 223509 (humerus)
Locality: Fort Sill/Richards Spur Quarry (UCMP locality V99051, horizon FEP 60-C), Comanche Co., OK, USA.
Formation and age: Fissure fill deposits (no formation name), Early Permian (possibly Leonardian)

Prior histological analyses: Enlow and Brown (1957) made general histological observations on *Captorhinus* based on a series of sections of different elements. They figured a rib, long bone, and humerus and also examined cranial elements and ribs. Peabody (1961) briefly described the histology of the humerus, vertebrae, and dentary as part of a broader study of reptilian zones and annuli. One of the humeral sections, UCMP 223509, was figured and described by Peabody (1961), and I redescribe it here. Warren (1963) described the annuli of the vertebral zygapophyses, and Enlow (1969) reviewed the general osteohistology of the

species. de Ricqlès (1974) described the humeral and ulnar histology, the largest discussion of *Captorhinus* histology to date. Finally, de Ricqlès and Bolt (1983) further described the histology of the jaws and teeth, as part of a larger study on skull growth and tooth replacement.

Histological observations: The humerus of UCMP 223509 is nearly oval in cross section, with a somewhat rounder, centrally situated medullary cavity. One side is pinched in cross section, at the base of either the ectepicondylar crest or the deltopectoral crest, both of which just reach the humeral mid-diaphysis in *Captorhinus* (Fox and Bowman 1966). As noted by Enlow and Brown (1957), Enlow (1969), and de Ricqlès (1974), the medullary cavity lacks trabeculae at mid-diaphysis, though a few small erosion rooms are present in this section. The medullary cavity is lined with a layer of endosteal lamellae that varies in thickness between ~50-130 μm, but is generally about 100 μm thick. As Peabody reported (1961), there are three LAGs (LAG packets) present in this section, all of which lie in the outer cortex (Figure 2.2A; note arrows).

The innermost cortex has been secondarily remodeled by a few oval erosion rooms. The largest of these is 230 μm along its major axis. Around most of the circumference of this section, the erosion rooms lack a lining of lamellar bone. However, on the side of the section opposite the ectepicondylar/deltopectoral crest, the rooms are more mature and are each lined with 5-15 lamellae. No other secondary osteons are present. The primary bone of the inner cortex is composed of moderately vascularized parallel-fibered bone. All of the canals in this region are longitudinally oriented, and fewer than ten anastomose circumferentially or obliquely with another canal. Most of these are simple primary canals. However, some primary osteons are also present. The canals are arranged circumferentially and locally form radial rows (Figure 2.2A: follow endosteally from top arrow). The osteocytes in this region are generally oriented perpendicular or oblique to the long axis of bone and have no preferred arrangement relative to each other. Some appear to orbit the vascular canals at the edge of the lamellae, but these generally do not look flattened, especially when compared to the osteocytes in the lamellae surrounding erosion rooms.

The outer cortex is not preserved as well as the inner cortex; it looks like the coverslip has separated from a slide here. Consequently, osteocytes were difficult to count in this region. The innermost LAG (actually a LAG "packet" of 2-4 lines) is coincident with a sharp histological transition at midcortex. External to this LAG, the primary bone is entirely composed of poorly-vascularized lamellar bone. All canals are simple primary canals. In this region, osteocytes appear smaller and generally run perpendicular or slightly oblique to the long axis of the bone. Osteocytes are much sparser here, and regionally line up along lamellae. They do not change orientation near the canals. The second LAG is a single LAG that locally splits or disappears. The outermost LAG lies close to the periosteal surface and is regionally hard to detect where the slide is thin. The locations of the LAGs are consistent with Peabody's (1961) description. They are closely spaced relative to each other.

Discussion: The microstructure of UCMP 223509 is most consistent with that described and figured by de Ricqlès (1974). That humerus was slightly smaller than UCMP 223509 (3 x 3 mm vs. 4.08 x 2.69 mm), but otherwise its proportions are similar. The humerus described by Enlow and Brown (1957) and Enlow (1969) differs in appearance somewhat; the published

images indicate short radial or radially oblique anastomoses connecting simple primary canals. However, Enlow and Brown (1957) describe the canals as following "a general longitudinal course" (p. 188), so this may be a slightly oblique section. It is clear from the images they provide that two distinct LAGs are present: one at 3/4 the diameter of the cortex, and another very close to the periosteal surfaces. As in UCMP 223509, the density of both canals and osteocytes decreases external to the inner LAG. It is possible that this specimen is younger or smaller than the section I examined, but no measurements were provided.

Huttenlocker and Rega (2011) and Reid (2012) both say that Enlow (1969) stated that *Captorhinus* has fibrolamellar bone. It does not, and Enlow (1969) did not claim that it did. He described "primary osteons" and suggested that vascular patterns and collagen orientation were reminiscent of some small mammals. However, he also noted that the primary cortical tissue of *Captorhinus* is composed of either coarse lamellar bone or parallel-fibered bone tissue, and in his original publication (Enlow and Brown 1957) he noted that the same specimen has a layer of lamellated bone near the periosteum. Enlow and Brown (1957) and Enlow (1969) did not differentiate between simple primary canals and primary osteons as de Ricqlès (1975) and Francillon-Vieillot et al. (1990) did; canals were called either primary or secondary osteons (also called Haversian canals). I suggest that Huttenlocker and Rega (2011) and Reid (2012) simply misinterpreted terms used in a time before they were standardized.

DIAPSIDA

All remaining taxa in this study are part of the clade Diapsida (see Figure 2.1: yellow star for phylogenetic position).

DIAPSIDA: LEPIDOSAUROMORPHA: LEPIDOSAURIA: RHYNCHOCEPHALIA

(See Figure 2.1, lineages A and B for phylogenetic position)

***Sphenodon punctatus* (Tuatara)**

Specimen numbers and elements: CMC 047, JC A, JC 57, JC 58, JC 807, JC 833 (all femora)
Locality: Stephens Island, New Zealand
Age: Recent

Prior histological analyses: Foote (1916) briefly described the mid-diaphyseal femoral microstructure of CMC 047, a specimen obtained from the AMNH. David Kizirian (Herpetology Collections Manager, AMNH) and I have determined that the sectioned specimen is no longer in the AMNH Herpetology or Paleontology collections. Castanet et al. (1988) described the bone microstructure of the phalanges of 78 *Sphenodon* from Stephens and Lady Alice Islands, New Zealand. The femoral histology was also described for seven of these individuals (JC A, B, 57, 58, 807, 808, 833); I redescribe them here, and add new information on cortical dimensions and measurements of osteocyte density. All of these specimens are currently in the personal collection of Jacques Castanet.

Histological observations: The cortical microstructure of all six femora is extremely similar.

Consistent with previous descriptions and images of these specimens' femoral histology (Foote 1916; Castanet et al. 1988), the femoral cortex of *Sphenodon punctatus* is thick and its medullary cavity small, relative to the periosteal circumference. The medullary cavity is irregularly shaped, and lined with a broad layer of endosteal bone that varies in thickness around its circumference. The shape of the medullary cavity is different in each individual, and in more proximal or distal sections may extend radially toward the periosteum. The layer of endosteal bone comprises as many as 25 lamellae at its thickest point and may be perforated by oval erosion rooms up to 0.5 mm in diameter. These were clearly formed after the endosteal lamellae were deposited, because they cut through the original tissue and are generally lined with a few lamellae of their own.

The transition from medullary cavity to cortical bone is abrupt; trabecular bone (whether primary or formed secondarily) is not present in any specimen. The cortices show no primary vascularity and no secondary osteons. In all specimens but JC A, a few large oval erosion rooms perforate the primary tissues of the cortex; these may be unlined, partially lined by a few lamellae, or completely lined with lamellae. These were clearly formed after the initial deposition of the cortex; they cut through the original tissue and osteocyte lacunae do not change orientation near them. Erosion rooms are limited to the inner third of the cortex. They do not appear external to the fifth preserved LAG in CMC 047, JC 57, or JC 833, and straddle the tenth LAG in JC 58 and JC 807. None of our histological specimens was sampled from juveniles, but it is likely that these erosion rooms began as primary or secondary canals. Based on the distribution of erosion rooms, I hypothesize that *Sphenodon* does not form new primary canals after (approximately) the tenth year of growth.

As reported previously (Foote, 1916; Castanet et al. 1988), the LAGs are fairly concentric. However, in all specimens it is clear that the geometric centroid of the bone migrates somewhat through ontogeny. Growth is slightly uneven around the periphery of the bone, depositing slightly more new bone along one end of the major axis compared to the opposite side. However, it is evident from looking at the position of the LAGs and from comparing their circularity that the overall shape or outline of the cross section remains consistent through ontogeny. Given the expansion of the medullary cavity and deposition of the endosteal bone, it is possible that the innermost LAGs of all JC specimens are missing. In CMC 047, a small region of densely packed osteocytes lies just internal to the first preserved LAG (see below). Castanet et al. (1988) found no evidence of a hatching line in the phalanges of the *Sphenodon* hatchlings, so it is possible that this corresponds to faster bone growth in the first year. In the outermost cortex of JC 58, JC 807, and JC 833, LAGs are packed very closely together and form an external fundamental system (EFS), signifying the end of the active phase of skeletal growth.

Most of the cortex is composed of primary parallel-fibered bone. Contrary to Castanet et al. (1988), I observe lamellae in the outer third of the cortex of each JC specimen (Figure 2.3; note thin purple lines between arrows). These form alternating bands of differential staining (lighter and darker, though the darker lamellae never stain as darkly as the LAGs). These lamellae are most clearly visible at higher magnification in regions where LAGs are more widely spaced. The transition to lamellar bone occurs before the tightly packed LAGs that form the EFS. Collagen fibers do not change their organization on either side of the LAG.

All osteocytes are oriented with their longest axis more or less perpendicular to the long axis of the femur (i.e., they appear elliptical in cross section). They do not show any

preferential organization/arrangement relative to each other in any region of the cortex. In the regions where lamellae are visible, the osteocytes do not line up along lamellae. I estimate an average osteocyte density of 440/mm^2 (standard deviation 74.71) based on all transects/specimens. In all JC specimens, osteocyte density fluctuates slightly through the cortex, but remains fairly constant throughout and shows no general trend of decreasing periosteally. In CMC 047, there is a narrow region of the innermost cortex (between the endosteal lamellae and the first preserved LAG) where osteocytes are much denser. This region may correspond to the first year of growth (before the first hibernation), or to embryonic bone; it is extremely similar to embryonic bone described in iguanid lizards by Hugi and Sánchez-Villagra (2012). If this is embryonic bone, then what I describe as the first LAG is likely a hatching line.

DIAPSIDA: LEPIDOSAUROMORPHA: LEPIDOSAURIA: SQUAMATA
(See Figure 2.1, lineages A and C for phylogenetic position)

***Iguana iguana* (Green Iguana)**
Specimen numbers and elements: UCMP 68286 (humerus); UCMP 68288 (tibia). These sections likely belong to the same individual.
Locality: none available, presumed wild-caught
Age: Recent

Prior histological analyses: Foote (1916) briefly described the femoral histology of this species (as *Iguana tuberculata*). Enlow (1969) figured the microstructure of the mid-diaphyseal femur of *Iguana* sp. as part of a general discussion of lepidosaurian bone structure. Germain and Laurin (2005) examined the microanatomy of the radius of *I. iguana* as part of a larger study of amniotes, but only reported the bone compactness and did not describe its microstructure. A similar study of amniote tibiae (Kriloff et al. 2008) included *I. iguana* but also did not report its histology. Hugi and Sánchez-Villagra (2012) described the microstructure of the humerus, radius, ulna, femur, tibia, and fibula of the marine iguana, *Amblyrhynchus cristatus*, and compared it to other terrestrial iguanids, including a captive adult male *I. iguana* (NMB 13801; the paper reports two different specimen numbers for the same individual). However, they did not describe the microanatomy of *I. iguana* in detail or figure its histology.

Histological observations: UCMP 68286 was excessively ground on one edge (the edge appears sheared off on the slide), requiring the circumference and major axis length to be estimated rather than measured directly. The specimen or the coverslip adhesive varies in thickness, making osteocytes difficult to image and estimates of osteocyte density impossible. UCMP 68288 is badly cracked under the coverslip, which also requires the circumference to be estimated.

The mid-diaphyseal cortex of the humerus is oval to subtriangular in cross section, and the central medullary cavity is subtriangular (Figure 2.4). The mid-diaphyseal cortex and central medullary cavity of the tibia are both oval in cross section (Figure 2.5). In both

elements, the medullary cavity lacks trabeculae and is lined by endosteal lamellae. This lining is thicker in the humerus than in the tibia (85-105 μm vs. 45-75 μm) and its osteocyte density is much lower than in the primary tissue of the innermost cortex, which it cuts across. The humerus preserves at least three LAGs (Figure 2.4, note arrows), and the tibia preserves four (Figure 2.5, note arrows). My estimate of RBT is consistent with that of Botha and Chinsamy (2004) for this species (listed as *I. tuberculata* in that paper).

As Foote (1916) noted and Enlow (1969) figured, the mid-diaphyseal cortex of adult *Iguana* is quite uniform. In both UCMP 68286 and UCMP 68288, the entire cortex consists of generally avascular, mostly lamellar bone punctuated by LAGs and annuli. As Hugi and Sánchez-Villagra (2012) reported for other large-bodied terrestrial iguanids, outside each LAG is a region ("growth zone") of mostly lamellar bone with patches of weakly parallel-fibered bone. In these areas, the lamellae are usually fairly distinct, and the osteocyte lacunae are elongate (their long axis is perpendicular to the long axis of the bone), but not flattened. Outside these regions is an annulus of lamellar bone with much more flattened osteocyte lacunae. The osteocyte density is higher in the "growth zone" region (*sensu* Hugi and Sánchez-Villagra 2012) compared to the annuli, but they share the same arrangement relative to each other. In both regions, osteocyte lacunae run parallel or subparallel to each other; however, they do not line up along the lamellae. Each annulus terminates in a LAG, and does not appear on the other side of the LAG. Four LAGs are visible in this specimen. Because the tibia slide is poorly preserved, these are most easily visible under polarized light; they birefringe more intensely than the adjacent zones. Enlow (1969: Fig. 21) provides an excellent example of LAG and osteocyte appearance and arrangement in *Iguana*.

In both UCMP 68286 and UCMP 68288, one region differs markedly from the general histological trend of this section. In the humerus, this region is radially thicker and extends around the circumference of the innermost cortex for a greater extent than in the tibia. In the humerus, the region is mostly avascular; there are two longitudinal simple primary canals and one radial canal extending from the medullary cavity to the periosteum. The collagen fibers here form large swaths of parallel-fibered bone that are generally oriented circumferentially, but locally they are oriented radially. In the tibia, this region of bone is punctuated by at least seven longitudinal vessels, and is extremely dense in osteocytes compared to the rest of the cortex (Figure 2.6, center of both top and bottom images). Most of these canals are secondary osteons lined with many lamellae that cut across primary osteons or the outermost lamellae of other secondary osteons. In these cases, the osteons have migrated through the cortex and left a "trail" through the cortex marking their past positions. However, at least two are primary vessels of some sort. These do not have even a single lamella but do have a thick region of osteocyte-dense, primary bone that circumnavigates the canal. One of these canals appears to have extended and cut into the endosteal lamellae. In this odd region of the bone, the osteocytes are dense and disorganized. They show no preferred orientation relative to the long axis of the bone, nor any preferential arrangement relative to each other. Locally they may appear to loosely encircle the canals, or form large clusters. The presence of vascular canals and the extremely disorganized appearance of the osteocytes are similar to the remnants of embryonic bone described by Hugi and Sánchez-Villagra (2012).

***Varanus niloticus* (Nile Monitor)**

Specimen numbers and elements: VdB uncatalogued, femur and tibia (same individual); UCMP 223456 (femur)
Locality: The sections made by de Buffrénil are from Sudano-tropical region of Africa (between 10° and 16° N); UCMP 223456 was collected in Ngamiland, Botswana. All specimens were wild-caught.
Age: Recent

Prior histological analyses: The bone histology of *Varanus niloticus* has been described extensively in the literature, and I discuss only the major studies that describe or analyze the microstructure of the major long bones here. Peabody (1961) first examined the humeral and femoral microstructure of wild-caught *V. niloticus*, but the most extensive work on this species (and varanid lizards in general) has been performed by Vivian de Buffrénil and his colleagues. The most descriptive of these works are de Buffrénil and Castanet (2000), a skeletochronological study of wild-caught Nile monitors that included bone labeling; de Buffrénil and Francillon-Vieillot (2001), which examined cortical histology, remodeling, and bone compactness; and de Buffrénil et al. (2008), which examined variation in vascularity across Varanidae. Botha and Chinsamy (2004) included *V. niloticus* in a comparative study of femoral bone wall thickness. Most importantly, this species has also been included in a series of quantitative works relating bone microstructure to bone growth in living amniotes (Cubo et al. 2005, 2008, 2012; Montes et al. 2007, 2010). These studies analyzed bone growth using measures of bone depositional rate (via labeling studies), osteocyte density and cell size, and vascular orientation, patterning, and density. UCMP 223456 was described by Peabody (1961). The other specimens I describe here were sectioned for the de Buffrénil and Castanet (2000) study, and are part of the personal collection of well de Buffrénil.

Histological observations: Both femora are circular or slightly oval in cross section, with a circular medullary cavity that lies centrally. The tibia is subrhomboidal in cross section, with a medullary cavity of the same shape. The tibial medullary cavity lies centrally, but is rotated ~30° relative to the external shape. All samples have a free medullary cavity, as expected based on a much larger sample (de Buffrénil and Francillon-Vieillot 2001), but each preserves some marrow in the slide (most obvious in the tibia). Each element preserves a very thin layer of endosteal lamellae, 30-70 μm in diameter. The de Buffrénil sections are ground very thin, making identification of LAGs difficult even in elliptically polarized or cross plane polarized light. For this reason, I did not estimate the number of LAGs for either element. UCMP 223456 preserves four LAGs; the first three are spaced similarly to the condition illustrated in figure 4B of de Buffrénil and Castanet (2000; lower growth rate earlier in life followed by a higher growth rate in a later year).

As noted by de Buffrénil and Castanet (2000) and de Buffrénil and Francillon-Vieillot (2001), the histology of the cortex is fairly uniform. This is true for all three elements I examined, but especially so in the femora. Both femora are moderately vascularized by radial primary osteons throughout the entire cortex, but in the tibia, vascular canals become increasingly sparse moving medially. This was also noted by de Buffrénil and Castanet (2000). Osteocyte density is higher in *V. niloticus* (1472 cells/mm^2 across all elements) than *Sphenodon* or *Iguana*, and does not change moving periosteally. The cortex of both elements is composed mostly of parallel-fibered bone, but in the deep cortex of UCMP 223456 and

regionally in the femur of the de Buffrénil sections, the osteocytes are more disorganized, suggesting that the tissue may be intermediate between parallel- and woven-fibered bone. Elsewhere, the osteocytes are generally oriented perpendicular to the long axis of the bone (i.e., they appear elongated in cross section). Throughout the cortex, osteocytes show no preferential arrangement relative to each other.

Discussion: My estimates of osteocyte density (1414 cells/mm^2 for the femur, 1579 cells/mm^2 for the tibia) are higher than Cubo et al. (2012) reported for *Varanus niloticus* (1000 cells/mm^2 for the femur, 1200 cells/mm^2 for the tibia; I converted these values from cells/μm^2, as they reported them), but they used slightly different methods to estimate cell density. Cubo et al. (2012) estimated osteocyte density by focusing on a single layer of osteocytes, counting all the cells in that layer, and dividing by the area of the surface they examined. Our methods are methodologically similar in that we both count a single layer of osteocyte lacunae, but my method averages values along the major and minor axes. Cubo et al. (2012) do not report where in the cortex they observed or how many replicates they made. However, as described in Chapter 1, individual and ontogenetic variation in osteocyte density for reptiles is unknown. Additionally, growth rates between wild and lab-bred animals are likely to differ. The estimates for *V. niloticus* in Cubo et al. (2012) are similar to those for other lizards and much lower than they report for birds and mammals, which is consistent with the results of my study (although see comments for some extinct taxa, below).

My estimate of femoral RBT, 29.7%, is much higher than that cited by Botha and Chinsamy (2004) for this species (15.5-19%). In *V. niloticus*, femoral compactness increases ontogenetically in males and females, and dramatically so in males (de Buffrénil and Francillon-Vieillot 2001), so it is possible that those estimates are based on a young individual.

de Buffrénil and Castanet (2000) described the collagen fiber orientation of *V. niloticus* as woven-fibered based on the monorefringence of the collagen fibers, osteocyte density, and abundant osteocyte canaliculi. This contrasts with the assessment of de Buffrénil and Francillon-Vieillot (2001), who described the bone as lamellar-zonal (implying lamellar or parallel-fibered bone tissue), and the assessment of de Buffrénil et al. (2008), who described it as parallel-fibered based on the pattern of birefringence. I agree with the latter two studies, based on the specimens I examined. Though the osteocyte density is higher compared to that of *Sphenodon* or *Iguana*, it is comparable to other larger-bodied reptiles that also exhibit parallel-fibered bone (see below; Table 2.2). Also, all three elements are anisotropic under polarized light, though this is certainly weaker in the de Buffrénil specimens, because the slides are so thin. Finally, both femora additionally exhibit a weak 'Maltese cross' pattern under elliptically and crossed plane polarized light at low magnification (Figure 2.7, bottom image: note the four darker regions that form a cross). This is characteristic of lamellar and parallel-fibered bone, but never occurs in woven bone unless the dominant fibrillar orientation is circumferential (Reid 1984, Francillon-Vieillot et al. 1990).

DIAPSIDA: ARCHOSAUROMORPHA

All remaining taxa in this study are part of the clade Archosauromorpha (see Figure 2.1, node 1 for phylogenetic position).

Trilophosaurus buettneri

Specimen numbers and elements: humerus: TMM 31025-849; ulna: TMM 31025-928; femora (growth series, six elements in total): TMM nos. 31025-787, 31025-67-01, 31025-67-02, 31025-885, 31025-862, 31025-876; tibiae (growth series, four elements in total): TMM nos. 31025-788, 31025-747, 31025-887, 31025-741.
Locality: Otis Chalk, Howard County, Texas, USA (TMM VPL locality 31025). All elements are from the same large, monodominant bone bed containing numerous articulated and disassociated *Trilophosaurus* bones.
Formation and age: Colorado City Formation (Dockum Group), early Norian
Prior histological analyses: None

General histological observations: The bone microstructure of *Trilophosaurus* is remarkable in its uniformity across skeletal elements and through ontogeny. The long bones of *Trilophosaurus* have thinner walls than those of *Sphenodon*, *Varanus*, and *Captorhinus* (Table 2.2). The medullary cavity is free of trabecular bone at the mid-diaphysis in every specimen except TMM 31025-862 (femur), which has several, and TMM 31025-928 (ulna), which has one. In both cases, the trabeculae are lined with two or three lamellae and project only a short distance into the medullary cavity. Though most specimens were filled in with mudstone or crystalline matrix, the mid-diaphyseal region likely lacked trabeculae in life. A single lamella (occasionally two or three) lines the endosteal margin of most specimens, cutting across the primary cortical tissues and forming a clear boundary between the medullary cavity and the cortex. The endosteal lamellae do not project into the medullary cavity, and often are similar in shape to the periosteal surface and to the LAGs, suggesting little shape change at the mid-diaphysis through ontogeny.

Cancellous bone is commonly preserved in the tibial mid-diaphysis (all tibiae sampled) and in the only ulna sampled, but is only present in one femur (TMM 31025-862), and absent in the only humerus sampled. Where present, cancellous bone is restricted to one small region of the bone (always less than 1/4 the circumference of the innermost cortex, and usually less than 1/10). In all cases it is formed by the resorption of the primary compact tissue of the innermost cortex, resulting in oval erosion rooms of various size. These erosion rooms are usually lined with 1-3 lamellae of variable thickness and may anastomose with adjacent erosion rooms. In the tibiae, this region of cancellous bone is always secondarily remodeled (even in the smallest specimen), and additional (as many as five or six) endosteal lamellae separate this region from the medullary cavity.

In all elements sampled, the cortex is composed of highly organized, poorly or moderately vascularized primary lamellar bone. Lamellae are distinct throughout the cortex. At least one LAG (usually many more; see Table 2.2) is visible in all specimens. In most cases, these LAGs occur as single, double, triple, or more LAG “packets”, separating zones that generally decrease in width periosteally. In the largest specimens, the outermost LAGs are separated by only a few lamellae.

All primary vascular canals are simple canals oriented longitudinally (i.e., parallel to the long axis of the bone), although in areas these may be slightly oblique. Except in the humerus, the primary vascular canals never anastomose with each other. The primary canals are often arranged randomly relative to each other, but regionally may align radially in rows. Primary osteons are never observed, but rarely, small isolated erosion rooms or secondary osteons are present. Canal density varies ontogenetically and by element, but decreases toward the periosteal surface even in the smallest individuals (TMM 31025-787, 31025-788).

The osteocytes are always oriented perpendicular to the long axis of the bone and appear elongated and very thin in cross section. In the interstitial spaces between vascular canals, the osteocytes are highly organized, lining up in rows between/along the lamellae. They do not change their orientation near the vascular canals. Osteocyte density in *Trilophosaurus* (1197 cells/mm^2 across all elements, standard deviation = 318) is comparable to that of *Iguana* and lower than that of *Varanus*. Along most radial transects, osteocyte density does not change appreciably within a section. However, when ontogenetic series are examined, it is clear that osteocyte density decreases with age. Because the bones are so hollowed at mid-diaphysis, too much ontogenetic history is obscured to make this trend obvious within a single individual.

Histological observations by element:

Humerus

TMM 31025-849 is among the largest humeri in the TMM collection (personal observation), the only museum with a substantial collection of *Trilophosaurus buettneri* postcrania. It is presumably from an adult, based on size and histology. The mid-diaphysis of TMM 31025-849 is roughly circular or D-shaped in cross section (Figure 2.8, top image). The medullary cavity is oval and sits at an oblique angle relative to the major and minor axes of the bone. No trabeculae are preserved, and four endosteal lamellae line much of the medullary cavity's circumference. The cortex preserves at least 15 LAGs. The zones between these are roughly similar in width until the outermost cortex. In this region, the borders between lamellae are quite pronounced, making LAG identification difficult. I identify this region as an EFS (Figure 2.8, bottom image: note closely-spaced lines to the left side of the image).

The vascular canals of TMM 31025-849 are mainly short radial canals, different from the general trend for *Trilophosaurus*. Some of these clearly connect two longitudinal canals, but most of these are not anastomoses. Although it is possible that this section was not cut precisely perpendicular to the long axis of the bone, re-examination of the cut blocks makes this seem unlikely. Because this occurs around the entire circumference of the bone, I think it is more likely that the canals may have been subparallel to the long axis of the humerus in life, making them appear more radial in cross section. The inner cortex is moderately vascularized, but the outer cortex is poorly vascularized. Here, the canals begin to "break up" (more canals are seen, but they are shorter and more widely spaced). The outermost cortex (including the EFS) is avascular.

Ulna

TMM 31025-928 is among the largest ulnae in the TMM collection (personal observation), and is presumably from an adult based on size. The mid-diaphyseal cortex and medullary cavity are essentially triangular in cross section (Figure 2.9, top image). The

medullary cavity lies centrally. A single trabecula arcs into the medullary cavity, and the lamellae that form it are continuous with the lamellae that line the medullary cavity. This specimen preserves at least 14 LAGs, and the zones between them vary in width throughout the cortex. Based on the shape of these LAGs, the mid-diaphysis probably did not change in shape throughout life.

The ulna of *Trilophosaurus* is remarkable for its extensive avascularity (Figure 2.9, bottom image: note lack of vascular canals). When canals are present, there are usually three or four canals within ~1 mm^2, but these very poorly vascularized regions are separated by at least five millimeters of avascular bone. In the outer half of the cortex, there are no vascular canals at all. Most of the vascularity in the ulna is limited to one small region of remodeled bone near the single trabecula. This region includes many secondary osteons and small erosion rooms, but they are confined to a thin strip extending most of the way through the cortex. None of the secondary osteons or erosion rooms is lined by more than three lamellae; some are unlined. However, in all cases, they clearly cut across primary tissues.

Femur

TMM 31025-787 is a complete femur. TMM 31025-1064 is nearly complete, missing the proximal metaphysis and epiphysis. TMM 31025-1063 and TMM 31025-862 are both complete. TMM 31025-885 preserves ~3/4 of the total length and is missing the distal end. Some distortion of the midshaft is visible in that specimen, as well as some antero-posterior crushing of the proximal metaphysis. In TMM 31025-786, both ends and the midshaft are preserved, but the contact between the diaphysis and distal end is crushed and could not be reconstructed. This specimen is among the largest in the TMM collection (personal observation), and is an adult based on size and ontogenetic changes in histology.

The femur of *Trilophosaurus* is round at mid-diaphysis, with a round medullary canal that sits centrally (Figures 2.10 and 2.11, top images). In all specimens, the medullary cavity cuts across the internalmost LAGs on one side. Additionally, each zone varies in thickness between adjacent LAGs around the circumference of the bone. This suggests that *Trilophosaurus* remodeled the femur through life, adding and resorbing bone on one side preferentially to maintain the position of the medullary cavity through ontogeny. Additionally, RBT decreases ontogenetically (Table 2.2) except in the largest specimen. Thus, the femur becomes progressively hollower as the animal grows.

In smaller specimens, annual growth marks are single LAGs (Figure 2.10, bottom image: note arrows), but LAG packets of 3-5 lines are more common in larger individuals (Figure 2.11, bottom image: note arrows). The zonal width is highly variable even within one individual; only TMM 31025-786 shows progressively decreasing zonal widths (Figure 2.11, bottom image: note that spacing between arrows decreases moving to left of image), and only in the outer cortex. Among the rest of the femora, there is no clear pattern of growth from year to year. In wider zones, the bone tends to be moderately vascularized; in thinner zones, the bone is poorly vascularized or even avascular. When canals are more numerous, they tend to align circumferentially and in radial rows, though regionally they may be arranged randomly relative to each other. When canals are sparse, they are distributed randomly.

The average osteocyte density for all femora is 1135 cells/mm^2 (standard deviation = 265). The two smallest individuals exhibit a higher osteocyte density compared to the

average, and the largest individual exhibits a lower than average osteocyte density (the other three approximate the average). Osteocyte density varies little within a single transect.

Tibia

TMM 31025-788 is a complete tibia. It is of similar size and preservation as TMM 31025-788 (femur). Their subsequent field numbers indicate they were collected on the same day from the same part of the quarry, so they may represent the same individual. TMM 31025-747 is complete, and TMM 31025-887 is missing only a small piece on the lateral side of the distal end, though it somewhat crushed at the mid-diaphysis. TMM 31025-741 is complete, and among the largest in the TMM collection (personal observation). It is presumably an adult based on ontogenetic changes in size and histology.

The tibia of *Trilophosaurus* is almond-shaped in cross section at the mid-diaphysis, with an oval medullary canal that sits centrally (Figures 2.12 and 2.13, top images). As in the femur, the medullary cavity cuts across the internalmost LAGs on one side. This is also the side to which the tibia adds more bone periosteally, as in the femur. On the opposite side of the section, bone is secondarily remodeled close to the endosteal surface in all tibiae except TMM 31025-887. This occurs in two ways. In TMM 31025-788 (the smallest individual), a thin layer of endosteal lamellae cuts across the original primary cortex (Figure 2.12, bottom image accompanies this discussion). Internal to these lamellae is a region of remodeled bone where thick trabeculae extend inwards radially. Their origin is difficult to discern; erosion rooms have formed within them and these have been subsequently lined with their own lamellae. At some point after this region was deposited, a new, thicker layer of endosteal lamellae was deposited on the inner surface of the odd-looking bone, and this layer is continuous with the lamellae around the rest of the endosteal margin. Subsequently, secondary osteons formed in the remodeled region, and these cut across that bone and the internal layer of endosteal lamellae. In TMM 31025-747 and TMM 31025-741, the innermost cortex is remodeled by secondary osteons and larger erosion rooms in the same position as TMM 31025-788. However, this appears to be remodeled in a more typical fashion, and there is only one layer of endosteal lamellae (Figure 2.13, bottom image, note only one band of endosteal lamellae at lower left of image).

The primary vascular canal density is lower in the tibia than in the femur at all ontogenetic stages, and the vascular canals are almost always randomly arranged when present. There is a small region of the inner cortex in TMM 31025-747 where canals are arranged in radial rows. Vascularity in the tibia is concentrated to one side; most canals occur on the side that experiences greater growth, and the opposite side is always avascular or nearly so. Where canals are present in the smaller two specimens, the spacing between them suggests moderate vascularization. In the larger two specimens, these regions are poorly vascularized in the inner cortex and nearly avascular in the outer cortex.

Unlike the femur, tibial RBT is similar throughout ontogeny (i.e., the hollowness of the bone is fairly constant). As in the femur, zonal width is variable through much of the cortex. Unlike the femur, single and paired LAGs are more common than LAG packets of higher numbers. In the two larger specimens, zonal width decreases periosteally in the outer cortex. In TMM 31025-741, the largest individual, a series of closely-spaced LAGs is apparent in the avascular bone near the periosteal surface. I identify this as an EFS. The tibia

has a higher average osteocyte density than all other elements (1349 cells/mm^2 across all tibiae, standard deviation = 330). The smallest tibia has a higher osteocyte density.

ARCHOSAUROMORPHA: ARCHOSAURIFORMES

All remaining taxa in this study are part of the clade Archosauriformes (see Figure 2.1, node 2 for phylogenetic position).

Vancleavea campi

Specimen number and element: UCMP 152662 (femur)
Locality: UCMP locality V82250 (Inadvertent Hills/Dinosaur Hill), Petrified Forest National Park, Arizona, USA
Formation and age: Petrified Forest Member of the Chinle Formation, middle Norian (Riggs et al. 1996)
Specimen number and element: GR 250 (femur)
Locality: Hayden Quarry 4, Ghost Ranch, Rio Arriba County, New Mexico, USA
Formation and Age: Petrified Forest Member, Chinle Formation, ~213 MYA, middle Norian (Irmis et al. 2011)

Prior histological analyses: Nesbitt et al. (2009b) described the histology of UCMP 152662, which I redescribe here, and add new information on cortical dimensions and osteocyte density. UCMP 152662 is figured well by Nesbitt et al. (2009b); I do not refigure it here (although images are available on MorphoBank). The histology of *Vancleavea* from Ghost Ranch has not been described previously. I describe and illustrate it here.

Histological observations: As Nesbitt et al. (2009b) noted, the mid-diaphysis of UCMP 152662 is roughly circular in cross section. This specimen has a large cancellous medulla, rather than a single medullary cavity. This is consistent with the aquatic or semi-aquatic lifestyle proposed for the species (Nesbitt et al. 2009b). The medulla sits centrally and has the same overall shape as the cortex in cross section. The thickness of the cortex is relatively uniform around the section, and it preserves at least three LAGs.

The erosion rooms of the innermost medulla are large and are either oval or irregular in shape. These become more circular and decrease in size periosteally. These erosion rooms are confined to the medulla; no additional erosion rooms are found in the cortex. As noted in Nesbitt et al. (2009b), the medullary trabeculae are formed by the resorption of primary bone tissues, and all but the smallest, outermost erosion rooms are lined with multiple endosteal lamellae. The primary bone preserved in the interstices between erosion rooms is poorly vascularized parallel-fibered bone, and the longitudinal canals are primarily simple primary canals (a few primary osteons are present). Only a few short radial and oblique anastomoses are present.

In the inner cortex (between the inner and middle LAGs), primary vascular density is slightly higher just external to the inner LAG, and decreases moving toward the middle LAG. These are all longitudinal primary osteons, and they are arranged in circumferential rows. Anastomoses are short and generally connect only two longitudinal canals, and are

predominantly radial. Osteocyte density is highest in the interstices between canals, but they also encircle the osteons, albeit at lower densities. When viewed under polarized light, the collagen fibers do not appear uniformly oriented throughout the inner cortex. Close to the inner LAG, they are weakly woven and become more parallel-fibered moving periosteally, but there is some variation in this transition around the section. The bone tissue of the outer cortex (between the middle LAG and the periosteal surface) is entirely composed of poorly vascularized or lamellar bone. Canal density decreases external to the middle LAG, and again external to the outer LAG. Where present, canals form a single circumferential row of longitudinal canals. Between the middle and outer LAG, the majority of these are primary osteons, and some are simple primary canals. External to the outer LAG, all are simple primary canals. Osteocyte density decreases throughout the outer cortex, but on average is higher than in *Trilophosaurus*, *Iguana*, and *Captorhinus*.

As in UCMP 152662, the femoral mid-diaphysis of GR 250 is roughly circular in cross section with a central, circular medulla, and the cortex is fairly uniform in thickness (Figure 2.14). The medulla has fewer trabeculae than UCMP 152662 does, but crystal growth may have destroyed some trabeculae in GR 250. These crystals make it difficult to estimate the size of the larger medullary erosion rooms; of the ones preserved, most are comparable to the largest of UCMP 152662. However, there are almost no small or medium-sized circular rooms. Because its medulla is smaller, this specimen has a much thicker cortex than UCMP 152662 does. It has no true LAGs, but two annuli composed of parallel-fibered bone are present. These lie approximately ½ mm and ¾ mm from the periosteal surface, and are each ~0.05 mm thick (Figure 2.15, note arrows).

Within the medulla, some of the larger erosion rooms are lined with one to three lamellae, and some are unlined. In the core of some trabeculae, non-lamellar primary bone tissue is visible. Internal to the first annulus, the cortex is composed of woven bone, which is well vascularized by longitudinal primary osteons. Anastomoses are common throughout the cortex and usually connect two or three longitudinal canals and sometimes up to five canals. In the inner cortex, anastomoses may be radial, oblique, or circumferential, and sometimes form small reticulations (Figure 2.15, bottom third of image). In the outer cortex, they are mostly radial, with fewer oblique and circumferential connections, and no reticulation (Figure 2.15, top third of image). Although there are fewer anastomoses in the outer cortex, when present, they tend to connect three or four canals. Throughout most of the cortex, the longitudinal and radial canals are organized into radial rows, but there are isolated regions where the pattern becomes more disorganized. The bone is woven between the annuli but grades from woven to parallel-fibered external to the outer annulus. In this region, the longitudinal canals are organized in circumferential rows. Around the periosteal surface of the bone (approximately every 2/3 to ¾ mm), short radial canals open to the periosteal surface.

Throughout the cortex, osteocytes are oriented randomly relative to the longitudinal axis of the bone. There is a much higher density of osteocytes within the interstitial spaces between canals than in the lamellae surrounding the primary osteons. Although there is no preferred arrangement in the interstices, immediately adjacent to the osteons there is almost always a ring of osteocytes surrounding the canal's outermost lamella. Osteocyte density is higher in GR 250 than UCMP 152662

Discussion: Nesbitt et al. (2009b) described a fourth LAG between our inner and middle

LAGs, but I cannot find a local break in bone tissue deposition there, nor trace it around the circumference.

The histology of these two femora is quite distinct, despite being similar in size and identical in morphology. The microstructure of GR 250 suggests much faster growth than experienced by UCMP 152662; there are no breaks in bone deposition (no true LAGs), the bulk of the cortex is woven bone rather than lamellar or parallel-fibered bone, and vascular canals exhibit higher density and connectivity, and more complex patterning. Whether the difference in bone microstructure represents extreme developmental plasticity within a single species, or species differences between the two localities, will need to be tested with additional specimens.

Proterochampsia

Specimen number and element: MCZ 4038 (nearly complete femur)
Locality: Argentina
Formation and age: Chañares Formation, Middle Triassic (Rogers et al. 2001)

Taxonomic comment: The specimen originated from a large concretion containing the remains of *Chanaresuchus bonapartei*. The size and morphology of MCZ 4038 matches that of *Chanaresuchus bonapartei* closely. However, a similarly sized proterochampsid, *Gualosuchus reigi*, also occurs in the same beds and has identical femoral morphology. Therefore, I assign this specimen to the least inclusive clade that contains both *Chanaresuchus bonapartei* and *Gualosuchus reigi*, the Proterochampsia.

Prior histological analyses: de Ricqlès et al. (2008) described the microstructure of a long bone shaft as part of a larger study of Triassic archosauriforms. That specimen (MCZ 4036) was referred to *Chanaresuchus* because it was obtained from the same concretion as MCZ 4038. Because that specimen cannot be identified to element, I did not include it in my analysis. Its histology is similar to that of MCZ 4038 in some regards.

Histological observations: The diaphysis of MCZ 4038 was partially crushed (Figure 2.16, top image); however, digital reconstruction reveals an oval cross section, with a round, central medullary cavity (Figure 2.16, bottom image). The medullary cavity preserves no trabeculae at mid-diaphysis and it is lined by several endosteal lamellae. Cortical thickness varies somewhat around the circumference, but not dramatically. The RBT of this specimen is comparable to the femora of *Trilophosaurus*. Regionally, bacterial or fungal invasion obscures parts of the inner cortex, but the main histological details are still observable. No LAGs are preserved in this specimen.

The inner cortex is composed of weakly woven, moderately to well-vascularized bone tissue. This grades to moderately vascularized parallel-fibered bone in the outer cortex. All canals in MCZ 4038 are simple primary canals (Figure 2.17A, B: no lamellae are visible around canals). In the inner cortex, they anastomose in all directions and commonly form reticulations among ten or more longitudinal canals. Locally, a radial or circumferential pattern may dominate. This is not a true plexiform pattern; there are no true circumferential canals (the reticulations form by short anastomoses) and thus true laminae do not develop. In

the outer cortex, anastomoses are less extensive, linking only 2-8 longitudinal canals, and some isolated canals are present. Osteocyte density declines through the section, and osteocyte organization increases. In the inner cortex, the lacunae are oriented randomly with respect to the long axis of the bone and to each other. In the outer cortex, at least half are oriented perpendicular to the long axis of the bone, though they show no preferred arrangement relative to each other. Throughout the section, the osteocytes maintain the same orientation, arrangement, and density regardless of their proximity to canals.

Discussion: Overall, my observations of the femur match those of de Ricqlès et al. (2008) fairly well, with two main differences. First, MCZ 4038 shows no LAGs or other evidence of growth cycles. This may result from inter-elemental variation in bone microstructure, or differences in age or body size; their specimen was much larger than mine (1.9 x 1.5 cm diameter vs. 1.1 x .95 cm, respectively). The trends I observe in vascularization and osteocyte density match what they figure leading up to the first (inner) LAG of MCZ 4036 (de Ricqlès et al. 2008: Plate 2, Figure 3), and this supports my age/size hypothesis. The second difference is that I observe only simple primary canals in MCZ 4038, whereas de Ricqlès and colleagues (2008) imply primary osteons by using the term "fibrolamellar bone". However, it is clear from the same figure that all of the canals in MCZ 4036 are simple primary canals. Without a lamellar component from primary osteons, neither MCZ 4036 nor MCZ 4038 can be considered to exhibit true fibrolamellar bone tissue.

Euparkeria capensis
Specimen number and element: AMNH FARB 2238 (femur)
Locality: *Euparkeria* type locality, South Africa
Formation and age: *Cynognathus* Assemblage Zone B, Beaufort Group; Anisian (Rubidge 2005)

Prior histological analyses: de Ricqlès et al. (2008) described the histology of *Euparkeria* based on a stylopodial (humerus or femur), rib, and osteoderm from the same individual (SAM-PK-7868). The stylopodial was re-analyzed by Legendre et al. (in press), who identified it as a humerus based on its cross-sectional geometry, bone size, and histological age. Based on this analysis, they also estimated that the section was taken from the proximal metaphysis rather than the mid-diaphysis. Because the elemental identification and sampling location are in question, I did not reanalyze this specimen, though digital images of SAM-PK-7868 are reposited on MorphoBank (project p880, accession numbers M153039, M153042, M153043) in association with Legendre et al. (in press). Botha-Brink and Smith (2011) described the histology of the humerus, femur, tibia, and fibula of *Euparkeria* (three individuals) as part of a larger study of archosauromorph histology and growth. These materials are still under research and were not available for my study. The bone microstructure of *Euparkeria* is well illustrated by de Ricqlès et al. (2008), Botha-Brink and Smith (2011), and Legendre et al. (in press); I do not illustrate it here.

Histological observations: These particular sections were made by Sterling Nesbitt for use in this project. The preservation of the bone is such that it ground differentially, and the resulting slides vary in thickness around the section.

The mid-diaphyseal femur is oval in cross section, with a circular medullary cavity that sits centrally. The medullary cavity lacks trabeculae, and is lined with a relatively thick (0.2-0.4 mm) layer of endosteal lamellae. Secondary remodeling is isolated to five erosion rooms in the innermost cortex, all of which are unlined, and some isolated secondary osteons. Five annuli, which only locally form LAGs, are preserved in this section.

The majority of the cortex is composed of parallel-fibered bone, consistent with previous descriptions of the femoral histology (Botha-Brink and Smith 2011). In the innermost cortex, the fiber bundles are somewhat coarser but are not woven. The parallel-fibered bone becomes progressively more organized moving periosteally. External to the fifth (outermost) annulus, the bone is lamellar. Vascular density also decreases periosteally. The bone tissue of the innermost cortex is poorly (along the minor axis) to moderately (along the major axis) vascularized by longitudinal primary osteons. These are arranged circumferentially and generally form radial rows. Short anastomoses connect two or rarely three longitudinal canals, and these may be radial, circumferential, or oblique in orientation. In the mid- and outer cortex, the bone is nearly avascular along the minor axis. Along the major axis, it is poorly vascularized. Primary osteons are arranged in circumferential rows, although some simple primary canals are also present. These are not poorly organized. Between the fourth and fifth annuli, there is one region of thicker growth in which longitudinal primary osteons form four circumferential rows. At least half of these anastomose radially with one or two other canals. External to the fifth annulus, the bone is nearly avascular around the entire circumference. The only canals present are short, radial, simple primary canals that open to the bone surface.

Osteocytes in the innermost cortex are generally oriented perpendicular or oblique to the long axis of the bone, but a few are oriented parallel to it. In this region, they show no preferred arrangement or spacing relative to each other in the interstices between canals. Closer to the canals, osteocyte density is lower and they orbit the primary osteons. External to the first annulus, all osteocytes are oriented perpendicular to the long axis of the bone. Throughout the cortex they are arranged more or less circumferentially, but the spacing between cells is irregular. External to the outermost annulus, they are highly organized and align along lamellae. Osteocyte density is much higher compared to any other taxon examined in this study so far (Table 2.2.), and it neither increases nor decreases through the section, despite increasing osteocyte organization.

Discussion: My histological observations on *Euparkeria* are largely consistent with those described by Botha-Brink and Smith (2011) for the femur in terms of the types of vascular canals present and the collagen fiber orientation. AMNH FARB 2238 differs in the number of annuli (five, even though it is a smaller specimen than either of the femora examined by Botha-Brink and Smith), in the presence of lamellar bone in the outermost cortex, and in the decreasing number of canals moving periosteally. Though it was a smaller animal, the histology of AMNH FARB 2238 suggests it was older than those specimens at the time of death.

Consistent with the observations of Botha-Brink and Smith (2011) for the femur of *Euparkeria*, I see no evidence of woven bone in my section. Under polarized light, most of the cortex of AMNH FARB 2238 is weakly anisotropic, and the osteocytic organization is more consistent with parallel-fibered bone than with woven bone. de Ricqlès et al. (2008, p. 65) described "an ill-defined fibrolamellar complex" in which the woven component was both finely bundled and well organized. Legendre et al. (in press) illustrate the cortex of SAM-PK-7868 in regular transmitted light in addition to polarized light (MorphoBank p880:M153039), and show isotropy (suggesting woven bone) in the inner cortex, with parallel-fibered bone forming the outer cortex. Additionally, a high resolution image of the entire section (MorphoBank p880:M153043) shows osteocytes with no preferential orientation relative to the long axis of the bone or arrangement relative to each other in the inner cortex, and confirms the observations by de Ricqlès et al. (2008). This may result from inter-elemental differences between the femur and the humerus, but I think it is more likely the result of positional differences between the mid-diaphysis and the proximal metaphysis. Bone at the metaphyses forms endochondrally, whereas bone at the mid-cortex forms appositionally by the periosteum, without a cartilage precursor.

The differences between growth at the metaphysis vs. the mid-diaphysis in *Euparkeria* are also suggested by the presence of growth marks in AMNH FARB 2238 and all elements figured in Botha-Brink and Smith (2011), and their absence in SAM-PK-7868 (de Ricqlès et al. 2008). In the mid-diaphysis of AMNH FARB 2238, some of these are difficult to detect at low magnification, because the annuli are very thin and only locally become LAGs. Annuli and LAGs are much clearer in the specimens figured by Botha-Brink and Smith (2011). However, the mid-diaphysis is used for growth analyses precisely because it preserves the longest record of appositional bone growth (Sander 2000; Stein and Sander 2009). Because the estimates of growth rate for SAM-PK-7868 were based on a model of humeral growth derived from data taken from the mid-diaphyseal humeri of living animals (Legendre et al. in press), the results of their growth rate analysis may be problematic.

Phytosauria

Specimen number and element: UCMP 25921 (femur)
Locality: *Placerias* Quarry (UCMP locality A269), near St. Johns, Arizona, USA
Formation and age: Blue Mesa Member of the Chinle Formation; early Norian (age constraints from Irmis et al. 2011)

Taxonomic comments: This specimen was previously identified as a femur of *Rutiodon* sp. (de Ricqlès et al. 2003b; Cubo et al. 2012, Legendre et al. n press). The genus *Rutiodon* is now restricted to *R. carolinensis*, a species known only from the Newark Supergroup (Stocker and Butler in press). The femur lacks apomorphies that would allow it to be identified beyond Phytosauria. Therefore, I opt for the conservative approach and identify it only to the clade level.

Prior histological analyses: UCMP 25921 was sectioned and first described by de Ricqlès et al. (2003b), described therein as a proximal femur. I have observed the specimen and clarify that the proximal half of the femur was preserved (not only the proximal end), and that the

section was taken from the mid-diaphysis. In the same paper, de Ricqlès et al. (2003b) described the microstructure of a phytosaur femur (taxon indeterminate), UCMP 2186. The published specimen number is incorrect; UCMP 2186 is a camelid petrosal from the Eocene Rattlesnake Formation of Oregon. I think this refers to UCMP 32186, listed in the UCMP catalog as a reptilian femur from the *Placerias* Quarry, but I was not able to locate the original specimen to confirm its taxonomic identity or sampling location, nor the histological slide to confirm microstructural observations. To date, these two specimens represent all the published research on phytosaur limb histology. In a conference abstract, Bronowicz (2009) reported the histology of *Paleorhinus* from the Late Triassic of Poland, but this work has not yet been published. I redescribe the histology of UCMP 25921 here, and add new information on cortical dimensions and measurements of osteocyte density.

Histological observations: This section is complete from the endosteal margin to the periosteal surface for over half the section, but the externalmost cortex is broken off along a LAG for about 1/4 of the circumference, and the entire cortex is missing adjacent to that region. The missing portion extends for less than 1/8th the circumference.

My histological observations are largely consistent with those of de Ricqlès et al. (2003b). The mid-diaphyseal femur of this phytosaur is oval in cross section. The medullary cavity is also oval and slits slightly off center along the minor axis. The cortex is relatively thick-walled compared to *Chanaresuchus* or *Trilophosaurus*, but the missing portion precludes an estimation of RBT. As noted by de Ricqlès et al. (2003b), no trabeculae are preserved within the medullary cavity. A layer of lamellae 0.15-0.45 mm thick is visible around most of the endosteal circumference, and these do not appear to change direction in the areas where the internal surface is abraded by matrix infill. This suggests that trabeculae were not present in life. Large erosion rooms (some as large as 1.6 mm along their longer axis) are common in the deep cortex, and smaller rooms regionally invade the midcortex. However, erosion rooms do not invade the bone past the innermost LAG, except in one region along the minor axis. Most of the erosion rooms are lined with 3-5 lamellae, but a few in the innermost cortex are unlined, suggesting at least some active resorption at the time of death. The section preserves multiple growth cycles spanning the transition from faster growth as a young individual, to slow growth later in life.

Even in the areas where erosion rooms are present, they are separated enough to observe and characterize the primary tissues around the entire section (Figure 2.18A,B,C: large spaces on right size of image). A small region of woven bone is present in the inner cortex (Figure 2.19, bone tissues to the left of the third arrow), but this does not characterize most of the section (though, see osteocyte description below). Given the size of the medullary cavity, it is possible that woven bone was more common in younger individuals but that these tissues have been resorbed by adulthood. The femoral microstructure is fairly uniform throughout much of the rest of the cortex, consisting mainly of well vascularized parallel-fibered primary bone tissue (Figure 2.18B,C: note patterns of refringence under polarized light) in the zones, which transitions to finer parallel-fibered bone or lamellar bone in the annuli. The outermost cortex is composed of lamellar bone.

At least eight LAGs separating zones that decrease in width periosteally are visible in this section. The innermost LAG locally grades into an annulus. The second LAG is a distinct,

single LAG, and the remaining LAGs are a double LAG (locally triple or quadruple) that locally grade into annuli. Additionally, an EFS is preserved in the outermost cortex.

Internal to the innermost LAG, the cortex is well vascularized by circumferential primary osteons. Short radial anastomoses connect adjacent canals to form a plexiform or subplexiform pattern. This vascular pattern remains dominant until the third preserved LAG. External to this, vascularity decreases. The canals of this region are predominantly longitudinal, and may be primary osteons or simple primary canals. These tend to form circumferential rows, and may anastomose with one or two other canals (usually circumferentially). The outermost cortex is avascular.

Osteocytes are numerous throughout the cortex. Internal to the first LAG, they show no preferred orientation relative to the long axis of the bone or arrangement relative to each other in the interstices between vascular canals. Around the primary osteons, they are equally dense and line up along and between the 1-3 poorly-defined lamellae encircling each vessel. Between the first and third LAGs, the interstitial osteocytes are organized as above, but the lacunae that encircle canals occur at a lower density. Periosteal to the fourth LAG, osteocytes are oriented perpendicular to the long axis of the bone and arranged circumferentially, although they do not line up parallel to or along lamellae until the outermost cortex. This region is largely avascular.

Discussion: An EFS is preserved in the outermost cortex, suggesting the active phase of growth was complete in this individual at the time of its death. However, this is not an especially large individual compared to other phytosaur femora found in this quarry (personal observation). This suggests one of several possibilities: first, that growth was quite variable among phytosaurs (i.e., developmental plasticity); second, that more than one species was present; or third, that one dimorphic species was present. These questions cannot be resolved without additional sampling of multiple size classes coupled with a re-examination of the phytosaur material from the *Placerias* Quarry.

ARCHOSAURIFORMES: ARCHOSAURIA

All remaining taxa in this study are part of the clade Archosauria (see Figure 2.1, node 3 for phylogenetic position).

ARCHOSAURIA: PSEUDOSUCHIA

(See Figure 2.1, node 14 for phylogenetic position)

Revueltosaurus callenderi

Specimen number: PEFO 33843 (femur)

Locality: *Revueltosaurus* Quarry (Petrified Forest National Park fossil vertebrate locality 297), Petrified Forest National Park, Arizona, USA

Formation and age: Petrified Forest Member of the Chinle Formation (Parker et al. 2005), Middle Norian. A maximum age for the quarry of 213±1.7 Ma is provided by Riggs et al. (2003).

Prior histological analyses: None

Histological observations: The femur of PEFO 33843 is sub-oval or almond-shaped in cross section (Figure 2.20, note blue border). It is squared off posteromedially and shows a slight pinching posterolaterally. The medullary cavity is oval and centrally located. Many erosion rooms are visible, but these are largely confined to a band running along the major axis. Although the endosteal margin has been destroyed in places by crystal growth in the medullary cavity, 2-12 lamellae are visible lining the preserved parts of the endosteal margin (Figure 2.21B, bottom of image). These lamellae are secondarily deposited; they cut at angles across the primary tissues of the inner cortex. Five LAG packets punctuate the cortex (Figure 2.20, note white lines; Figure 2.21D, note yellow arrows).

The cortex is fairly uniform in appearance throughout the section, which consists of poorly vascularized, largely unremodeled parallel-fibered bone (Figure 2.21B,C,D: note overall lack of secondary osteons). The erosion rooms are confined to the inner cortex. Most of these are small (0.1-0.2 mm diameter), but some reach 0.8 mm in diameter. These vary in stages of maturity; some are lined with 1-3 lamellae, and others are unlined. However, there is no clear relationship between the size of the erosion room and the number of lamellae.

Primary canal density in the inner cortex is very low, with only a few longitudinal simple canals (Figure 2.21 D, note white triangles). Some are oriented slightly oblique relative to the long axis of the bone and resemble very short radial canals. Secondary osteons are absent from the inner cortex. The primary bone tissue type in the midcortex is parallel-fibered bone. The midcortex is slightly better vascularized compared to the inner cortex, except for the anterior side of the bone, which is poorly vascularized. Nearly all of the canals are isolated longitudinal primary simple canals, but very short anastomoses may connect two canals. These anastomoses are usually radial, but may be circumferential or oblique. The canals are arranged circumferentially. The outer cortex shows more organized parallel-fibered bone compared to the midcortex, and locally may be lamellar. Vascular density is extremely low, and the longitudinal (or very slightly oblique) simple primary canals resemble those of the inner cortex. The outermost cortex is nearly avascular and composed of highly organized parallel-fibered bone (*sensu* Stein and Prondvai 2013) or lamellar bone (Figure 2.21D: see lamellae at top of image).

The osteocytes of the inner cortex are generally round in cross-section and oriented parallel or oblique to the long axis of the bone. They are not spaced evenly, and do not change orientation or arrangement with proximity to the vascular canals. However, they are more disorganized in the primary tissues between erosion rooms. In the midcortex, osteocytes occur in similar densities compared to the inner cortex, but they are better organized. In the outer cortex, the osteocytes are not evenly spaced, but they are arranged more centripetally than in the midcortex.

Each LAG is a packet of 2-5 annuli and rest lines, some of which grade into annuli of parallel-fibered tissue at some point around the circumference. The zones between the LAG packets decrease in width periosteally, but no external fundamental system (EFS) is visible. The LAGs reveal an ontogenetic shift in cross sectional shape. Early in ontogeny, the mid-diaphysis is more oval, and it becomes progressively more flattened (compressed anteroposteriorly), more pinched posterolaterally and more squared-off posteromedially with age.

Aetosauria

Specimen numbers and elements: UCMP 32178 (humerus, section taken from the proximal diaphysis), UCMP 25914 (femur), GR 252 (juvenile tibia)

Locality: Both UCMP specimens are from the *Placerias* Quarry (UCMP locality A269), near St. Johns, Arizona, USA. GR 252 is from Hayden Quarry 2, Ghost Ranch, Rio Arriba County, New Mexico, USA.

Formation and age: The Placerias Quarry is in Blue Mesa Member of the Chinle Formation, early Norian (age constraints from Irmis et al. 2011). Hayden Quarry is from the Petrified Forest Member of the Chinle Formation, ~213 MYA, middle Norian (Irmis et al. 2011).

Taxonomic comments: None of these elements preserves diagnostic apomorphies that would allow identification beyond Aetosauria. The UCMP specimens were previously diagnosed as *Desmatosuchus* sp. [UCMP 32178; de Ricqlès et al. 2003b, Woodward et al. 2011 (as UCMP 3218)], *Stagonolepis* sp. (UCMP 25914; de Ricqlès et al. 2003b), and *Calyptosuchus* sp. (UCMP 25914, Cubo et al. 2012; Legendre et al. in press). At least three different aetosaur are present in the *Placerias* Quarry (Long and Murry 1995; Parker 2008), and so to be conservative, I do not assign either specimen to a more inclusive clade than Aetosauria. Based on the morphology of osteoderms and fibulae, there are at least two aetosaurs present in the Hayden Quarry (Randall Irmis and Sterling Nesbitt, personal communication), and so I also opt to refer this specimen only to Aetosauria until the materials are described. UCMP 25905, previously described both as *Typothorax* sp. radius (de Ricqlès et al. 2003b) and as *Typothorax* sp. femur (Cubo et al. 2012; this results from an error on the slide label), is here re-identified as a phytosaur fibula lacking both proximal and distal ends. I do not include it in my analysis.

Prior histological analyses: UCMP 32178 and UCMP 25914 were previously described by de Ricqlès et al. (2003b) as part of a larger discussion of pseudosuchian bone histology. UCMP 25914 was analyzed by Cubo et al. (2012) as part of a study of amniote growth and bone depositional rates. I redescribe UCMP 25914 here, and add new information on cortical dimensions and measurements of osteocyte density. This section has been extensively illustrated (de Ricqlès et al. 2003b, Cubo et al. 2012; Legendre et al. in press); I do not illustrate it here (though images are available on MorphoBank). UCMP 32178 is not a mid-diaphyseal section; although I figure it on MorphoBank and make brief comments, I do not provide an extended description. The histology of aetosaur osteoderms has received comparatively greater attention in the literature (e.g., Parker et al. 2008, Cerda and Desojo 2011), because they are diagnostic both to taxon and to carapace region. I describe and illustrate GR 252 for the first time here.

Histological observations:

My histological observations are generally concordant with those of de Ricqlès et al. (2003b). The femur of UCMP 25914 is oval in cross section, with an oval to rectangular medullary cavity that lies off center along the minor axis. Crushing precludes external measurements in the absence of digital reconstruction, but it is a large animal. The ACT is

close to 7 mm (Table 2.2) and in places greater than 10 mm (as noted by de Ricqlès et al. 2003b), and the diameter likely exceeded 40 mm along the minor axis. Though some of the original endosteal surface has been destroyed by matrix and crystal infilling of the medullary cavity, endosteal lamellae are visible around much of the circumference. In the areas where these are preserved, bone spicules do not extend into the medullary cavity, but may have been lost diagenetically.

The innermost cortex of UCMP 25914 is composed of cancellous bone formed by the resorption of primary cortical bone tissues. There are many erosion rooms, each lined with multiple lamellae despite great variability in size. A few secondary osteons are preserved, but these all may be incipient erosion rooms. The endosteal lamellae separate the medullary cavity this region of cancellous bone; the erosion rooms are almost never confluent with the medullary cavity. In some regions, this secondary remodeling obscures much of the primary cortical tissue. Where visible, the primary tissue is composed of woven bone, which grades to parallel-fibered bone and lamellar bone approaching the innermost LAG. As de Ricqlès et al. (2003b) observed, the woven component is not as strongly woven as are those of theropod dinosaurs, but collagen fiber bundles are clearly oriented in several directions.

The cycle of initial disorganized bone followed by a broad annulus of more organized bone repeats itself throughout the cortex, but in the outer third of the cortex, it changes from parallel-fibered to lamellar bone without a woven component. Although individual lamellae can be discerned, these may locally grade into parallel-fibered bone. In the inner third of the cortex, the annuli terminate in a LAG, and the bone tissue immediately external to the LAG is always woven bone. Moving periosteally, the annulus may flank both sides of the LAG. Eighteen of these cycles are preserved; all end in LAGs except the third (annulus). LAG packets are more common in the outer cortex than in the mid- or inner cortex, where single LAGs dominate. The zones between LAGs generally decrease in width periosteally, but there is some variation, even in the outermost cortex.

The transitions between disorganized and organized collagen fibers are mirrored by transitions in vascular density and connectivity, as well as osteocyte organization. Where the woven fibers occur, the cortex is well vascularized, but the annuli are almost avascular. In the woven regions, the canals are predominantly longitudinal primary osteons, but these usually anastomose with 2-10 other canals. The anastomoses often show no lamellae; i.e., they look more like simple canals than primary osteons. The anastomoses of the aetosaur femur are more similar in extent and pattern to those observed in the proterochampsian described above than to the phytosaur, despite having a much larger body size than the proterochampsian and exhibiting more woven bone than the phytosaur. Moving periosteally through the section, vascular density and connectivity both decrease.

Where woven bone is common, the interstitial osteocytes show no preferred orientation relative to the long axis of the bone and (or) preferred arrangement relative to each other, although they do encircle the primary osteons along their lamellae. The osteocytes are more organized in parallel-fibered bone, but in the lamellar regions of the cortex, they are never as regularly oriented or arranged as those of the endosteal lamellae, or the lamellar bone of other taxa, and lamellae locally fade out. de Ricqlès et al. (2003b) also noticed the relative disorganization of these tissues and interpreted them as coarse lamellar bone, but it may be described more accurately as highly-organized parallel-fibered bone (*sensu* Stein and Prondvai 2013). Osteocyte density varies through the section, but not in any consistent way.

The juvenile aetosaur tibia (GR 252) is the first juvenile from an extinct pseudosuchian taxon to be sectioned and described. The tibia is subtriangular in cross section (Figure 2.22), with a triangular medullary cavity that sits at a slight angle compared to the cortical perimeter. The medullary cavity appears relatively large, but some of the innermost cortex has been eaten away because crystals have filled in the marrow cavity, so the ACT may be an underestimate. Endosteal lamellae are visible lining the medullary cavity in one region; these form a layer ~0.1 mm thick.

The tibia of GR 252 has very porous bone tissue that strongly resembles that of perinatal archosaurs, and is especially similar to perinatal birds and nonavian dinosaurs (Horner et al. 2001). The entire cortex is composed of well-vascularized woven bone. As in the adult, the woven tissues are not as strongly woven as those of dinosaurs. Where intact, the inner cortex preserves a scaffold of bone that separates large vacuities (Figure 2.22, note large spaces in inner cortex on left and bottom sides of both images). Unlike the cancellous bone of most elements described in this study, these spaces were not formed by resorption of primary cortical tissues, but rather the primary deposition of very porous bone (Figure 2.23, top image; note primary tissues having high osteocyte density between vascular spaces). Some of these spaces are lined or partly lined with a single lamella, but it is never clearly demarcated from the adjacent tissues.

Most of the vascular canals in this specimen are longitudinal primary osteons, although simple primary canals are present throughout the section. The single "lamella" surrounding these canals is usually composed of parallel-fibered tissue and its edges are never distinct from the surrounding interstitial tissue. These osteons vary in diameter and obliquity, and may anastomose with one or two other canals in any direction. There is no overall pattern in canal arrangement, but regionally, some canals are organized into circumferential rows. In the interstices between vascular canals, osteocyte density is high and the lacunae show no preferred orientation relative to the longitudinal axis of the bone, nor a preferred arrangement relative to each other. Closer to the canals, the osteocytes are still randomly oriented relative to the longitudinal axis of the bone, but encircle the canals. These lacunae occur just outside the primary osteons; the parallel-fibered bone lining each osteon is surrounded is almost acellular.

Discussion: GR 252 shows an overall histological signal of high growth rates, consistent with other perinatal archosaurs (Horner et al. 2001). In the adult (UCMP 25914), there are two growth signals: one of declining growth rate with age (signified by narrower zones, and an increasingly large lamellar component relative to the entire annual growth cycle), and an alternating faster-slower growth signal that repeats each year. This signal is not itself surprising (indeed, it has been associated with seasonal shifts in food resources in extant artiodactyls; Köhler et al. 2012); rather, the proportion is unusual. In the aetosaur, 20%-50% of each zone is composed of the slower-growing tissue. The section from the proximal diaphysis of the humerus (UCMP 32178) shows a similar alternation between avascularized, parallel-fibered bone and avascular, lamellar bone, but here the annuli are much narrower. This may result from positional differences between the mid-diaphysis and proximal diaphysis, where the cortex is thinner overall. Because so few aetosaurs have been sectioned, and there is no overlap in size categories between the two localities, it is hard to determine the overall growth pattern for Aetosauria. The presence of woven bone throughout much of the

cortex suggests that aetosaurs were capable of rapid growth throughout their ontogeny, but the broad annuli suggest that it was not sustained throughout the growth cycle. Whether this results from seasonal shifts in resources, as seen in living animals, or physiological differences between aetosaurs and other clades cannot be resolved without further sampling.

Cubo et al. (2012) estimated an osteocyte density of 2200 cells/mm^2 for UCMP 25905, (reidentified above as a fibula) and 3700 cells/mm^2 for UCMP 25914 (femur). My estimate of average osteocyte density for the femur of UCMP 25914 is considerably lower than their estimate (971 cells/mm^2), though the juvenile tibia (GR 252) is higher at 1287 cells/mm^2. This may in part result from methodological differences. Cubo et al. (2012) estimated osteocyte density by focusing on a single layer of osteocytes, counting all the cells in that layer, and dividing by the area of the surface they examined. Our methods are similar in that we both count a single layer of osteocyte lacunae, but my method averages values along the major and minor axes. Cubo et al. (2012) do not report replications or where their observations were made.

Average osteocyte density will always be lower than the highest observed values, but the difference will be especially dramatic in taxa with much higher densities in the innermost cortex compared to the rest of the sample (as one might expect for individuals whose mid-diaphyseal cortex includes embryonic or perinatal bone). However, though osteocyte density varied from boxplot to boxplot on the radial transects I examined, it did not decrease progressively through the section in either specimen. Furthermore, of the 22 transect boxplots I counted for GR 252, only two (3100 and 3200 cells/mm^2) approach the Cubo et al. (2012) estimates, and both of these were in the mid- or outer cortex (i.e., not in the embryonic tissues preserved). Of the 39 transect boxplots I counted for UCMP 25914, none exceeds 2000 cells/mm^2. After I made these measurements, I went back to the original slide from UCMP 25914, and could not find any region of primary bone tissue with exceptionally high osteocyte density, though some areas of secondarily remodeled bone appear to show higher osteocyte density compared to primary bone tissues.

Effigia okeeffeae

Specimen number and element: AMNH FARB 30589 (femur, *Effigia okeeffeae* paratype)
Locality: *Coelophysis* (= Whitaker) Quarry (UCMP locality V75128), Ghost Ranch, Rio Arriba County, New Mexico, USA
Formation and age: 'Siltstone member' of the Chinle Formation, Rhaetian (Nesbitt 2007)

Prior histological analyses: Nesbitt (2007) described the femoral histology of this individual as part of his monograph on the anatomy and relationships of *Effigia*. The section was taken from a portion of the diaphysis between the mid-diaphysis and the fourth trochanter (much closer to the midshaft than to the metaphysis). I re-examined his slide and revise his diagnoses here, and add new information on cortical dimensions and measurements of osteocyte density. This section is well illustrated in Nesbitt (2007), but I include illustrations of parallel-fibered bone in the outer cortex (additional images available on MorphoBank).

Histological observations:

This section is oval in cross-section, but one side along the major axis is crushed and abraded, making circumferential measurements difficult. The ACT is small relative to the size of the medullary cavity, which is also oval in cross section and is positioned centrally. Nesbitt (2007) reported that the medullary cavity lacked trabeculae, but this is difficult to ascertain. Small splinters of bone are visible in the medullary cavity close to the cortex. Some of these have clearly peeled inwards from the innermost cortex, but others are show lamellar bone on one edge and may represent trabecular fragments.

Large, oval erosion rooms are common in the innermost cortex; the largest of these exceed 5 mm in diameter. These are all lined by several, well-defined lamellae. In some areas, they cut across primary cortical bone and in other areas, they cut through remodeled tissue. Regionally around the circumference, the inner cortex is heavily remodeled; secondary osteons are dense, overlap, and have replaced all primary bone tissues. In other areas, the secondary osteons have enough space between them to observe the primary cortical condition (Figure 2.24, bottom of images). Throughout the inner cortex, many of the secondary osteons have anastomosed with two or three adjacent osteons, which may be primary or secondary, depending on the region.

Most of the rest of the cortex is very similar histologically; the primary bone is mainly composed of well-vascularized woven bone. This becomes regionally less prominent external to the third LAG. In the outermost cortex (external to the fifth LAG), parallel-fibered bone is preserved along most of the circumference. The cortex preserves six annuli/LAGs, confirming the observations of Nesbitt (2007) (Figure 2.24; note arrows). The annuli are narrow. In the inner and midcortex, they are composed of parallel-fibered bone. In the outer cortex they are more organized, but never form distinct lamellae. The innermost annulus regionally has tissue breaks to become a LAG, and the outer five annuli have either a single LAG or LAG packet of 2 or 3 lines lying halfway through the width of the annulus. The zones between growth marks decrease in width periosteally (Figure 2.24; note spacing between arrows).

Most of the cortex is well vascularized; it is moderately to poorly vascularized external to the sixth LAG and poorly vascularized near the periosteal surface. Internal to the sixth LAG, Most of the canals are longitudinal primary osteons with one or two well-defined lamellae; about half of these anastomose with two or more other osteons. These anastomoses may occur in any direction. In one region of the bone, the canals form extensive circumferential anastomoses in a subplexiform to plexiform arrangement. In the rest of the cortex, small reticulations similar to those observed in the proterochampsian and in the fast-growth portion of the aetosaur annual cycle. External to the sixth LAG, about half of the canals in the outermost cortex are primary osteons bearing a single lamella; the rest are simple canals. In this region, canals generally do not anastomose.

Osteocyte density is high throughout most of the cortex. In the interstices between canals they show no preferred orientation relative to the long axis of the bone and no preferred arrangement relative to each other. Around the canals, the osteocytes are usually oriented perpendicular to the long axis of the bone and follow the boundaries of the lamellae. There is no difference in osteocyte density between the interstices and the area immediately surrounding the canals. In the annuli and in the outermost cortex (external to the sixth LAG), interstitial osteocytes here are generally organized perpendicular to the long axis of the bone, and more or less line up circumferentially, although lamellae are not discernible. In this region, osteocytes do encircle canals, but not as densely as in the inner cortex. Additionally, in

this region there is a noticeable decrease in osteocyte density compared to the inner and mid-cortex.

Discussion: I generally agree with the assessments of Nesbitt (2007), except that I do not observe clear lamellar tissue in the outermost cortex. I think this region is likely composed of parallel-fibered bone, though regionally it may be more properly termed highly organized parallel-fibered bone. Distinct lamellae are never visible. Additionally, I think the woven component of the bone is much more disorganized, and its extent much greater than most of the taxa above (an exception is the GR *Vancleavea*), than reported by Nesbitt (2007). I think some of this confusion results from his use (common at the time) of the fibrolamellar/lamellar-zonal dichotomy to describe these tissues. Although the inner and mid-cortex deposit true fibrolamellar bone (with both woven and lamellar components), "lamellar-zonal" inaccurately describes the outer tissues (which are zonal, but not lamellar).

Loricata, possibly *Postosuchus*
Specimen number and element: UCMP 28353 (humerus), UCMP 25906 (femur)
Locality: *Placerias* Quarry (UCMP locality A269), near St. Johns, Arizona, USA
Formation and age: Blue Mesa Member of the Chinle Formation, early Norian (age constraints from Irmis et al. 2011)

Taxonomic comments: UCMP 25906 was previously identified by de Ricqlès et al. (2003b) as *Postosuchus* sp., tibia. However, I re-identify this element as the distal half of a right femur. UCMP 28353 was also identified as *Postosuchus* in that study. Though no diagnostic apomorphies allow either element to be identified beyond Loricata, they are of comparable size to diagnostic *Postosuchus* material found in the quarry. *Postosuchus* is the only loricatan of similar body size currently known from the *Placerias* Quarry (Long and Murry 1995). I redescribe this slide, and that of UCMP 28353, in this section, and add new information on cortical dimensions and measurements of osteocyte density.

Prior histological analyses: The femoral microstructure of *Postosuchus* was first figured by Chinsamy (1994), but she did not describe the material in the text or include a specimen number. de Ricqlès et al. (2003b) described the microstructure of an isolated humerus and femur (tibia in that publication; see above) of *Postosuchus* in detail as part of a larger study of pseudosuchian histology. Since then, the humerus (UCMP 28353) has been analyzed as part of larger studies of amniote growth rates (Cubo et al 2012, Legendre et al. in press). *Postosuchus* osteoderms have also been sectioned and described (Scheyer and Desojo 2011, Cerda et al. in press).

de Ricqlès et al. (2008) described the femoral microstructure of '*Mandasuchus*', a Tanzanian rauisuchian that has yet to be formally described or analyzed phylogenetically, and a section from a long bone shaft of ?*Luperosuchus*, a rauisuchian for which postcranial material is currently undescribed (Nesbitt et al. 2013). Because it is not possible to place '*Mandasuchus*' taxonomically or to confirm the element of ?*Luperosuchus* that was sampled, I do not include these materials in my analysis.

Histological observations: In general, my observations agree with those of de Ricqlès et al. (2003b). Both sections are oval in cross section, each with one "corner" that is more angular than round. In both elements, the medullary cavity sits centrally and is lined with a band of distinct endosteal lamellae 0.1-0.25 mm thick. In the humerus, the cortical wall is proportionately much thicker than the femur in reconstructed cross section. The inner cortex of both elements preserves cancellous bone formed by the resorption of primary or secondary cortical tissues. In the humerus, this region varies between 1.5-2.5 mm thick, but in the femur, it is thicker, generally 3-5 mm, and in one region almost 6 mm. In both elements, the erosion rooms closest to the endosteal margin are oval in cross section; the long axis runs circumferentially. They are all lined with 2-3 distinct lamellae. These rooms become more circular periosteally. The interstices between erosion rooms are unremodeled around most of the circumference, though in both elements there are localized regions where the interstices are composed of heavily remodeled secondary bone. Both sections preserve numerous LAGs, which separate zones that decrease in width periosteally. LAGs in both specimens are most commonly preserved as LAG packets of five or more lines, but at least one LAG in the innermost cortex of each specimen is single around most of the preserved circumference (locally double). The externalmost cortex of the humerus preserves an EFS.

In the humerus, the primary bone tissue is fairly well organized throughout the cortex. The inner and midcortex are composed of parallel-fibered bone tissue that does not form lamellae here except in the annuli. In the outer ~1 mm of the cortex, nearly all of the cortex is composed of lamellar bone, though thin bands of parallel-fibered bone are also visible. Throughout the cortex, the annuli always flank both sides of each LAG packet. In the inner cortex, these packets contain only two or three LAGs; in the mid and outer cortex, five or more lines are common. There are 15 LAGs preserved in the cortex, and another 10 or more in the EFS (although lines in the EFS are not reliably construed as annual).

The preserved primary tissue of the humerus is never well or even moderately vascularized. Circumferential rows of longitudinal primary osteons occur through the cortex; these are usually spaced widely and may anastomose with one or two other canals. The anastomoses may occur in any direction, but most are circumferential. Some of these anastomoses are lined with lamellae, and some are simple primary canals. The pattern does not change throughout the cortex; in the internal cortex, there may be two or three rows of osteons, but in the mid- and outer cortex, there is only one row per zone.

Osteocytes in the regions of parallel fibered bone are only slightly less organized than those in lamellar bone. They are always organized perpendicular to the long axis of the bone and always line up more or less circumferentially in the interstices between canals. The osteocyte lacunae rarely orbit vascular canals, and the areas just outside the primary osteons usually have fewer lacunae than in the interstices. A similar pattern occurs in the lamellar bone of the annuli and outer cortex, except that here, osteocytes tend to line up along lamellae. Osteocyte density is always slightly lower in the outermost cortex than in the inner and mid-cortex.

In the femur, the primary tissues of the inner cortex are composed mainly of parallel-fibered bone, though, as de Ricqlès et al. (2003b) noted, localized regions of weakly woven bone are also present. Most of the rest of the cortex is composed of parallel-fibered bone that repeatedly grades into annuli of more organized parallel-fibered or lamellar bone. These

annuli flank both sides of the LAG packet. The outermost 1.5 mm of the cortex is composed entirely of lamellar bone. The pattern of tissue organization is especially difficult to discern under regular transmitted light, because mineralization has stained the bone differentially. As a result, many dark bands are visible that do not always correspond to LAGs or annuli. Therefore, at lower magnification under regular light, the bone looks like it has far more zones than it does when LAGs are examined under higher magnification or polarized light. At least 10 LAGs are present; in the outermost cortex; these are spaced more closely and it is difficult to determine where one LAG packet ends and the next begins. I agree with de Ricqlès et al. (2003b) that the femur does not preserve an EFS; the closely spaced lines of the outermost cortex resemble the more internal LAG packets.

In the inner third of the cortex, the bone is moderately vascularized by longitudinally oriented primary osteons, each lined by 1-2 lamellae. These commonly form anastomoses with five or more canals in any direction. In the midcortex, 2-4 longitudinal canals may anastomose circumferentially (usually) or obliquely. The outer cortex transitions from moderate levels of vascularization to regions of alternating moderate vascularity and avascularity. The outermost 0.2 mm of the cortex is more or less avascular, but the isolated canals present are longitudinal simple primary canals.

Osteocytes in the woven bone of the innermost cortex show no preferred orientation relative to the long axis of bone and no preferred arrangement relative to each other, at least in the interstices between canals. Closer to the vascular canals, they orbit the canals, but in densities equal to that of the interstices. In the parallel-fibered bone that comprises most of the cortex, most osteocytes are oriented perpendicular to the long axis of the bone and tend to be oriented circumferentially in the interstices between primary osteons. As in the regions of woven bone, osteocytes encircle vascular canals, but they do so in lower densities compared to the interstitial areas. In the lamellar bone of the outermost cortex, all osteocytes are oriented perpendicular to the long axis of the bone and arranged circumferentially along lamellae. Along all transects, osteocyte density varies by about 300 cells/mm^2 among boxplots, but overall, there is no increasing or decreasing trend moving periosteally. The femur shows higher osteocyte density compared to the humerus, which is similar to most extant taxa sampled by Cubo et al. (2012).

Discussion: de Ricqlès et al. (2003b) argued that the cortex of UCMP 28353 (humerus) was mainly composed of lamellar bone and that the outermost cortex did not preserve an EFS. Rather, they posited that this region was merely a continuation of progressively slowing growing bone tissue. I disagree with both conclusions. First, the bone does not show true lamellae except in the annuli and the outermost cortex. Second, the pattern of refringence under polarized light is more similar to parallel-fibered bone than lamellar (Figure 2.25: note refringence pattern in right image). Regarding the EFS, at least 10 closely spaced lines are visible in the outermost cortex (Figure 2.26 accompanies this discussion). These lines are more numerous, more regularly spaced, and much more distinct (darker and with a more even surface) than the lines of the LAG packets, even the most external ones. This area is nearly avascular; the only osteons present appear to form tiny “dents” in the LAG surfaces, as if they were lying external to the bone surface at one point before being “walled in” by periosteal deposition. In contrast, the primary osteons of the outermost cortex most frequently occur between LAG packets, not within them. Finally, the outermost region is nearly 0.5 mm in

width, whereas LAG packets rarely exceed 0.1 mm in width. I agree with de Ricqlès et al. (2003b) that this animal had progressively slowed growth leading to the outermost cortex; however, I think that the differences I describe above are more consistent with an EFS than a wide LAG packet at the periosteal surface.

Cubo et al. (2012) estimated osteocyte density for UCMP 28353 to be 3800 cells/mm^2, four times my estimate for that specimen, and double my estimate for UCMP 25906 (femur). As for the aetosaurs, I cannot explain the difference in my results compared to those of Cubo and his colleagues, except to suggest that their point sample(s) may have focused on a region showing atypically high osteocyte densities. However, I can find no region of primary bone in the original slide from UCMP 28353 that shows such a high osteocyte density relative to the areas of my sampled transects (though again, some remodeled regions show higher osteocyte densities). Among the 42 transect boxplots I counted for UCMP 28353, none exceed even 1400 cells/mm^2, and there is no consistent pattern of increasing or decreasing osteocyte density moving periosteally. In the femur, osteocyte density is more variable, and seven (of 65) boxplots exhibit osteocyte densities comparable to Cubo et al. (2012)'s estimates for the humerus. However, the average osteocyte density for the femur is only 1857cells/mm^2.

Chinsamy (1994: Fig.1C) figured but did not describe a ~1.6 x ~1.4 mm portion of the outermost femoral cortex of *Postosuchus*. Much of this region is moderately vascularized by primary osteons that form small reticulations. These grade to isolated longitudinal canals in the outermost cortex. Three single LAGs are visible in this image, and they do not appear to be flanked by annuli. The LAGs are separated by two zones of equal width (~0.6 mm). Given the single LAGs and small vascular reticulations, its tissues are most similar to those of the innermost cortex in UCMP 25906 (femur). I suggest that Chinsamy's specimen may have been ontogenetically younger than UCMP 25906. Based on the histological assessments described above, the humerus (UCMP 28353) has more LAGs and appears histologically quite a bit older than UCMP 25906. Whether these differences reflect true ontogenetic differences, taxonomic differences among large loricatans, or intraelemental variation cannot be determined without further sampling.

de Ricqlès et al. (2003b) described most of the femoral (tibial, in that paper) cortex of *Postosuchus* as lamellar-zonal tissue. Based on the patterns of birefringence they described in the zones between annuli, their description is consistent with my observations of parallel-fibered bone tissue. Their use of lamellar-zonal bone in this manner is consistent with the classification of Francillon-Vieillot et al. (1990), who included lamellar and parallel-fibered tissues in their definition of lamellar-zonal bone.

Crocodylia: *Alligator mississippiensis*

Specimen numbers and elements: UCMP 68331 (femur), UCMP 68314 (tibia), UF FWC 40723 (humerus, femur, and tibia), UF FWC 40583 (humerus, femur, and tibia), and UF FWC LGS1 (femur). The UCMP specimens are from juveniles (4-5 years), nearing the end of the time of fastest growth for this species (Magnusson et al. 1989), and may have been sampled from the same individual. UF FWC 40723 was a male (snout-vent length = 995 mm, total length = 2030 mm, femur length = 134.77 mm, mass = 71 kg). UF FWC 40583 was a female of similar body and femoral length but smaller mass (snout-vent length = 1000 mm, total

length = 1990 mm, femur length = 139.48 mm, mass = 61 kg; Ross et al. 2002; Tumarkin-Deratzian 2007). Sex and field measurements are unknown for UF FWC LGS1

Based on body length, UF FWC 40723 (male) was at or near the age of sexual maturity at the time of death, and UF FWC 40583 (female) and UF FWC LGS1 (sex unknown) were sexually mature adults (Magnusson et al. 1989; Ross et al. 2002; Tumarkin-Deratzian 2007). These five are the specimens that are described in detail; brief comments on additional specimens are also provided below.

Locality: All specimens are wild caught. Specific locality for UCMP specimens is unknown. UF specimens were collected from Lake Griffin, Lake County, Florida, USA, and were healthy at time of capture (Ross et al. 2002; Tumarkin-Deratzian 2007).
Age: Recent

Prior histological analyses: Bone histology from extant *Alligator mississippiensis* (American alligator) is well described in the literature (e.g., Enlow 1969, Peabody 1961, Chabreck and Joanen 1979, Ferguson et al. 1982, Ferguson 1984, Reid 1984, Wilkinson and Rhodes 1997, Horner et al. 2001, de Ricqlès et al. 2003b, Lee 2004, Padian et al. 2004, Schweitzer et al. 2007, Tumarkin-Deratzian 2007, Wilkinson 2008, Klein et al. 2009, Woodward et al. 2011). However, most of these studies relied on captive-bred or captive-reared individuals, which are known to grow much faster than their wild counterparts (Coulson et al. 1973). A few other extant crocodylians have been described histologically. These include *Crocodylus* sp. (Enlow 1969), *Crocodylus niloticus* (e.g., Hutton 1986) and *C. siamensis* (de Buffrénil 1980). Additionally, Chinsamy-Turan (2005: Fig. 7.1.B) figured the histology of *C. porosus*, and Cubo et al. (2012) quantified some aspects of *C. niloticus* microstructure. Similar histological patterns are also described for the extinct alligatoroid *Leidyosuchus* (Padian et al. 2004). In all taxa, the overall patterns of growth and long bone microstructure are similar to those described for *A. mississippiensis*.

In this study, I limit my observations to wild-caught individuals that were never reared in captivity. These include specimens previously examined by Tumarkin-Deratzian (2007): UF FWC 40723, UF FWC 40583, and UF FWC LGS1. For those slides, I redescribe the histology, and add new information on cortical dimensions and measurements of osteocyte density. As the osteohistology of *Alligator* has been fairly well illustrated in the literature, I limit my figures to those that show important details of the femur and tibia at higher magnification, as well as some comparative images that illustrate differences between sexes.

General histological observations: I summarize my main observations here, then describe the histology of individual elements below. The mid-diaphyseal histology of the humerus, femur, and tibia does not vary substantially within an individual; ontogenetic and especially sex differences are greater than interelemental ones. In all individuals and growth stages examined, the mid-diaphyseal cortex is thick relative to the diameter of the bone (30-40% in all specimens for which RBT could be estimated; Table 2.2). The medullary cavity of each element is lined with distinct endosteal lamellae, which do not give rise to bony trabeculae at the mid-diaphsysis. Erosion rooms are visible in the innermost cortex of all elements examined except UCMP 68331 and UCMP 68314 (juvenile femur and tibia, respectively), but secondary remodeling is otherwise rare. All sampled elements show multiple growth marks,

which always include an annulus but may or may not exhibit a distinct LAG. Osteocyte densities are fairly stable along transects, but decline slightly with age. In the primary tissues of the zones, collagen fiber organization, vascular density and vascular patterning are more variable, and this variability correlates with sex even more than age. This results in histological sexual dimorphism, with males showing stronger indicators of faster growth compared to females.

Histological observations by element:

Humerus

The mid-diaphyseal humerus was examined in detailed two individuals: UF FWC 40723 and UF FWC 40853. At the mid-diaphysis, the cortex is circular in cross section, with a circular medullary cavity that sits off center. The two humeri are quite different histologically despite similar bone proportions.

In UF FWC 40723, the inner cortex is separated from the medullary cavity by a layer of endosteal lamellae ~0.14-0.2 mm thick. The primary bone tissue of the inner cortex is difficult to discern between the large erosion rooms. Just external to the endosteal lamellae is a region of parallel-fibered bone that corresponds to an annulus, but it is difficult to see except in polarized light. No LAG is visible here. External to the annulus, the bone transitions to a zone of woven-fibered bone ~1.4 mm thick. The cycle repeats itself twice more (a total of four concentric annuli), with the outermost annulus close to the periosteal border. The second and third annuli divide the cortex into three zones of roughly equal width. The annuli become progressively wider moving periosteally.

In the inner cortex, several erosion rooms are visible. These are all lined with several lamellae, but the boundaries between them are difficult to discern in regular transmitted light. Most of the other canals in this inner cortex are primary osteons (their lamellae do not cut across primary tissues). The primary osteons of the inner cortex are generally longitudinal, but frequently they anastomose radially (sometimes obliquely) with several other canals. The lamellae surrounding these osteons are not distinct except under polarized light. Four wide (diameter ~3-4 times greater) radial primary osteons extend from the innermost cortex past the second annulus; these are lined and extend many short anastomoses circumferentially. In the mid and outer cortex, the bone is moderately to well vascularized, comparable to the proterochampsian, but not reaching the level of *Effigia* or theropod dinosaurs (see below). The outer cortex shows a similar density of longitudinal canals compared to the midcortex, but there are fewer anastomoses between them. The periosteal surface is not smooth; many canals open to it directly.

In the woven-fibered regions (i.e., in the zones), the osteocytes are more organized closer to the primary osteons, which they tend to orbit. They do not occur within the lamellar bone lining the osteon, however. In the interstices between canals, the osteocytes are show no preferred orientation relative to the long axis of the bone or preferred arrangement relative to each other. In the annuli, the osteocytes are all oriented perpendicular to the long axis of the bone, though the spacing between them is variable.

The mid-diaphyseal cortex of UF FWC 40853 is much different than UF FWC 40723, despite a difference in total length of only 40 mm and similar proportions at the mid-diaphysis (UF FWC 40853 is smaller; Tumarkin-Deratzian 2007). Endosteal lamellae are present, but they are thinner (~0.1 mm) and discontinuous around the circumference. This does not appear

to be a preservational problem; the endosteal margin was likely under active resorption at the time of the animal's death. As in the other humerus, the inner cortex of UF FWC 40853 shows several erosion rooms, which may be lined or unlined. The secondary remodeling is visible in the innermost three zones. Primary cortical tissue is visible between erosion rooms. Internal to the 14th (externalmost) annulus, each zone is composed entirely of organized parallel-fibered bone, and adjacent zones are separated by thin annuli of even more organized parallel-fibered or lamellar bone. Some of these annuli (e.g., the third and fourth) terminate in a LAG, but these are discontinuous around the circumference. The 14th annulus is broad, with distinct lamellae. External to it, there is a wide zone of parallel-fibered bone that extends to the periosteal surface.

The mid-diaphyseal humeral cortex in UF FWC 40853 is poorly to moderately vascularized, depending on the zone. Internal to the third annulus, about half the canals are longitudinal primary osteons, and the rest are large secondary osteons. The latter appear to have formed by expansion of primary canals and subsequent redeposition of lamellae, because they occur in circumferential rows along with primary osteons. The secondary osteons often anastomose with each other, usually circumferentially, but may extend a radial anastomosis to connect with one or two osteons in the adjacent zone. Between the third and fifth annulus, the bone is almost avascular. Most of the canals in this region are longitudinal or extremely short radial primary osteons, but a few simple primary canals are also present. Between the fifth and 14th annulus, the canals are quite uniform. The inner half of the zone is usually avascular, and the outer half bears a single row of longitudinal primary osteons (regionally, two rows in some zones). Most of these canals are isolated, but some extend a single radial anastomosis to the nearest osteon in the adjacent zone. Along the antero-posterior axis, long, crack-like anastomoses connect primary osteons circumferentially every few zones. These circumferential canals may be simple primary canals or primary osteons, and may connect with some radial anastomoses. However, the overall signal is one of isolated longitudinal canals rather than circumferential connections or short reticulations.

Osteocytes throughout the cortex are well organized. They are all oriented perpendicular to the long axis of the bone and arranged more or less circumferentially. However, spacing between osteocytes are irregular and distinct lamellae are uncommon, except in the outer annuli. The osteocytes show no general pattern with regards to the vascular canals; they orbit some and not others. They rarely line up along the lamellae that surround each osteon.

I briefly examined the bone microstructure of three other humeri, UF FWC 35119, UF FWC LGS4, and UF FWC 40854. The first two specimens were described by Tumarkin-Deratzian (2007), and the third was part of the same sample set but not reported in that study. However, the sex, size, and locality data for that individual were reported by Ross et al. (2002). UF FWC 35119 is also a male and of similar body length to UF FWC 40723 (20 mm shorter), and exhibits seven annuli in the humerus. UF FWC LGS4 is a large individual of unknown sex (3182 mm estimated total length), and I observe seven annuli in its humerus (contra Tumarkin-Deratzian 2007, who reported 10). UF FWC 40854 is a male (snout vent length = 1480, total length = 2920 mm, mass = 83.5 kg) salvaged from Lake Woodruff, FL, after it died from environmental contamination (Ross et al. 2002). Its humerus shows 13-15 annuli, some of which include distinct LAGs. In all cases, the general histological profile was much more similar to that of UF FWC 40723 (the male described first above) than to UF

FWC 40583 (the female described second above). However, in UF FWC 40854, the outer cortex shows a decrease in vascularity that corresponded to an increase in osteocyte organization and a transition to more lamellar bone. The outermost cortex (external to the 12th annulus/LAG) is entirely composed of nearly avascular, lamellar bone. This may represent an incipient EFS or a slowdown in growth resulting from disease at the time of death (Ross et al. 2002).

Femur

The mid-diaphyseal femur was examined in detail in four individuals: UCMP 68331, UF FWC 40723, UF FWC 40853, and UF FWC LSG1. The femoral histology of UF FWC 40723 and UF FWC 40853 is extremely similar to that of their associated humeri, so I only make brief comments on those individuals. The mid-diaphyseal cortex is nearly circular in cross section in younger individuals (Figure 2.27). This becomes more oval with age and ultimately rhomboidal in adults (see Schweitzer et al. 2007: Fig. 2). The medullary cavity sits centrally and retains an oval to subrectangular shape throughout ontogeny.

The femur of UCMP 68331 was ground too thin in places, and thus the external dimensions cannot be measured. This specimen preserves no endosteal lamellae, trabeculae, or secondary remodeling at mid-diaphysis. The entire cortex is composed of woven-fibered zones that alternate with relatively broad annuli (i.e., at least half the width of the zones) of parallel-fibered bone (Figure 2.27, bottom image: note arrows; Figure 2.28). The innermost and outermost annuli lie very close to the endosteal and periosteal surfaces, respectively. Four annuli are preserved, despite the small size of UCMP 68331 (~6-7 mm diameter), none of which terminate in a LAG. Because of the relative prominence of the parallel-fibered annuli in this section, the section shows a "Maltese cross" effect in polarized light (Figure 2.27, bottom image). Beginning with the innermost zone and moving periosteally, the widths of the zones are approximately 0.75 mm, 0.3 mm, and 0.5 mm.

The cortex of UCMP 68331 is well vascularized compared to larger femora, though it shows lower vascular connectivity. Most of the canals in this section are longitudinal primary osteons, which are somewhat organized into loose circumferential rows in each zone. This organization is regionally apparent in the inner two zones, and clearest in the outermost zone, which preserves two distinct rows. Regionally, the primary osteons show a secondary pattern of radial rows. Especially in the innermost zone, the canals may anastomose radially with one to three other canals.

Osteocytes in this specimen are very disorganized compared to those of the larger individuals. They show no preferred orientation relative to the long axis of the bone or to each other, even within the annuli, and spacing between them is highly variable. Within the zones, the osteocyte density is regionally high (osteocytes appear bunched together). The average osteocyte density is 974 cells/mm^2, higher than any of the other individuals sampled.

The femur of UF FWC 40723 (Figure 2.29, top image: note arrows) is at least twice as large as that of UCMP 68331, despite preserving the same number of annuli. Because of the similarity in the cortical histology between the femur and humerus (and tibia, see below) of UF FWC 40723, I think this results more from differences in growth strategy between the two individuals, rather than differences in age alone. The medullary cavity of UF FWC 40723 is not large enough that it would obscure much of the cortex of UCMP 68331 if the sections

were superimposed, and the width of the two innermost zones of UF FWC 40723 are substantially wider than any of the zones in UCMP 68331.

The femoral mid-diaphysis of UF FWC 40723 is extremely similar to that of the humerus, even down to the patterns of remodeling in the innermost cortex. I observe the same number of annuli (four) in the femur as in the humerus, with the externalmost annulus again lying at the periosteum. Each of the three zones is at least 1.5 mm wide. The main difference between the humerus and femur is that the vascular patterning is more complex in the lateral half of the femur than in the medial half, whereas both sides were similar in the humerus. The lateral half shows a higher number of radial anastomoses. These generally link canals across the width of a single zone, but a couple span nearly the entire width of the cortex. Other than this, the two elements are quite similar.

As in UF FWC 40723, the femoral mid-diaphyseal cortex of UF FWC 40583 is extremely similar to that of the associated humerus. Fifteen annuli are preserved in the femur (the humerus clearly showed 14); the outer three are very closely spaced (Figure 2.29, bottom image: note arrows). The spacing between more internal annuli is always < 1 mm, and usually less than 0.5 mm. In this regard, it is more similar to UCMP 68331 than to UF FWC 40723. As in the humerus, a thicker, better vascularized zone lies between the outermost annulus and the periosteal surface. In the femur, there is also a secondary signal of canal pattern; in addition to primary osteons being organized in circumferential rows, there is a secondary signal of organization into radial rows.

The femur of UF FWC LGS1, an individual of unknown sex, is histologically very similar to UF FWC 40723, except that it preserves eight annuli rather than four, and that radial anastomoses are present in roughly similar proportions on the medial and lateral halves of the femur. As in UF FWC 40723, the externalmost annulus lies close to the periosteal surface. One other difference is that whereas in UF FWC 40723 the zones were all about the same width, in UF FWC LGS1, the three outermost zones are approximately half the width of the more internal zones. This indicates a decrease in annual bone deposition after the fifth preserved annulus. In these zones, the woven component is a much smaller component of the bone relative to the parallel-fibered component. External to the sixth LAG, vascularity decreases in this individual.

I briefly examined the mid-diaphyseal femoral microstructure of UF FWC 40854 (male, same individual as described for the humerus), as well as UF FWC LGS4 (sex unknown) and UF FWC LGS6 (male), two individuals previously described by Tumarkin-Deratzian (2007). These individuals were both large adults (3182 and 3150 mm estimated total length, respectively). UF FWC 40854 preserves 16 annuli (the outermost annuli appear to merge along. In the medial half of the cortex, the histological condition strongly resembles that of UF FWC 40723. In the lateral half of the cortex, this is true internal to the 12th annulus; external to it, the bone is more like that of UF FWC 40583. This mirrors a similar decrease in vascularity and a similar increase in fibrillar and osteocyte organization in the outermost cortex as seen in the humerus. In UF FWC LGS4, the pattern is similar, with the transition to more organized, less vascular bone occurring after the tenth of 12 annuli. UF FWC LGS 6 preserves no such transition (the entire cortex resembles that of UF FWC 40723), but the outermost three zones (nine or ten annuli are preserved) are much narrower than the inner zones.

Tibia

The mid-diaphyseal tibia was examined in detail in three individuals: UCMP 68314, UF FWC 40723, and UF FWC 40853. The tibial histology of UCMP 68314 is very similar to that of UCMP 68331 (they may be the same individual), and UF FWC 40723 and UF FWC 40853 are extremely similar to that of their associated humerus and femur, so I only make brief comments on tibial histology for all elements. Throughout ontogeny, the mid-diaphyseal tibia remains more or less circular in cross section, though there may be a slight pinching on the posterior (flexor) surface of the tibia at the insertion of the M. flexor tibialis externus in some individuals. In each individual, endosteal lamellae line the medullary cavity and no trabeculae are present at mid-diaphysis. The medullary cavity is more or less circular and lies off center.

The tibia of UCMP 68314 is preserved as a half section, retaining the anterior (extensor) section based its on cortical outline. The innermost cortex preserves a thick band of lamellar bone, which is much thicker in one direction and shows a medial or lateral migration of the medullary cavity. Just internal, a few secondary osteons are visible. As in the humerus of UF FWC 40583 (adult female), most of these form a single circumferential row, and may have formed by the expansion of primary osteons and subsequent deposition of additional lamellae. A few additional, isolated secondary osteons are present and cut across the primary tissues of the innermost cortex. As in the femur of UCMP 68331, the cortex preserves well vascularized, woven-fibered zones that alternate with parallel-fibered annuli. These annuli are not as broad as those of the femur, and in the direction of the medullary canal migration they split slightly, with a narrow band of vascularized woven tissue between the split annuli (a double annulus). The externalmost annulus does not lie along the periosteal surface; if this animal is indeed the same individual as UCMP 68331, then more of the periosteal surface was ground from the slide than I estimated above.

The mid-diaphyseal tibial histology in UF FWC 40723 is very similar to that of the associated humerus and femur. It differs from the femur in preserving a similar level of anastomoses around the circumference of the bone, and from both the humerus and femur in showing lower vascular density and very few anastomoses in the outermost zone (medial half only). Here, the bone is only poorly vascularized (locally, moderately vascularized) by longitudinal primary osteons. These hug the border of the previous annulus, and do not anastomose with other canals. In the lateral half of the bone, the outermost zone is histologically indistinct from more internal zones.

Discussion:

Woven Bone Controversy

There is still disagreement in the literature over whether or not wild American alligators commonly produce woven-fibered primary bone tissues after the perinatal stage. Some of this disagreement seems to stem from inconsistent use of terms, both before and after the terminological standardization by de Ricqlès (1975) and Francillon-Vieillot et al. (1990). As noted by Reid (1984), this problem extends even to basic terms such as laminae, primary osteon, or primary bone. Another problem is that none of the studies that have illustrated woven bone in adult alligators (Reid 1984, Chinsamy and Hillenius 2004, and Tumarkin-Deratzian 2007) provided adequate imagery to support or refute their claims. When Reid (1984: Fig. 1d) illustrated the mid-diaphyseal femur of *A. mississippiensis*, the woven regions

of the bone were too dark to view any structures. Chinsamy and Hillenius (2004: Fig. 28.5) illustrated both *A. mississippiensis* and *C. johnstoni* to illustrate "abundant fibrolamellar bone" (p. 656), but both images are reproduced at a size where vascular canal pattern and zones are difficult to discern, much less canal type, fiber organization, or cellular characters. Tumarkin-Deratzian (2007: Fig. 1) illustrated five humeral and femoral sections at a magnification sufficient to see several zones, but not at a level at which cellular, fibrillar, or vascular details could be observed (though it is clear that these sections are better vascularized than a comparative image of lamellar-zonal bone. Furthermore, none of these studies illustrated their sections in polarized light, making confirmation of fibrillar organization difficult.

I found unambiguous woven bone in both the juvenile femur (UCMP 68331; Figures 2.27, 2.28) and tibia (UCMP 68314), though this is not unexpected given previous work on perinatal and juvenile archosaurs (Horner et al. 2001, Padian et al. 2004). In the same specimens as Tumarkin-Deratzian (2007) examined, I confirmed woven bone in the mid-diaphyseal cortex of UF FWC 40723 (humerus, femur, tibia), UF FWC 40854 (humerus and femur), UF FWC LGS1 [humerus and femur (Figures 2.30, 2.31), but primarily in the inner and midcortex], LGS4 (femur), and UF FWC LGS6 (femur), a sample that includes subadults and large adults. At least some alligators, therefore, are certainly capable of maintaining woven fibered bone past the juvenile fast-growth stage and sexual maturity.

The woven bone observed in adult *A. mississippiensis* is not as strongly woven as the woven bone of the juveniles, Ghost Ranch *Vancleavea,* aetosaurs, *Effigia*, or dinosaurs (see below). Furthermore, the woven component of primary bone in adult *A. mississippiensis* decreases relative to the parallel-fibered component, especially later in ontogeny, suggesting that the more rapid growth rates were not sustained for as much of each annual growth cycle (Figure 2.31). This differs greatly from the condition in juvenile alligators (see above) and from some dinosaurs that deposit woven bone for most or all of their annual growth cycle (see below). However, it is similar to the condition I observed in the aetosaur femur (though the adult aetosaur exhibited a greater ratio of woven- to parallel-fibered bone, especially in the deep cortex). In all cases where woven bone occurs, vascular density is higher, anastomoses are more common, and osteocytes are less organized.

It is worth noting that many of the adult crocodylians sampled in previous studies (whether captive or wild caught) show a pattern that suggests much slower growth. These animals exhibit moderately to poorly vascularized parallel-fibered or lamellar bone in the zones, which are separated by lamellar annuli or LAGs (see, for example, de Ricqlès et al. 2003b: Plate 7, Fig. 2). This is similar to the bone observed in UF FWC 40583 (humerus, femur, tibia) and the outer cortex of UF FWC LGS4 (humerus and femur). Because this pattern is also common, I suggest that *A. mississippiensis* commonly produces two histological patterns of growth, and discuss the two most likely influences (ontogeny and sex) below.

Ontogeny

As in other pseudosuchians and archosauromorphs, the histology reflects a transition from faster growth in younger individuals to slower growth in adults. Perinatal and juvenile *Alligator* deposit poorly organized, coarse parallel-fibered or woven bone (Horner et al. 2001, Padian et al. 2004, this study), although the degree of disorganization varies among

individuals and decreases with age. After the perinatal stage, there seem to be two developmental "tracks" in *Alligator*. One is similar to that of UF FWC 40723, and one is similar to that of UF FWC 40583 (Figure 2.29 accompanies the following discussion). The first track shows more disorganized tissues (woven bone or coarse parallel-fibered bone), high vascularity (both in terms of canal density and vascular pattern complexity), and wide zones through at least the fifth year of growth. After this, the zones narrow in width and the proportion of parallel-fibered bone increases, though vascularity remains high. After 10-12 years of growth, the bone transitions again, becoming much less vascular and much more organized, with narrow zones of poorly-vascularized or avascular, weakly parallel-fibered or lamellar bone. These zones are separated by thin annuli or LAGs. In the second track, the bone tissue resembles the last phase of track one throughout much of ontogeny. After the juvenile stage, the bone shows narrow zones of poorly vascularized parallel-fibered or lamellar bone throughout the cortex, and secondary remodeling of the inner cortex is more extensive. In the outermost cortex, lamellar bone and distinct LAGs indicate a functional cessation of growth. Woodward et al. (2011) have recently identified an EFS in wild caught *Alligator*, and this is consistent with their findings.

Sex

I propose that the main factor influencing the histological differences between these two tracks is the sex of the individual, rather than the ontogenetic stage or environment, though these certainly play a role as well. In American alligators, both sexes hatch at the same body length (Magnusson et al. 1989) and reach sexual maturity at approximately the same length (Joanen and McNease 1975, 1980; Wilkinson and Rhodes 1997), but the adults exhibit sexual size dimorphism. Male alligators are 20-100% larger than mature females of the same age (Chabreck and Joanen 1979, Woodward et al. 1995, Cox et al. 2007) and have steeper growth curves (Chabreck and Joanen 1979, Wilkinson and Rhodes 1997). The result is that even though both sexes are sexually mature at the same size, they are not at the same age at maturity; females reach sexual maturity several years after males. In some cases, females may take almost twice as long to reach sexual maturity as males (Magnusson et al. 1989). Furthermore, whereas female growth rate declines rapidly after maturity, males continue to grow rapidly for at least ten years more (Chabreck and Joanen 1979). Although adult body size and size at sexual maturity are known to vary geographically (Rootes et al. 1991, Woodward et al. 1995, Dalrymple 1996, Wilkinson and Rhodes 1997), the pattern of larger, faster growing males is consistent across the entire range of *A. mississippiensis*. This is true even in captive-reared alligators (Elsey et al. 1992).

Given that such drastic differences in growth rate are observed between male and female American alligators, these should be expressed in the bone tissues. Males should exhibit histological signs of faster growth (e.g., more disorganized collagen fibers, higher vascular density, more complex vascular patterning, and wider zones) compared to females, especially in the first five-ten years of growth. Additionally, one would expect the histological signature of slowed growth (e.g., a transition to more organized tissues or an EFS) to occur later in males than in females, because they reach their growth asymptote later (Chabreck and Joanen 1979). Furthermore, these differences should persist regardless of collection site (though comparing them may be difficult), and should be visible in both captive and wild-caught animals.

My sample contains six individuals of known sex: five males and one female, all collected from the same location at the same time (Tumarkin-Deratzian 2007). As expected, the males (UF FWC 35199, UF FWC 40723, UF FWC 40854, UF FWC LGS6, UF FWC LGS8) all show the faster ("track one") histological growth pattern, and the only female (UF FWC 40583) shows the slower ("track two") histological growth pattern (see Figure 2.29 for comparison). Granted, this is a small sample size, and only one female is included. However, I contacted a colleague with a much larger sample set (over 30 wild-caught and captive American alligators of known sex, collected and reared in Louisiana), and she has also observed differences in the bone tissues of male and female alligators. In her sample set, male alligators always show more disorganized collagen fibers, greater vascular density and pattern complexity, and wider zones compared to females of similar size or age. Females show more remodeling of the inner cortex. These results are true for both wild and captive reared individuals (Holly Woodward, personal communication, June 2013).

Previous studies have shown sexual differences in crocodylian bone histology. Both Hutton (1986) and Tucker (1997) noted marked differences in the amount of secondary remodeling in osteoderms between adult male and female *Crocodylus* (*C. niloticus* and *C. johnstoni*, respectively). The females exhibited much more remodeling compared to the males, and these differences only presented once females reached sexual maturity. Similarly, Wink and Elsey (1986) and Wink et al. (1987) noted seasonal changes in porosity, robusticity, and resorption in the mid-diaphyseal femora of egg-laying female *A. mississippiensis*. These changes were not observed in juveniles, males or non-egg-laying females. Finally, Klein et al. (2009) noted increased remodeling in the osteoderm and femur of a captive female *A. mississippiensis* and attributed this to physiological changes during egg-laying. However, none of these studies examined sexual differences in histology reflecting differences in ontogenetic growth trajectory.

Based on my results, I think that the 3-4 unsexed individuals in my sample include both male and female individuals. I predict that UCMP 68331 and UCMP 68314 (possibly the same individual) are females of 4-5 years, based on the narrowness of their zones, the lack of anastomoses between canals even in fast-growing tissues, and the presence of remodeling in the tibia. I predict that UF FWC LGS1 and UF FWC LGS4 are male, based on their broad zones, higher vascular density, and high levels of vascular connectivity. Furthermore, I predict that UF FWC LGS4 is an individual at or just after the point of transition between faster and slower growth regimes, based on the differences in microstructure in the outermost cortex.

ARCHOSAURIA: ORNITHOSUCHIA: ORNITHODIRA

All remaining taxa in this study are part of the archosaurian stem-group Ornithosuchia (Gauthier 1984, 1986; Gauthier and Padian 1985) (i.e., they are all bird-line archosaurs), later mistakenly discarded by some workers in favor of the junior synonym Avemetatarsalia, and its subclade the node-group Ornithodira (= Pterosauria + Dinosauria; see Figure 2.1, node 4 for phylogenetic position). To determine whether or not elevated growth rates evolved independently in pterosaurs and dinosaurs, it would be ideal to sample the successive sister taxa of Ornithodira within Ornithosuchia, as well as stem pterosaurs and stem dinosaurs. However, the only ornithosuchian thought by some to lie outside Ornithodira is

Scleromochlus taylori. This small-bodied taxon is only known from natural molds of skeletal elements preserved in coarse sandstone (Benton 1999), making it difficult to assess the morphological details of critical but extremely small elements such as the tarsals (Nesbitt 2011). It has been regarded variously as a sister-taxon to pterosaurs (Huene 1916, Padian 1984), a possible sister taxon to dinosaurs (Sereno 1991), and as an unresolved basal member of Ornithodira (Benton 1999). Benton's cladistic analysis has been the most thorough, but he found it difficult to resolve the relationships of *Scleromochlus*, usually by as few as one character in either direction.

In any event, the preservation of the bones of *Scleromochlus* as molds eliminates the possibility of histological sampling and analysis. Although non-dinosaurian dinosauromorphs exist, definitive stem pterosaurs have yet to be recognized (Nesbitt 2011). For this study, I examined the successive outgroups to Dinosauria, including non-dinosaurian dinosauromorphs and non-dinosaurian dinosauriforms. Among the pterosaurs, I examined *Eudimorphodon* and *Dimorphodon*, two early-diverging lineages that lie far outside Pterodactyloidea, the main radiation of pterosaurs.

ORNITHODIRA: PTEROSAUROMORPHA: PTEROSAURIA

(See Figure 2.1, lineage D for phylogenetic position)

Eudimorphodon cromptonellus

Specimen number and element: MGUH VP 3393 (MCZ field no. 13/91G; femur). This is part of the holotype and only known specimen of *Eudimorphodon cromptonellus*. The slide is reposited at the MCZ.

Locality: Lower part of the Carlsberg Fjord beds, Jameson Land, East Greenland

Formation and age: Ørsted Dal Member of the Fleming Fjord Formation, Scoresby Land Group, Late Norian (Jenkins et al. 2001, Clemmensen et al. 1998).

Taxonomic comments: Some recent analyses disagree on the phylogenetic affiliations of this species. Dalla Vecchia (2009) recovered a paraphyletic *Eudimorphodon*, and advocated the removal of *E. cromptonellus* from the genus. A much larger analysis (in terms of taxon and character sampling) of pterosaur affiliations (Andres 2012) recovered a monophyletic *Eudimorphodon*. I use the Andres (2012) taxonomy here, but both analyses placed this specimen outside a group that includes *Rhamphorhynchus*, *Dimorphodon*, and pterodactyloids. Because the only other pterosaurs examined in this dissertation are *Dimorphodon* and *Pterodactylus*, the generic affiliation of this individual is not critical to the rest of my study.

Prior histological analyses: The femur of *Eudimorphodon cromptonellus* was sectioned as part of the species description of (Jenkins et al. 2001). It was subsequently reanalyzed as part of a larger study of growth in pterosaurs and small dinosaurs (Padian et al. 2004), who modified the observations of the prior study in some regards. I redescribe the same slide here, and add new information on cortical dimensions and measurements of osteocyte density.

Histological observations: As noted by both Jenkins et al. (2001) and Padian et al. (2004), this specimen shows extensive diagenetic alteration. Calcite crystals fill the entire medullary cavity, and local recrystallization is visible throughout most of the cortex, especially near the vascular canals and close to both the periosteal and endosteal surfaces (Figure 2.32, note colorful spots on lower images where recrystallization has occurred).

The original endosteal margin of the bone has been eroded by crystal infilling of the medullary cavity. As such, my estimates of ACT and RBT should be taken as minimum estimates until more specimens are found and sectioned. Although it is not possible to confirm whether endosteal lamellae or endosteal lamellae were present at the mid-diaphysis in life, longitudinal sections through the metaphysis and epiphysis do show that trabeculae were present in those regions (Padian et al. 2004).

The microstructure of the cortex is fairly uniform throughout the section. The primary tissues are parallel-fibered throughout the section; I see no evidence of localized lamellae. No annuli or LAGs, or an EFS are visible in this section. However, recrystallization makes it impossible to assess the innermost and outermost cortex for these traits, and recrystallization near the canals would make it difficult to trace them around the midcortex if they were present.

The bone is moderately vascularized around most of the circumference, but one region along the minor axis is poorly vascularized to avascular (Figure 2.32, lower image). Nearly all of the canals are longitudinally oriented, but in a few cases close to the endosteal surface, short radial anastomoses are visible. The canals show no other pattern of arrangement. Further classification of the vascular canals is difficult; nearly all canals were diagenetically altered by recrystallization of adjacent tissues. In most cases, crystals form a circular ring around the canal, superficially reminiscent of a secondary osteonal outline. However, by focusing through the section, I can see evidence of 1-2 lamellae surrounding some canals, and these are limited to just the area closest to the lumen. Therefore, I cautiously describe them as primary osteons.

The bone tissue in the interstices between canals is less altered than the tissue surrounding them. The osteocytes in these regions vary in their orientation relative to the long axis of the bone. Most are oriented more or less perpendicular to the long axis of the bone, and the rest are oriented oblique to the long axis. The former cluster locally and in these regions they tend to line up somewhat circumferentially. However, regardless of orientation, the osteocyte lacunae usually show no pattern of arrangement relative to each other and are always spaced irregularly.

Discussion: In general, my observations are more similar to those of Padian et al. (2004) than those of Jenkins et al. (2001). For example, Padian et al. (2004) described the canals as primary osteons, whereas Jenkins et al. (2001) found no evidence of primary osteonal development and referred to them as simple primary canals. By focusing through the section, it is clear that lamellae are present. Additionally, I find no evidence of localized lamellar bone tissue (contra Jenkins et al. 2001). I disagree with Padian et al. (2004) regarding the osteocyte lacunae in this section. Whereas that study described these as flattened, I find that focusing through the section often reveals changes in both orientation and girth. Ultimately, however, I agree with Padian et al. (2004) that the specimen does not show signs of mature bone

(indicating an older individual) or of the very fast-growing tissues that tend to characterize juveniles. The parallel-fibered bone, vascularization and osteocyte density are consistent with moderately fast-growing tissues, but without older or younger individuals for comparison, it is difficult to assess whether the inferred depositional rates characterize the entire ontogeny of this taxon.

It is worth noting that this specimen is among the smallest pterosaur specimens known, and several features of the skeleton suggest it was immature. For example, the individual long bones of the wing and hindlimb are all more or less equal in length (Jenkins et al. 2001). Pterosaur limb elements elongate at different rates during ontogeny, and by adulthood vary significantly in size (the ratios between limb elements are diagnostic to genus). Additionally, the epiphyses show a rough, unfinished texture (Jenkins et al. 2001), rather than a smooth lamina of calcified cartilage, suggesting that they had not finished ossifying their limbs (Holliday et al. 2010). Additionally, if MGUH VP 3393 is a juvenile, its basal phylogenetic position among pterosaurs should be questioned. When included with phylogenetic analyses of morphological data, juvenile specimens often are placed at the base of clades, rather than with adults of their own or closely-related species (e.g., Evans et al. 2011, Fowler et al. 2011, Tsuihiji et al. 2011).

Dimorphodon macronyx

Specimen numbers: YPM 350B (tibia-fibula), YPM 9182E (tibia-fibula). Of these, YPM 350B is the larger individual (l04 mm vs. 85 mm tibia-fibula length; Padian et al. 2004).
Locality: YPM 350B: Lyme Regis, Dorset, England. YPM 9182: Aust Cliff (south bank of River Severn), Gloucester, England (see Padian 1983 for locality discussion)
Formation and age: Lower Subgroup, Lias Group, Hettangian-Sinemurian (Hallam 1960)

Prior histological analyses: Several elements of *Dimorphodon macronyx* were briefly described as part of a larger survey of pterosaur growth (de Ricqlès et al. 2000), including the second and third wing phalanges and the tibiae-fibulae. These specimens represent three individuals. In that study, the tibiae-fibulae slides were misidentified in Table 1 as ulnae, but were correctly identified as tibiae-fibulae in the text. The microstructure of these elements was further described by Padian et al. (2004), as part of a larger study of growth in pterosaurs and small dinosaurs. I redescribe the tibiae-fibulae sections of two individuals here, and add new information on cortical dimensions and measurements of osteocyte density. Because these individuals were extensively illustrated by de Ricqlès et al. (2000) and Padian et al. (2004), I do not refigure them here (though images are available on MorphoBank).

Histological observations: de Ricqlès et al. (2000) and Padian et al. (2004) were consistent in their descriptions of these specimens, and my observations concur with theirs. I summarize these findings and add a few additional observations regarding osteocyte density, arrangement, and orientation.

Both specimens are crushed at midshaft. In YPM 350B, about 75% of the circumference is preserved, and in YPM 9182E, most or all of it is present. In both individuals, the endosteal margin of the cortex is lined with lamellar bone about 0.05 mm thick. This region is very distinct from the cortex, and in many places separated from it

slightly because of crushing. No trabeculae are visible in the medullary cavity of either specimen.

In both specimens, the preserved cortical microstructure of the tibia-fibula at mid-diaphysis is fairly uniform around the circumference. In YPM 9128E, the cortex is composed of mostly woven-fibered or weakly-woven bone tissue that grades into parallel-fibered bone regionally. The parallel-fibered bone is fairly well organized and seems limited to a thin band in the midcortex, which does not extend all the way around the circumference. For this reason, I do not call it an annulus. In YPM 350B, the cortex is mainly composed of parallel-fibered tissue.

Both specimens are moderately vascularized by longitudinal primary osteons. These osteons are more distinct in YPM 350B than in YPM 9182E. In the former case, the osteons all have 1-2 lamellae and are slightly brighter compared to the surrounding interstices. In the latter case, some canals in the outer cortex appear to be simple primary canals under regular light. It is only under polarized light that the parallel fibers of these osteons are more clearly differentiated. In YPM 9182E, the osteons align in neat radial rows, and often form short radial anastomoses with one adjacent canal. The anastomoses are more common on the medial side of the bone and closer to the fibular region. The primary osteons of YPM 350B never anastomose.

Osteocytes near the canals are oriented perpendicular to the long axis of the bone and may orbit the canals. They show no preferred orientation relative to the long axis of the bone or preferred arrangement relative to each other in the interstices between canals. Osteocyte lacunae occur in higher density in the interstices than in the areas immediately surrounding the canals. The osteocyte density is much higher overall in YPM 9182E than in YPM 350B (2518 vs 1634 cells/mm^2, respectively), but in both cases, it decreases gradually from the innermost cortex to the periosteal surface. Notably, osteocyte densities in the outer cortex of YPM 9182E are similar to those of the inner cortex of YPM 350B (1700-2000 cells/mm^2, see Appendix).

Discussion: Even though neither specimen shows clear annuli or LAGs, I agree with Padian et al. (2004) that the histological differences between these individuals probably reflect ontogenetic changes in bone growth rates. Compared to YPM 350B, the collagen fibers and osteocytes of YPM 9128E are more disorganized, vascular connectivity is higher, and osteocyte lacunae typically occur in much higher densities (except in the outer cortex, where they occur in similar densities). These changes are somewhat consistent with the findings of the only two other studies to have examined (at least partial) ontogenetic series of pterosaurs. Chinsamy et al. (2009) examined a growth series of the pterodactyloid *Pterodaustro* and found similar ontogenetic shifts in collagen fiber organization and vascular connectivity in every element examined (including the tibia), but the changes were more pronounced and occurred early in ontogeny. Prondvai et al. (2012) also noted early ontogenetic shifts in the fibrillar organization and vascular density of *Rhamphorhynchus*, with larger individuals also exhibiting more histological variability. Both studies found LAGs at the midcortex of several elements sampled from individuals of different sizes.

Padian et al. (2004) suggested that the histology of both *Dimorphodon* specimens supported relatively slower growth compared to some pterosaurs such as *Pterodactylus* (see below). However, the presence of woven-fibered bone in YPM 9182E, not likely to be a

juvenile based on its size and lack of typical perinatal tissues, suggests that faster growth was sustained for a longer portion of ontogeny in *Dimorphodon* than in *Pterodaustro* or *Rhamphorhynchus*. This hypothesis was also advanced by Prondvai et al. (2012).

Pterodactylus
Specimen number and element: CM 11430 (femur, tibia)
Locality: Solnhofen Beds, Bavaria, Germany
Formation and age: Solnhofen Limestone, Kimmeridgian-Tithonian (Schweigert 2007)

Taxonomic comments: Padian et al. (2004) noted that this specimen is misidentified in the CM catalogue as *Rhamphorhynchus*, but that the proportions of the metacarpal and the limb ratios are diagnostic of *Pterodactylus.* This correction has not yet been updated in the CM catalog. Further supporting this hypothesis, Prondvai et al. (2012) examined the tissues of a growth series of unambiguous *Rhamphorhynchus* from the Solnhofen Limestone, and at no size category do its tissues resemble those of the *Pterodactylus* sections described below.

Prior histological analyses: The ulna, first wing phalanx, femur, and tibia of *Pterodactylus* were described as part of a larger study of growth in pterosaurs and small dinosaurs (Padian et al. 2004). I redescribe the femoral and tibial sections here, and add new information on cortical dimensions and measurements of osteocyte density.

Histological observations: Neither the femur nor the tibia of CM 11430 is crushed at the mid-diaphysis. The medullary cavities of both elements have been infilled completely with crystals. Each section preserves a small region of endosteal lamellae, but these regions are not preserved around most of the circumference of the medullary cavity. Neither section preserves trabecular bone extending into the medullary cavity, but it is clear that the calcite crystals have at least partially eroded the original endosteal margin and some of the cortex in each element (more so in the femur than in the tibia). Therefore, I cannot determine whether they were originally absent or lost diagenetically.

Internal to the endosteal lamellae, neither element shows secondary remodeling. In the femur, woven-fibered bone can be found throughout the cortex (Figure 2.32, Figure 2.33). However, though fibers are aligned in all directions, more are oriented circumferentially than longitudinally or radially. Therefore, the bone tissue refringes in a manner intermediate to woven-fibered and parallel-fibered bone under polarized light (Figure 2.32: note description of color pattern in elliptically polarized light). A ‘Maltese’ cross is clearly visible, but so are fibers traveling in perpendicular directions. In one region of the femur, the cortex is more intensely woven and fibers show no preferred orientation (Figure 2.34, lower left of all images). In the tibia, the bone shows no preferred fiber orientation. Neither section preserves an annulus or LAG.

There are many simple primary canals throughout the femoral and tibial sections, especially periosteally, but the canals of the inner and midcortex are neither simple primary canals nor typical primary osteons [contra Padian et al. (2004), who described them as primary osteons]. Though the tissue immediately surrounding the canals is better organized than that of the interstices, it is parallel-fibered or woven-fibered, not lamellar. The typical

'Maltese crosses' are not visible under polarized light, no cement lines are present between layers, and osteocytes are not oriented perpendicular to the longitudinal axis of the bone. It may be more accurate to describe the canals as primary Haversian cavities (*sensu* Francillon-Vieillot et al. 1990) that were subsequently filled with parallel-fibered bone, rather than with the more common lamellae or acellular, heavily mineralized bone. However, the use of this term is somewhat unsatisfactory; the vascular canals of *Pterodactylus* clearly formed by the same process as normal primary osteons (a woven "scaffolding" is deposited, and later, other bone is deposited between that initial scaffold and the canal, compacting it), but parallel-fibered or woven-bone was used for compaction, rather than lamellae. I discuss this idea further in the Discussion section below.

The cortex of the femur is well vascularized. The longitudinal canals usually anastomose with several other canals in more than one direction, forming small reticulations that regionally grade into areas where radial or circumferential anastomoses dominate (Figure 2.34A, note canal patterns on right side of image). Although it seems from initial examination that at most only four or five canals are connected by short anastomoses, focusing through the plane of the section reveals far more connectivity in three dimensions. In the tibia, most of the canals are isolated, and they tend to be oblique relative to the longitudinal axis of the bone, rather than purely longitudinal. Where anastomoses are present, nearly all are radial connections linking two canals.

In both elements, the osteocyte lacunae orbit the vascular canals, frequently in several layers, but they occur at low density and they are irregular in their spacing and orientation. In the interstices between canals, they show no preferred orientation relative to the long axis of the bone and no preferred arrangement relative to each other. The density of osteocyte lacunae in the tibia is comparable to that of the smaller *Dimorphodon* tibia-fibula (YPM 9182E; ~2500 cells/mm^2), and only slightly higher in the femur (2817 cells/mm^2). In the femur, the region of most intensely woven bone corresponds to the region of highest osteocyte density (Figure 2.34A, note lower left of image).

The femur also preserves a small region of endosteally derived, possibly primary bone tissue internal to the endosteal lamellae (Figure 2.35 accompanies this discussion). This tissue is composed of woven- and parallel-fibered bone. The canals in this region are longitudinal or oblique canals of the same type as occur in the cortex (primary Haversian cavities subsequently filled with parallel-fibered bone), but because they are so large they superficially resemble secondary osteons. However, the fibers of the parallel-fibered bone surrounding the canals are coarser and less organized compared to those of the cortex, and in some areas may be composed of woven bone. The bone of the interstices is also more strongly woven than the cortex, with many more osteocytes, although it is no better vascularized. It is clear that the woven region must have been deposited after the deposition of the original endosteal lamellae because it cuts across some of the lamellae (a resorption line is visible between the woven bone and the original endosteal lamellae). After its deposition, a second layer of lamellae was deposited that cuts into the woven region. This same tissue is visible in a wing phalanx of CM 11430, described as "secondarily compacted coarse cancellous tissue" by Padian et al. (2004: p. 565). Its presence in two elements potentially indicates a systemic condition.

Discussion: I disagree with Padian et al. (2004) in their diagnosis of this tissue as fibrolamellar bone. Though woven fibers are certainly present, I find that the cortical bone of

both the femur and the tibia of CM 11430 lack a true lamellar component. Rather, their vascular canals are lined with parallel-fibered bone.

Chinsamy et al. (2009) described and figured an endosteally derived primary tissue in the pterodactyloid pterosaur *Pterodaustro*, which they identified as medullary bone. Medullary bone is an ephemeral tissue rapidly deposited in the medullary cavity of female birds and dinosaurs in advance of egg-laying, which serves as a labile calcium reserve for eggshells (Schweitzer et al. 2005, Lee and Werning 2008). Though the tissue in that specimen was likewise endosteal in origin and bounded by two layers of lamellar bone, it is difficult to determine whether it is medullary bone, a pathology, or a result of cortical drift. The *Pterodaustro* tissue was described as compacted coarse cancellous bone, but no details of the matrix fiber organization, canal type, or osteocyte organization were given, making direct comparison difficult. It is unfortunate that the *Pterodaustro* sections were not illustrated at a size or resolution that allow the determination of these characteristics. It is therefore difficult to assess whether these *Pterodaustro* specimens exhibit a homologous tissue to that of CM 11430.

The presence of similar endosteally derived tissues in both the femur and the wing phalanx of CM 11430 is consistent with a hypothesis of medullary bone, which is present simultaneously in many elements of the skeleton (Simkiss 1967). In birds, medullary bone is not as compact as the bone of the cortex (Simkiss 1967), but in the four nonavian dinosaurs in which it has been observed, it is always fairly compact (Schweitzer et al. 2005, Lee and Werning 2008, Hübner 2012). Medullary bone in dinosaurs and birds shows radial spicules, but this bone shows no clear depositional orientation. This may result from secondary compaction of originally radial spicules, but it is difficult to determine. It is also possible that the tissue represents a pathology, which in birds sometimes resembles medullary bone and also may occur systemically (Chinsamy and Tumarkin-Deratzian 2009). Finally, this tissue may result from cortical drift, a process in which the bone resorbs tissue on one side of the medullary cavity and simultaneously deposits or remodels it on the opposite side. If that is the case, then its presence in two bones only indicates that two bones underwent the same process simultaneously. For these reasons, I hesitate to diagnose it as medullary bone homologous with that of birds or dinosaurs, but its presence warrants further investigation.

ORNITHODIRA: DINOSAUROMORPHA

All remaining taxa in this study are part of the clade Dinosauromorpha (see Figure 2.1, node 5 for phylogenetic position).

Dromomeron romeri

Specimen numbers and elements: GR 221 (femur), GR 253 (tibia), GR 254 (tibia). GR 221 is part of the type series of *Dromomeron romeri* (Irmis et al. 2007). GR 254 is a smaller individual than GR 253, and the GR 254 section was made slightly distal to the mid-diaphysis. GR 221 and GR 253 are among the largest *Dromomeron* femora and tibiae recovered from the Hayden Quarry to date (personal observation). None of these specimens is likely to be from the same individual; the two larger specimens are from different quarries, and GR 221 and GR 254 were not found in the same part of the quarry.

Locality: Hayden Quarry 3 (GR 221, GR 254), Hayden Quarry 4 (GR 253), Ghost Ranch, Rio Arriba County, New Mexico, USA
Formation and age: Petrified Forest Member of the Chinle Formation, ~213 MYA, middle Norian (Irmis et al. 2011)
Prior histological analyses: None

General histological observations: The bone tissue of all three individuals is similar in most respects. All three elements exhibit crystal infilling of the medullary cavity, which has eroded part of the original endosteal margin. A thin band of endosteal lamellae (~ 0.04 - 0.1 mm thick) is visible in all specimens, but none of the specimens preserve trabeculae at mid-diaphysis. I describe the histology by element below.

Histological observations by element:
Femur

The femur (GR 221) is circular in cross section, with a round, central medullary cavity (Figure 2.36). This element is relatively thin walled; its RBT (14.9%) is between that of the pterosaurs *Eudimorphodon* and *Pterodactylus* (Table 2.2). There are three LAGs in this section (Figure 2.37; note arrows). The inner LAG lies very close to the endosteal surface. In some areas it is hard to distinguish, and in others it has been resorbed by medullary cavity expansion and (or) mineral infilling. Where present, it presents as a double LAG. The middle LAG lies 0.75 mm from the inner LAG and 0.45 mm from the periosteal surface, and sits within an annulus of lamellar bone. It is the most distinct growth mark in the section and occurs as two pairs of double LAGs, spaced similarly to the two lines of the inner LAG. The outer LAG occurs 0.1 mm from the periosteal surface. It is a single LAG that regionally grades into an annulus or double LAG. The inner half of the cortex is composed of woven-fibered bone tissue, which transitions rapidly to highly-organized parallel-fibered bone (*sensu* Stein and Prondvai 2013) and then lamellar bone approaching the middle LAG (Figure 2.37, bottom image, note change in refringence at one third the cortical width). External to the second LAG, the bone is lamellar within the annulus. External to the annulus, it becomes slightly less organized (i.e., returns to highly organized parallel-fibered bone) but quickly returns to a lamellar state, and stays this way to the periosteal surface.

In the regions of woven-fibered bone, the femur is well vascularized, and in the areas of parallel-fibered and lamellar bone it is moderately to well vascularized. External to the outer LAG, the bone is regionally poorly vascularized or nearly avascular. Nearly all the canals are longitudinal primary osteons, with just a few longitudinal simple primary canals in the outermost cortex. The primary osteons all exhibit a single, very distinct lamella and are arranged in radial rows (Figures 2.36 and 2.37, top image). Given the vascular density, it is surprising that so few of the canals anastomose; other ornithodirans show more vascular connectivity compared to *Dromomeron*. Where anastomoses occur, they are radial and connect two or three longitudinal canals (Figure 2.37, above middle arrow). Secondary osteons are absent in this element.

In the regions of woven-fibered bone, the osteocyte lacunae show no preferred orientation relative to the long axis of the bone and no preferred arrangement relative to each other. This is true near the canals, which they generally do not orbit, and in the interstices between canals. In the areas of highly-organized parallel-fibered bone, the lacunae are more

or less perpendicular to the long axis of the bone, but the spacing between them is less regular. In the lamellar regions, they are highly organized. Every osteocyte in this region is aligned along a lamella and the spacing between them is more regular. Osteocyte density declines moving periosteally in some regions, and remains constant throughout the cortex in others.

Tibia

The cortex of GR 254 (smaller specimen) is circular in cross section, with a round medullary cavity that sits centrally (Figure 2.38). Its RBT is similar to that of *Trilophosaurus* and *Pterodactylus* (18.3%; Table 2.2). It shows two definite annuli and one area between them that regionally forms slightly more organized tissue. The inner annulus lies about 1 mm from the periosteal surface (about 1/3 of the preserved cortex from the endosteal margin). Locally, this annulus splits into a double annulus, and will also show regional breaks in tissue (i.e., a LAG). Near the periosteal surface is a second annulus punctuated by a double LAG. Between these definitive growth marks is another region that is brighter under regular light and refringes differently under elliptically polarized light compared to the tissue that flank it. Regionally, this tissue is more organized than the surrounding tissues, but it does not continue all the way around the circumference and it is difficult to discern under cross plane-polarized light. I do not think it is an annulus, but I refer to it as the "bright region" below.

GR 254 preserves lamellar bone around at least half the endosteal circumference. It is similar in width and appearance to that of GR 221. The cortex of GR 254 is mostly composed of woven-fibered bone tissue (Figure 2.39, bottom image). Woven-fibered bone occurs internal to the inner annulus, and between this annulus and the outer growth marks, except in the bright region described above. The inner annulus regionally varies in composition; it is sometimes parallel-fibered and sometimes lamellar. Where it is lamellar, a LAG lies along its inner margin. This suggests that bone deposition slowed abruptly at the end of the first preserved season, and was slower at the start of the subsequent growth season. The bone tissue of the bright region is parallel-fibered. Halfway between the bright region and the outer annulus/LAG, the bone transitions from woven-fibered to parallel-fibered bone. The bone is lamellar within the double LAG, and lamellar in the small region between the outer line and the periosteal surface.

Except between the two lines of the double LAG, this tibia is well vascularized by longitudinal primary osteons. As in the femur, they each bear a single distinct lamella. Within the double LAG, canals are sparse and are usually simple primary canals. Internal to the inner annulus, the canals show no clear pattern. External to the annulus, the canals of the tibia form radial or radially oblique rows. In the femur, the radial rows are very straight, but in GR 254 they are not so perfectly aligned (Figure 2.39, note the "waviness" of radial rows in the bottom image). This gives the appearance of narrower spacing between rows. As in the femur, there is little vascular connectivity, but in the inner cortex, a few canals anastomose radially or obliquely when another canal is very close. Secondary osteons are absent.

Osteocytes throughout the cortex are fairly disorganized. In the woven regions, the osteocyte lacunae show no preferred orientation relative to the long axis of the bone and no preferred arrangement relative to each other. They do not orbit the primary osteons. In the inner annuli, many are oriented perpendicular to the long axis of the bone, but at least a third are not. In the lamellar bone of the outer annulus, they align along the lamellae and show

more regular spacing. Osteocyte lacunae occur in slightly higher densities in GR 254 compared to the femur (2080 vs. 1756 cells/mm^2, respectively).

In GR 253, the larger tibia, the cortex and medullary cavity are more oval at mid-diaphysis (Figure 2.40), but the RBT (19.4%) is similar to that of the smaller tibia. Endosteal lamellae are visible in two patches, one small band on the medial side, and the other extending for approximately one fourth of the endosteal circumference in the anterolateral quadrant. A single LAG is visible 0.55 mm from the periosteal surface (Figure 2.41, note arrow). The inner half of the cortex is composed entirely of woven-fibered bone. This transitions to coarse parallel-fibered bone in the midcortex (not right at the LAG, however), and it remains this way until the periosteal surface.

As in the femur and smaller tibia, the vascular canals of GR 253 are longitudinal primary osteon that each bear a single, distinct lamella. This element is well vascularized throughout the cortex, but vascular density does appear to decrease very slightly at the transition between woven-fibered bone and again external to the LAG. There are very few anastomoses present in this tibia; they most commonly occur in the parallel-fibered bone internal to the LAG. Where present they connect two canals radially. As in the other individuals, the primary osteons are organized in radial rows (Figure 2.41) and secondary osteons are absent.

Osteocytes show similar patterning in GR 254 as in the other tibia and femur sections. The density (1978 cells/mm^2) is only slightly lower compared to the younger individual.

Discussion: Based on the high vascular density and woven bone present in all three individuals sampled, *Dromomeron romeri* was clearly capable of relatively fast growth during at least the first few years of life. All three bones show a transition from woven-fibered to parallel-fibered bone after the first or second preserved LAG, and GR 221 and GR 253 both show a decrease in vascularity in the outer cortex. This, in combination with the LAG spacing and lamellar bone in the outer cortex of GR 221, suggest that growth in *D. romeri* slowed or stopped after only a few years. That GR 221 is among the largest femora known for this taxon further supports this hypothesis. However, because the bones are so thin-walled, growth curves cannot be reconstructed based on these specimens alone. Fortunately, ontogenetic series of the femora and tibiae of both *D. romeri* and its sister taxon, *D. gregorii*, have been collected (Nesbitt et al. 2009a; personal observation), so it would be possible to sample these elements ontogenetically in the future.

DINOSAUROMORPHA: DINOSAURIFORMES

All remaining taxa in this study are part of the clade Dinosauriformes (see Figure 2.1, node 6 for phylogenetic position).

DINOSAURIFORMES: SILESAURIDAE

(See Figure 2.1, lineage E for phylogenetic position)

The bone histology of one silesaurid, *Silesaurus opolensis*, was described by Fostowicz-Frelik and Sulej (2010). Their sample set included several femora (ZPAL Ab III/411/4, ZPAL Ab III/405, and ZPAL Ab III/2380) and tibiae (ZPAL Ab III/414, ZPAL Ab

III/1270, and ZPAL Ab III/1885) from the *Silesaurus opolensis* holotype locality. I attempted several times to contact Drs. Fostowicz-Frelik and Sulej to borrow these specimens for comparison, but never received a reply.

Asilisaurus kongwe

Specimen numbers and elements: NMT RB45 (femur), NMT RB46 (femur), NMT RB47 (femur). These specimens are part of the type series of *Asilisaurus kongwe* (Nesbitt et al. 2010). All three femora are from individuals of approximately the same size (based on the midshaft proportions). Both larger and smaller individuals are known from the holotype locality (Sterling Nesbitt, personal communication).

Locality: *Asilisaurus kongwe* holotype locality, near the town of Litumba Ndyosi, Ruhuhu Basin, Tanzania

Formation and age: Lifua Member of the Manda Beds, Late Anisian (Rubidge 2005, Nesbitt et al. 2010)

Prior histological analyses: None

Histological observations: All three femora experienced a significant amount of diagenetic alteration. The medullary cavity of each has been infilled with mineral crystals. The cortex suffered from post-depositional bacterial or fungal invasion, extensive compressive cracking post-fossilization, and subsequent mineral invasion of some of these cracks. Despite these problems, it is still possible to describe the histology of these elements. They are all quite similar, and I describe them together.

All three individuals show a circular or oval cortical outline at mid-diaphysis and have a central medullary cavity of the same shape as the cortical outline (Figure 2.42). The endosteal margin is eroded in NMT RB45 and NMT RB46, but a strip about 1 mm long and 0.05 mm thick is visible in NMT RB47. No trabeculae are visible in the femoral mid-diaphyseal cortex in any specimen, but as in *Dromomeron*, the crystal infilling makes it impossible to determine whether they were absent in life or lost diagenetically.

What can be seen of the cortical microstructure is fairly uniform throughout. No LAGs can be discerned in any of the sections. It is possible that the cortex is too fragmented to provide adequate assessment of LAGs, but enough undamaged radial "transects" across the cortex are available that the lack of LAGs is probably real. The bone tissue is woven-fibered throughout, but as in *Pterodactylus*, circumferential fibers are more common than longitudinal, radial, or oblique fibers. The entire cross sectional diameter of both NMT RB46 and NMT RB47 show weak "Maltese crosses" under polarized light, indicating that circumferential fibers are most common, but fibers oriented in other directions are also visible (Figure 2.42, bottom image).

The cortices of all three individuals are moderately to well vascularized by primary osteons. Some exhibit one or two distinct but acellular lamellae, but in general the lamellar border is indistinct in regular transmitted light. Under polarized light, the lamellae are easily to distinguish. Some primary osteons show additional encircling fibers, too coarse to be lamellar bone, external to the lamellae. These regions are composed of parallel-fibered bone, based on their patterns of refringence and osteocyte orientations (see below). In all three individuals, the primary osteons are predominantly longitudinal, but very often they

anastomose with several other canals. These anastomoses may occur in any direction and often form small reticulations (Figure 2.43, note vascular canals in the mid and outer cortex), comparable to those of the proterochampsian described above. As in *Dromomeron*, all three bones lack secondary osteons.

Osteocyte lacunae encircle the primary osteons in all three individuals, sometimes in several layers. These are associated with the regions of parallel-fibered bone. At least half of these are oriented perpendicular to the long axes of the bones, and the remaining lacunae are oriented more obliquely. The lacunae that orbit canals are spaced irregularly. In the interstices between vascular canals, the lacunae show no preferred osteocyte orientation relative to the long axes of the bones, and no preferred arrangement relative to each other. In all three individuals, osteocyte lacunae occur at higher densities than in *Dromomeron* or any taxon described so far except *Euparkeria*.

Discussion: Although NMT RB45, NMT RB46, and NMT RB47 were all of similar size or slightly larger (in terms of both ACT and diameter) compared to GR 221, the *Dromomeron* femur I sampled, none showed any signs of slowed growth moving periosteally, and none showed LAGs. The more complex vascular patterning, presence of woven bone throughout the cortex, and greater osteocyte density in *Asilisaurus* suggest more rapid growth rates and higher metabolic rates compared to *Dromomeron*. However, Nesbitt et al. (2010) reported that most individuals in the type series of *Asilisaurus* (including these specimens) were probably juveniles or subadults, as they were only 60-80% the size of the largest individual recovered. Based on their size and the histology described above (perinatal tissues are not visible, and there are no annuli, LAGs, or signs of declining growth rate), I agree that these three femora are likely from subadult individuals. Although these individuals may have been at an ontogenetic stage comparable to GR 254, the smaller of the *Dromomeron* tibiae I sampled, the difference in adult body size between the two taxa may influence the difference in growth rate and cortical microstructure.

Silesauridae indet.
Specimen numbers and elements: GR 255 (humerus), GR 190 (tibia).
Locality: Hayden Quarry 2 (GR 190) and Hayden Quarry 3 (GR 255), Ghost Ranch, Rio Arriba County, New Mexico, USA
Formation and age: Petrified Forest Member of the Chinle Formation, ~213 MYA, middle Norian (Irmis et al. 2011)

Taxonomic comments: Irmis et al. (2007) and Nesbitt et al. (2009a, Supplementary Information) reported a silesaurid from the Hayden Quarry based on isolated materials. The material is currently under study and has yet to be described formally. It shares a number of apomorphies with *Silesaurus* and *Sacisaurus* (features not present in *Asilisaurus*) that places it in a clade nested within Silesauridae (i.e., it is more derived than *Asilisaurus*; Nesbitt et al. 2009a).

Prior histological analyses: None

Histological observations: As with all the Hayden Quarry material, the medullary cavity of both the humerus (GR 255) and tibia (GR 190) are infilled by crystals. In the humerus, these crystals to not contact the endosteal margin, and it is preserved intact. In the tibia, about a third of the original endosteal margin is preserved. In both elements, the endosteal lamellae form a layer 0.05-0.10 mm thick. Both elements preserve indications of trabecular bone in the medullary cavity at mid-diaphysis, but because of the crystals, their true extent cannot be known. In both specimens, the collagen fibers do not refringe brightly under polarized light, but this may result from preservational or preparational alteration (both elements were especially dark ground unevenly; they had to be ground thinner than normal and by hand to achieve optical clarity).

In the humerus, the cortex is triangular at mid-diaphysis, with a subpentagonal medullary cavity that sits centrally (Figure 2.44). The only indication of mid-diaphyseal trabecular bone is a single small patch of osteonal bone that lies within the crystal infill close to the endosteal margin (Figure 2.44, note arrow). It looks like a sole secondary osteon, floating among the crystals. Most of the cortex is composed of unremodeled woven-fibered bone tissue. A single LAG is visible 0.5 mm from the periosteal surface (Figure 2.45, note arrows). It regionally becomes a double LAG, with the second line about 0.2mm external to it. The LAG lies within an annulus of parallel-fibered bone; no change in tissue is visible around the second line. In the areas where a second line is visible, the periosteal surface shows two to four thin layers of parallel-fibered bone. However, this is not laterally extensive, and the bone surface elsewhere does not show this tissue.

Most of the humerus is well vascularized by longitudinal primary osteons (Figure 2.45). Individual canals are similar in appearance to those of *Dromomeron*; the single lamella is very distinct. However, in GR 255 they are arranged randomly or in circumferential rows, rather than radial rows. In this region, anastomoses tend to be circumferential or oblique, and connect two to five longitudinal osteons. Approaching the LAG, vascular density and connectivity do not decrease noticeably. External to the LAG, most canals do not anastomose.

Around most primary osteons, osteocytes line up along the outside of lamellae. In these regions they are mostly (not exclusively) oriented perpendicular to the long axis of the bone. In the interstices between canals, osteocytes are disorganized, with no preferred orientation relative to the long axis of the bone and no preferred arrangement relative to each other. The osteocyte lacunae of GR 255 occur in high densities throughout the section (1995 cells/mm^2, comparable to the tibiae of *Dromomeron*), and are highest in the innermost cortex.

The external surface of GR 190 (tibia) is abraded. This likely reflects natural weathering rather than overpreparation; it was found close to the surface of the bonebed in the first year of excavation at Hayden Quarry 2. Because so much of the original surface is missing, I do not estimate circumference or RBT for this element. The estimate of ACT is based on the preserved cortex; it underestimates the thickness in life. The mid-diaphyseal cortex of the tibia is triangular in cross section at mid-diaphysis (confirmed on other Hayden Quarry specimens; personal observation) with a subcircular medullary cavity that sits centrally (Figure 2.46). In this element, the crystals filling the medullary cavity are separated somewhat from the preserved endosteal margin. A trabecular fragment, about 5-6 mm long, is visible in the anterior (extensor) quadrant (Figure 2.46, note arrow). This served as the endosteal margin for at least three large, oval erosion rooms. The remnants of the walls of these erosion rooms show that they were lined by lamellae. A few smaller, circular, and

unlined erosion rooms are visible in the innermost cortex of this region, along with some secondary osteons. The posterior part of the endosteal margin also shows large, circular erosion rooms lined by lamellae but preserves only a small trabecular fragment.

The tibia preserves three LAGs (Figure 2.47, note arrows). The inner LAG sits at midcortex and is a double LAG. The inner line of that double LAG locally grades into an annulus. The middle LAG occurs approximately 0.45-0.5 mm external to the inner LAG, and the outer LAG occurs 0.78 mm external to the middle LAG, close to the periosteal surface. The tissue is generally woven-fibered. An annulus of parallel-fibered bone straddles the inner LAG. After this annulus, the bone is again woven-fibered and remains that way until about halfway through the zone between the middle and outer LAG. In the outer half of that zone, the bone gradually transitions into coarse parallel-fibered bone. The outer LAG lies in the center of an annulus of parallel-fibered bone. Very little bone tissue is preserved external to the third LAG, and where it is visible it seems to be part of this annulus.

The entire cortex is well or very well vascularized by primary osteons. As in *Asilisaurus*, *Dromomeron*, and GR 255, these are mostly longitudinal primary osteons arranged randomly. However, there is far more connectivity between canals in GR 190 than in any of those elements. In the innermost cortex, the lamellae surrounding each canal are very distinct, but they become less so periosteally. Internal to the inner LAG, most of the canals anastomose with several other canals, forming small reticulations. These may link to as many as eight longitudinal canals, but more commonly, they connect three to five canals. Just internal to the inner LAG, canal diameter, density, and connectivity all decrease noticeably (Figure 2.47). This occurs throughout the region of parallel-fibered bone identified as an annulus above. In the woven-fibered tissues between the inner and middle LAG, the canals form circumferential rows and are more likely to anastomose circumferentially than to form reticulations. This is especially the case in the anterior and posterior quadrants, where the vascular patterning looks almost plexiform. The last row of canals, just internal to the middle LAG, shows fewer anastomoses compared to the other rows in this zone, but not as few as in the annulus surrounding the inner LAG. On the other side of the middle LAG, the canals are very similar in their arrangement, but reticular anastomoses are again common. That the canals show similar density and connectivity on both sides of the middle LAG is probably related to the lack of a parallel-fibered annulus here. The zone between the middle and outer LAG shows two vascular patterns. The inner half is very similar in canal density and patterning to the zone between the inner and middle LAGs. The outer half appears less vascular because the canals are narrower in diameter and anastomose less frequently compared to the inner half (Figure 2.47). Very little bone tissue is preserved external to the third LAG, but what canals are visible are isolated longitudinal canals.

Around the primary osteons of the tibia, the osteocytes orbit the canals and line up along the outside of their lamellar border. In the interstices between canals, osteocytes are much more disorganized, with no preferred orientation relative to the long axis of the bone and no preferred arrangement relative to each other. In general, osteocyte density is very high throughout the section. Osteocyte density is similar in the inner two zones, but decreases slightly external to the second LAG. This shift in osteocyte density occurs at the same point in the cortex as the transition from woven-fibered to parallel-fibered bone and the decrease in vascular connectivity described above. Even with this decrease in osteocyte density external to the second LAG, osteocytes occur in high numbers throughout the section in both elements,

especially compared to the other taxa described above. The average osteocyte density across the entire section is 3005 cells/mm^2, higher than any taxon examined so far in this study.

Discussion: The histology of these elements suggests that the Hayden Quarry silesaurid experienced several years of sustained, relatively fast growth. Both elements preserve several growth cycles; the histology in adjacent zones is overall very similar and does not change much (even between zones), except in the annuli. Given that the tibia shows a histological transition in the outer zone that suggests decreasing growth rates over a longer period of time (compared to a normal annulus), it is possible that this specimen preserves the main growth inflection point between accelerating and decelerating growth rates. Vascular connectivity and vascular density are higher in the Hayden Quarry silesaurid compared to the other ornithodirans examined, but these differences in growth rate could reflect differences in body size (larger animals grow at absolutely faster rates, but may grow relatively slower when corrected for body size). However, osteocyte density is also higher in the Hayden Quarry silesaurid compared to the other ornithodirans, suggesting higher metabolic rates. Given that mass tends to scale inversely with metabolic rate, this could reflect a biological difference beyond size.

The histology of the Hayden Quarry silesaurid is similar in some regards to what is reported for *Silesaurus opolensis*, the only other silesaurid whose bone microstructure has been published. In a study of several individuals and across several elements, Fostowicz-Frelik and Sulej (2010) found woven-fibered bone through much of ontogeny, but grading into parallel-fibered bone later in life. Similar to both elements sampled for the Hayden Quarry silesaurid, vascular canals are mainly primary osteons and occur in high densities, but unlike what is observed in the Hayden Quarry tibia, the canals do not anastomose extensively.

Unlike other ornithodirans examined to this point, the Hayden Quarry silesaurid remodeled its inner cortex. This may reflect differences in body size compared to the pterosaurs and *Dromomeron*, and ontogenetic differences compared to *Asilisaurus*. It could also reflect the higher RBT; the other ornithodirans have proportionately hollower bones and would have resorbed the inner cortex before it could be remodeled.

DINOSAURIFORMES: ?DINOSAURIA

(See Figure 2.1, node 7 for phylogenetic position)

Nyasasaurus parringtoni

Specimen number and element: NHMUK R6586 (humerus). This section is from the holotype humerus of *Nyasasaurus parringtoni*.

Locality: *Nyasasaurus parringtoni* holotype locality (Parrington's locality B36), Ruhuhu Basin, southern Tanzania

Formation and age: Lifua Member of the Manda beds, late Anisian (Middle Triassic; Nesbitt et al. 2013)

Taxonomic comment: *Nyasasaurus* is either the sister taxon to Dinosauria or the earliest known member of that clade (Nesbitt et al. 2013). It possesses characters of the humerus and

vertebrae considered autapomorphic for dinosaurs, but the incomplete nature of the holotype specimen (humerus and six vertebrae) makes it difficult to determine whether or not it is a true dinosaur.

Prior histological analyses: Nesbitt et al. (2013) described the microstructure of the mid-diaphyseal humerus of *Nyasasaurus*. I wrote that analysis and include a modified version here. For this study, I include additional histological measures (e.g., RBT, osteocyte density), but as we figured this element extensively in Nesbitt et al. (2013), I do not include additional images here (more images are published on MorphoBank at http://www.morphobank.org/index.php/Projects/ProjectOverview/project_id/485

Histological observations: The humerus of NHMUK R6856 is almond- or eye-shaped in cross section (somewhat pinched at the edges, along the major axis). The medullary cavity is elliptical in cross section and sits centrally, though it lies at a small angle (< 5º) to that of the section as a whole. Much of the original endosteal surface has been secondarily altered and destroyed by matrix and crystal infilling of the medullary cavity. However, localized areas of the original endosteal margin remain, and preserve four or five endosteal lamellae. In these same regions, small amounts of cancellous tissues are preserved just external to the endosteal lamellae. This cancellous bone was clearly formed by the secondary resorption of primary bone tissues, and its erosion rooms vary in size. There are no secondary osteons in this region.

The inner cortex and mid-cortex are almost entirely composed of unremodeled primary woven-fibered bone. In the outer cortex, there are some signs of slightly slowed growth relative to the inner and midcortex. Approximately 0.9-1.2 mm from the periosteal surface, the bone transitions to parallel-fibered bone tissue, forming an annulus. No LAG is visible within this annulus. Approximately 0.5 mm from the periosteal surface, the parallel fiber bundles become coarser and less organized. This type of bone continues to the periosteal surface.

The vascular canals of the inner cortex are all primary osteons. Many of these are longitudinal canals, but locally, short radial canals may dominate. The diameters of these canals tend to be larger than canals closer to the periosteal surface, but this may be diagenetic expansion resulting from the crystals that infill of many of these canals. At least half of the longitudinal canals anastomose with at least one other canal. These anastomoses may travel in any direction (circumferential, oblique, or radial). All canals are surrounded by 1-2 distinct lamellae. Though the cement lines between lamellae are distinct, there are no resorption surfaces surrounding these vascular canals. The number and diameter of the vascular canals decrease slightly in the midcortex. Within the annulus, vascular canal density decreases dramatically. The canals here are primary osteons lined by 1–2 lamellae, but they are much smaller in diameter and rarely anastomose. They are arranged more or less into circumferential rows, and each row is spaced somewhat widely. External to the annulus, most of the canals are primary canals similar in morphology to the midcortex, but very close to the periosteal surface, some simple primary canals can be observed.

In the inner cortex, the osteocyte lacunae associated with the lamellae surrounding primary osteons tend to be elongate and oriented perpendicular to the long axis of the bone. Some are more globular and oriented parallel or oblique to the long axis of the bone; these generally occur closer to the endosteal surface. The distances between osteocytes in the

osteonal lamellae vary. The osteocytes of the interstices between canals show no preferred alignment or orientation relative to the long axis of the bone and no preferred arrangement relative to each other. Osteocyte density decreases slightly in the mid-cortex, but the orientation and arrangements are the same. Within the annulus, osteocytes are still numerous, but they are more organized compared to the inner and midcortex. Here they are more elongate, tend to be oriented perpendicular to the long axis of the bone, and are arranged more or less circumferentially. Spacing between osteocytes in the annulus remains very irregular. External to the annulus, the osteocyte lacunae become less organized, similar to those just internal to the annulus. Osteocyte density in *Nyasasaurus* is lower than the other dinosauromorphs described above, but falls within the range of unambiguous dinosaurs.

Discussion: Nesbitt et al. (2013, Supporting Information) discussed the bone microstructure of *Nyasasaurus* in relation to silesaurs and unambiguous dinosaurs. *Nyasasaurus* is well vascularized and shows high vascular connectivity throughout the cortex (i.e., throughout the entire preserved ontogeny), and the canals anastomose in all directions. Compared to the other taxa examined so far in this study, it is most similar to the tibial inner cortex of the Ghost Ranch silesaurid (rather than the humerus, which shows less connectivity overall). Nesbitt et al. (2013) also noted that the bone microstructure of *Nyasasaurus* was also similar to that of *Megapnosaurus rhodesiensis* (described below) in its vascular density and in its patterns of anastomoses/connectivity, osteocyte orientation and arrangement, and woven-fibered bone tissue.

DINOSAURIFORMES: DINOSAURIA

All remaining taxa in this study are unambiguously part of the clade Dinosauria (see Figure 2.1, node 8 for phylogenetic position).

DINOSAURIA: ORNITHISCHIA

(See Figure 2.1, lineage F for phylogenetic position)

Fruitadens haagarorum

Specimen numbers and elements: LACM 115727 (femur), LACM 120478 (femur). Both femora are part of the paratype material of *Fruitadens haagarorum*. LACM 115727 is a larger and older individual than LACM 120478; the smaller individual is not much larger than the medullary cavity of the larger individual (Butler et al. 2010).
Locality: LACM Fruita Paleontological Area, northwest of Grand Junction, Colorado, USA
Formation and age: base of the Brushy Basin Member of the Morrison Formation, early Tithonian (Kirkland 2006)

Prior histological analyses: Both specimens were sectioned and described by Butler et al. (2010) as part of the original description of *Fruitadens haagarorum*. I redescribe both sections here, and add new information on canal type, cortical dimensions, and measurements of osteocyte density.

Histological observations: My observations largely concur with those of Butler et al. (2010). The femoral mid-diaphysis of LACM 120478 is slightly oval in cross section, with a subpentagonal medullary cavity that sits centrally (Figure 2.48). In the larger individual, LACM 115727, the mid-diaphysis is oval, with an oval to subtriangular medullary cavity (Figure 2.49). Both individuals show a crystalline infill of the medullary cavity and a region of endosteal bone that lines the medullary cavity. In LACM 120478, this layer is about 0.15 mm thick and continues around nearly the entire circumference along the endosteal margin. It is formed of parallel-fibered bone, with a distinct line separating it from the primary cortical tissue. In LACM 115727, a thin (0.07 - 0.1 mm) layer of lamellar or parallel-fibered bone lines the endosteal border. This layer is less distinct from the cortex than in LACM 120478 and it is discontinuous around the circumference of the medullary cavity. LACM 115727 also preserves several thin trabeculae that project ~0.75 mm into the medullary cavity and enclose long erosion rooms (Figure 2.49). These trabeculae and erosion rooms were clearly formed by the resorption of primary cortical tissues. The trabeculae preserve tissues similar to those of the inner cortex of LACM 120478 and are not lined with endosteal lamellae. The outer (more periosteal) margin of the erosion rooms is lined by endosteal lamellae, but not the portion of their margin formed by trabeculae.

Butler et al. (2010) noted that the mid-diaphyseal cortex of LACM 120478 is mostly composed of parallel-fibered primary bone tissue (Figure 2.50), with a single localized area of woven bone in the thickest portion of the cortex (Figure 2.51, note multicolored region in bottom image). The cortex of this individual preserves a single distinct LAG, which is visible ~0.05-0.15 mm from the periosteal margin. In LACM 115727, the cortex is composed of parallel-fibered bone that regionally grades into lamellar bone, especially just internal and external to the growth marks (Figures 2.52). The parallel-fibered component becomes more organized moving periosteally. As Butler et al. (2010) reported, four growth lines are visible in this individual (Figure 2.52, note yellow arrows). The innermost is a very distinct annulus that is only preserved in one small region (it is resorbed by medullary cavity expansion elsewhere). External to this, there are two LAGs in the inner cortex that locally grade into annuli. The outer one of these lies at midcortex. There is also a LAG close to the periosteal surface, which regionally disappears. I find an additional annulus between the second and third growth marks [i.e., the inner two growth marks Butler et al. (2010) illustrate in Figure 3f (p. 378)] in some regions of the bone (Figure 2.52, note white triangle). This may reflect a temporary change in bone depositional rate in the middle of the growth cycle; it is only as distinct as the regions where the LAGs just internal and external to it grade into annuli and disappears regionally. Halfway between the LAG at midcortex and the outermost LAG, there is thin region of 1-2 lamellae that locally degrades into an accretionary “bright line” (*sensu* Currey 1962). As noted by Butler et al. (2010), the outermost cortex (external to the fourth/outermost LAG) is composed of parallel-fibered tissue. This tissue is similar in organization to the parallel-fibered regions of endosteal lining bone.

LACM 120478 is well vascularized to moderately vascularized. The majority of the canals are radial or radial-oblique (Figure 2.50), but there is an isolated region where most are either longitudinal or short, circumferential canals (Figure 2.51). This is the same region where longitudinal canals and short radial canals are most common. The radial canals extend for most of the cortical width; however, at low magnification, they may appear shorter or

segmented because they weave in and out of the plane of section (Figure 2.50). In this individual, both simple primary canals and primary osteons are present. The longitudinal canals are nearly all primary osteons; radial canals are always simple primary canals. LACM 115727 is moderately to poorly vascularized by canals that are all longitudinal or slightly oblique (Figure 2.52). In regular light, these all have a lighter band around them, suggesting that they might be primary osteons, but lamellar bone is not visible. Under polarized light, it is clear that lamellae do not line most of the canals; rather, the primary bone of the cortex continues around the canal opening. Therefore, I diagnose most of the canals as simple primary canals, but a handful of primary osteons is visible in the innermost cortex. Across the section, there is no regular pattern of canal arrangement, but locally they may occur in pairs or form short radially oblique rows, four or five canals long. Vascular density and canal diameter both decrease periosteally, and the parallel-fibered tissue periosteal to the outermost LAG is avascular. As Butler et al. (2010) reported, neither shows any evidence of secondary osteons.

The osteocytes of LACM 120478 are difficult to see in some regions because the slides are too thick. They are easiest to discern in the inner and mid-cortex. In the woven region, osteocytes are disorganized and show no preferred orientation relative to the long axis of the bone and no preferred arrangement relative to each other. Close to the primary osteons, the lacunae orbit the canals. In the parallel-fibered regions, most of the osteocyte lacunae are oriented perpendicular to the long axis of the bone and do not orbit the canals. In LACM 115727, osteocytes are visible only in small patches except in the avascular, parallel-fibered region at the periosteal surface). Where visible, they are similar in appearance to the parallel-fibered bone of LACM 120478. Osteocyte density is very high in both specimens - 3409 cells/mm^2 in LACM 120478 and 3265 cells/mm^2 in LACM 115727. These values are higher than any taxon examined previously, and among the highest in this dataset.

Discussion: I agree with Butler and his colleagues (2010) that growth rate in LACM 115727 had slowed appreciably compared to the smaller LACM 120478, and that it would not likely have increased much in size had it lived longer. This taxon appears to have grown relatively fast in its first year, slowed growth and bone deposition rates in its second year, and grew steadily at a similar rate for several more years.

Neornithischia (outside Cerapoda), cf. *Lesothosaurus* or *Stormbergia*
Specimen number and element: NM QR 3076 (femur)
Locality: Spitskop Farm, Jamestown, Eastern Cape, South Africa
Formation and age: Upper Elliot Formation, Hettangian-Sinemurian (Olsen and Galton 1984)

Taxonomic comments: The taxonomic affiliation of NM QR 3076, a partially articulated skull and postcrania, has been discussed in detail by Butler (2005) and Knoll et al. (2010). Butler agreed with previous assessments that this specimen was not a heterodontosaurid, but he could not assign this specimen conclusively to a genus, because the skull of *Stormbergia* has not been described and because almost all of the postcranial material of this specimen "shows equal similarity to material of both *Lesothosaurus* or *Stormbergia*" (Butler 2005: p188). In contrast, Knoll et al. (2010) concluded based on histological evidence that *Stormbergia* should be regarded as a mature form of *Lesothosaurus*. This hypothesis has not been

subjected to further testing, and so in this study I follow the more conservative approach of Butler 2005 and other, more recent phylogenetic analyses of Ornithischia (e.g., Butler et al. 2007, Butler et al. 2008) that place this specimen as an early-diverging neornithischian that falls outside Cerapoda.

Prior histological analyses: The femur histology of NM QR 3076 was first described by Knoll et al. (2010). I redescribe that section here, and add new information on cortical dimensions and measurements of osteocyte density. I do not extensively figure this specimen here, because it has been illustrated adequately in the literature (Knoll et al. (2010). Additional materials described as *Lesothosaurus* were described histologically by de Ricqlès et al. (2008) and by Knoll et al. (2010). These specimens, MNHN IG 23, 24, 25, 27, and 30, will not be discussed in this study because their taxonomic affiliation is in question. The original description of these materials (Knoll and Battail 2001) does not list apomorphies that would conclusively place them into either *Lesothosaurus* or *Stormbergia*. MNHN IG 24, 25, and 30 are not identifiable to element, and therefore their identification even to Ornithischia is risky. Furthermore, none of those specimens could have been sampled at the mid-diaphysis (see Knoll and Battail, Fig. 1). Because they are not sampled at homologous locations and their taxonomic affinity is uncertain, I do not discuss these materials here.

Histological observations: The mid-diaphyseal femoral cortex of NM QR 3076 forms a rounded triangle in cross section. The medullary cavity is similarly shaped and sits off center, such that the cortical walls vary in thickness around the section. This variation is further enhanced by abrasion of the periosteal surface, which may be diagenetic or result from overpreparation.

The medullary cavity is infilled with a mudstone or claystone matrix and does not show crystalline growth. Small fragments of bone are scattered throughout the matrix within the medullary cavity; these resemble broken bits of the cortex more than trabeculae. A band of lamellar bone ~0.15 mm thick is visible around the endosteal margin, forming a somewhat 'wavy' border. This waviness is exacerbated by breaks in the bone wall. The endosteal surfaces of these lamellae appear fairly smooth, and do not suggest any location where trabeculae may have extended into the medullary cavity in life.

Around most of the circumference, endosteal lamellae form a distinct internal edge to a region of cancellous and or heavily secondarily remodeled bone. Oval erosion rooms are common in the remodeled area; these reach 0.66 mm in length and may have formed by resorbing either primary or secondary bone tissue. Where present, the erosion rooms and secondary osteons in this region are well developed; they are each lined with several distinct lamellae. I agree with Knoll et al. (2010) that in some regions, these tissues appear to be compacted coarse cancellous bone, but note that they are not laterally extensive. Knoll et al. (2010) suggested that these tissues may have been endosteally derived, but I can find no trace of the original endosteal margin. However, the remodeling through most of this region is heavy enough that few traces of the original primary tissues remain, so the original margin may have been obliterated. The endosteal lamellae must have been deposited after remodeling of the inner cortex began, because they cut across several secondary osteons and small erosion rooms.

The mid- and outer cortex are composed mainly of coarsely-woven parallel-fibered primary bone tissue. Knoll and colleagues (2010) describe these tissues as fibro-lamellar, but I do not observe woven-fibered bone anywhere in the section (Figure 2.53, note refringence patterns more suggestive of parallel-fibered bone). Separating the mid-cortex from the outer cortex is an annulus of more organized parallel-fibered tissue surrounding a LAG. Locally within the annulus, the parallel-fibered tissues become weakly lamellar. Periosteal to the annulus/LAG is a thick zone (1.3-1.8 mm) of coarsely parallel-fibered bone tissue. This zone abruptly transitions to lamellar bone in the outermost cortex (Figure 2.54). The lamellar region is punctuated by four LAGs (Figure 2.54, note arrows), one of which locally becomes a double LAG. Knoll et al. (2010) suggested this outermost region could represent an EFS. If so, this transition is exceptionally abrupt compared to those observed in the taxa described above.

In the coarsely parallel-fibered regions, the bone is well or very well vascularized. The vascular canals of the mid-cortex tend to be primary osteons; these grade into simple primary canals periosteally. Throughout the section, the most common canal orientation is longitudinal. However, nearly all of these are linked by long, circumferential anastomoses, such that a circumferential pattern is most obvious. The inner annulus is less well-vascularized compared to surrounding tissues, although a band of closely-spaced longitudinal canals lies just external to the LAG. In the outermost cortex, the tissue is more or less avascular, supporting the EFS hypothesis of Knoll et al. (2010).

Osteocytes throughout the primary tissues of the cortex are oriented perpendicular to the long axis of the bone. They are arranged more or less circumferentially relative to each other, though spacing is irregular everywhere except the outermost cortex. Osteocytes tend to orbit the canals, whether they are primary osteons or simple primary canals. In the outermost cortex, they are spaced more regularly and line up along lamellae. Osteocyte density varies little throughout the section (~ 2300 cells/mm^2 on average). Although this value is lower than that of *Fruitadens*, it is comparable to that of the silesaurids, despite being a much larger animal.

Scutellosaurus lawleri

Specimen numbers and elements: UCMP 130580 (humerus and tibia), UCMP 170829 (femur). UCMP 130580 and 170829 are both known from partial skeletons, and UCMP 170829 is about 20% larger than 130589 (Rosenbaum & Padian 2000).
Locality: UCMP localities V85010 (UCMP 130580) and V85013 (UCMP 170829), Adeii Eechii Cliffs, Coconino Co., Arizona, USA
Formation and age: Sinemurian-Pliensbachian (Peterson and Pipiringos 1979)

Prior histological analyses: The microstructure of the femur and tibia of *Scutellosaurus* were first described by Padian et al. (2004) as part of a larger study of small-bodied dinosaurs and pterosaurs. A section of the mid-diaphyseal humerus was made from UCMP 130580, but was never described. I redescribe the femoral and tibial sections here, adding new information on cortical dimensions and measurements of osteocyte density. I also describe the humeral section for the first time. The femur and tibia are adequately illustrated in the literature; I do not figure them here (although images are available on MorphoBank).

Histological observations by element:

Humerus

The humerus of UCMP 130580 is triangular in cross section at the mid-diaphysis (Figure 2.55). Its medullary cavity is slightly more oval, and lies centrally. It is fairly thick-walled (RBT = 26.3%) compared to most other archosaurs examined in this study (Table 2.2). The medullary cavity is infilled with crystals, as are the erosion rooms of the inner cortex. The endosteal margin is lined with lamellar bone along much of its circumference. Most of the original endosteal margin appears to have been eaten away somewhat by the crystal infill; the band of endosteal lamellae is 0.1 mm at its thickest point, but even here the internal surface appears to be somewhat eroded. No trabeculae are preserved at mid-diaphsysis, but a broad patch of lamellar bone floats among the crystals. Given its position, appearance, and coloration, this could be a remnant of trabeculae, or a thick piece of endosteal bone.

A circumferential row of 8 oval and circular erosion rooms occupy the innermost cortex, very close to the endosteal margin. These are each quite large, and appear to have a somewhat regular spacing. They are all lined with 2-5 lamellae of irregular width, but the crystal infill of these chambers may have altered their original inner surface. The erosion rooms formed by resorption of primary cortical tissues and least some formed before the endosteal lamellae were deposited, because the endosteal lamellae cut across the outermost lamellae of one of these rooms. The rest appear to have been separated from the medullary cavity by a thin bridge of endosteal lamellae and some primary cortical tissues, but these bridges have mostly been eroded by crystalline infill.

The inner half of the cortex is composed almost entirely of parallel-fibered primary bone tissue, with local areas grading into more lamellar tissue. It becomes more organized leading up to midcortex. After that, the cortical tissue is exclusively lamellar. Five growth marks are visible in this section (Figure 2.55 and 2.56; note colored lines and arrows). The inner two show localized breaks in tissue and elsewhere grade into annuli. Of these, the innermost lies close to the endosteal margin and the second sits about one third of the cortical thickness from the endosteal margin. The third and fourth growth marks are double LAGs; one lies at midcortex and the other halfway between the third growth mark and the periosteal edge. The outermost growth mark is a faint double annulus that lies very close to the periosteal margin, and is mostly visible on the anteromedial half of the bone.

The humerus of UCMP 130580 is generally poorly vascularized (Figure 2.56), with small regions of moderate vascularity in the inner cortex (Figure 2.57, triangles indicate canals). The vascular canals are nearly all simple primary canals (a few primary osteons are visible in the innermost cortex), and almost all are longitudinally oriented. Internal to the second growth mark, a few anastomoses connect up to three longitudinal canals (mostly two), and while these generally extend radially, a few circumferential and oblique anastomoses are visible. Between the third and fourth growth marks, there are three to four circumferential rows of longitudinal canals. External to the fourth growth mark, the cortex is very poorly vascularized, and in some regions avascular. In the ventro-lateral region of the cortex, very short radial anastomoses can be seen at semi-regular intervals in this last row. A single circumferential row of longitudinal canals can be found just internal to the outermost annulus in some regions of the bone.

In the parallel-fibered regions of the bone, many osteocytes tend to be oriented perpendicular to the long axis of the bone, but at least a quarter are oriented parallel or slightly oblique to the long axis of the bone. They are arranged circumferentially in the interstices of the bone, but spacing is not regular. The osteocytes in the outer half of the cortex are highly organized and always lie perpendicular to the long axis of the bone. Locally, the lamellae are very distinct. The osteocytes rarely change orientation near the vascular canals. Usually the areas closest to the canals are more or less acellular. The average osteocyte density in the humerus (2732 cells/mm^2) is comparable to that of pterosaurs and some silesaurids.

Femur

The femur of UCMP 170829 is difficult to image because it is has been ground to variable thicknesses across the slide and shows evidence of peeling. About a third of the cortex is missing from the original specimen, and the opposite side along the long axis is ground very thin. The mid-diaphysis is oval or almond shaped in cross section, with a oval or subrectangular medullary cavity. The medullary cavity sits centrally, but its major axis is angled slightly relative to the major axis of the cortical outline. As in the humerus of UCMP 130580, the medullary cavity is filled with crystals that have eaten away at the endosteal margin in some areas. It is difficult to ascertain whether or not the mid-diaphysis would have exhibited trabeculae. Where the endosteal margin is preserved, there is no indication of trabecular extension, except the base of a single strut is preserved.

External to the lamellae, there is one region of compacted coarse cancellous tissue and a few isolated secondary osteons. In this area, the band of endosteal lamellae is thicker and cuts across the compacted coarse cancellous tissue in places. The compacted coarse cancellous bone formed endosteally; there is a sharp resorption boundary demarcating it from the primary cortical tissues, which it cuts across. Outside of this region of compacted coarse cancellous bone and the adjacent tissues, no secondary osteons occur. The bone added to the endosteal margin here lies at the opposite end of the medullary cavity to an area that has expanded deeper into the cortex. In other words, the medullary cavity is expanding on one side of the bone and adding bone to the opposite side, changing its shape and position relative to the external outline of the cortex.

The primary tissue of the femoral inner cortex is woven-fibered bone, which transitions to mostly parallel-fibered bone (there are small regions of woven bone) at midcortex. Padian et al. (2004) reported no LAGs in this individual, but I observe six annuli. These are more visible under crossed plane polarized light, but changes in mineralization and osteocyte density are visible under regular light. However, the nature of the slide preservation makes these differences more difficult to see in the femur than in the humerus. The innermost annulus lies just outside the resorption line at the edge of the area of compacted coarse cancellous bone. The second annulus lies 0.5 mm external to the innermost, and is preserved as an arc because the medullary cavity cuts across it. The third annulus lies 0.5 to 0.9 mm external to this and also forms an arc because of medullary cavity expansion. The fourth annulus sits at midcortex and can be traced around much of the preserved circumference. The fifth annulus lies halfway between the fourth and the sixth, which lies very close to the periosteum. In the inner half of the cortex, the annuli are very thin bands of parallel-fibered bone. The fifth and sixth annuli are lamellar.

The inner cortex is moderately to well vascularized (more so than the humerus or tibia) and many short anastomoses can be seen connecting two or three longitudinal canals. These anastomoses may occur in any direction. The canals of the inner cortex are mixed in type; many are primary osteons exhibiting one or two lamellae, but some are simple canals. These generally show no preferred arrangement relative to each other, but in some regions, they form short radial rows. As in the inner cortex, the canals of the outer cortex are a mix longitudinal simple primary canals and primary osteons, but here they align in roughly circumferential rows and rarely anastomose. Vascular canal density in the outer cortex decreases slightly moving periosteally. Vascular canal diameter is larger in the outer cortex; this may reflect the immaturity of the canals (Starck and Chinsamy 2002).

In the inner cortex (regions of woven bone), the osteocytes near primary osteons often encircle them. These lacunae tend to line up along lamellae as well as orbiting the canal outside the osteonal margin. In the interstices between canals, they show no preferred orientation relative to the long axis of the bone, and no preferred arrangement relative to each other. In the outer cortex, the osteocyte lacunae become more organized; they generally lie perpendicular to the long axis of the bone, and are arranged circumferentially (though spacing between them is irregular). Osteocyte density in the femur of UCMP 170829 is half that of the humerus of UCMP 130580 (1408 cells/mm^2 vs. 2732 cells/mm^2, respectively).

Tibia

I generally agree with the assessments of Padian et al. (2004) regarding the tibia of UCMP 130580. This section is more difficult to characterize histologically because the bone experienced post-depositional fungal or bacterial invasion. This appears as dark regions that do not refringe in polarized light and do not preserve cellular details. This invasion obscures most of the endosteal margin, and much (but not all) of the cortex. The mid-diaphysis is crushed, and some small pockets of crystal infilling are present in the medullary cavity. These are not extensive and some of the endosteal surface is intact. Where this surface is visible, the lamellae are distinct and form a band that varies between 0.1 and 0.2 mm in thickness. The individual lamellae undulate somewhat within the band. The innermost cortex preserves a few erosion rooms near the endosteal margin, but unlike those of the humerus, they are not regular in size, shape, or spacing. The largest of these is 0.6 mm wide and shaped like a B. All are lined with one or two lamellae.

Based on the non-invaded regions, most of the primary cortex is composed of parallel-fibered bone. Five growth marks are visible; the inner two are annuli, and the outer three (all very close to the periosteal surface are LAGs. The innermost annulus lies about halfway between the endosteal margin and mid cortex; it is separated from the endosteal margin by a band of invaded tissues. This annulus is composed of lamellar bone, and locally becomes a double annulus. The second annulus lies at midcortex, approximately 0.5 mm external to the innermost annulus. Both annuli are broad and locally bear a bright line (*sensu* Currey 1962) at the center. The third growth mark is a LAG around most of the section but locally shows no break in tissue. It lies about 0.5 mm external to the second annulus, and is slightly closer the periosteal surface than to midcortex. The second and third growth marks are separated by a band of invaded tissue. External to the third growth mark, the tissue is far more organized; here is it either lamellar or weakly parallel-fibered. The outer two LAGs and the periosteal

surface are evenly spaced. The fourth growth mark is 0.13 mm external to the third, the fifth/outermost is 0.11 mm from the fourth growth mark, and the periosteal surface is 0.10 from the outermost growth mark. Locally, the outermost LAG is a double LAG.

Internal to the third growth mark, longitudinal vascular canals are visible even in the invaded regions and usually preserve a single thin lamellae. As in the other elements, there is a mix of simple primary canals and primary osteons in the inner cortex, and some of these connect with another canal via short radial or oblique anastomosis. Although the annuli are avascular, the zones between them are moderately vascularized. External to the third growth mark, the bone is poorly vascularized to avascular.

Osteocytes cannot be characterized in most of the section because they are obscured by bacterial or fungal invasion. However, in the gaps between invaded regions, the bone tissue is very similar to that of the humerus. In the parallel-fibered regions, osteocytes tend to be oriented perpendicular to the long axis of the bone, but some are oriented parallel or slightly oblique to the long axis of the bone. Osteocyte lacunae are arranged circumferentially in the interstices of the bone, but spacing is not regular. The osteocytes in the lamellar regions (the annuli and external to the third growth mark) are highly organized and always lie perpendicular to the long axis of the bone. The spacing between the lacunae is far more regular and the osteocytes line up along lamellae. Osteocyte density is high in this tibia; at 3200 cells/mm^2, it is similar to the silesaurids and the Ghost Ranch coelophysoid (see below), despite a much smaller body size.

Discussion: Growth in *Scutellosaurus* is somewhat difficult to characterize because the elements sampled for the two individuals were non-overlapping. Based on the femur of UCMP 170829, *Scutellosaurus* was definitely capable of making moderately vascularized woven bone. However, none of the elements sampled is as densely vascularized or displays the complex vascular patterning of the other neornithischian and saurischian (see below) dinosaurs. Padian et al. (2004) suggested that the larger specimen (UCMP 170829) was near the end of its active growth phase, but I think this statement equally characterizes UCMP 130580 (the smaller specimen). The larger specimen has six annuli in its femur, and the smaller specimen has five growth marks in both its tibia and humerus. The outermost zones of the humerus and especially the tibia of UCMP 130580 are very closely spaced, certainly comparable to those of the femur.

Padian et al. (2004) commented that there was “very little if any typical fibro-lamellar bone in most of these elements” (p. 559). Certainly this is true in the tibia and humerus of UCMP 130580, but not in the femur, where half the cortex is composed of woven-fibered bone vascularized by primary osteons. Similarly, that study referred to these tissues as poorly vascularized overall, whereas I classify most of these elements as moderately vascularized. I think this reflects in part the comparative sample examined for that paper. Most of the taxa Padian et al. (2004) examined are well vascularized or very well vascularized, and *Scutellosaurus* seems poorly vascularized by comparison. However, compared to *Sphenodon*, *Trilophosaurus*, or adult female *Alligator*, *Scutellosaurus* would seem relatively well vascularized. This highlights the importance of consistency in diagnoses, especially when using qualitative descriptors.

Psittacosaurus mongoliensis
Specimen numbers and elements: PIN 1369/1-11/1948 (humerus), PIN 698/4-22/1946 (femur, tibia), PIN 698/5-9/2/1946 (tibia)
Locality: Khamaryn Us [=Khamrin-Us of Erickson and Tumanova 2000; earlier literature refers to it as Gashuuny Khudag (Kurochkin and Barsbold 2000)], southeastern Gobi Desert ~150km southeast of Sainshand, Dornogovi Province, Mongolia
Formation and age: Züünbayan (= Dzun Bayan) Formation, Hühteeg (= Sainshand) Svita; Aptian-Albian (Hicks et al. 1999)

Prior histological analyses: An extensive study of the microstructure and growth patterns of *Psittacosaurus mongoliensis* was completed by Erickson and Tumanova (2000), who examined the mid-diaphyseal and diaphyseal histology of the humerus, femur, and tibia based on ontogenetic series of each element. Lee (2007) constructed growth curves for *P. mongoliensis* using the original sections of Erickson and Tumanova (2000), but did not examine other aspects of the bone microstructure. A closely related taxon, *P. lujiatunensis*, has also been examined. Erickson et al. (2009b) figured the fibular histology and constructed growth curves and life tables for that taxon, but the focus of that paper was not histological. Zhao et al. (2013) described the histology of the humerus, femur, tibia, and fibula of *P. lujiatunensis* based on ontogenetic series of each element. I redescribe four of Erickson and Tumanova's (2000) sections here, and add new information on cortical dimensions and measurements of osteocyte density. The microstructure of these sections was illustrated, but the full cross sections were not, so I include those here (Figures 2.57, 2.58, 2.59, 2.60).

Histological observations by element:
Humerus

The slide preserved for PIN 1369/1-11/1948 is not ground to optical clarity in all area of the slide and so not all details are visible throughout. About one third of the cortex is missing from this specimen, and much of the periosteal surface is abraded or chipped away. The section was too thick to view under polarized light, even when wet, so I cannot verify the collagen fiber orientation. It is also too thick to observe or count osteocytes. As Erickson and Tumanova (2000) noted, the contrast of the dark minerals filling the canals and the lighter bone tissue makes it easy to track canal orientation in three dimensions. However, because three dimensions of vasculature can be seen, the apparent vascularity is higher than the actual vascularity at the plane of the section's surface. Erickson and Tumanova (2000) examined humeri from two individuals with the same specimen number; one at growth stage B and one at stage E. This section is the growth stage B section, and was estimated to be four years old when it died.

At mid-diaphysis, the humerus of PIN 1369/1-11/1948 is circular to subtriangular in cross section, with a circular medullary cavity that sits centrally (Figure 2.57). The matrix in the medullary cavity is a mix of dark ferrous minerals (Erickson and Tumanova 2000) and a few patches of clear crystals. Fragments of bone are preserved within the matrix that fills the medullary cavity. Some of these clearly detached from the endosteal margin, but for others it is less clear.

Three LAGs are visible (Figure 2.57, note colored lines); these occur near the endosteal margin, at midcortex, and near the periosteal margin. The inner two LAGs show a

break in tissue so distinct it is visible even on the thick slide. Each of these is a double LAG, and the distance between the two lines of the double LAG is approximately 0.4 mm in both cases. Each line lies within an annulus; it is visible as a thin avascular band on both sides of the LAGs. The outermost LAG is visible only in the outermost cortex in two regions; not enough bone is preserved external to determine whether this is a single or double LAG.

The entire cortex is moderately vascularized at the plane of the section's surface. A light-colored "halo" of even width is visible around each canal. In the sections ground thinner (see below), this "halo" is also visible and corresponds to lamellar bone surrounding each canal. I diagnose these canals as primary osteons following Erickson and Tumanova (2000). Between the two lines that make up the inner LAG, the canals are oriented longitudinal to slightly oblique. External to the first LAG, the bone is reticular, but with a strong radial component ("radiating reticular") in the internal part of the zone. It becomes more reticular approaching the second LAG. Between the lines of the second LAG, the canals *at the plane of the section's surface* are longitudinal or oblique/radial, with a few anastomoses. However, it is clear that they reticulate *in three dimensions*. External to the second LAG, the canals are similarly organized; they become a mix of radial and reticulating canals approaching the outer LAG.

Femur

This specimen is preserved in much better condition than the humerus of PIN 1369/1-11/1948. It was ground thinner and more evenly, and is missing only a small portion of the cortex. Additionally, the external surface is not nearly as abraded as PIN 1369/1-11/1948. Unfortunately, osteocytes are preserved only at the endosteal and periosteal margins, and along some of the vascular canals, making estimates of their density impossible. This individual was assigned to growth stage A by Erickson and Tumanova (2000), who estimated it to be three years old at the time of death.

The femur of PIN 698/4-22/1946 is circular at mid-diaphysis, with a circular medullary cavity that sits centrally (Figure 2.58). The medullary cavity is filled with a dark matrix that does not appear crystalline. It does not preserve trabeculae. Parallel-fibered bone lines the endosteal margin along a small portion of its circumference; this region is between 0.1 and 0.3 mm thick, and is not especially distinct from the primary tissue of the cortex. A few secondary osteons are visible in the innermost cortex; the endosteal lining bone cuts across some of them. A few small oval and circular erosion rooms are also visible; the largest of these is 0.46 mm across its longer axis. Some of these are lined with lamellar bone or parallel-fibered bone.

Three growth marks are preserved in this section (Figure 2.58, note colored lines). The inner two are double annuli that locally form LAGs; the outer is a LAG. The growth marks roughly divide the cortex into thirds. The inner double LAG lies about one third the width of the cortex from the endosteal margin (0.8 mm), the middle growth mark lies 0.66 mm external to the inner one, and the outer LAG lies very close to the periosteal surface (0.6 mm from the middle mark). The pattern and spacing of the LAGs in this femur is very similar to that of the humerus of PIN 1369/1-11/1948. Except in the annuli, the cortex is composed of woven-fibered bone. As in *Pterodactylus* and *Asilisaurus*, more circumferential fibers are present than radial, oblique, or longitudinal. Additionally, the annuli (which are parallel-fibered) are relatively broad. Because of this, the whole section gives a 'Maltese cross' appearance under

polarized light, despite being predominantly woven-fibered. In both double LAGs, the outer line refringes more brightly under polarized light than the inner one.

The femur is moderately to well vascularized by primary osteons. Internal to the inner double annulus, the dominant canal orientation is longitudinal, but many canals anastomose with one or two other canals, most often forming short radial connections (Figure 2.58). Within the double annulus, radial and circumferential anastomoses are equally common. In the zone between the double annuli, short reticulations are common, similar to those of the proterochampsian described above. Again, the radial direction is the most common direction of anastomosis. In the second double annulus, both component annuli are less vascularized compared to the surrounding bone, and canals are much less likely to connect with other canals. The zone between the middle growth mark and the outer LAG is similar in appearance to the previous zone. External to the outer LAG, which does not lie within an annulus of parallel fibered tissue, the bone is dark from fungal or bacterial invasion and hard to diagnose. Where canals are visible, they are either radial canals or longitudinal canals arranged in radially oblique rows.

Osteocyte lacunae are numerous in this section but difficult to image; in most regions of the bone, they lack any infilling and are very similar in color to the bone tissues in which they lie. In a few areas the lacunae take on a contrasting color, but these patches are not large enough to place a digital box plot for measuring, When I imaged the regions of non-contrasting osteocyte lacunae, it was not possible to determine from the images which cells lay in the plane of focus and which did not (usually there are color differences in addition to clarity of the outline; here, everything was the same color). By focusing through the section, it was possible to observe two or three layers of osteocytes orbiting each canal in the regions of woven-fibered bone. In the interstices between canals, osteocytes are very disorganized; they show no preferred orientation relative to the long axis of the bone. The spacing between osteocytes in these regions is irregular, and they do not show a preferred arrangement relative to each other.

Tibia

PIN 698/4-22/1946 [smaller individual; growth stage A of Erickson and Tumanova (2000)] and PIN 698/5-9/2/1946 [larger individual; growth stage E of Erickson and Tumanova (2000)] are both mid-diaphyseal sections, but have much different cortical outlines. The smaller individual is oval at mid-diaphysis (Figure 2.59), whereas the larger individual is somewhat bilobed on one side (Figure 2.60, note shape of surface at top of image). The medullary cavity of the smaller individual is hard to define because of internal fracturing; in the larger specimen, the medullary cavity is more or less triangular. This is because *Psittacosaurus mongoliensis* underwent significant changes in diaphyseal bone proportions through ontogeny (Erickson and Tumanova 2000). Not only did the tibia experience differential bone growth around the circumference of the section (cortical drift), but these differences in bone growth rate became greater as the animal aged. Similar changes were observed in the related taxon *P. lujiatunensis*, which corresponded to changes in forelimb to hindlimb ratios as that species made the transition from quadrupedal to bipedal posture (Zhou et al. 2013).

Both slides vary slightly in thickness (depth) across the slide. Fortunately, there was one region in both sections where the slide was thin enough and the osteocytes distinct

enough to measure osteocyte density. PIN 698/4-22/1946 has heavy cracking around much of the perimeter and into the medullary cavity; for this reason I do not estimate MSC, minor axis MSD or minor axis MCD for this specimen. In both specimens, the medullary cavity was filled by a dark mineral, as in the other specimens described above. PIN 698/4-22/1946 does not appear to have a free medullary cavity at mid-diaphysis; several trabeculae extend inward. However, there are so many cracks on one side of the element that it is impossible to determine whether these struts would have spanned the medullary cavity in life, or whether they would have connected to an endosteal border of lamellar bone. Along one side of the medullary cavity, the trabeculae are very thick; many lamellae have been added to each strut. In PIN 698/5-9/2/1946, the medullary cavity is more open; no trabeculae extend inward, and along part of the circumference, a thin (~ 0.7 mm) band of lamellar bone is preserved. Both specimens have circular and oval erosion rooms in the innermost cortex; these are often confluent with the medullary cavity (again, preservation makes it difficult to tell whether they would have been walled off by endosteal lamellae in life).

As Erickson and Tumanova (2000) reported, the primary cortex of both elements is composed of woven-fibered bone tissue. The annuli in PIN 698/4-22/1946 are composed of parallel-fibered bone, and the annuli in PIN 698/5-9/2/1946 are composed of either parallel-fibered or lamellar bone. The inner two of these are single LAGs that lie in the center of thin annuli; the outermost is an annulus that only regionally grades into a LAG (Figure 2.59, note colored lines). In PIN 698/5-9/2/1946, six growth marks are present (Figure 2.60, note colored lines). The innermost is partially eroded by medullary cavity expansion. It is a double LAG for most of the circumference, but on the anterior (extensor) surface these lines merge into a single LAG. This LAG lies within a thin annulus of parallel-fibered bone. It is very similar in appearance to the second growth mark, which lies 0.5 mm to 1.8 mm external to the innermost LAG (depending where around the circumference one measures). The third growth mark is a single LAG that grades regionally into an annulus of parallel-fibered bone. This LAG lies at midcortex in one region of the bone, but in the deep cortex elsewhere; it is 0.5 to 1.3 mm external to the second LAG. The fourth growth mark is similar to the third histologically, except that the annulus is locally lamellar. The fourth growth mark shows changes in the orientation of the external outline of the bone at time of deposition; here, one lobe of the posteromedial (flexor) surface begins to enlarge, and the other experiences less growth. The fifth and six growth marks exaggerate this trend further. The fifth and six growth marks are single LAGs that locally become annuli and even disappear. The fifth is just internal to a region of radially vascularized bone near the periosteal surface; the sixth is just external to it, very close to the periosteal surface.

Nearly all canals in both individuals are primary osteons, as Erickson and Tumanova (2000) noted. The smaller individual is well vascularized by longitudinal primary osteons throughout the cortex. These canals anastomose to a varying extent around the circumference of the bone. In some areas they tend to be isolated; in others, they anastomose radially or obliquely, or form small reticulations. Some of these reticulations are simple primary canals. The larger individual is also well vascularized. In this specimen, longitudinal osteons are relatively uncommon. These are limited to one part of the flexor surface of the bone, where they occur from the endosteal margin to the periosteal surface. Most of the cortex shows reticular or short radial canals. Just external to the fourth growth marks, there is a band of slightly longer radial canals that form in the direction of the widest part of the zone (i.e., the

lobe that began to enlarge at that point of ontogeny). Radial canals are quite long and pronounced in the zone between the fifth and sixth growth marks, especially in the lobes (Figure 2.60, note white triangles). Elsewhere in this zone, the canals are reticular or longitudinal.

As in the femur, two or three layers of osteocyte lacunae orbit most canals in both tibial sections. In the larger specimens, only one layer of lacunae orbit canals in the radially vascularized regions. In the woven-fibered regions of both sections, the osteocytes in the interstices between canals are very disorganized; they show no preferred orientation relative to the long axis of the bone and no preferred arrangement relative to each other. These become more organized in the parallel-fibered and even more so in the lamellar regions. In both cases, the osteocytes are all organized perpendicular to the long axis of the bone; the main difference here is that the spacing between osteocytes is more regular in the lamellar regions. Surprisingly, osteocyte density is lower in the smaller (younger) individual than in the larger one (1844 cells/mm^2 vs. 2167 cells/mm^2, respectively). This is likely because I only was able to measure osteocyte density along one transect for each individual. I strongly suspect that with additional transects, the numbers would be more consistent between growth stages.

Discussion: Erickson and Tumanova (2000) estimated age at death to be three years for the smaller individual (PIN 698/4-22/1946) and eight for the larger individual (PIN 698/5-9/2/1946). Erickson and Tumanova (2000) noted that the larger individual required estimation of missing growth marks. These estimates match my observations closely; I observe three growth marks in the former and six in the latter.

The tibial sections illustrate an unexpected pattern for *Psittacosaurus* growth: namely, that older individuals show vascular correlates of faster growth compared to younger individuals. The innermost zones show mostly longitudinal osteons; outer canals show first reticular and then strongly radial canals. These canal orientations have been shown to correlate with progressively faster bone depositional rates in many taxa (Castanet et al. 2000; Cubo et al. 2012), though not in others (e.g., de Margerie et al. 2002). In *P. lujiatunensis*, zones at all stages show a mixture of longitudinal canals and reticular canals, but the proportion of reticular canals decreases with age (Zhou et al. 2013). However, the reduction in reticular canals occurs earlier in forelimb elements than in hindlimb elements. The timing of this histological transition in the forelimb corresponds to a postural transition from quadrupedal to bipedal posture (Zhou et al. 2013). In *P. lujiatunensis*, only one element (a humerus from a young individual) showed radial vascularization similar to that observed in the larger tibia of *P. mongoliensis* (and several large femora); Zhou et al. (2013) concluded that either the two species showed a very different growth trajectory, or some of the larger elements of *P. mongoliensis* sectioned by Erickson and Tumanova (2000) were pathological.

The radial vascularization observed in the tibia of PIN 698/5-9/2/1946 does appear similar to the reactive tissues observed in the periosteal tissues of both living birds with avian osteopetrosis and a dinosaur bone with visible external pathologies (Bell and Campbell 1961; Campbell 1966; Chinsamy and Tumarkin-Deratzian 2009). This similarity led Chinsamy and Tumarkin-Deratzian (2009) to hypothesize a pathological origin for the tissues figured in Erickson and Tumanova (2000). However, in both of the specimens examined by Chinsamy and Tumarkin-Deratzian (2009), extensive erosion rooms were visible throughout the cortex

and radial spicules also grew from the endosteal margin into the medullary cavity. Neither of these is present in PIN 698/5-9/2/1946. Additionally, the specimens examined by Chinsamy and Tumarkin-Deratzian (2009) showed a resorption/reversal line just internal to the region of radial bone. A LAG is present in PIN 698/5-9/2/1946, close to the radial tissues, but it does not share the scalloped appearance that characterizes resorption surfaces.

It is difficult to characterize this tissue; it does not share all the diagnostic criteria of pathological bone reported by Chinsamy and Tumarkin-Deratzian (2009), and it occurs in at least four individuals sampled by Erickson and Tumanova (2000). On the other hand, the late ontogenetic appearance of such fast-growing tissues is also unexpected, and just because the tissues do not conform precisely to those associated with avian osteopetrosis does not mean they are not pathological. Because I only had one of these sections available to examine and my specialization is not pathology, I opt to reserve judgment on this matter until I see additional specimens.

DINOSAURIA: SAURISCHIA

All remaining taxa in this study are part of the clade Saurischia (see Figure 2.1, node 9 for phylogenetic position).

SAURISCHIA: SAUROPODOMORPHA

(See Figure 2.1, lineage G for phylogenetic position)

Plateosaurus engelhardti

Specimen number and elements: SMNS F48-1 (femur), SMNS F14A (femur and tibia). Both are subadults or adults that have not finished growing (Klein 2004, Klein and Sander 2007)
Locality: Trosselbach (Trossel Creek), Trossingen, within the Black Forest, Baden-Württemberg, Germany
Formation and age: Trossingen Formation (formerly considered part of the Knollenmergel Formation), Middle Keuper (≈ latest Norian) (Sander 1992, Nitsch 2005)

Prior histological analyses: The osteohistology of *Plateosaurus engelhardti* is well described. Seitz (1907) and Gross (1934) both described the microstructure of the tibia as part of larger studies of fossil reptiles. de Ricqlès (1968) summarized their findings, compared the histology of *Plateosaurus* to that of other sauropodomorphs, and added additional comments in context of his larger work on vertebrate histology. Foelix and Fischer (1999) illustrated the ribs of *Plateosaurus* as part of a larger study of the application of X-rays in museum research, but did not comment extensively on their histology. The most comprehensive work on this taxon was completed by Nicole Klein and Martin Sander (Klein 2004; Sander and Klein 2005; Klein and Sander 2007), whose sample includes several partial ontogenetic series of several elements (including the humerus, femur, and tibia) from localities in Germany and Switzerland. These localities do not preserve juveniles, so the Klein/Sander dataset includes subadults and adults only. Because of the incredible size of most sauropodomorph taxa, the Sander lab has developed a core drilling technique that samples a radial or diametrical transect through the

cortex at mid-diaphysis (Stein and Sander 2009); no cross sections are available for this taxon. For this study, I redescribe three elements originally sampled by Klein (2004) from the Trossingen locality, and add new measurements of osteocyte density. The microstructure of these elements has been well illustrated, but the cored transects were not, so I include those here (Figures 2.61, 2.62, 2.63). The microstructure of all three elements is similar, so I describe them together.

Histological observations: As Klein (2004) reported, the *Plateosaurus* material from Trossingen is often highly fractured internally, especially at the mid-diaphysis. This cracking often results in the loss of portions of the cortex (especially cancellous regions) during the coring process. These cracks are visible in all three specimens I examined (Figures 2.61, 2.62, 2.63; note cracks). Klein (2004) and Klein and Sander (2007) also reported large medullary cavities in both the femur and tibia throughout the preserved ontogeny (accounting for approximately half of the mid-diaphyseal diameter), and that secondary remodeling was usually visible in the innermost cortex. These factors generally obliterated or obscured the juvenile histology.

Klein & Sander (2007) described the border of the medullary cavity in the femur and tibia as well-defined, but endosteal lamellae are preserved only in one femur (not a specimen I observed). The inner cortex of the femur and the tibia are usually remodeled with erosion rooms and some secondary osteons, but the amount and thickness of this zone of remodeled tissue varies by element. This remodeling is visible in only one of the specimens I examined (SMNS F48-1; see Figure 2.61, bottom third of image), in which numerous erosion rooms have eaten into the primary cortical tissue. In this specimen, the erosion rooms are circular or slightly oval, and are generally smaller than 0.5 mm in diameter (the largest is 1.3 mm along its long axis).

In all elements I examined, the primary cortical tissues were composed of woven-fibered, or a mixture of both woven-fibered and parallel-fibered bone tissue (Figure 2.64, note arrows and triangles). In the femur of SMNS F48-1, most of the bone is woven. In the tibia of SMNS F14A, there is proportionately more woven bone in the inner cortex compared to the outer cortex, but there is not a clear transition from one tissue type to another. Rather, adjacent laminae might show different fibrillar organization (Figure 2.64). In the largest specimens (not in my sample), the outer cortex is composed of lamellar bone (Klein and Sander 2007) and sometimes preserves an EFS. Growth marks in these elements tend to be expressed as annuli of parallel-fibered bone, rather than true LAGs showing a break in tissue. LAGs are only present in the outer cortex in the elements I observed. This is consistent with the reports of Klein (2004) and Klein and Sander (2007) for *Plateosaurus*, as well as sauropodomorphs in general (Sander 2000, Sander and Clauss 2008). The annuli I observe are almost exclusively single bands, but the LAGs of the outer cortex locally become double LAGs. In other individuals sampled by Klein (2004) and Klein and Sander (2007), double, triple, and quadruple LAGs occur.

Throughout the cortex of all three elements I observed, the vascular canals are exclusively primary osteons. Most of these are either longitudinal canals linked by long circumferential anastomoses or true circumferential canals. In the inner cortex of SMNS F48-1 (femur) and SMNS F14A (tibia), some short radial and oblique anastomoses also occur. Klein and Sander (2007) show additional elements in which regions dense in radial canals are

preserved. This type of tissue is never laterally extensive in its deposition, and it may interfinger with regions showing more typical histology. In some specimens, this tissue was deposited in the same area in the outer cortex in successive growth cycles. Klein and Sander (2007) also report that in the largest individuals, the lamellar regions of the outermost cortex show only longitudinal primary osteons, which occur in lower densities. In areas where an EFS is visible, the bone is avascular.

Average osteocyte density (1100-1300 cells/mm^2; see Table 2.2) is much lower in *Plateosaurus* compared to any other ornithodiran observed above (see Discussion section below). Osteocyte organization varies with fibrillar organization (Figure 2.64, note arrows and triangles). In regions of woven-fibered bone, osteocyte lacunae show no preferred orientation relative to the long axis of the bone, and show no preferred arrangement relative to each other. In regions of parallel-fibered bone, osteocytes are oriented more or less perpendicular to the long axis of the bone, and are organized circumferentially. They also occur in slightly lower densities compared to regions of woven-fibered bone.

Discussion: Klein and Sander (2007) reported fibro-lamellar bone as the commonest primary bone tissue observed in the long bones of *Plateosaurus*, and they did not discuss the parallel-fibered component in detail. However, given that all primary canals are primary osteons, that the bone is either woven-fibered or a mix of woven- and parallel-fibered tissue, and that their sample size was larger than mine, I do not think our diagnoses are in disagreement. However, this highlights an issue with the use of terms such as "fibro-lamellar bone", which do not include the precision necessary to address the complexity of some bone tissues adequately.

The low osteocyte densities observed in *Plateosaurus* may result from differences in adult body mass (the two sauropodomorphs are the largest taxa examined in this study), in addition to the lack of juveniles in the dataset. *Massospondylus* (see below) shows comparable osteocyte densities in an adult specimen (BPI 5241a), but the juvenile (BPI 5253a) shows a much higher average osteocyte density (2692 cells/mm^2).

Massospondylus carinatus

Specimen number and elements: BPI/1/5253a, BPI/1/5241a, BPI/1/4777a (all femora)
Locality: Farm Upper Drumbo, Barkly East District, Eastern Cape Province, South Africa
Formation and age: Upper Elliot Formation, Hettangian-Sinemurian (Olsen and Galton 1984)

Taxonomic comment: A second species, *Massospondylus kaalae*, is also known from the Upper Elliot Formation of Eastern Cape Province, South Africa (the holotype locality is near Voyizane village in Herschel District; Barrett 2009), but this species is known only from one specimen. It is possible that the specimens I examined may include individuals of *M. kaalae*, but the sections I examined are taken from partial (BPI/1/5253, BPI/1/4777) or very complete skeletons (BPI/1/5241) that have always been regarded as *M. carinatus*. Furthermore, BPI/1/5241 was included by Barrett (2009) as an exemplar of *M. carinatus* in the original description of *M. kaalae*. Future work, including the discovery and description of any postcranial material of *M. kaalae*, will need to be completed before this question is resolved, but in this study I refer these materials to *M. carinatus* following previous authors.

Prior histological analyses: Reid (1990) briefly described the femoral and rib histology of *Massospondylus* as part of a larger study on zonal growth in dinosaurs. Chinsamy (1993a) was the first to describe the histology of this taxon in detail, based on an ontogenetic series of femora. Subsequently, she has reanalyzed the materials as part of several studies of dinosaur and ornithodiran growth (Chinsamy 1993b, 1994, Chinsamy-Turan 2005). Lee (2007) constructed growth curves for *Massospondylus* using Chinsamy's original sections, but did not examine other aspects of its microstructure. I redescribe three of Chinsamy's original sections here, and add new information on cortical dimensions and measurements of osteocyte density. Additionally, I figure the histology in cross section for the first time.

Histological observations: The femoral mid-diaphysis is subtriangular (BPI/1/5253a, BPI/1/4777a) to subrectangular (BPI/1/5241a) in cross section, with a circular to oval medullary cavity that sits centrally (Figures 2.65, 2.66, 2.67). No cancellous bone is visible in the medullary cavity of BPI/1/5253a (Figure 2.65), but erosion rooms are visible around the endosteal margin in both BPI/1/4777a (Figure 2.66) and BPI/1/5241a (Figure 2.67). These regions clearly formed by the resorption of primary cortical tissues; primary bone is visible between erosion rooms and shows no secondary osteons. Erosion rooms are more numerous and extend further into the inner cortex of BPI/1/5241a; this may relate to its larger size and presumably older age.

In the smallest specimen, BPI/1/5253a, the cortical histology is fairly uniform. The primary tissue of the cortex is almost entirely composed of woven-fibered bone (Figures 2.68, 2.69); only at the periosteal surface does it become more parallel-fibered (2.69, bottom image). Nearly all vascular canals are primary Haversian cavities (the earliest stage of primary osteonal development, in which the initial scaffold has been deposited but the canals have not yet been compacted, see Francillon-Vieillot et al. 1990 and Discussion section below), but a few primary osteons are visible in the innermost cortex. Though at low magnifications, the dominant canal orientation seems circumferential (Figure 2.65), the majority of canals in this specimen are actually longitudinal. These extensively anastomose in a circumferential direction to form a laminar pattern. At higher magnifications, it is clear that the longitudinal canals form first (Figure 2.68, note triangles) and later anastomose, usually circumferentially. Radial canals are also visible in this femur (Figure 2.65; Figure 2.69, top image), some of which extend nearly the entire breadth of the cortex (Figure 2.65). In the inner cortex, canal diameter is much larger than in the outermost cortex (Figure 2.69). Osteocytes in the woven-fibered portions of the bone are very disorganized; osteocyte lacunae show no preferred orientation relative to the long axis of the bone, and show no preferred arrangement relative to each other (Figure 2.69, top image). Close to the periosteal surface, osteocytes show more organization, they tend to be arranged circumferentially and encircle canals. In this region, most osteocyte lacunae are oriented more or less perpendicular to the long axis of the bone, but at least 20% are oriented obliquely. As mentioned above, osteocyte density (2692 cells/mm^2) is high compared even to most other ornithodirans examined in this study.

The mid-diaphyseal femoral microstructure of the larger individuals is quite similar among specimens. In contrast to the description of Chinsamy (1993), most of the cortex in each individual is not woven, but composed of parallel-fibered bone. This is easily confirmed in polarized light (Figure 2.70, note lack of colorful cross-hatching in lower image) and

consistent with patterns of osteocyte orientation and arrangement (Figure 2.71). Some regions of the inner cortex of BPI/1/4777a show a mix of woven-fibered and parallel-fibered bone as in *Plateosaurus* (see above), and the outermost cortex of BPI/1/5241a is lamellar. Ten growth marks are preserved in BPI/1/4777a and 13-14 are visible in BPI/1/5241a. These are usually LAGs, but locally they may become annuli of organized parallel-fibered bone or disappear.

Most of the vascular canals in this section are simple primary canals, but primary osteons are also scattered throughout the entire cortex. As in BPI/1/5253a, longitudinal canals anastomose circumferentially with many other canals, giving a plexiform appearance at low magnification (Figure 2.70). In the inner half of the cortex, these laminae appear somewhat wavy. They become straighter periosteally. In the outermost cortex, canal diameter, density, and connectivity all decrease dramatically (Figure 2.71). Here, isolated canals are common, many of which are primary osteons. Where anastomoses occur, they may link up to five canals in any direction and form small reticulations.

Osteocyte density is higher in the inner cortex than in the outer cortex (Figure 2.70), but in both regions, all the lacunae are oriented perpendicular to the long axis of the bone and align circumferentially. Although osteocytes commonly encircle vascular canals, they rarely form distinct lamellae. Compared to the inner cortex, osteocyte lacunae are more evenly spaced in the outer cortex, and line up along lamellae (Figure 2.71, bottom of lower image). As in *Plateosaurus*, BPI/1/5253a shows much lower average osteocyte densities (1191 cells/mm^2) compared to most other ornithodirans examined in this study. Osteocyte density was not measured in BPI/1/4777a, but appears intermediate to those observed in the larger and smaller individual.

Discussion: I disagree with Chinsamy (1993) about the tissue type visible in *Massospondylus*. While I agree that woven-fibered bone is common in the cortex of BPI/1/5253a, and present locally in the inner cortex of BPI/1/4777a, most of the cortex in the two larger individuals is parallel-fibered. Additionally, though primary osteons are present, most of the canals seem to be simple primary canals. Therefore, I do not agree with her assessment that this taxon is characterized by fibrolamellar tissue, at least based on these individuals. The woven component is not present in the larger individuals, and the lamellar component is not commonly present except in the outermost cortex of the largest individual sampled. It is also clear from these three individuals that no single histological type characterizes the entire ontogeny of *Massospondylus*. As in the other archosaur taxa described above, an ontogenetic transition to the deposition of slower-growing tissues is observed. Finally, Chinsamy (1993) reported that secondary osteons were common throughout the cortex of some individuals; I do not observe them. However, she observed more specimens than I did, including several larger individuals.

SAURISCHIA: THEROPODA

All remaining taxa in this study are part of the clade Theropoda (see Figure 2.1, node 10 for phylogenetic position), although the position of *Herrerasaurus* has been disputed because some do not recognize it as a saurischian or even a dinosaur (refs).

Herrerasaurus ischigualastensis
Specimen number and elements: MCZ 7064 (humerus and tibia)
Locality: A.S. Romer 1958 site, 1 km northwest of Arroyo de Agua, San Juan Province, Argentina.
Formation and age: Ischigualasto Formation, late Carnian (Martinez et al. 2011)

Prior histological analyses: The bone histology of the humerus and tibia of *Herrerasaurus* was analyzed but not described by Padian et al. (2001) as part of a study of dinosaurian growth rates. Later, these specimens were briefly described by de Ricqlès et al. (2003b) and additionally figured by Padian et al. (2004). Additional long bone material was also briefly described by de Ricqles et al. (2008) as part of a larger study of archosaur growth and histology. Unfortunately, the material used in the 2008 study was not identifiable to element, so I cannot confirm its assignment to this taxon or that its sampling position is homologous. Here, I provide the first detailed description of the original humeral and tibial slides described by de Ricqles et al. (2003b), and add new information on cortical dimensions and measurements of osteocyte density. Because I only had access to the specimens for a few days, I was only able to image each section in regular transmitted light.

Histological observations: Only half of the cortex is preserved for both the humerus and the tibia of MCZ 7064. In both specimens, the medullary cavity was filled by a mudstone or claystone matrix after deposition and the endosteal margin is lined with a band of lamellae. The maximum preserved thickness of this band is 0.25 mm in the humerus and 0.54 mm in the tibia. In the humerus, cracks are visible running through this endosteal layer; these run along lamellae and are so distinct that they might initially be confused with growth or resorption lines. At least in the half of the bone preserved, trabeculae do not extend into the medullary cavity in either element. There is no indication that trabecular struts branched off the endosteal lamellae, and no trabecular remnants are visible within the matrix infill. Resorption of at least some tissue from earlier ontogenetic stages has taken place in both elements; neither preserves neonatal tissues. Additionally, the endosteal lamellae cut across primary cortical tissues at such as strong angle (based on the orientation of vascular canals) that they could not possibly be following the original endosteal margin. Secondary osteons are not visible in either element.

The microstructure of the humerus of MCZ 7064 is fairly uniform throughout the cortex. Only woven-fibered primary bone tissue is present. This tissue is well vascularized by primary osteons. In the innermost cortex, these almost always anastomose with several other canals, forming reticulations and regions of plexiform bone. In the midcortex, fewer canals anastomose in general, and the vascular pattern changes along the circumference. In one region, reticulations or radial anastomoses link five to seven canals amid many isolated longitudinal primary osteons, but on the other side of the section, the pattern is more laminar and few radial anastomoses are present (the “more circumferentially oriented” region of de Ricqlès et al. [2003b: p. 94]) . In the outer cortex, the humerus is cracked heavily around at least half of the preserved section. Where the original cortex is visible, half of the preserved section is formed of laminar bone as in the midcortex. Moving around the circumference, the circumferential canals become shorter and shorter until the pattern becomes one of mostly isolated canals, with very few reticulations linking three or four canals. Most of the surface is

abraded; however, in one region, 2 mm of a single LAG is preserved very close to the periosteal surface. This LAG does not lie within an annulus of lamellar or parallel-fibered bone, and the surface is abraded external to it. It is possible that more LAGs were present in life. I do not observe a thin avascular layer resembling an EFS at the periosteal surface, in contrast to the observations of de Ricqlès et al. (2003b).

Throughout the humeral cortex, osteocyte lacunae orbit canals along lamellae (1-3 per primary osteon). In the interstices between canals, the osteocytes show no preferred orientation relative to the long axis of the bone and no preferred arrangement relative to each other. In more laminar regions, the osteocytes tend to cluster at the center of the lamina, but where the primary osteons are reticular or longitudinal, they are evenly distributed among the canals. Osteocyte density in this element (1709 cells/mm^2) is higher than that observed in the sauropodomorphs, but lower than that of most other ornithodirans. Osteocyte density is similar throughout much of the cortex; it declines only in the outermost cortex.

The tibia of MCZ 7064 is fairly similar histologically. It is mainly composed of woven-fibered bone and is well vascularized by primary osteons through much of the cortex. As in the humerus, about half of the cortex shows more vascular connectivity than the other half; however, there are more isolated longitudinal canals throughout the section than observed in the humerus, and the anastomoses (reticular or circumferential) link fewer canals. As in the humerus, 1-3 lamellae surround each primary osteon, and osteocytes align along these lamellae. The osteocytes in these regions are all oriented perpendicular to the long axis of the bone. In the interstices between canals, the osteocytes show no preferred orientation relative to the long axis of the bone and no preferred arrangement relative to each other. This is the case regardless of the vascular pattern observed. Overall, osteocyte density is higher in the tibia (1972 cells/mm^2) than in the humerus. As in that element, osteocyte density is fairly similar throughout much of the cortex, declining only in the outermost cortex.

The main difference between the tibia and humerus is visible in the outermost ~1mm of the tibia. At that point, there is a thin (~.5mm) band of short, radially-oriented primary canals extending around most of the preserved circumference. This region is similar to the radial canals observed external to the fourth LAG in the larger *Psittacosaurus* tibia (PIN 698/5-9/2/1946) described above; they are much shorter than the long radial canals visible close to the periosteum in that specimen. Here, the interstitial tissue surrounding the radial canals shows higher osteocyte density compared to the inner and midcortex, and the canals are slightly larger in diameter. These features are all consistent with faster growth regimes during the time of deposition of this bone tissue. An annulus of parallel-fibered to lamellar bone is preserved on each side of this band of short radial canals. They extend laterally and eventually merge, and show only short, regional breaks in the tissue. External to the annulus, the density and pattern of the vascular canals change. A thin zone separates the annulus from a double LAG; this zone preserves two circumferential rows of longitudinal canals, most of which are simple primary canals. A few primary osteons are present in this region, which are surrounded by a single lamella. This double LAG is separated from the next double LAG by a zone approximately 0.1 mm thick; it contains a single circumferential row of longitudinal primary osteons. The bone here is more organized; it is parallel-fibered in some areas and lamellar in others. This cycle repeats itself at least once and possibly twice more; the external surface is abraded and it is difficult to trace LAGs circumferentially. In total there are either

four or five growth marks, which are closely packed near the surface and likely constitute an EFS.

Discussion: Although only the tibia of MCZ 7064 shows evidence of an EFS (contra de Ricqlès et al. 2003b), both elements show a vascular indication of slowed growth approaching the outermost cortex. As de Ricqlès et al. (2003b) noted, no LAGs are visible in the deep cortex of either element, though the medullary cavities are large enough that early growth marks may have been eroded. Additionally, de Ricqlès et al. (2003b) figured several bright lines in the tibial cortex that might at first seem to indicate cyclical growth. These are not "bright lines" *sensu* Currey 1962 - they are not visible at higher magnification and are not associated with any histological change (e.g., in fibrillar organization, canal pattern, or osteocyte density). Therefore, I follow de Ricqlès et al. (2003b) and do not consider them annual. Regardless of whether the medullary cavity expansion obliterated an earlier LAG, it is clear that this individual of *Herrerasaurus* finished the active phase of skeletal growth in a relatively short time relative to the other dinosaurs examined so far.

Tawa hallae

Specimen number and elements: GR 155 (femur), GR 257 (tibia). GR 155 is part of an associated individual and one of the paratype specimens of *Tawa hallae* (Nesbitt et al. 2009a). These elements were found in different sites within the Hayden Quarry and were not likely from the same individual.
Locality: Hayden Quarry 2 (GR 155) and Hayden Quarry 3 (GR 257), Ghost Ranch, Rio Arriba County, New Mexico, USA
Formation and age: Petrified Forest Member, Chinle Formation, ~213 MYA, middle Norian (Irmis et al. 2011)
Prior histological analyses: None

Histological observations: As in the other Hayden Quarry elements described above, the medullary cavities (and some of the larger vascular canals) of both GR 155 and GR 257 are filled with crystals. Both specimens preserve only a single, small region of endosteal lamellae. In GR 155 (femur), this border is visible along the medial quadrant of the endosteal margin, but is very thin (0.02 mm; one lamella). In GR 257 (tibia), this region is confined to a 0.7 mm strip along the lateral portion of the endosteal margin and is 0.05 mm thick (four distinct lamellae). It is not clear how much of the original endosteal margin was lost to crystallization of the medullary cavity in either specimen; the regions that preserve endosteal lamellae are comparable in cortical thickness to the rest of the cortex. No trabeculae extend into the medullary cavity at mid-diaphysis (again, this could be a result of crystal infill). No secondary osteons are visible in cortex of either specimen.

The femoral cortex of *Tawa hallae* is subcircular at mid-diaphysis, with a large circular medullary cavity that sits centrally (Figure 2.72). The inner cortex is composed of woven-fibered primary bone tissue and shows three growth marks (two annuli and a LAG; note arrows in Figure 2.73). The inner annulus is composed of parallel-fibered bone and lies about one third the distance between the endosteal margin and the periosteal border (this is the case on the anterior, medial, and posterior sides; it is close to the endosteal border laterally).

External to this annulus, the bone again is woven-fibered until midcortex. Here, the bone again transitions to a parallel-fibered (regionally, lamellar) annulus. Laterally, this growth mark becomes a double annulus, but these merge back into a single annulus around the rest of the circumference. External to the second annulus, the bone is generally parallel-fibered or very weakly woven. Close to the periosteal border (0.15-0.25 mm internal to it), a distinct single LAG is visible. External to the LAG, the bone is regionally lamellar or weakly parallel-fibered.

In the woven-fibered regions internal to the first growth mark, the bone is well vascularized by primary osteons and a few simple primary canals. As in most of the other Hayden Quarry specimens, the primary osteons are each ringed by a single distinct lamella. The canals are predominantly longitudinal, but many anastomose with one to five other canals. These anastomoses occur in all directions and form small reticulations in the anteromedial quadrant. Within the inner annulus, vascular density and connectivity decrease slightly. In the zone between the first and second annuli, the canals of the woven-fibered region are very similar to the one in the woven-fibered region internal to the first annulus. The density of longitudinal canals does not decrease approaching the second annulus, but connectivity between canals does. The longitudinal canals closest to the second annulus are more likely to be simple primary canals than primary osteons. The second annulus is nearly avascular; only a few longitudinal simple primary canals pierce it. Between the second annulus and the LAGs, the bone is moderately vascularized and most canals are longitudinal simple primary canals. These align in circumferential rows in the anterior cortex, and here they sometimes anastomose circumferentially. Elsewhere they are more irregularly distributed. External to the LAG, the canals are all simple primary canals. Most of these are longitudinal and very few anastomose. Moving from the anterior cortex to the posterior cortex in this region, the bone changes from moderately vascularized to poorly vascularized.

Osteocyte lacunae noticeably decrease in density and increase in organization between the innermost and outermost cortex. In the woven-fibered regions, a single row of osteocytes encircles the primary osteons along their lamellar border. However, these may be organized perpendicular or parallel to the long axis of the bone. In the interstices between canals, they show no preferred orientation relative to the long axis of the bone and no preferred arrangement relative to each other. In the parallel-fibered regions, most are oriented perpendicular to the long axis of the bone, although spacing between them may be irregular. In lamellar regions, they are very highly organized and spaced regularly along lamellae. The average osteocyte density in GR 155 (1487 cells/mm^2) is the lowest observed among all theropods; it is most comparable to *Varanus* and some individuals of *Trilophosaurus*.

The tibia of *Tawa* is circular in cross section, with an oval medullary cavity that sits centrally (Figure 2.74). The walls of the cortex are proportionately thicker than in the femur. As in the femur, three growth marks are visible. All three of these are double LAGs for much of their circumference; the innermost becomes a single LAG along posteriorly, and the outermost becomes indistinct posteromedially and again laterally (Figures 2.75 and 2.76, note arrows). Internal to the inner LAG, the zone shows woven-fibered bone in the innermost cortex; this becomes more parallel-fibered in the outer half of this zone (Figure 2.75, note color change in upper left of bottom image). Approaching the inner LAG, the bone forms a thin annulus of parallel-fibered bone. This annulus is also visible on the other side of the inner LAG, but here it looks more lamellar. The zone between the inner and middle LAGs is

mostly composed of parallel-fibered bone, but some weakly woven bone is visible in the anterior cortex. Approaching the middle LAG, the bone becomes lamellar; the annulus remains lamellar on the other side of the middle LAG. The zone between the middle and outer LAG is mostly composed of parallel-fibered bone. This becomes more lamellar approaching the outer LAG. The outer LAG lies very close to the periosteal surface and regionally shows no break in tissue. Not much bone tissue is preserved between the outer LAG and periosteal surface; all of it is lamellar.

Internal to the first LAG, all the vascular canals are primary osteons surrounded by a single distinct lamella. Infrequently, they anastomose circumferentially with another canal. The canals of the woven-fibered region (i.e., the innermost cortex) have a larger diameter than those in the outer half of this zone. These canals are usually only two to three times wider than the canals in the rest of the cortex, but in the region closest to the endosteal lamellae, they may be up to five times the width of the other canals (compare canal diameter in upper right of Figure 2.75 with those in the lower left of Figure 2.76). It is not likely that these canals were enlarged as a result of crystal infilling; each preserves its lamella and does not show any indications of resorption. Additionally, these are the oldest canals preserved in the section and have had the longest time to mature; one might expect these to have the narrowest diameter (Starck and Chinsamy 2002). It is possible that this woven-fibered region preserves perinatal tissues; the medullary cavity of this specimen is only 3.33 mm wide. In the parallel-fibered portion of this zone, the bone is only moderately vascularized around most of the circumference (it remains well vascularized in the anterior quadrant).

The zone between the inner and middle LAG is moderately vascularized around most of the circumference (it is well vascularized in the anterior quadrant). The canals are nearly all longitudinal; they are primary osteons everywhere but the medial quadrant, where they are simple primary canals. The canals form radial rows in the anterior quadrant but show no pattern elsewhere. Very few canals anastomose in this zone. The zone between the middle and outer LAG is moderately vascularized by longitudinal simple primary canals (mostly) and primary osteons. These are more or less arranged into two or three circumferential rows. External to the outer LAG, the bone is poorly vascularized by a single row of longitudinal simple primary canals, or locally avascular.

The osteocytes of the tibia are generally better organized than those of the femur; this results from a greater proportion of parallel-fibered and lamellar bone in this section. As in the femur, the woven-fibered regions of the tibia show a single row of osteocytes encircling each primary osteon along its lamella. They may be organized perpendicular or parallel to the long axis of the bone. In the woven-fibered interstices between canals, they show no preferred orientation relative to the long axis of the bone and no preferred arrangement relative to each other. In the parallel-fibered regions, the osteocytes are oriented perpendicular to the long axis of the bone, although spacing between them is irregular (as in the femur). In lamellar regions, lacunae are oriented perpendicular to the long axis of the bone and align along lamellae with regular spacing between them. Osteocyte density is higher in this tibia than in the sampled femur (1708 cells/mm^2), but still lower than all other theropod elements sampled except the humerus of *Herrerasaurus* (if it is a theropod).

Discussion: The femoral and tibial histology of *Tawa hallae* suggests different ontogenetic trajectories for these elements. The femur (GR 155) preserves woven bone in its inner two

zones; this type of tissue is largely confined to the innermost cortex of the tibia, within its innermost zone (GR 257). The femur shows higher levels of vascular connectivity throughout the cortex compared to the tibia, and vascular density decreases less dramatically in the femur compared to the tibia. Additionally, the inner two growth marks are annuli in the femur (indicating a slowdown but not complete stoppage of growth), whereas all growth marks are LAGs in the tibia (indicating growth stoppages at the end of each year). Together, these histological indicators suggest that the femur maintained relatively faster growth than the tibia throughout much of its ontogeny.

Assuming that the tibia does preserve perinatal tissues in its innermost cortex, GR 257 was in its fourth year at the time of death. Estimating age for GR 155 is more difficult; perinatal tissues are not preserved, and the element has a lower RBT (i.e., it is hollower and may have resorbed more of the bone deposited early in ontogeny). The femur of *Tawa* is more robust externally than the tibia at mid-diaphysis (personal observation), but establishing whether or not it was similarly hollow would require sectioning both elements from the same individual. Neither specimen shows an EFS, but both show decreasing vascular density and connectivity, along with increasing fibrillar and osteocyte organization. This suggests suggest that growth rates were markedly slower in *Tawa* after its first or second year of growth. However, although the third zone (i.e., the zone between the second and third LAGs) is narrower than the second in both individuals, it is not dramatically so in either case. Given that larger individuals of *T. hallae* are known from the Hayden Quarry (Nesbitt et al. 2009a), it is likely that growth continued for several years after an initial 1-2 years of faster growth.

Coelophysis bauri

Specimen number and elements: AMNH FARB uncatalogued (tibia). Slides were made by Sterling Nesbitt for use in this study.
Locality: *Coelophysis* (= Whitaker) Quarry (UCMP locality V75128), Ghost Ranch, Rio Arriba County, New Mexico, USA
Formation and age: 'Siltstone Member' of the Chinle Formation, Rhaetian (Nesbitt 2007)

Prior histological analyses: The shaft of a long bone of *Coelophysis bauri* (from the Ghost Ranch *Coelophysis* Quarry) was figured by Colbert (1995), but neither the element nor the sampling position was identified. Nesbitt et al. (2006) described the histology of the femoral proximal metaphysis of a juvenile specimen of *C. bauri*. That section was not sampled at a homologous location to most of the specimens in this study, so I do not re-examine it here. Chinsamy (1994) figured the tibial histology of *C. bauri*, but no information as to specimen number or sampling location was given. Additionally, its histology looks very different than the section figured by Colbert (1995). de Ricqles et al. (2003) and Padian et al. (2004) described the mid-diaphyseal femoral histology of a *Coelophysis* specimen from Petrified Forest National Park, AZ. This specimen, UCMP 129618, was referred by Padian (1986) to *C. bauri*, who noted that it was larger and more robust than the material from the Ghost Ranch *Coelophysis*/Whitaker Quarry. I describe this section, but refer it to "Coelophysoidea indeterminate", not *C. bauri* (see below). Chinsamy-Turan (2005) briefly described new material she sectioned from a femoral growth series of *Coelophysis*. However, the specific

epithet, locality, specimen numbers, and sampling locations were not provided. I emailed Dr. Chinsamy-Turan to request these data, but have not received a response.

Histological observations: The tibia of *Coelophysis bauri* is slightly oval in cross section, with an oval medullary cavity that sits slightly off center (Figure 2.77). The medullary cavity shows mineral crystals and signs of either bacterial or fungal invasion. However, this is largely confined to the medullary cavity, and most of the endosteal margin is preserved. A thin band of 10-11 endosteal lamellae borders the medullary cavity, and no trabecular spicules are preserved among the calcite crystals at the center of the bone. However, given the extent of the calcite and bacterial/fungal invasion, it is impossible to determine conclusively whether or not they would have been present in life.

The microstructure of the cortex is fairly uniform and is almost entirely composed of woven-fibered primary bone tissue (Figure 2.78, note color pattern in bottom image); only the outer 0.5 mm is composed of parallel-fibered bone. Two growth marks are visible in this section (Figure 2.77, note arrows); the first lies in the inner cortex and is an annulus that only regionally grades into a LAG. The second annulus sits 0.1 mm from the periosteal surface and shows a break in the tissue around more of the circumference. All but the outermost 0.5 mm is well vascularized; that region is only moderately vascularized. Nearly all of the canals are longitudinal primary osteons, and each canal is lined with a single distinct lamella. Rarely, short anastomoses connect two longitudinal canals circumferentially or slightly obliquely (Figure 2.78, upper left of both images; Figure 2.79, lower half of image). These anastomoses occur more frequently in the inner cortex. Osteocytes encircle the outer margin of the lamellae of each vascular canal. These show no preferential orientation relative to the long axis of the bone. The osteocytes of the interstices between canals tend to be arranged parallel to the long axis of the bone, although oblique and perpendicular osteocytes are also present. These interstitial osteocytes show no preferred arrangement relative to each other and are spaced irregularly. Average osteocyte density is high in this specimen (1849 cells/mm^2); it is consistent through most of the cortex except for the parallel-fibered region external to the second growth mark, where it decreases slightly.

Megapnosaurus rhodesiensis

Specimen number and elements: Figured and analyzed for osteocyte density: NMZB QG 715, NMZB QG 726. I also examined a growth series of femora including BPI QC6T and the following NMZB specimens: QG 45, QG 174, QG 715, QG 726, QG 727, QG 753, but do not figure them or report osteocyte densities.

Locality: Chitake River quarry, near Nyamandhlovu, Tsholotsho District, Matabeleland North, Zimbabwe

Formation and age: Forest Sandstone Formation, Karoo Group; Hettangian-Sinemurian (Olsen and Galton 1984)

Prior histological analyses: Raath (1977) described the bone tissues of a growth series of tibiae, and Chinsamy (1990) described the microstructure of a growth series of femora of *Megapnosaurus* (formerly *Syntarsus*) *rhodesiensis*. Later, Chinsamy (1993b, 1994) reanalyzed the femoral sections as part of larger studies of dinosaurian vascularization and

growth. Raath (1977) did not report where on the tibia his sections were made, so I do not discuss the tibial histology. Some but not all of these specimens made by Chinsamy were cut precisely at mid-shaft; the remaining were cut from more distal locations on the diaphysis. Based on the cross-sectional geometry and mid-diaphyseal measurements provided by Raath (1977) and Chinsamy (1990), I confirmed that several specimens were sampled at the femoral mid-diaphysis. I redescribe these slides, adding new information on cortical measurements and osteocyte density. I include illustrations for comparison with the other coelophysoids in this sample, but because Chinsamy has illustrated this taxon extensively, I do not figure *M. rhodesiensis* extensively.

Histological observations: The femur of *Megapnosaurus rhodesiensis* is subtriangular at the mid-diaphysis in cross section, with a slightly rounder medullary cavity that lies more or less centrally (Figure 2.80). None of the femoral specimens of *M. rhodesiensis* sectioned preserve trabeculae at the mid-diaphysis (Chinsamy 1990). In all specimens examined, invasion of the medullary cavity by mineral crystals and mudstone matrix destroyed most of the original endosteal surface. However, in most individuals (e.g., NMZB QG 174, NMZB QG 726, NMZB QG 727, and NMZB QG 753), endosteal lamellae do line the intact portion of the inner bone surface.

The smallest individual (NMZB QG 45) has extensive post-fossilization compressive cracking and matrix infill of the medullary cavity and vascular network. The cortical microstructure is quite uniform. Almost the entire cortex consists of woven primary bone tissue. As Chinsamy (1990) reported, there is one LAG, which sits at midcortex on the outer margin of a narrow annulus of parallel-fibered bone. The bone is well vascularized by longitudinal primary Haversian cavities. In the innermost cortex, canals anastomose circumferentially (sometimes radially or obliquely) with one or two other vessels. In the mid- and outer cortex, the canals do not anastomose. Throughout most of the cortex, the osteocyte lacunae show no preferred orientation relative to the long axis of the bone, and no preferred arrangement or spacing relative to each other. This is true for the interstitial areas between canals and also around the vast majority of the canals; most canals are not orbited by osteocytes. Within the annulus, the osteocytes are all oriented perpendicular to the long axis of the bone and arranged circumferentially, although spacing between cells remains irregular. Because this individual lacks lamellar tissue surrounding its canals, I disagree with Chinsamy's (1990) assessment that *C. rhodesiensis* produced true fibrolamellar bone, at least in its first two years.

In individuals approximately twice the mid-diaphyseal diameter of NMZB QG 45 (BPI QCT6, NMZB QG 174, NMZB QG 715, NMZB QG 727), the cortex is also mainly composed of woven primary bone tissue. In the outermost cortex of these specimens, parallel-fibered bone is visible (either regionally or around the entire circumference, depending on the specimen). I observed a single LAG in NMZB QG 727 (very close to the periosteal surface), and two LAGs in both NMZB QG 174 and BPI QC6T (one in the inner/midcortex and one close to the outer surface). I could not find any LAGs preserved in BPI QG 715. At low magnification, three bands are visible in this specimen (Figure 2.80, note arrows) but no break or change in tissue can be observed at higher magnifications (Figure 2.81). However, the bands refringe brightly under polarized light at lower magnification, and the outer two bands can be traced around the entire circumference (the medullary cavity cuts across the inner

band). Because there is no change in tissue type or deposition (although there may be a change in mineralization), I do not consider these bands to be annuli.

In all four individuals, longitudinal primary osteons are the dominant canal type (Figure 2.81), though some simple primary canals are visible in each specimen, especially in the outer cortex. Additionally, canals anastomose more frequently compared to QG 45 (again, generally these are circumferential), and the area where anastomoses are present usually extends into the outer cortex. Within this size class, the number of canals that anastomose, and the number of canals linked by anastomoses both increase with size. The smallest individual in this group, NMZB QG 715, shows the least amount of vascular connectivity and the fewest primary osteons. In this specimen, anastomoses connect 2-4 longitudinal canals and, averaged across the entire section, about half the canals are true primary osteons with a distinct lamella. The primary osteons are regionalized in their distribution; in some areas they are rare, and in others, most of the canals are primary osteons (the latter situation is the case for the region shown in Figure 2.81). NMZB QG 727 is similar in vascular patterning compared to NMZB QG 715, but a greater percentage of its canals are primary osteons, and these are more evenly distributed around the section. In the inner and midcortex of BPI QC6T, most longitudinal primary osteons anastomose circumferentially with 3-8 other canals, and many anastomose radially as well. In the inner cortex, the anastomoses are more similar in extent to those observed in NMZB QG 715 and NMZB QG 727. In these specimens, nearly all of the longitudinal canals bear a single lamella, but most of the anastomoses are unlined. NMZB QG 174 is most similar histologically to that of NMZB QG 715 and NMZB QG 727 in terms of its canal type and vascular patterning

Throughout the entire cortex, specimens in this size category usually have multiple layers of osteocytes encircling longitudinal and circumferential primary osteons, even though there is only one lamella with a distinct cement line for each. In woven-fibered regions, the osteocytes in the interstices between canals have no preferred orientation relative to the long axis of the bone, and no preferred organization or arrangement relative to each other.

Bordering its medullary cavity, NMZB QG 174 preserves one small region of endosteally derived primary woven bone tissue between two layers of lamellar bone. This tissue is somewhat similar histologically to the endosteal woven-fibered region in the femur of *Pterodactylus* (CM 11340, described above). As in CM 11340, this region is composed of well-vascularized compacted cancellous bone and lined with a second set of endosteal lamellae. Each canal is longitudinal and surrounded by many lamellae to form a large osteonal unit. These lamellae never overlap each other and the resorption line separating them from the interstitial bone is not scalloped. The interstices between canals are composed of primary woven bone tissue. It is difficult to ascertain the order of deposition for this region relative to the cortical bone. Unlike CM 11340, the innermost lamellae cut across the endosteally derived tissues and are confluent with the endosteal lamellae that border the adjacent regions. The more periosteal set of lamellae cuts across some of the osteons within the endosteal woven bone, but also, one of the endosteal osteons cuts into that same lamellar region, confusing the order of deposition. Because the innermost layer of lamellar bone is confluent with the lamellae lining the rest of the endosteal border, I suggest that this region results from cortical drift.

The two largest specimens, NMZB QG 753 and QG 726, show signs of dramatically slowed growth late in life. These are the only specimens that show cortical remodeling at the

femoral mid-diaphysis. In NMZB QG 726, the longitudinal canals of the inner cortex are slightly expanded, with rough edges, suggesting incipient secondary osteon or erosion room formation (Figure 2.82, note large circular canal at bottom of image). In NMZB QG 753, erosion rooms, secondary osteons, and expanding canals (incipient secondary osteons) are visible in the inner third to half the cortical diameter. These are subcircular to subtriangular in shape and are usually lined with 1-3 lamellae.

In both specimens, a gradual transition in fibrillar organization occurs, from woven-fibered bone (in the deep cortex) to parallel-fibered bone (in the mid- and outer cortex) to lamellar bone in the outermost cortex. The region of lamellar bone is about twice as wide in NMZB QG 753 as NMZB QG 726. Two LAGs are preserved in NMZB QG 726; both are double LAGs around at least part of the circumference, although the inner one locally grades into an annulus (Figure 2.82, note arrows). In NMZB QG 753, two annuli and two LAGs are present. In both specimens, the primary bone of the inner cortex is moderately vascularized; as Chinsamy (1990) reported, the lamellar bone of the outer cortex is poorly vascularized or nearly avascular. As in the other specimens of *M. rhodesiensis*, both simple primary canals and primary osteons are present. In the inner and midcortex, primary osteons are more common than simple primary canals, and in the outer cortex, simple primary canals are more common than primary osteons (Figure 2.82; note change in canal type moving up the image). The canals of the outer cortex are smaller in diameter than in the inner and midcortex, and anastomoses are absent in this region.

Osteocytes encircle all canals throughout the section. The interstitial osteocytes of the deep cortex show no preferred orientation or arrangement, but they become progressively more organized moving periosteally, corresponding to the increase in fibrillar organization. Average osteocyte density is comparable in the two specimens examined (2473 cells/mm^2 in NMZB QG 715 and 2492 cells/mm^2 in NMZB QG 726); it does not change through the cortex. This is higher than that observed for *Coelophysis bauri*, and is more similar to that observed in silesaurids, ornithischians, and birds (see below).

Discussion: In general, the femora in this sample increasingly show signs of slowed growth with size, except the two largest femora, NMZB QG 753 and NMZB QG 726. NMZB QG 726 is slightly larger, but only has canal expansion in the inner cortex (incipient secondary remodeling). NMZB QG 753 has secondary osteons and a proportionately thicker layer of endosteal lamellae at the periosteal surface. Therefore, NMZB QG 753 was likely ontogenetically older than NMZB QG 726, even though the diameter of the latter is slightly larger.

I disagree with Chinsamy (1990) regarding the number of LAGs preserved in several of these specimens. She reported three LAGs in NMZB QG 715, and four in both BPI QCT6 and NMZB QG 727. I could not find any LAGs preserved in NMZB QG 715. I found one LAG preserved in NMZB QG 727 (very close to the periosteal surface) and two in BPI QC6T (one in the inner/midcortex, and one close to the outer surface). Chinsamy (1990) distinguished between LAGs (exhibiting a depositional hiatus and break in tissue) and annuli (exhibiting a tissue change but no break in tissue). I cannot account for these differences in LAG counts.

Chinsamy (1990) also reported extensive fibrolamellar bone at all stages of growth in this taxon. Here, I disagree somewhat. In NMZB QG 45, the bone is woven-fibered but nearly

all canals are simple primary canals (no lamellar component). In the four "mid-sized" specimens, fibrolamellar bone tissue is certainly present, but the use of this diagnosis implies that only primary osteons are present, when in actuality, simple primary canals are present as well. As in most taxa examined in this study, the bone microstructure changes in appearance and composition through ontogeny; one term cannot describe the animal through its lifespan.

***Coelophysoidea* indeterminate**
Specimen number and elements: GR 256 (femur)
Locality: Hayden Quarry 4, Ghost Ranch, Rio Arriba County, New Mexico, USA
Formation and age: Petrified Forest Member, Chinle Formation, ~212 MYA, middle Norian (Irmis et al. 2011)

Specimen number and elements: UCMP 129618 (femur)
Locality: UCMP locality V82250 (Inadvertent Hills/Dinosaur Hill), near Lacey Point, Petrified Forest National Park, Apache County, Arizona, USA
Formation and age: Petrified Forest Member, Chinle Formation, middle Norian (Riggs et al. 1996)

Taxonomic comment: Padian (1986) referred UCMP 129618 to *Coelophysis bauri*, but noted differences between this specimen and *C. bauri* from the *Coelophysi*s/Whitaker Quarry. At the time, the classic *Coelophysis* material was under study by E.H. Colbert, so extensive comparisons could not be made. With the recent discovery of new specimens from Petrified Forest, it is clear that these and UCMP 129618 are larger and more robust than the *Coelophysi*s/Whitaker Quarry specimens, in addition to being separated temporally (Nesbitt et al. 2007). Because of these differences, Nesbitt et al. (2007) referred UCMP 129618 to *Coelophysis* but did not assign a specific epithet, pending a thorough description of the new material. The same approach was taken by de Ricqlès et al. (2003b) and Padian et al. (2004). The Hayden Quarry coelophysoid is known from many isolated and associated elements from Hayden Quarry 4 (personal observation). It is has not been formally described, but based on postcranial evidence available at the time, Irmis et al. (2007) and Nesbitt et al. (2009a) noted that it was similar to *C. bauri* from the *Coelophysi*s/Whitaker Quarry. Given that the Hayden Quarry coelophysoid and the Petrified Forest coelophysoid both occur in the Petrified Forest Member of the Chinle Formation, these specimens could represent the same taxon. However, because neither has been included in a formal phylogenetic analysis, I adopt a more conservative approach and refer them both to Coelophysoidea indeterminate.

Prior histological analyses: Two other coelophysoids, *C. bauri* and *M. rhodesiensis*, have been described here and elsewhere (see above). The femur of GR 256 has not previously been described. UCMP 129618 was figured by Colbert (1995: Fig. 45, p. 153) but not described. The material was described in detail by de Ricqlès et al. (2003b, as *Coelophysis* sp.) as part of a larger study on the bone histology of Triassic archosaurs. The specimen was reviewed briefly by Padian et al. (2004) as part of a study on bone tissues and growth in small dinosaurs and pterosaurs. I redescribe the femoral histology of UCMP 129618, adding new information on cortical measurements and osteocyte density. I describe and illustrate the femoral histology

of GR 256 for the first time.

Histological observations: The mid-diaphyseal femur of GR 256 is suboval in cross section, with a subrectangular medullary cavity that sits centrally (Figure 2.83). As in the other Hayden Quarry specimens, the medullary cavity is filled with mineral crystals, which abut the endosteal margin. A thin band of lamellae is preserved around nearly the entire endosteal margin, suggesting that the crystals have not obliterated much of the original bone. There are no trabecular remnants preserved within the medullary cavity, but the extent of the crystal infilling means that I cannot exclude the possibility that they would have been present in life. Secondary osteons are present but restricted to one region of the inner cortex. The secondary osteons look somewhat indistinct in regular transmitted light, but birefringe distinctly in polarized light (Figure 2.84, note colorful region at bottom of left image).

GR 256 preserves two growth marks in the outer cortex (Figures 2.84, 2.85; note arrows). The inner mark is an annulus or double annulus around most of the section, but locally regions shows small breaks in tissue (Figure 2.85, note lower arrow). Most of the cortex internal to and between these growth marks is composed of primary woven-fibered bone; parallel-fibered bone is restricted to the annulus and the region external to the second growth mark. Most of the cortex is well vascularized by primary osteons that commonly form short anastomoses, at least internal to the growth marks. These are generally circumferential or oblique, but may also be radial. External to the outer LAG, the bone is parallel-fibered and anastomoses are not present. As in other Hayden Quarry specimens, each primary osteon exhibits a single distinct lamella. In woven-fibered regions, osteocytes in the interstices between canals show no preferred orientation relative to the long axis of the bone and no preferred arrangement relative to each other, and are irregularly spaced. Closer to canals, they tend to follow the outline of the canal (including anastomoses), but do not always orbit them. In the parallel-fibered regions of the cortex, the osteocyte lacunae are oriented more or less perpendicular to the long axis of the bone, but at least a third of them are slightly oblique. They are arranged circumferentially relative to each other, but are still spaced irregularly. Average osteocyte density for GR 256 (3364 cells/mm^2) is the highest observed for any coelophysoid.

The femur of UCMP 129618 is badly crushed at mid-diaphysis (Figure 2.86). Additionally, the original periosteal surface is abraded or missing in several regions, making it impossible to measure MSC, MSD, and MCD for this individual. However, the entire cortex is visible in some areas (e.g., Figure 2.86), so an estimate of ACT is possible. The endosteal margin is clearly lined by a thin band of lamellar bone. No trabeculae appear to extend into the medullary cavity from the endosteal border, but the fragmentation of the inner cortex has resulted in the presence of thin splints of bone scattered throughout the medullary cavity. Therefore, I am cautious in inferring a lack of trabeculae in life.

The femoral microstructure of this individual is remarkably uniform. The entire cortex is composed of primary woven bone tissue, although it is more weakly woven in the outer cortex. I could not find conclusive growth marks in this section; the fractured nature of the cortex makes it difficult to trace any lines around the circumference of the bone. The canals of the inner and midcortex are all primary osteons; these are predominantly longitudinal, but many anastomose. In the inner cortex, nearly every canal anastomoses with several others to form a subplexiform pattern (Figure 2.86, bottom third of image). In the midcortex, about one

third of the primary osteons are isolated; the rest anastomose with 1-7 other canals (this varies around the circumference of the bone). These anastomoses are most commonly circumferential or radial, and may form small reticulations (Figure 2.86, middle third of image). In the outer cortex, most of the canals are simple primary canals, though primary osteons are also visible. Here, the canals anastomose radially or obliquely, rather than circumferentially (Figure 2.86, top third of image), and generally form small reticulations. Osteocyte density is highest in the inner cortex; it decreases slightly moving periosteally. The average osteocyte density for the section is 2001 cells/mm^2, more similar to *C. bauri* than to *M. rhodesiensis* or the Hayden Quarry taxon. Though osteocyte density decreases periosteally, the osteocytes never show a preferred orientation relative to the long axis of the bone, nor are they ever regularly spaced. The lacunae only orbit canals in the inner and mid cortex.

THEROPODA: AVES: PYGOSTYLIA

All remaining taxa in this study are part of the clades Aves and Pygostylia (see Figure 2.1, node 11 for phylogenetic position).

The bones of living and fossil birds commonly form three distinct layers within the cortex (Enlow and Brown 1957). The innermost is the inner circumferential layer (ICL), a band of circumferentially oriented lamellar or parallel-fibered bone that forms the endosteal margin. The ICL is often moderately vascularized by radial canals. Similarly, an outer circumferential layer (OCL) forms periosteally, and is also composed of circumferentially oriented lamellae or parallel-fibered bone. The OCL is nearly always avascular, and it is homologous to the EFS of other tetrapods. However, unlike the EFS of reptiles examined above, the OCL of birds usually forms over a period of weeks or months, rather than years (Chinsamy-Turan 2005). Between these regions is a middle layer of periosteally deposited bone, usually reported as woven-fibered and always vascularized. Ornithuran birds do not generally produce growth marks in the middle, woven-fibered layer, because most reach full body size within a year, usually a matter of weeks or months (Chinsamy-Turan 2005); when growth marks are present, they almost always occur in the OCL (though there are exceptions, usually among birds that continue to grow after a year; see Chinsamy-Turan 2005; Turvey et al. 2005; Bourdon et al. 2009). Following established conventions of avian histology, I refer to the ICL and OCL, rather than endosteal lamellae and EFS (respectively) for the remaining taxa.

Confuciusornis sanctus

Specimen number and elements: NGMC 98-8-2 (skeleton) and MOR 1063 (thin sections; humerus, femur, tibia)
Locality: unknown; presumed to be western Liaoning Province, China
Formation and age: this specimen unknown; presumed to be Yixian Formation; Early Cretaceous (131-120 Ma; Zhou 2006)

Prior histological analyses: The bone histology of *Confuciusornis* has received considerable attention in the literature. This taxon was first sampled by Zhang and colleagues (1998, 1999),

who described the femoral microstructure and cortical dimensions, and compared it to that of three extant birds (Zhang et al. 1998) and to *Alligator sinensis* and a small theropod (Zhang et al. 1999). Later, de Ricqlès et al. (2003a) sampled most of the limb bones from a single specimen, as well as the pubis and pygostyle, in order to better characterize inter-elemental variation. The mid-diaphyseal femoral microstructure of the same specimen was reviewed by Padian et al. (2004) as part of a larger discussion of growth in pterosaurs and small dinosaurs. The tibia of a third specimen of *Confuciusornis* was figured but not described by Erickson et al. (2009a) as part of a study of paravian and avian bone histology and growth rates. Most recently, Chinsamy et al. (2013) reported medullary bone in the humerus and ulna of a fourth specimen (a tibia was also examined). For this study, I review the bone histology of *Confuciusornis sanctus* based on the materials sampled by de Ricqlès et al. (2003a), because mid-diaphyseal samples from all three major long bones used in my study were available for that specimen. I add new information on osteocyte density. Because this taxon has been so thoroughly described and illustrated in the literature, I do not figure it extensively, although I do provide representative images of each element (Figures 2.87, 2.88, and 2.89).

Histological observations: All elements examined are crushed at mid-diaphysis. de Ricqlès et al. (2003a) digitally reconstructed the humerus, femur, and tibia and found that all were round to slightly subtriangular in cross section, with a circular to subtriangular medullary cavity (de Ricqlès et al. 2003a: Figure 2B). They also established that ACT (termed bone wall thickness, or BWT, in that paper) was quite thin (0.45-1.1 mm) in *Confuciusornis*, and that its bones were much hollower than those of most nonavian dinosaurs. No trabeculae extend into the medullary cavity in any of these elements, and no broken struts of bone are visible either. Because the medullary cavity was not filled by crystals post-fossilization, I think their absence is probably real, and that they would not have been present in life in these elements at the stage of growth that was sampled. Trabeculae are not preserved at midshaft in any of the other *Confuciusornis* specimens sampled to date (Zhang et al. 1998, 1999; Erickson et al. 2009a; Chinsamy et al. 2013).

As noted by de Ricqlès et al. (2003a), the macrohistology of all three elements is similar. In each, the ICL is much thicker than the OCL, with the middle layer comprising approximately half of the cortical thickness (Figures 2.87, 2.88, and 2.89; note the relative thickness of each layer). In all three specimens, both the ICL and OCL are composed of parallel-fibered bone. The parallel-fibered bone of the ICL is better organized than that of the OCL. The middle layer is mostly composed of woven bone, but this tissue transitions to parallel-fibered bone ~0.1 mm internal to the OCL (Figures 2.87, 2.88, and 2.89; note white triangles). All three specimens preserve two LAGs; the inner LAG separates the middle layer and the OCL, and the outer LAG lies within the OCL, close to the periosteal surface (Figures 2.87, 2.88, and 2.89; note yellow arrows).

In each specimen, the ICL is crossed by several radial simple primary canals that extend from the middle layer to the medullary cavity. The woven-fibered portion of the middle layer is moderately vascularized by longitudinal primary osteons. These anastomose with other canals via short simple primary canals, which may extend in any direction and form small reticulations. In the humerus, nearly every canal in this region anastomoses with at least two other canals, but only about half of them anastomose in the femur and tibia. In the humerus, canal density is lower in the parallel-fibered region of the middle layer, but canal

patterning is similar (Figure 2.87). In the femur (Figure 2.88) and tibia (Figure 2.89), canal density decreases dramatically in the parallel-fibered region of the middle layer, and no canals anastomose.

In the ICL and OCL, the osteocyte lacunae are oriented perpendicular to the long axis of the bone, and are arranged circumferentially. Here, they are fairly evenly spaced along the long axis, but do not form even rows. In the middle layer, several layers of lacunae orbit each longitudinal canal, but they do not encircle any of the anastomoses. Some lacunae appear confluent with the anastomoses, suggesting that the anastomoses formed after the initial deposition of bone. In the woven-fibered interstices between canals, the lacunae show no preferred orientation relative to the long axis of the bone and no preferred arrangement relative to each other. They are better organized in the parallel-fibered portion of the middle layer, with most lacunae oriented perpendicular to the long axis of the bone, but they tend to be irregularly spaced relative to each other (especially compared to the ICL and OCL). Osteocyte density is consistent through the entire cortex within each element; among specimens, average osteocyte density varies. In the humerus, it is 1878 cells/mm^2, lower than the either the femur (2056 cells/mm^2) or the tibia (2341 cells/mm^2).

PYGOSTYLIA: ORNITHURAE

All remaining taxa in this study are part of the clade Ornithurae (see Figure 2.1, node 12 for phylogenetic position).

Hesperornis

Specimen number and elements: YPM PU 22443
Locality: Worland, Washakie County, Wyoming, USA
Formation and age: Teapot Sandstone Member, Mesaverde Formation; late Campanian, ~72 Mya (Gill and Cobban 1966)

Prior histological analyses: The histology of *Hesperornis* was first illustrated and the vascular patterns first described by Houde (1987), as part of a larger study of the role of histological characters in interpreting avian phylogenetic relationships. Chinsamy et al. (1998) sectioned two femoral fragments of *Hesperornis regalis* from the Niobrara Chalk (Late Cretaceous) of Kansas and provided the first in-depth description of *Hesperornis* histology. These works were reviewed by Chinsamy (2002). Because Chinsamy did not examine the histology of the tibiotarsus, I describe the histology of the section made by Houde (1987) in detail, and add new information on cortical measurements and osteocyte density.

Histological observations: Houde's (1987) original section is complete but has experienced bacterial or fungal invasion that has made some regions of the bone very dark (Figure 2.90), so microstructural observation is difficult. To compensate for this, it appears that the slide was ground somewhat thin in other areas.

In cross section, the tibiotarsus of *Hesperornis* (YPM PU 22443) is subpentagonal at mid-diaphysis, with a triangular projection on the lateral side (Figure 2.90). This projection is the fibular crest, which is very distinct and extends to midshaft in *Hesperornis* (Martin and

Cordes-Person 2007). The medullary cavity is also subpentagonal, and sits centrally. Similar to the femur of *Hesperornis*, the RBT of this taxon is relatively thick compared to other birds (Table 2.2); this likely relates to its aquatic ecology and diving habits (Chinsamy et al. 1998).

The OCL is very thin in this specimen. It is visible as a thin band external to the only LAG (Figure 2.91, note arrow), and is composed of parallel-fibered bone. This LAG separates the OCL from the middle layer, as in *Confuciusornis* (see above). The interstices between canals in the middle layer are composed of woven-fibered bone, but there is a large lamellar component surrounding the osteons (see below). The separation between the middle layer and the ICL is not distinct, but can be resolved by examining changes in osteocyte and fibrillar organization. The ICL (Figure 2.92, note darker brown region at bottom of image) is composed of poorly organized parallel-fibered bone, and is much thicker than the OCL.

The tibiotarsus is moderately to well vascularized in the ICL and middle layer. Short radial simple primary canals cross the ICL, connecting the middle layer to the medullary cavity. These are sometimes linked by longer circumferential anastomoses. In the inner half of the middle layer, primary and secondary osteons are common. These are difficult to distinguish because many layers of osteocytes surround both types of osteons, but secondary osteons overlap another and show distinct resorption borders. In both primary and secondary osteons, the osteocytes surrounding them orbit in layers, but do not exhibit distinct lamellae. In the outer half of the middle layer, only primary osteons are present, and these have fewer surrounding layers than those in the inner half. Throughout the middle layer, osteons anastomose with each other via simple primary canals that may extend in any direction to form reticulations. These reticulations are more extensive in the inner half of the middle layer. The OCL is poorly vascularized or avascular, depending on the region examined. Where canals are present, they are longitudinal simple primary canals that do not anastomose.

Osteocyte organization is different in all three cortical layers. In the ICL, most (~60-70%) of the osteocyte lacunae are oriented perpendicular to the long axis of the bone. These lacunae are arranged more or less circumferentially, but there is no regularity in their spacing, and they look much more disorganized than the parallel-fibered bone of the OCL. In that region, nearly all of the lacunae are oriented perpendicular to the long axis of the bone, and their orientation is more regular (though they are not uniformly spaced). Within the middle layer, several layers of lacunae orbit each osteon. As noted above, the primary and secondary osteons of the inner half of the middle layer are surrounded by many more layers than those in the outer half. As a result, the osteonal units (not the canals themselves) are much larger in diameter. The interstices among canals represent the original woven scaffolding of the bone, and the lacunae here are extremely disorganized. They show no preferred orientation relative to the long axis of the bone, and no preferred alignment or arrangement relative to each other. Average osteocyte density is high (nearly 2800 cells/mm^2); this specimen shows the highest osteocyte density of all the birds examined.

Discussion: My observations are similar to those of Chinsamy et al. (1998) and Chinsamy (2002) regarding the mid-diaphyseal femur of *Hesperornis*. In that specimen, most of the canals were longitudinal, though short reticular and circumferential anastomoses were also present, especially in the midcortex (see Chinsamy et al. 1998: Figure 2, p. 228). The main difference between the mid-diaphyseal tibiotarsus I observed and the mid-diaphyseal femur used in that study was that femoral inner cortex was more heavily remodeled by secondary

osteons. The femur examined by Chinsamy et al. (1998; Chinsamy 2002) appears to be histologically older than the tibiotarsus based on the lack of extensive reticulation and the presence of more extensive secondary remodeling. To determine whether these reflect ontogenetic differences between specimens or histological differences between elements will require further sampling. A recent dissertation (Wilson 2012) on hesperornithiform paleobiology included histological analyses.

Houde (1987) disregarded the importance of ontogeny and body size in avian histology; he did not think either was an important factor driving histological variation. Instead, he argued (Houde 1986, 1987) that phylogeny was the main influence. This argument was based on previous work by Amprino and Godina (1947) and Zavattari and Cellini (1956), who noted some differences in vascular canal patterning between ratites and other birds. Houde (1986, 1987) associated different vascular patterns with different major groups: tinamous with isolated longitudinal canals, ratites with plexiform/laminar canals, and neognaths with reticulating canals. Because he considered them diagnostic, Houde (1987, 1988) used vascular patterns to place problematic taxa such as *Hesperornis* phylogenetically.

The studies by Amprino and Godina (1947) and Zavattari and Cellini (1956) did not examine many bird taxa, but even with their small sample sets, Houde's typology can be refuted. Amprino and Godina (1947) examined several elements from six bird species, including the ostrich (a palaeognath) and five neognaths. The cortices of these taxa were illustrated in enough detail (Amprino and Godina 1947: Figures 26 through 45) to show that neognaths can produce all three types of vascular patterns, sometimes in one element and sometimes in several elements. Furthermore, these illustrations established that branching or reticulating patterns are not present in some taxa (at least in the elements they observed). Amprino and Godina (1947) reported that age, size, element, and cursoriality were highly associated with microstructural characteristics. Zavattari and Cellini (1956) examined three ratites, three tinamous, and thirteen neognaths. Although they did find striking differences between the microstructure of ratites and those of other birds, they primarily examined differences in osteonal structure and trabecular architecture, rather than vascular patterning.

I agree with Chinsamy et al. (1998; Chinsamy 2002) that the phylogenetic signal Houde observed was in part influenced by the ontogenetic stages of the specimens he examined. As Chinsamy (2002) noted, all three vascular patterns can be observed within one *Hesperornis* section. Other recent studies (e.g., Castanet et al. 1996) have confirmed that vascular pattern changes with age within the same element of a single individual. These changes reflect decreasing growth rate as the animal approaches its growth asymptote; reticular and plexiform patterns are common during times of relatively faster growth, and isolated longitudinal canals are common during times of relatively slower growth. This is the same histological trajectory, moving periosteally, within the *Hesperornis* tibiotarsus that Houde observed.

ORNITHURAE: NEORNITHES

All remaining taxa in this study are part of the clade Neornithes (see Figure 2.1, node 13 for phylogenetic position).

NEORNITHES: PALAEOGNATHAE

Much of the previous work on palaeognath bone histology has examined the ratites (the living Struthionidae, Rheidae, Casuariidae, Dromaiidae, and Apterygidae, plus the extinct †Dinornithidae). Compared to tinamous (Tinamidae), ratites are thought by some to be better ecological proxies for dinosaurs because they are (mostly) large and flightless, and they are often more accessible to researchers because they are farmed for meat and leather. However, large body size and flightlessness are derived conditions within Palaeognathae. For this study, I examined two lithornithiforms (*Lithornis celetius* and *Paracathartes howardae*) and a tinamou (*Rhynchotus rufescens*). *Lithornis celetius* is the earliest known unambiguous palaeognath (Houde 1988, Dyke and van Tuinen 2004), and all three taxa show the plesiomorphic conditions of relatively smaller body size and flightedness (Dyke and van Tuinen 2004).

Lithornis celetius

Specimen number and elements: USNM 290554 (tibiotarsus)
Locality: Bangtail Quarry, western Crazy Mountain Basin (east side of Bridger Range), Park County, Montana, USA
Formation and age: Fort Union Formation, earliest Tiffanian (Gingerich et al. 1983)

Prior histological analyses: The histology of *Lithornis* was illustrated and the vascular patterning briefly described by Houde (1986, 1987, 1988) as part of larger studies on the role of histological characters in interpreting avian phylogenetic relationships. Using Houde's original slide, I describe the histology in detail for the first time here, and add new information on cortical dimensions and measurements of osteocyte density.

Histological observations: The mid-diaphysis of the tibiotarsus of *Lithornis* is almond-shaped in cross section, with an oval medullary cavity that lies centrally (Figure 2.92). The more pointed end corresponds to the fibular crest, as in *Hesperornis* (see above). The medullary cavity is almost completely filled with crystals (similar to the Hayden Quarry specimens), and a thin dark "halo" separates the crystals from the ICL. Part of the ICL is intact around the entire circumference; however, some of the original endosteal margin has been resorbed. A second thin layer of lamellar bone is visible in one region of the bone, within the dark "halo" (Figure 2.92, note arrows), and it is possible that more of this layer would have been present during life. Because crystals have filled the medullary cavity, it is impossible to determine whether or not trabeculae would have been present there in life. No erosion rooms are visible in this specimen.

The ICL is uneven in thickness around the circumference. It is very distinct from the middle layer, with a clear resorption line that cuts across canals of the innermost cortex (Figure 2.93, note top arrow). The ICL shows several of these resorption lines, which are thicker and less even than lamellae (Figure 2.93, note bottom two arrows). Most of the ICL is composed of lamellar bone, but patches of parallel-fibered bone are also visible where the lamellae become indistinct. The OCL is very thin (Figure 2.94, bottom image; note OCL); it is not preserved around the entire circumference. This may have resulted from abrasion of the outer surface of the bone. The OCL is composed of lamellar bone. The middle layer is

composed of woven bone throughout (Figure 2.94, note woven texture most visible in bottom layer), but it becomes slightly more organized near the OCL. No LAGs are visible in this section.

As in *Hesperornis*, simple primary radial canals cross the ICL, connecting the middle layer to the medullary cavity. However, there are many fewer canals in the ICL of *Lithornis* than in *Hesperornis*. As Houde reported (1986, 1987), the middle layer is moderately to well vascularized by longitudinal primary osteons, each with one (occasionally two) lamellae. These lamellae are most distinct in crossed plane polarized light (Figure 2.94, note canals in bottom image). In the inner half of this layer, nearly all the canals anastomose with one other canal circumferentially or obliquely. In the outer half of this layer, canal density decreases slightly, and most of the canals do not anastomose. Canal density continues to decrease periosteally. Close to the OCL, there are a few simple primary canals. The OCL is nearly avascular; only a few radial simple primary canals cross it.

Osteocyte lacunae are better organized in *Lithornis* than in *Hesperornis*. In the parallel-fibered regions of the ICL and OCL, the osteocytes are all oriented perpendicular to the long axis of the bone and aligned circumferentially. However, the spacing between them is irregular and they do not line up along lamellae. In the middle layer, osteocytes orbit the canals but only in one or two layers. In the interstices between canals, they do not show a preferred orientation relative to the long axis of the bone, and no preferred arrangement relative to each other. Osteocyte density does not change centrifugally within the middle layer. Average osteocyte density is approximately 2200 cells/mm^2.

Paracathartes howardae

Specimen number and elements: USNM 361407 (tibiotarsus)
Locality: UMMP locality SC-210 (Sand Coulee 210), near the Badland Hills, northern Clark Fork Basin (= Clark's Fork Basin), Park County, Wyoming, USA
Formation and age: Willwood Formation, early Eocene (Winkler 1983)

Prior histological analyses: The histology of *Paracathartes* was illustrated and the vascular patterning briefly described by Houde (1986, 1987, 1988) as part of larger studies of the role of histological characters in interpreting avian phylogenetic relationships. Using Houde's original slide, I describe the histology in detail for the first time here, and add new information on cortical dimensions and measurements of osteocyte density.

Histological observations: The mid-diaphyseal tibiotarsus of *Paracathartes* (USNM 361407) is D-shaped in cross section, with a similarly shaped medullary cavity that sits centrally (Figure 2.95). As in the specimen of *Lithornis* described above, the surface is somewhat abraded in areas. Additionally, some small pieces of the outer cortex were lost during preparation of the slide. As a result, the OCL is not well preserved around most of the circumference. No erosion rooms are visible in this section, and no trabeculae extend into or across the medullary cavity.

The ICL in this specimen is composed of lamellar and parallel-fibered bone, depending on the region examined. In some areas, there are no lamellae (Figure 2.96), whereas in others (Figures 2.97 and 2.98, note bottom images), the lamellae are quite distinct.

One to three reversal lines are always visible within this region. Where the OCL is preserved (Figure 2.97, note label), it is a very thin band of parallel-fibered bone external to the only distinct LAG (Figure 2.97, note arrow). The middle layer also varies in composition around the section but always contains both parallel-fibered and woven-fibered bone. However, within a region of the bone, one or the other type is more prevalent (see Figure 2.97 for an example of dominant parallel-fibered bone and Figure 2.98 for an example of dominant woven-fibered bone). In some regions, woven bone is present in the core of a lamina, and the bone tissue becomes more organized moving toward the canal (Figure 2.96; note condition in the three laminae closest to the ICL, especially how osteocytes are organized). There is one definite and one possible growth mark in this section. A LAG is present very close to the surface of the bone (Figures 2.96, 2.97, 2.98; note arrows), just internal to the boundary between the middle layer and the OCL. Approximately halfway through the middle layer is a potential growth mark. Around most of the circumference, there is a decrease in osteocyte density at this point (Figure 2.97, note white triangle), and in some regions this is accompanied by a thin dark line (Figure 2.96, note white triangle). This region may be an annulus, but if so, it is not present in at least one part of the bone (Figure 2.98).

In contrast to *Hesperornis* and *Lithornis*, the ICL of *Paracathartes* is crossed by very few radial canals. Where present (Figure 2.97), they are simple primary canals, and generally do not extend along the entire width of this region. The OCL is avascular. Nearly all of the canals in this section are primary osteons arranged circumferentially; no secondary osteons are present and there are only a few simple primary canals in the outermost portion of the middle layer (Figures 2.96, 2.97, 2.98). These osteons are sometimes surrounded by a lamella with a distinct cement line, and at other times, the surrounding tissue looks more parallel-fibered. Through the middle layer, the cortex changes centrifugally from well vascularized in the inner half to moderately vascularized and then poorly vascularized to avascular in the outermost portion. Most of the canals in this specimen are longitudinal. In the inner cortex, they almost always anastomose circumferentially (occasionally slightly oblique or radial), but moving centrifugally, anastomosis is less common.

The osteocytes in the lamellar regions of the ICL and OCL are all oriented perpendicular to the long axis of the bone and aligned circumferentially along lamellae. In the parallel-fibered regions of the ICL, most are oriented perpendicular to the long axis and the spacing between lacunae is irregular. In the middle layer, osteocyte organization is much more variable. As in *Lithornis*, the lacunae orbit the canals, but only ever in one or two layers. The interstices between canals show several conditions: in regions where woven-fibered bone is dominant, they do not show a preferred orientation relative to the long axis of the bone, and no preferred arrangement relative to each other (Figure 2.98, top image). In regions where parallel-fibered bone is dominant, two possibilities are common. In one type, the osteocyte density and disorganization is high at the center of laminae, but are sparser closer to the canals (Figure 2.96; note condition in the three laminae closest to the ICL). In the regions closer to canals, most lacunae are oriented perpendicular to the long axis of the bone, but at least a third of them are not. In the second type, there is no concentration of disorganized osteocytes at the center of the laminae, and the bone shows the 2:1 mix of perpendicular: randomly oriented lacunae described above. Osteocyte density does vary through the cortex, but not in any regular way. Average osteocyte density for this specimen is 1924 cells/mm^2. This is relatively low among the sampled birds.

Discussion: Houde (1986) reported that the primary osteons in this specimen were "predominantly arranged in concentric rings that lie in the transverse plane of the bone, as in the tibiotarsus of ratites" (p. 564). Around the entire circumference (Figure 2.95), this seems generally true, but does not take into account the extent of variation in vascular patterns, especially in the outer cortex (Figures 2.97 and 2.98, but particularly 2.96). He also equated the condition of *Paracathartes* (in which most canals are longitudinal and circumferential anastomoses do not link more than a few canals) with that of *Rhea* and other large ratites, in which true circumferential canals are present, or circumferential anastomoses link dozens of canals (Houde 1986). This approach ignores ontogenetic signal in this individual of *Paracathartes*, which, at least based on vascular connectivity and vascular density, experienced a progressive slowing in growth approaching the end of its first year (as opposed to a more abrupt slowdown).

***Rhynchotus rufescens* (Red-winged Tinamou)**

Specimen number and elements: PU 728 (tibiotarsus). The Princeton Museum of Natural History transferred its ornithological holdings to the FMNH in 1980. This specimen was not transferred at that time. I contacted Houde to find out where the specimen was returned (personal communication; 26 June 2013), but he did not recall where he sent the specimen. It is not in the FMNH, YPM, or USNM collections; therefore, I could not verify the identification of this specimen. Because of this, inferences based on this specimen should be made with caution.

Locality: Species restricted to central and eastern South America; no locality information available.

Age: Recent

Prior histological analyses: The first histological study of tinamous was undertaken by Zavattari and Cellini (1956), who examined the tibiotarsal microstructure of *Nothoprocta cinerascens* (Brushland Tinamou) and *Nothura maculata* (Spotted Nothura) in addition to that of *Rhynchotus rufescens*. That study focused on differences in osteonal structure between ratites and other birds, and as such the samples were only illustrated at the osteonal level. Later, Houde (1986, 1987, 1988) described and illustrated vascular patterns in the tibiotarsus of *Rhynchotus* as part of larger studies on the role of histological characters in interpreting avian phylogenetic relationships. Using Houde's original slide, I describe the histology in detail for the first time here, and add new information on cortical dimensions and measurements of osteocyte density.

Histological observations: Houde made two slides for this specimen, one of which is too thick to image. The other is thin enough to see microstructure, but is missing the medial side. I made measurements of MSD, MCD, and RBT using the thicker slide, and measured ACT using the thinner slide.

The tibiotarsus of PU 728 is oval or slightly almond-shaped in cross section, with a large medullary cavity of the same shape that sits centrally (Figure 2.99). No erosion rooms are visible in this section, and no trabeculae extend into or across the medullary cavity.

Fracturing in the outermost cortex makes it difficult to determine whether the outermost portion represents an OCL, or whether it is not preserved in this specimen. The ICL is relatively thick (approximately ¼ of the cortical thickness) and is histologically distinct from the middle layer, though a distinct reversal line is not present (Figure 2.100). It is mostly composed of parallel-fibered bone. This tissue varies slightly in osteocytic organization around the circumference, but true lamellae are rare. As in the other neornithines, the ICL of *Rhynchotus* shows two or three reversal lines, but these are local and do not extend around the entire cortex. The middle cortical layer is composed mostly of woven-fibered bone. Two growth marks are visible in this section; one is a midcortical annulus of parallel-fibered and weakly woven bone that lies about 1/3 of the cortical width from the preserved periosteal margin. This annulus shows differences in vascularity (Figure 2.100, note lower arrow) and birefringence (Figure 2.99, note lower arrow) compared to the rest of the cortex.

As in the other birds, the ICL of PU 728 is crossed by a few short radial simple primary canals, some of which connect the middle layer to the medullary cavity (Figure 2.99). The ICL is poorly vascularized compared to *Hesperornis*, but similar to the other birds described above. Internal to the midcortical annulus, the middle layer is well vascularized by longitudinal primary osteons and a few simple primary canals (Figure 2.100, note area between ICL and lower arrow). These canals show no preferred arrangement relative to each other. As noted by Zavattari and Cellini (1956), these are orbited by one or several layers of osteocytes, but the osteocytes are not well organized and the layers do not exhibit distinct lamellae or cement lines, even around the border of the osteon. As in *Pterodactylus*, these canals seem to be surrounded by parallel-fibered bone or even woven-fibered bone in places, rather than lamellae. A few anastomoses connect one to three canals, generally obliquely. Between the annulus (which is poorly vascularized to avascular) and the LAG, the canals are longitudinal primary osteons with more distinct borders. Very little bone tissue is preserved external to the LAG, and no canals are visible in what bone remains.

Osteocytes in the ICL are generally oriented perpendicular to the long axis of the bone, and somewhat sloppily aligned circumferentially around the bone. Within regions of lamellar bone, they line up along lamellae. The lacunae of the ICL appear much larger than those of the middle layer (Figure 2.100). Within the middle cortical layer, it is difficult to distinguish between the osteocytes of the primary osteons (primary Haversian cavities compacted by parallel- or woven-fibered bone) and the osteocytes of the interstitial region, at least internal to the annulus. As noted above, lacunae seem to orbit the canals loosely in one or two layers, but they do not form clear ring structures, and no lamellae or cement lines are visible. Additionally, they only show a preferred orientation regionally relative to the long axis of the bone (perpendicular; though at least half the lacunae are parallel or oblique). In the interstices between canals, the osteocytes show no preferred orientation relative to the long axis of the bone, and no preferred arrangement relative to each other. Between the annulus and LAG, the interstitial osteocytes are similarly disorganized, but the ones closest to canals form definite rings around the primary osteons, and are oriented perpendicular to the long axis of the bone. Average osteocyte density is 2524 cells/mm^2, which is relatively high compared to most birds examined in this study.

Discussion: Though Zavattari and Cellini (1956) noted that the primary osteons did not show distinct lamellae or cement lines, it is clear from their illustration (Plate 4, Figure 8) that the

primary osteons they observed in *Rhynchotus rufescens* were better organized than those visible in PU 728. These are similar in terms of the number of loose "layers" around the canal, and in the lack of cement lines, but the rings of lacunae are slightly more distinct. In the specimen examined by Zavattari and Cellini (1956), the osteons seem to be compacted by a spiral of bone that advances inward toward the vessel from the surrounding interstitial scaffold, rather than being composed of concentric layers of bone.

NEORNITHES: NEOGNATHAE

All remaining taxa in this study are part of the clade Neognathae. This radiation encompasses most of the known species of both living and fossil birds. No study of the present scope could adequately describe bone microstructure across the diversity of living neognaths. To incorporate comparative measurements from living neognaths, I examined one galliform, *Crax rubra*, and two neoavians (*Buteo jamaicensis* and *Corvus corax*).

***Crax rubra* (Great Curassow)**

Specimen number and elements: USNM 19918 (tibiotarsus)
Locality: wild caught (1907); Panama Canal Zone (United States administered territory), Panama
Age: Recent

Prior histological analyses: Houde (1987) sampled and analyzed the tibiotarsus of *Crax rubra* as part of a larger study of the role of histological characters in interpreting avian phylogenetic relationships. However, he did not illustrate this section or describe it (beyond a general description of the "neognath" condition). Using Houde's original slide, I describe the histology in detail for the first time.

Histological observations: The tibiotarsus of *Crax* is more or less oval in cross section at the mid-diaphysis, with a flattened anterior surface. My observation of the cortical shape is based on examination of unsectioned skeletal material (MVZ 85574). Houde's original section preserves slightly less than half of the cortical circumference (Figure 2.101), and so it is difficult to determine which region of the cortex is preserved in this slide. The thickness of the cortex is consistent around the preserved portion, and so I suspect that the medullary cavity is of similar shape as the cortical outline and sits centrally, as in the other birds examined in this study.

The ICL is not preserved around most of the section, but traces of it are visible (Figure 2.102, note white triangle). Based on these isolated regions, the ICL appears to be composed of parallel-fibered bone. The middle layer is composed of woven-fibered bone (Figure 2.103, note colors in inner cortex). The tissue transitions to coarse parallel-fibered bone about half to two thirds of the way through the cortex (Figure 2.103, note change in colors) and remains parallel-fibered until the periosteal surface. Two LAGs are visible in the outermost cortex (Figures 2.102 and 2.103, note yellow arrows). The transition from the middle cortical layer to the OCL likely occurs at or just external to the inner LAG, rather than

at the transition between woven-fibered and parallel-fibered bone. This is because the bone remains vascularized until the inner LAG.

The inner third of the cortex (within the middle layer) is well vascularized by longitudinal primary osteons. A few short radial canals also extend inwards from the medullary cavity (Figure 2.103, note radial canal at center of image). These primary osteons (rather than simple primary canals, as in the other birds examined so far) anastomose circumferentially and obliquely with up to five other canals. In some regions, isolated small reticulations are visible. The middle third of the cortex is moderately vascularized by primary osteons that either do not anastomose or connect circumferentially with one or two other canals. The canals are arranged randomly in both regions. External to the inner LAG, the cortex is functionally avascular, but a few longitudinal simple primary canals are also visible.

Within the middle layer, osteocyte lacunae orbit each primary osteon in several layers. In the outer layers of each osteon, the osteocytes are less organized compared to the inner layers. Only about half of them are organized perpendicular to the long axis of the bone, and the spacing between them is irregular. Additionally, the outer layers are not true lamellae, such that the outer layers look much like those of *Rhynchotus*. In the inner layers of each osteon, all the lacunae are oriented perpendicular to the long axis of the bone, and they align along true lamellae. In the woven-fibered interstitial regions between canals, the osteocytes show no preferred orientation relative to the long axis of the bone, and no preferred arrangement relative to each other. Within the parallel-fibered regions, most of the lacunae are oriented perpendicular to the long axis of the bone and align more or less circumferentially. However, the spacing between them is irregular. Osteocyte density does not change appreciably through the cortex, and average osteocyte density is 2540 cells/mm^2. This is relatively high compared to most birds examined in this study.

Discussion: Houde (1987) stated that all neognaths that he examined show a "randomly branching pattern" (p. 127) throughout the cortex. Although this characterizes some small regions where canals form small reticulations, it does not characterize most of the cortex. In general, only two or three canals are linked by anastomoses, and these do not branch or reticulate.

NEOGNATHAE: NEOAVES

All remaining taxa in this study are part of the clade Neoaves.

***Buteo jamaicensis* (Red-tailed Hawk)**

Specimen number and elements: UWBM 82968 (humerus). This slide is catalogued in the Vertebrate Paleontology collection in the UWBM.
Locality: (wild-salvaged) Washington, USA
Age: Recent

Prior histological analyses: Enlow and Brown (1957) described and illustrated the microstructure of the femoral mid-diaphysis of a *Buteo* species. The canalicular organization in the humerus of *Buteo jamaicensis* was described by Rensberger and Watabe (2000) as part

of a larger study of these structures in mammals and dinosaurs (including birds). However, other characters were not addressed. More recently, the humeral microstructure of *B. jamaicensis* was figured by Simons and O'Connor (2012) as part of a study on canal laminarity in bird wing bones. As in the Rensberger and Watabe study, the microstructure was not described in detail (only a laminarity index was provided). I describe the histology in detail for the first time here, using the slide produced by Rensberger and Watabe (2000).

Histological observations: The mid-diaphysis of the humerus of *Buteo jamaicensis* is subtriangular in cross section, with a subrhomboidal medullary cavity that sits centrally (Figure 2.104). Several oval erosion rooms are visible in the inner cortex of the anteromedial quadrant of the bone; all of these are lined with lamellae. The endosteal margin of the largest of these (2.9 mm long) forms a trabecular strut across the inside of the medullary cavity (Figure 2.104). The lamellae lining this room cut across vascular canals in the primary cortical tissues adjacent to it, suggesting that this chamber formed by resorption rather than as a result of trabecular extension across the medullary cavity. Secondary osteons are present in the inner cortex (Figure 2.105, white triangles), but they do not extend more than a third of the way around the cortex (Figure 2.104; note region bracketed by white triangles). In all cases, the secondary osteons are bordered by a resorption line that cuts across other tissues. Additionally, secondary osteons are shaped irregularly (rather than circular).

An ICL and OCL are both present in this specimen (Figure 2.105, note labels); both are composed of parallel-fibered bone. A faint reversal line separates the ICL from the woven-fibered middle layer, but no line separates the middle layer from the OCL. No LAGs are present in this specimen. As in most taxa examined in this study, vascularity decreases periosteally. The inner cortex is moderately to well vascularized by primary osteons, secondary osteons, and even a few simple primary canals. Many of these are longitudinal, and nearly all of them anastomose with several other canals. In the inner half of the middle layer, these anastomoses are extensive and may occur in any direction. In some regions around the circumference, they form reticulations (Figure 2.105, note condition in lower half of image), whereas in others, the canals are nearly subplexiform in pattern (see Figure 2.104 for variation around the circumference). Where secondary osteons are present, the anastomoses often connect canals of different types (e.g., primary osteons with secondary osteons), suggesting either that the secondary remodeling process begins early, or that anastomoses continue forming after the bone is deposited and compacted. If the latter case is true, it would suggest that a number of these anastomoses are not primary, but secondary (having cut through original primary tissue), even though they are not ringed by compacted bone. In the outer half of the middle layer, vascular density and connectivity decrease progressively moving towards the OCL, and all of the canals are primary osteons or simple primary canals. At least a third of the canals do not anastomose with another canal in this region. Most of the rest anastomose circumferentially with a few other canals, but do not reticulate.

In the parallel-fibered bone of the ICL and OCL, most osteocytes are oriented perpendicular to the long axis of the bone and are arranged circumferentially. In these regions, the spacing between osteocytes is irregular. In the woven-fibered tissue of the middle cortical layer, osteocyte lacunae orbit the primary and secondary osteons, but only in the outermost cortex are distinct lamellae visible. Many of layers of osteocytes encircle each secondary osteons; only 1-4 layers are visible around any of the primary osteons. In the interstices

between canals, osteocytes show no preferred orientation relative to the long axis of the bone, but are more or less evenly spaced. As a result, osteocytes appear somewhat organized relative to each other, compared to other birds examined in this study. Osteocyte density is consistent through the cortex, and average osteocyte density for this element is 2285 cells/mm^2.

Discussion: Enlow and Brown (1957) reported that the femur and tibiotarsus of *Buteo* showed a reticular network of vascular canals throughout most of the cortex. In some regions of the cortex, secondary osteons were only sparsely present, but in others, secondary remodeling had obscured most of the primary tissues. They illustrated mid-diaphyseal sections of the femur and the tibiotarsus. The femur (Plate XXV, Figure 9: p. 209) is poorly to moderately vascularized in the region they illustrate, and the reticulations are not well developed; the anastomoses link only 2-5 canals, and most of the canals are circumferential or oblique. The tibiotarsus (Plate XXVI, Figure 8: p. 211) is moderately to well vascularized by circumferential canals. The humerus I examined has regions that resemble each of Enlow and Brown's (1957) illustrations.

Another humerus of *Buteo jamaicensis* was illustrated by Simons and O'Connor (2012: Figure 7, p. 394). The primary osteons of that specimen were laminar or subplexiform throughout the entire middle cortical layer, at least in the region figured, and no secondary osteons were present in either *B. jamaicensis* specimen they examined. Simons and O'Connor (2012) found a higher laminarity index (a measure of the proportion of laminar and plexiform canals in the cortex) in both specimens of *B. jamaicensis* than in all the other specimens they examined. In the specimen I examined, laminar canals were more common in the inner cortex than in the outer cortex. Without further natural and life history information, it is impossible to determine whether this is a result of individual variation, or reflects differences in sex, age, or geographic location. Regardless, the presence of laminar/subplexiform canals in two specimens of *B. jamaicensis* confirms that at least some neognaths commonly exhibit non-reticular vascular patterns.

***Corvus corax* (Common Raven)**

Specimen number and elements: UWBM 90537 (humerus). This slide is catalogued in the Vertebrate Paleontology collection in the UWBM.
Locality: (wild-salvaged) Washington, USA
Age: Recent

Prior histological analyses: Enlow and Brown (1957) briefly described and illustrated the femoral microstructure of a crow (another *Corvus*). The canalicular organization in the humerus of *Corvus corax* was described by Rensberger and Watabe (2000) as part of a larger study of these structures in mammals and dinosaurs (including birds). I describe the humeral histology in detail for the first time here, using the slide produced by Rensberger and Watabe (2000).

Histological observations: This section is preserved well enough to see cellular and lamellar details, but it was ground so thin that it does not refringe well under polarized light.

Additionally, numerous small cracks are visible in this section; these run circumferentially (especially in lamellar areas) or radially, and often connect at nearly right angles. Unfortunately, they may be mistaken for vascular canals because they stain similarly dark and often run between canals. They can be distinguished from blood vessels because they are smaller, they appear angular at high magnification (especially where the crack changes direction), and jagged edges are visible when focusing through the plane of section.

The mid-diaphyseal humerus of *Corvus corax* is more or less circular in cross section, with a circular medullary cavity that sits centrally (Figure 2.106). The cortex is slightly thicker on the posterior side. The medullary cavity is lined by a band of endosteal lamellae that varies in thickness (0.1-0.2 mm) around the section. No trabeculae extend inward into the medullary cavity or bisect it at mid-diaphysis, but a single strut hugs the medial border. It is very similar to the strut observed in the humerus of *Buteo* (UWNM 82968). Like the *Buteo* specimen, the strut in UWBM 90537 is formed by the resorption of original primary tissues, rather than primary extension across the medullary cavity. The border of the oval erosion room just internal to this strut shows an uneven resorption surface, with lamellae that cut across vascular canals in the adjacent primary tissues. This erosion room is approximately 2.3 mm long and 0.4 mm wide. The core of the trabecular strut is composed of primary bone tissue that is confluent with adjacent cortical tissues.

The cortex varies in appearance around the circumference of this section, but in any given area it tends to be fairly uniform in appearance moving radially through the section. This specimen preserves a clear ICL and an OCL, but each varies in thickness around the circumference of the bone. The ICL is composed of lamellar bone, whereas the OCL is composed of parallel-fibered bone. A distinct and uneven resorption surface separates the ICL from the middle layer. The primary tissue of the middle cortical layer generally grades from woven-fibered bone in the innermost cortex to parallel-fibered bone periosteally, but there is some variation around the circumference of the bone. Depending on the region of the bone examined, parallel-fibered bone or woven-fibered bone may occupy more of the cortical width. There is no distinct transition between the middle layer and the OCL around most of the circumference.

As in all of the birds I examined, the ICL is crossed by short radial simple primary canals that connect the innermost cortex to the medullary cavity. The many long, circumferential cracks running through the ICL often begin or end at one of these radial canals. Similar radial canals cross the OCL (Figure 2.107, note radial canal at top of image), but these are uncommon, and the OCL is generally avascular. The middle layer is vascularized by both primary and secondary osteons. The secondary osteons (Figure 2.107, note white triangles) are distributed throughout the cortex, but do not cluster in one region of the bone. As in *Rhynchotus*, the primary osteons are surrounded by several layers of parallel-fibered bone (rarely, lamellae), and the outer border tends to be indistinct from the surrounding interstitial tissues. Some of the primary osteons are so broad that little interstitial space exists between them (Figure 2.107, note canals in center of image).

The vascular density, connectivity, and patterns of the primary osteons all vary dramatically around the section. For example, the anteromedial quadrant (Figure 2.106, upper left of image) is very poorly vascularized by isolated longitudinal canals, whereas the anterolateral quadrant is well vascularized by canals that extensively anastomose to form a subplexiform pattern. The posterior portion (Figure 2.106, right side of image; 2.107) grades

from poorly to well vascularized; in some regions, longitudinal canals are isolated or anastomose with one other osteon (as in Figure 2.107), whereas in other regions, canals anastomose with several other canals to form small reticulations. Throughout the section, the bone appears to be better vascularized than it actually is, because of small cracks that run throughout the cortex and often intersect with canals (Figure 2.107, green arrow).

In the ICL, all osteocytes are oriented perpendicular to the long axis of the bone and align circumferentially along the lamellae. Most of the lacunae in the OCL are also oriented perpendicular to the long axis of the bone and arranged circumferentially, but the spacing between them is less regular and they do not look as flattened in cross section as the lacunae of the ICL. In the middle layer, osteocyte organization and orientation vary with fiber type. Several layers of osteocyte lacunae orbit each primary or secondary osteon. As noted above, the outer layers of primary osteons are somewhat indistinct from the surrounding interstitial tissue because they are composed of parallel-fibered bone (rarely, the inner layers are true lamellae). In the parallel-fibered layers, osteocytes are more globular in cross section and are generally oriented perpendicular to the long axis of the bone. In the lamellar layers, the lacunae are flattened, and are always oriented perpendicular to the long axis of the bone. The orientation and arrangement of interstitial osteocytes correlate with fibrillar organization. In parallel-fibered regions, the orientation is similar to the parallel-fibered layers of the primary osteons. In woven-fibered regions, they are randomly oriented relative to the long axis of the bone and show no preferred arrangement relative to each other. Osteocyte density does not change radially through the cortex or around its circumference. The average osteocyte density of this specimen (1706 cells/mm^2) is the lowest of any of the birds I examined.

Discussion: Enlow and Brown (1957) briefly described and illustrated the femoral microstructure of a crow (another *Corvus*). They reported extensive and elaborate vascular reticulating primary canals, each orbited by osteocyte lacunae. In the interstices between canals, osteocytes were disorganized. However, the femur they illustrated (Plate XXVII, Figure 5: p. 213) is only moderately vascularized (at least in the region pictured); it is slightly better vascularized than the *Buteo* femur that they also described (see above). As in their femur of *Buteo*, the reticulations are not well developed; they have short circumferential or oblique anastomoses that link only 2-5 canals. Additionally, isolated longitudinal canals are visible.

DISCUSSION

In this section, I first discuss the major phylogenetic trends in histological characters observed in this study, based on the observations described above. I then discuss new insights into the histological characters themselves. I conclude my discussion by examining the effects of sampling on my results, especially those related to interpretations of ontogenetic, interelemental, phylogenetic, and individual variation.

Phylogenetic Trends in Histology

As mentioned above, among living tetrapods, birds and mammals have relatively high growth and metabolic rates compared to amphibians, turtles, crocodylians, and lepidosaurs (Ricklefs 1973, Case 1978a, 1978b, Arendt 1997, Starck and Ricklefs 1998a).The plesiomorphic condition for all tetrapods is assumed to be relatively slow growth and low metabolic rates. Because the extant sister taxon to birds (crocodylians) has the plesiomorphic condition, the derived conditions of faster growth and higher metabolic rates may have originated along the lineage leading to birds, after the avian lineage split from the lineage leading to crocodylians. The inclusion of fossil taxa allows us to examine this question at a finer scale. If the origination of higher rates occurred after the avian-crocodylian split, where along the avian lineage did it occur? There are several possibilities: for example, after the lineage leading to birds diverged from other theropods, near the base of Dinosauria, within Dinosauromorpha, or near the base of Ornithodira. The inclusion of fossil taxa also allows us to test alternative hypotheses about the phylogenetic position of these rate changes; rather than occurring within the avian lineage, higher rates of growth and metabolism may have originated anywhere between the node Archosauria and among any other total group archosaurs. This would imply a secondary loss of these elevated growth and metabolic rates somewhere on the lineage leading to Crocodylia.

As noted in Chapter 1, some osteohistological characters are associated with elevated growth rates in living amniotes (most notably woven-fibered bone, high vascular density, extensive vascular connectivity, complex vascular patterning, and high bone depositional rates). These characters are common in mammals and birds, and among embryos of other taxa. Similarly, osteocyte density is thought to be correlated with metabolic rate (although reptiles are poorly sampled for this character). I have summarized the histological conditions relating to fast growth for each taxon in Table 2.3. For several characters, I include two assessments; one that reflects the highest levels of fibrillar disorganization, canal development, or vascularity, and a second that indicates the dominant state around most of the cortex. This dual assessment reflects a common situation in my dataset: a taxon may be capable of producing a certain type of tissue, but that tissue does not predominate in its microstructure. For example, the younger individual of *Fruitadens* (LACM 120478) has woven-fibered bone in one region of the cortex, but most of that section (and that of the other individual, LACM 115727) is composed of parallel-fibered primary bone tissue. Also, although I did not use the term “fibrolamellar bone” when describing the microstructure of each taxon, I include a column in Table 2.3 assessing its presence. This diagnosis is based on whether I observed the combination of both woven-fibered bone and primary osteons in the same area. In other words, it is a conclusion or diagnosis derived from my observations on fibrillar organization and canal type, rather than a direct observation. Finally, I assess the presence of intracortical growth marks (as opposed to all growth marks in the cortex and OCL/EFS).

In this section, I first discuss the histological condition I observed in birds, and then compare it to the condition in the successive outgroups, moving away from the crown. Because the ontogenetic stage of comparison is the time of active (most rapid) growth, I limit my discussion of birds to the microstructure of the primary bone tissues in the middle cortical layer, and do not discuss the histological condition of the ICL or OCL. The ICL is homologous to the endosteal lamellae observed in nearly every taxon examined in this study; it is a secondary tissue (Francillon-Vieillot et al. 1990) and plesiomorphic for this group. The

OCL is a primary tissue, but it is homologous to the EFS of other tetrapods (Chinsamy-Turan 2005), and therefore does not characterize the active phase of growth in birds. In non-avian taxa, I discuss only the primary tissues of the cortex deposited during times of active growth. Therefore, I do not discuss the endosteal lamellae or EFS.

Each of the eight birds examined in this study has woven-fibered bone in the interstitial primary bone tissue between canals. However, none of the taxa I observed had woven-fibered bone around the entire circumference. In some taxa (*Paracathartes*, *Crax*, and *Corvus*), parallel-fibered bone composes a significant proportion of these interstitial tissues; it may also functionally constitute much of the cortex through compaction of the vascular canals (as in *Hesperornis*, *Rhynchotus*, and some regions of the *Corvus* humerus). Except in *Confuciusornis*, all taxa are well vascularized around at least part of the circumference. Most taxa are only moderately vascularized in most regions, especially in the outer half of the middle cortical layer. Vascular connectivity also varied among birds; it was rare in some samples (*Rhynchotus, Crax*), and variable around the section in others (*Buteo, Corvus*). In the remaining four taxa, anastomoses are common but not extensive (i.e., they connect only a few canals, at least in two dimensions) except in *Paracathartes*. Vascular pattern also varied among these taxa: half showed some level of vascular reticulation and the rest showed circumferential or oblique anastomosis.

Of the four extant birds examined in this study, true fibrolamellar bone is common in two taxa (*Crax, Buteo*); it is present but uncommon in a third (*Corvus*). The fourth taxon, *Rhynchotus*, shares with *Corvus* a different type of primary osteon, in which the vascular canals are lined by parallel-fibered bone rather than lamellar bone (I discuss this type of canal in the Histological Characters section below). Among the fossil birds, *Confuciusornis* and *Lithornis* produce true fibrolamellar bone, but *Hesperornis* produces tissue much like that of *Rhynchotus* and *Buteo*. Because they do not have a lamellar component, it is not appropriate to refer to the tissues of *Hesperornis*, *Rhynchotus* and *Corvus* as true fibrolamellar bone. However, as I discuss below, the absence of true fibrolamellar bone in these taxa probably does not imply the same slow growth rates as in taxa that either lack a woven component or do not compact canal).

Osteocyte density is variable among the taxa examined; it ranges from 1706 cells/mm^2 in the humerus of *Corvus* to 2778 cells/mm^2 in the tibiotarsus of *Hesperornis*. Most taxa have densities of 2200 cells/mm^2 or higher. The available data on osteocyte densities for birds are poor, but my estimates are comparable to or higher than those observed in the primary woven-fibered bone of small mammals (Hernandez et al. 2004). Finally, intracortical growth marks are rare among birds; in this sample, a single mark is present within the middle layer only in *Rhynchotus* and possibly *Paracathartes*. Growth marks separate the middle layer from the OCL in these taxa, as well as *Confuciusornis*, *Hesperornis*, and *Crax*. As many others have noted, ornithuran birds do not generally produce intracortical growth marks (Chinsamy 2002; Chinsamy-Turan 2005; Turvey et al. 2005; Bourdon et al. 2009), although these marks are more common in early birds (Chinsamy et al. 1995a, 1995b; Padian et al. 2001; de Ricqlès et al. 2003a; Chinsamy 2002; Chinsamy-Turan 2005; Cambra-Moo et al. 2006; Erickson et al 2009a; Chinsamy et al. 2013)

The microstructure of the birds described above is fairly variable, even when considering only the crown or extant taxa. Several factors may influence this. First, none of these taxa are especially closely related and that they vary in body size. Furthermore, their

cortices are relatively thin compared to most nonavian taxa examined in this study (Table 2.2); much of the earliest record of growth has been lost to medullary cavity expansion. Given that the remaining cortex also includes the ICL and OCL, this leaves only a small amount of bone to record the tail end of the active growth phase.

How, then, to describe the avian condition? It is clear from this study and earlier ones (e.g., de Margerie 2002, de Margerie et al. 2002, 2004; Starck and Chinsamy 2002) that birds regularly produce woven-fibered bone. However, many early studies of bird histology did not consider fibrillar organization (e.g., Foote 1916, Amprino and Godina 1947; Zavattari and Cellini 1956; Enlow and Brown 1957; Houde 1986, 1987, 1988). It is also common for birds to have primary osteons, though my results suggest that these vary in structure more than previously considered. For at least part of their ontogeny, birds deposit moderately to well vascularized bone tissue, but vascular density clearly varies by element and bone region, and likely with age and body size. Among extant birds, body size is known to play at least some role in determining vascular density and connectivity; small birds produce poorly vascularized bone with few anastomoses (Foote 1916; de Ricqlès et al. 2001; Padian et al. 2001; Erickson et al. 2009a). Based on my sample, patterns of vascular connectivity and vascular patterning are not clear, and seem variable. Studies of early birds and their dinosaurian ancestors (e.g., de Ricqlès et al. 2001; Padian et al. 2001; Erickson et al. 2009a) establish body size as a key influence on vascular density, connectivity, and pattern in these taxa, but few studies have examined the distribution of vascular connectivity and patterning among extant birds, especially neognaths. Zavattari and Cellini (1956) and Houde (1986, 1987) proposed phylogenetic influences, but in these studies, body size was certainly a component because the large-bodied taxa that they examined were mostly ratites. Ecology and biomechanics are known to influence vascular patterning in some neognaths (Simons and O'Connor 2012), but the extent of these influences has not yet been studied.

None of the characters mentioned above are found exclusively in birds. Woven-fibered bone is present among several nonarchosaurian archosauriforms (*Vancleavea*, the proterochampsian, and phytosaurs), all the pseudosuchians examined except *Revueltosaurus*, and every ornithodiran examined except *Eudimorphodon* and the Neornithischian (cf. *Lesothosaurus* or *Stormbergia*). Outside Archosauriformes, I did not observe woven-fibered bone. Even if we restrict our samples to those taxa whose dominant fibrillar organization is woven-fibered bone, it is still present in *Vancleavea*, most pseudosuchians (including male *Alligator* for part of its ontogeny), *Pterodactylus*, and most dinosauromorphs.

Primary osteons are similarly distributed throughout Archosauriformes; within that clade, all taxa have primary osteons except *Revueltosaurus* and the proterochampsian, and it is generally the dominant canal type among archosauriforms. This character is not restricted to archosauriforms, however; primary osteons also occur in *Varanus* and *Captorhinus*. From other studies, it is clear that *Varanus* is atypical among lepidosaurs in this regard; most lizards and *Sphenodon* are either avascular or have only simple primary canals (Enlow and Brown 1957; Peabody 1961; Castanet et al. 1988; Castanet and de Ricqlès 1986-1987; de Buffrénil et al. 2008). Given that *Trilophosaurus*, most lepidosaurs, and amphibians exhibit simple primary canals, primary canals may have evolved independently in *Captorhinus*, *Varanus*, and archosauriforms.

Most taxa examined in this study produce at least moderately vascularized bone tissue at some point during their ontogeny. These include nearly every archosauromorph (all except

Revueltosaurus), as well as *Captorhinus* and *Varanus* (although, as stated above, *Varanus* is better vascularized compared to most lepidosaurs). However, only archosauriforms produced well vascularized or very well vascularized tissue. Among these, only *Euparkeria*, *Revueltosaurus*, *Eudimorphodon*, and *Dimorphodon* do not have well vascularized bone in at least the inner cortex. However, well vascularized bone is not the dominant canal density observed for many taxa, including several birds. Among nonavian Ornithodira, these include some taxa that rarely produce well vascularized bone (*Fruitadens, Scutellosaurus*), and some that produce moderately vascularized and well vascularized tissue in more or less equal amounts (*Dromomeron, Asilisaurus, Tawa*). Among Ornithodira, these are all small-bodied taxa compared to other theropods, the sauropodomorphs, and the Ghost Ranch (Hayden Quarry) silesaurid. Outside Ornithodira, the size pattern is not as clear: some large-bodied taxa (phytosaurs, *Postosuchus*, female and older male *Alligator*) are only moderately vascularized, in addition to smaller bodied taxa such as the proterochampsian.

The vascular connectivity of all nonavian archosauriforms is similar to birds in that they show at least some anastomoses among canals, although these may be restricted to the inner cortex or to early ontogenetic stages. In few taxa in my sample did extensive anastomosis dominate much of the cortex; this pattern was mostly found in *Postosuchus*, phytosaurs, one element of *Herrerasaurus*, and *Paracathartes*. All of these are large-bodied taxa within their clades. Regarding vascular patterning, plexiform, laminar/circumferential, and long radial canals were all fairly rare within this sample. However, many archosauriform taxa had small reticulations or short anastomoses traveling in several directions, as seen in most birds. The first taxon to show this pattern is the proterochampsian, and the pattern is common crownward of that point on the tree.

Osteocyte orientation is tightly linked with fibrillar organization; I discuss this in more detail below. Because it is strongly correlated with woven-fibered bone, only taxa that produce woven-fibered bone exhibit this trait. Osteocyte density is harder to assess; the birds in my study generally show average osteocyte densities over 2200 cells/mm^2. Outside Archosauriformes, no taxon exceeds 1500 cells/mm^2, and within Ornithodira, many exceed 2000 cells/mm^2 or even 3000 cells/mm^2. Nonarchosaurian archosauriforms and pseudosuchians are mixed in the distribution of these traits; all these except *Euparkeria* have average densities under 2000 cells/mm^2 (some taxa, such as *Effigia*, phytosaurs, and *Vancleavea*, have higher densities than what is observed in *Corvus*). Metabolic rate carries a phylogenetic signal (Montes et al. 2007, 2010), but it is also inversely correlated with mass. Without assessing mass and phylogeny more explicitly, it is impossible to determine whether lower metabolic rates equate to lower mass-specific metabolic rates for these taxa. It is interesting, therefore, that the birds in my sample have osteocyte densities (an indicator or metabolic rate) similar to or lower than several much larger taxa (e.g. silesaurids, ornithischians, some coelophysoids). Larger taxa might be expected to have lower BMR (and therefore lower osteocyte densities) even if their physiologies were otherwise similar to those of extant birds. Given this, my results could suggest that some extinct archosauriforms had higher BMRs than are observed among living taxa, including birds.

As noted above, the presence of intracortical LAGs is uncommon in ornithuran birds, although some early birds (outside Ornithurae) are known to have produced them. This suggests a change in growth duration (the length of time spent in active growth) in extant birds compared to the plesiomorphic condition for Aves. No ornithodiran examined here has

more than six LAGs, and none of the theropods have more than three. However, this is likely an artifact of sampling. The dataset includes only early-diverging members of the primary lineages, all of which are small-bodied compared to the more derived forms with longer growth durations (Padian et al. 2004). For example, although none of the sampled theropods have more than three LAGs, studies of larger taxa (e.g., tyrannosaurids, *Allosaurus*) have established that many theropods grew for ten years of longer (Erickson et al. 2004; Horner and Padian 2004; Lee 2007; Lee and Werning 2008). None of the pterosaurs examined here have LAGs, but LAGs are known from other taxa (Chinsamy et al. 2009; Prondvai et al. 2012). Teasing out the evolution of avian growth duration will require better constraints on body size and growth duration and longevity. Ideally, transitions in this character would be assessed using growth curves based on ontogenetic series for the successive outgroups, but these are not available for most taxa.

My results suggest that most of the histological characters that we associate with the avian condition of faster growth (woven bone moderately to well vascularized by primary osteons that form short anastomoses, either reticulating or in several directions) are not exclusive to birds. Rather, these are common to all ornithodirans, most pseudosuchians, and most non-archosaurian archosauriforms examined in this study. Although *Alligator* does not have all of these characteristics throughout ontogeny, they are present in earlier ontogenetic stages in both sexes and persist after sexual maturity in males. Furthermore, all of the early-diverging pseudosuchians examined except *Revueltosaurus* exhibit them. The presence of histological indicators of faster growth in pseudosuchians, ornithodirans, and stem archosaurs indicates that these conditions evolved before the avian and crocodylian lineages diverged. If this is the case, then the slower growth that characterizes adult female and older male *Alligator* (and other crocodylians) must be secondarily derived, rather than a reflection of the plesiomorphic condition.

My histological results supporting fast growth in dinosaurs and other ornithodirans are not controversial. Erickson et al. (2009b) found that dinosaurian (specifically, maniraptoran theropods) histology and growth rates were identical to those of *Archaeopteryx* and other birds when body size was taken into account. The findings of Erickson et al. (2009b) echoed the results of de Ricqlès et al. (2001) and Padian et al. (2001, 2004), who found that most of the histological diversity observed in birds and other dinosaurs could be attributed to size. Published estimates of dinosaurian bone deposition rates also support this hypothesis, but these estimates rely on the same histological characters used to infer fast growth, so this is not surprising. For example, using the relationship between canal pattern and bone deposition rate established by Castanet et al. (1996; 2000) for ducks and ratites, Padian et al. (2001) estimated bone deposition rates in dinosaurs, pterosaurs, and pseudosuchians. They found that dinosaurs (and some pterosaurs) deposited bone as fast as or faster than extant birds. Cubo et al. (2012) measured histological characters of extant amniotes and created a multivariate model to predict bone deposition rate. They estimated that bone deposition in two theropods and *Lesothosaurus* occurred at similar or higher levels compared to what is known experimentally in extant birds. Finally, studies that reconstruct age-mass growth curves for dinosaurs also support a hypothesis for faster growth in that clade. By comparing maximum growth rates across a number of taxa, Erickson and Tumanova (2000) and Erickson et al. (2001) showed that dinosaurs grew at rates comparable to those of mammals and precocial birds, much faster than extant fish or reptiles.

Prior to my study, only two previous works examined the histology of non-dinosaurian dinosauriforms: Nesbitt et al. (2013) examined the histology of *Nyasasaurus*, and Fostowicz-Frelik and Sulej (2010) examined the histology of *Silesaurus*. *Nyasasaurus* is sister to Dinosauria but shares synapomorphies of that clade (making it either the earliest dinosaur or the closest sister taxon), and silesaurids are sister to the *Nyasasaurus* + Dinosauria clade (Nesbitt et al. 2013). Both studies found the histology of their respective study organisms to be similar to that of dinosaurs. My examination of two additional silesaurids and the nondinosauriform dinosauromorph *Dromomeron* is consistent with both earlier reports. Among pterosaurs, most studies have found histological support for fast growth in most taxa, at least earlier in life (de Ricqlès et al. 2000; Sayão 2003; Chinsamy et al. 2008, 2009; though see Padian et al. 2004 and Prondvai et al. 2012 for discussion of slower-growing taxa). Quantitative estimates of bone deposition or whole body growth rates have not yet been estimated for *Nyasasaurus*, silesaurids, and *Dromomeron* using either histological methods or by constructing growth curves. However, it would be possible to do so for most of these taxa.

de Ricqlès et al. (2003b) hypothesized that pseudosuchians may have secondarily evolved slow growth grates because the condition of the immediate outgroups to Archosauria were unclear. Furthermore, some of the pseudosuchians they examined (e.g., *Terristrisuchus*, a sphenosuchian crocodylomorph) retained histological indicators of fast growth. By reexamining some of their histological materials using strict diagnostic criteria, as well as incorporating other early pseudosuchians (e.g. *Effigia*) and additional ontogenetic stages (*Alligator*, aetosaurs), I show that histological indicators of fast growth are more common among pseudosuchians than previously realized. My results are supported by those of Cubo et al. (2012) and Legendre et al. (in press), who estimated bone depositional rates in the aetosaur femur (UCMP 25914; see histological description above) in addition to dinosaurs. Cubo et al. (2012) found depositional rates in this aetosaur to be much higher than those observed in extant crocodylians (which in turn grow faster than lepidosaurs), and similar to the rates observed in the Mallard (*Anas platyrhynchos*). They predicted much lower depositional rates in another aetosaur, but that specimen (UCMP 25905) has since been shown to be a phytosaur fibula (see above). Their models are element-specific, so this specimen would need to be reanalyzed using a fibula model to establish bone depositional rate.

My results for most of the remaining archosauromorphs show no clear pattern for the group as whole, but most taxa exhibit some or all of the "avian" characteristics. Few studies have estimated growth rates in nonarchosaurian archosauriforms, because appropriate specimens were not available for sectioning until recently (de Ricqlès et al. 2003b). The exception is a study by Botha-Brink and Smith (2011), who examined the histology of *Prolacerta* (an archosauromorph, but closer to the Archosauriformes than *Trilophosaurus*), and three archosauriforms (*Proterosuchus*, *Euparkeria*, and *Erythrosuchus*). *Prolacerta* is generally characterized by parallel-fibered bone tissue moderately vascularized by longitudinal primary osteons, but sometimes also has woven-fibered bone. *Proterosuchus* elements are composed of a mix of woven-fibered and parallel-fibered early in life, but the tissues become better organized (parallel-fibered and lamellar) later in ontogeny. The tissues are well vascularized by radial or radially anastomosing primary osteons earlier in life, but these transition to radial rows of longitudinal primary osteons and simple primary canals. The microstructure of *Euparkeria* suggests is comparatively slow growing, with only parallel-fibered bone and low levels of vascular density and connectivity. *Erythrosuchus*, however,

shows all of the features found in extant birds: woven-fibered bone well vascularized by primary osteons that anastomose in all directions and even form reticulations. Thus, the results of Botha-Brink and Smith (2011) are similar to mine in that they found some histological characters associated with fast growth in several taxa, but no consistent patterns in the group.

Studies of bone deposition rate in nonarchosaurian archosauromorphs show that this character is also variable among stem archosaurs. Botha-Brink and Smith (2011) estimated bone deposition rates using a method similar to the one I describe in Chapter 1. They found that *Prolacerta* deposited bone at rates similar to those of extant crocodylians, but that *Proterosuchus* and *Erythrosuchus* had bone deposition rates several times that of crocodylians, but still lower than those of extant birds. Botha-Brink and Smith (2011) and Legendre et al. (in press) both estimated low bone deposition rates in *Euparkeria* relative to extant birds. However, the latter study estimated a higher rate than observed in extant crocodylians, whereas the former estimated rates similar to crocodylians.

Regardless of where among archosauromorphs the histological indicators of fast growth first evolved, it is clear that several taxa outside Archosauria were capable of much faster growth than is observed among extant lepidosaurs and crocodylians. Among nonarchosaurian archosauriforms, the histological indicators of fast growth are variably present. For example, *Vancleavea* has woven-fibered bone, but simple vascular patterns, whereas *Euparkeria* shows greater anastomosis but does not have woven-fibered bone. It is possible that these characters did not evolve simultaneously; future work is needed to determine whether the origins of all histological indicators of faster growth resolve to one node on the phylogenetic tree.

Histological Characters

In this study, I avoided tissue-level descriptors such as fibrolamellar bone, and instead examined each component character individually. My results have several implications for the study and assessment of bone histology, at least among archosauromorph reptiles. I discuss three main points below.

1. *The amount of woven-fibered bone varies within fibrolamellar bone*.

In the mid-diaphyseal cortex of extant vertebrates, nonpathological periosteally-deposited primary woven-fibered bone is commonly associated with a lamellar component (Amprino and Godina 1947; de Ricqlès 1975; Francillon-Vieillot et al. 1990). This relates to the way woven-fibered bone is thought to form underneath the periosteum. First, a scaffold of woven-fibered bone matrix forms between adjacent vascular canals, enclosing them in a three-dimensional latticework (Amprino and Godina 1947; de Ricqlès 1975; Francillon-Vieillot et al. 1990; de Ricqlès et al. 1991; Ferretti et al. 2002; Hall 2005; Marotti 2010). This bone tissue is highly disorganized: collagen fibers and osteocytes show no preferred orientation relative to the long axis of the bone. Because the initial scaffold of disorganized bone is thin, the girth of the bone can increase rapidly (de Ricqlès 1975; Francillon-Vieillot et al. 1990; Hall 2005; Marotti 2010). Although the bone surface is still expanding under the periosteum, the scaffold itself expands inwards, compacting the canals. The compacting tissue may be woven-fibered, parallel-fibered, or lamellar (de Ricqlès 1975; Francillon-Vieillot et al.

1990; de Ricqlès et al. 1991; Hall 2005; Stein and Prondvai 2013). In fibrolamellar bone, most of the compacting bone is woven-fibered, but the compaction is ultimately finished by lamellar bone, which is deposited at a slower rate compared to the woven-fibered component (de Ricqlès 1975; Francillon-Vieillot et al. 1990; de Ricqlès et al. 1991; Hall 2005; but see Stein and Prondvai 2013). By definition, fibrolamellar bone has both a woven-fibered component and a lamellar component, and the primary vascular canals in it are primary osteons (de Ricqlès 1975; Francillon-Vieillot et al. 1990).

The two-phase deposition of woven-fibered bone allows rapid expansion in the radial direction, but compaction is not necessarily as fast. For example, Stein and Prondvai (2013) observed that the woven-fibered component in the bone tissue of sauropodomorph dinosaurs was restricted to the center of the interstitial bone between canals. This core of woven-fibered bone corresponded to the initial scaffold of woven-fibered bone; much of the non-lamellar compacting tissue was actually composed of parallel-fibered bone, rather than woven-fibered bone. A similar condition was found in the bones of large-bodied mammals (horse and sheep; Kerschnitzki et al. 2011), which Stein and Prondvai (2013) considered an independent evolutionary innovation.

The relative amount of woven-fibered component of the compacting tissue varies within my sample as well. For example, the tibia of *Plateosaurus* (SMNS F14A; Figure 2.64) has a mix of parallel-fibered bone and woven-fibered bone; woven-fibered bone often forms the inner core of the interstitial bone between canals. This is perhaps to be expected, given that *Plateosaurus* is a sauropodomorph, as were the Stein and Prondvai (2013) samples. However, I also observe this in some of the birds in my sample. Regionally within the tibiotarsus of *Paracathartes*, woven bone is restricted to a thin core at the center of the lamina, and parallel-fibered bone composes the regions between the woven-fibered core and the lamellae surrounding the primary osteon. The primary osteons in the humerus of *Corvus* (Figure 2.107) have one or two clear lamellae surrounding the vascular canal. Surrounding these lamellae are many layers of parallel-fibered tissue, which make the total osteonal diameter much larger. However, the transition from the woven-fibered bone of the initial scaffold to the parallel-fibered bone surrounding the osteon is indistinct.

This phenomenon is not limited to the birds in my study. I have observed identical patterns of parallel-fibered compacting bone between the woven-fibered core in the interstitial bone and the lamellae of the primary osteon in the some of the birds in the Foote Collection [e.g., the femora of the turkey (*Meleagris*; CMC 109), *Rhea* (CMC 114), ibis (CMC 138)]. This condition is also apparent in the tibiotarsi of *Rhea* and a moa that Houde sampled for his 1986 and 1987 studies (personal observation).

Stein and Prondvai (2013) concluded that the presence of parallel-fibered tissue in the fibrolamellar complex called into question the rapid growth rates that had been estimated for sauropods and possibly other dinosaurs, and suggested that perhaps canal pattern was a better histological proxy for growth. I disagree with that conclusion; the presence of parallel-fibered bone reflects a lower bone *compaction* rate, not a lower bone deposition rate. Bone deposition rates (reported in µm/day) measure *radial* deposition under the periosteum; i.e., the rate of radial expansion of the initial bone scaffold. Furthermore, these rates are already known to be correlated with the fibrillar organization of the bone, even in taxa that do not produce fibrolamellar bone (e.g., Montes et al. 2007, 2010; Cubo et al. 2008, 2012).

The rate of canal compaction and the proportion of woven-fibered bone in fibrolamellar bone may be correlated with other aspects of an animal's physiology, ecology, or life history. For example, Stein and Prondvai (2013) noted that variations in the rate of bone compactness and the fibrillar organization of that compacting tissue have implications for biomechanics, especially regarding the structural integrity of the bone under different loading regimes. I agree with them that the proportion of woven-fibered tissue actually present in fibrolamellar bone should be noted in future descriptions.

2. *The presence of woven-fibered bone does not always imply fibrolamellar bone*.

Just as I observed primary osteons in lamellar, parallel-fibered, and woven-fibered bone, I also observed simple primary canals in lamellar, parallel-fibered, and woven-fibered bone. Although de Ricqlès (1975) and Francillon-Vieillot et al. (1990) acknowledged that both types of canals can occur in tissues of all three fibrillar organizations, their categorization (e.g., Francillon-Vieillot et al. 1990: Figure 14, p. 509) tends to limit discussion of canals in woven-fibered bone to primary osteons. Admittedly, this is a common situation (probably the most common), but since that typology came into regular use, the paleohistological literature has tended to synonymize woven-fibered bone and fibrolamellar bone. Below, I discuss three situations that I observe in my dataset in which nonpathological woven-fibered bone is not associated with lamellar bone (i.e., it is not vascularized by primary osteons).

The first situation is found in juvenile tissues, in which primary woven-fibered bone has been deposited (the initial scaffold and possibly woven-fibered compaction), but the compacting tissue has not yet been finished with lamellar bone. This is an early stage in the ontogeny of primary osteons; if the bone had been allowed to continue developing, primary osteons eventually would have formed. de Ricqlès (1975) and Francillon-Vieillot et al. (1990) discussed this type of tissue, and referred to these canals as "primary Haversian cavities", "primary Haversian spaces", or "primitive Haversian spaces". However, the term has largely been ignored in the histological and paleohistological literature [Ferretti et al. (2002), Marotti (2010), and Reisz et al. 2013 are exceptions], even in discussions of embryonic, perinatal, and juvenile tissues, where this type of canal is most likely to be found (e.g., Chinsamy 1990; Chinsamy 1993; Horner et al. 2001; Horner et al. 2009; Werning 2012).

In woven-fibered bone, primary Haversian cavities can be distinguished from simple primary canals by the relative size of the canals; the former range in size between 50 and 250 μm, whereas the latter are much narrower in diameter (Francillon-Vieillot et al. 1990). Primary Haversian cavities also can be distinguished from (mature) primary osteons not only by the size of the canal, but also because mature primary osteons are finished by lamellar bone close to the vessel. Primary Haversian cavities can be distinguished from the expanded canals that precede secondary osteon deposition by the lack of a resorption surface.

Because these canals represent an early phase in primary osteonal development, they are most common in the tissues of juveniles of rapidly growing taxa. Among my samples, I only observed primary Haversian cavities in the femora of of juvenile *Massospondylus* (BPI/1/5253a; Figure 2.68) and *Megapnosaurus* (NMZB QG 45; not figured). However, in the literature describing the bone tissue of perinatal archosaurs, a few additional examples are available. These include a perinatal femur of *Dryosaurus*, an ornithopod dinosaur (MWC 1473-F3-2; Horner et al. 2009: Figure 4B, p. 739), a tibia of a full-term embryonic emu (*Dromaius novaehollandiae*; MOR 98-5-T/F-L3; Horner et al. 2001: Figure 2G, p.43), and the

long bones of embryonic sauropodomorphs (Reisz et al. 2013: Supplementary Figure 3). Notably, I did not observe primary Haversian cavities in juvenile *Alligator* (UCMP 68331, UCMP 68314; Figure 2.28) despite the presence of woven bone; these specimens had already developed true primary osteons, with a lamellar border surrounding each canal (this is expected; Horner et al. [2001] observed primary osteons even in embryonic *Alligator*). Based on the available examples, primary Haversian cavities are most likely to be found in embryos, and in perinates or juveniles of large-bodied, fast growing taxa.

Although these canals are rare, I argue that the term "primary Haversian cavities" should be used when it applies, because it carries important information about the ontogeny of the canals and their stage of maturity. It is a potentially useful term for discussions about the rate of canal compaction, as well (see points 1 and 3).

In the second situation, nonpathological woven-fibered bone may occasionally be vascularized by canals other than primary osteons, even in subadult and adult individuals. For example, the femoral cortex of a proterochampsian (MCZ 4038) is composed of woven-fibered bone and vascularized by simple primary canals (Figure 2.17). Admittedly, this is a rare combination of histological characters (this is the only example), but it is not an isolated case; de Ricqlès et al. (2008: Plate 2, Figure 3, p. 66) illustrate the identical condition in another proterochampsian (likely the same taxon). Francillon-Vieillot et al. (1990) comment that woven-fibered bone is nearly always vascularized by primary osteons, but it is worth noting that some exceptions exist.

The third situation in which nonpathological woven-fibered bone is vascularized by canals other than typical primary osteons can be observed in the long bones of *Pterodactylus*, *Crax*, and *Rhynchotus*. In *Pterodactylus*, most of the bone compacting the vascular canals is woven bone, similar in relative amount to the primary osteons of typical fibrolamellar bone. However, the bone is finished by a thin parallel-fibered bone, rather than lamellar bone (Figures 2.34, 2.35). Similarly, in *Rhynchotus* and *Crax*, woven-fibered bone comprises the interstices between canals, but the canals are compacted by several layers of parallel-fibered bone, and lamellae are absent (Figures 2.100, 2.102, 2.103). This type of canal is not described by de Ricqlès (1975) and Francillon-Vieillot et al. (1990); I have not found reference to it elsewhere in the literature.

This condition could result from either relatively faster or relatively slower compaction of vascular canals, depending on the relative proportion of parallel-fibered bone present. *Pterodactylus* seems to represent the first scenario: most of the compaction involves woven-fibered bone, but the compaction is finished with parallel-fibred bone (which has faster bone deposition rates compared to lamellar bone). In *Crax* and *Rhynchotus*, the condition seems developmentally similar to that observed in sauropodomorphs (see Point 1; Stein and Prondvai 2013) and *Corvus* (Point 1), in which much of the compaction is completed with parallel-fibered bone, rather than woven-fibered bone (which has faster bone deposition rates than parallel-fibered bone). The main difference seems to be that in *Crax* and *Rhynchotus*, the canals are never finished by lamellar bone.

The construction of these canals again highlights the need for further research into how canals are compacted in woven-fibered bone, after the initial scaffold is deposited. This process is clearly more variable than previously appreciated, at least among archosauromorph reptiles. The most common state is that described by de Ricqlès (1975) and Francillon-Vieillot et al. (1990), in which the interstices between canals are composed of woven-fibered

bone, which is finished by one or two lamellae as the bone tissue approaches the canal. However, in some taxa, this finishing tissue may be parallel-fibered rather than lamellar (as in *Pterodactylus*). If one allows that the compaction might be finished using the same type of tissue as initially deposited, as in the proterochampsian, this same process would result in simple primary canals rather than primary osteons (*sensu* Francillon-Vieillot et al. 1990). Similarly, the type of compacting tissue is also variable; in many taxa it is woven-fibered, but for some, much of the compacting tissue is composed of parallel-fibered bone (as in the sauropodomorphs, *Rhynchotus*, *Crax*, and *Corvus*), which may be further finished by lamellae (as in *Plateosaurus* and *Corvus*).

In all cases described above, compaction clearly occurs by the same process; it is only the rate of deposition of the compacting and finishing tissue (as expressed by the different tissue types during each phase of deposition) that differ among the taxa. We tend to think of primary osteons and simple primary canals as different structures because they look different. From a developmental perspective, however, it is easy to see that merely by varying the rates of deposition during formation of the initial scaffold, subsequent compaction towards the canal, and final finishing phase, a common process could result in entire known range of primary canal types.

3. *Osteocyte orientation is highly correlated with fibrillar organization.*

de Ricqlès (1974, 1975,1976,1980) and Francillon-Vieillot et al. (1990) noted that osteocytes in woven-fibered bone tended to be globular or round in cross section, whereas osteocytes in lamellar and parallel-fibered bone tended to appear flattened in cross section. Using mouse, horse, and sheep models, Hirose et al. (2007) and Kerschnitzki et al. (2011) recently established that osteocyte orientation and canalicular arrangement all reflect the organization of the extracellular matrix. These observations correspond to the way bone forms under the periosteum. In bone formed by static osteogenesis, mesenchymal stem cells differentiate into osteoblasts and then further develop into osteocytes at the same position. The osteoblasts secrete matrix independent of each other, and develop into osteocytes after enclosing themselves in their own matrix (Ferretti et al. 2002; Palumbo et al. 2004; Marotti 2010). This method of bone deposition always yields woven-fibered bone with globular osteocytes that vary in orientation relative to the long axis of the bone (Ferretti et al. 2002; Marotti 2010). When bone forms by dynamic osteogenesis, osteoblasts move in a coordinated fashion along the osteogenic lamina of an ever-thickening layer of bone. They develop into osteocytes after they are enclosed by matrix produced by other osteoblasts, and thus appear flatter than the osteocytes produced by static osteogenesis. Because these osteoblasts are coordinated in their movements, they are all more or less aligned during matrix deposition, and this alignment persists after enclosure within the matrix (Ferretti et al. 2002; Marotti 2010). This type of bone deposition tends to produce more organized bone tissue (lamellar or parallel-fibered bone).

My reptilian dataset shows the same relationship between osteocyte lacunar orientation and collagen fiber orientation that was established in mammals. In all cases, the osteocytes in primary woven-fibered bone tissue show no preferred orientation relative to the long axis of the bone, and no preferred orientation or arrangement relative to each other. This is easily established by focusing through the slide, which allows the observer to assess and compare the orientation of nearby osteocytes simultaneously. Although osteocytes often

appear circular in cross section, they are always somewhat ellipsoid, and a long axis can be determined by noting changes in the outline of the osteocyte as the plane of focus moves through the section. In primary lamellar bone, osteocytes are much better organized. In all cases, osteocytes are oriented perpendicular to the long axis of the bone and are aligned circumferentially, forming rows along lamellae. The spacing between osteocytes in lamellar bone was fairly regular, as well.

The osteocytes of parallel-fibered bone were better organized than those of woven-fibered bone, and less so than those of lamellar bone. In every case in which I observed parallel-fibered bone, at least two-thirds of the osteocytes were oriented perpendicular to the long axis of the bone. The rest were generally oriented oblique to the long axis. There was also variability in the arrangement of lacunae relative to each other; osteocytes were arranged circumferentially, but not aligned perfectly and generally with somewhat irregular spacing between lacunae.

I found osteocyte orientation to be a better predictor of fibrillar organization than canal type, canal density or vascular patterning. Within this dataset, I observe primary osteons and simple primary canals in parallel-fibered bone and woven-fibered bone (Table 2.3), and both canal types are also known to occur in lamellar bone (e.g., de Ricqlès 1974, 1975,1976,1980; Francillon-Vieillot et al. 1990). I also observed higher canal densities in taxa whose cortices were mainly composed of parallel-fibered (*Massospondylus*; Neornithischia, cf. *Lesothosaurus* or *Stormbergia;* the outer cortex of *Effigia*), weakly woven-fibered (e.g. Loricata, cf. *Postosuchus*) and woven-fibered bone (many taxa, see Table 2.3). Finally, some specimens have complex vascular patterns (i.e., anastomosis in more than one direction) even within parallel-fibered bone. Examples of this condition include small reticulations in the outer cortex of the proterochampsian, extensive circumferential anastomoses in Neornithischia, cf. *Lesothosaurus* or *Stormbergia*; and plexiform and subplexiform patterns throughout the parallel-fibered cortex of adult *Massospondylus* (BPI/1/5241a; Figures 2.70; 2.71, bottom image).

In fossil bone, birefringence patterns reflect either the presence of original collagen or the replacement of them by apatite or quartz crystals (Lee and O'Connor 2013). As I noted in Chapter 1, this is the most common way of diagnosing fibrillar organization in Recent and fossil bone. However, in some specimens, collagen fibers or their replacement crystals are lost to diagenetic alteration, and no birefringence pattern can be observed under polarized light. In other specimens, the fossilized cortex may contain dark or dark-staining minerals, such that the bone must be ground very thin to observe structures like osteocytes and vascular canals. In these cases, even though collagen or replacement crystals are present, but the specimen is so thin that a birefringence pattern cannot be observed under polarized light. The relationship between osteocyte lacunar orientation and fibrillar organization provides an alternate way of diagnosing fiber orientation in fossil bone when birefringence patterns cannot be observed, or when the signal is difficult to resolve.

Sampling

Paleohistological studies often rely on one or two elements or individuals and extrapolate species-level or clade-level growth dynamics from these. For example, de Ricqlès et al. (2003b) sectioned two phytosaurs from the *Placerias* Quarry (UCMP locality A269),

and these two specimens (one of which could not be re-located for this study) represent all that is known about the bone histology and growth of phytosaurs. UCMP 25921 has been re-examined by Cubo et al. (2012) and Legendre et al. (In press), as well as this study, but no additional materials have been described in the decade since de Ricqlès and his colleagues published their initial study. This problem will be ameliorated somewhat once the *Paleorhinus* study mentioned above (Bronowicz 2009) is published. Additionally, I have obtained phytosaur materials from the Hayden Quarry for future analysis. Unfortunately, until these studies are published, our understanding of phytosaur growth, ontogeny, and metabolism is essentially based on one specimen.

This is not a criticism of the de Ricqlès et al. (2003b) study, an overview of pseudosuchian bone microstructure that was never intended to be a detailed analysis of phytosaur growth dynamics, or the subsequent studies that analyzed the original materials using new methods. However, the case of phytosaurs illustrates a general problem with paleohistological studies, namely that for most taxa, the available materials are not sufficient to address questions of histological variation. Horner et al. (2000) described four main influences on osteohistology: phylogeny, ontogeny, biomechanics, and the environment (other influences, such as pathology, were considered important but not universal influences). Increasing the size of the sample examined would do much to address the variation resulting from all four factors. Unfortunately, although many studies (especially of dinosaurs) have addressed the first two factors, the latter two influences have received far less attention.

Although the focus of my study is on phylogenetic variation, I include comments below on how sampling affects my interpretations of growth and metabolic rates of these taxa, especially in regard to ontogeny, intra- and interelemental variation, phylogeny, and environment.

Sampling: Ontogenetic variation

For comparative purposes, I attempted to sample individuals of comparable ontogenetic stage for this study. Whenever possible, I used specimens whose histological record of ontogeny included the time of peak postnatal growth rates (equivalent to the point of inflection on a sigmoidal growth curve), and avoided specimens whose size or skeletal development suggested senescence or juvenile stages (although these were sometimes included to complement additional specimens). Because bone is deposited over time, its histological record always preserves at least a partial ontogenetic trajectory of that individual. This allows direct observation of the ontogenetic changes in bone tissue over the length of that record. For most taxa in this study, this record comprises several years of growth. Additionally, for some taxa (e.g., *Trilophosaurus*, *Alligator*, *Megapnosaurus*, *Massospondylus*), partial ontogenetic series were available for sampling and examination, allowing observations to be made for a greater portion of ontogeny and individual variation to be assessed.

Nearly all taxa examined in this study show a decrease in the histological indicators of fast growth with age, not only among individuals within an ontogenetic series, but also within individual elements moving periosteally through a section. For example, the bone tissue in juvenile *Alligator* is woven-fibered. The bone of sexually mature males is woven-fibered and well vascularized, with extensive anastomoses that form complex vascular patterns. However, as these animals age, the new bone they deposit is proportionately less woven-fibered.

Instead, parallel-fibered bone makes up a greater proportion of each zone. Vascular density decreases and the anastomoses between canals become less extensive, such that in older individuals, only isolated longitudinal canals are visible. This pattern is true even for *Trilophosaurus*, the taxon I examined that shows the least histological variation among individuals. The smallest *Trilophosaurus* femur, TMM 31025-787, shows higher canal density compared to the largest, even though fibrillar organization and vascular patterns are the same.

Within individuals, these same trajectories can be observed. For example, in a tibia of the Hayden Quarry silesaurid (GR 190; Figure 2.47), well vascularized woven-fibered bone can be observed internal to the first LAG. In this region, canals anastomose with several others and form small reticulations. Near the periosteal surface, isolated longitudinal canals are the most common canal type, canal density is lower than the innermost cortex, and the bone is parallel-fibered. These patterns are to be expected; histological characters that vary with growth rate should show signs of slower growth rate as the animal approaches its growth asymptote. This observation has been made for many extant and extinct taxa (e.g., Amprino and Godina 1947; Enlow and Brown 1958; Francillon-Vieillot et al. 1990; Castanet et al. 1993; Horner et al. 1999, 2001).

Sampling ontogenetic series is important because some histological characters may only be expressed at some points during ontogeny, or may be obscured by later remodeling. For example, as described above, female *Alligator* produce woven-fibered bone only in the first few years of life; during most of their ontogeny, they produce parallel-fibered bone. To complicate matters, female *Alligator* remodel the inner cortex earlier and more extensively than males do, destroying the record of earliest ontogeny. A study that included only older females might incorrectly conclude that *Alligator* were incapable of producing this type of tissue.

One character that might initially seem less affected by ontogeny is osteocyte density. In most of the elements I observed, osteocyte density does not progressively decrease centrifugally within a single section (although it may vary within that transect, or moving around a section). The only exceptions are the proterochampsian and *Dromomeron*, which have decreases in osteocyte density within single sections. This apparent lack of variation might at first seem to suggest that metabolic rate stayed stable through ontogeny. However, I think this may result from a sampling artifact. In nearly every taxa where partial ontogenetic series of the same elements were sampled [e.g., *Trilophosaurus, Alligator, Dimorphodon, Fruitadens,* and *Massospondylus*; see Table 2.2], younger individuals showed higher osteocyte densities than larger/older ones. One exception is *Megapnosaurus*, in which both specimens analyzed had nearly identical average osteocyte densities. Because osteocyte density correlates with basal/standard metabolic rate, this suggests that metabolic rates decline with age, but perhaps over a longer time scale compared to growth rates. As described in Chapter 1, my transect sampling method is somewhat time-transgressive; perhaps if box plots were restricted to single zones rather than allowed to cross between them, this could be resolved at a finer scale.

The ontogenetic differences in osteocyte density between juveniles and adults might reflect an interesting aspect of metabolic ontogeny (for description of this section, see Figure 2.108, top panel; note black line). In mammals, basal metabolic rate (BMR) progressively increases during embryonic, perinatal, and early juvenile stages. In birds, a similar pattern of

increase in standard metabolic rate (SMR) occurs during embryonic growth, but just before hatching, SMR decreases slightly. Post-hatching, SMR again increases dramatically (Vleck and Vleck 1996). Notably, in both clades, juvenile BMR/SMR is substantially higher than that of adult conspecifics (at least twice as high in some taxa; Nagy 2000). This reflects increased energetic demands during times of active growth in these clades, which is associated with greater foraging costs and heat increment of feeding costs in growing endotherms (Blaxter 1989; Wieser 1994; Nagy 2000). Later (but still while juveniles), BMR/SMR and mass-specific BMR/SMR begin to decrease to adult levels (Hill and Rahimtulla 1965; Kleiber 1975; Adolph 1983; Wieser 1994). Once adulthood is reached, these rates are maintained at fairly consistent levels through reproductive life (Adolph 1983).

If metabolic rates in the extinct taxa described above followed a similar ontogenetic trajectory in metabolism to mammals and birds, then the histological indicator of metabolic rate (osteocyte density) should be higher (even substantially higher) in juveniles compared to adult conspecifics, and most adults should show stable osteocyte densities through several zones. This is the pattern I observed in nearly all the extinct taxa where both juveniles and adults were sampled.

Given that this ontogenetic decline in BMR/SMR may occur relatively quickly, and that BMR/SMR is maintained through non-senescent adulthood, it is possible that a statistical difference in metabolism (as reflected in osteocyte density) would not be detectable without sampling the earliest stages of growth. This may explain why I see these differences primarily in taxa for which I have analyzed ontogenetic series of the same element.

In contrast to mammals and birds, studies of neonatal lizards, snakes, and turtles (Bennett and Dawson 1976; Brown et al. 2005) have shown that SMR and mass-specific SMR are similar in neonates, juveniles, and adults of the same population, even when temperature is experimentally adjusted (see Figure 2.108, bottom panel; note black line). If extinct taxa followed an ontogenetic trajectory in metabolic rate similar to those of squamates and turtles, then we would expect osteocyte density to be very similar throughout an ontogenetic series. In *Sphenodon*, the only non-archosauromorph for which I had a partial ontogenetic series available, osteocyte densities varied by less than 100 cells/mm^2 across all individuals, and by less than 150 cells/mm^2 for all within-individual transects and all box plot samples except one (standard deviation = 74.71 across all samples). Among the six specimens I examined, the only area where osteocyte density was visibly higher than the rest of the cortex was in CMC 047, in the region of potential embryonic bone internal to the first LAG/hatching line. Among the extinct taxa observed, this was also the case in *Megapnosaurus*, but only two specimens were analyzed.

Ontogenetic variation in osteocyte density could be another line of evidence to support hypotheses of metabolism in fossil taxa. If, when juveniles are included in the sample set, osteocyte density showed a dramatic decrease through ontogeny, it would suggest an ontogenetic trend in metabolism similar to that observed in living mammals and birds. If osteocyte densities were consistent throughout ontogeny even when juveniles are included, it would suggest an ontogenetic trend in metabolism more similar to those of extant lepidosaurs and turtles. Notably, these trends would be distinct from trends in histological indicators of growth rate or body size, which have different ontogenies (Figure 2.108).

Sampling: Variation among different skeletal elements

My study was designed to minimize the effects of interelemental variation by examining the histology of only three bones: the humerus, femur and tibia. Because of specimen availability, I was unable to sample all three elements for most taxa, and often, different elements were taken from different individuals (as opposed to sampling all three elements for several individuals, which would be ideal).

As earlier authors noted (e.g., Amprino and Godina 1947; Francillon-Vieillot et al. 1990; Castanet et al. 1993; Horner et al. 1999), different skeletal elements experience different growth trajectories and thus may show differences in histology. For example, in the ornithopod dinosaur *Tenontosaurus* (Werning 2012), in which I examined ontogenetic series of five limb bones (humerus, ulna, femur, tibia, and fibula), I noted that the ulna and fibula experienced greater secondary (Haversian) remodeling than the other three elements. Within a single individual, secondary remodeling also began at an earlier age in both the ulna and fibula, such that those bones looked histologically older. This makes sense given that different elements are subject to different biomechanical and physiological influences. Additionally, studies of extant animals have established that different cells, organs, and organ systems have different metabolic requirements (see for example Hulbert and Else 2000, and references therein). Inter-elemental ontogenetic differences in growth rate and histology also have a phylogenetic signal; for example, in ornithopod dinosaurs, the tibia experiences the least remodeling among the major limb bones (Horner et al 2000; Werning 2012), whereas in all tyrannosaurids (theropod dinosaurs), the fibula was the least remodeled (Erickson et al. 2004).

Despite this understanding, few studies have attempted to show systematically how bone histology varies by element across a wide phylogenetic sample. The most thorough of these is by Cubo et al. (2012), who sampled the humerus, femur, and tibia in 16 extant amniotes and quantified various histological characters. The characters they examined included vascular density, osteocyte density, osteocyte size, and osteocyte shape. Additionally, they calculated indices of canal orientation, representing the proportion of radial, oblique, and circumferential anastomoses. The focus of that study was to examine how these factors varied with bone depositional rate; they did not seek to explain how these characters varied by element. However, their data tables (Supplemental Information: Table 1) show that whereas most characters examined varied quite a bit among the elements of a single individual, they did not do so in a consistent pattern. For example, no one element consistently showed higher depositional rates than the other two across taxa, even though it was common for these rates to vary from element to element. The only exception was osteocyte density, which was generally quite similar among all three elements examined. However, when the data were controlled for phylogeny, Cubo et al. (2012) found that all of the characters reported in their Table 1 could be used in a multivariate model to predict bone depositional rate, and that the equations for these models differed by element.

Although most taxa in my study include examples of different elements and different individuals, very few individuals are represented by more than one element. Among these, I do not observe any consistent pattern of variation, although nonhomologous elements often show differences in vascularity, vascular patterning, and osteocyte density. In this way, my data are similar to those of Cubo et al. (2012). It is possible that patterns of variation in inter-elemental ontogeny are only apparent at finer phylogenetic scales, or that statistical methods that account for phylogeny are needed to discover them. Regardless, without sampling several

elements from ontogenetic series, individual variation cannot be distinguished from interelemental variation in my study.

Even though interelemental comparisons of ontogenetic variation in bone histology have been made for a handful of extinct taxa, such a study has not yet been done for extant animals. Cubo et al. (2008, 2012) used only neonates and young juveniles in their work because their focus was to examine the relationship between histological characters and bone depositional rate during times of fastest growth. These basic ontogenetic data are needed before phylogenetic trends in variation can be discussed.

Sampling: Phylogeny

Although my study focused on phylogenetic variation among archosauromorph reptiles, it is worth mentioning that large phylogenetic gaps in our knowledge of reptilian growth and histology are still present, even within this clade.

In my histological descriptions above, I mentioned that Neognathae, the most diverse clade among extant tetrapods, is undersampled from a histological perspective. The historical studies of bird osteohistology (e.g., Quekett 1849a, 1849b; Foote 1916; Amprino and Godina 1947; Zavattari and Cellini 1956; Enlow and Brown 1957; Meister 1965) were limited in their taxonomic (and ontogenetic) sampling. None except Foote (1916) included more than 20 taxa, and only some of these studies examined several elements. In the last two decades, comparative studies of Mesozoic and Cenozoic bird microstructure (e.g., Chinsamy et al. 1995a, 1995b, 1998; Chinsamy and Elzanowski 2001; Chinsamy 2002; Erickson et al. 2009a) have been more common than comparisons of extant bird microstructure. These recent studies of extant birds have tended to focus either on one taxon, or one or two histological characters rather than describing microstructure at the tissue level (e.g., Houde 1986, 1987, 1988; Rensberger and Watabe 2000; de Margerie 2002; de Margerie et al. 2002, 2004; Starck and Chinsamy 2002; Simon and O'Connor 2012; though see Castanet et al. 2000 for an exception). For birds, we still lack large comparative studies that examine ontogenetic, phylogenetic, populational/geographic, or ecological variation in bone histology, especially among neognaths. Sampling all 10,000+ extant species of birds is likely impossible (or at the very least, highly impractical), but this type of study would be beneficial even at the ordinal or familial level.

Another large gap in our understanding of reptilian growth is that of pseudosuchian archosaurs. Despite a rich fossil record, only a few of the earliest lineages and living species have been examined. Although the incredible level of avian diversity places practical limits on sampling among birds, this is not the case for extant crocodylians, of which there are approximately 24 extant species (Schmitz et al. 2003; Hekkala et al. 2010, 2011), many of which are well represented in museum collections. As noted above, bone histology from extant *Alligator mississippiensis* is well described in the literature (e.g., Enlow 1969, Peabody 1961, Chabreck and Joanen 1979, Ferguson et al. 1982, Ferguson 1984, Reid 1984, Wilkinson and Rhodes 1997, Horner et al. 2001, de Ricqlès et al. 2003b, Lee 2004, Padian et al. 2004, Schweitzer et al. 2007, Tumarkin-Deratzian 2007, Wilkinson 2008, Klein et al. 2009, Woodward et al. 2011), although most of these studies relied on captive-bred or captive-reared individuals, which grow faster than wild alligators (Coulson et al. 1973). Only three other extant crocodylians have been histologically described or figured in the literature:

Crocodylus niloticus (Hutton 1986, Cubo et al. 2012), *C. siamensis* (de Buffrénil 1980), and *C. porosus* (Chinsamy-Turan 2005).

Though living pseudosuchians are all medium- and large-bodied aquatic ambush predators (Brochu 2001, 2003), historically this clade has been more diverse taxonomically (Hutchison 1982; Brochu 2003; Nesbitt 2011) and more disparate ecologically. Mesozoic and Cenozoic pseudosuchians included bipedal species that mimicked theropod dinosaurs in form and physiology (e.g., *Effigia* and other poposaurs; Nesbitt and Norell 2006; Nesbitt 2007; Gauthier et al. 2011), large armored herbivores (aetosaurs), and both fully terrestrial and fully marine predators (champsosaurs and thalattosuchians, respectively; Hutchison 1982; Nesbitt 2011). In short, most of the diversity and disparity within Crocodylomorpha is preserved in the fossil record. Despite this great diversity and an excellent fossil record, sampling among fossil pseudosuchians is only slightly better than among extant crocodylians. Although several taxa outside Crocodylomorpha have been sampled (see my descriptions above), most lineages within Crocodylia have not been examined. The exceptions are thalattosuchians (Hua and de Buffrénil 1996) and some extinct taxa that fall within crown Crocodylia [e.g., the alligatoroid *Leidyosuchus* (Padian et al. 2004)].

Although skeletochronological methods are commonly used to assess age and population structure in lepidosaurs, their osteohistology is rarely described beyond LAG counts, and their growth is rarely assessed using histological methods (Hugi and Sánchez-Villagra 2012).

Extensive sampling among extant reptiles is critical in order to better calibrate our understanding of how bone microstructure relates to growth rates and metabolic rates. Furthermore, if crocodylians have secondarily derived their slow growth and metabolic rates, as seems likely from the distribution of histological characters relating to faster growth and higher metabolic rates, fossil taxa are critical to establishing when that transition occurred.

Sampling: environmental variation

The relative influence of environmental variation on bone histological variation is largely unknown, even among extant taxa. However, it should have at least some effect; variation in factors such as temperature and seasonality are known to affect growth rates in many living vertebrates (particularly “ectotherms”), and the characteristics of bone microstructure reflect variations in growth rate. Although not extensively studied, in a few cases, environmental differences are associated with differences in the appearance of bone tissue among different individuals or populations.

Population-level differences in growth rate and histology were established for the salamandrid *Triturus marmoratus* (Caetano et al. 1985; Caetano and Castanet 1993). Those studies compared growth in three populations in Portugal, whose habitat varied in average air and water temperatures, altitude, rainfall, and dry season duration. The three populations varied in body size, growth rate, and longevity; the population experiencing the lowest temperatures, highest rainfall, and shortest dry season grew largest and at the fastest rate, and lived longest. Additionally, the LAGs varied in appearance among the three populations, and each group had different levels of medullary cavity expansion. However, several environmental variables differed among these populations; it is not clear which one(s) had the greatest influence on growth rates and histological features.

Another potential example is the American alligator, *Alligator mississippiensis*, described above. Sex in *A. mississippiensis* is determined by incubation temperature (Ferguson and Joanen 1982), and sexual differences in growth rate and time to maturity are reflected in the different appearance of male and female bone tissue (see above). Growth rates, age and size at sexual maturity, and asymptotic size are known to vary across the range of *A. mississippiensis* (Wilkinson and Rhodes 2007), but complementary studies of histological variation have not been undertaken to determine whether microstructure is sensitive enough to record these differences.

Several paleohistological studies suggest that differences in environment cause histological differences. For example, Scheyer and Sander (2007) established that the bone microstructure of turtle carapacial bones could be used to establish an aquatic or terrestrial habitat. Sander and Klein (2005) found differences in body size between two populations of *Plateosaurus*, with high levels of developmental plasticity in both groups (i.e., age did not correlate with size, with no evidence of taxonomic or sexual differences). A recent histological study by Sanchez and Schoch (2013) showed marked differences in fibrillar organization, bone compactness, presence of calcified cartilage, bone deposition rate, number of LAGs, and extent of remodeling in specimens of the Triassic temnospondyl *Gerrothorax* from two fossil lake localities in Germany. Sedimentological and faunal evidence suggest that one of these lakes was nutrient-poor and experienced fluctuations in both salinity and water depth (it was possibly ephemeral). At this locality, there is far greater variation in histology and growth among individuals than at the other locality, which is thought to have been more stable and favorable.

In my dataset, very few taxa are sampled from more than one locality. These include the aetosaurs, *Vancleavea*, and potentially the coelophysoids from Petrified Forest and Ghost Ranch (which may represent the same taxon; Irmis et al. 2007). All three taxa show marked histological differences between the two samples, despite morphological similarity. The aetosaurs clearly represent different ontogenetic stages and are possibly different species, and so histological differences may represent taxonomic, ontogenetic, or environmental differences (or a combination of all three). The coelophysoids differ in cortical thickness, number of LAGs, and osteocyte density despite similar size; however, the Ghost Ranch specimen has yet to be described anatomically and neither has been analyzed phylogenetically, so it is not possible to assess whether these differences result from taxonomic or phylogenetic differences. The *Vancleavea* specimens from Ghost Ranch are morphologically indistinguishable from those found at Petrified Forest, and the sampled femora were nearly identical in size. However, their histology could not be more different: GR 250 is composed of well vascularized woven-fibered bone with a small medullary cavity, whereas UCMP 152662 has much more parallel-fibered and lamellar bone, fewer canals, and a larger medulla. Unfortunately, even with two specimens from different localities that show different histological profiles, the question of environmental variation cannot be answered, because the geological work to establish differences in paleoenvironment has not yet been completed.

Even in studies in which ontogenetic and taxonomic differences can be eliminated, it is difficult to determine how much variation to attribute to environmental differences, and how much to attribute to individual variation. For example, Werning (2012) described the histology of 18 individuals of *Tenontosaurus*, an ornithopod dinosaur. These specimens were

recovered from several localities in two geological formations separated by over twelve degrees of paleolatitude. I did not observe any striking differences in bone microstructure between the specimens in each formation, but noted that individuals varied in the extent of secondary remodeling, vascular patterning, and the ratio of simple canals to primary osteons. Whether these reflected individual or environmental differences specific to each locality could not be determined.

We lack the data to resolve these issues for extant reptiles (including birds), but they could be assessed through long-term captive studies, in which single environmental variables (e.g., temperature, humidity, seasonality) were altered. Establishing how histological variation was influenced by environmental variation in the fossil record requires a better knowledge of how these variables influence microstructure in living taxa, but also better sampling: more specimens from more localities, but also geological work to establish paleoenvironment.

CONCLUSIONS

This extensive study of the bone microstructure of archosauromorphs has resulted in a number of insights and conclusions:

First, the microstructural indicators of faster growth and high metabolic rates in birds can also be identified in most of the ornithodirans, pseudosuchians, and non-archosaurian archosauriforms examined in this study. Their presence in basal pseudosuchians and stem archosaurs indicates these conditions evolved before the avian and crocodylian lineages diverged sometime during the Triassic, and that the slower growth exhibited in living crocodylians must be secondarily derived.

Second, the comparative analysis of a large histological dataset allows observation of a number of infrequently reported microstructural conditions, many related to the rate of tissue compaction towards vascular canals. As others have noted (Stein and Prondvai 2013), the relative proportion of woven-fibered bone varies within fibrolamellar bone. However, I also observed several cases in which woven-fibered bone was not associated with a lamellar component. These include primary Haversian cavities in the juveniles of fast-growing, large-bodied taxa; simple primary canals in woven-fibered tissue; and primary osteons in which parallel-fibered tissue rather than lamellar bone is used as a finishing tissue. These observations invite new thoughts about the nature of bone compaction in woven-fibered bone after the initial scaffolding is deposited. I observed great variation in the appearance of simple canals and primary osteons in the archosauromorphs observed, despite a common process and pattern of bone deposition. I suggest that this variation in appearance can be achieved merely by varying the rates of bone deposition during formation of the initial scaffold, subsequent compaction towards the canal, and final finishing phase.

Third, small sample sizes in paleohistological studies likely obscure important trends related to the influence of ontogeny and environment on bone microstructure. The taxa for which I had larger sample sizes all provided new insights into how these factors impact bone microstructure. For example, ontogenetic differences in growth rate between male and female *Alligator mississippiensis* result in markedly different histological profiles for the two sexes. In the absence of larger sample sizes, one might infer exceptionally high or low growth rates

for the taxon as a whole, rather than the more nuanced reality. Paleohistological studies often extrapolate species-level or clade-level growth dynamics from one or two elements or individuals, often taken from a single locality. Doing so limits the conclusions that can be drawn about natural levels of variation among individuals, but also impedes our ability to discover the relationships between environment and bone microstructure. An understanding of the latter relationship would be especially important in determining the long-term biological impacts of environmental change on growth and metabolic physiology.

Finally, these relationships cannot be established without a much better understanding of bone microstructural variation among and within extant taxa. Sampling skeletal tissues is not always necessary to measure or assess growth and metabolism in living animals. However, they are the only vertebrate tissues that regularly record cellular- and tissue-level physiological processes in the fossil record. A better understanding of bone histological variation could unlock over 300 million years of vertebrate growth and metabolic physiology, allowing researchers to test hypotheses about the abiotic influences and biological innovations that drive their evolution in deep time.

ACKNOWLEDGMENTS

This project was completed over several years as part of a larger collaborative work on the biology, paleoecology, and systematics of Triassic archosaurs. Seven colleagues in particular provided much assistance, support, discussion and commentary: Randy Irmis, Sterling Nesbitt, Kevin Padian, Bill Parker, Nate Smith, Alan Turner, and Jessica Whiteside. Without them, this work could not have been completed. Equally important to the success of this project, many people and institutions offered help and specimen access. I am most indebted to Carl Mehling and Mark Norell (AMNH); Alex Downs (GR); Ellen Lamm, Holly Woodward, and Jack Horner (MOR); Bill Parker and Matt Smith (PEFO); Matt Brown, James Sagabiel, and Tim Rowe (TMM); and Pat Holroyd and Mark Goodwin (UCMP). The UCMP VP Lunch and Fossil Coffee seminars and the MVZ Herp Group seminar saw earlier versions of this research, and were important in shaping how I thought about this project and explained it. I thank the MOR, UCMP, April Carr, and Kevin Padian for access to preparation and imaging facilities. I grateful to the following institutions for funding and financial support of this project: Geological Society of America (Graduate Student Research Grant); Jurassic Foundation; MVZ (Louise Kellogg research award); University of California, Berkeley (Graduate Division Summer Fellowship); University of California Department of Integrative Biology (Gray Research Award, Resetko Summer Research Scholarship); UCMP (Annie M. Alexander Fellowship; Doris O. and Samuel P. Welles Fund; Peabody Fellowship).

This chapter is dedicated to my URAPs and undergraduate volunteers, who made many slides and counted an obscene number of osteocytes. I am privileged to have worked with the following students on this and other histology projects: Dana Baba, Dominique Bertrand, Michael Cheng, Yasmine Colque, Jonathan Ly, Zachary Morris, Rachel Tenney, and Sarah Tulga. Working with these talented students was a highlight of my time at Berkeley. Thank you all so much for your help and all you have taught me.

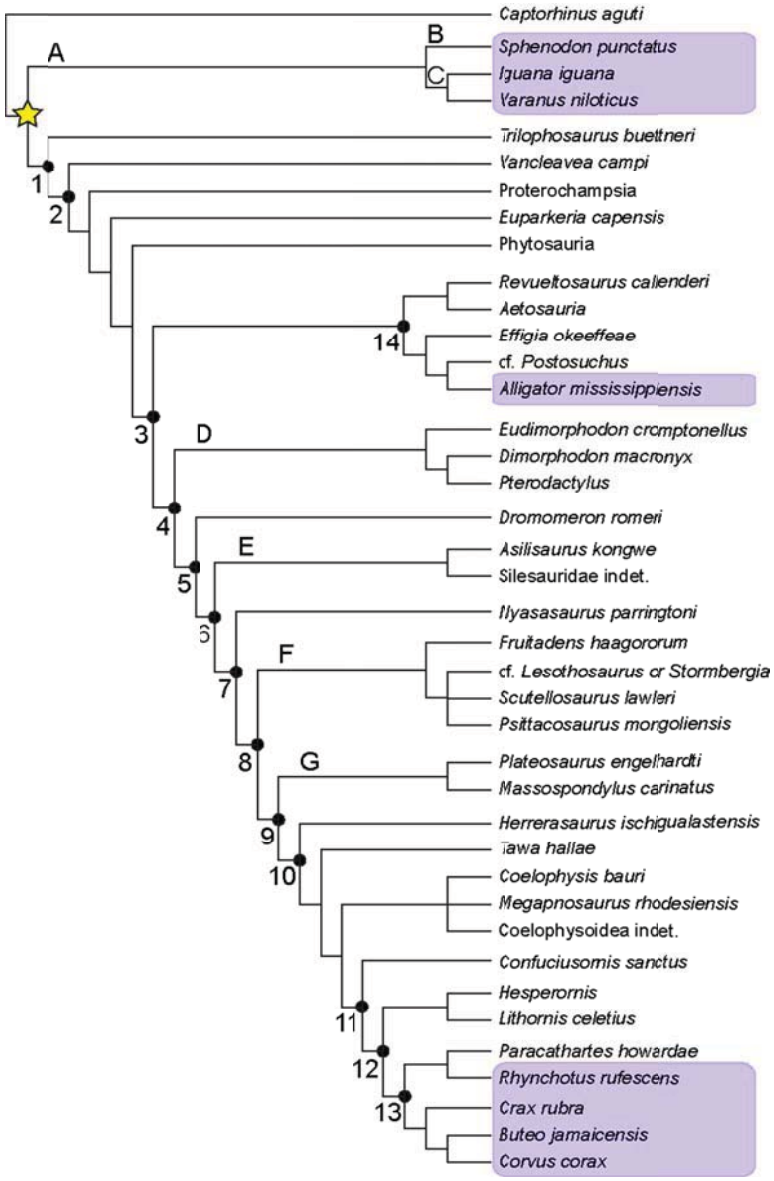

Figure 2.1 Phylogenetic relationships of the eureptilian taxa examined in this study. Extant taxa are indicated by purple boxes. The yellow star indicates the divergence between Lepidosauromorpha (A) and Archosauromorpha (1). Numbers indicate key nodes along the lineage leading to extant archosaurs: **1** Archosauromorpha, **2** Archosauriformes, **3** Archosauria, **4** Ornithodira, **5** Dinosauromorpha **6** Dinosauriformes, **7** or **8** Dinosauria (see text), **9** Saurischia, **10** Theropoda, **11** Aves: Pygostylia, **12** Ornithurae, **13** Neornithes, **14** Pseudosuchia. Letters indicate outgroup lineages also discussed in this study: **A** Lepidosauromorpha, **B** Rhynchocephalia, **C** Squamata, **D** Pterosauromorpha: Pterosauria, **E** Silesauridae, **F** Ornithischia, **G** Sauropodomorpha. Tree is ultrametric (branch lengths do not represent evolutionary distance) and is based primarily on the analyses of Nesbitt (2011) and Nesbitt et al. (2009a, 2010, 2013), with pterosaurs relationships from Andres (2012) and ornithischian relationships from Butler et al. (2007, 2008).

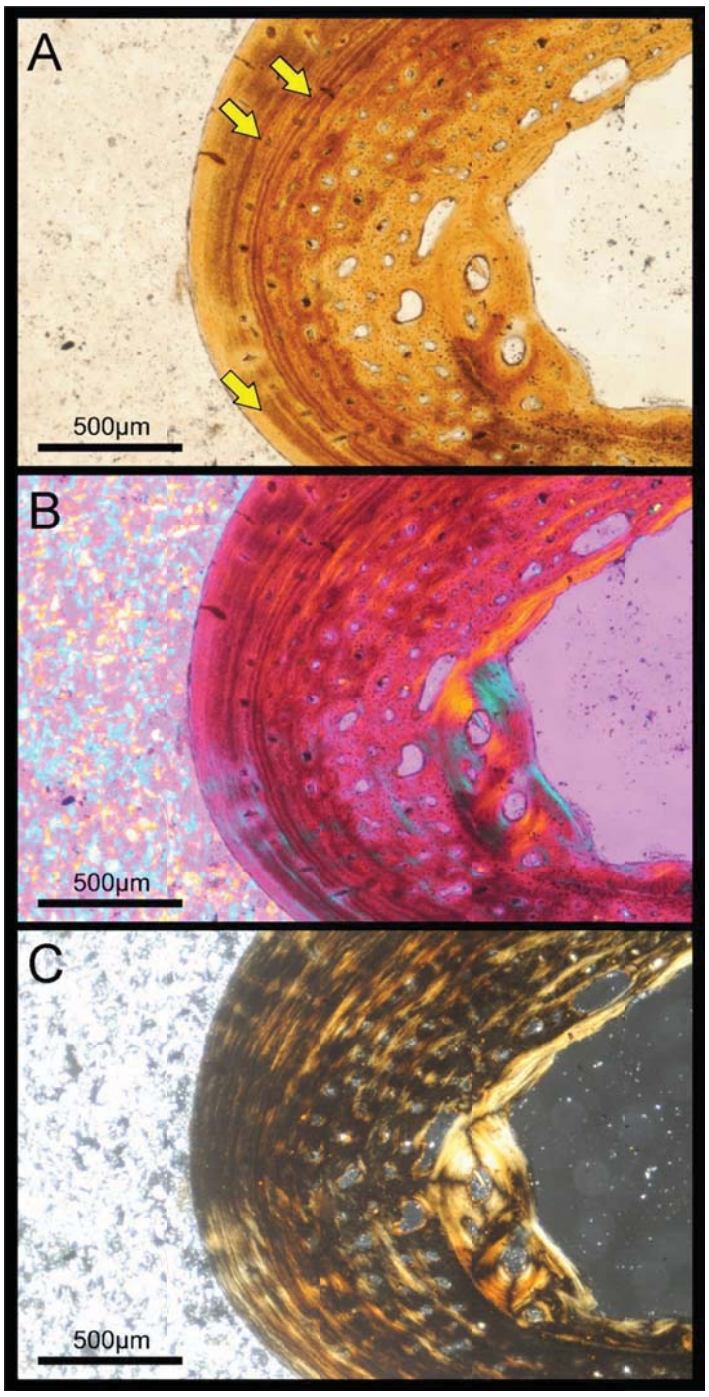

Figure 2.2 Cortical histology of the mid-diaphyseal humerus of *Captorhinus aguti* (UCMP 223509) in A) regular transmitted light, B) elliptically polarized light, and C) crossed plane-polarized light. In C, coarse parallel-fibered bone is visible in the inner cortex of the section (internal to the inner LAG packet), which grades to lamellar bone in the outermost cortex. The periosteum lies to the left in all images, and arrows indicate lines of arrested growth.

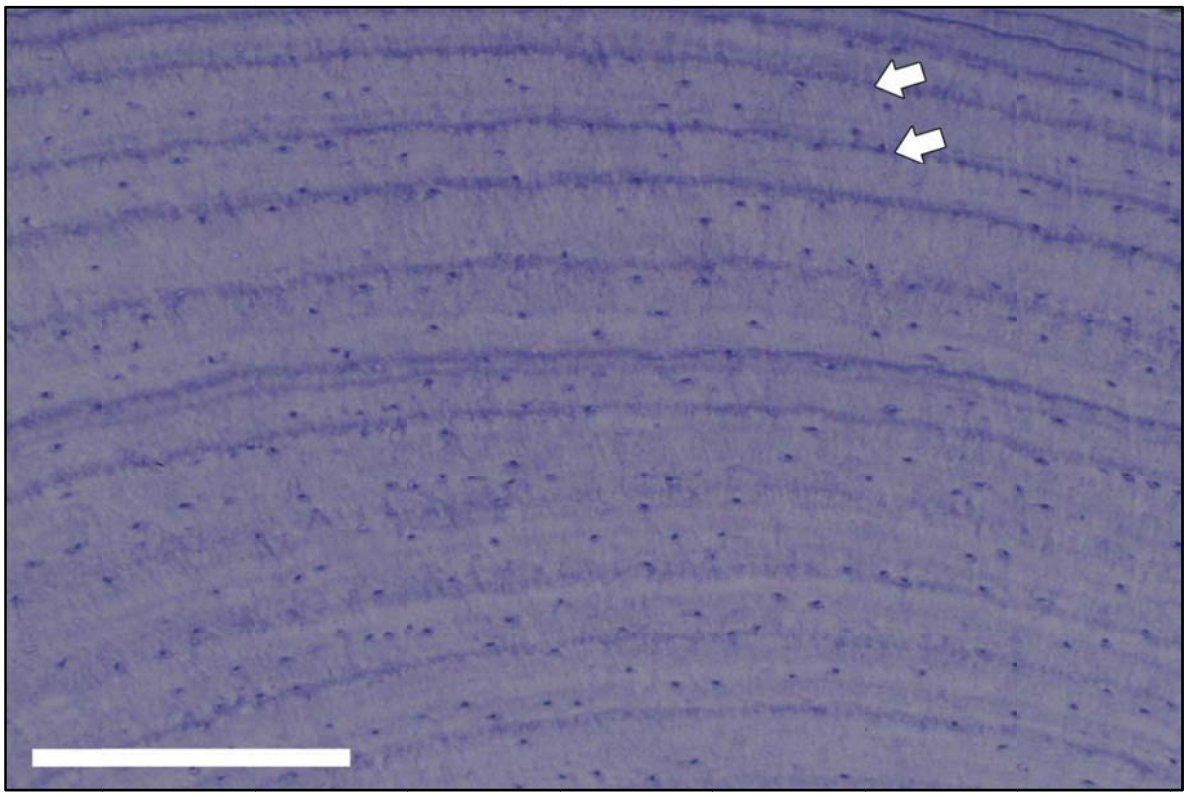

Figure 2.3 Lamellar bone in the mid-diaphyseal femoral cortex of *Sphenodon punctatus* (JC A, demineralized section stained with hematoxylin) in regular transmitted light. Arrows indicate two lines of arrested growth (LAGs), which stain darkly. Between the LAGs, alternating bands of differential staining (light and slightly darker) indicate lamellae (lamellar bone). Periosteum to top of image, scale = 250 μm.

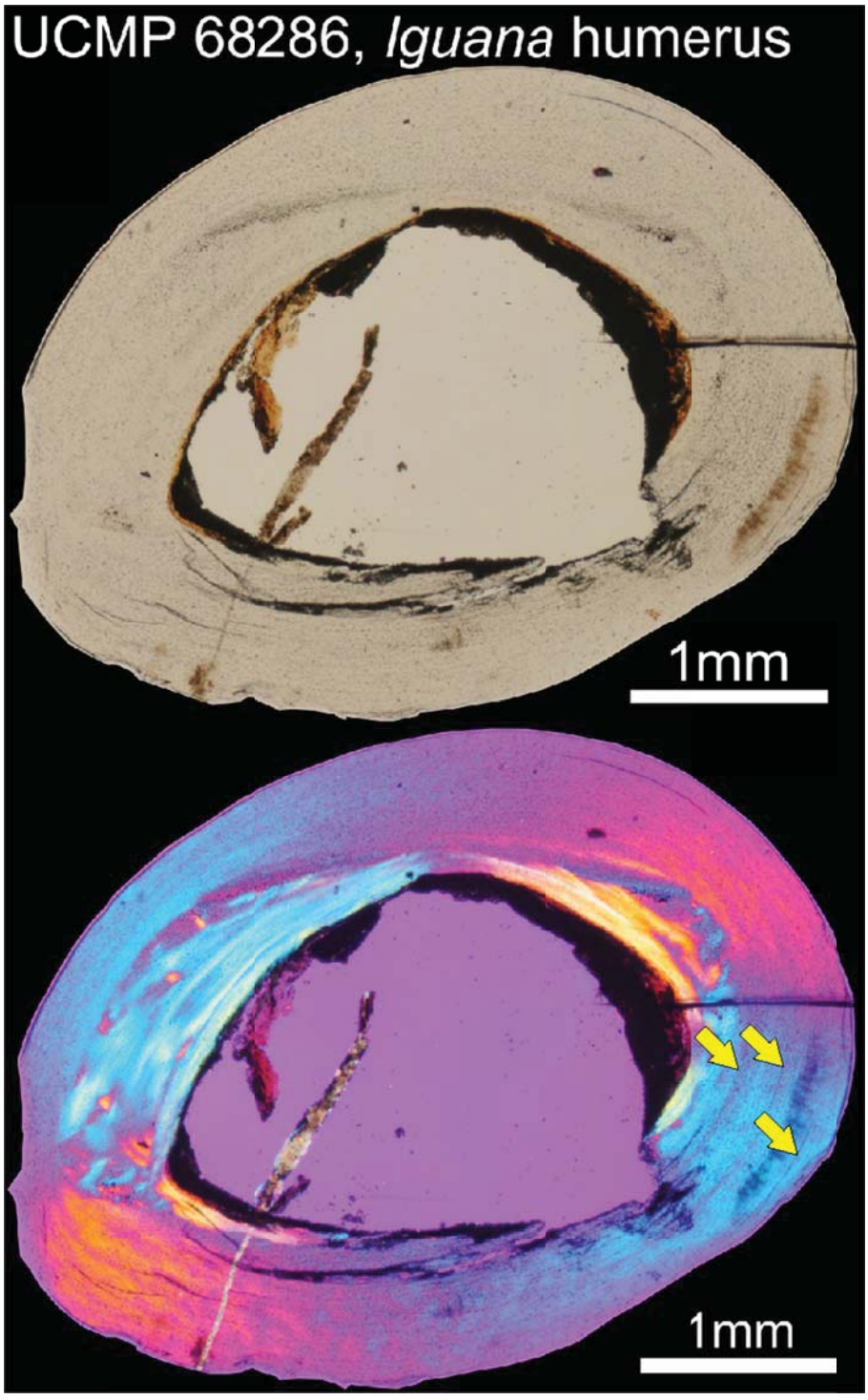

Figure 2.4 Bone microstructure of the mid-diaphyseal humerus of *Iguana iguana* (UCMP 68286) in regular transmitted light (top) and elliptically polarized light (bottom). The humerus is comprised of nearly avascular lamellar bone. Arrows indicate lines of arrested growth.

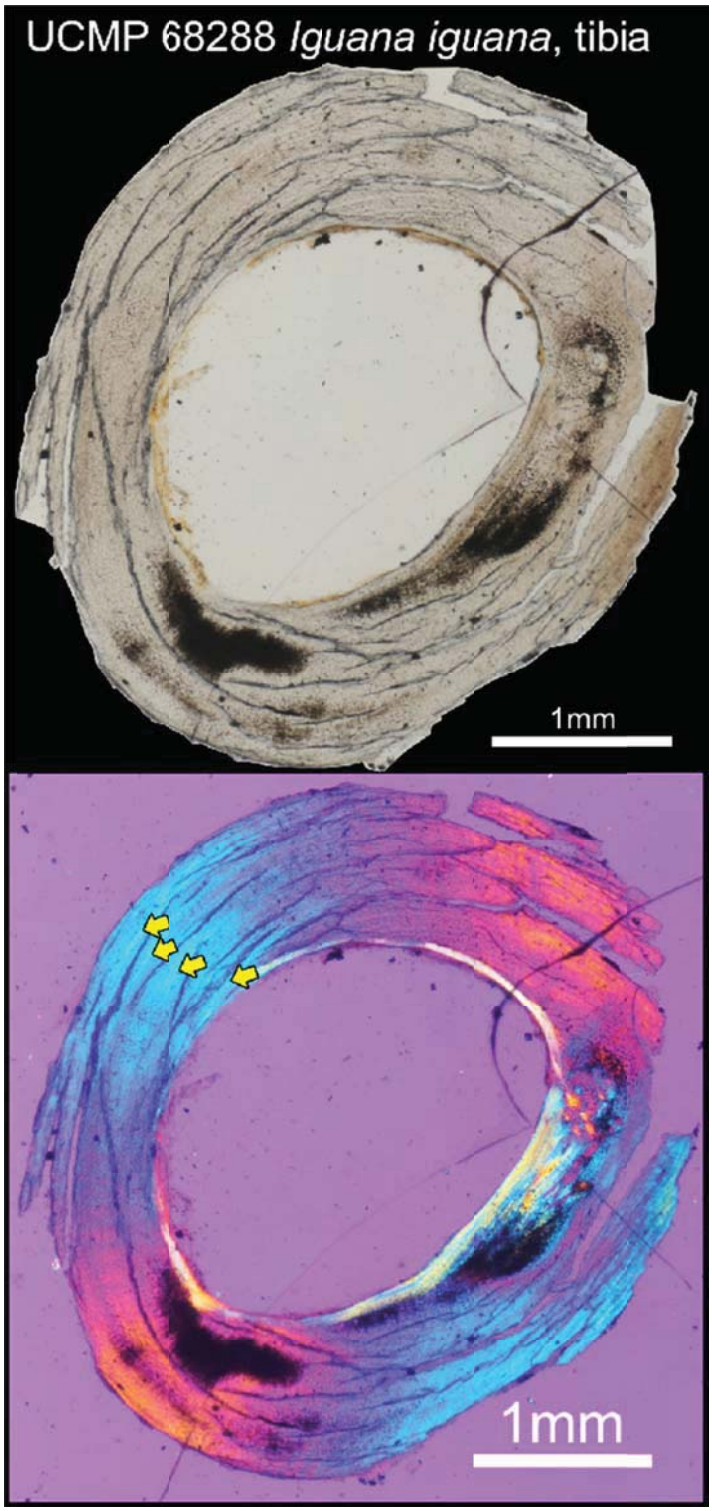

Figure 2.5 Bone microstructure of the mid-diaphyseal tibia of *Iguana iguana* (UCMP 68288) in regular transmitted light (top) and elliptically polarized light (bottom). The tibia is entirely comprised of avascular lamellar bone. Arrows indicate lines of arrested growth.

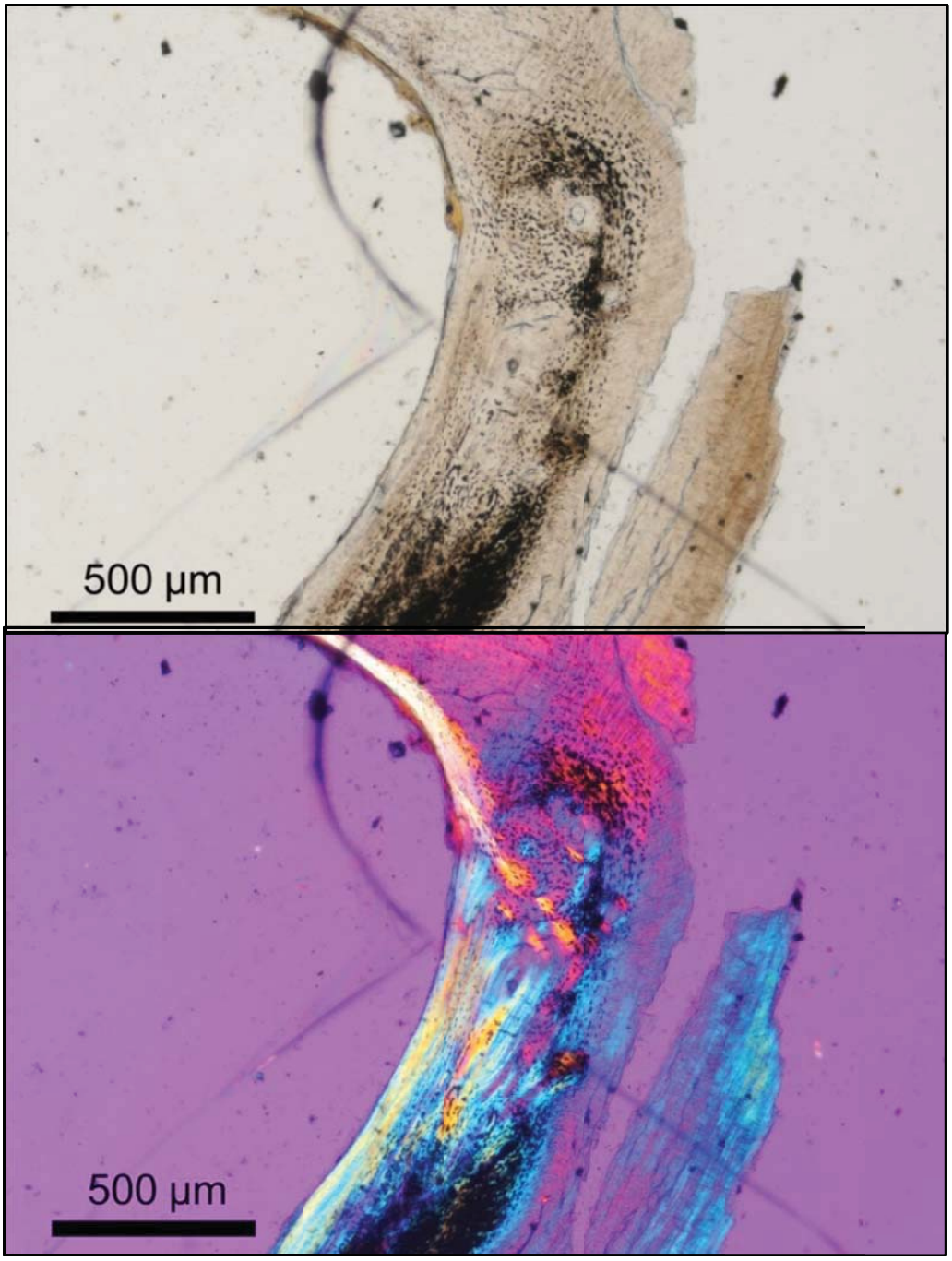

Figure 2.6 Cortical bone microstructure of the mid-diaphyseal tibia of *Iguana iguana* (UCMP 68288) in regular transmitted light (top) and elliptically polarized light (bottom). In this region, osteocyte density is much higher compared to the rest of the cortex, and there are several simple primary canals and secondary osteons. Based on descriptions of other iguanid lizards (e.g., Hugi and Sánchez-Villagra 2012), this region may correspond to embryonic bone, some of which subsequently remodeled.

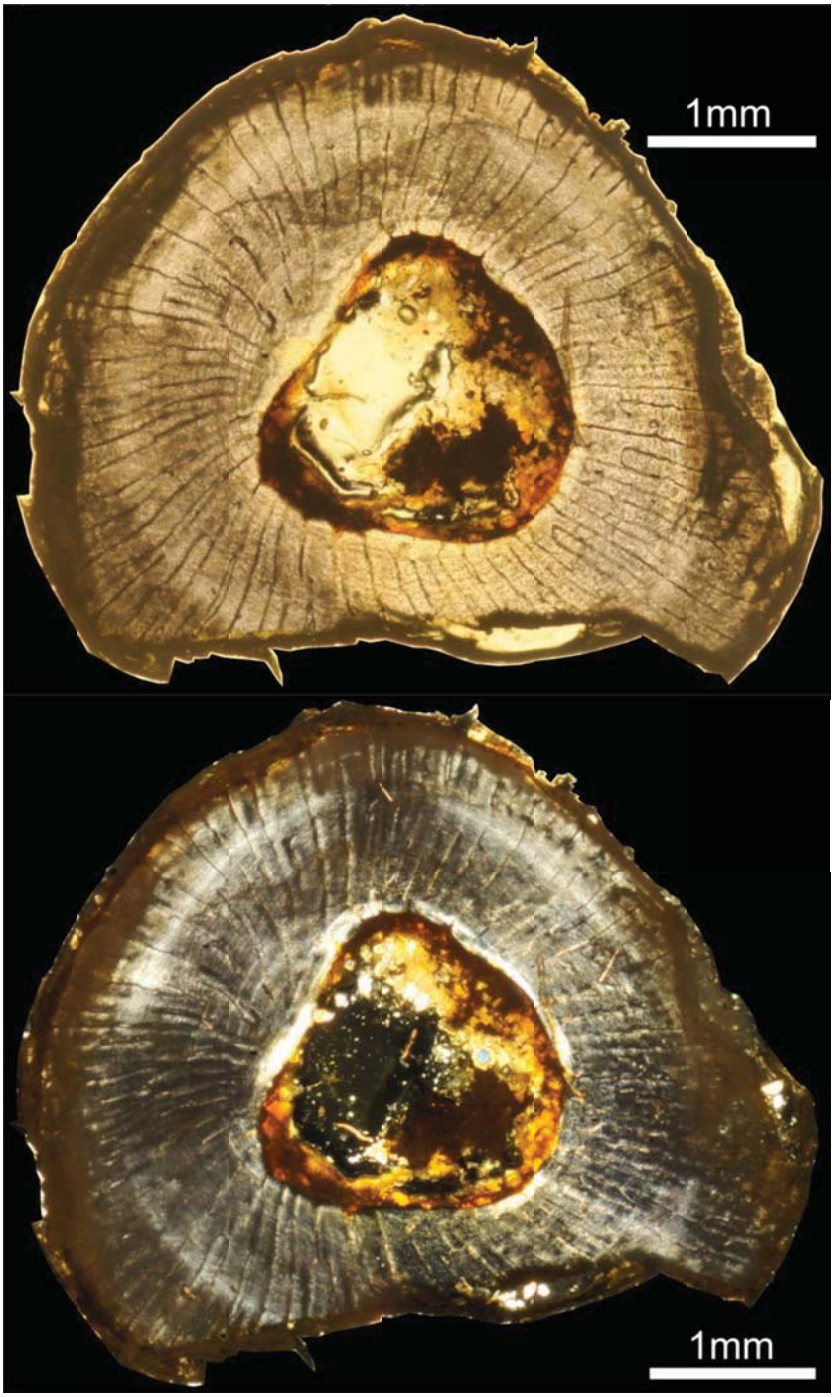

Figure 2.7 Cross section through the mid-diaphyseal femur of *Varanus niloticus* (UCMP 223456) in regular transmitted light (top) and cross plane polarized light (bottom). Under polarized light, the entire section shows a "Maltese cross" extinction pattern, which only forms when bone tissue is lamellar or parallel-fibered and the element is more or less circular in cross section.

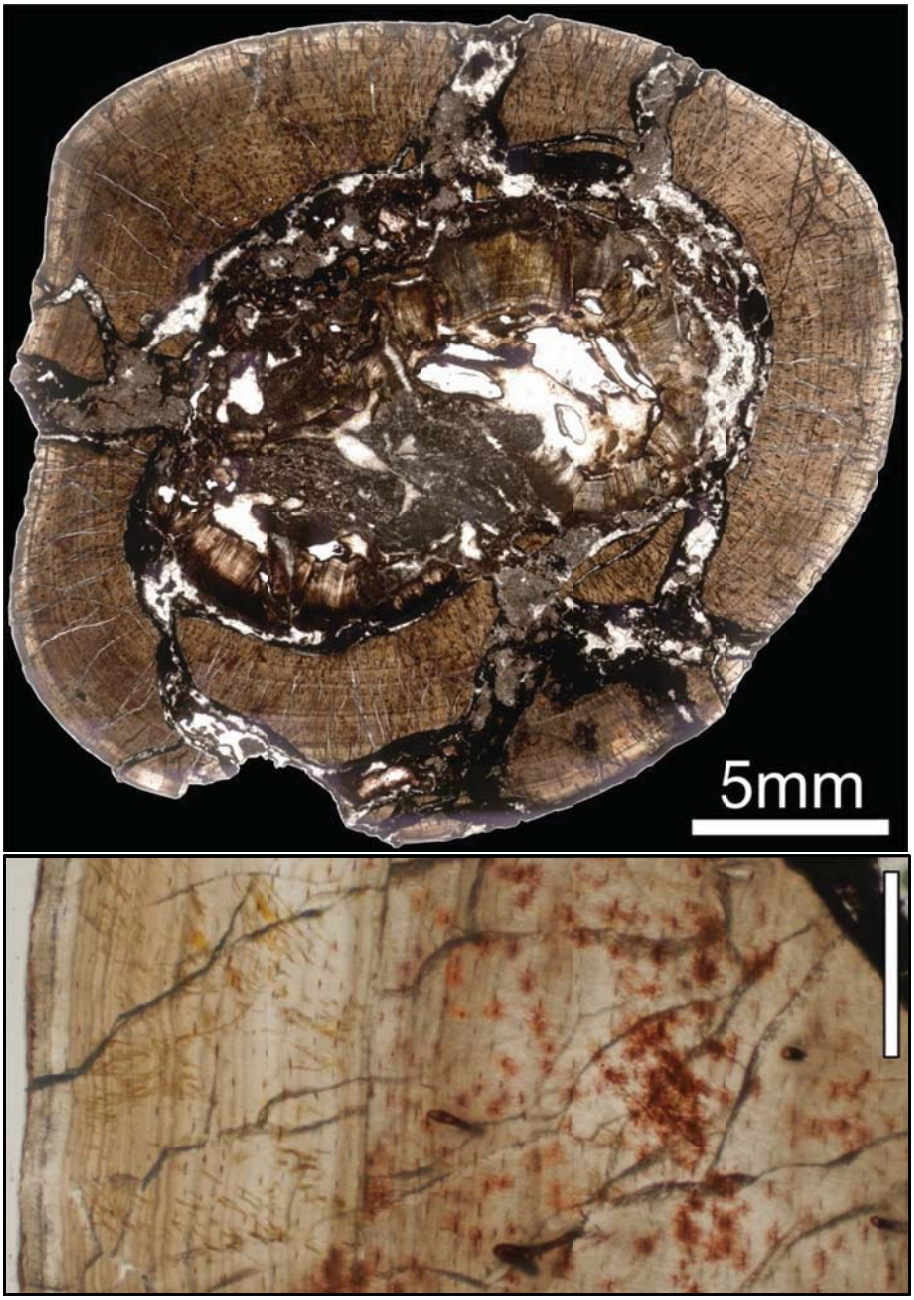

Figure 2.8 Cortical bone microstructure of the mid-diaphyseal humerus of *Trilophosaurus buettneri* (TMM 31025-849; adult) in regular transmitted light. The top image shows the entire cortex in cross-section, and the bottom image illustrates the histology of the outer cortex (periosteum to left of image, scale = 250 μm). As for all elements of *Trilophosaurus*, the mid-diaphyseal humerus is comprised entirely of lamellar bone. The closely-spaced thin lines to the left of the bottom image are the external fundamental system, which signifies the animal had reached the end of the active phase of skeletal growth at the time of death.

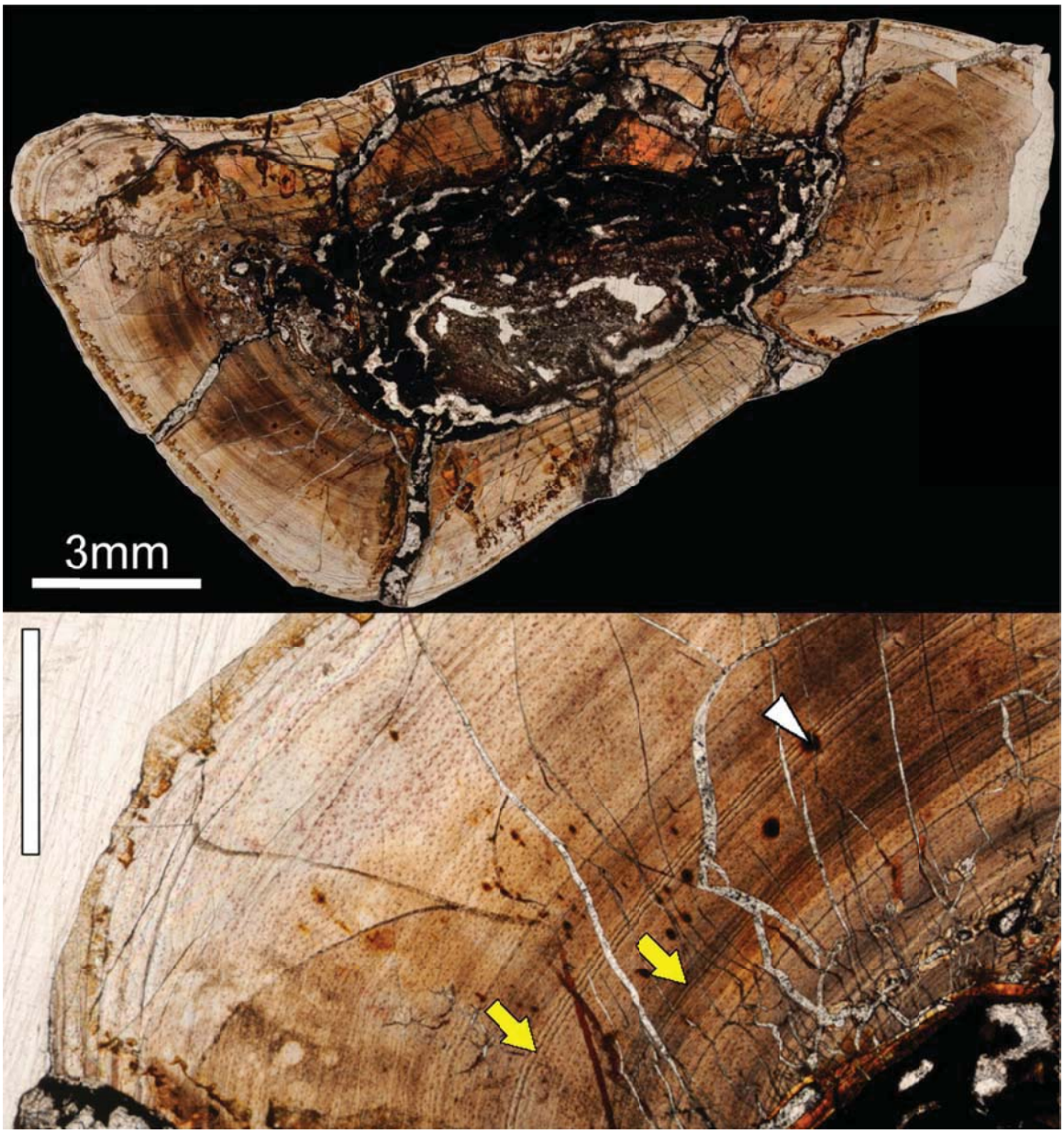

Figure 2.9 Cortical bone microstructure of the mid-diaphyseal ulna of *Trilophosaurus buettneri* (TMM 31025-928; adult) in regular transmitted light. The top image shows the entire cortex in cross-section, and the bottom image illustrates the histology of the cortex (periosteum to upper left of image, scale = 1 mm). Most elements of *Trilophosaurus* are poorly vascularized at the mid-diaphysis, but the ulna is nearly avascular. In this image, the white triangle points to a rare vascular canal, and the yellow arrows point to lines of arrested growth (LAGs). In *Trilophosaurus*, annual growth marks most frequently occur in a small packet comprised of 3-5 lines, rather than as a single LAG.

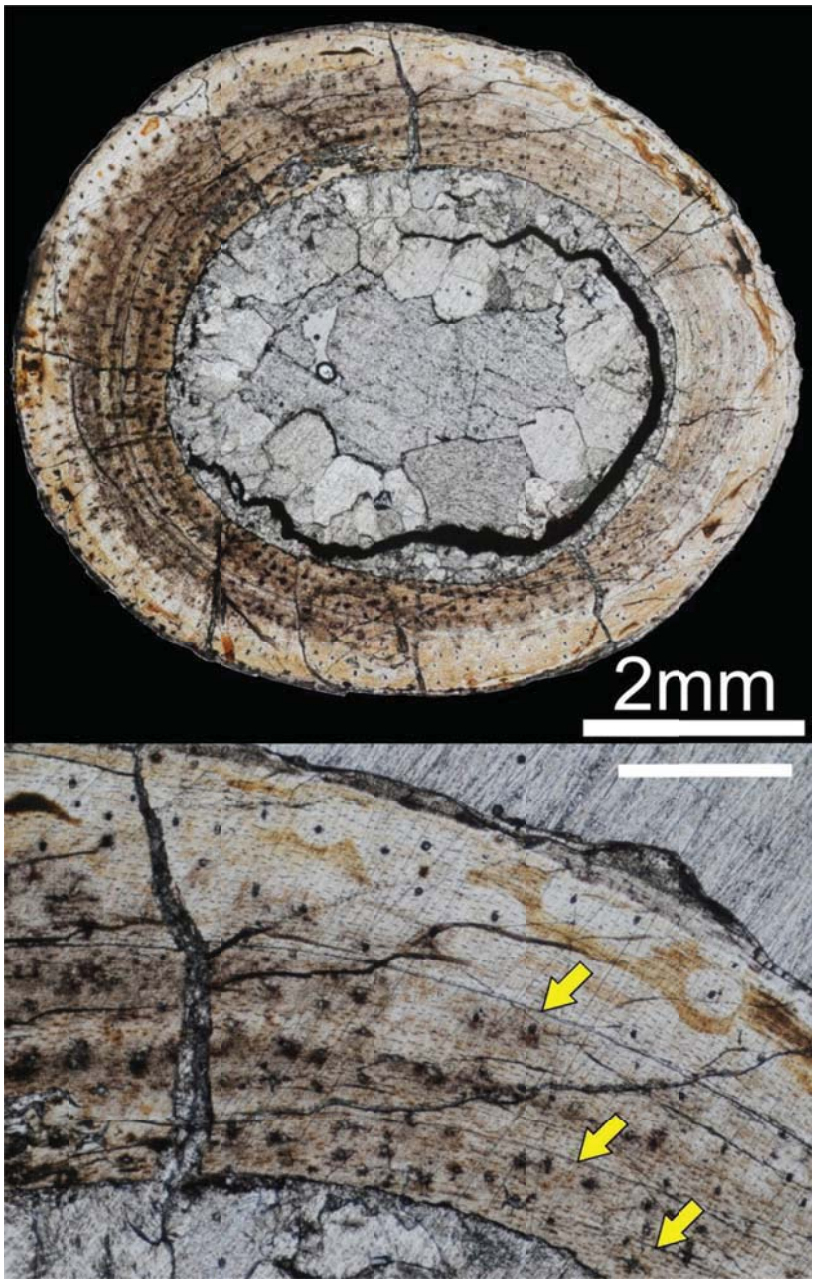

Figure 2.10 Cortical bone microstructure of the mid-diaphyseal femur of *Trilophosaurus buettneri* (TMM 31025-787; smallest femur) in regular transmitted light. The top image shows the entire cortex in cross section, and the bottom image illustrates the histology of the cortex (periosteum to upper right of image, scale = 500 μm). In this image, the arrows point to lines of arrested growth (LAGs). In smaller *Trilophosaurus* femora, annual growth marks most frequently occur as a single LAG, rather a small packet comprised of 3-5 lines, as in larger individuals.

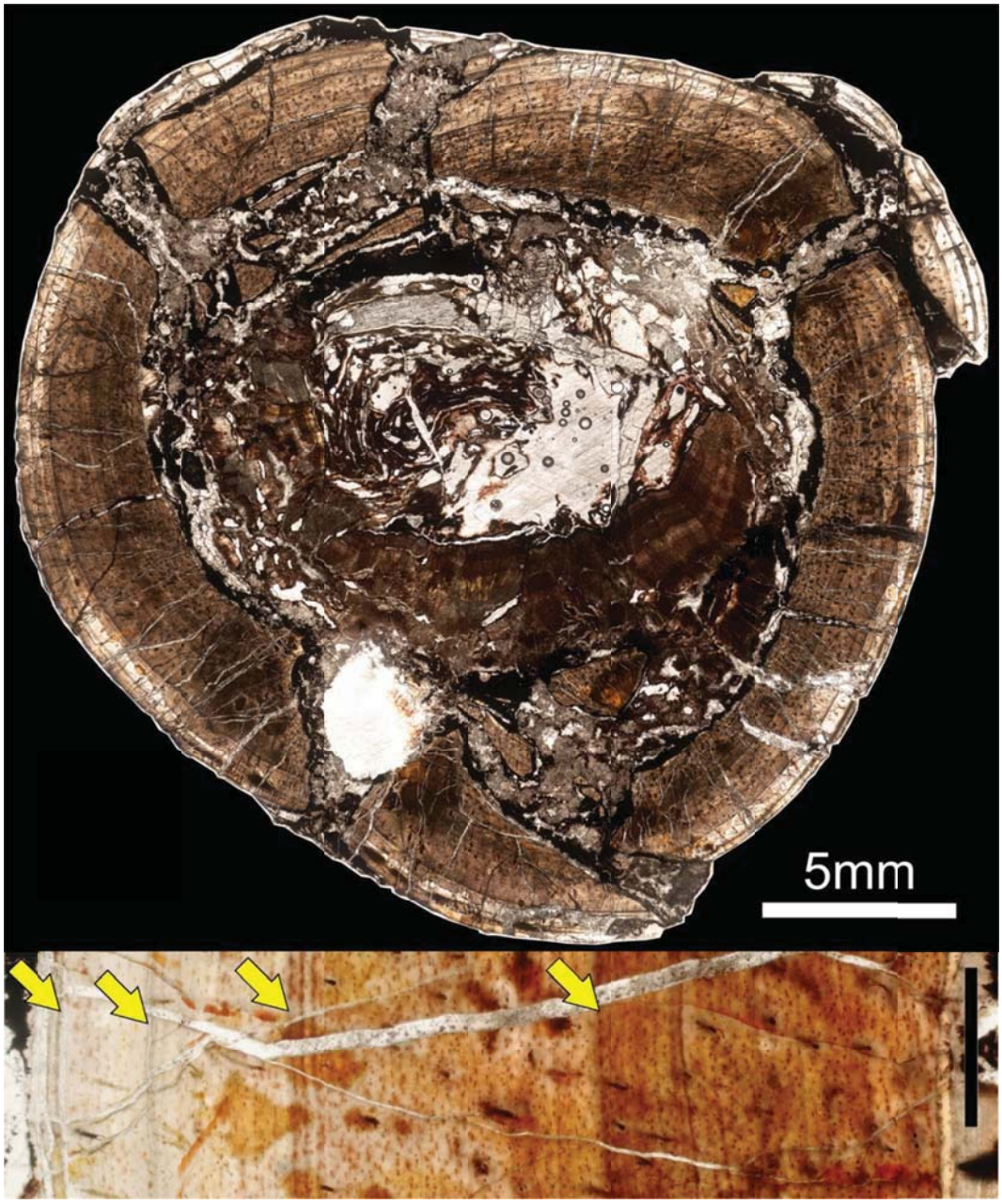

Figure 2.11 Cortical bone microstructure of the mid-diaphyseal femur of *Trilophosaurus buettneri* (TMM 31025-786; largest femur) in regular transmitted light. The top image shows the entire cortex in cross section, and the bottom image illustrates the histology of the cortex (periosteum to left of image, scale = 500 μm). In this image, the arrows point to lines of arrested growth (LAGs). In larger *Trilophosaurus* femora, these annual growth marks most frequently occur as LAG packets comprised of 3-5 lines. This is the only individual to show zones that decrease in width periosteally throughout the section (note arrow spacing decreasing to left).

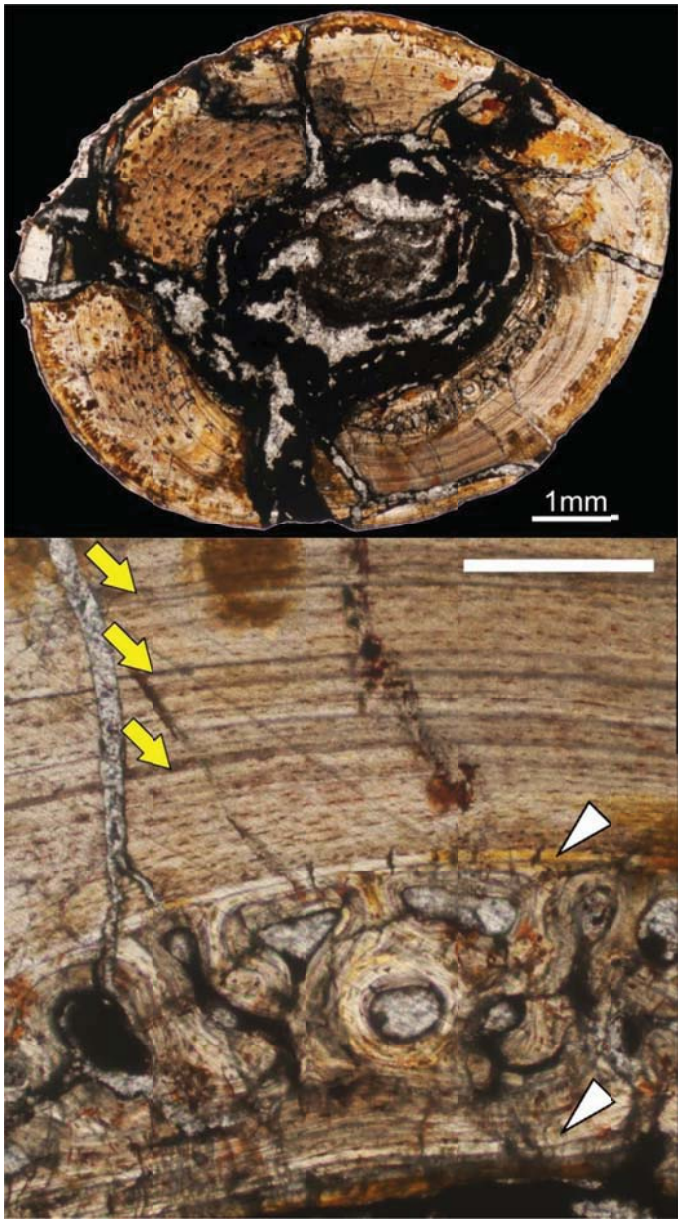

Figure 2.12 Cortical bone microstructure of the mid-diaphyseal tibia of *Trilophosaurus buettneri* (TMM 31025-788; smallest tibia) in regular transmitted light. The top image shows the entire cortex in cross section (scale = 1 mm), and the bottom image illustrates the histology of the inner and midcortex (periosteum towards top of lower image; scale = 250 μm). In this image, yellow arrows point to lines of arrested growth, and white triangles indicate endosteal lamellae (EL). Between the EL, a region of cancellous bone has formed. It abuts the outer EL (top triangle) and must have formed after deposition of the outer EL. Later, the inner EL (bottom triangle) lined the medullary cavity, including the region of cancellous bone. Finally, the cancellous region began to secondarily remodel across both EL (not pictured).

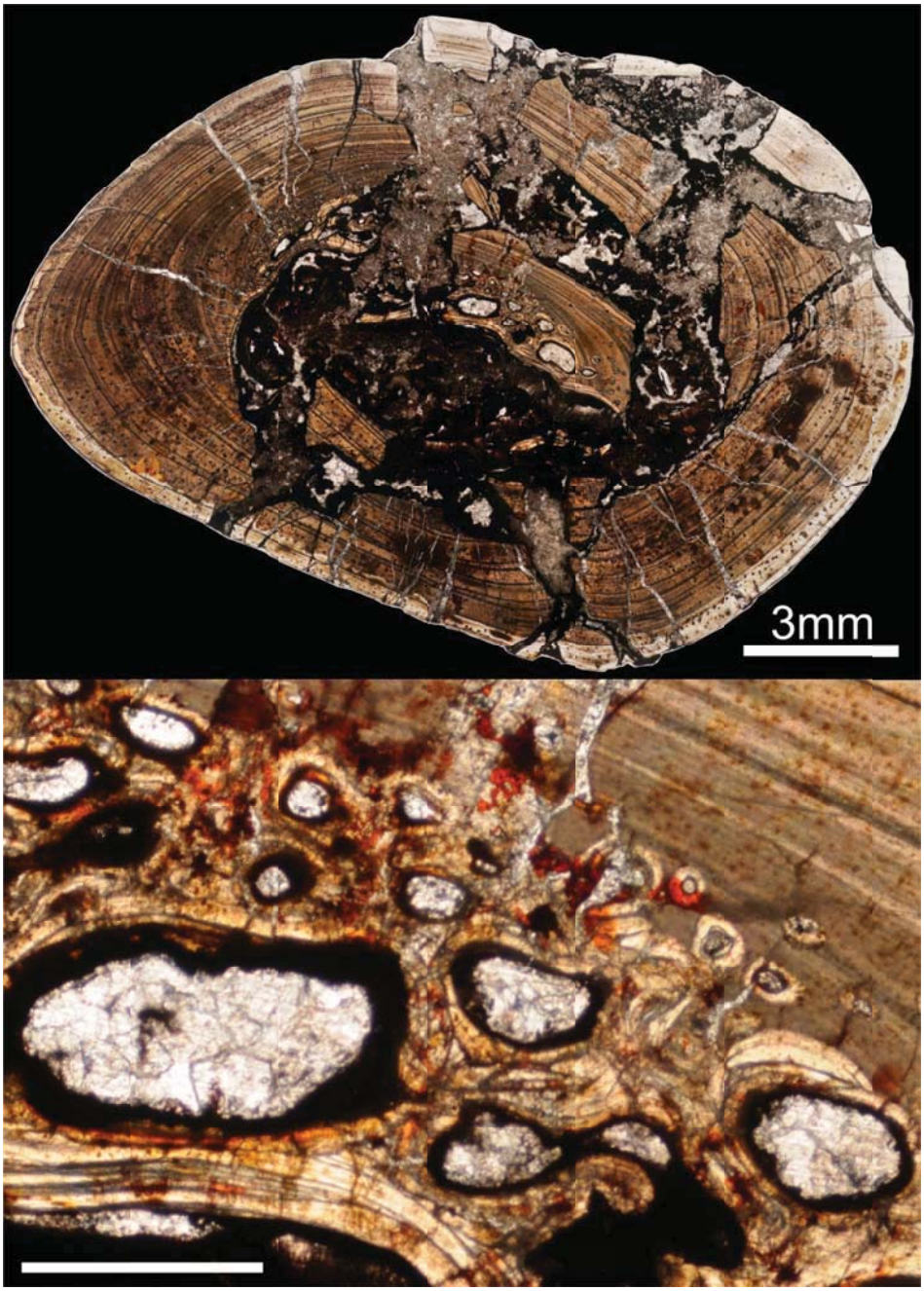

Figure 2.13 Cortical bone microstructure of the mid-diaphyseal tibia of *Trilophosaurus buettneri* (TMM 31025-741; largest tibia) in regular transmitted light (scale = 3 mm). The top image shows the entire cortex in cross section, and the bottom image illustrates the histology of the inner and midcortex (periosteum towards top right of image, scale = 500 μm). In larger adults, a region of cancellous bone is found in the same position as the cancellous bone in TMM 31025-741 (Figure 2.12), but there is only one layer of endosteal lamellae (lower left corner). In these specimens, resorption rooms form through the resorption of primary cortical tissues.

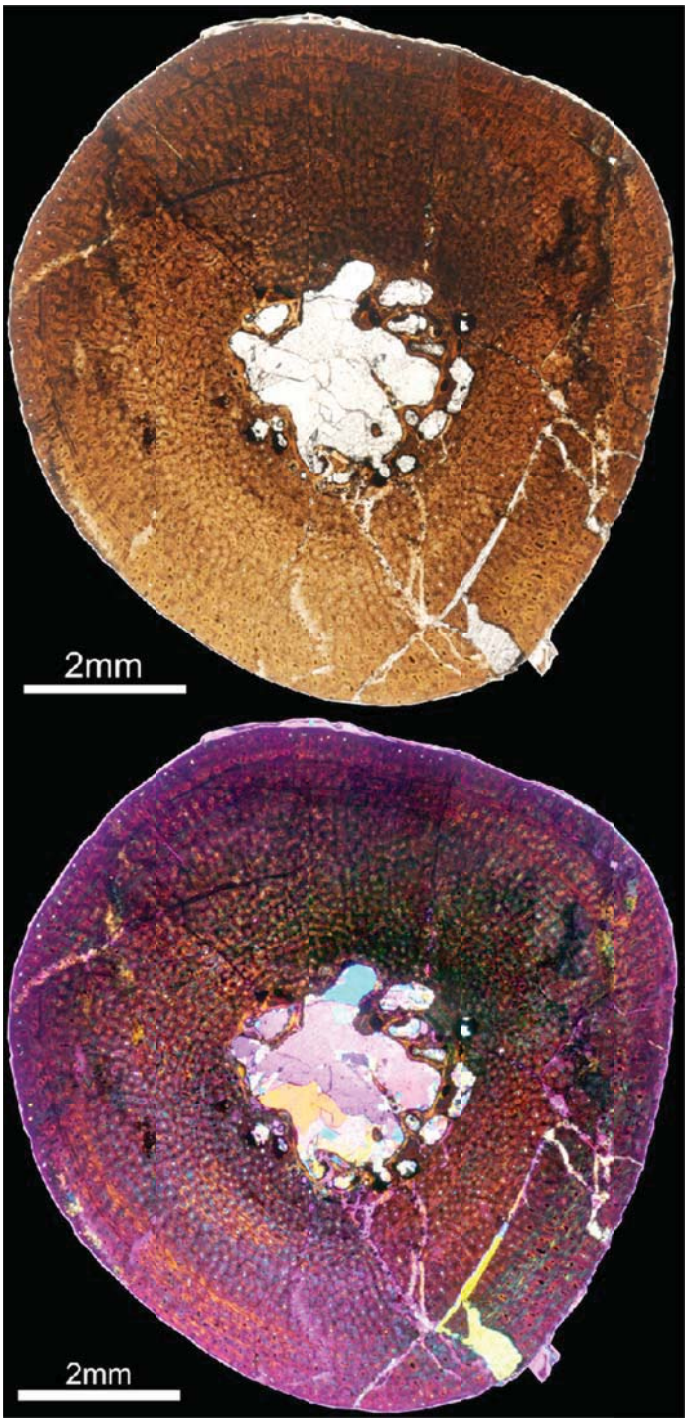

Figure 2.14 Bone microstructure of the mid-diaphyseal femur of *Vancleavea campi* (GR 250) in regular transmitted light (top) and elliptically polarized light (bottom). The cortex is thick relative to the diameter, and is largely comprised of well vascularized woven bone. No LAGs are present in this section, but two annuli are visible close to the periosteum (see Figure 2.15).

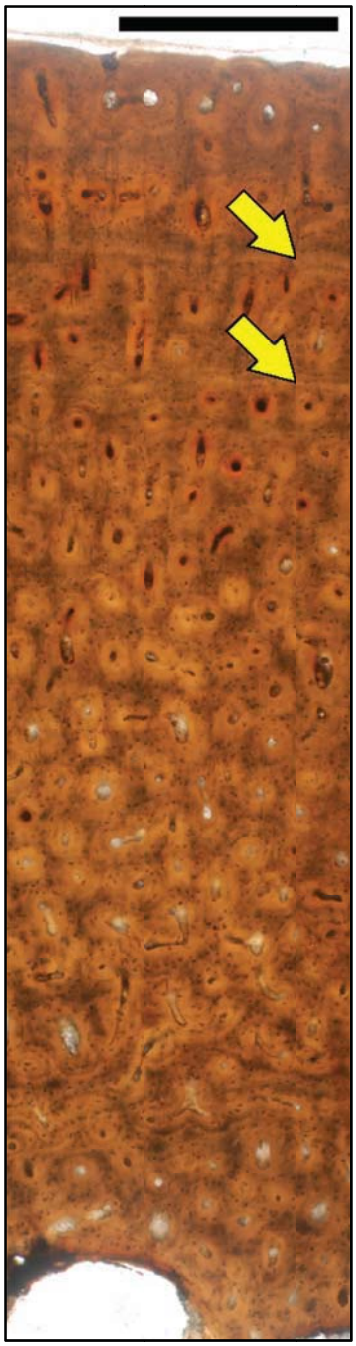

Figure 2.15 Bone microstructure of the mid-diaphyseal femur of *Vancleavea campi* (GR 250) in regular transmitted light. Most primary osteons are longitudinal and anastomose with several others. Anastomoses may be reticular in the inner cortex (bottom third of image) but are radial in the outer cortex (top third of image). Osteocytes (small black flecks) are disorganized and show no preferred arrangement relative to each other. Arrows indicate annuli. Periosteum to top of image, scale = 500 μm.

Figure 2.16 Cortical histology of the mid-diaphyseal femur of a proterochampsian (possibly *Chanaresuchus*; MCZ 4038). The top image shows the specimen as preserved; the bottom image was reconstructed digitally in Adobe Photoshop to approximate the original cross sectional geometry. No LAGs or annuli are visible in this section.

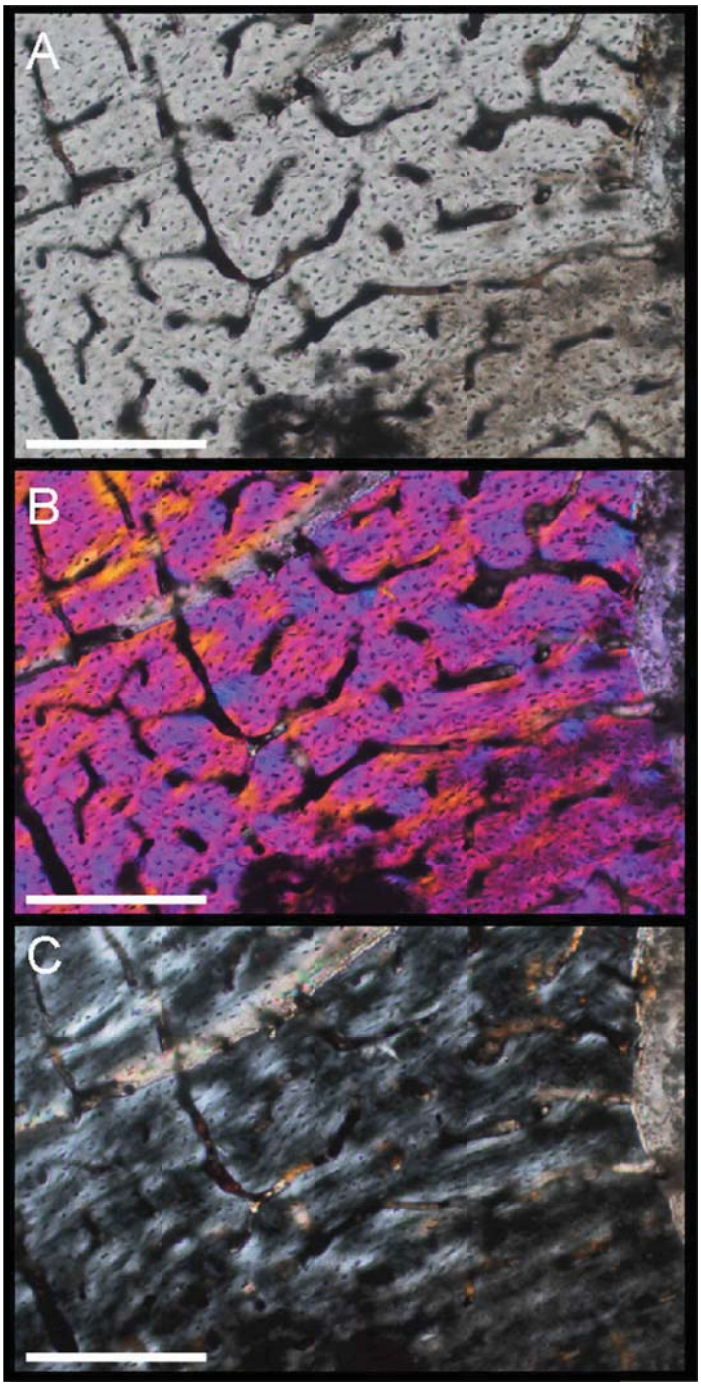

Figure 2.17 Cortical histology of the mid-diaphyseal femur of a proterochampsian (possibly *Chanaresuchus*; MCZ 4038) in A) regular transmitted light, B) elliptically polarized light, and C) crossed plane-polarized light. The inner cortex (pictured here) is comprised of weakly woven, moderately to well-vascularized bone tissue, which grades to parallel-fibered bone tissue in the outer cortex (not pictured). All canals are simple primary canals, and lack a lamellar border (see A and B). All scale bars = 500 μm.

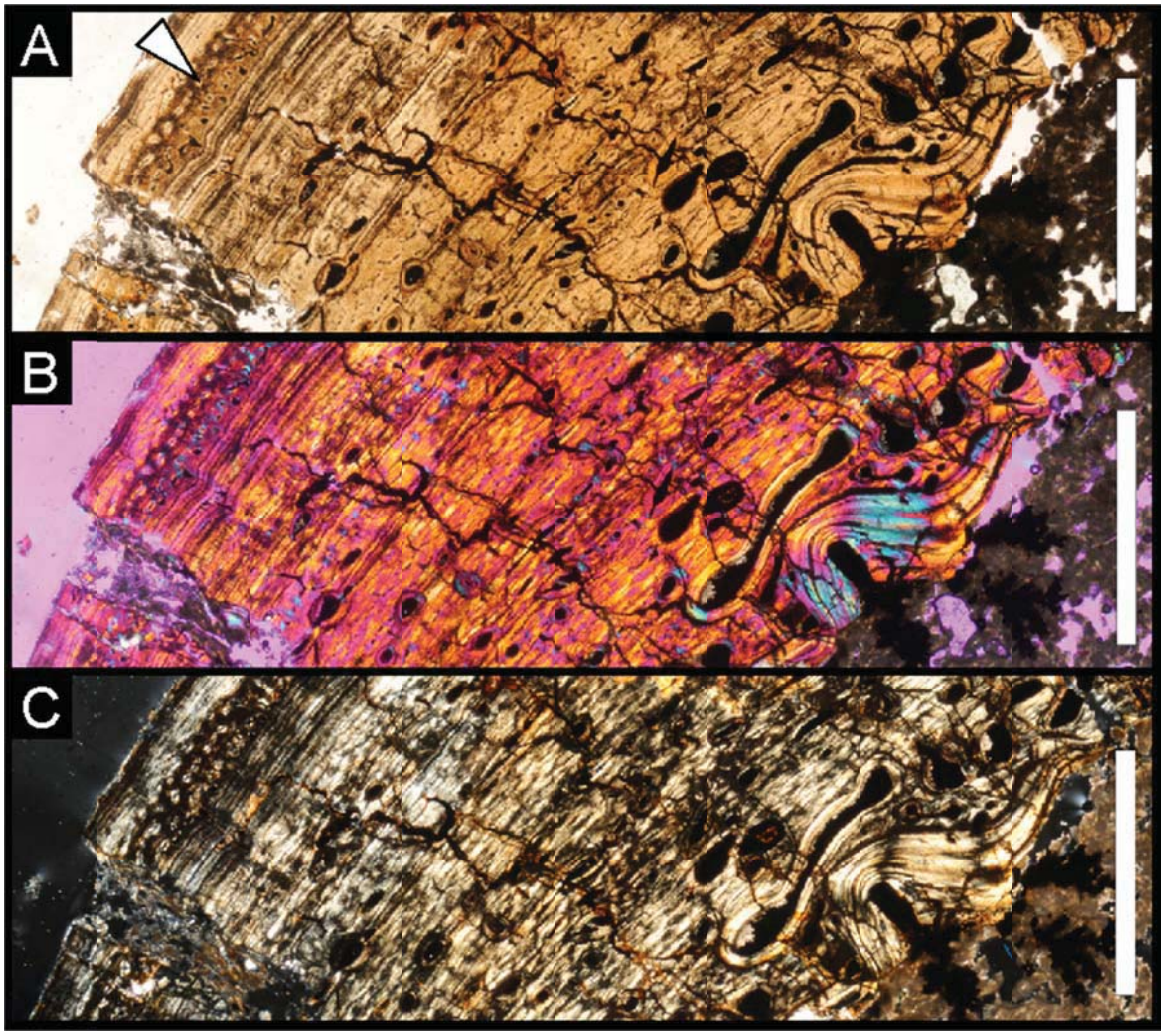

Figure 2.18 Cortical histology of the mid-diaphyseal femur of a phytosaur (UCMP 25921) in A) regular transmitted light, B) elliptically polarized light, and C) crossed plane-polarized light. Arrows indicate the inner three lines of arrested growth (LAGs). This image shows the typical histology of the cortex, which is mainly comprised of parallel-fibered bone. Toward the periosteum (to the left in all images), this grades into lamellar bone. Close to the periosteum, there is a single row of longitudinal canals (triangle). External to this, the bone is again comprised of parallel-fibered bone. This suggests that phytosaur growth was at least somewhat labile late into ontogeny. All scale bars = 2 mm.

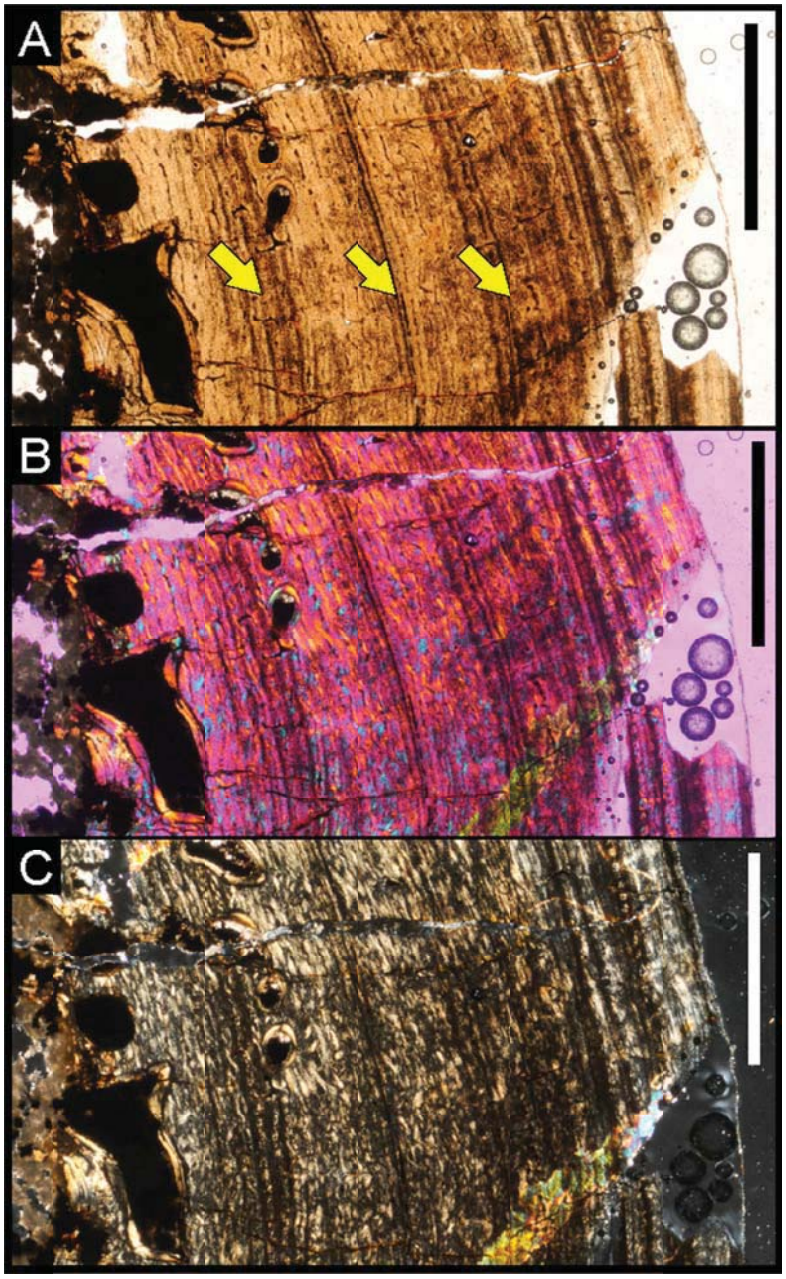

Figure 2.19 Cortical histology of the mid-diaphyseal femur of a phytosaur (UCMP 25921) in A) regular transmitted light, B) elliptically polarized light, and C) crossed plane-polarized light. Arrows indicate the inner three lines of arrested growth (LAGs). This image shows the only part of the cortex where weakly woven bone can be observed in this specimen. The woven bone does not extend past the third LAG. Note that each image is scaled slightly differently, with the first LAG shifted slightly to the left in each subsequent image. Periosteum to the right in all images. All scale bars = 2 mm.

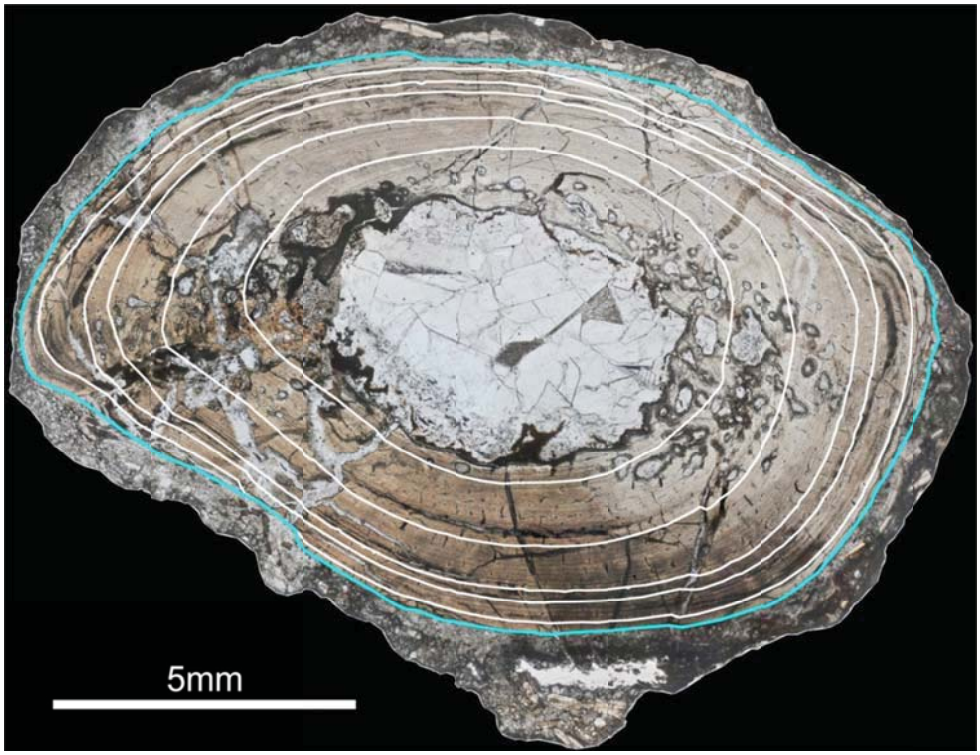

Figure 2.20 Cortical histology of the mid-diaphyseal femur of *Revueltosaurus callenderi* (PEFO 33843) in regular transmitted light, showing relative positions of LAGs (white lines) and periosteal border (blue line). Scale = 5 mm.

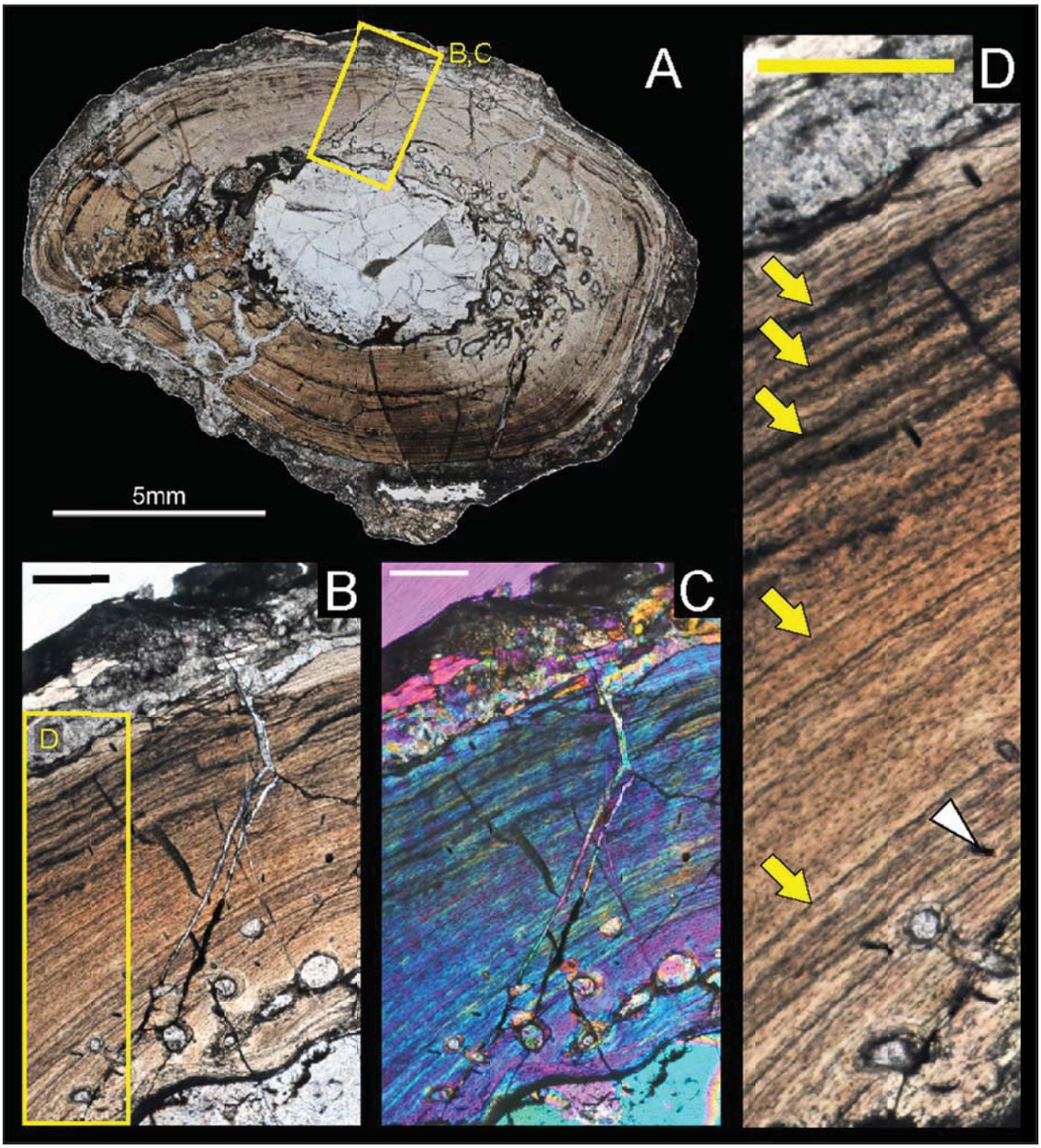

Figure 2.21 Cortical histology of the mid-diaphyseal femur of *Revueltosaurus callenderi* (PEFO 33843) in regular transmitted light (A,B,D) and elliptically polarized light (C). The cortex is fairly uniform in appearance throughout the section. Most of it is composed of poorly vascularized (note canal appearance; white triangle in D) or avascular parallel-fibered bone. This transitions to nearly avascular lamellar bone in the outer cortex (D, top of image). Five LAGs are visible in the cortex (yellow arrows). The periosteum lies to the top of the image in B,C,D. Scale bars: A = 5 mm; B,C, D = 500 μm.

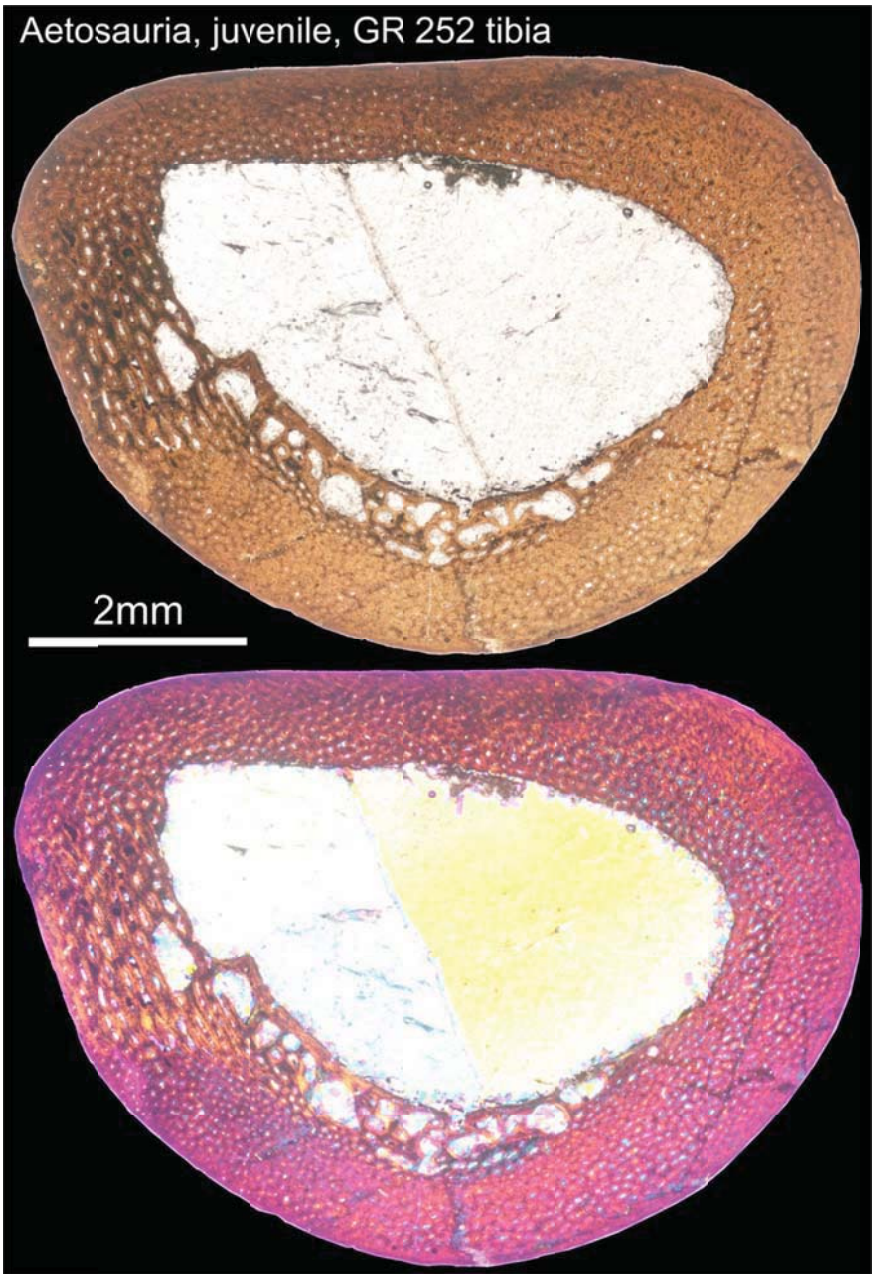

Figure 2.22 Cortical histology of the mid-diaphyseal tibia of a juvenile aetosaur (GR 252) in regular transmitted light (top) and elliptically polarized light (bottom). The entire cortex is composed of well-vascularized woven bone. The inner cortex preserves a woven scaffolding of primary bone separated by large vacuities. This porous tissue is very similar to that of other perinatal archosaurs, including birds and nonavian dinosaurs (Horner et al. 2001). Elsewhere in the cortex, much smaller longitudinal primary osteons are visible. Scale = 2 mm.

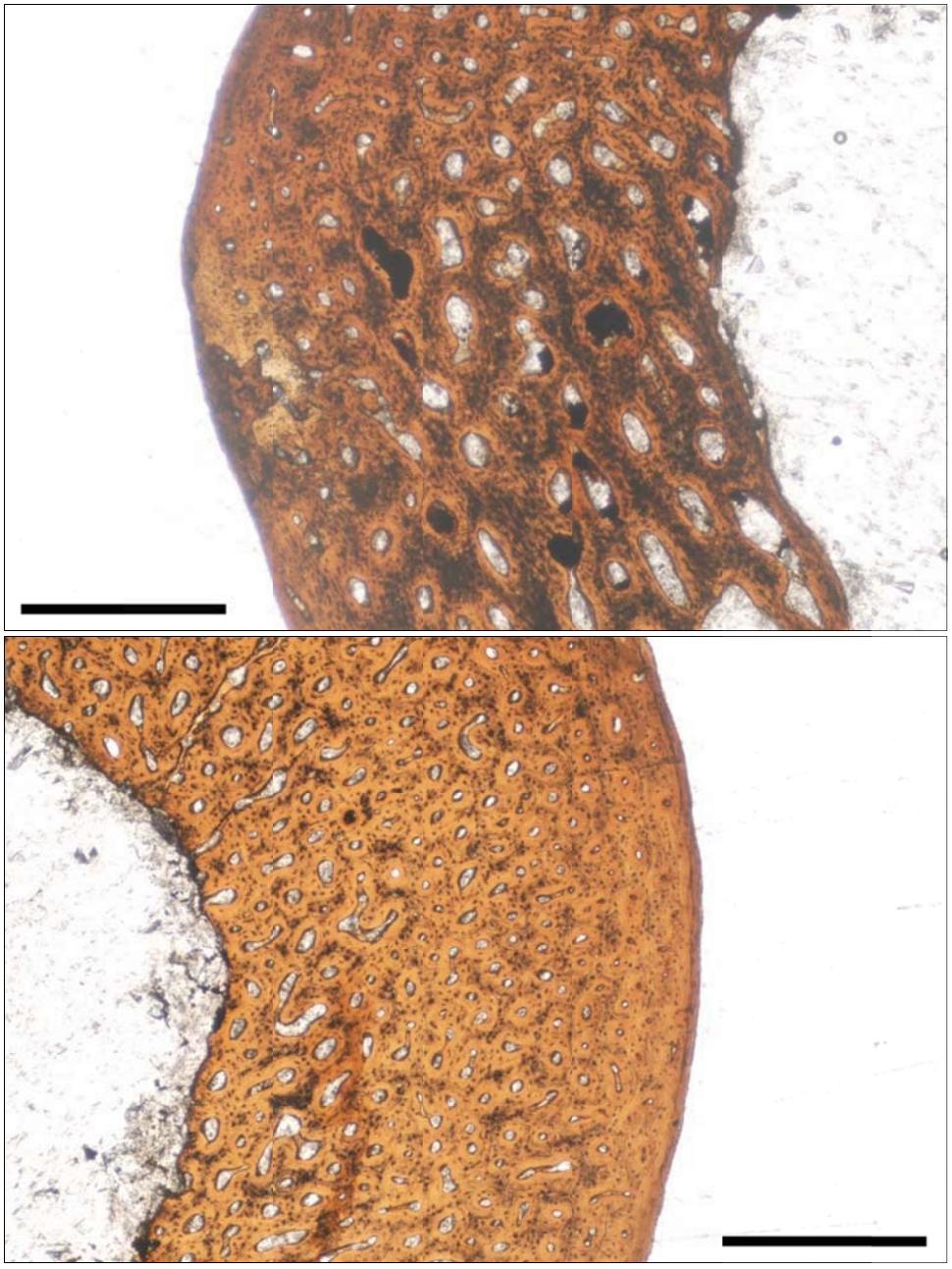

Figure 2.23 Cortical histology of the mid-diaphyseal tibia of a juvenile aetosaur (GR 252) in regular transmitted light, comparing preserved perinatal tissues (top) to the opposite side of the cortex (bottom). The top image shows a bony scaffolding composed of woven-fibered bone. In this region, osteocytes (small black flecks) occur in very high densities, and the struts of the bony scaffolding are separated by large vascular spaces. In the bottom image, vascular canals are much narrower in diameter, osteocytes occur in lower densities, and lamellae surrounding primary osteons are more distinct. Scale bars = 500 μm.

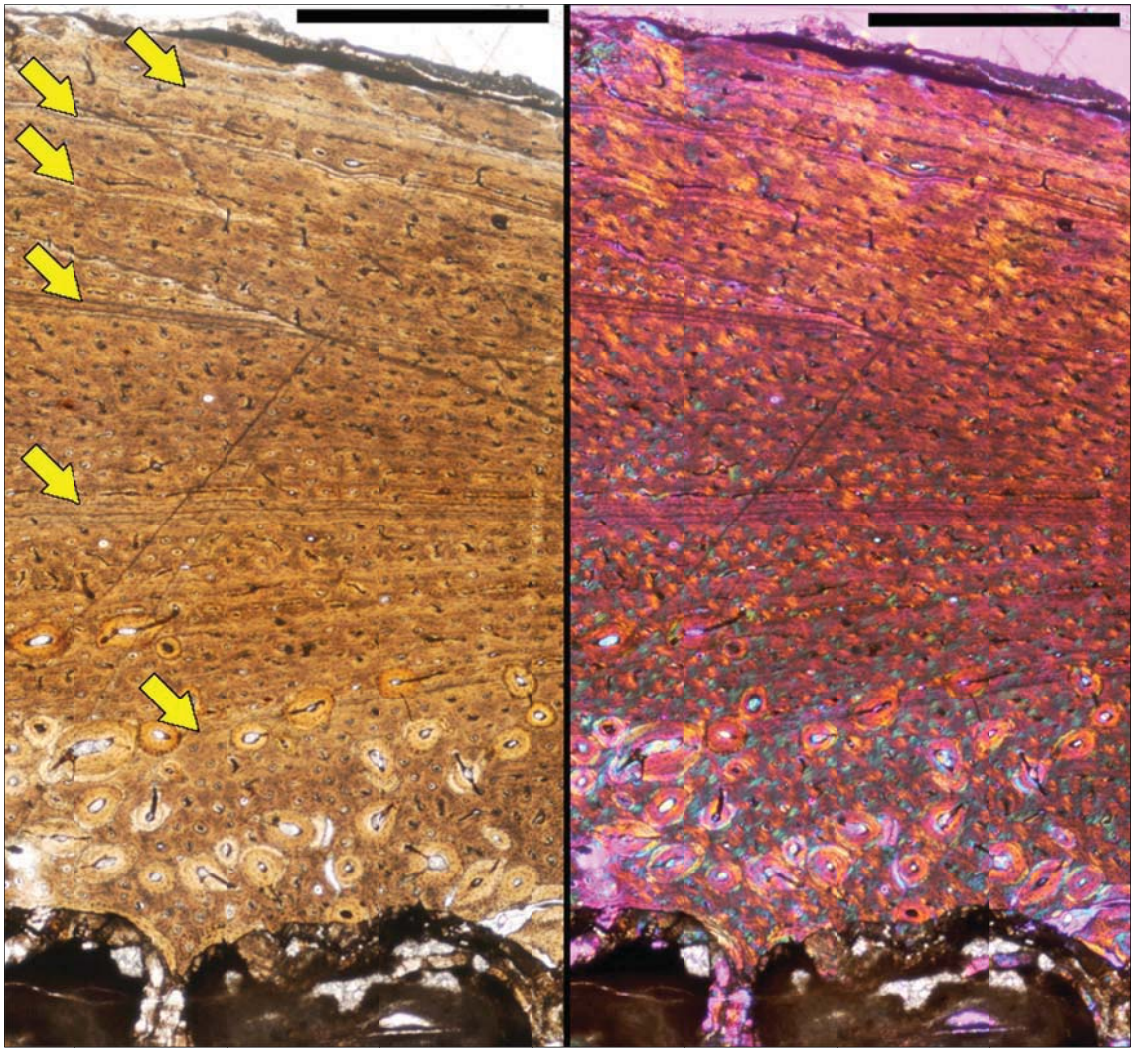

Figure 2.24 Cortical histology of the mid-diaphyseal femur of *Effigia okeeffeae* (AMNH FARB 30587; holotype specimen) in regular transmitted light (left) and elliptically polarized light (right). Arrows indicate LAGs. Internal to the third preserved LAG, the cortex is entirely composed of woven-fibered bone. Woven-fibered tissue forms the inner portion of the next zone, but external to the fourth LAG, most of the bone tissue is parallel-fibered. Periosteum to the top of both images; scale bars = 1 mm.

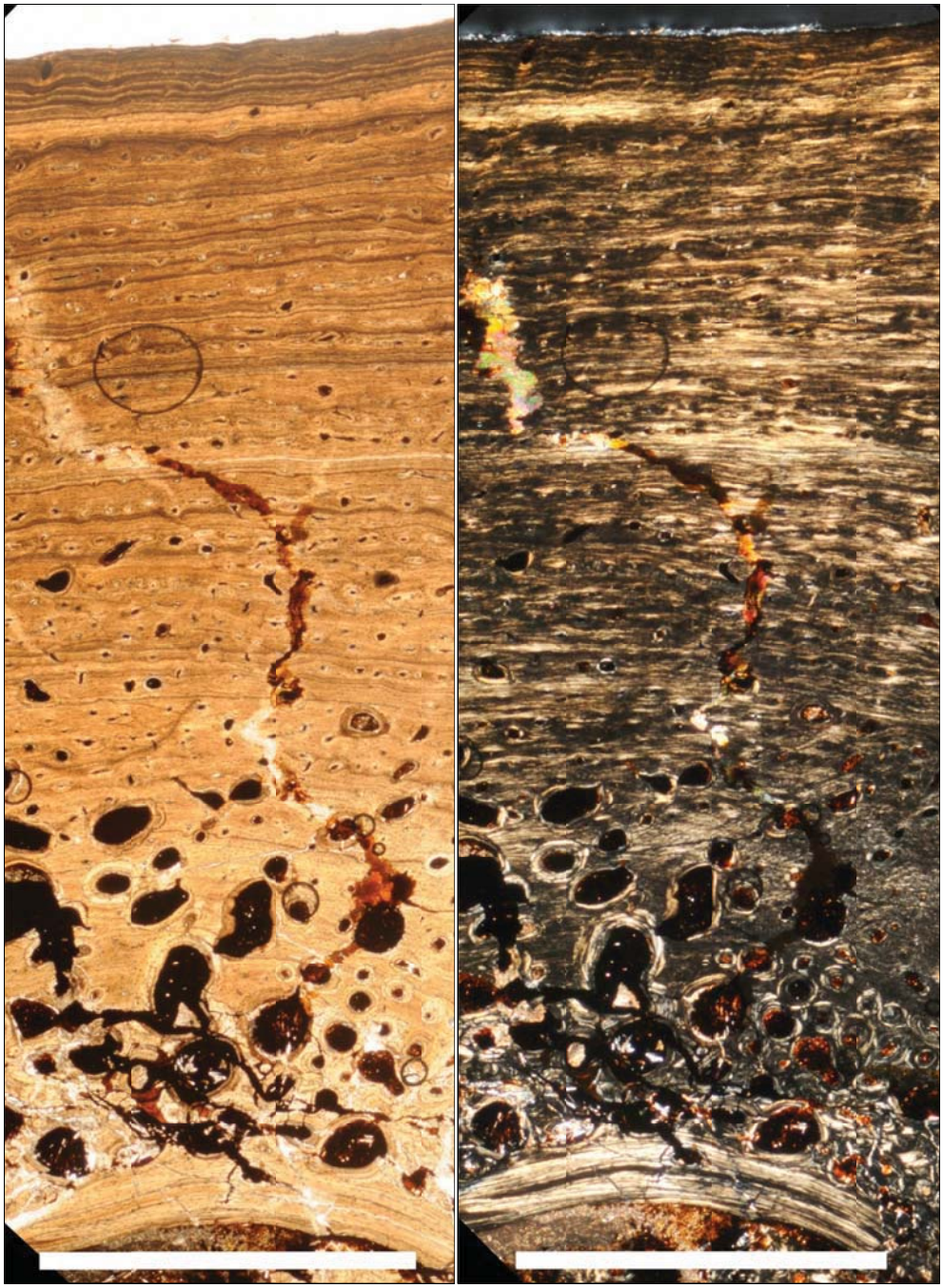

Figure 2.25 Cortical histology of the mid-diaphyseal humerus of a loricatan, cf. *Postosuchus* (UCMP 28353) in regular transmitted light (left) and crossed plane-polarized light (right). The refringence pattern in the right image is more consistent with parallel-fibered bone in the inner and midcortex. Lamellar bone is common only in the outermost cortex, where thin bands of regular width show alternating light and dark signal. Periosteum to the top of both images; scale bars = 2 mm.

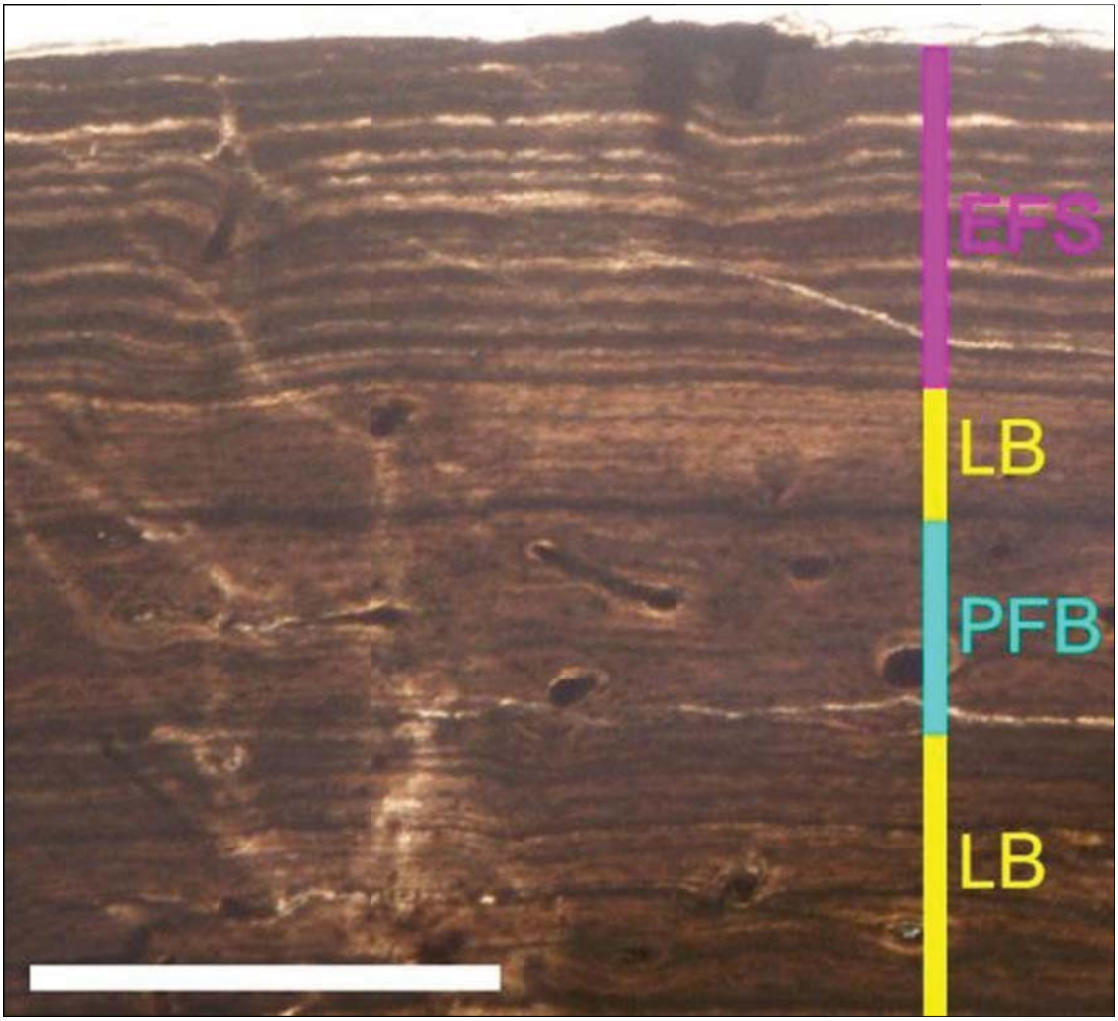

Figure 2.26 Externalmost cortex showing an EFS in the mid-diaphyseal humerus of a loricatan, cf. *Postosuchus* (UCMP 28353; image in regular transmitted light). In this image, the regions marked LB (lamellar bone) contain the outermost two LAG packets of the cortex. The region between them (marked PFB, parallel-fibered bone) is the outermost zone. In the EFS, at least 10 closely spaced lines are visible. These lines are more numerous, more regularly spaced, and much more distinct (darker and with a more even surface) compared to the lines of the two LAG packets. This area is also nearly avascular, whereas the LB and PFB of the cortex show several canals. Finally, the EFS is nearly 0.5 mm in width, whereas LAG packets rarely exceed 0.1 mm in width. The periosteum to the top of this images; scale = 500 µm.

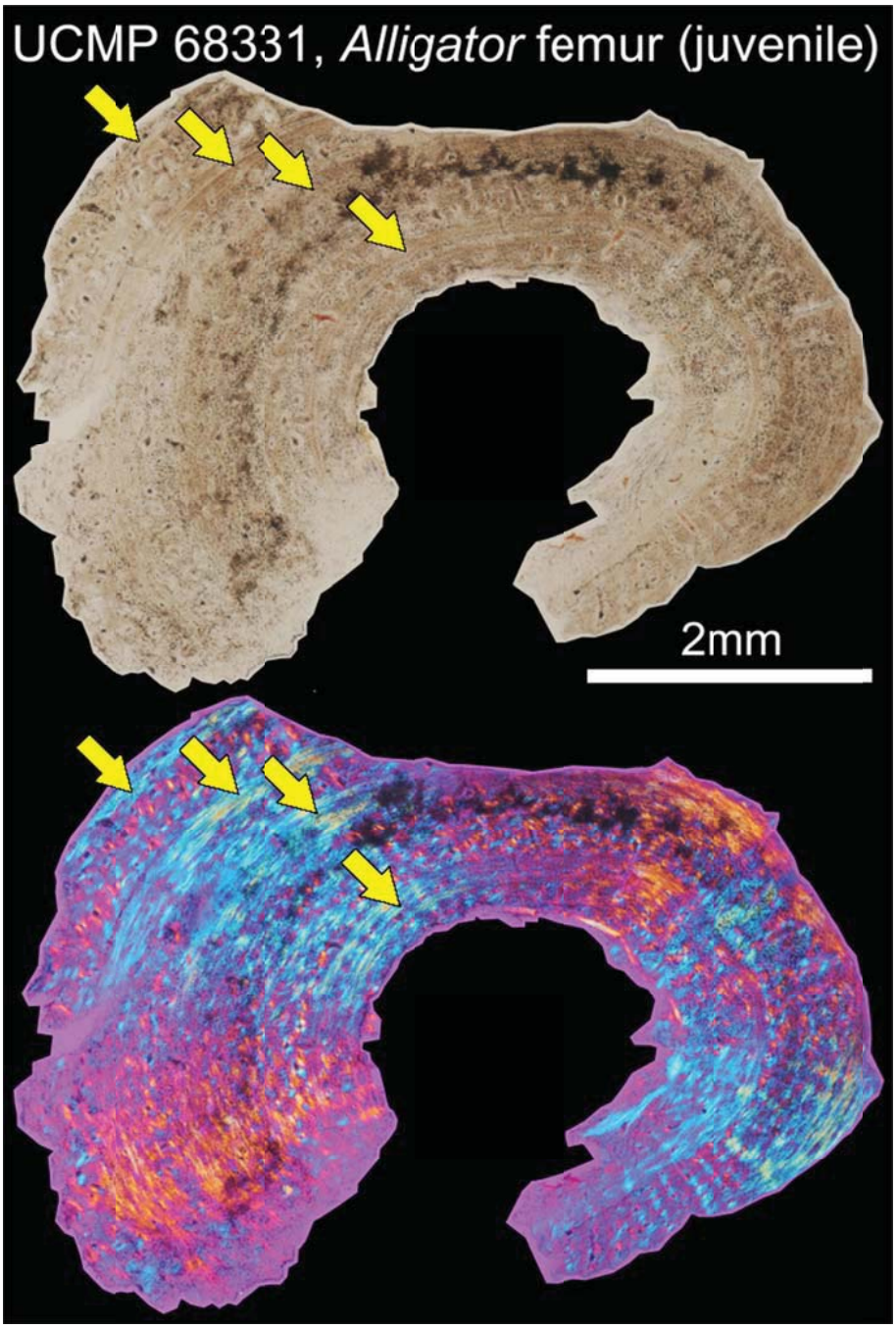

Figure 2.27 Cortical histology of the mid-diaphyseal femur of wild-sacrificed *Alligator mississippiensis* (UCMP 68331; juvenile) in regular transmitted light (top) and elliptically polarized light (bottom). Arrows indicate annuli. In this specimen, the annuli are composed of parallel-fibered bone (bottom image, blue regions) and are relatively broad. Between the annuli, woven-fibered bone tissue is visible (bottom image, multicolored regions between arrows). Scale = 2 mm.

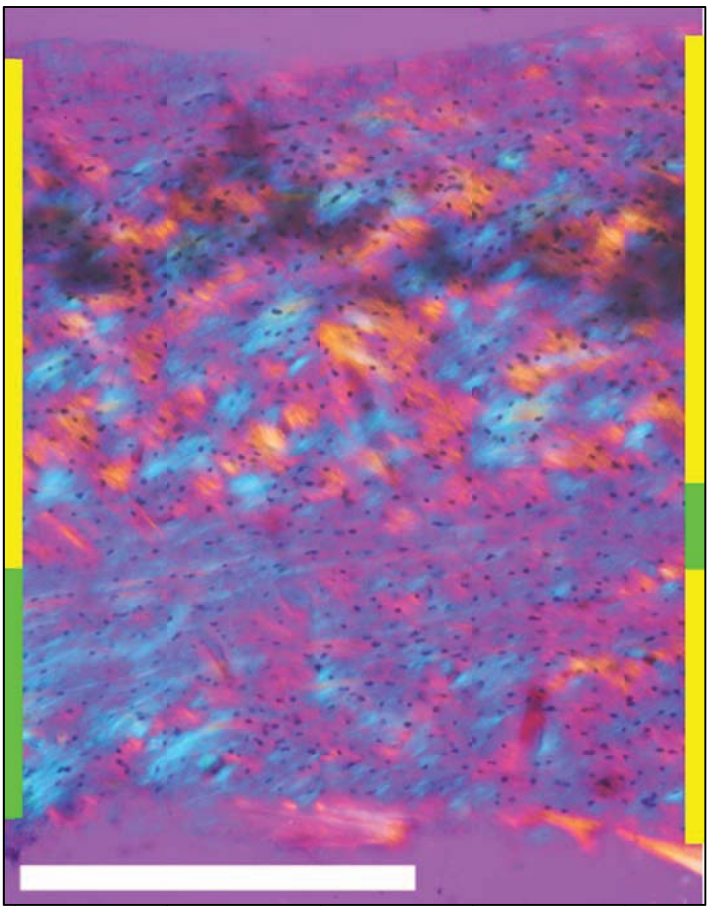

Figure 2.28 Cortical histology of the mid-diaphyseal femur of wild-sacrificed juvenile *Alligator mississippiensis* (UCMP 68331) in elliptically polarized light. Woven-fibered bone tissue (multicolored regions bracketed by yellow bars) is clearly visible in this specimen. Annuli of parallel-fibered bone tissue (blue-purple region bracketed by green bars) separate these woven-fibered regions. Woven bone has been reported previously in juvenile archosaurs, including alligators (Horner et al. 2001, Padian et al. 2004). Scale bar (white) = 500 μm. Periosteum to top of image.

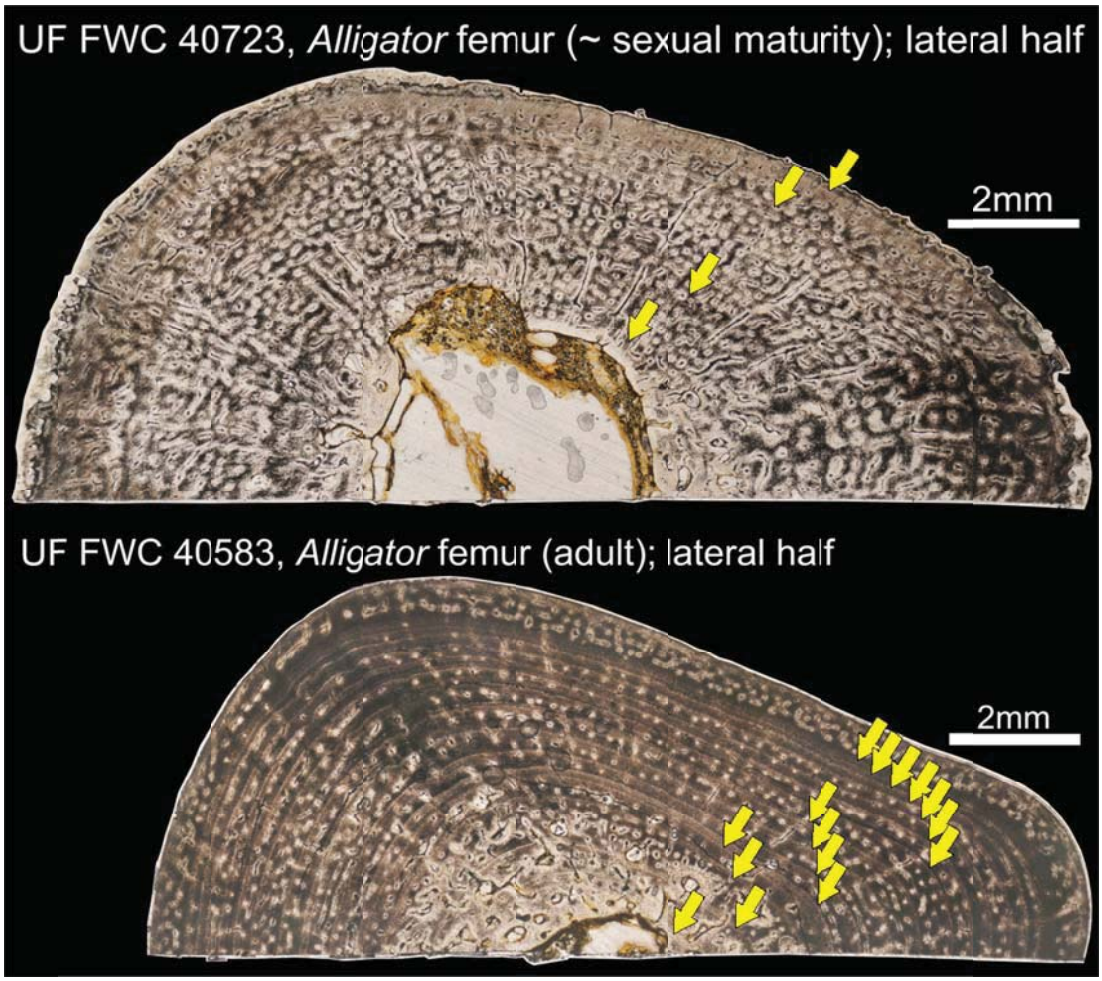

Figure 2.29 Cortical histology of the femur of two wild-sacrificed adult *Alligator mississippiensis* of similar body and femur length. Top image: UF FWC 40723, male near the age of sexual maturity (SVL = 995 mm, TL = 2030 mm, femur L = 134.77 mm, mass = 71 kg). Bottom image: UF FWC 40583, adult female (SVL = 1000 mm, TL = 1990 mm, femur L = 139.48 mm, mass = 61 kg). Both animals were from the same locality and healthy at time of death.

Despite similar body and femoral length, the male (top image) shows four indistinct annuli separating broad zones, whereas the female (bottom image) shows 15 annuli that separate narrow zones. Histological differences in vascular density and connectivity are also immediately apparent. Unlike females, males also produce woven-fibered bone after the juvenile stage. In general, the bones of male alligators are more robust and show greater vascularity and microstructural disorganization; females show more organized tissues and remodel the inner cortex more extensively. These histological differences result from differences in growth rate through ontogeny. Both images taken under regular transmitted light. Scale bars = 2 mm (both images are reproduced at the same scale). Periosteum to top of both images.

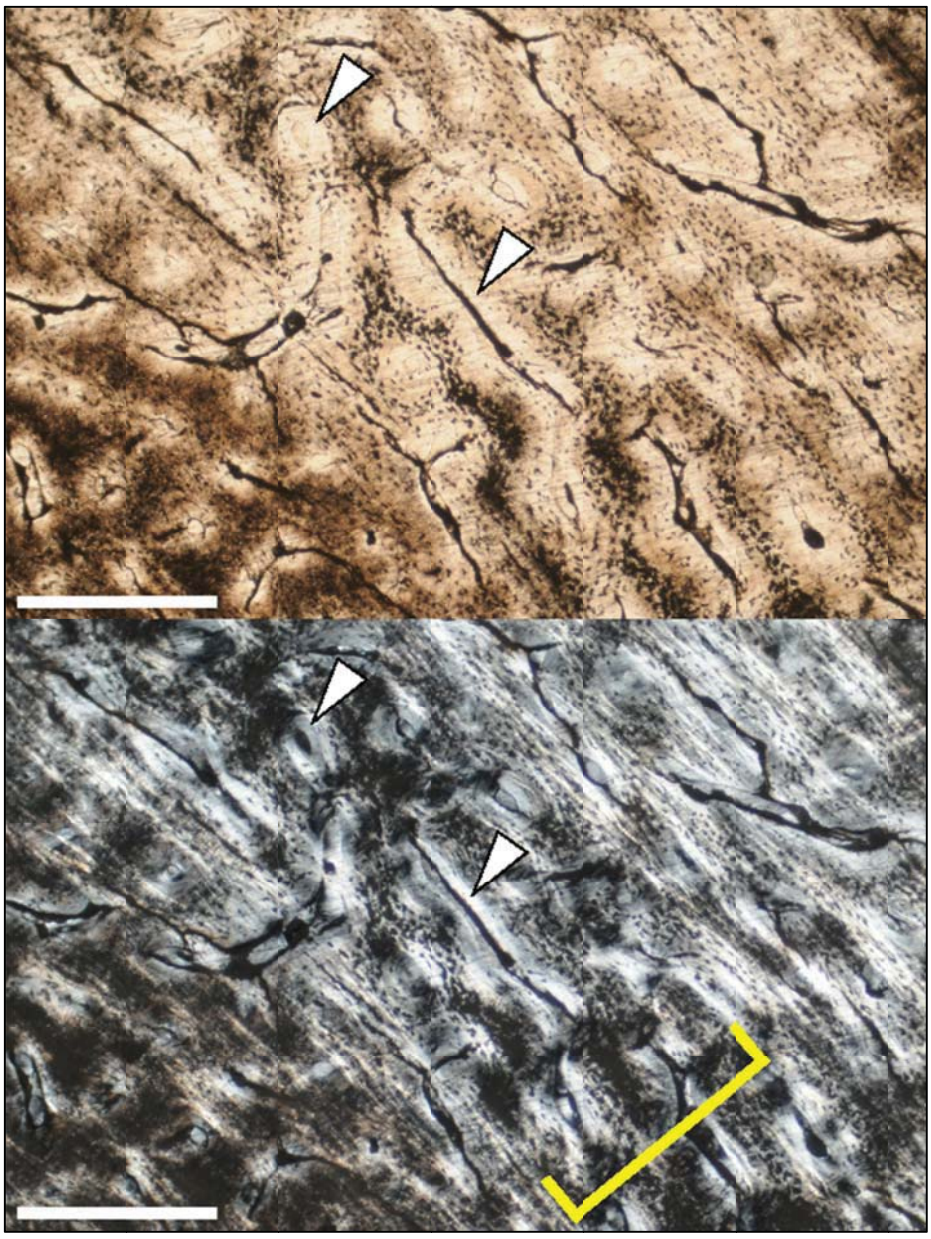

Figure 2.30 Woven-fibered bone in the outer cortex of the femur of a wild-caught adult male *Alligator mississippiensis* (UF FWC-LGS1) shown in regular transmitted light (top) and crossed plane-polarized light (bottom). Yellow bracket indicates a narrow band of woven bone; parallel-fibered bone is present on either side of this bracket. In regions of parallel-fibered bone, osteocyte lacunae are oriented in the same direction relative to the long axis of the bone and are aligned in the same direction relative to each other. Within the woven-fibered bone, osteocytes show much less organization and are less consistently oriented. White triangles indicate lamellae surrounding primary osteons, confirming a previous diagnosis of fibrolamellar bone in this individual (Tumarkin-Deratzian 2007). Scale bars = 500 μm.

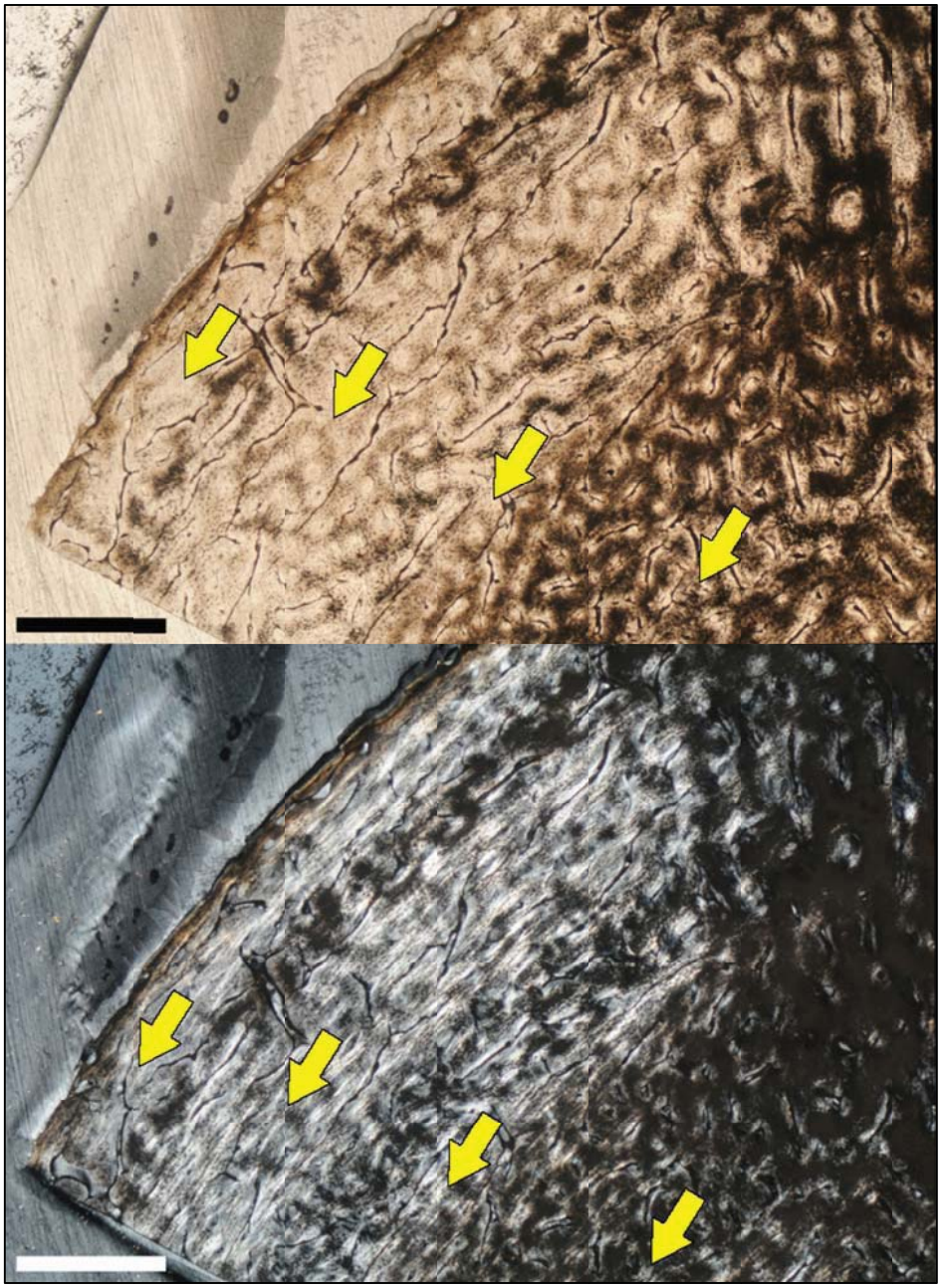

Figure 2.31 Woven-fibered bone in the outer cortex of the femur of a wild-caught adult male *Alligator mississippiensis* (UF FWC-LGS1) shown in regular transmitted light (top) and crossed plane-polarized light (bottom). This individual preserves eight annuli in the femoral cortex; the outer four are indicated here (yellow arrows). Under polarized light, the outer three annuli are bright; these regions are composed of parallel-fibered bone. The darker regions between them are composed of woven-fibered bone. After the fifth LAG (right-most arrow in this image), the woven-fibered component forms less of the zones between annuli than the parallel-fibered component. Scale bars = 1 mm.

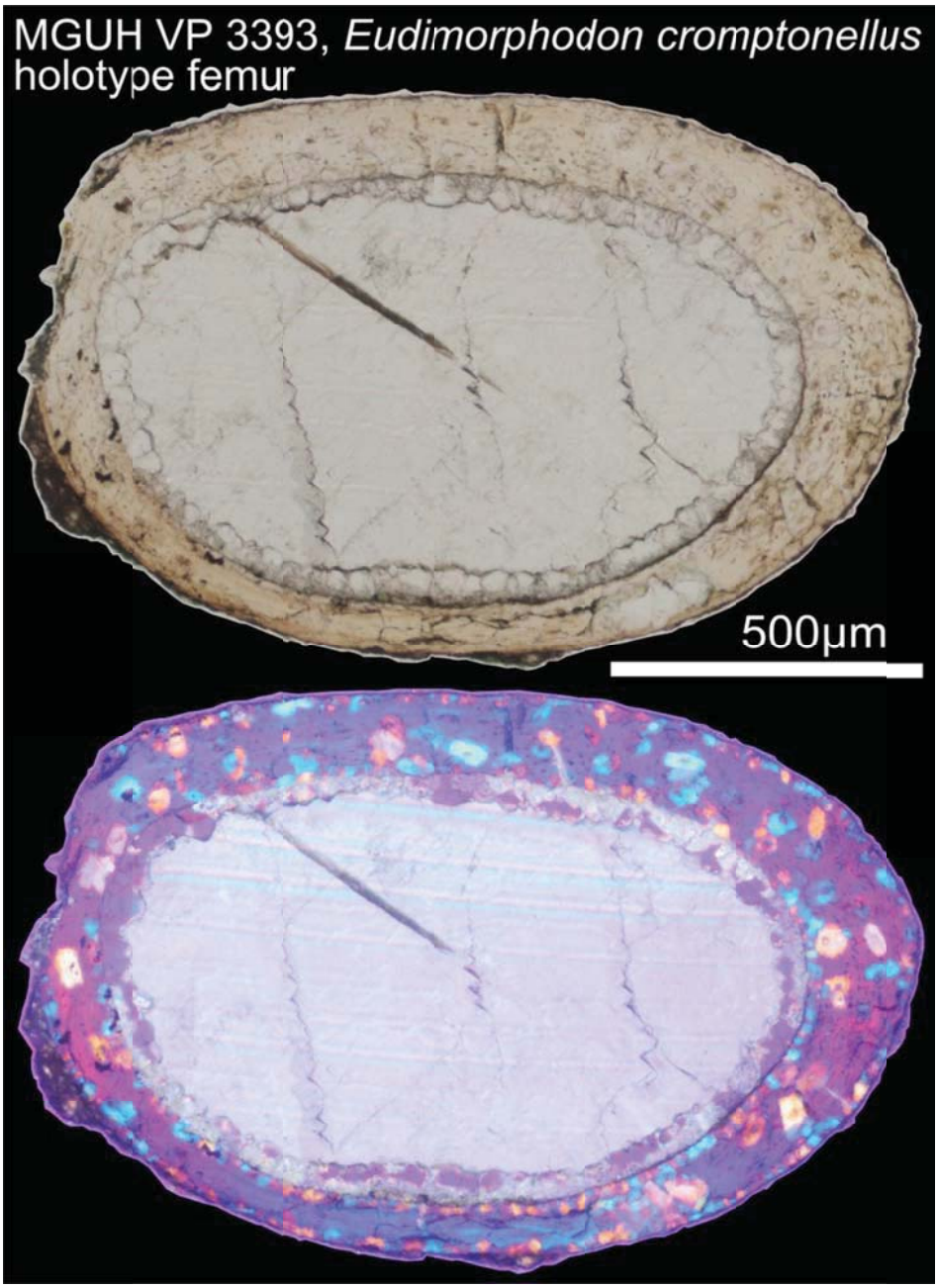

Figure 2.32 Cortical histology of the mid-diaphyseal femur of *Eudimorphodon cromptonellus* (MGUH VP 3393) in regular transmitted light (top) and elliptically polarized light (bottom). This figure illustrates the extent of diagenetic alteration in this specimen; the colorful spots within the cortex in the lower image are osteons which have been recrystallized, along with adjacent tissues. The bottom of each image shows the region of avascularity (no colorful osteons within the cortex). Scale = 500 µm.

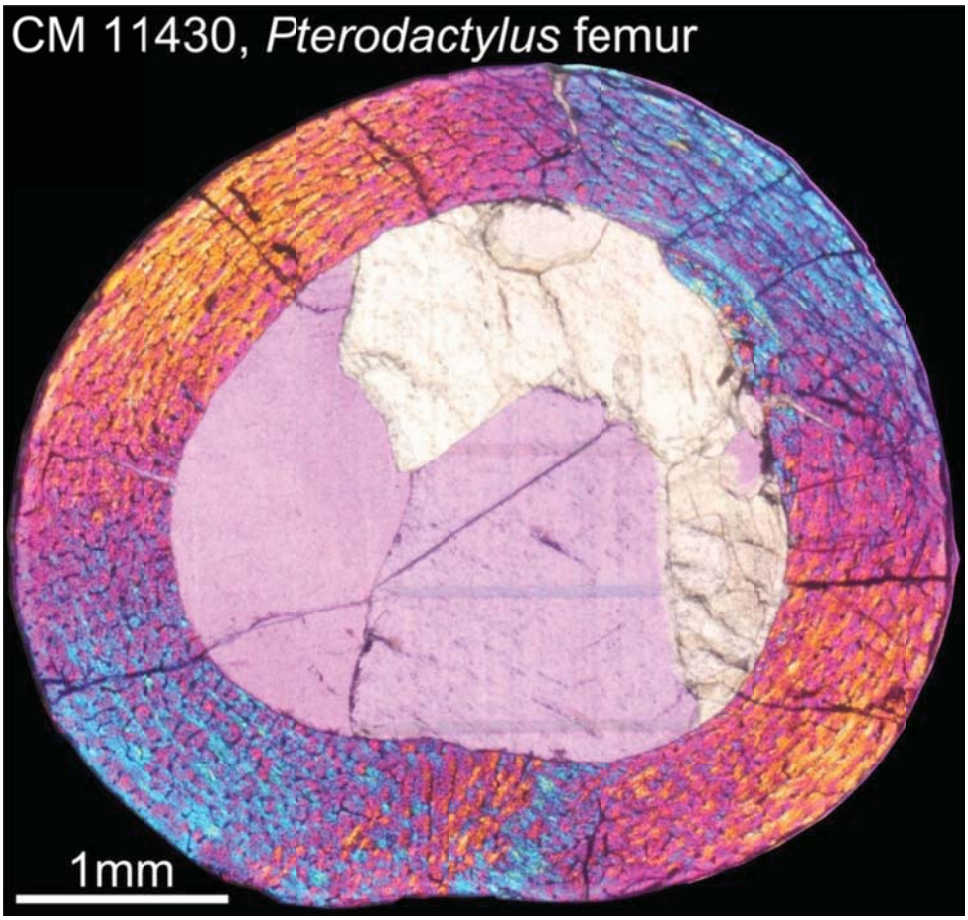

Figure 2.33 Cortical histology of the mid-diaphyseal femur of *Pterodactylus* (CM 11430) in elliptically polarized light. Woven-fibered bone can be found throughout the cortex. However, though the collagen fibers are aligned in all directions, more are oriented circumferentially than longitudinally, obliquely, or radially. Therefore, the bone refringes in a manner intermediate between woven-fibered and parallel-fibered bone under polarized light. Scale = 1 mm.

In elliptically polarized light, different colors represent positive or negative optical sign relative to the slow axis of the polarizer (the color and the sign depend on the material in question, which may be original collagen or apatite crystals that replaced them). What is most important in this image is the pattern of color (as opposed to the colors themselves). Bright regions of one color occur when many collagen fibers (or their replacement) are aligned in the same direction. Where more than one color is bright, but the colors travel in different directions, woven fibered bone is present. These regions often look like a multicolored patchwork (e.g., bottom of image; see also Figure 2.34). Around most of the section, the most intense colors travel circumferentially around the section. However, between these circumferential colors, other bright colors are visible, which are oriented in different directions (usually radially). The subtle nature of this patchwork reflects a greater proportion of circumferentially oriented fibers in this section.

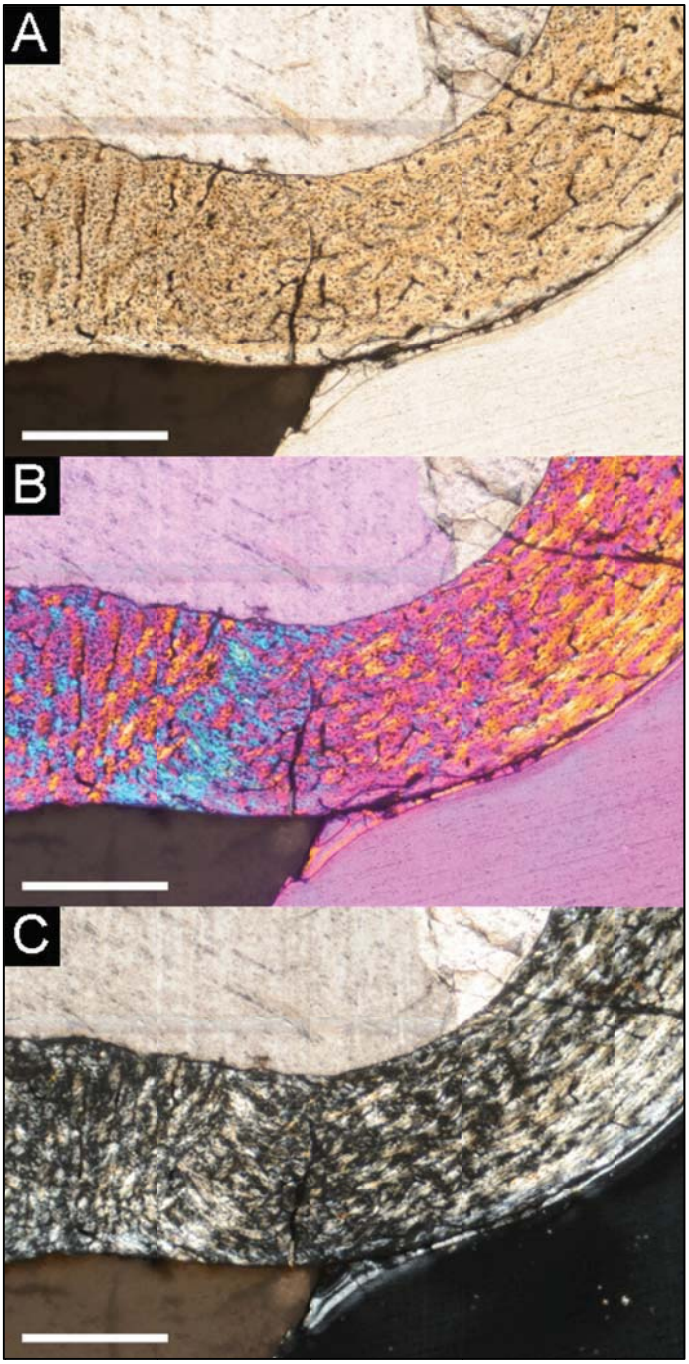

Figure 2.34 Cortical histology of the mid-diaphyseal femur of *Pterodactylus* (CM 11430) shown in A) regular transmitted light, B) elliptically polarized light, and C) crossed plane polarized light. This region is the most intensely woven region within the section, and also shows the highest density of osteocyte lacunae (see A, lower left corner of image). Periosteum to the bottom of all images. Scale bars = 500 μm.

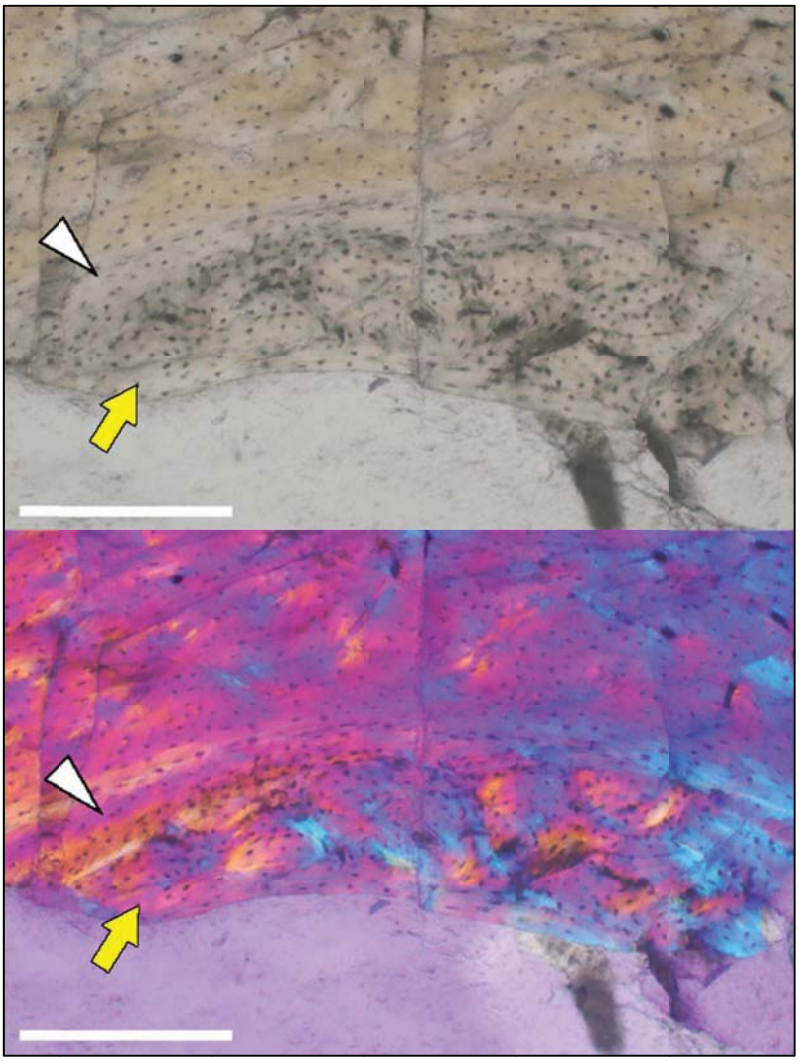

Figure 2.35 Endosteally-derived tissues of the mid-diaphyseal femur of *Pterodactylus* (CM 11430) shown in regular transmitted light (top) and elliptically polarized light (bottom). The original endosteal lamellae continue around the entire endosteal margin, and are indicated here by white triangles. A second layer of lamellae (yellow arrow) internally border a region of endosteally-derived woven-fibered bone. This woven-fibered region must have been deposited after the deposition of the original endosteal lamellae, because a resorption line is visible between the woven bone and the original endosteal lamellae (right side of image), and this cuts across some of the lamellae. The canals in this woven-fibered region are oriented in several directions and are lined by parallel-fibered bone. The second layer lamellae cuts across the woven-fibered region. A similar tissue is visible in a wing phalanx of this individual. Endosteal margin to bottom of each image; scale bars = 250 μm.

This region is histologically similar to an endosteally-derived primary tissue in the pterodactyloid *Pterodaustro* (Chinsamy et al. 2009), which those authors identified as medullary bone, an ephemeral tissue rapidly deposited in the medullary cavity of female birds and dinosaurs in advance of egg-shelling (Schweitzer et al. 2005).

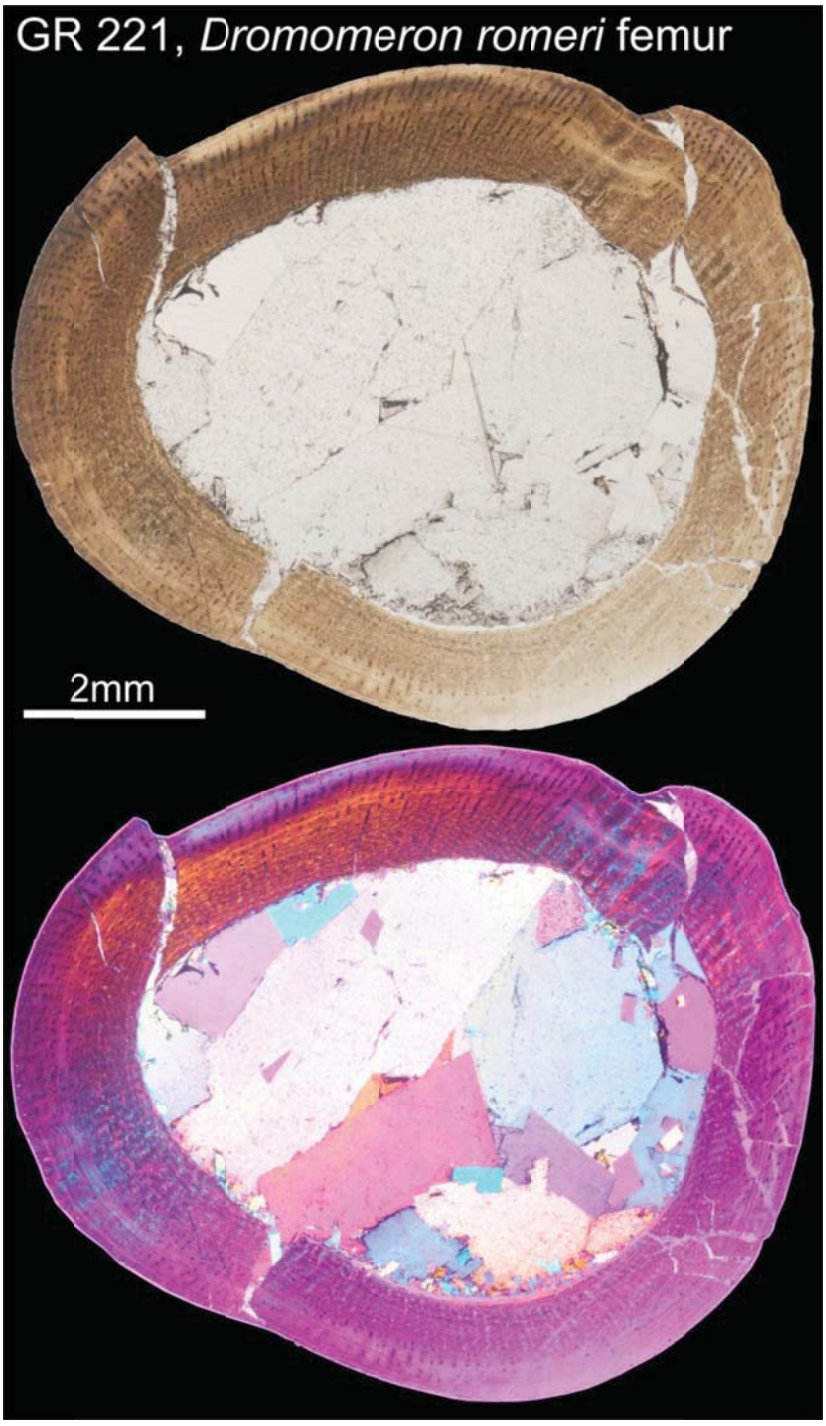

Figure 2.36 Cortical histology of the mid-diaphyseal femur of *Dromomeron romeri* (GR 221) shown in regular transmitted light (top) and elliptically polarized light (bottom). This section was ground thin (lower right of each image); collagen fiber orientation is more easily distinguished in thicker sections. Most vascular canals in this section are arranged in radial rows. Scale = 2 mm.

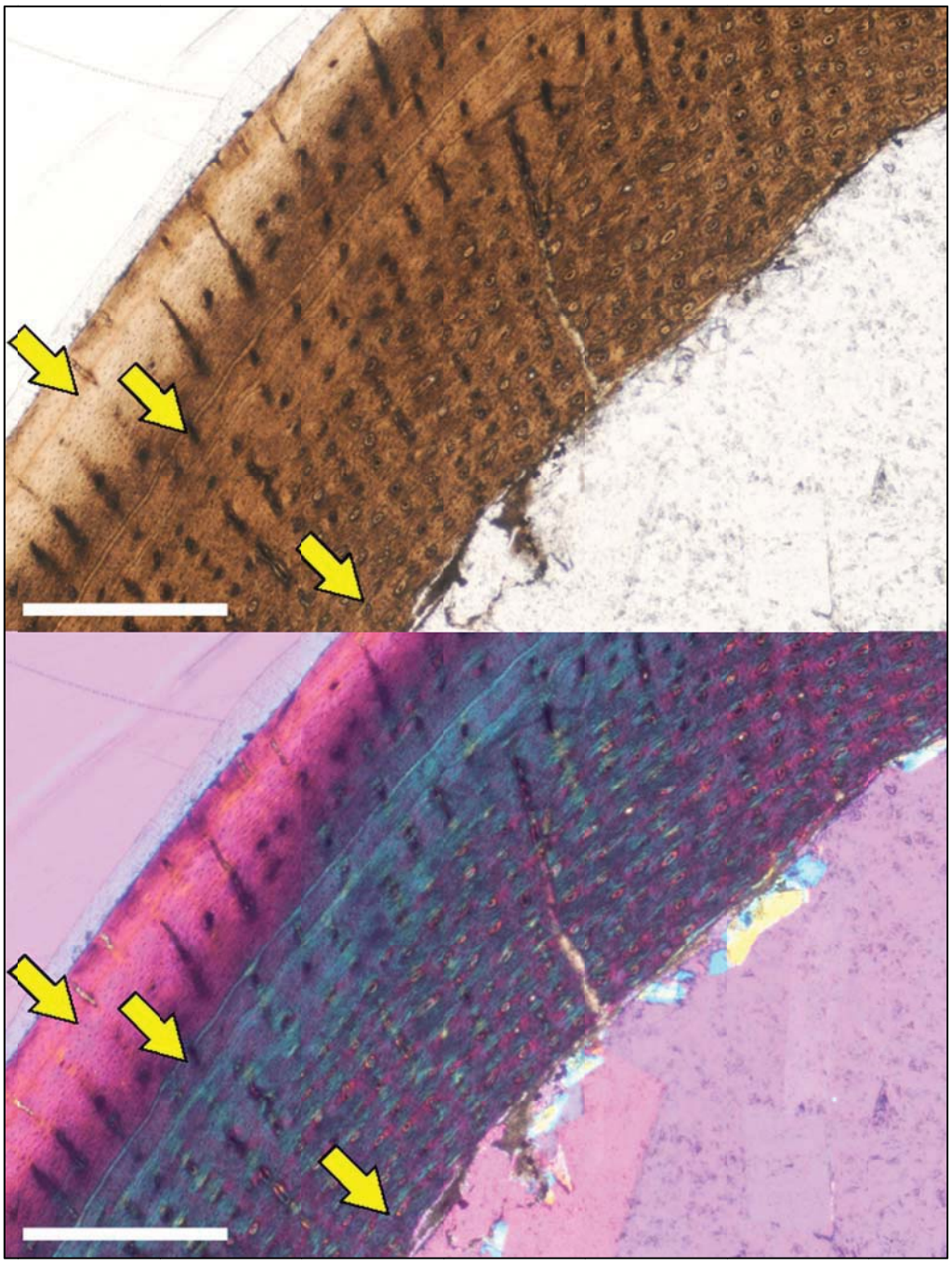

Figure 2.37 Cortical histology of the mid-diaphyseal femur of *Dromomeron romeri* (GR 221) shown in regular transmitted light (top) and elliptically polarized light (bottom). Three LAGs are visible in this section (arrows). The inner cortex is composed of woven fibered bone, but this transitions to lamellar bone approaching the middle LAG. In the zone between the middle and outer LAG, the bone is mostly lamellar. The cortex is moderately to well vascularized by primary osteons that align in radial rows. Periosteum to upper left of each image. Scale = 500 μm.

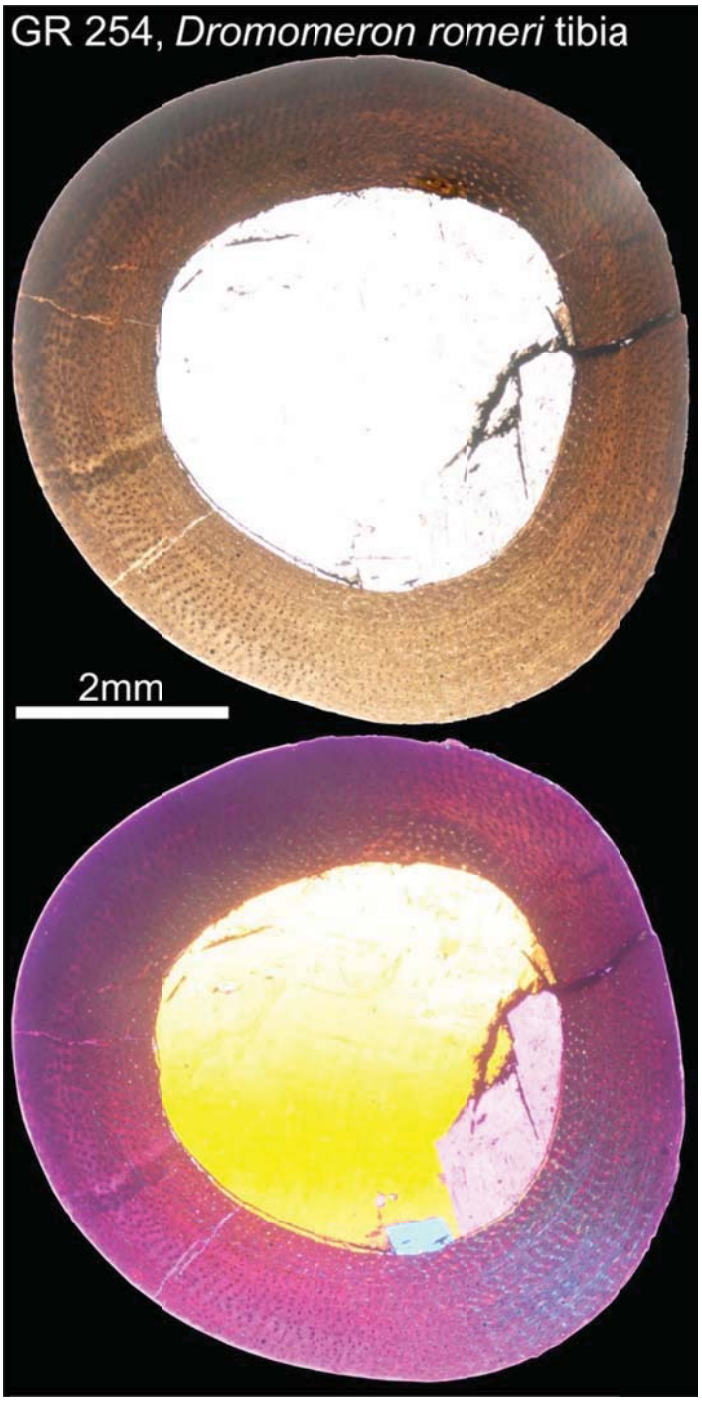

Figure 2.38 Cortical histology of the mid-diaphyseal tibia of *Dromomeron romeri* (GR 254) shown in regular transmitted light (top) and elliptically polarized light (bottom). As in the femur described above, most vascular canals are arranged in radial rows, but they are slightly less organized in the tibia than in the femur. Scale = 2 mm.

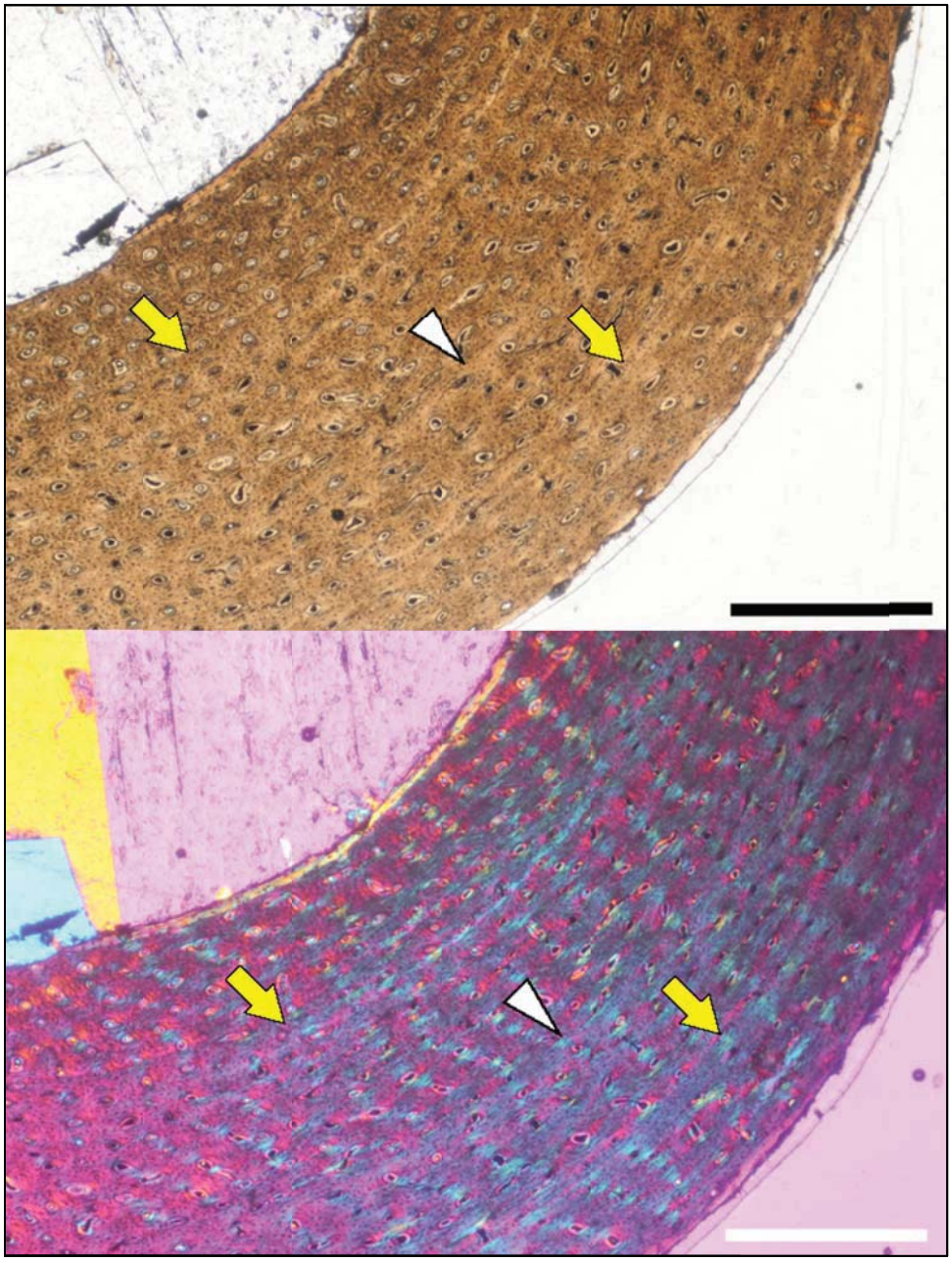

Figure 2.39 Cortical histology of the mid-diaphyseal tibia of *Dromomeron romeri* (GR 254) shown in regular transmitted light (top) and elliptically polarized light (bottom). Two annual growth marks are visible in this section (yellow arrows). Regionally, another line appers (white triangle) that brighter under regular light and refringes differently under elliptically polarized light compared to surrounding tissues. This line is not laterally extensive and I do not consider it a LAG or annulus. The cortex of GR 254 is mostly woven-fibered, and is well vascularized by longitudinal primary osteons that form radial rows. These canals generally do not anastomose. Periosteum to lower right of each image. Scale bars = 500 μm.

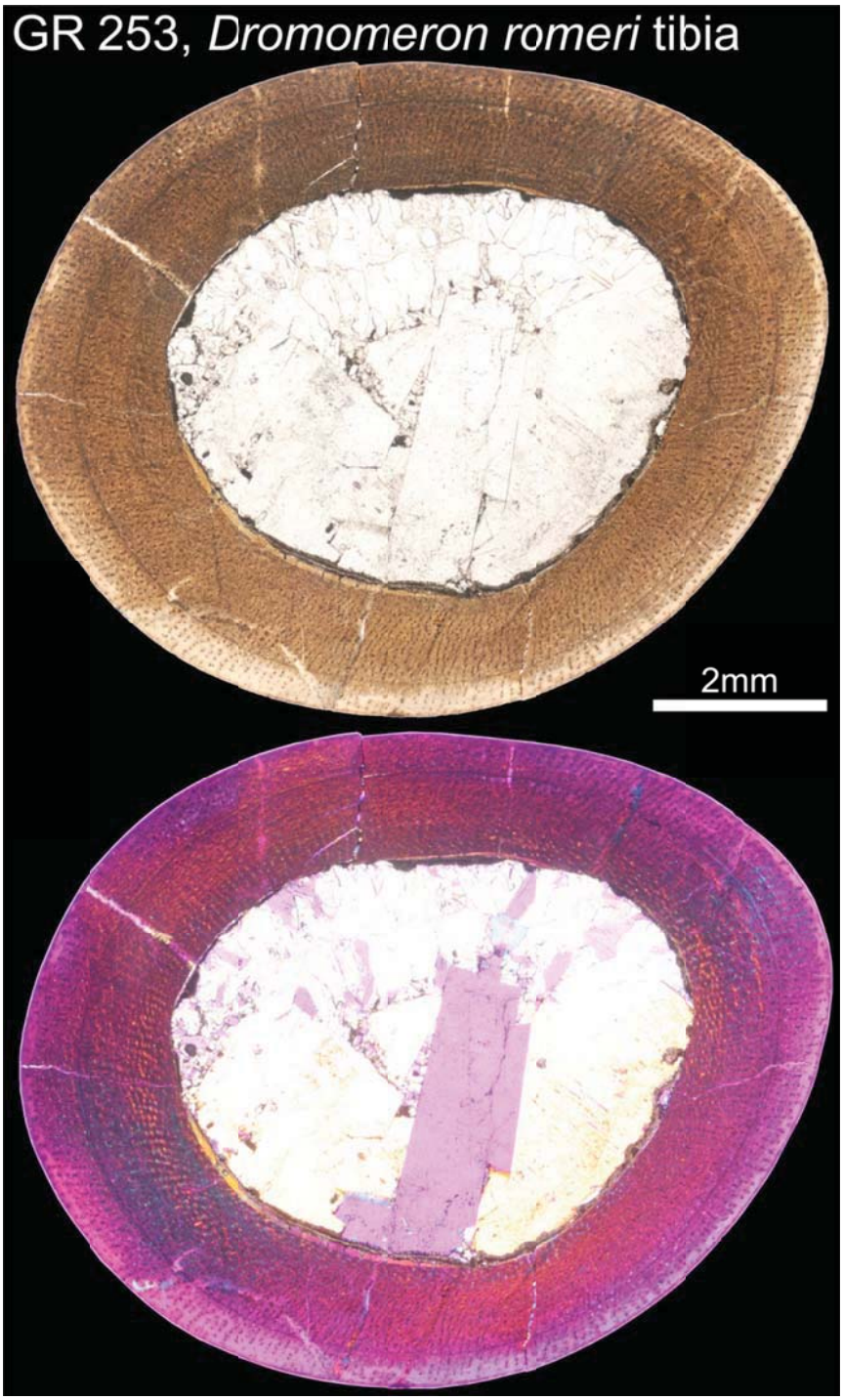

Figure 2.40 Cortical histology of the mid-diaphyseal tibia of *Dromomeron romeri* (GR 253) shown in regular transmitted light (top) and elliptically polarized light (bottom). As in GR 254 (smaller tibia), most vascular canals are arranged in radial rows, but they do not form straight rows as in the femur. Scale = 2 mm.

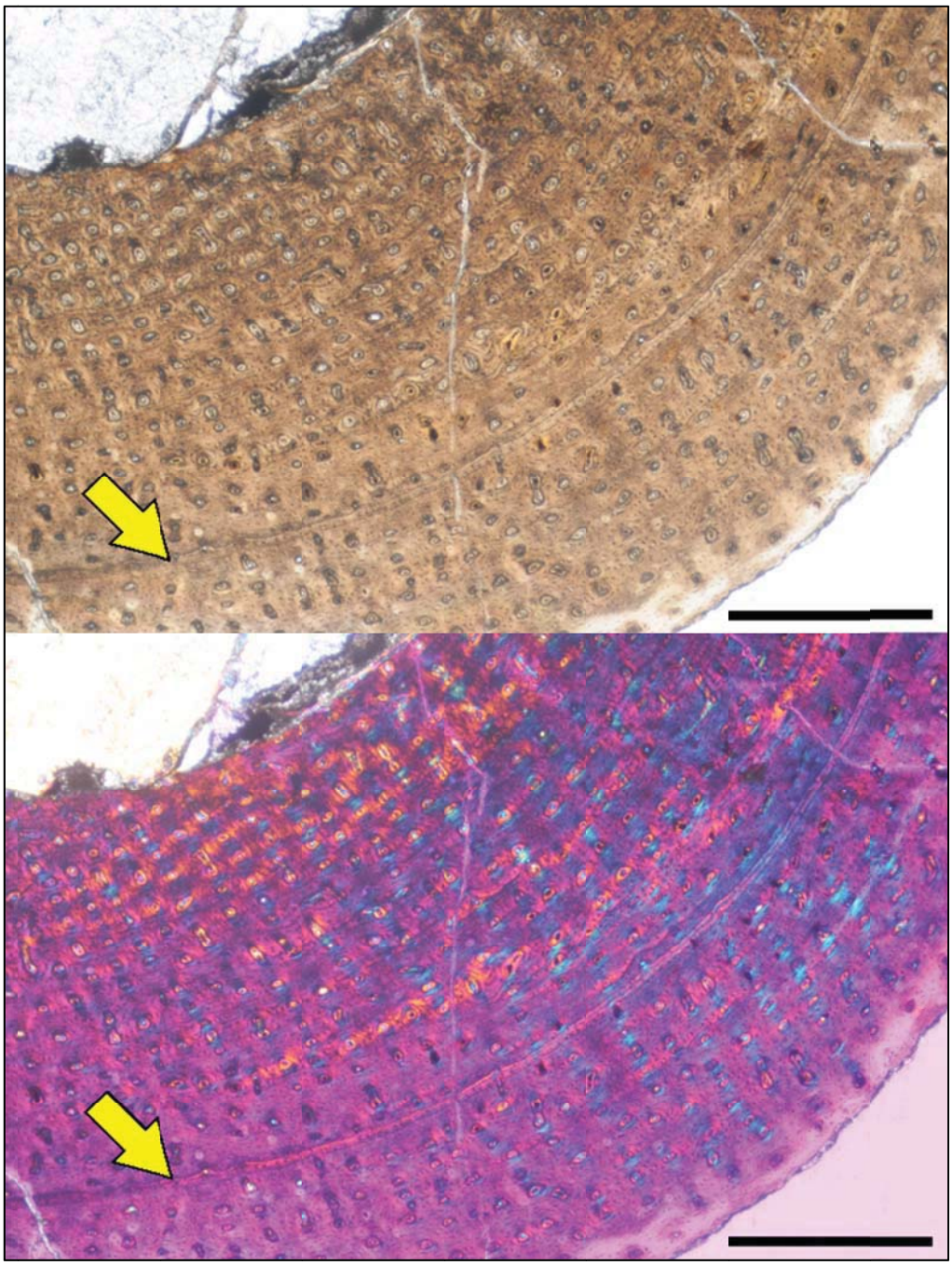

Figure 2.41 Cortical histology of the mid-diaphyseal tibia of *Dromomeron romeri* (GR 253) shown in regular transmitted light (top) and elliptically polarized light (bottom). A single LAG is visible in this section (yellow arrows). The inner cortex of GR 253 is mostly woven-fibered, but transitions to parallel-fibered bone at midcortex (near the LAG). It is well vascularized by longitudinal primary osteons that form radial rows. As in the smaller tibia (GR 254), these canals generally do not anastomose. Periosteum to lower right of each image. Scale bars = 500 μm.

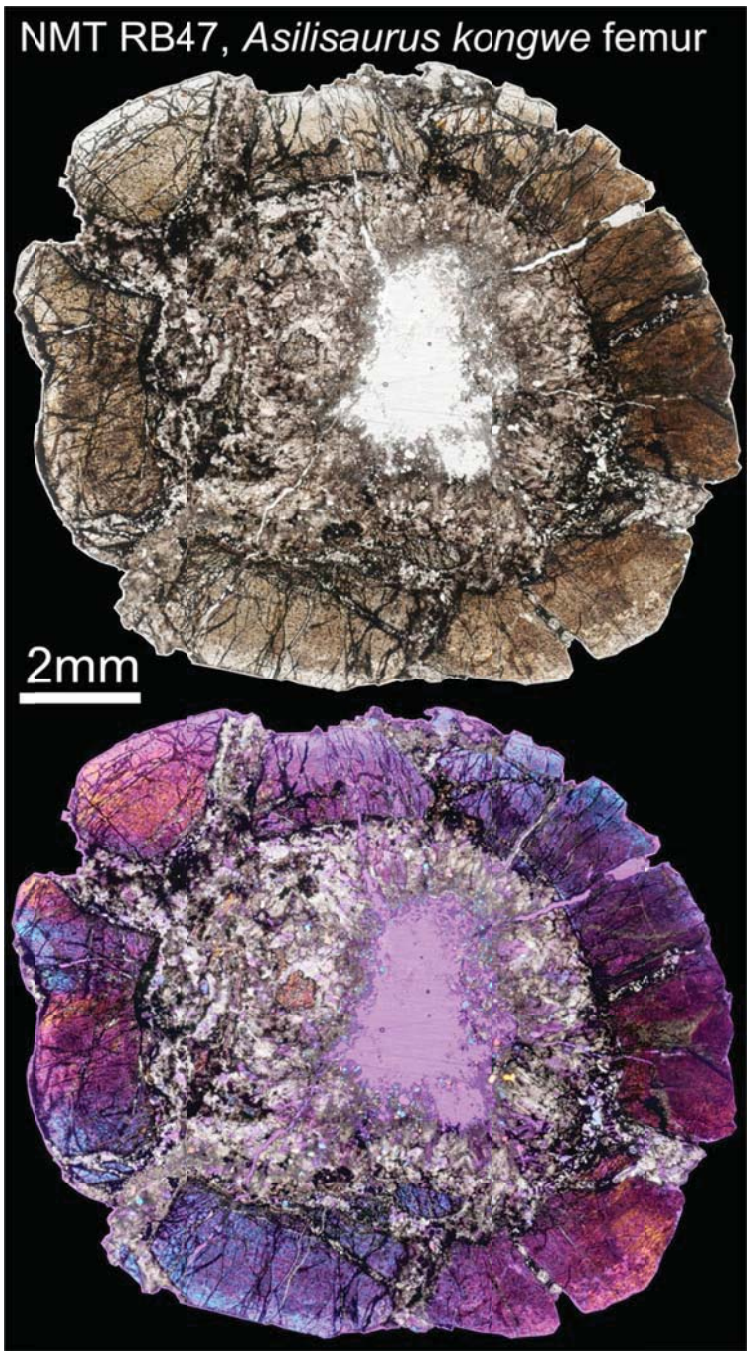

Figure 2.42 Cortical histology of the mid-diaphyseal tibia of *Asilisaurus kongwe* (NMT RB47) shown in regular transmitted light (top) and elliptically polarized light (bottom). All elements show extensive cracking of the cortex and mineral infilling of the medullary cavity. Scale = 2 mm.

Figure 2.43 Cortical histology of the mid-diaphyseal tibia of *Asilisaurus kongwe* (NMT RB46) in regular transmitted light. Extensive cracking is visible throughout the cortex. Primary osteons in this taxon are predominantly longitudinal, but they often anastomose with several other canals to form small reticulations. None of the sampled individuals preserves LAGs or annuli. The periosteum is to the top of this image. Scale = 500 μm.

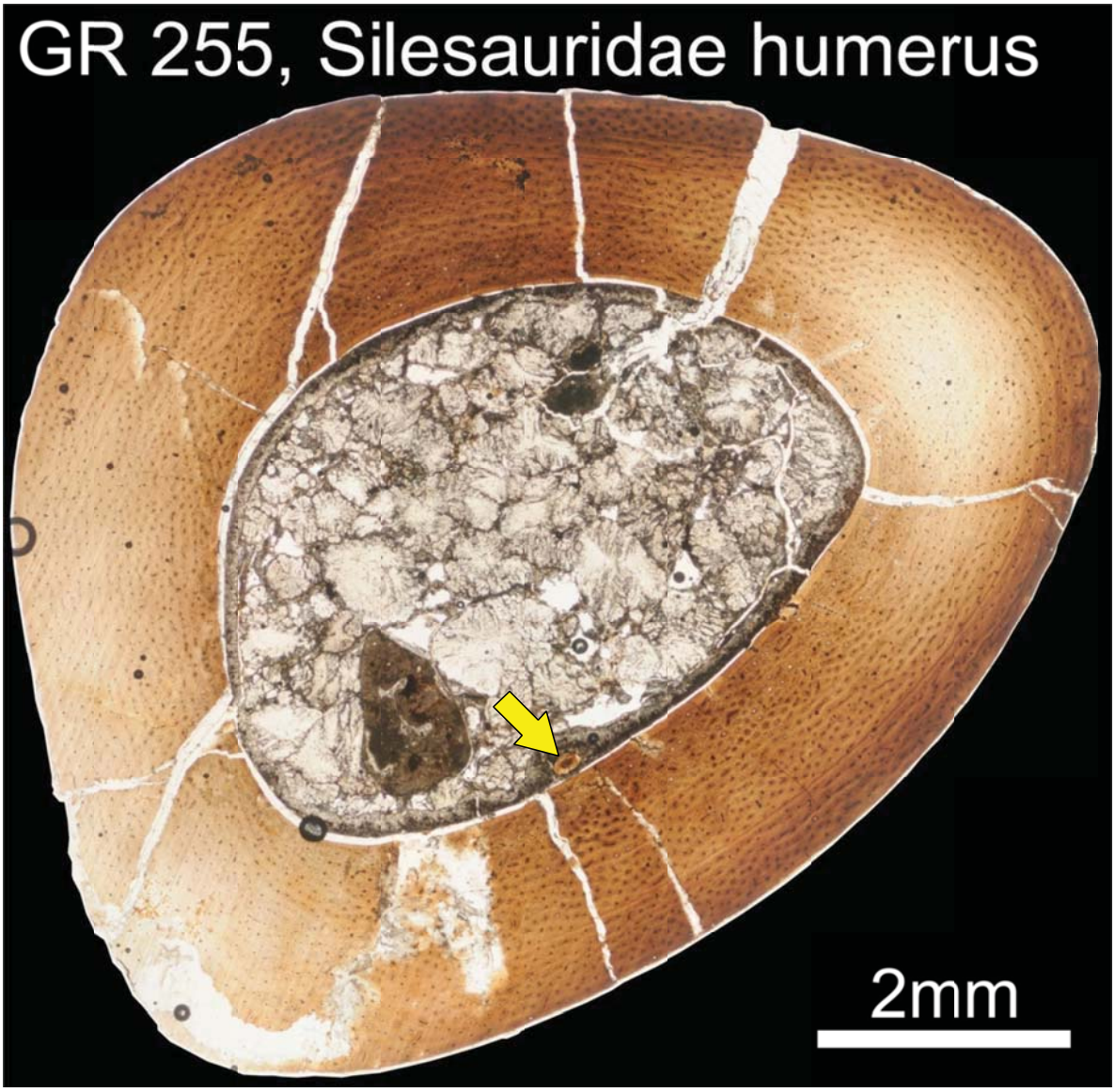

Figure 2.44 Cortical histology of the mid-diaphyseal humerus of the Hayden Quarry silesaurid (GR 255) shown in regular transmitted light. The medullary cavity of this element is free except for a single osteon "floating" among the crystals (arrow). Scale = 2 mm.

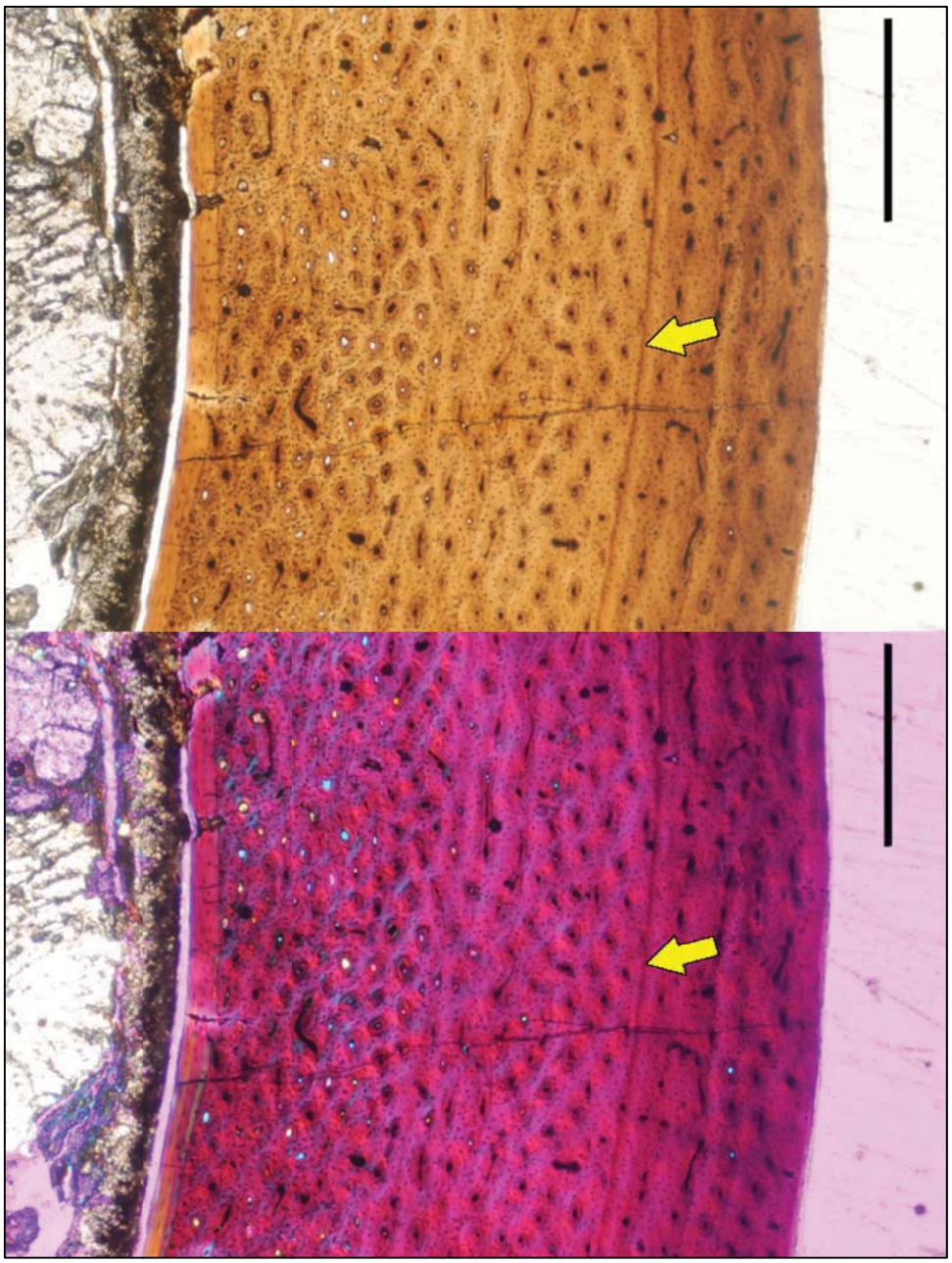

Figure 2.45 Cortical histology of the mid-diaphyseal humerus of the Hayden Quarry silesaurid (GR 255) shown in regular transmitted light (top) and elliptically polarized light (bottom). A single LAG is visible in this section (yellow arrows). The cortex of GR 255 is mostly composed of woven-fibered bone, but transitions to parallel-fibered bone in the annulus surrounding the LAG. It is well vascularized by longitudinal primary osteons that are arranged randomly in the inner cortex and form cicumferential rows in the outer cortex. Periosteum to right of each image. Scale bars = 500 μm.

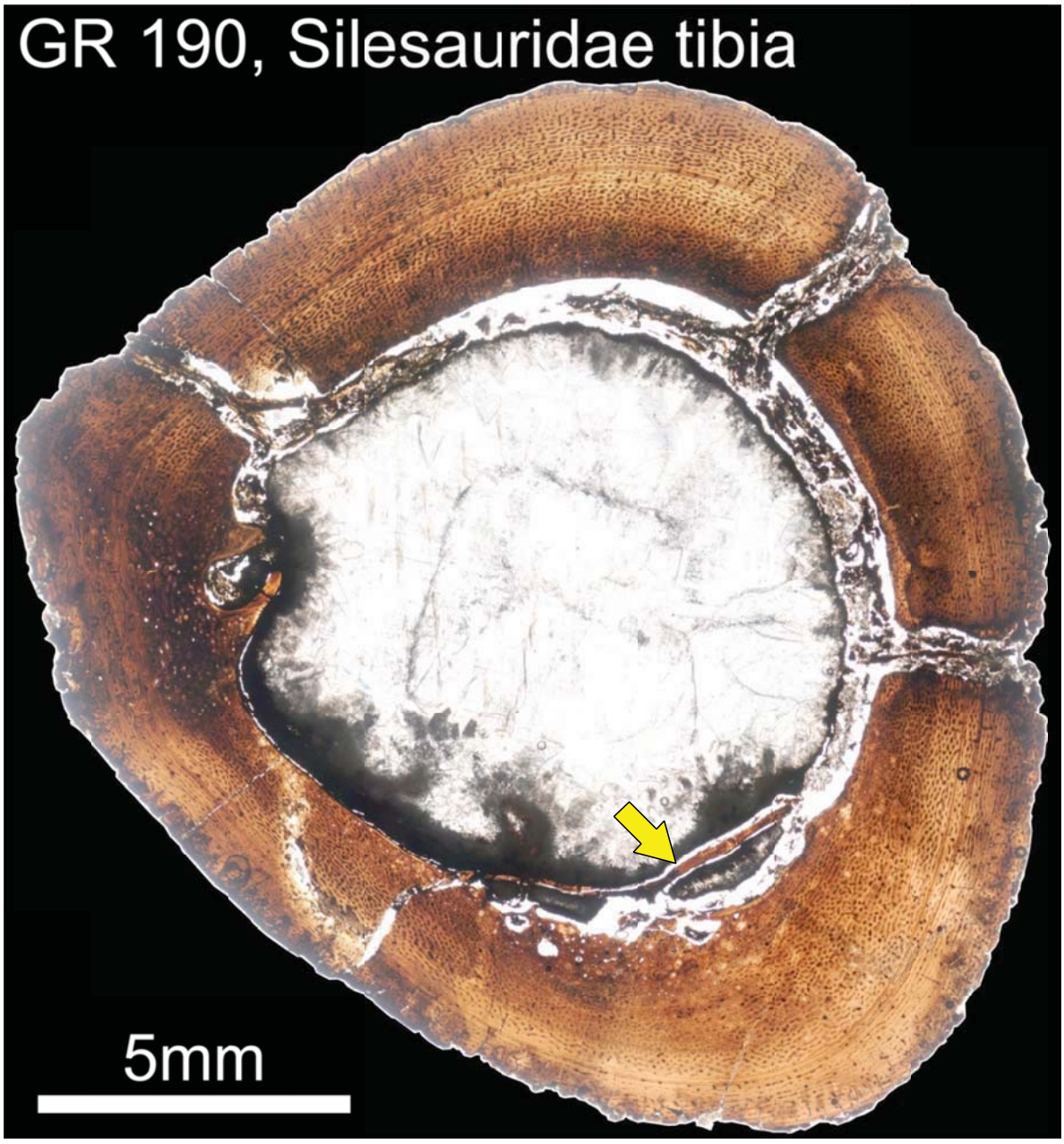

Figure 2.46 Cortical histology of the mid-diaphyseal tibia of the Hayden Quarry silesaurid (GR 190) shown in regular transmitted light. The external surface was abraded by natural weathering. In the anterior quadrant, a trabecular fragment (arrow) runs along the endosteal margin, forming a border between resorption rooms and the medullary cavity. Scale = 2 mm.

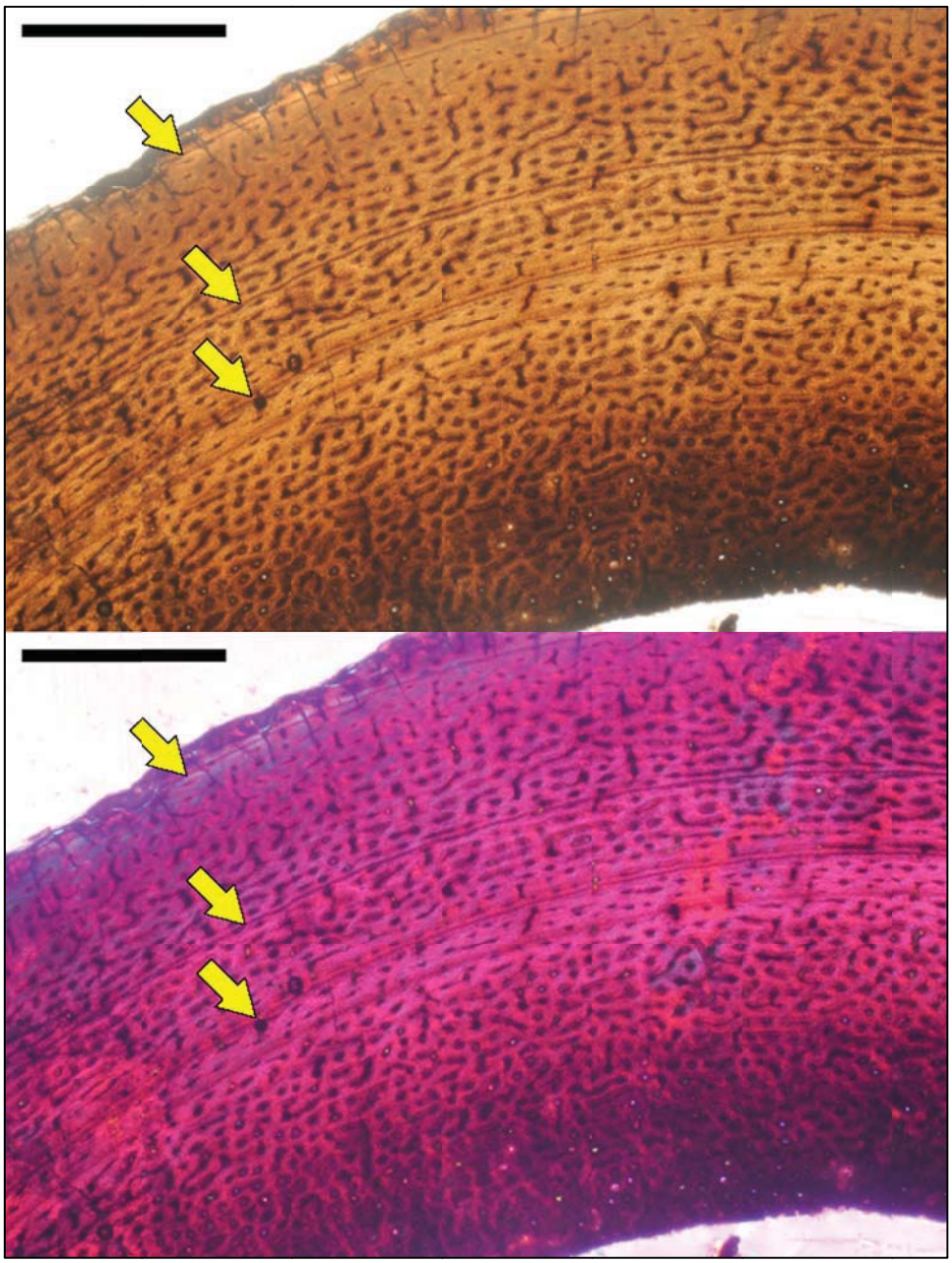

Figure 2.47 Cortical histology of the mid-diaphyseal tibia of the Hayden Quarry silesaurid (GR 190) shown in regular transmitted light (top) and elliptically polarized light (bottom). Three LAGs are visible in this section (yellow arrows). The cortex of GR 190 is mostly composed of woven-fibered bone, and it is well vascularized by primary osteons. Unlike the humerus (Figures 2.45, 2.46), the tibia shows extensive anastomosis between canals, and these connections may occur in any direction. Vascular connectvity, vascular density, and canal diameter all decrease approaching the inner and outer LAGs. Periosteum to top of each image. Scale bars = 1 mm.

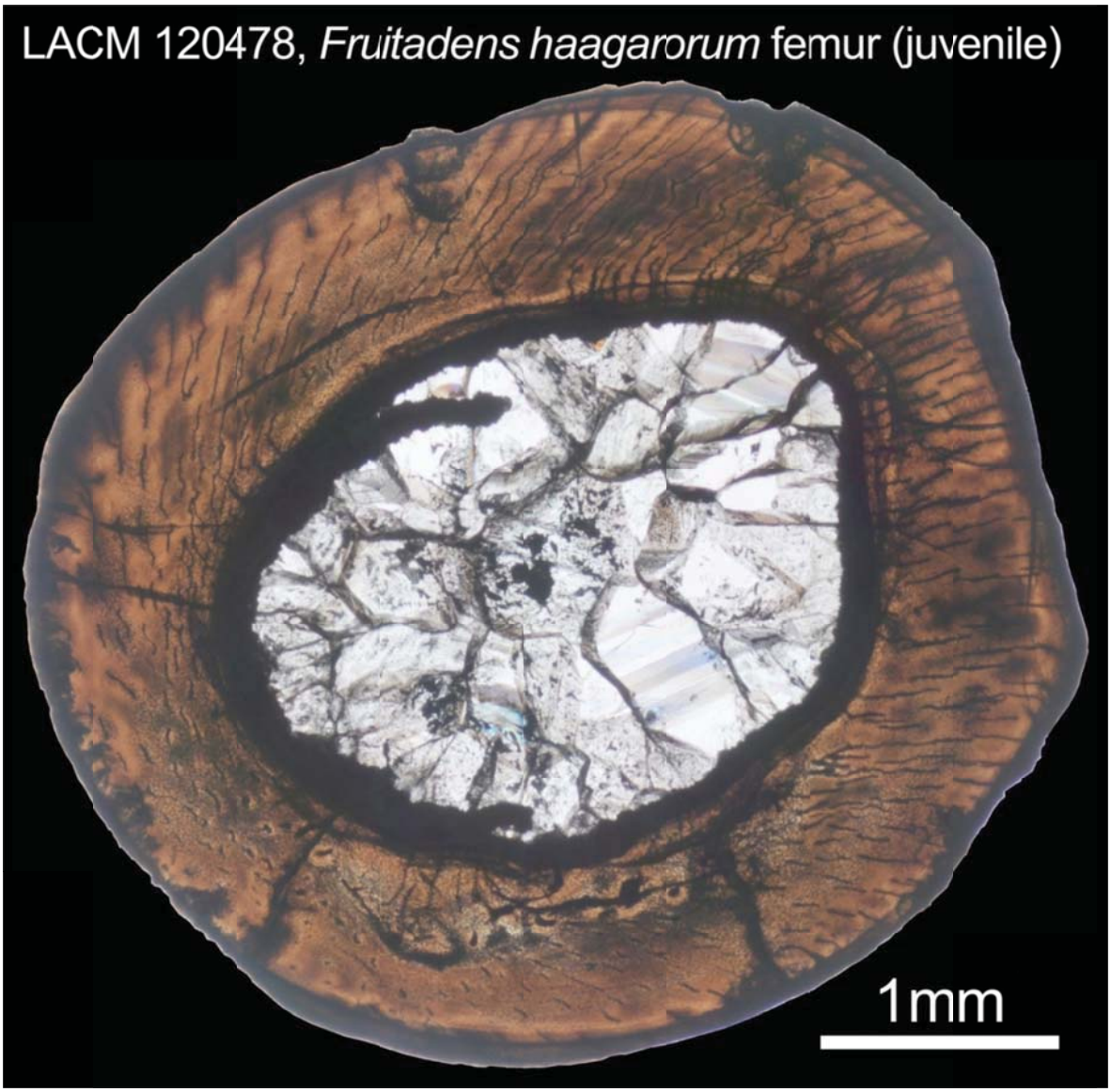

Figure 2.48 Cortical histology of the mid-diaphyseal femur of *Fruitadens haagororum* (LACM 120478; smaller individual). The cortex is moderately to well vascularized by radial primary osteons that span most of the width of the cortex. Scale = 1 mm.

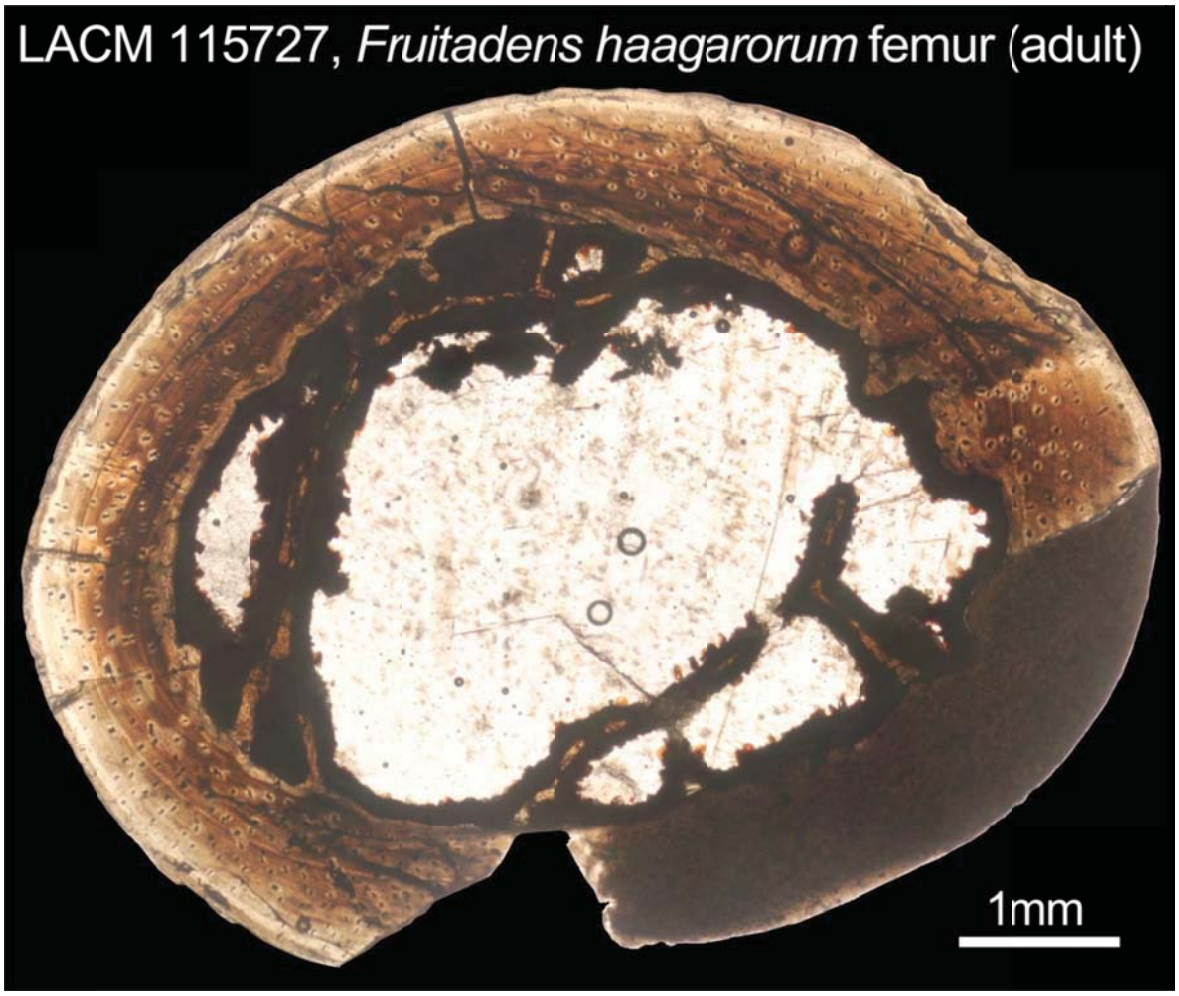

Figure 2.49 Cortical histology of the mid-diaphyseal femur of *Fruitadens haagororum* (LACM 115727; larger individual). This individual preserves trabeculae within the medullary cavity. The cortex is moderately vascularized by longitudinal primary osteons. Scale = 1 mm.

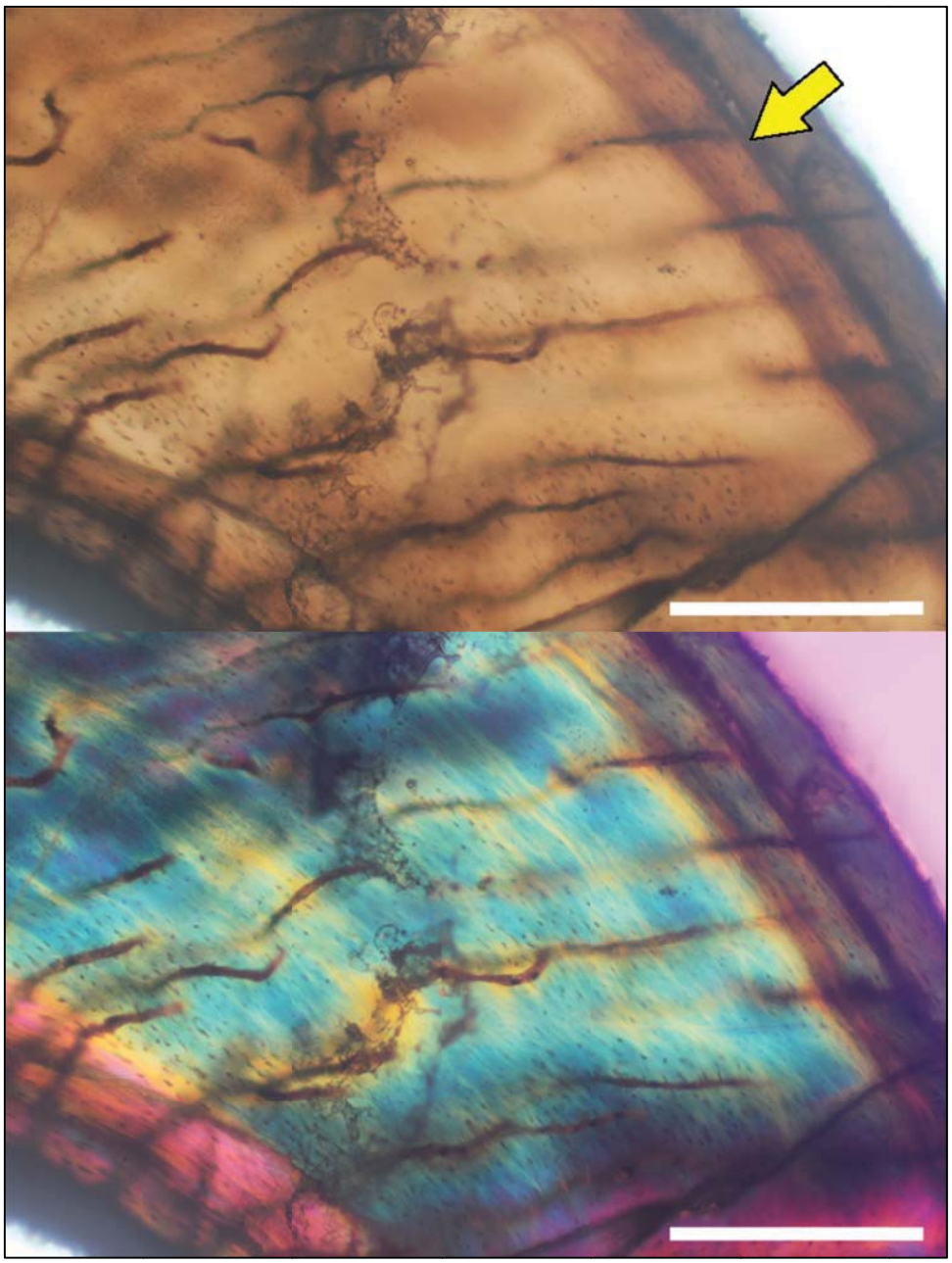

Figure 2.50 Cortical histology of the mid-diaphyseal femur of *Fruitadens haagororum* (LACM 120478) shown in regular transmitted light (top) and elliptically polarized light (bottom). The mid-diaphyseal cortex of this individual is mostly composed of parallel-fibered primary bone tissue. A single LAG is visible close to the periosteal surface (arrow). Radial primary osteons (thin dark lines) run the entire width of the cortex, but weave in an out of the plane of section Periosteum to the upper right in both images. Scale = 250 μm.

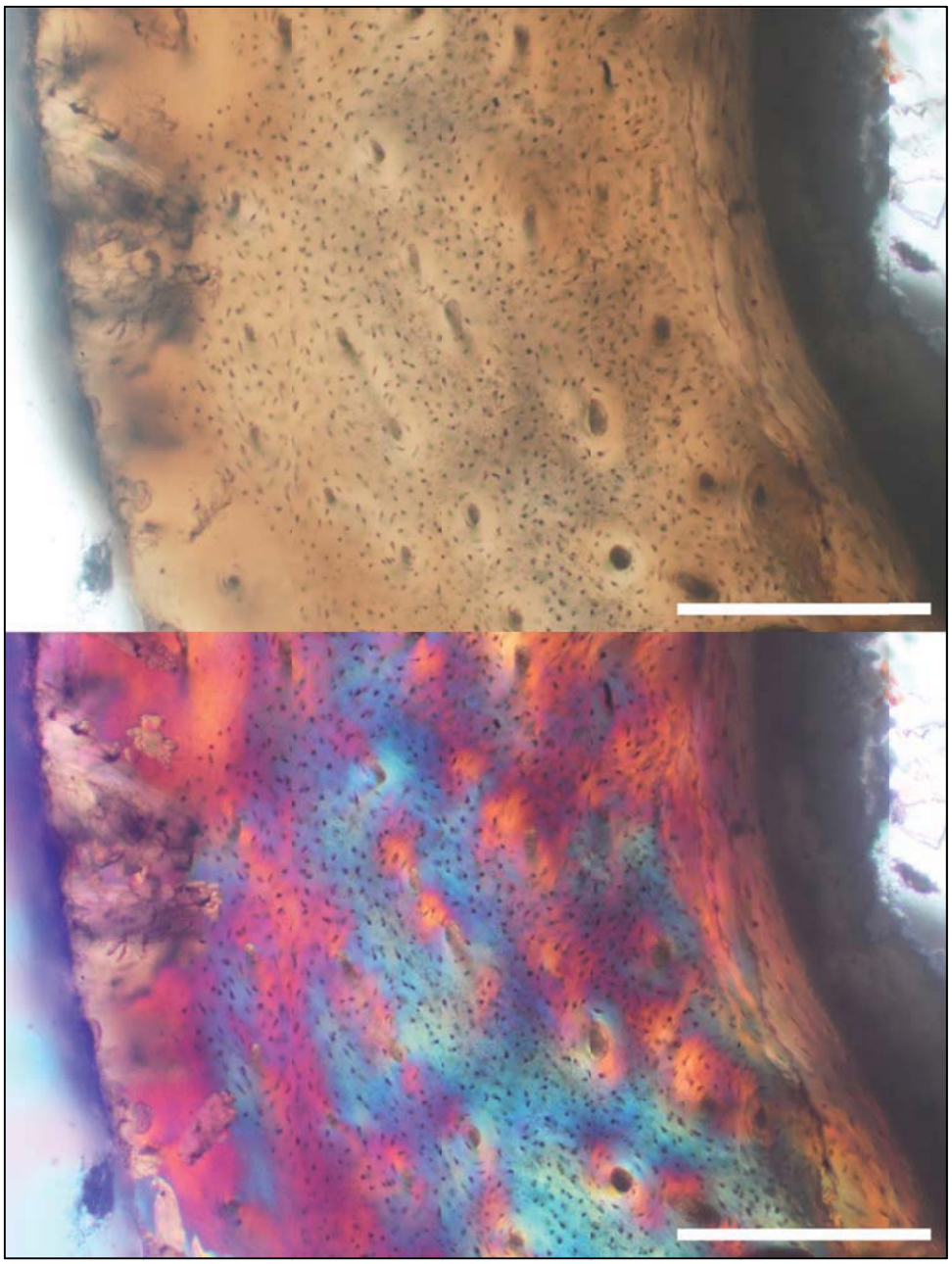

Figure 2.51 Cortical histology of the mid-diaphyseal femur of *Fruitadens haagororum* (LACM 120478) shown in regular transmitted light (top) and elliptically polarized light (bottom). The mid-diaphyseal cortex of this individual is mostly composed of parallel-fibered primary bone tissue (see Figure 2.50), but a single localized area of woven bone is present in the thickest portion of the cortex, pictured above (multicolored region, bottom image). In this region, primary osteons are oriented longitudinally. Periosteum to the left of both images. Scale = 250 μm.

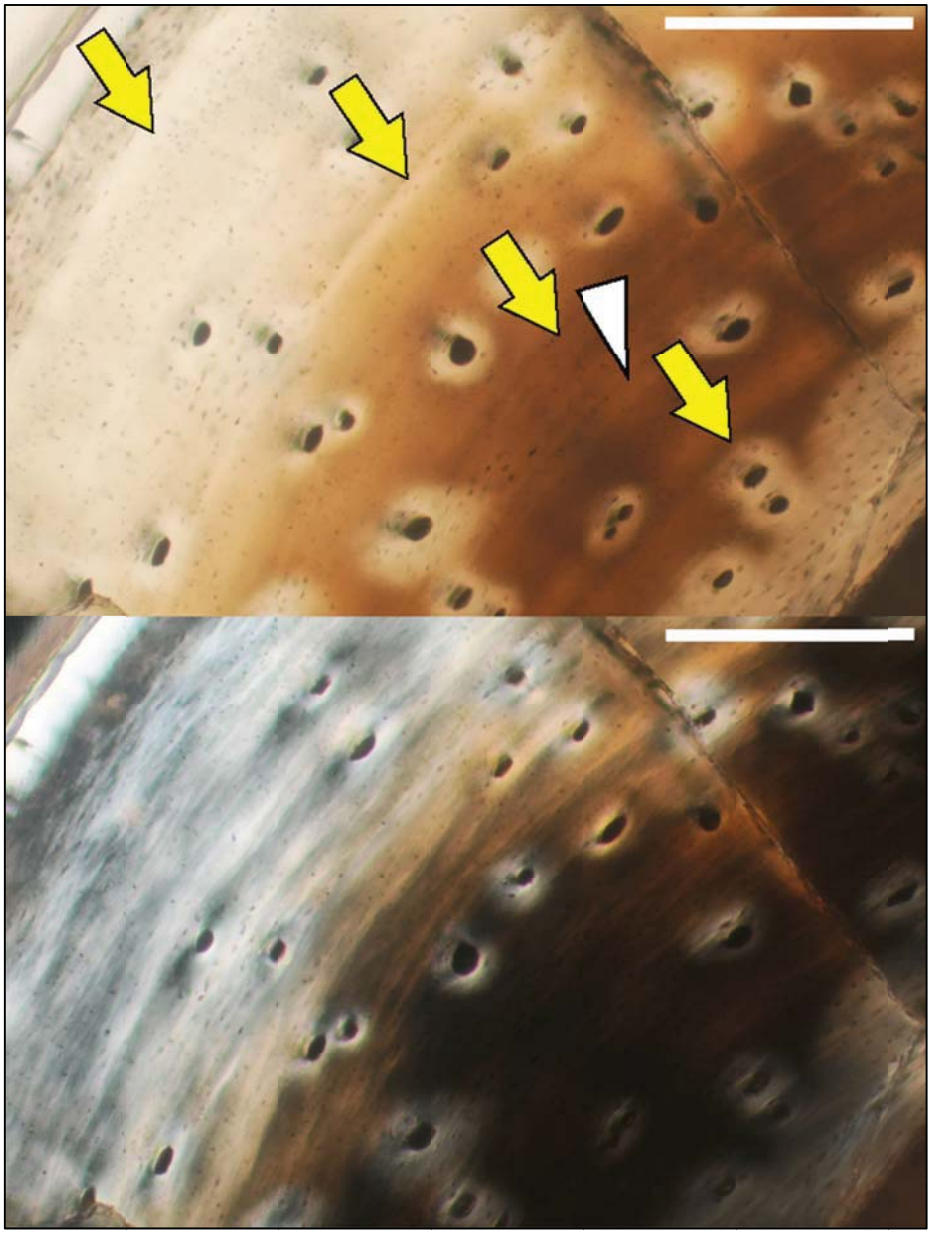

Figure 2.52 Cortical histology of the mid-diaphyseal femur of *Fruitadens haagororum* (LACM 115727) shown in regular transmitted light (top) and crossed plane polarized light (bottom). The mid-diaphyseal cortex of this individual is mostly composed of parallel-fibered primary bone tissue, and is moderately to poorly vascularized by mostly simple primary canals, though some primary osteons are present in the inner cortex. Four LAGs are visible in this section (yellow arrows), though an annulus (white triangle) is regionally present between the first and second LAGs. External to the fourth (outermost) LAG is a region of parallel-fibered bone similar to the tissues at the endosteal margin. Periosteum to upper left of image. Scale = 250 μm.

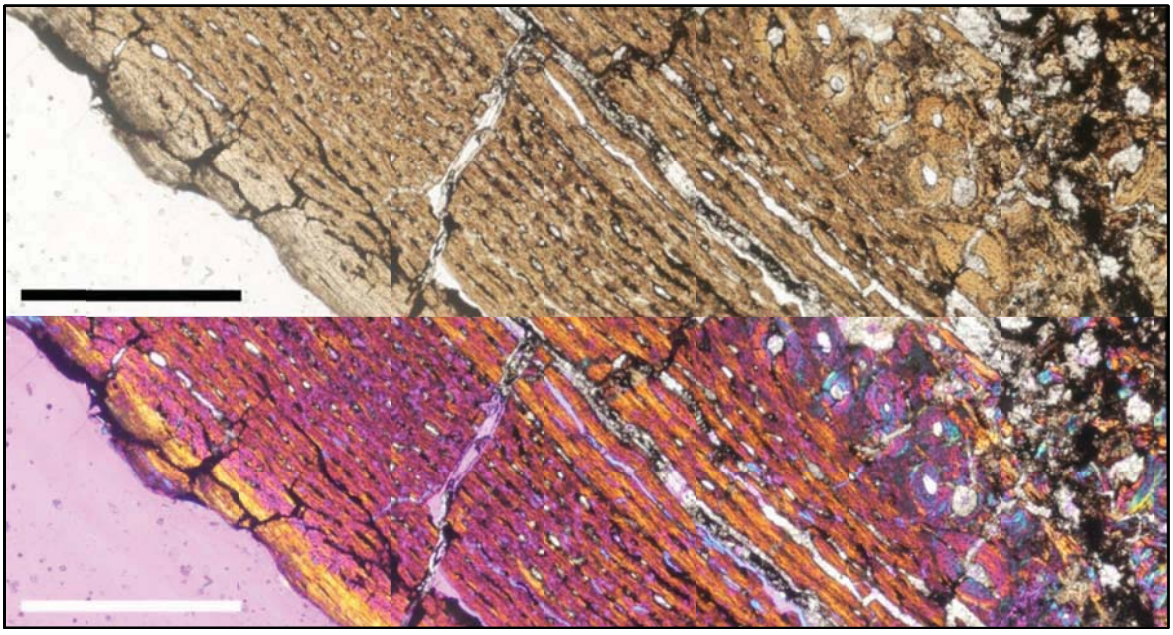

Figure 2.53. Cortical histology of the femur of a neornithischian dinosaur, cf. *Lesothosaurus* or *Stormbergia* (NM QR 3076) in regular transmitted light (top) and elliptically polarized light (bottom). The cortex of this individual is composed mainly of parallel-fibered tissue, and does not show a refringence pattern characteristic of woven bone (bottom image). Periosteum to left of both images. Scale = 1mm.

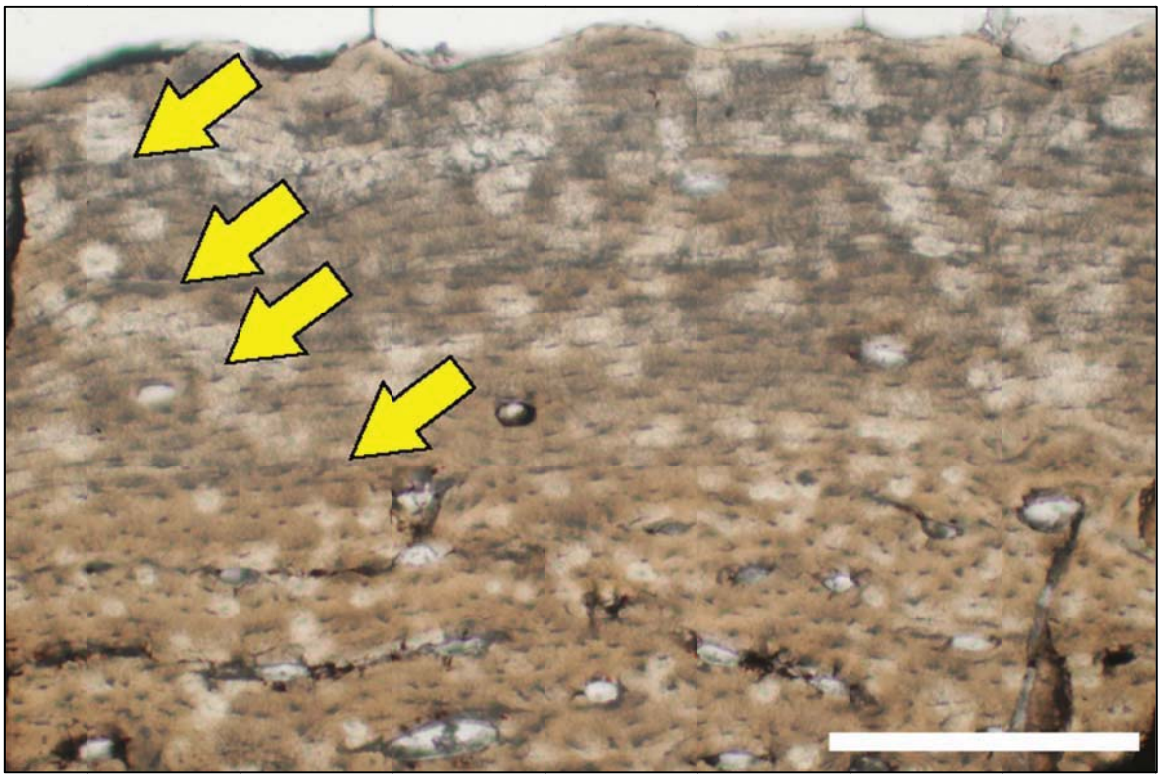

Figure 2.54. Outermost cortex of the mid-diaphyseal femur of a neornithischian dinosaur, cf. *Lesothosaurus* or *Stormbergia* (NM QR 3076) in regular transmitted light. This image shows the abrupt transition between the well vascularized, parallel-fibered cortical tissues (below bottom arrow) and the nearly avascular lamellar bone of the EFS. Arrows indicate the position of the four LAGs in the EFS. LAGs are difficult to see in this image because of the tradeoff between higher magnification and depth of field; the slide was slightly thick and I focused to highlight cells and canal borders rather than LAGs. Periosteum to the top of image. Scale = 250 μm.

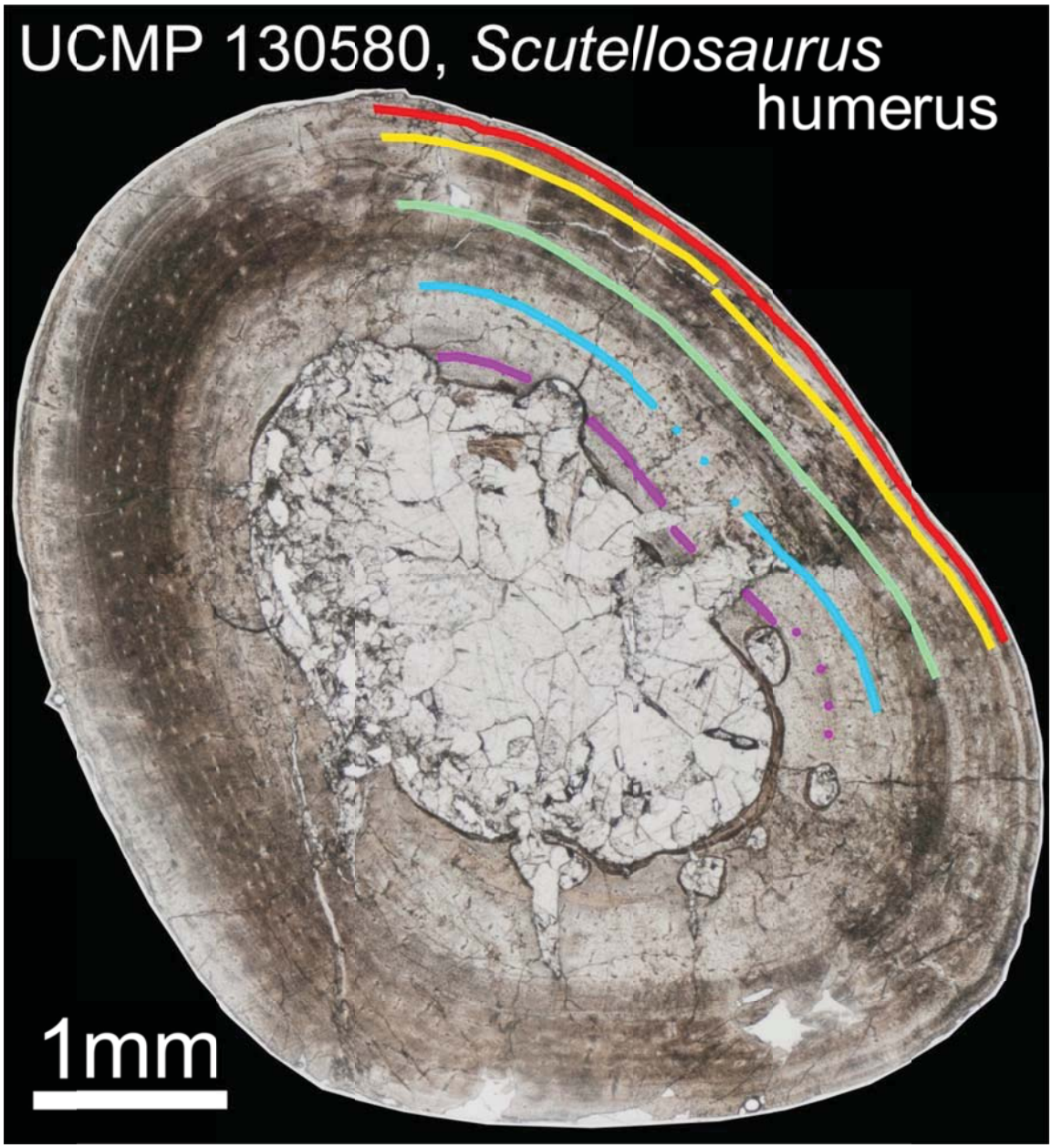

Figure 2.55. Cortical histology of the mid-diaphyseal humerus of the basal thyreophoran dinosaur *Scutellosaurus lawleri* (UCMP 130580) shown in regular transmitted light. Solid colored lines illustrate the path of LAGs in the anteromedial cortex (LAGs continue around th circumference, but are only illustrated in one region so as not to obscure all of the microstructure. Dotted lines show regions where the inner two LAGs locally grades into annuli. Scale = 1 mm.

Figure 2.56. Cortical histology of the mid-diaphyseal humerus of the basal thyreophoran dinosaur *Scutellosaurus lawleri* (UCMP 130580) shown in regular transmitted light. Five growth marks are visible in this section (arrows). The second growth mark (second arrow from bottom) is an annulus at this point in the circumference. The humerus is poorly vascularized by simple primary canals and is mostly composed of parallel-fibered bone tissue. Periosteum to top of image. Scale = 250 μm.

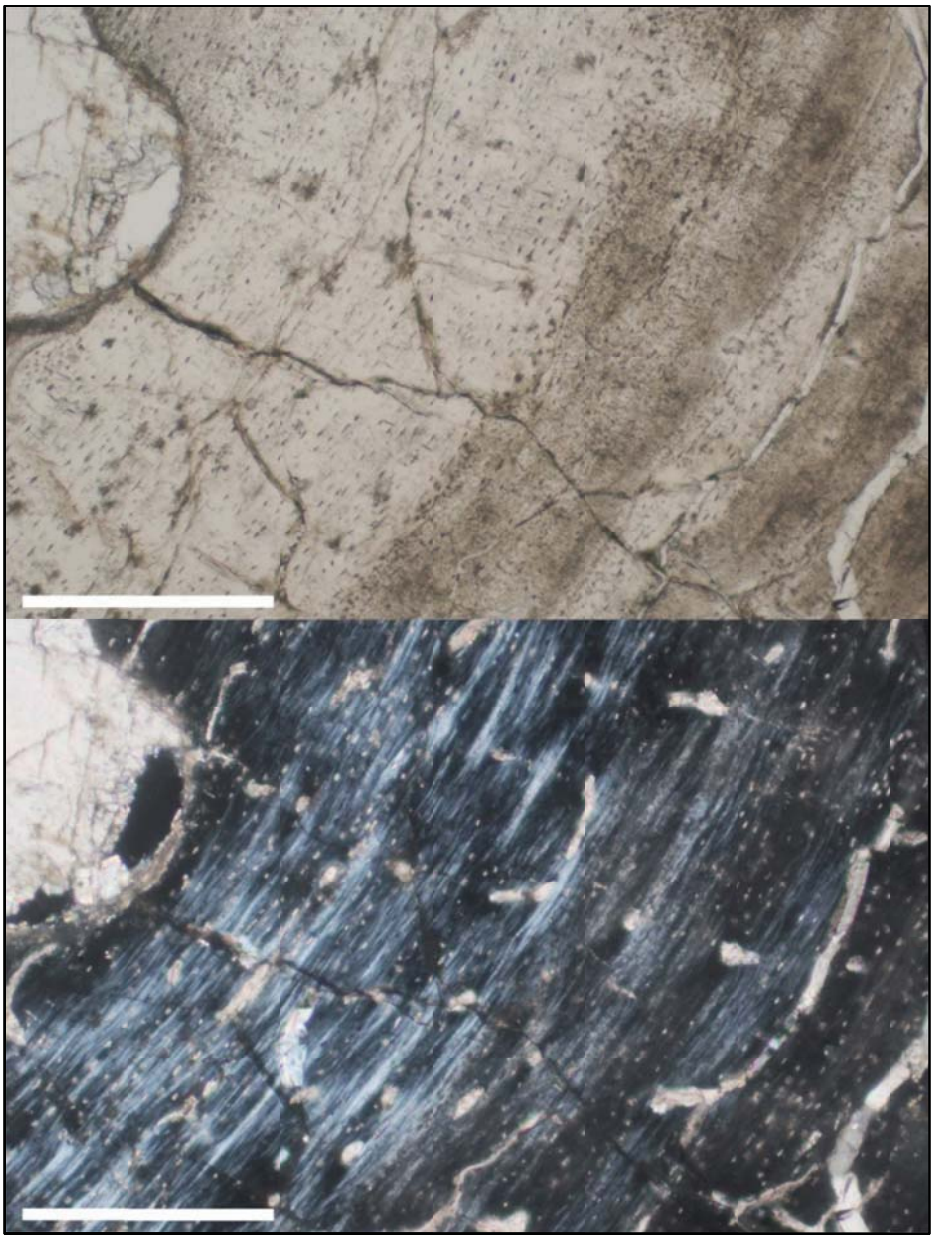

Figure 2.56. Innermost cortex of the mid-diaphyseal humerus of the basal thyreophoran dinosaur *Scutellosaurus lawleri* (UCMP 130580) shown in regular transmitted light (top) and crossed plane polarized light (bottom). This region of the humerus is moderately to poorly vascularized by simple primary canals (triangles) and is mostly composed of parallel-fibered bone tissue. Periosteum to top of image. Scale = 100 μm.

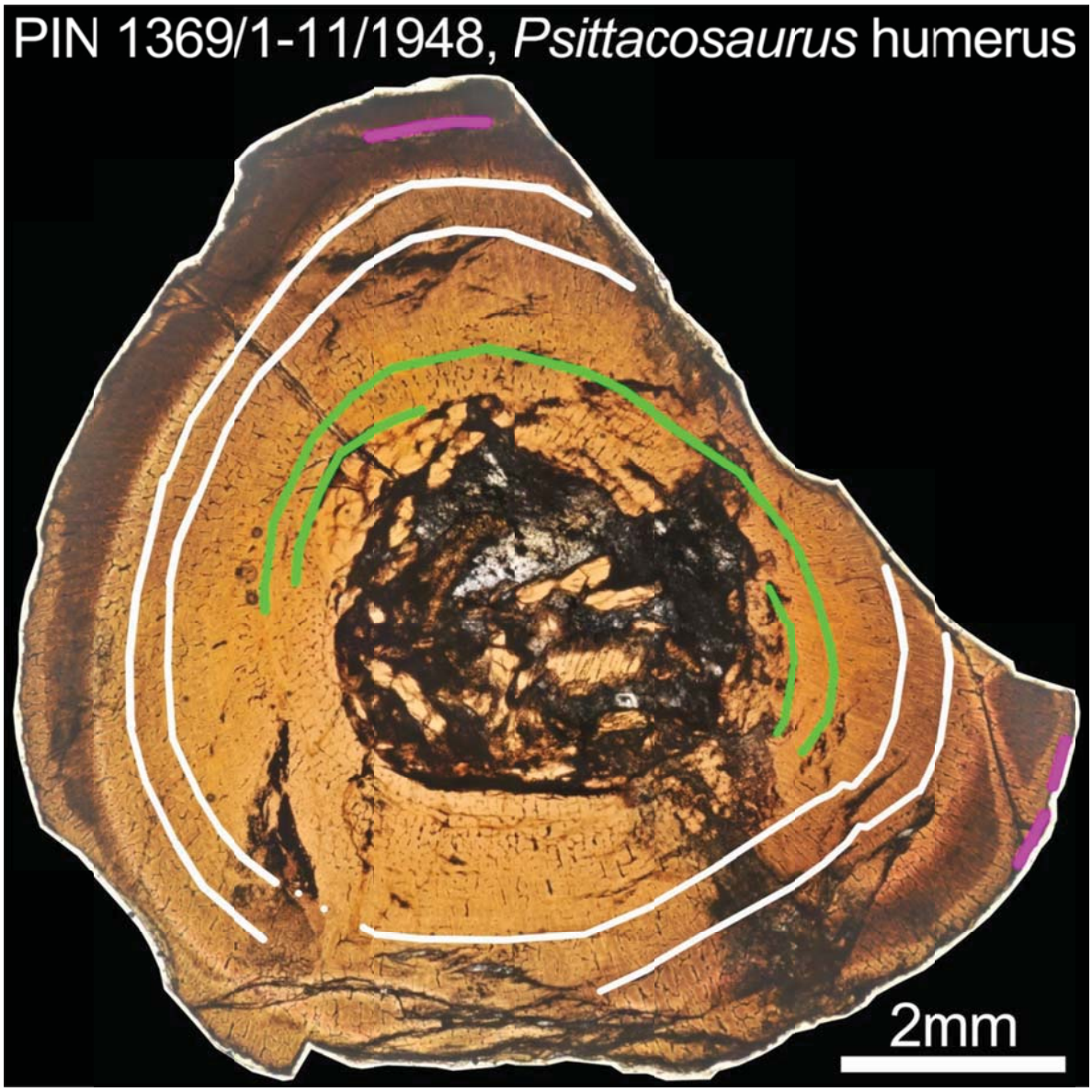

Figure 2.57 Cortical histology of the mid-diaphyseal humerus of *Psittacosaurus mongoliensis* (PIN 1369/1-11/1948) shown in regular transmitted light. This specimen shows three LAGs (colored lines); the inner LAG (green) and middle LAG (white) are double LAGs. Most canals in this section are longitudinal primary osteons that anastomose radially or form small reticulations. Scale = 2 mm.

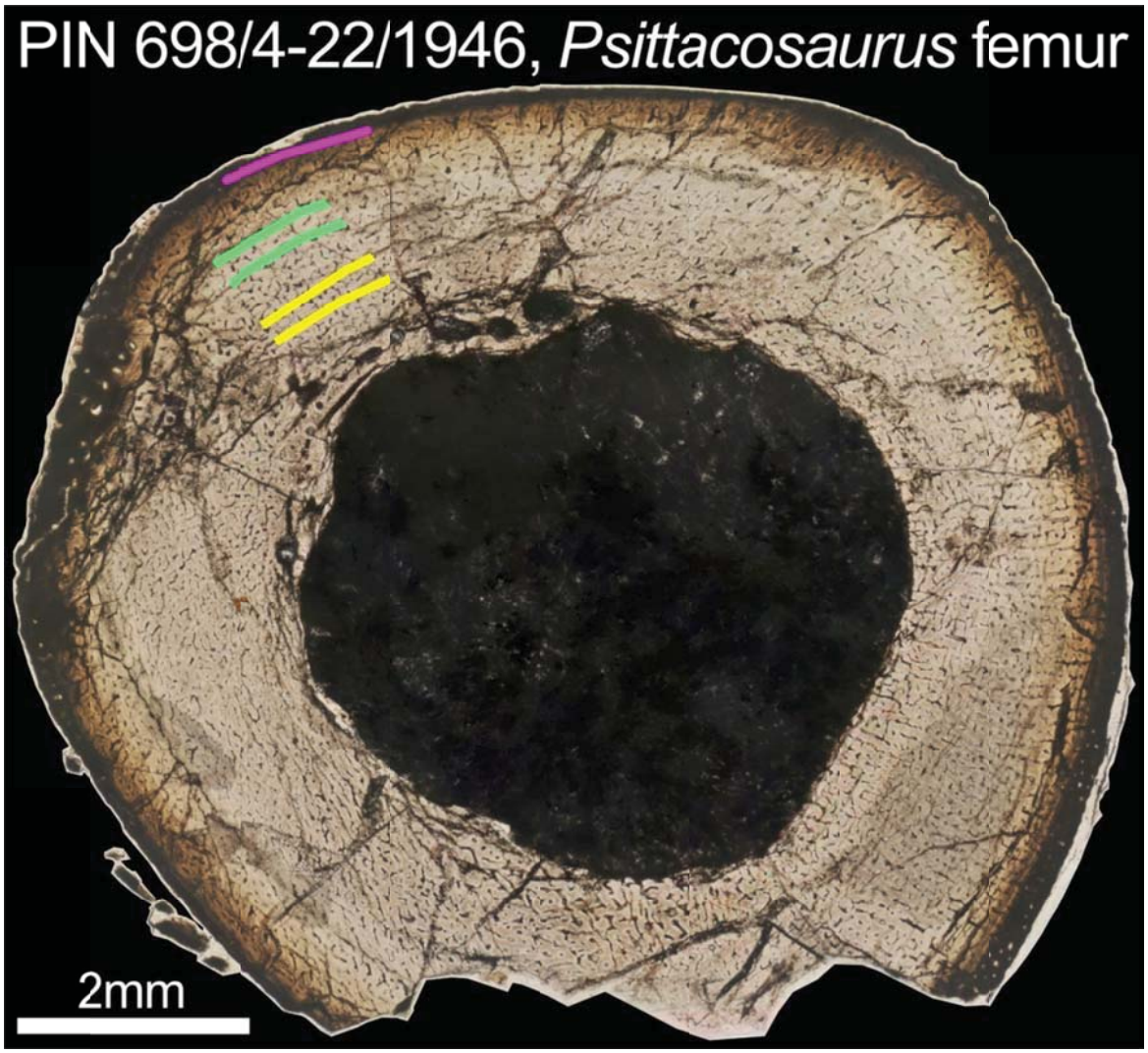

Figure 2.58 Cortical histology of the mid-diaphyseal femur of *Psittacosaurus mongoliensis* (PIN 698/4-22/1948) shown in regular transmitted light. This specimen shows three growth marks (colored lines); the inner annulus (yellow) and middle annulus (green) are double annuli. Most canals in this section are longitudinal primary osteons that may anastomose radially or obliquely. Scale = 2 mm.

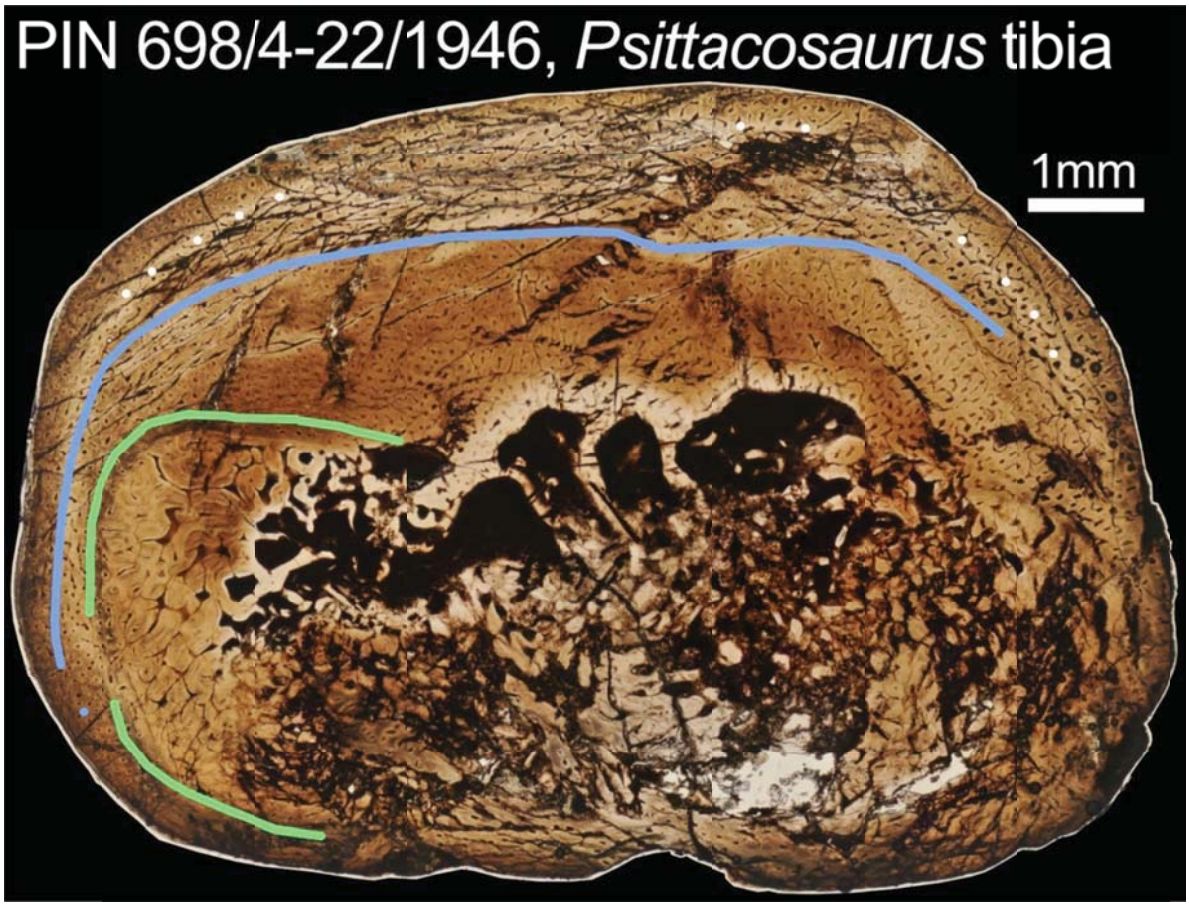

Figure 2.59 Cortical histology of the mid-diaphyseal tibia of *Psittacosaurus mongoliensis* (PIN 698/4-22/1948; same individual as in Figure 2.58) shown in regular transmitted light. This specimen shows three growth marks (colored lines and dotted line): an inner LAG (green line) and middle LAG (blue line), and an outer annulus (white dotted line). None are double annuli/LAGs. Most canals in this section are longitudinal primary osteons. These infrequently anastomose around most of the section. Spacing between growth marks varies dramatically around the circumference of this element because the mid-diaphysis changed shape during ontogeny. Scale = 1 mm.

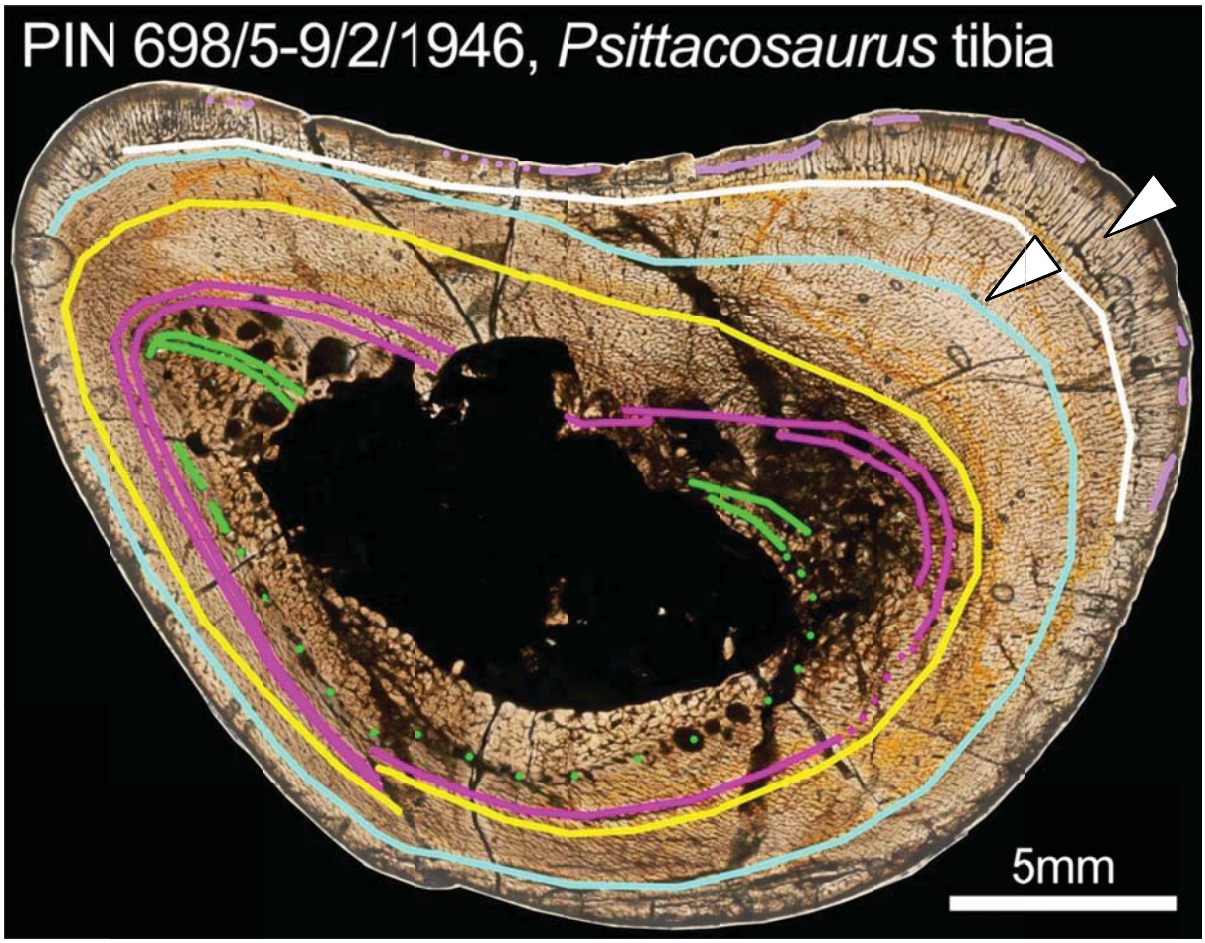

Figure 2.60 Cortical histology of the mid-diaphyseal tibia of *Psittacosaurus mongoliensis* (PIN 698/5-9/2/1946) shown in regular transmitted light. This specimen shows six growth marks (colored lines): the innermost LAG (green line/dotted line) and second LAG (pink line) form double LAGs around most of the circumference, but merge anteriorly. The innermost LAG becomes an annulus anteriorly as well. Spacing between growth marks varies dramatically around the circumference of this element because the mid-diaphysis changed shape during ontogeny. Just external to the fourth (turquoise) and especially the fifth (white line) LAGs, radial canals (tips of white triangles) signal periods of rapid bone deposition, but the bone does not expand equally around the circumference. Scale = 5 mm.

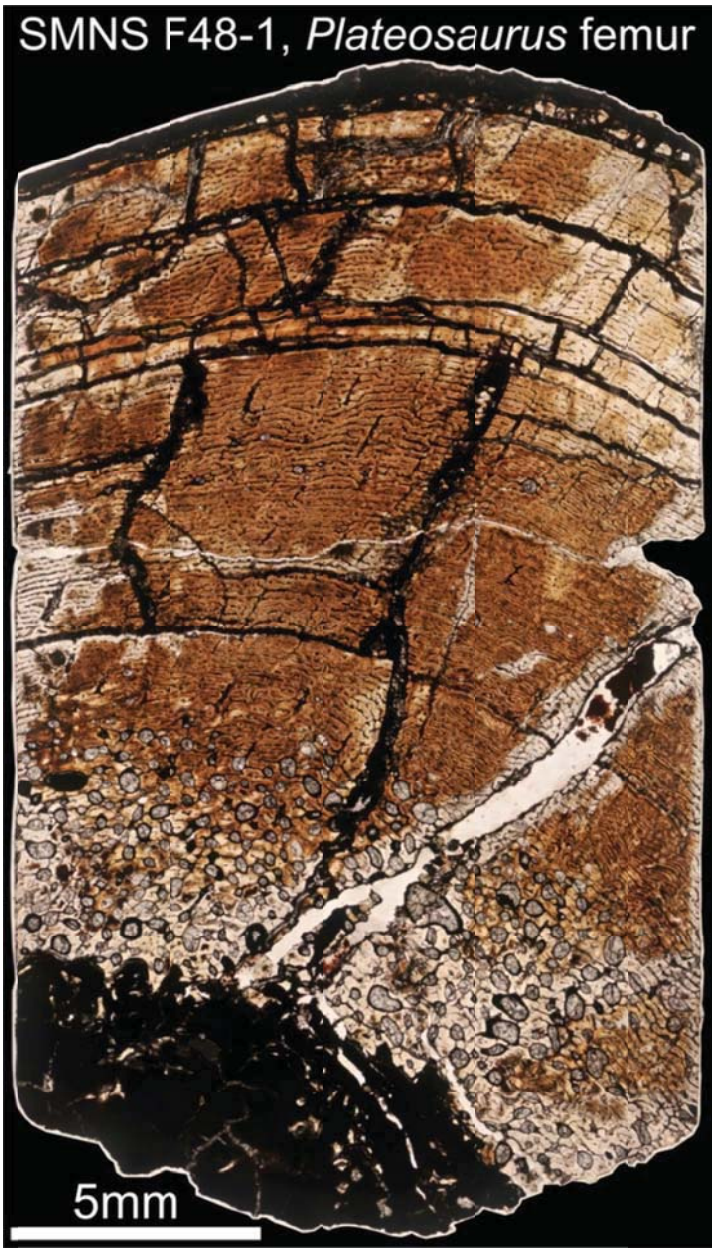

Figure 2.61 Cortical histology of the mid-diaphyseal femur of *Plateosaurus englhardti* (SMNS F48-1) shown in regular transmitted light. This section is a radial transect running from the periosteal surface (top of image) to the medullary cavity (bottom left; dark region) and shows several LAGs (thick black lines). Fracturing is common in Trossingen *Plateosaurus*; cracks often occur along LAGs or cut at angles through the cortex. This specimen preserves most of the inner cortex, which is often lost during the coring process. Most of the vascular canals in this specimen (thin black lines) are circumferential, locally forming laminar or plexiform patterns. At the bottom of the image, numerous circular resorption rooms eat into the primary cortical tissues. Scale = 5 mm.

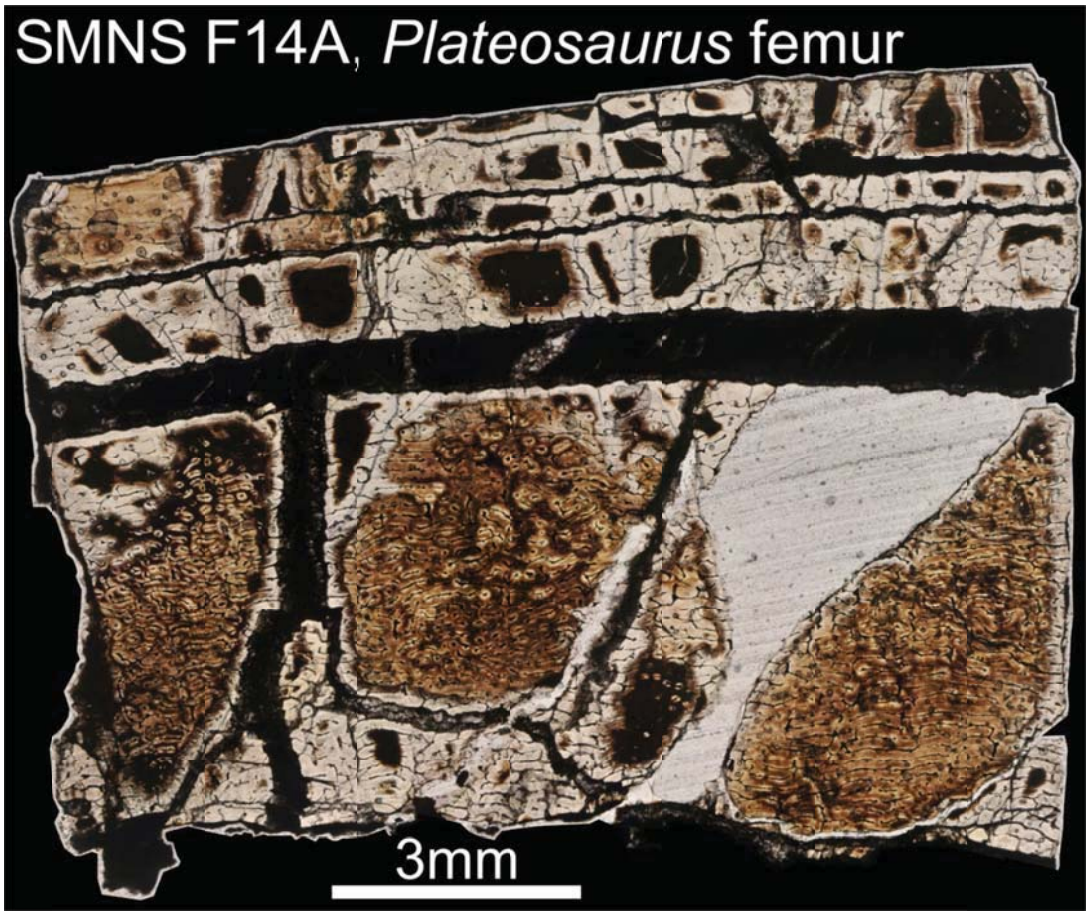

Figure 2.62 Cortical histology of the mid-diaphyseal femur of *Plateosaurus englhardti* (SMNS F14A) shown in regular transmitted light. This section is a partial radial transect running from the periosteal surface (top of image) to the inner/mid cortex (bottom) and shows several LAGs (thick black lines). Most of the vascular canals in this specimen (thin black lines) are circumferential, locally forming laminar or plexiform patterns. Scale = 3 mm.

Figure 2.63 Cortical histology of the mid-diaphyseal tibia of *Plateosaurus englhardti* (SMNS F14A) shown in regular transmitted light. This section is a partial radial transect running from the periosteal surface (top of image) to the inner cortex (bottom), close to the medullary cavity. Several annuli are visible in this section (green lines), but only the two outermost annuli are LAGs (confirmed by breaks in tissue). Most of the vascular canals in this specimen (thin black lines) are circumferential, and generally form a laminar pattern. Scale = 5 mm.

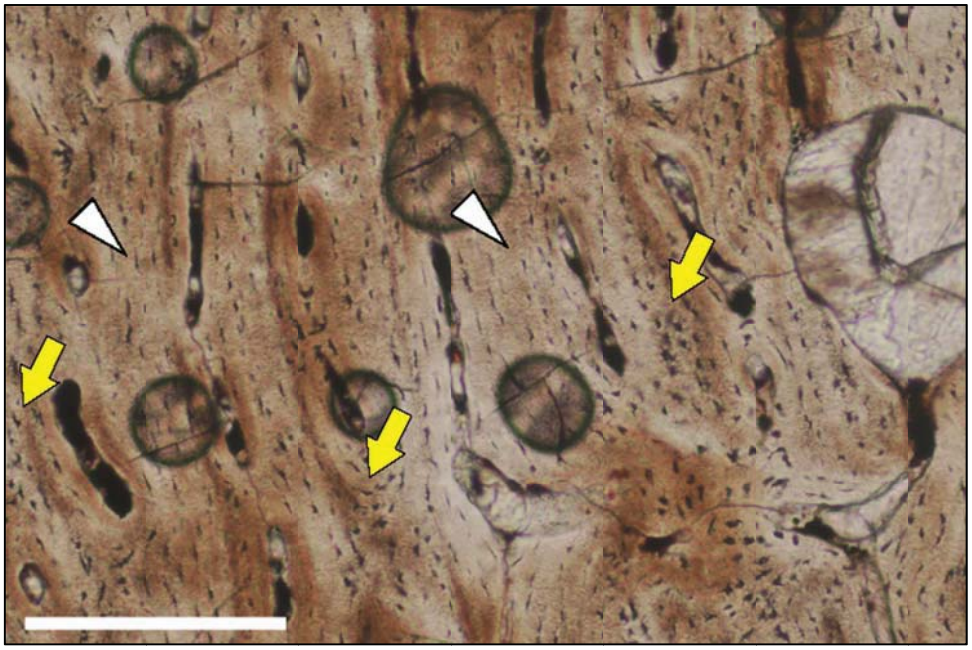

Figure 2.64 Cortical histology of the mid-diaphyseal tibia of *Plateosaurus englhardti* (SMNS F14A) shown in regular transmitted light. In *Plateosaurus*, the primary cortical tissues are often a mix of both woven-fibered and parallel-fibered bone. This image is from the midcortex and shows regions of woven bone (yellow arrows) and parallel-fibered bone (white triangles). No annulus is visible in this image. Osteocyte lacunae show no preferred orientation relative to the long axis of the bone or to each other in regions of woven-fibered bone. In regions of parallel-fibered bone, osteocytes are oriented more or less perpendicular to the long axis of the bone, and are organized circumferentially. They also occur in slightly lower densities compared to regions of woven-fibered bone. Periosteum toward the left of this image. Scale = 250 μm.

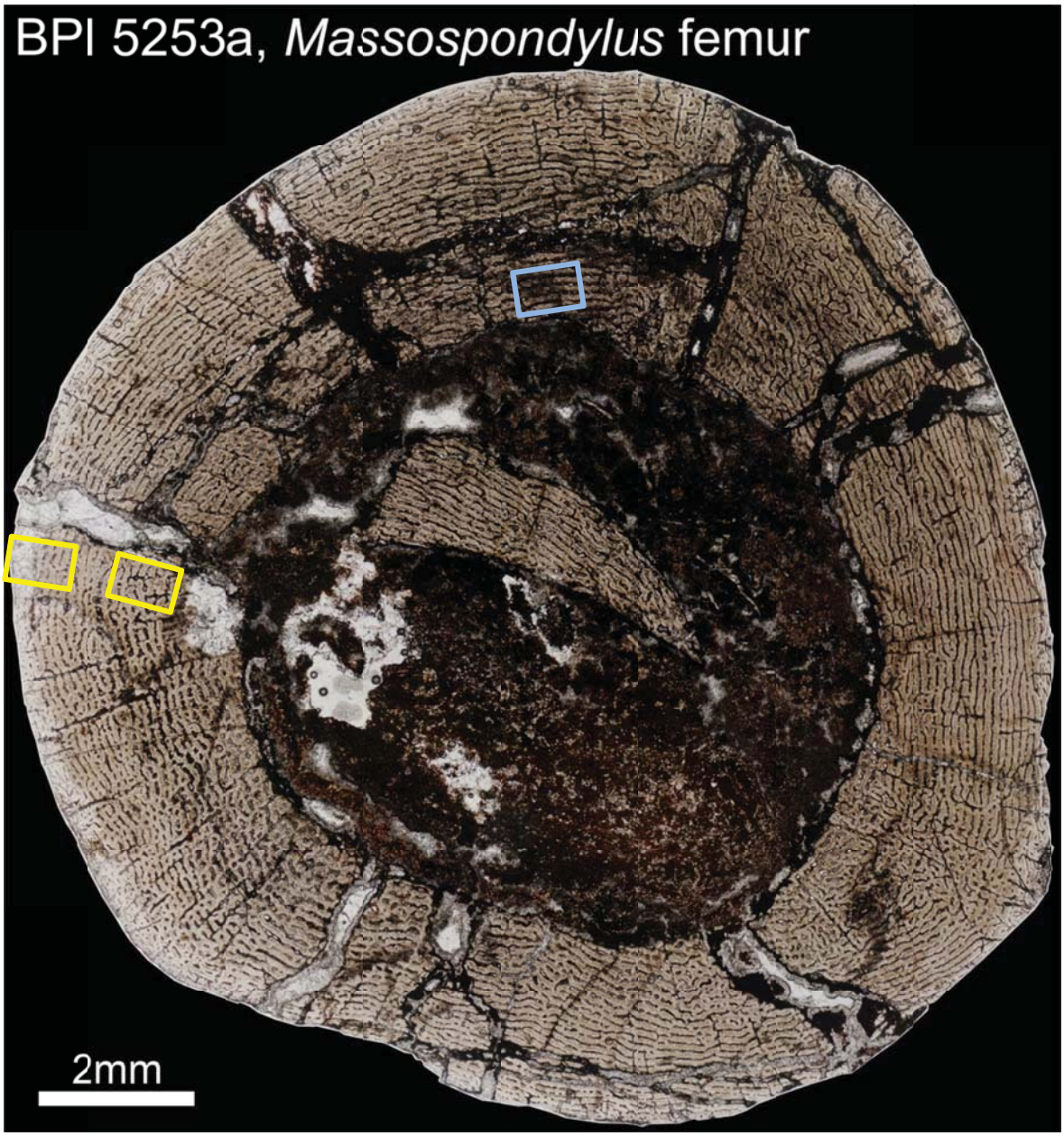

Figure 2.65 Cortical histology of the mid-diaphyseal femur of *Massospondylus carinatus* (BPI/1/5253a) shown in regular transmitted light. This specimen, a juvenile individual, shows no LAGs and no remodeling of the innermost cortex. Most of the vascular canals in this specimen (thin black lines) are actually longitudinal simple primary canals, which extensively anastomose in a circumferential direction to form a laminar to plexiform pattern. Radial canals are also visible around the circumference of this femur, some of which extend nearly the entire breadth of the cortex. Boxes show relative positions of the representative images shown in Figures 2.68 (blue) and 2.69 (yellow). Scale = 2 mm.

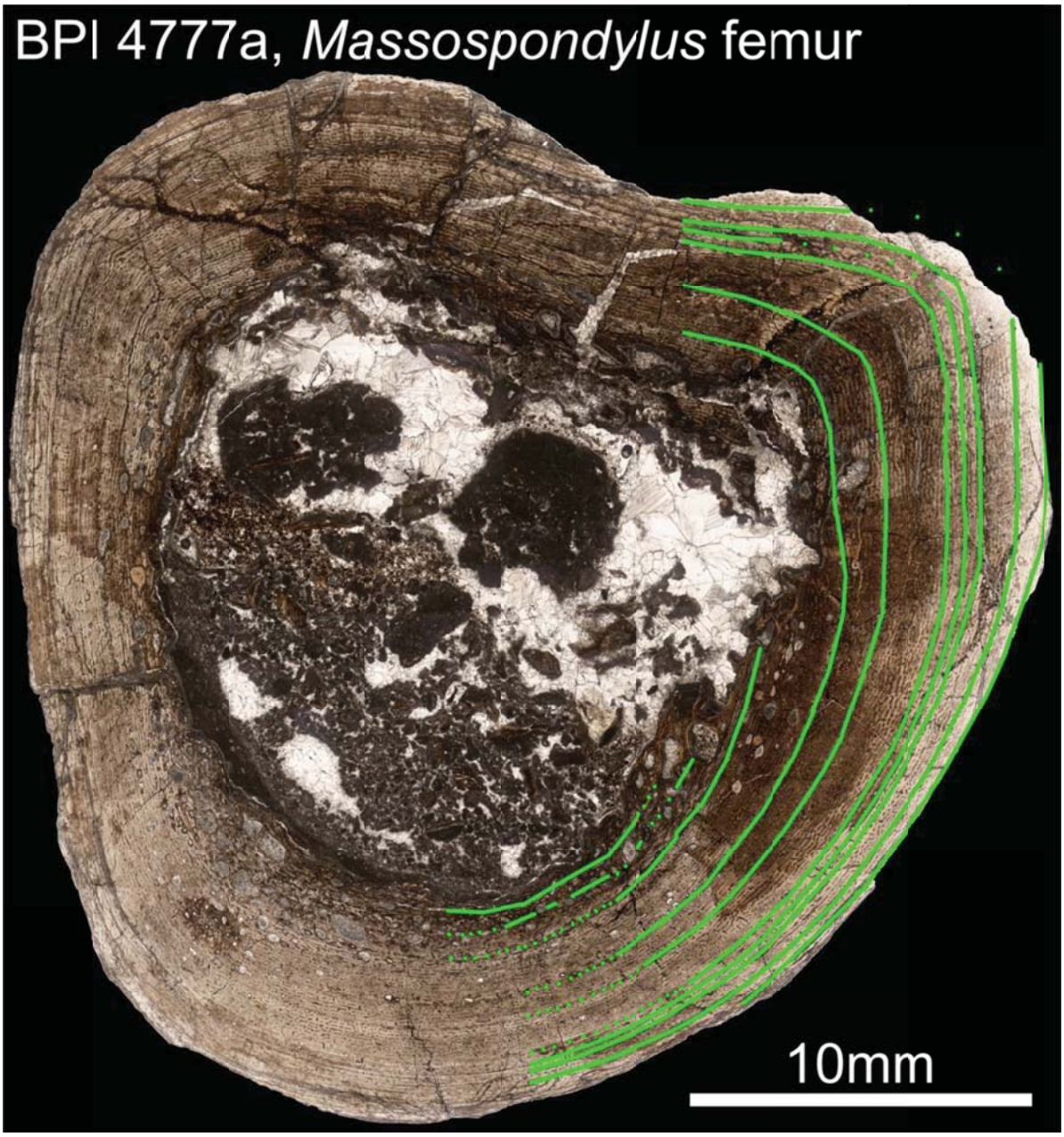

Figure 2.66 Cortical histology of the mid-diaphyseal femur of *Massospondylus carinatus* (BPI/1/4777a) shown in regular transmitted light. This specimen shows 10 LAGs (solid green lines). Locally, some of these become annuli (dotted lines at bottom of image). Resorption rooms are visible around the circumference of this specimen, close to the endosteal margin. Scale = 10 mm.

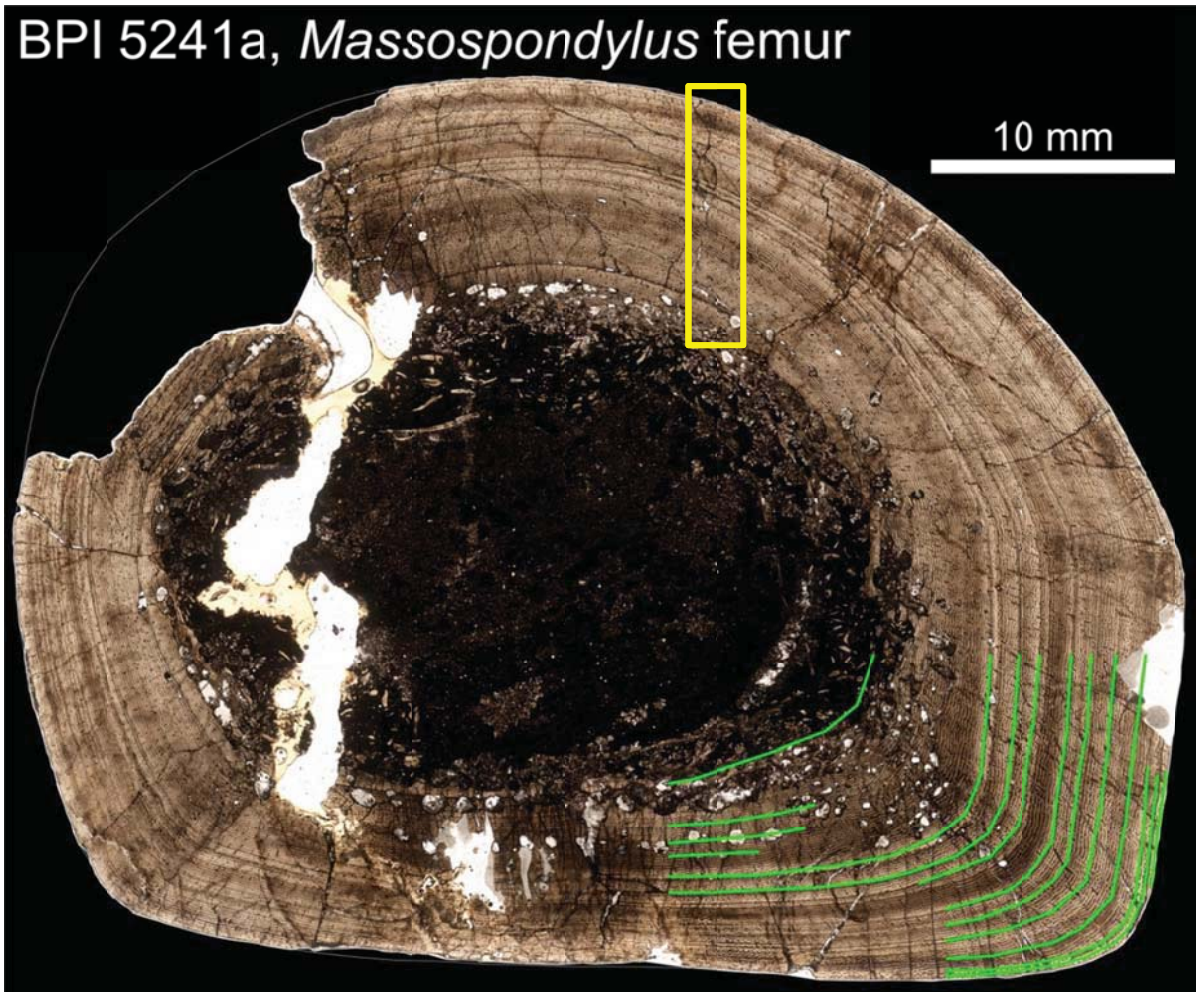

Figure 2.67 Cortical histology of the mid-diaphyseal femur of *Massospondylus carinatus* (BPI/1/5241a) shown in regular transmitted light. This specimen preserves 13-14 LAGs (green lines). Resorption rooms are visible around the circumference of this specimen, close to the endosteal margin. This type of remodeling is more extensive than in BPI/1/4777a. Yellow box corresponds to the position of the radial transect visible in Figure 2.70. Scale = 10 mm.

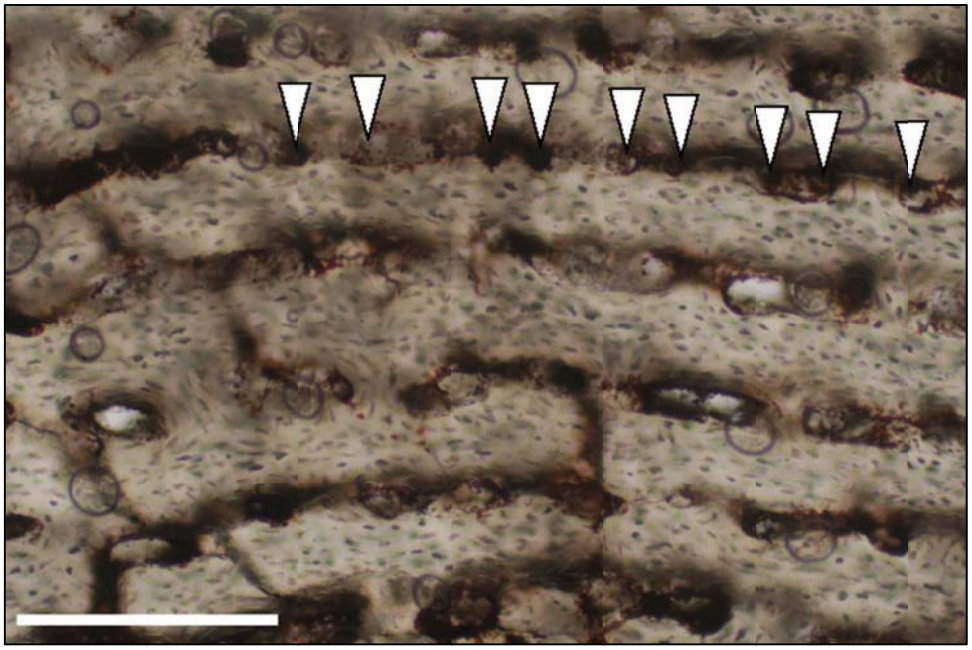

Figure 2.68 Cortical histology of the mid-diaphyseal femur of *Massospondylus carinatus* (BPI/1/5253a) shown in regular transmitted light. This image shows the process of canal pattern formation in the inner cortex (see blue box in Figure 2.65 for position). Longitudinal canals (triangles) form first and later anastomose, usually circumferentially. Periosteum toward the top in this image. Scale = 250 μm.

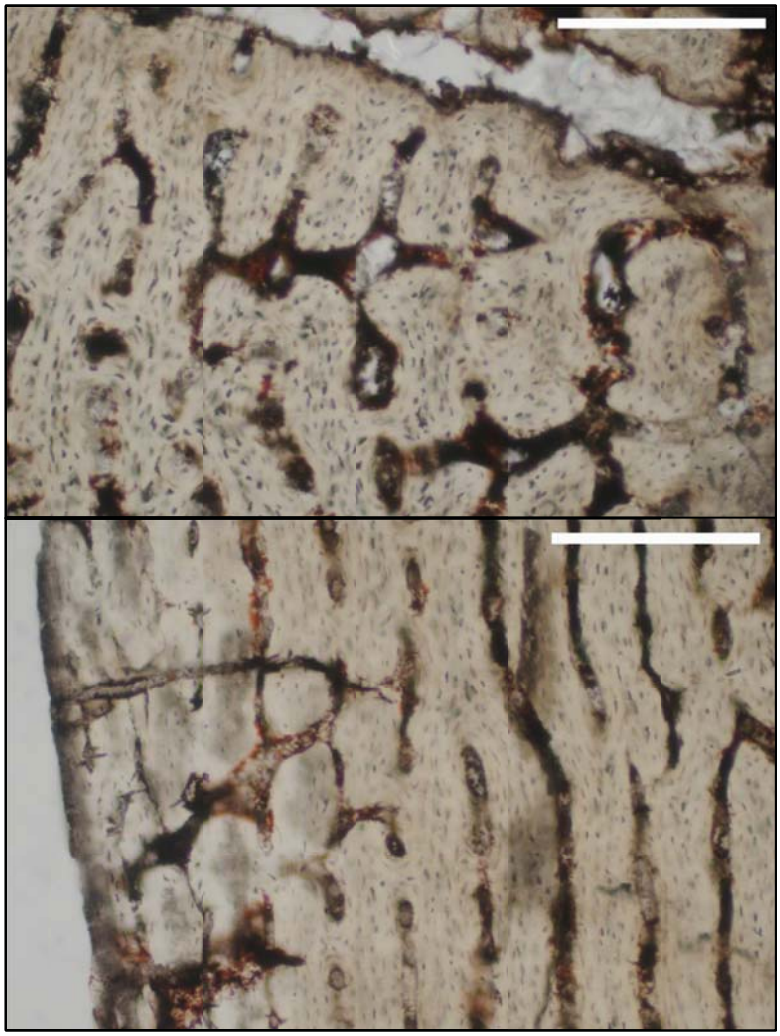

Figure 2.69 Cortical histology of the mid-diaphyseal femur of *Massospondylus carinatus* (BPI/1/5253a) shown in regular transmitted light. Representative images show the canal structure of the inner cortex (top) and outer cortex (bottom) from the same region of the bone (see yellow boxes in Figure 2.65 for position). Differences in vascular canals and osteocyte arrangement can be seen in the two images. In the inner cortex (top), canals are larger in diameter compared to those of the outer cortex, despite being older (they were deposited first and have had more time to fill in the initial bone scaffolding). In both images, it is clear that longitudinal canals form first, which later may anastomose radially (top; oriented horizontal in this image) or circumferentially (oriented top to bottom in both images). Osteocyte density is similar in both regions of the bone, but the cells are more organized in the outer cortex (bottom), where they are all aligned more or less circumferentially. Changes in osteocyte orientation occur with the transition from woven-fibered bone in the inner cortex to parallel-fibered bone in the outer cortex. Periosteum toward the left in both images. Scale bars = 250 μm.

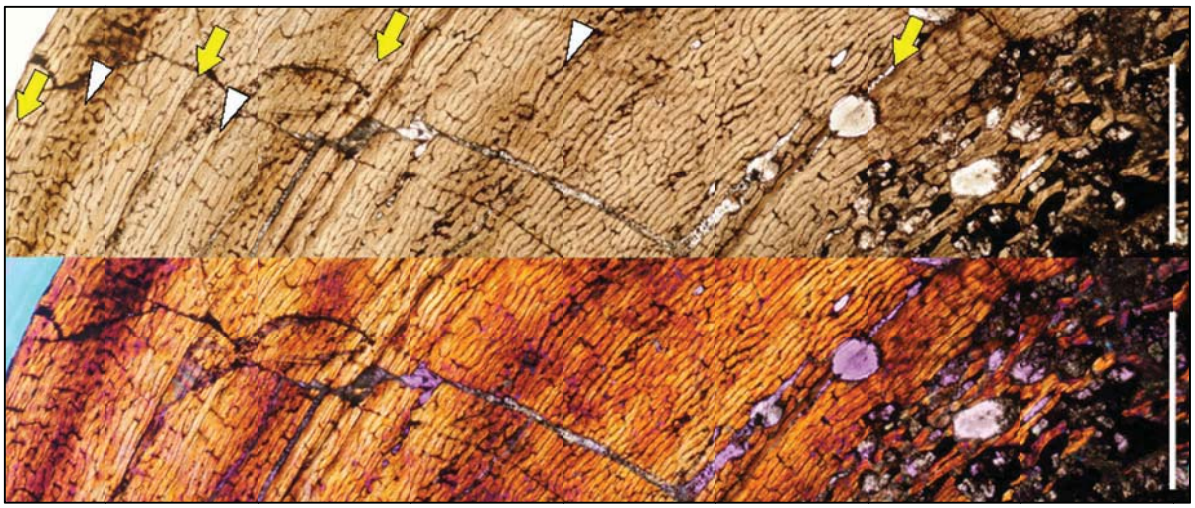

Figure 2.70 Cortical histology of the mid-diaphyseal femur of *Massospondylus carinatus* (BPI/1/5241a) shown in regular transmitted light (top) and elliptically polarized light (bottom). This image shows a radial transect through the cortex, from the periosteal surface (left) to the innermost cortex (right). See Figure 2.67 (yellow box) for position of transect. Most of the cortex is composed of parallel-fibered primary bone tissue, which grades into lamellar tissue periosteally. Endosteally, circular and oval resorption rooms can be seen eating into the tissues of the inner cortex. At least thirteen growth marks are preserved in this section; the positions of seven of these are noted above (several are most clearly distinguished on the opposite side of the section; see Figure 2.67. The yellow arrows represent LAGs that stay as LAGs around the entire circumference. The white triangles indicate LAGs that locally become annuli in this part of the section. Most of the vascular canals in this section are simple primary canals. As in BPI/1/5253a, these are longitudinal canals that anastomose circumferentially with many other canals. At low magnification, the canals of the inner half of the cortex take on a wavy laminar or plexiform appearance. These laminae become straighter periosteally. In the outermost cortex, canal density and connectivity both decrease. Periosteum to the upper left in both images. Scale = 2 mm.

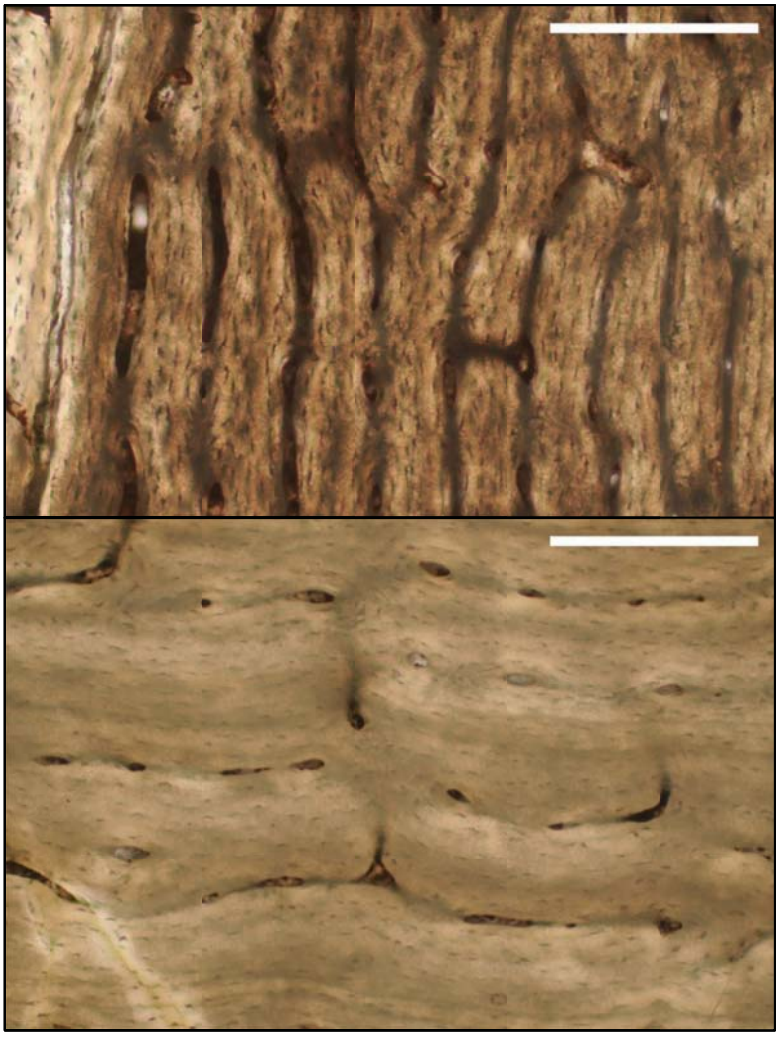

Figure 2.71 Cortical histology of the mid-diaphyseal femur of *Massospondylus carinatus* (BPI/1/5241a) in regular transmitted light. Images show the appearance of the canals and osteocytes in the inner cortex (top) and outer cortex (bottom). As in BPI/1/5253a (Figure 2.69), longitudinal canals anastomose circumferentially with many other canals (top image), forming a plexiform arrangement. In the outer cortex, canal diameter is smaller, and more canals are isolated. Osteocyte density is higher in the inner cortex compared to the outer cortex, but in both regions, all the lacunae are oriented perpendicular to the long axis of the bone and align circumferentially. Compared to the inner cortex, osteocyte lacunae are more evenly spaced in the outer cortex (bottom). Two lamellae (faint horizontal line) are visible in the bottom of the lower image. Periosteum is to the left in the upper image and to the bottom in the lower image. Scale bars = 250 μm.

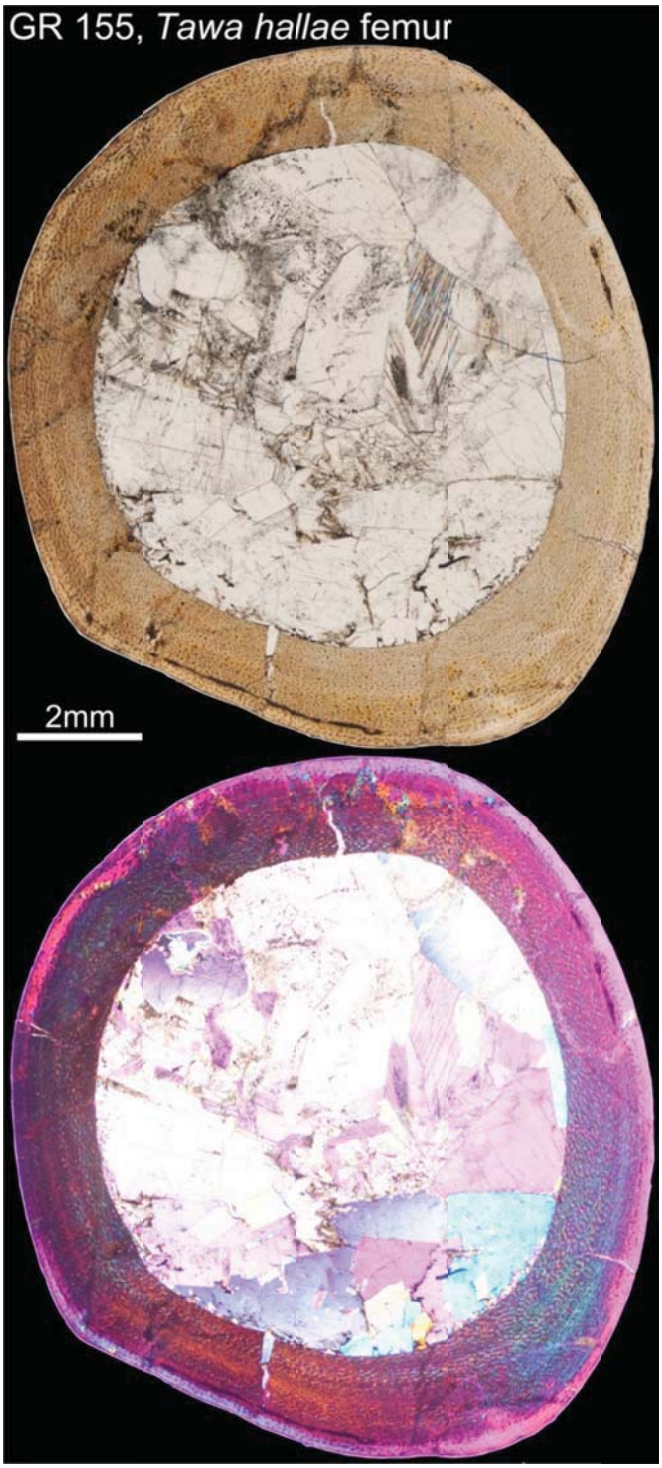

Figure 2.72 Cortical histology of the mid-diaphyseal femur of *Tawa hallae* (GR 155) in regular transmitted light (top) and elliptically polarized light (bottom). This image shows the shape of the cortex and thin nature of the cortical walls at mid-diaphysis. Scale = 2mm.

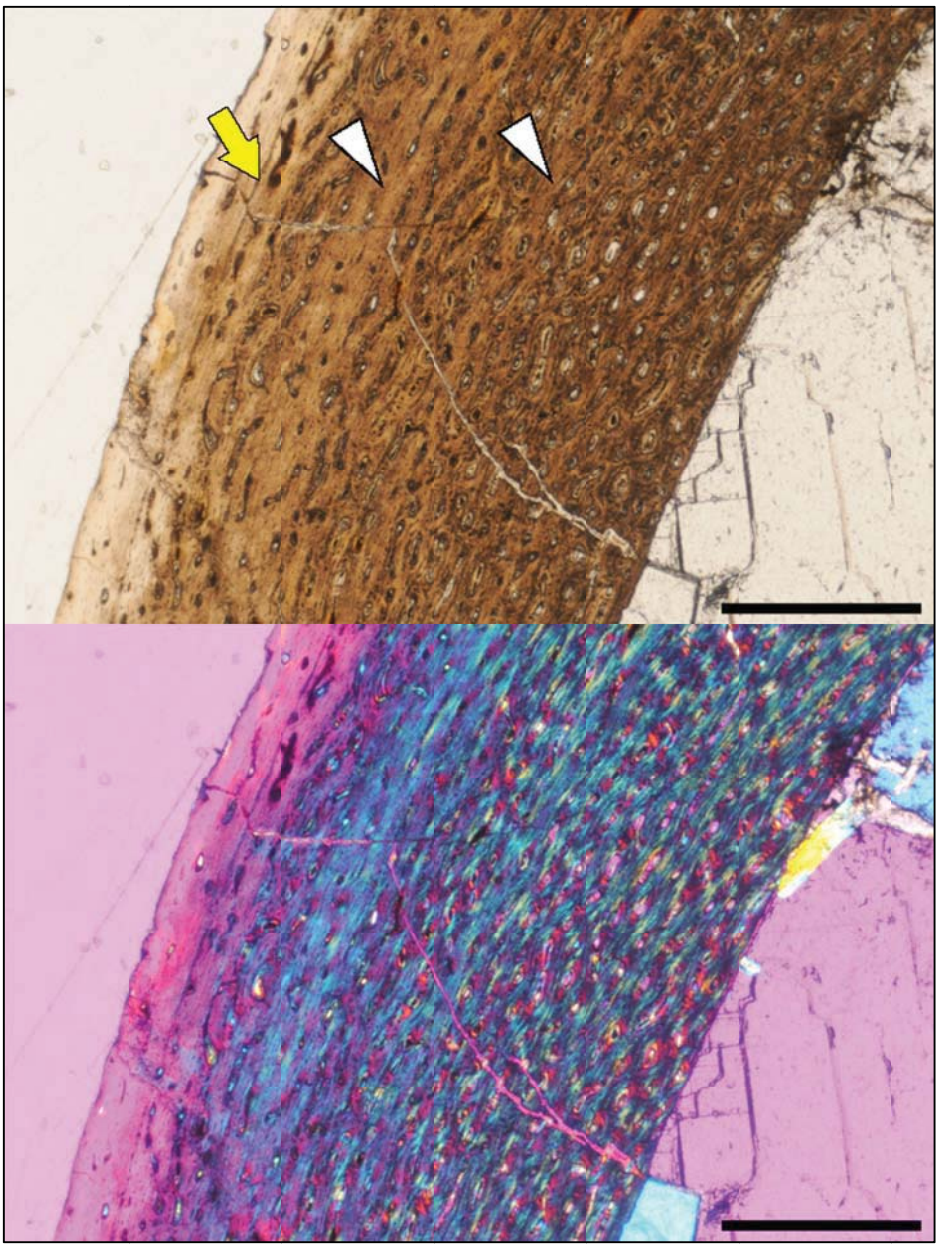

Figure 2.73 Cortical histology of the mid-diaphyseal femur of *Tawa hallae* (GR 155) in regular transmitted light (top) and elliptically polarized light (bottom). Yellow arrow indicates the position of the outer LAG; white triangles indicate the two annuli. This element is composed of woven bone internal to the first annulus, and between the first and second annuli. Between the second annulus and the LAG in the outer cortex, the bone is composed of parallel-fibered bone, and external to the LAG it is lamellar. Most vascular canals in this section are longitudinal primary osteons, which decrease in number periosteally. Periosteum to left of these images. Scale = 500 μm.

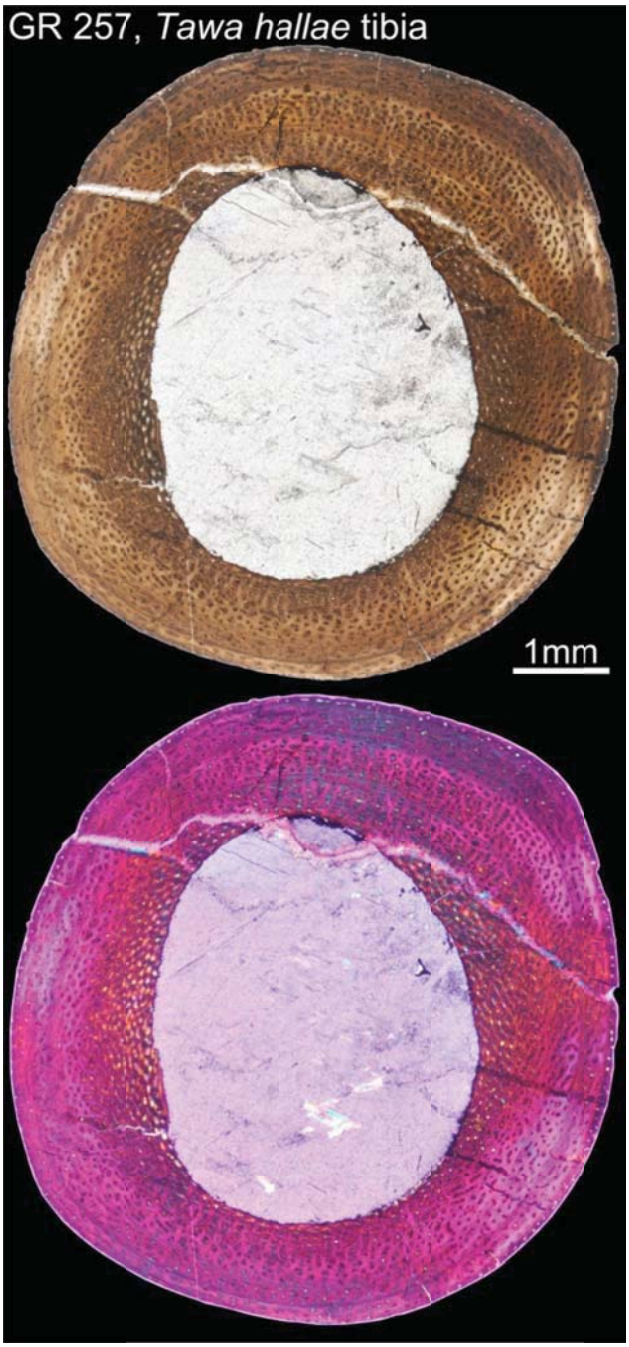

Figure 2.74 Cortical histology of the mid-diaphyseal tibia of *Tawa hallae* (GR 257) in regular transmitted light (top) and elliptically polarized light (bottom). This image shows the shape of the cortex at mid-diaphysis and the relatively thick cortical walls compared to the femur examined (see Figure 2.72 for comparison). Scale = 1 mm.

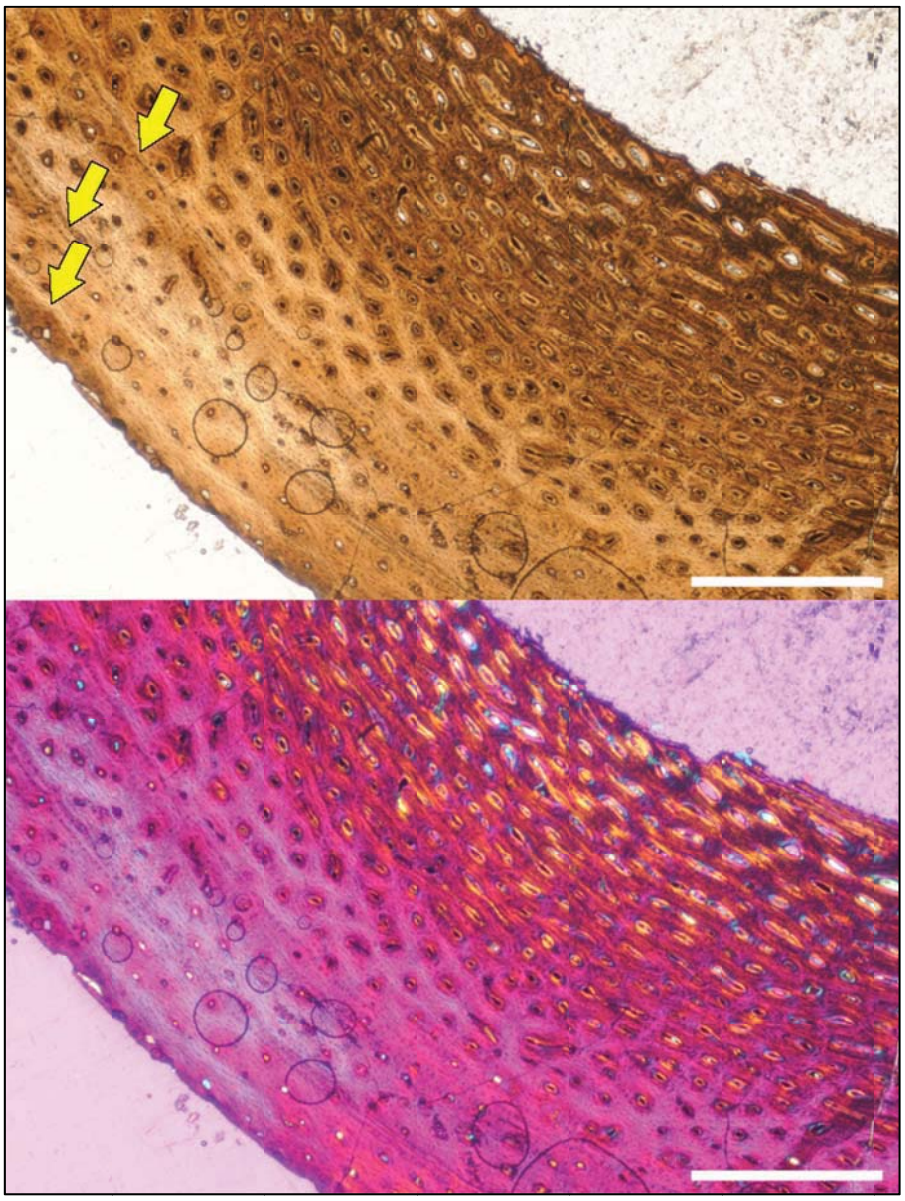

Figure 2.75 Cortical histology of the mid-diaphyseal tibia of *Tawa hallae* (GR 257) in regular transmitted light (top) and elliptically polarized light (bottom). Three LAGs are preserved in this section (arrows). Internal to the first LAG, the zone is composed of woven bone in the innermost cortex, with the rest of the zone composed of parallel-fibered bone. External to the first LAG, the bone is mostly parallel-fibered, until the third LAG, where it becomes lamellar. Most vascular canals are longitudinal primary osteons, but some anastomose with a few other canals. In the upper right of the image, canals have a much larger diameter than the canals that occur elsewhere in the cortex (compare with the woven-fibered regions of Figure 2.76). This region may preserve neonatal tissues. Periosteum to the lower left of these images. Scale bars = 500 μm.

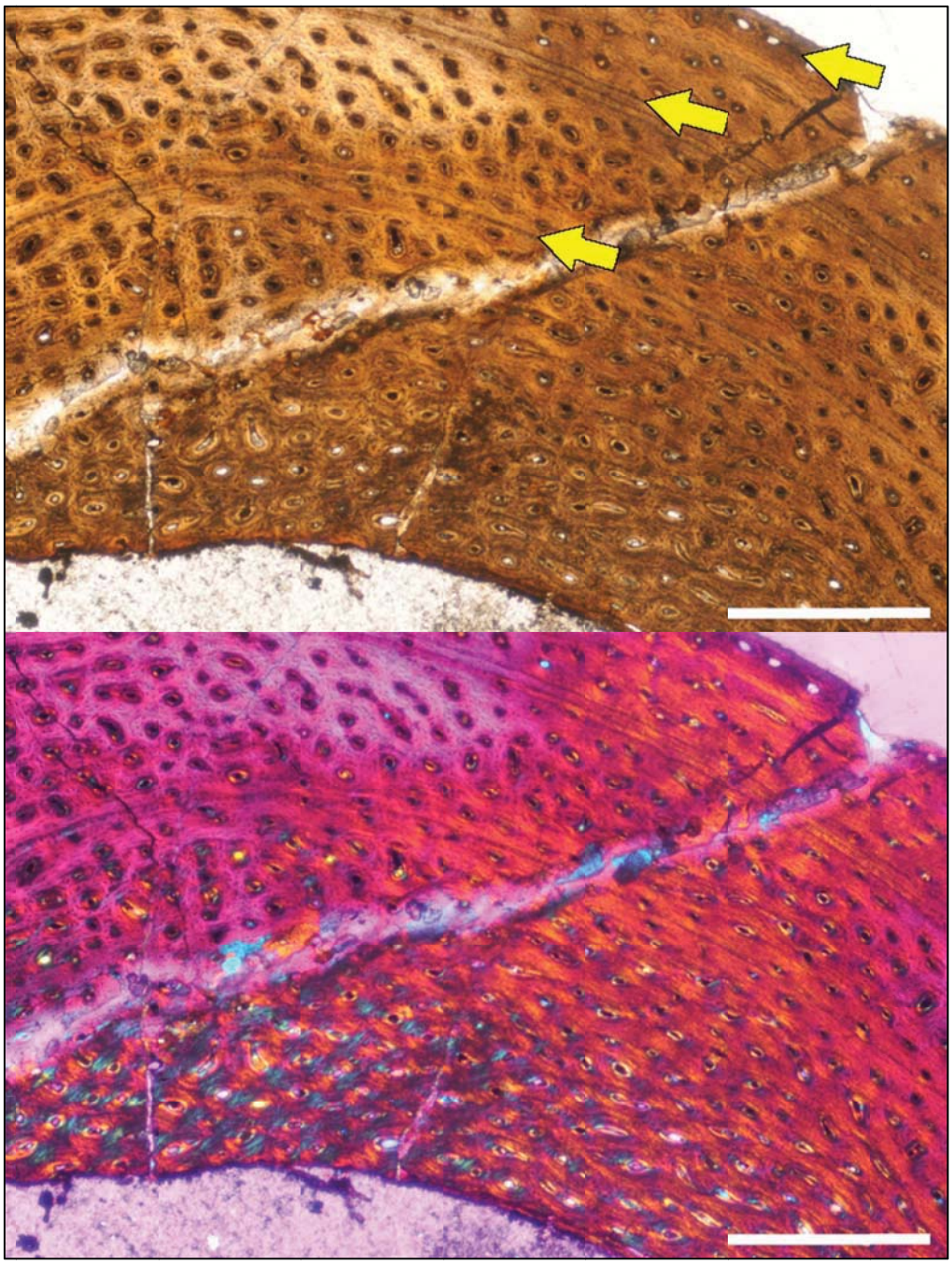

Figure 2.76 Cortical histology of the mid-diaphyseal tibia of *Tawa hallae* (GR 257) in regular transmitted light (top) and elliptically polarized light (bottom). Three LAGs are preserved in this section (arrows). The innermost cortex (multicolored region in lower left of bottom image) shows woven-fibered bone tissue as seen in Figure 2.75, but here the primary osteons are much narrower in diameter. Periosteum to top/upper right in these images. Scale bars = 500 μm.

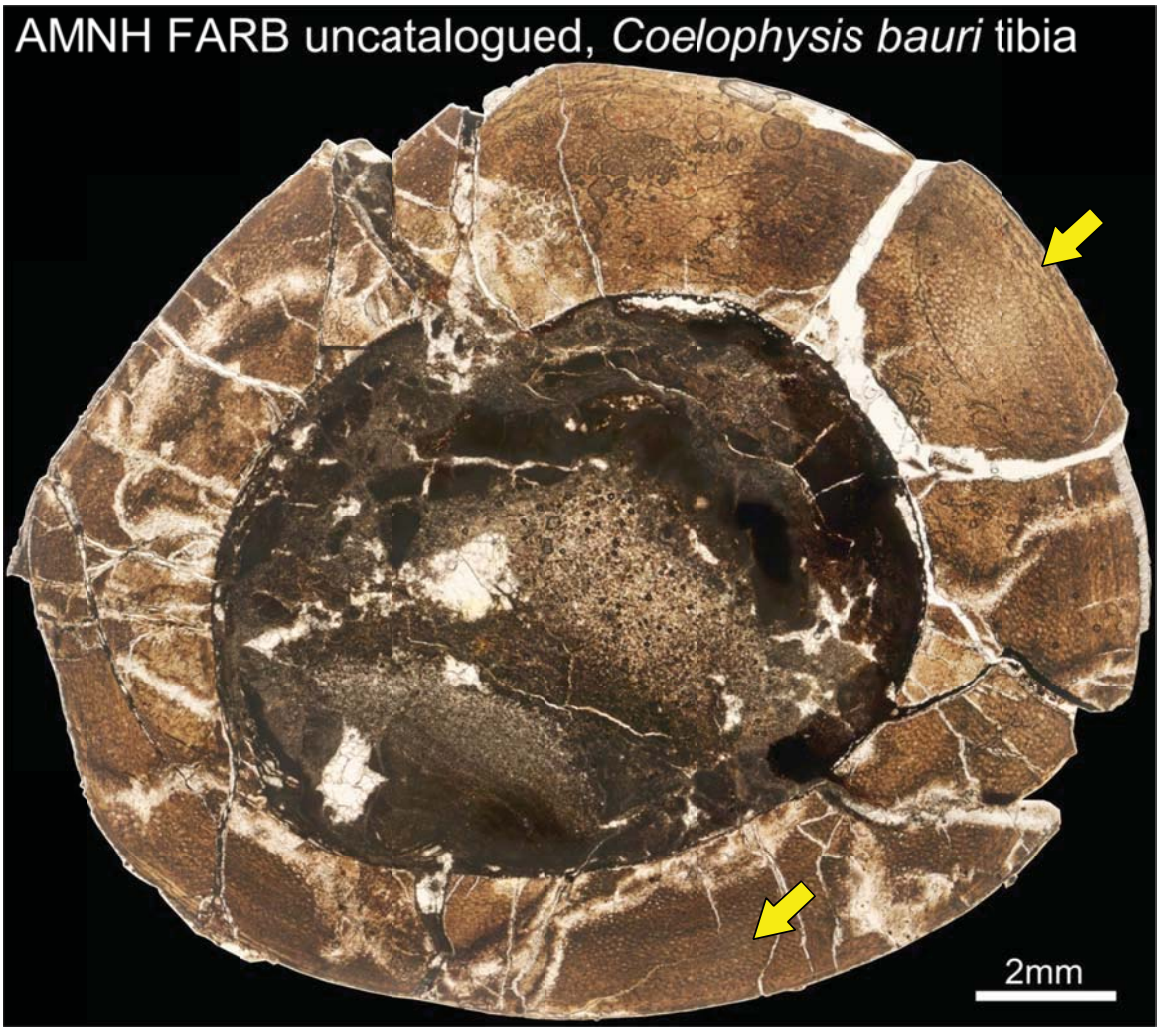

Figure 2.77 Cortical histology of the mid-diaphyseal tibia of *Coelophysis bauri* (AMNH FARB uncatalogued) in regular transmitted light. This image shows the relative positions of the two annuli (yellow arrows), which regionally become LAGs. Scale = 2 mm.

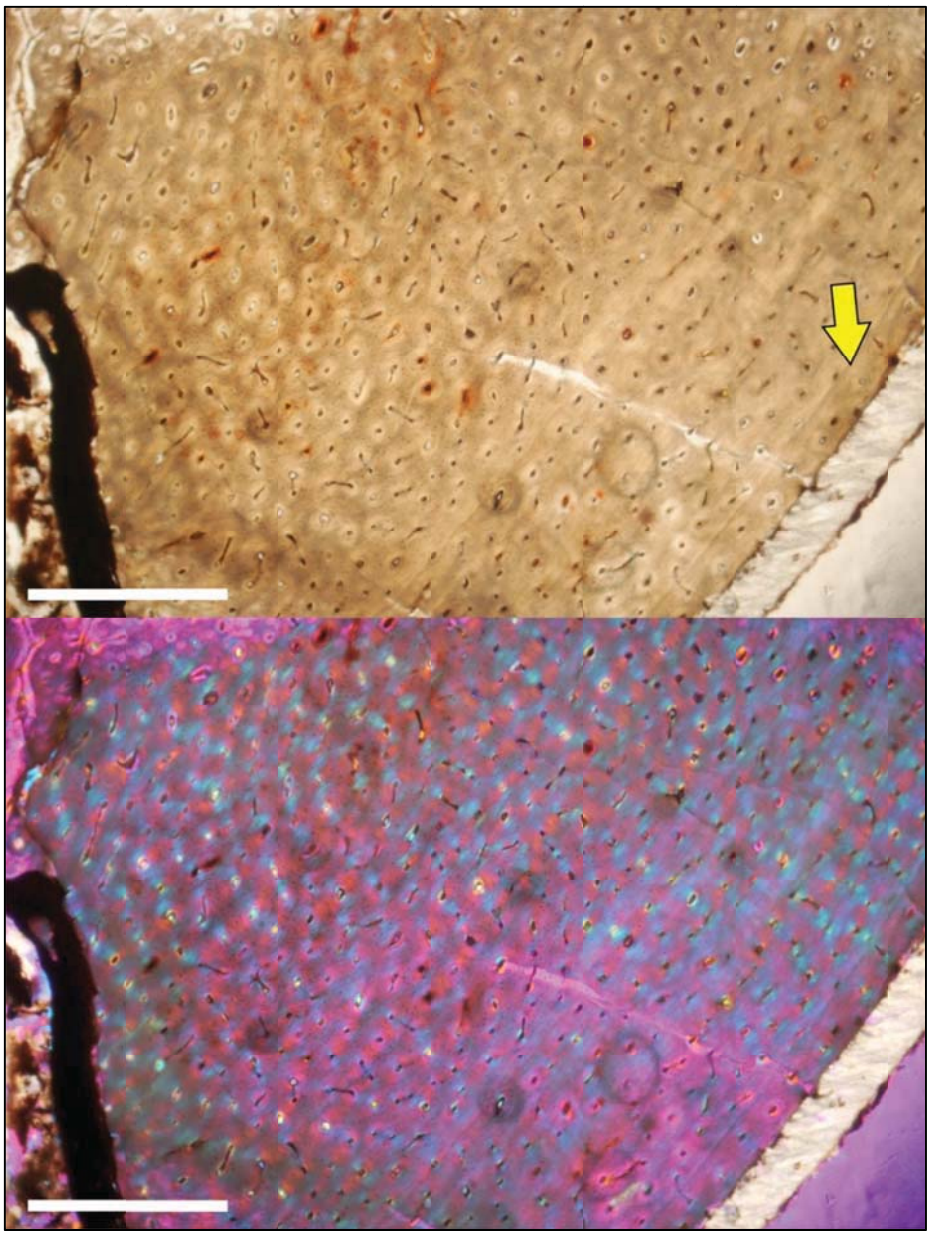

Figure 2.78 Cortical histology of the mid-diaphyseal tibia of *Coelophysis bauri* (AMNH FARB uncatalogued) in regular transmitted light (top) and elliptically polarized light (bottom). This image shows a partial transect extending from the periosteal surface (lower right) into the midcortex (upper left). The arrow indicates the position of the outer annulus (faint line). Most of the cortex is composed of woven-fibered bone (upper left of lower image); the outer 0.5 mm is composed of parallel-fibered bone (lower right). All the canals in this section are longitudinal primary osteons; in the inner cortex these are more likely to anastomose with one other canal in a radial or oblique direction. Periosteum to the lower right of both images. Scale = 500 μm.

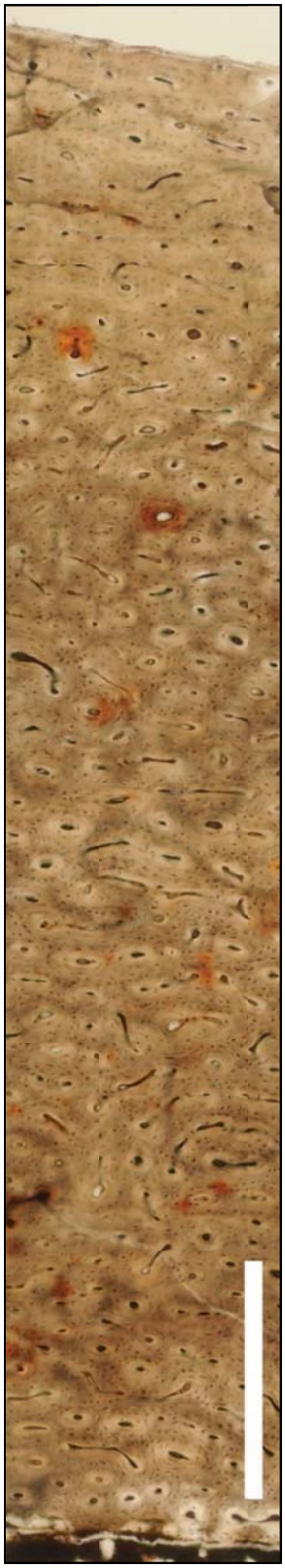

Figure 2.79 Cortical histology of the mid-diaphyseal tibia of *Coelophysis bauri* (AMNH FARB uncatalogued) in regular transmitted light. All of the canals in this section are longitudinal primary osteons; in the inner half of the cortex, they are more likely to anastomose with one other canal in a radial or oblique direction. Periosteum to the top of this image. Scale = 500 μm.

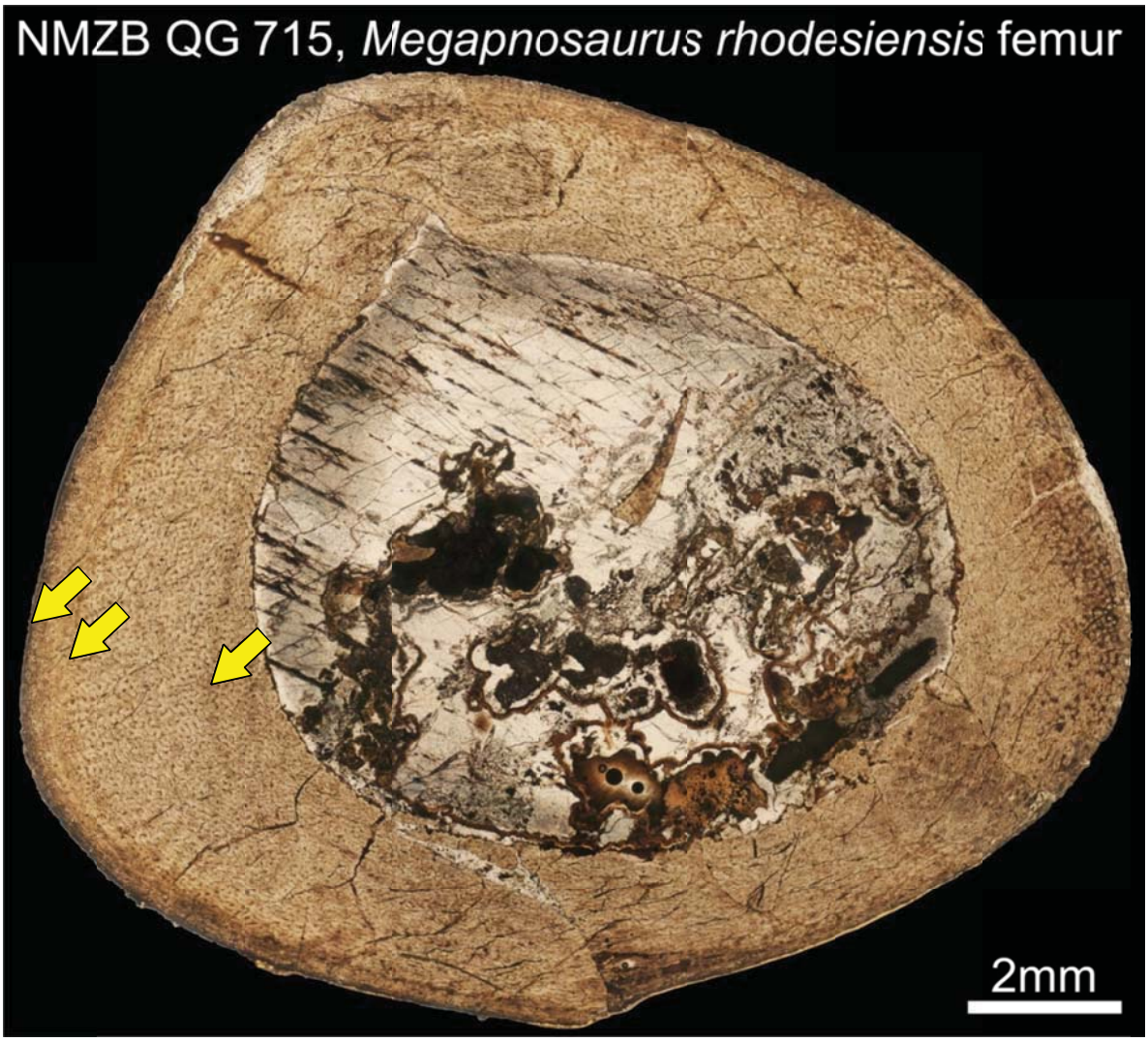

Figure 2.80 Cortical histology of the mid-diaphyseal femur of *Megapnosaurus rhodesiensis* (NMZB QG 715) in regular transmitted light. At low magnification, three bands are visible (arrows) but no break or change in tissue can be observed at higher magnifications (Figure 2.81). However, the bands refringe differently under polarized light (only at lower magnification) and the outer two can be traced around the entire circumference (the medullary cavity cuts across the inner band). These bands cannot be considered true annuli because there is no change in tissue deposition, although there may be a change in mineralization. Scale = 2 mm.

Figure 2.81 Cortical histology of the mid-diaphyseal femur of *Megapnosaurus rhodesiensis* (NMZB QG 715) in regular transmitted light. Compared to *Coelophysis bauri* (Figure 2.79), *M. rhodesiensis* shows more extensive anastomoses through most of the cortex, and primary osteons (rather than simple primary canals) are the dominant vascular canal type. Through most of the cortex, the bone is woven-fibered, but in the outermost cortex (darker region at top of image), it is parallel-fibered. No LAGs are visible in this section, but three bands are visible at low magnification (Figure 2.80). These are not associated with tissue changes and cannot be viewed at higher magnifications. Periosteum to the top of this image. Scale = 500 μm.

Figure 2.82 Cortical histology of the mid-diaphyseal femur of *Megapnosaurus rhodesiensis* (NMZB QG 726) in regular transmitted light. Two double LAGs are present in this specimen (arrows); the inner set (lower on this image) locally grades into a double annulus. As in the other specimens of *M. rhodesiensis*, both simple primary canals and primary osteons are present throughout the section. In the inner and midcortex, primary osteons are more common, but in the outer cortex, simple primary canals are more common. In this image, this can be seen by comparing canals in the inner cortex (bottom of image) with those nearer to the periosteal surface (top of image). The lighter halos sounding most canals in the inner cortex corresponds to the lamellae of primary osteons; these are absent in most canals of the outer cortex. Additionally, the canals of the outer cortex are smaller in diameter than in the inner and midcortex, and anastomoses are absent in this region. At the bottom of this image, just above the scale bar, a circular black region indicates the position of an incipient secondary osteon or resorption room. Periosteum to the top of this image. Scale = 500 μm.

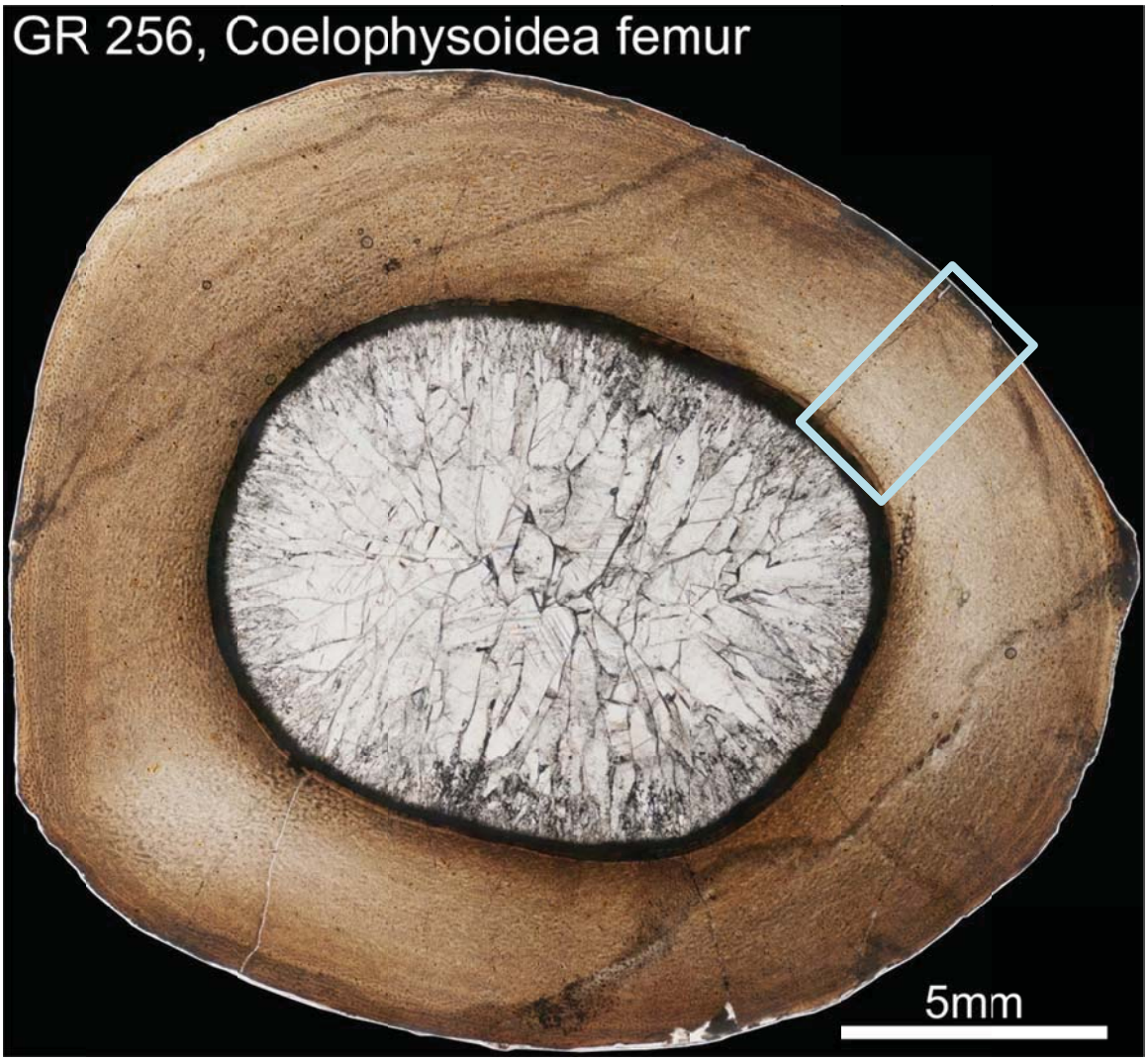

Figure 2.83 Cortical histology of the mid-diaphyseal femur of an undescribed coelophysoid from Hayden Quarry, Ghost Ranch, NM (GR 256), in regular transmitted light. This image shows the suboval shape of the cortex in cross section and the subrectangular shape of the medullary cavity. Blue box indicates the position of Figure 2.84. Figure 2.85 is from a different thin section taken from this element, but would lie approximately at the top of this image. Scale = 5mm.

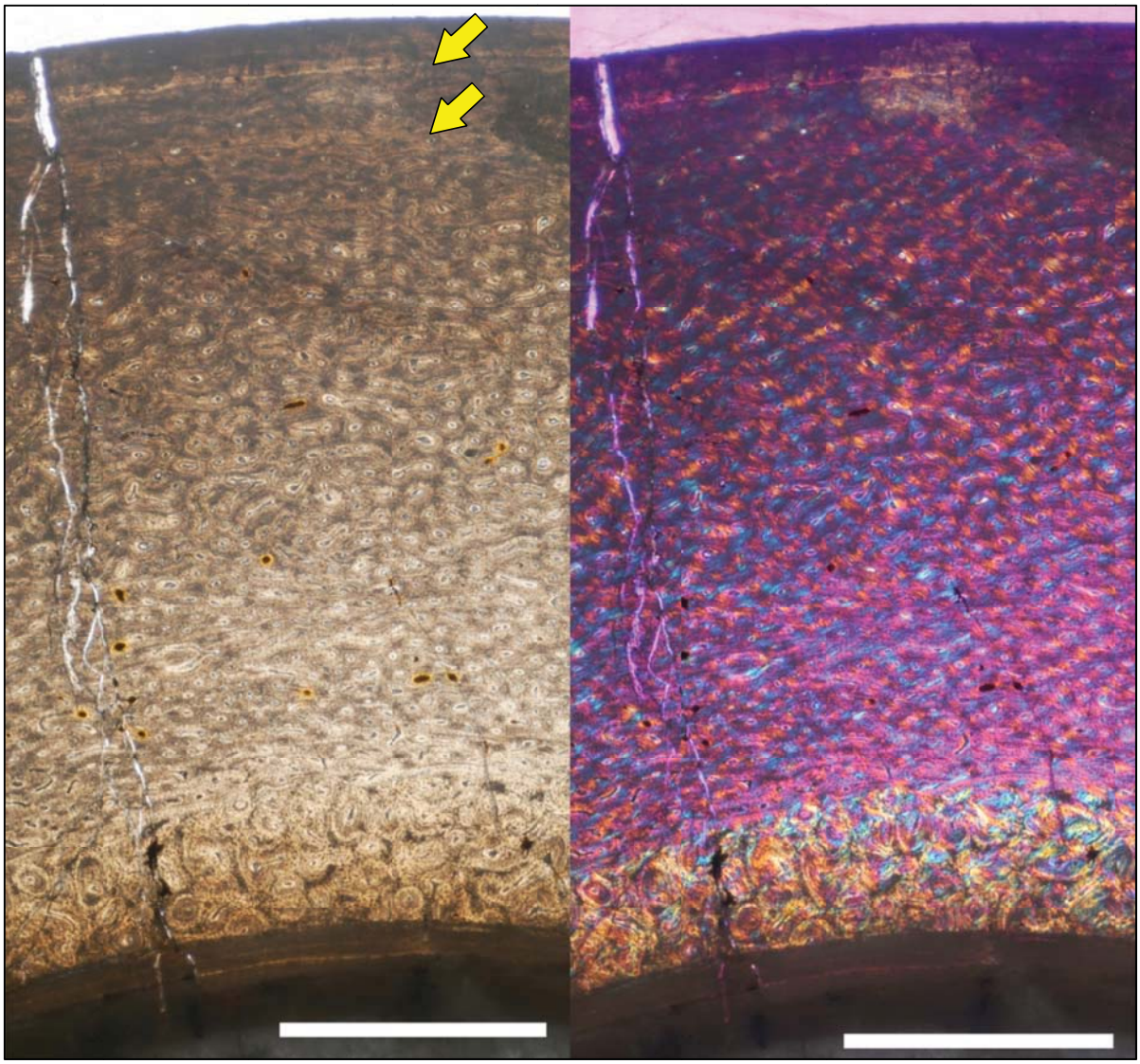

Figure 2.84 Cortical histology of the mid-diaphyseal femur of an undescribed coelophysoid from Hayden Quarry, Ghost Ranch, NM (GR 256), in regular transmitted light (left) and elliptically polarized light (right). The position of this radial transect through the cortex is indicated in Figure 2.83 (blue box). This section shows two growth marks (arrows) in the outer cortex (top of image). The inner mark is an annulus or double annulus around most of the section, but in small regions shows breaks in tissue (see Figure 2.85). A laterally restricted region of secondary remodeling is visible near the endosteal margin. The secondary osteons look somewhat indistinct in regular transmitted light, but are colorful in elliptically polarized light. Scale = 1 mm.

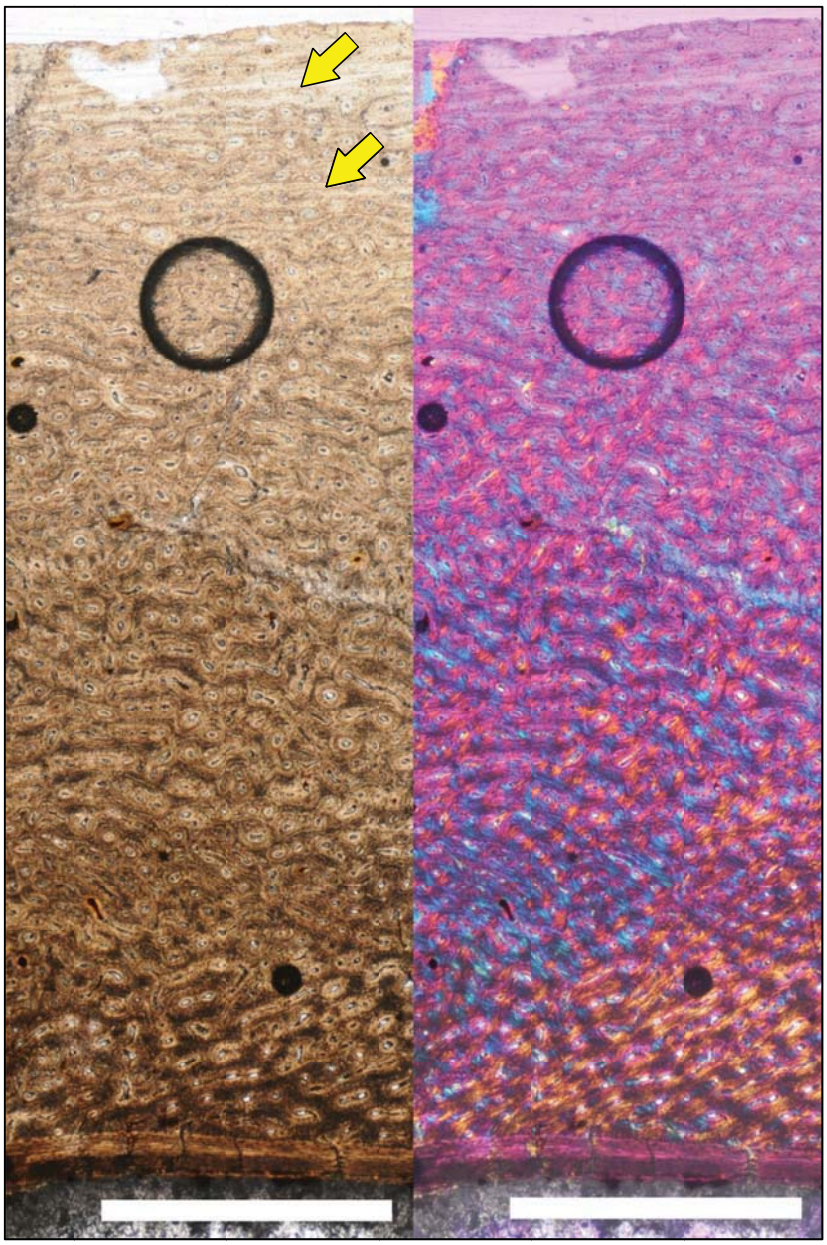

Figure 2.85 Cortical histology of the mid-diaphyseal femur of an undescribed coelophysoid from Hayden Quarry, Ghost Ranch, NM (GR 256), in regular transmitted light (left) and elliptically polarized light (right). Two growth marks are visible in outer cortex (arrows). The outer mark (upper arrow) is a double LAG around the circumference of the section, but the inner mark (lower arrow) is an annulus around most of the bone. In this femur, most of the cortex is composed of well vascularized woven–fibered bone, with primary osteons that form short anastomoses in all directions. External to the outer LAG, the bone is parallel-fibered and anastomoses are not present. The large circles in the top third of the images are bubbles in the slide, not microstructural features. Periosteum to the top of both images. Scale = 1 mm.

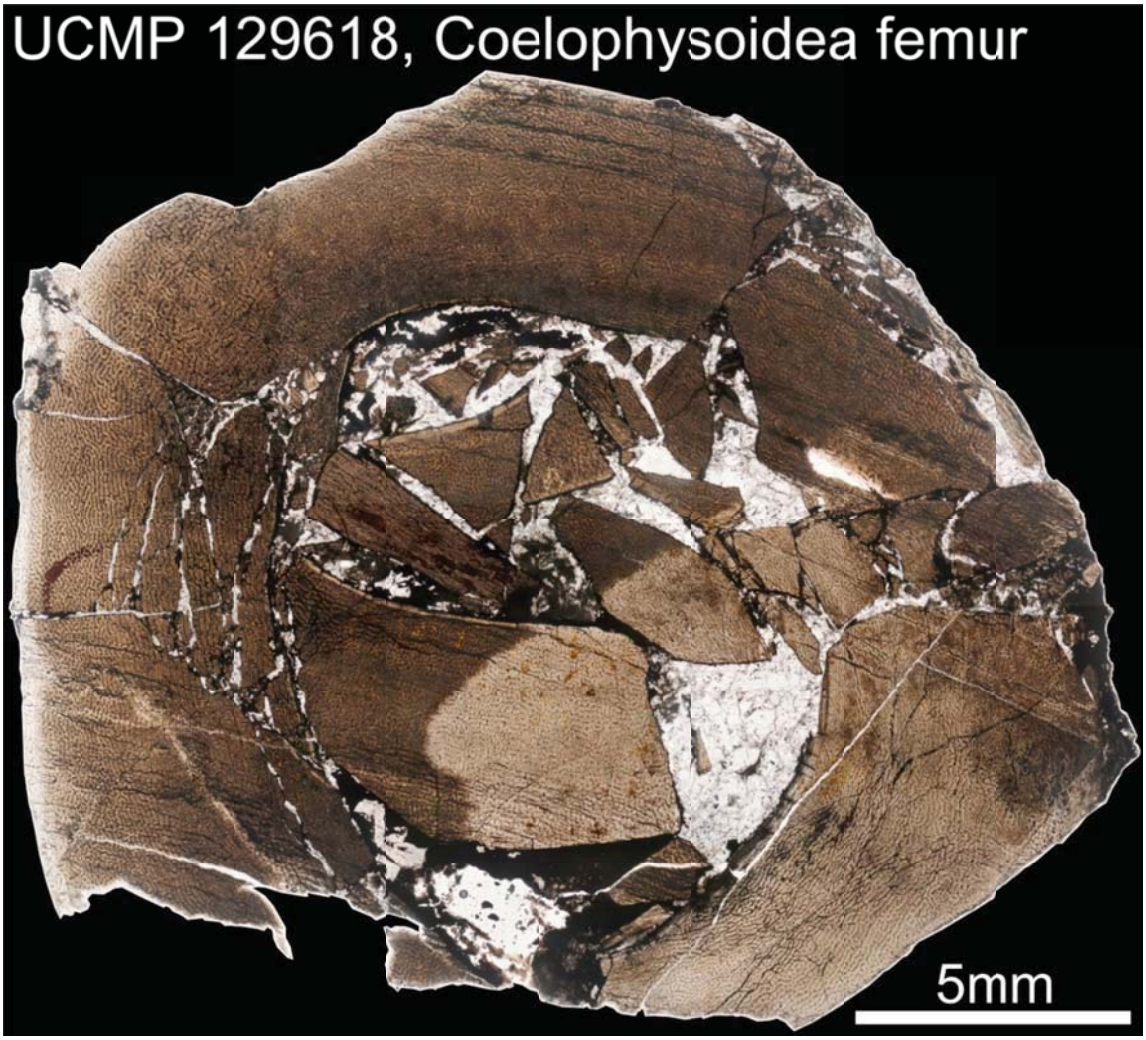

Figure 2.86 Cortical histology of the mid-diaphyseal femur of a coelophysoid from the Inadvertent Hills locality, Petrified Forest National Park, AZ (UCMP 129618), in regular transmitted light. This specimen was referred to *C. bauri* by Padian (1986), but subsequent studies have questioned whether or not this is truly *C. bauri* or a new coelophysoid species (de Ricqlès et al. 2003b; Padian et al. 2004; Nesbitt et al. 2007). The femur is badly crushed at midshaft, but suggests a circular or oval shape, with a central medullary cavity. Scale = 5 mm.

Figure 2.86 Cortical histology of the mid-diaphyseal femur of a coelophysoid from the Inadvertent Hills locality, Petrified Forest National Park, AZ (UCMP 129618), in regular transmitted light. The entire cortex is composed of primary woven bone tissue, although it is more weakly woven in the outer cortex (top of image). No growth marks are visible in this section. In the inner cortex, nearly every primary osteon anastomoses with several others to form a subplexiform pattern (bottom third of image). In the midcortex, about one third of the primary osteons are isolated; the rest anastomose with 1-7 other canals (the extent varies around the circumference of the bone; see Figure 2.85). These anastomoses are most commonly circumferential or radial, and may form small reticulations (middle third of image). In the outer cortex, most of the canals are simple primary canals, though primary osteons are also visible. Here, the canals anastomose radially or obliquely, rather than circumferentially (top third of image), and generally form small reticulations. Periosteum to the top of this image. Scale = 500 µm.

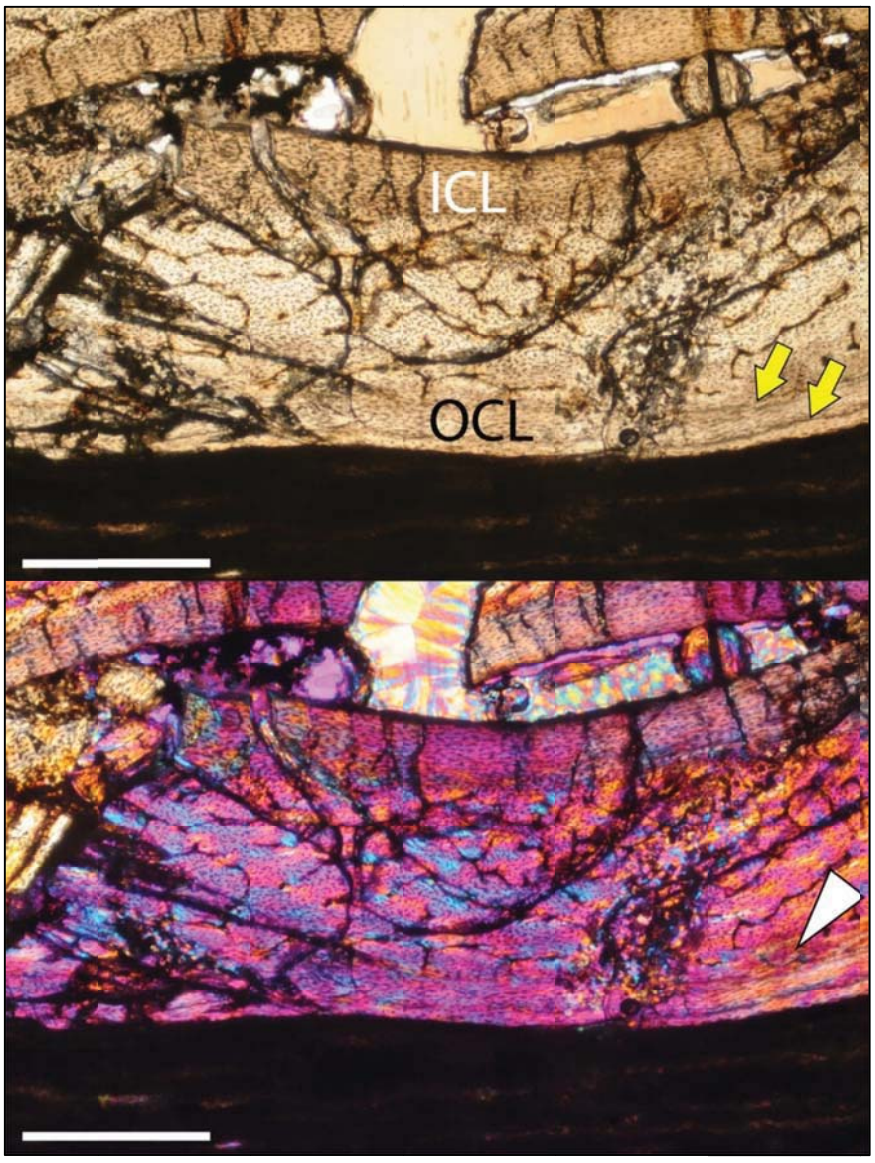

Figure 2.87 Cortical histology of the mid-diaphyseal humerus of *Confuciusornis santcus* (NGMC 98-8-2 / MOR 1063) in regular transmitted light (top) and elliptically polarized light (bottom). The inner circumferential layer (ICL) is thicker than the outer circumferential layer (OCL), and is crossed by radial canals extending from the middle layer to the medullary cavity. The middle layer is composed of woven-fibered bone internally, which grades into parallel fibered bone at the point of the white arrow. In the woven-fibered region, longitudinal primary osteons anastomose with each other via simple primary canals that extend in all directions. As the bone transitions to parallel-fibered bone, vascular canal density decreases, though vascular connectivity and pattern remain similar. Two LAGs are visible in this specimen (yellow arrows); the inner LAG separates the cortex from the OCL. Periosteum to bottom of both images. Scale = 500 μm.

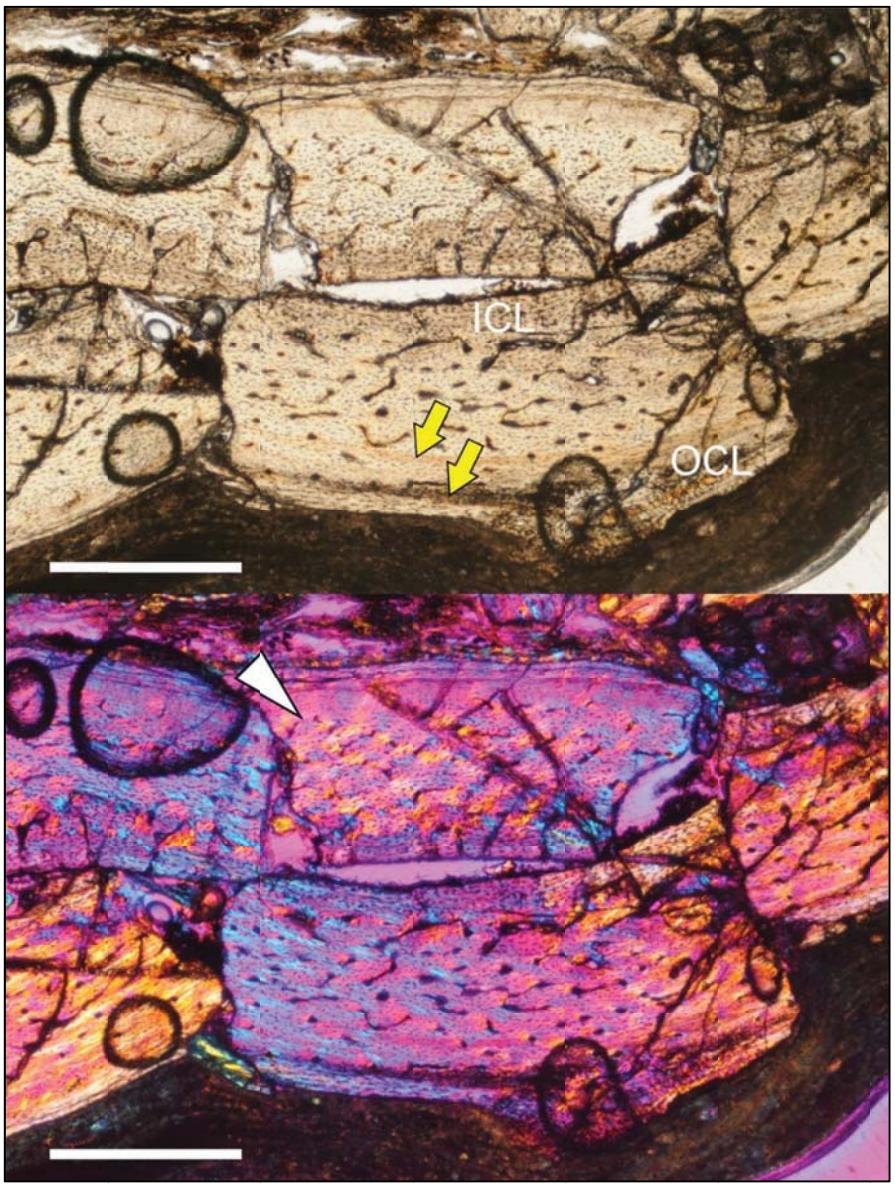

Figure 2.88 Cortical histology of the mid-diaphyseal femur of *Confuciusornis santcus* (NGMC 98-8-2 / MOR 1063) in regular transmitted light (top) and elliptically polarized light (bottom). The inner circumferential layer (ICL) is thicker than the outer circumferential layer (OCL), and is crossed by radial canals extending from the middle layer to the medullary cavity. The middle layer is composed of woven-fibered bone internally, which grades into parallel fibered bone at the point of the white arrow. In the woven-fibered region, longitudinal primary osteons anastomose with each other via simple primary canals that extend in all directions. As the bone transitions to parallel-fibered bone, vascular canal density and connectivity both decrease. Two LAGs are visible in this specimen (yellow arrows); the inner LAG separates the cortex from the OCL. Periosteum to top and bottom of both images (specimen is crushed). Scale = 500 μm.

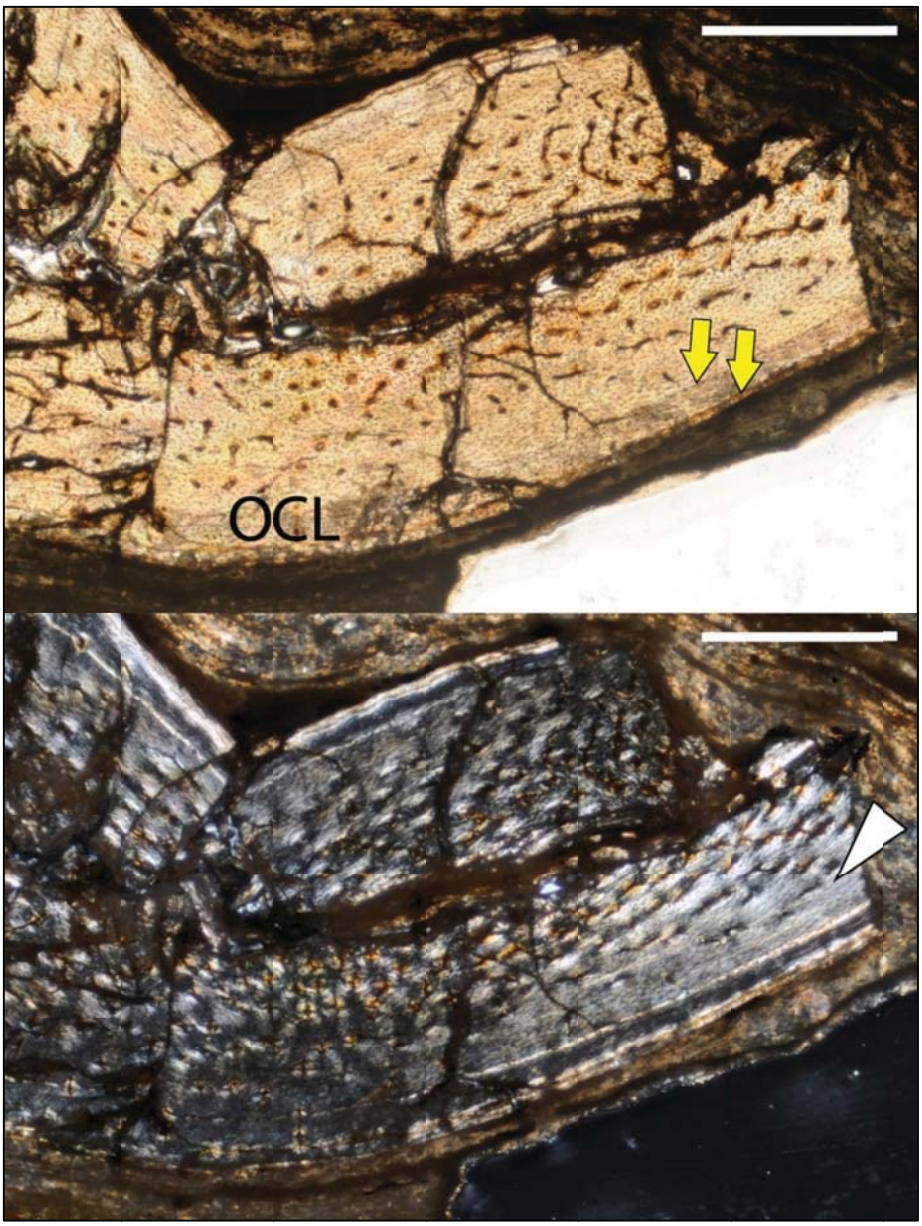

Figure 2.89 Cortical histology of the mid-diaphyseal tibia of *Confuciusornis santcus* (NGMC 98-8-2 / MOR 1063) in regular transmitted light (top) and crossed plane polarized light (bottom). The inner circumferential layer is not preserved in this region of the bone, but the outer circumferential layer (OCL) is visible. The middle layer is composed of woven-fibered bone internally, which grades into parallel fibered bone at the point of the white arrow. In the woven-fibered region, longitudinal primary osteons anastomose with each other via simple primary canals that extend in all directions. As the bone transitions to parallel-fibered bone, it becomes nearly avascular. Two LAGs are visible in this specimen (yellow arrows); the inner LAG separates the cortex from the OCL. Periosteum to top and bottom of both images (specimen is crushed). Scale = 500 μm.

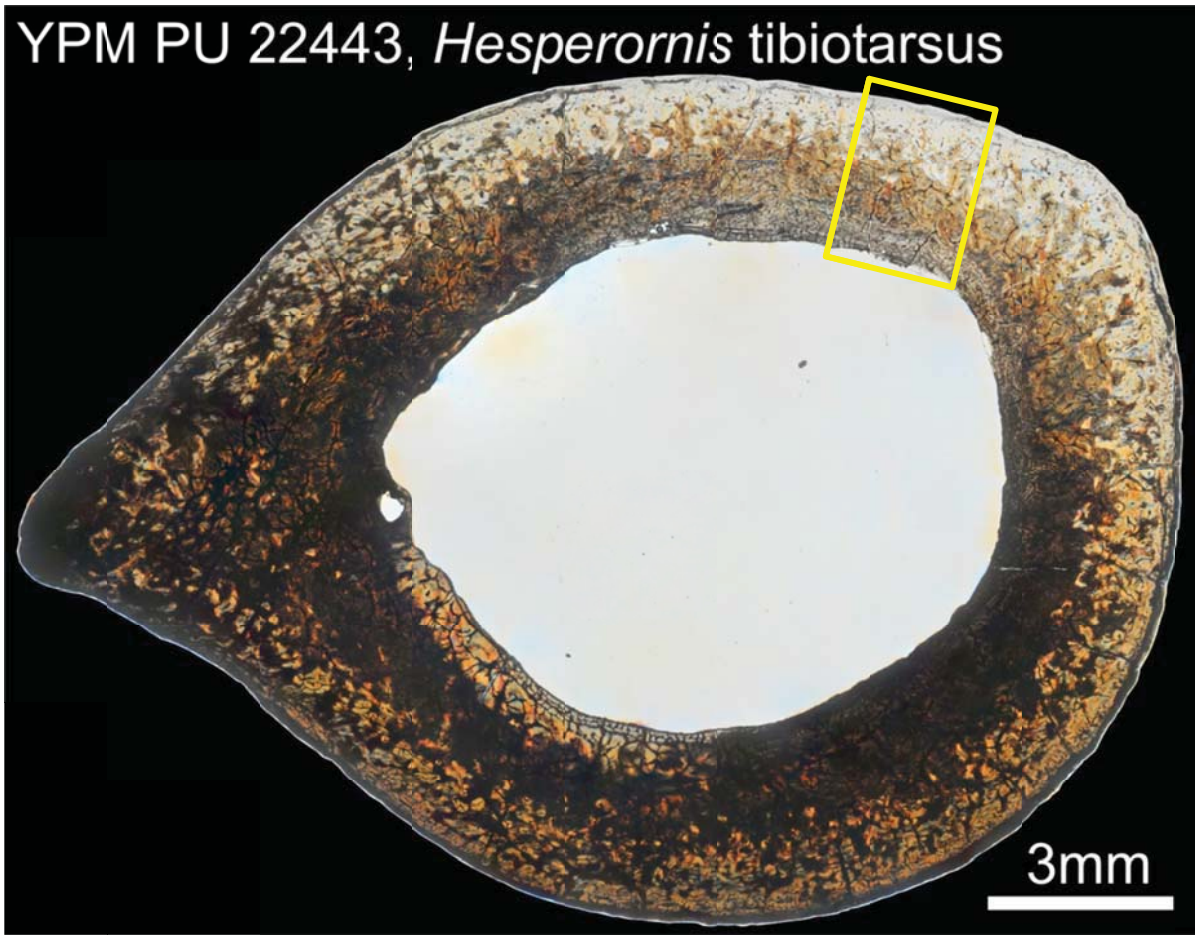

Figure 2.90 Cortical histology of the mid-diaphyseal tibiotarsus of *Hesperornis* (YPM PU 22443) in regular transmitted light. The bone experienced bacterial or fungal invasion, rendering some regions dark. In these regions, the microstructure is hard to assess. The projection on the lateral portion of the bone (left side of this image) is the fibular crest. The yellow box indicates the position of the image in Figure 2.91. Scale = 3 mm.

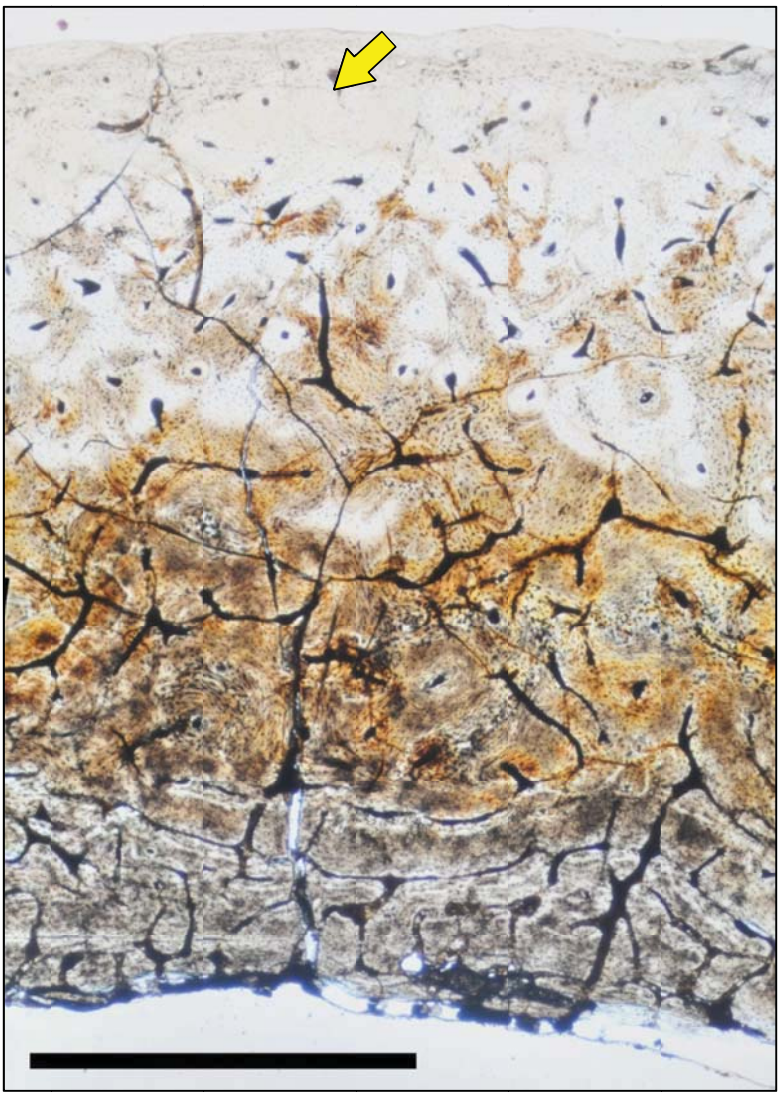

Figure 2.91 Cortical histology of the mid-diaphyseal tibiotarsus of *Hesperornis* (YPM PU 22443) in regular transmitted light. This image is a radial transect through the cortex and shows the pattern of vascular canals (thick black lines) in this element (see Figure 2.90 for position of image within the cross section). A single LAG is visible in this section (yellow arrow; note that LAG appears faint because the slide is thin near the edge); it separates the outer circumferential layer (OCL) from the middle, woven-fibered layer. The inner circumferential layer (ICL; darker brown region at bottom of image) is much thicker than the OCL. Short radial canals cross the ICL, connecting the middle layer to the medullary cavity. In the inner half of the middle layer, primary and secondary osteons are common. These are difficult to distinguish; many lamellae surround both types of osteons. Secondary osteons overlap another and show distinct resorption borders. In the outer half of the middle layer, only primary osteons are present. Throughout the middle layer, osteons anastomose with each other via simple primary canals that may extend in any direction to form reticulations. These reticulations are more extensive in the inner half of the middle layer. Scale = 1 mm.

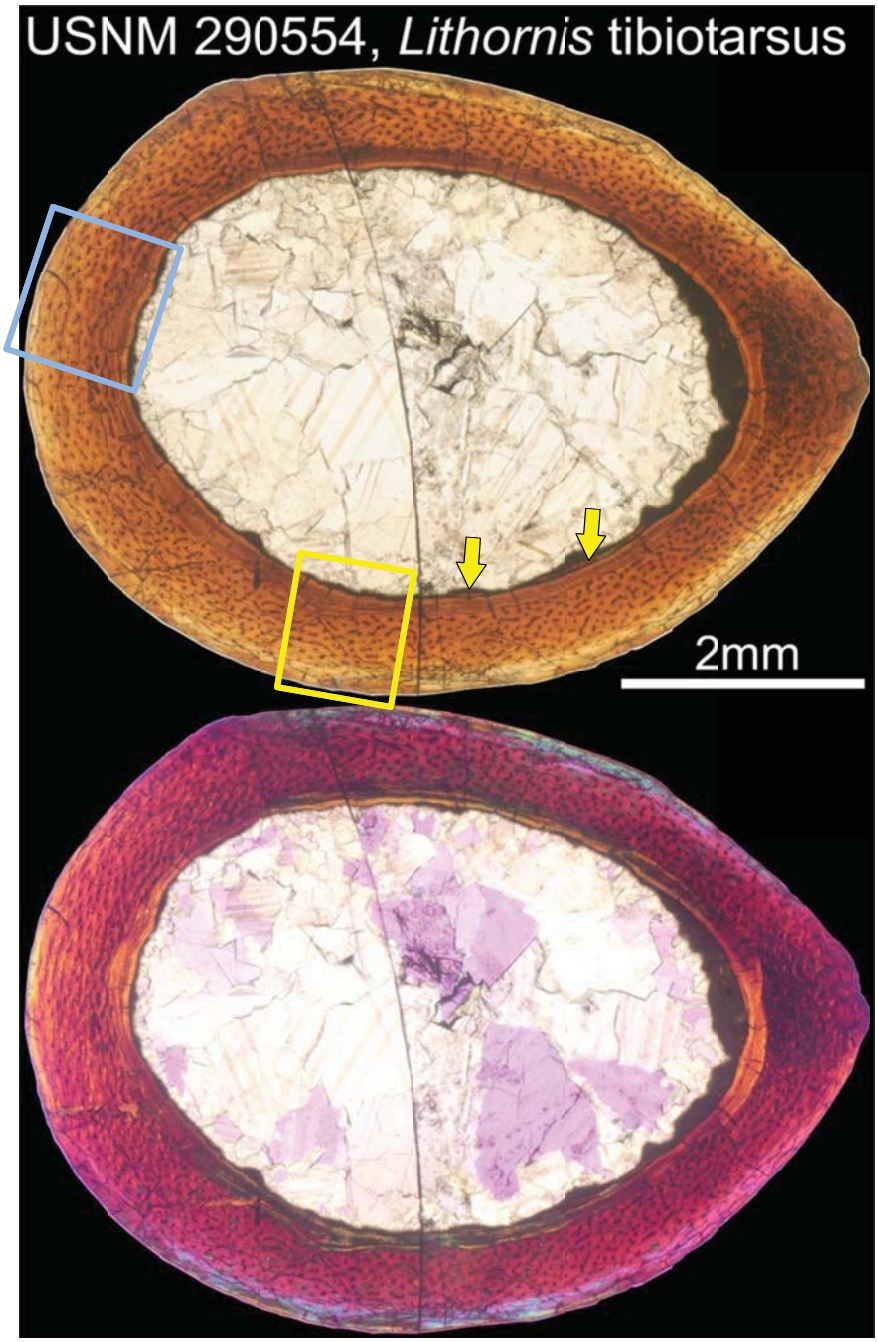

Figure 2.92 Cortical histology of the mid-diaphyseal tibiotarsus of *Lithornis celetius* (USNM 290554) in regular transmitted light (top) and elliptically polarized light (bottom). This image shows the shape and relative thickness of the cortex at mid diaphysis. The ICL appears intact around the circumference, but remnants of at least one more layer are visible (arrows), suggesting the crystals in the medullary cavity destroyed at least part of the original endosteal margin. The yellow box indicates the position of Figure 2.93, and the blue box indicates the position of Figure 2.94. Scale = 2mm.

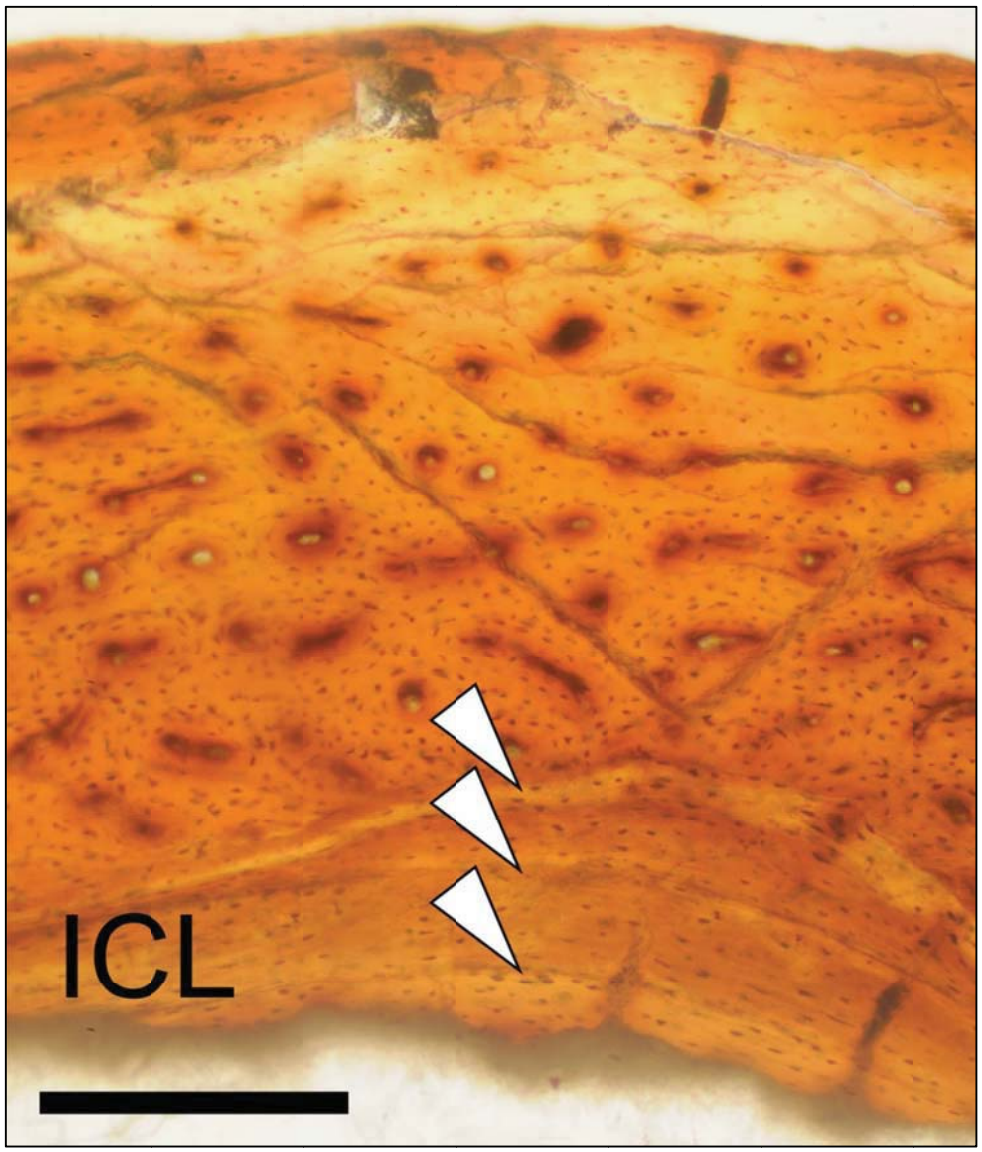

Figure 2.93 Cortical histology of the mid-diaphyseal tibiotarsus of *Lithornis celetius* (USNM 290554) in regular transmitted light. The position of this image is indicated by the yellow box in Figure 2.92. The inner circumferential layer (ICL) is composed of parallel-fibered and lamellar bone crossed by radial simple primary canals. This layer shows several reversal lines (white arrows) and cuts into the middle layer. The middle layer is composed of woven-fibered bone and is moderately to well vascularized by longitudinal primary osteons. In the inner half of this layer, most canals anastomose with one other either circumferentially or obliquely. In the outer half of this layer, canal density decreases slightly, and most of the canals do not anastomose. The outer circumferential layer is not visible in this image. No LAGs or annuli are present in this specimen. Periosteum to top of image. Scale = 250 μm.

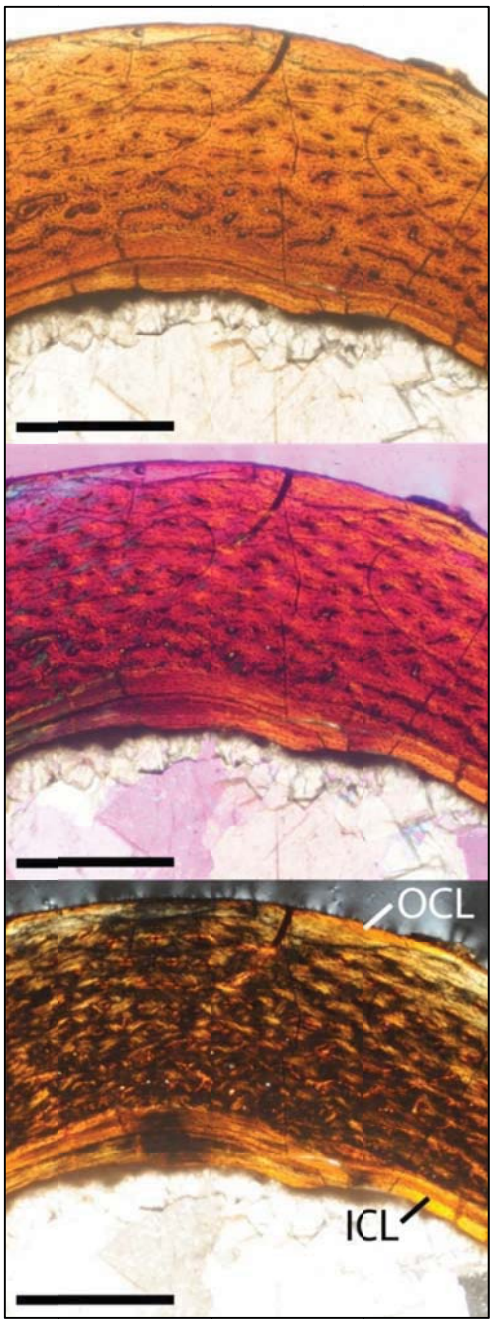

Figure 2.94 Cortical histology of the mid-diaphyseal tibiotarsus of *Lithornis celetius* (USNM 290554) in regular transmitted light (top), elliptically polarized light (middle), and crossed plane polarized light (bottom). The position of this image is indicated by the blue box in Figure 2.92. The outer circumferential layer (OCL) is most distinct in crossed plane polarized light. It is a very narrow band composed of lamellar bone, especially compared to the inner circumferential layer (ICL), and it is missing from some areas of the circumference (because of surface abrasion). Between the ICL and OCL, the middle layer is composed of woven-fibered bone. Periosteum to the top of all three images. Scale = 500 μm.

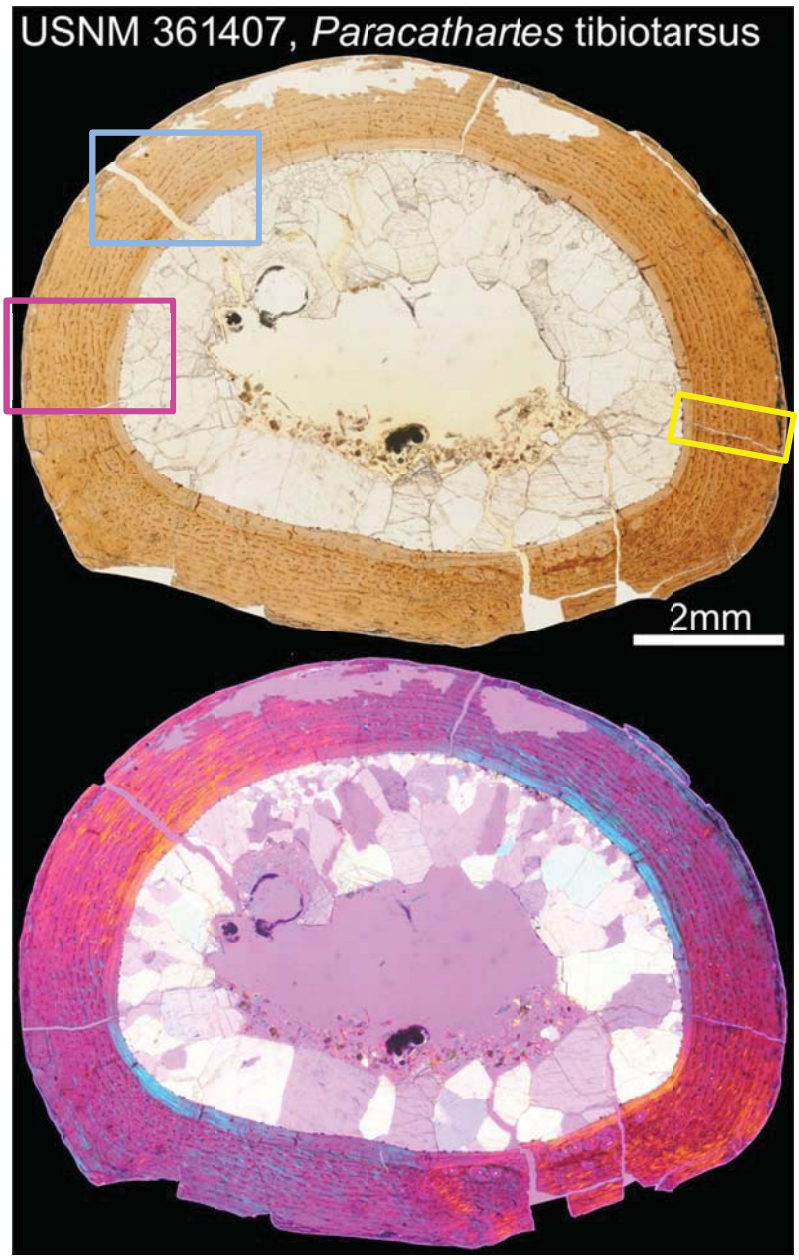

Figure 2.95 Cortical histology of the mid-diaphyseal tibiotarsus of *Paracathartes howardae* (USNM 361407) in regular transmitted light (top) and elliptically polarized light (bottom). This image shows the shape and relative thickness of the cortex at mid diaphysis. The outer circumferential layer is extremely thin and is not preserved around most of the circumference. The yellow box indicates the position of Figure 2.96, the blue box indicates the position of Figure 2.97, and the magenta box indicates the position of Figure 2.98. The anterior side of the element is at the bottom of both images. Scale = 2mm.

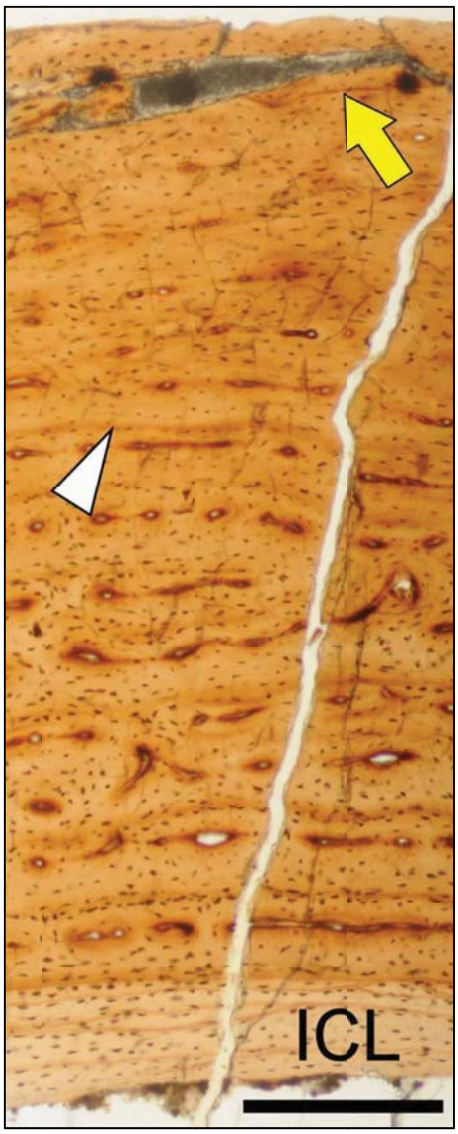

Figure 2.96 Cortical histology of the mid-diaphyseal tibiotarsus of *Paracathartes howardae* (USNM 361407) in regular transmitted light. The position of this radial transect through the cortex is indicated by the yellow box in Figure 2.95. The inner circumferential layer (ICL) shows several reversal lines (thin lines) but no lamellae or radial canals in this region. The middle layer shows a decrease in both the density and connectivity of primary osteons moving periosteally (towards top of image). Most primary osteons are longitudinal, but these anastomose circumferentially with up to six other canals in the inner cortex. In the innermost laminae, the osteocytes are concentrated at the core of each lamina, and are sparser closer to canals. This section also shows the one definitive LAG (yellow arrow) and a potential annulus (white triangle). Around most of the circumference of the bone, there is a dramatic decrease of osteocyte density at this position within the cortex. Here, a thin dark line is also present, but no break in tissue is observed. The outer circumferential layer is not preserved in this region of the bone. Scale = 250 μm.

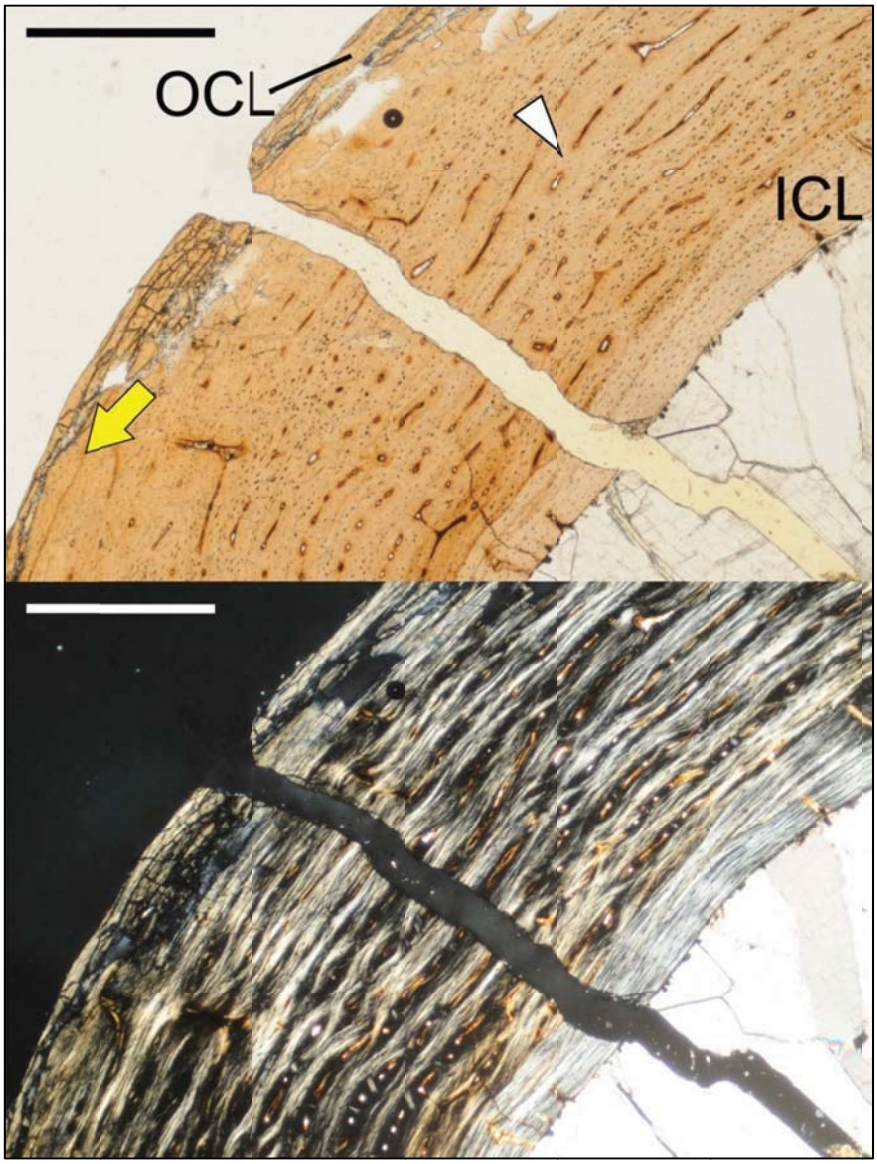

Figure 2.97 Cortical histology of the mid-diaphyseal tibiotarsus of *Paracathartes howardae* (USNM 361407) in regular transmitted light (top) and crossed plane polarized light (bottom). The position of this image is indicated by the blue box in Figure 2.95. This image shows one of the few regions around the circumference where short radial canals are visible in the inner circumferential layer (ICL). The outer circumferential layer (OCL) is visible only as a thin band in this region. A single LAG (yellow arrow) lies just internal to the boundary between the OCL and the middle layer. This image also shows a potential annulus; a region at midcortex where osteocyte density decreases dramatically around most of the circumference (white triangle).In this region, parallel-fibered tissue is more common within the middle layer than woven-fibered tissue. Periosteum to upper left of both images. Scale = 500 μm.

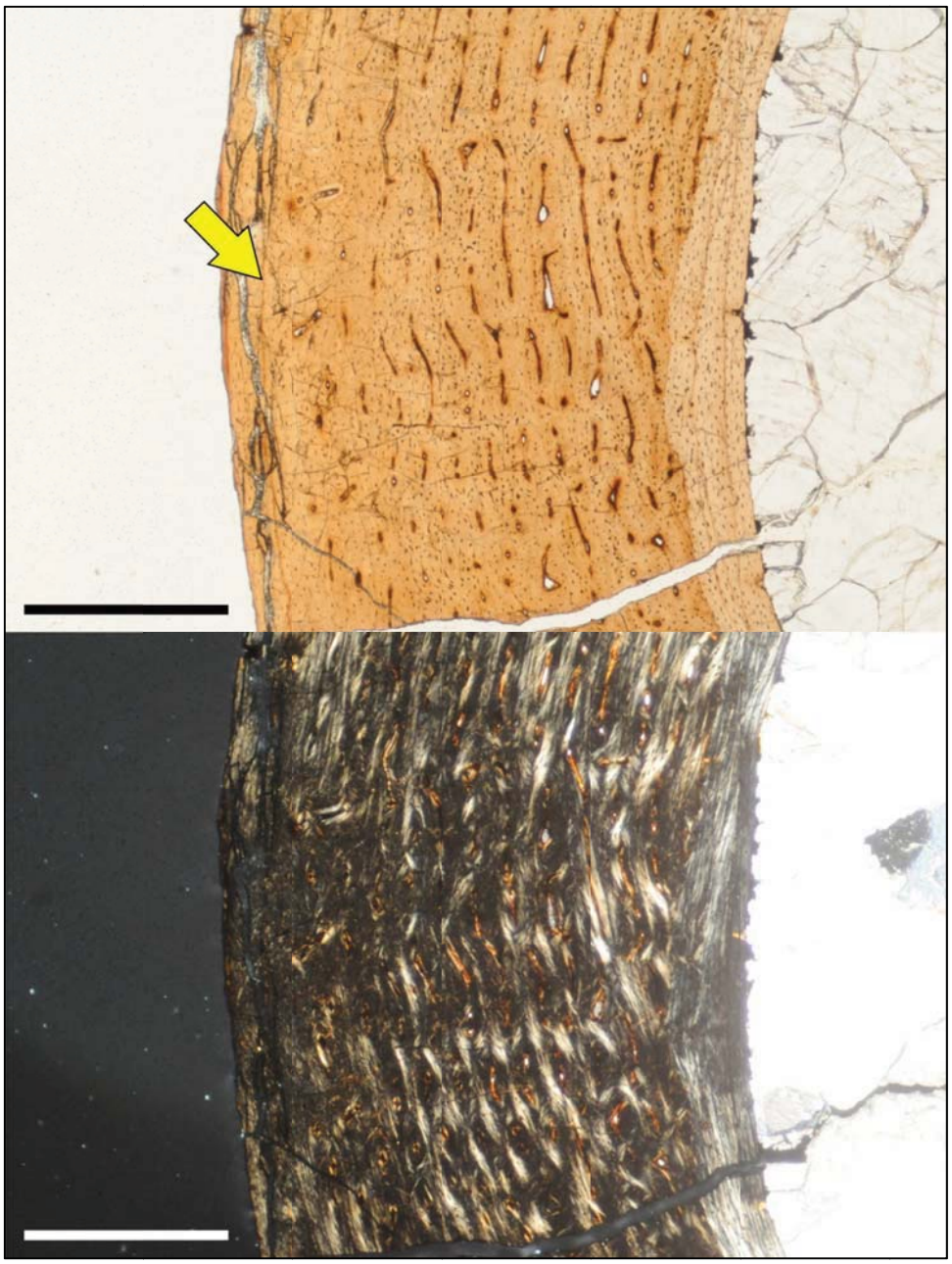

Figure 2.98 Cortical histology of the mid-diaphyseal tibiotarsus of *Paracathartes howardae* (USNM 361407) in regular transmitted light (top) and crossed plane polarized light (bottom). The position of this image is indicated by the magenta box in Figure 2.95. A single LAG (yellow arrow) is visible in this section, but the region of low osteocyte density that potentially represents an annulus (see Figures 2.96, 2.97) is absent. This image also shows the region at midcortex where osteocyte density decreases dramatically around most of the circumference (white triangle). In this region, woven-fibered tissue is more common in the middle layer than parallel-fibered tissue. Periosteum to left of both images. Scale = 500 μm.

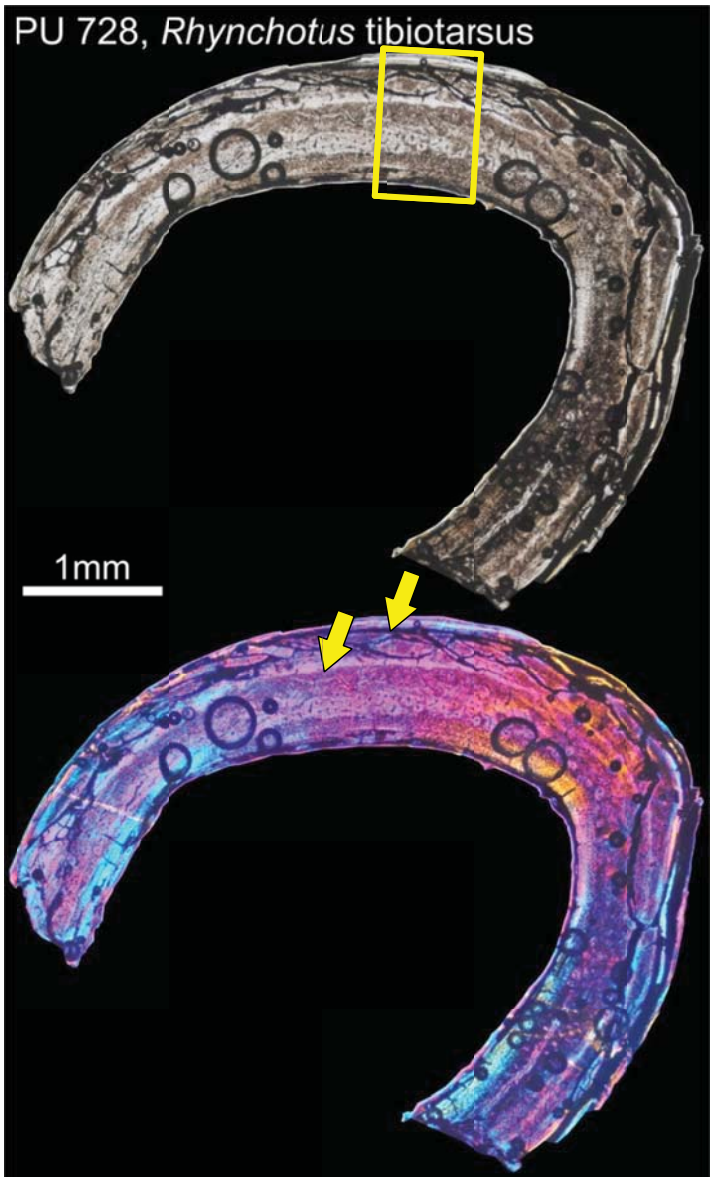

Figure 2.99 Cortical histology of the mid-diaphyseal tibiotarsus of *Rhynchotus rufescens* (PU 728) in regular transmitted light (top) and elliptically polarized light (bottom). This slide is missing the medial portion of the diaphysis (lower left of image), but the full cross section is oval or slightly almond shaped. The yellow box indicates the position of Figure 2.100. Two growth marks are present in this specimen (arrows). The inner mark is an annulus of parallel-fibered and weakly woven bone that shows differences in both vascularity and birefringence compared to the surrounding tissue. The second is a LAG in the outer cortex. A crack in the bone follows this LAG, and little bone is preserved external to it. Because of the fracturing in the outermost cortex, it is difficult to determine whether or not an outer circumferential layer is preserved. Scale = 1 mm.

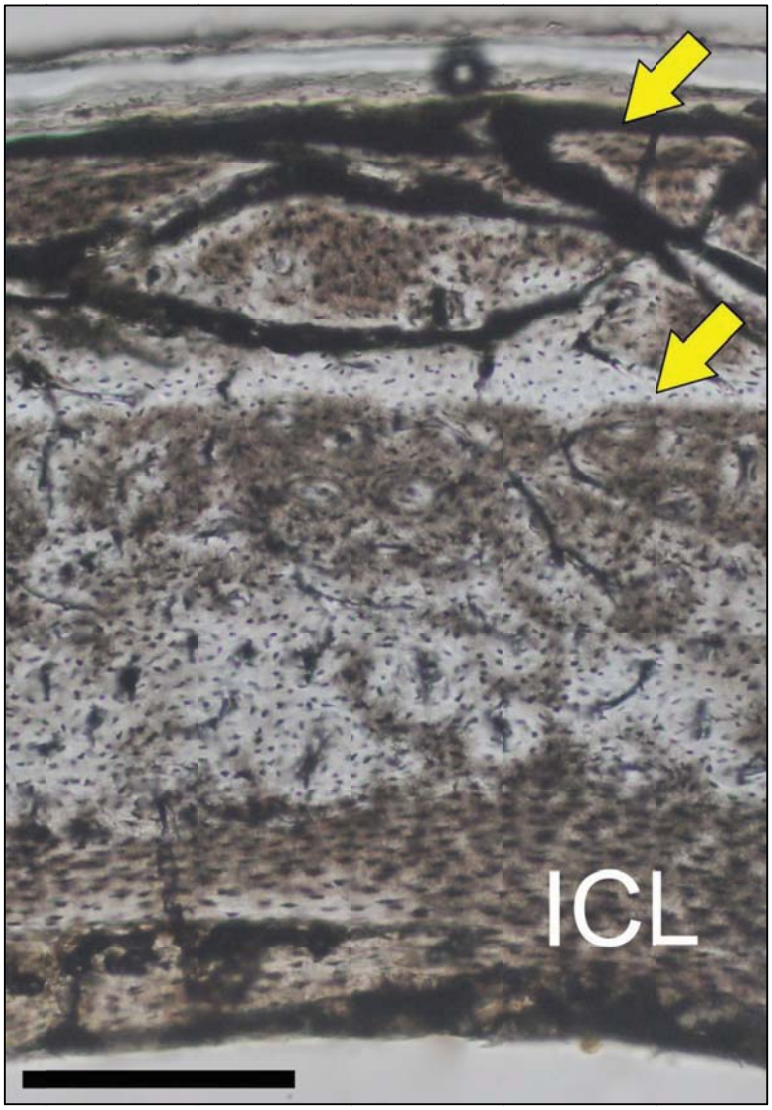

Figure 2.100 Cortical histology of the mid-diaphyseal tibiotarsus of *Rhynchotus rufescens* (PU 728) in regular transmitted light. The position of this cortical transect is indicated by the yellow box in Figure 2.99. Two growth marks are present in this specimen (arrows). The inner mark (lower arrow) is an annulus of parallel-fibered and weakly woven bone that shows differences in both vascularity and osteocyte organization compared to the surrounding tissue. The second is a LAG in the outer cortex. A major crack in the bone follows this LAG, and little bone is preserved external to it. Because of the fracturing in the outermost cortex (thick black lines at top of image), it is difficult to determine whether or not an outer circumferential layer is preserved. The inner circumferential layer (ICL) is mostly composed of parallel-fibered bone, with localized patches of lamellar bone. The border between the ICL and the middle layer is not marked by a distinct reversal line, but the histological transition from poorly vascularized parallel-fibered bone to moderately to well vascularized woven bone is clear. Periosteum to top of image. Scale = 250 μm.

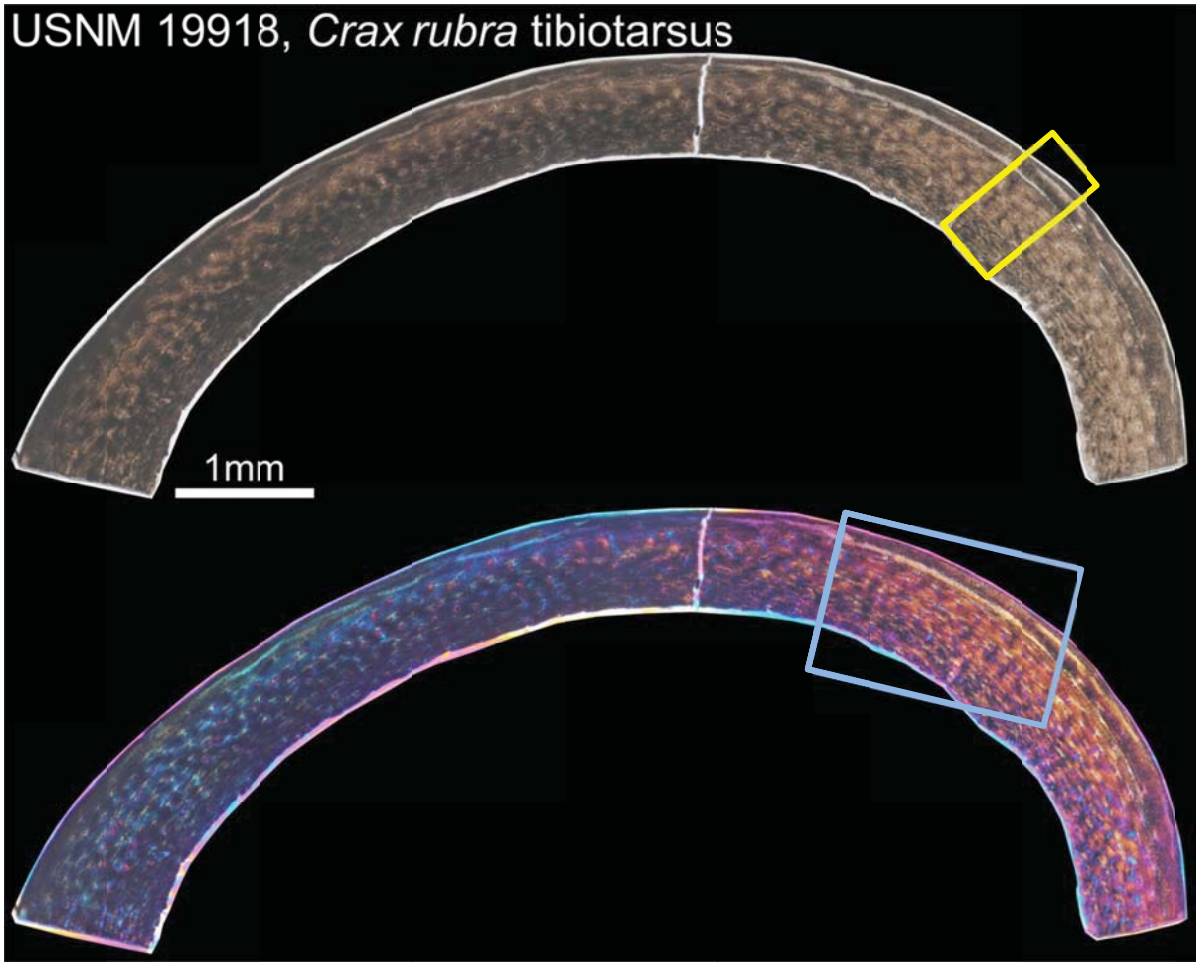

Figure 2.101 Cortical histology of the mid-diaphyseal tibiotarsus of *Crax rubra* (USNM 19918) in regular transmitted light (top) and elliptically polarized light (bottom). The yellow box indicates the position of Figure 2.102, and the blue box indicates the position of Figure 2.103. Scale = 1 mm.

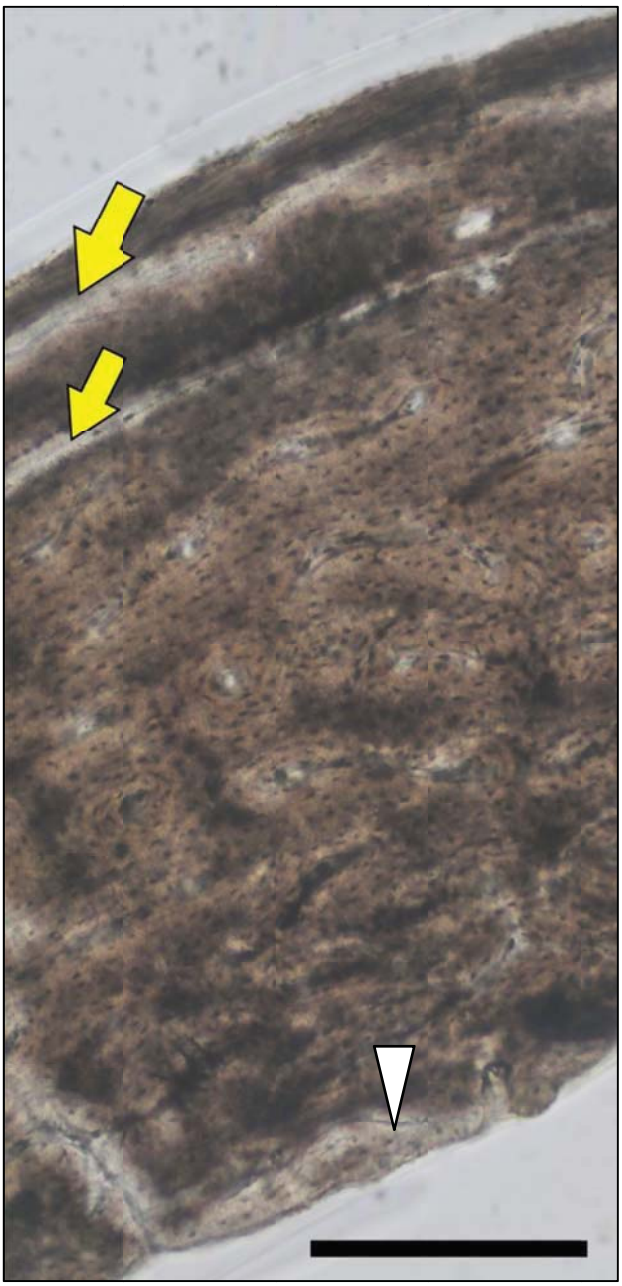

Figure 2.102 Cortical histology of the mid-diaphyseal tibiotarsus of *Crax rubra* (USNM 19918) in regular transmitted light. The position of this cortical transect is indicated by the yellow box in Figure 2.101. Only a few small traces of the inner circumferential layer are visible in this specimen (white triangle). The inner half of the middle layer is composed of well vascularized woven-fibered bone. In this region, the primary osteons anastomose circumferentially or obliquely. About halfway through the cortex, the bone transitions to parallel-fibered bone and vascular density and connectivity decrease slightly. Two LAGs (yellow arrows) are visible in the outer cortex. Scale = 250 μm.

Figure 2.103 Cortical histology of the mid-diaphyseal tibiotarsus of *Crax rubra* (USNM 19918) in elliptically polarized light. The position of this cortical transect is indicated by the blue box in Figure 2.101. The inner half of the cortex is composed of well vascularized woven-fibered bone (multicolored region). Here, the primary osteons anastomose circumferentially or obliquely. About halfway through the cortex, the bone transitions to parallel-fibered bone and vascular density and connectivity decrease slightly. Two LAGs (yellow arrows) are visible in the outer cortex. Scale = 500 μm.

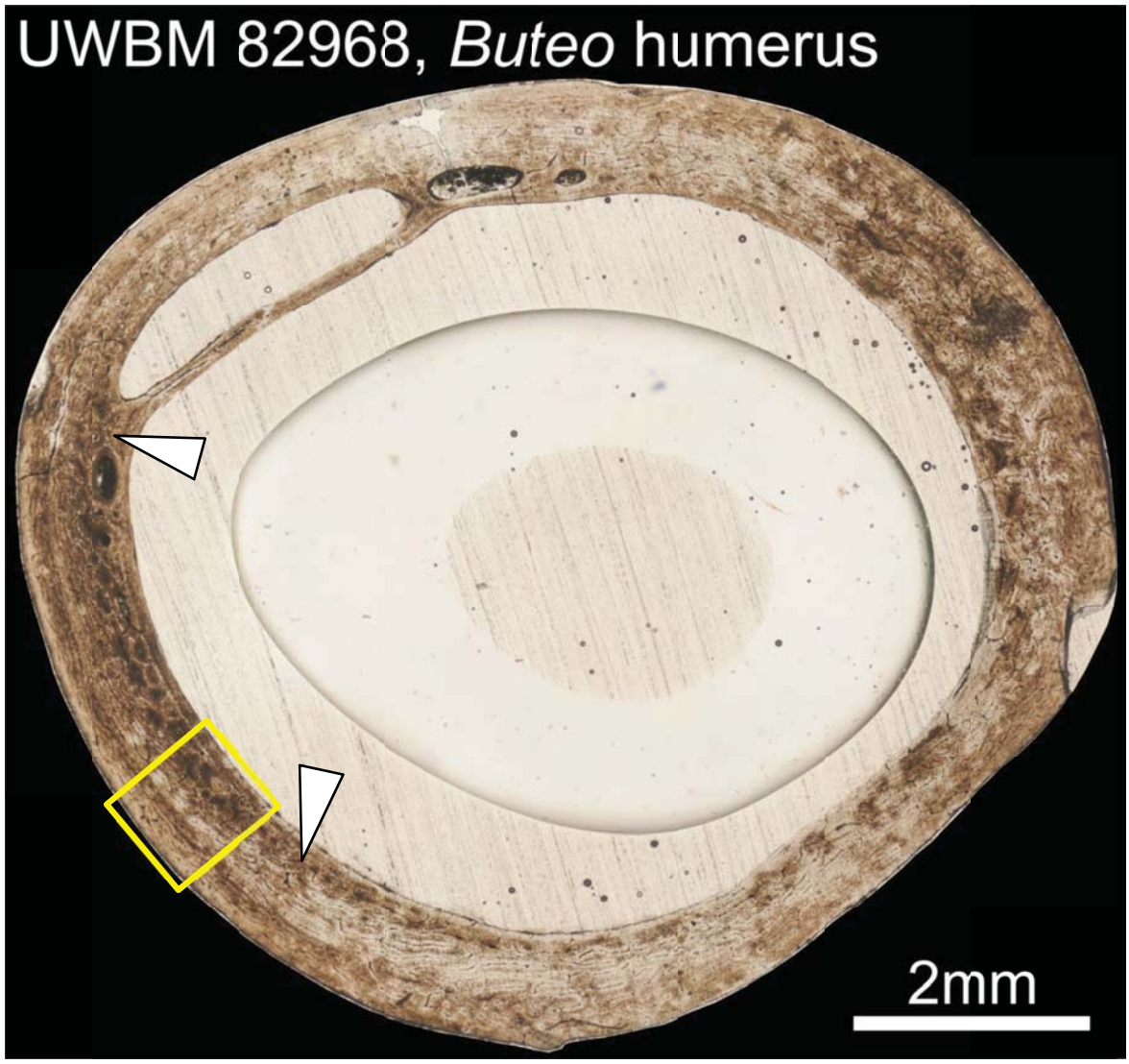

Figure 2.104 Cortical histology of the mid-diaphyseal humerus of *Buteo jamaicensis* (UWBM 82968) in regular transmitted light. The yellow box indicates the position of Figure 2.105. The humerus is subtriangular in cross section, with a thin cortex. The region bracketed by the two white triangles indicates the region where secondary osteons are most common. In the anteromedial quadrant of this bone, a large resorption room is visible (2.9 mm long). The inner margin of this room is a trabecular strut that forms a chord across the medullary cavity. Other resorption rooms are visible on each side of the largest one. Scale = 2 mm.

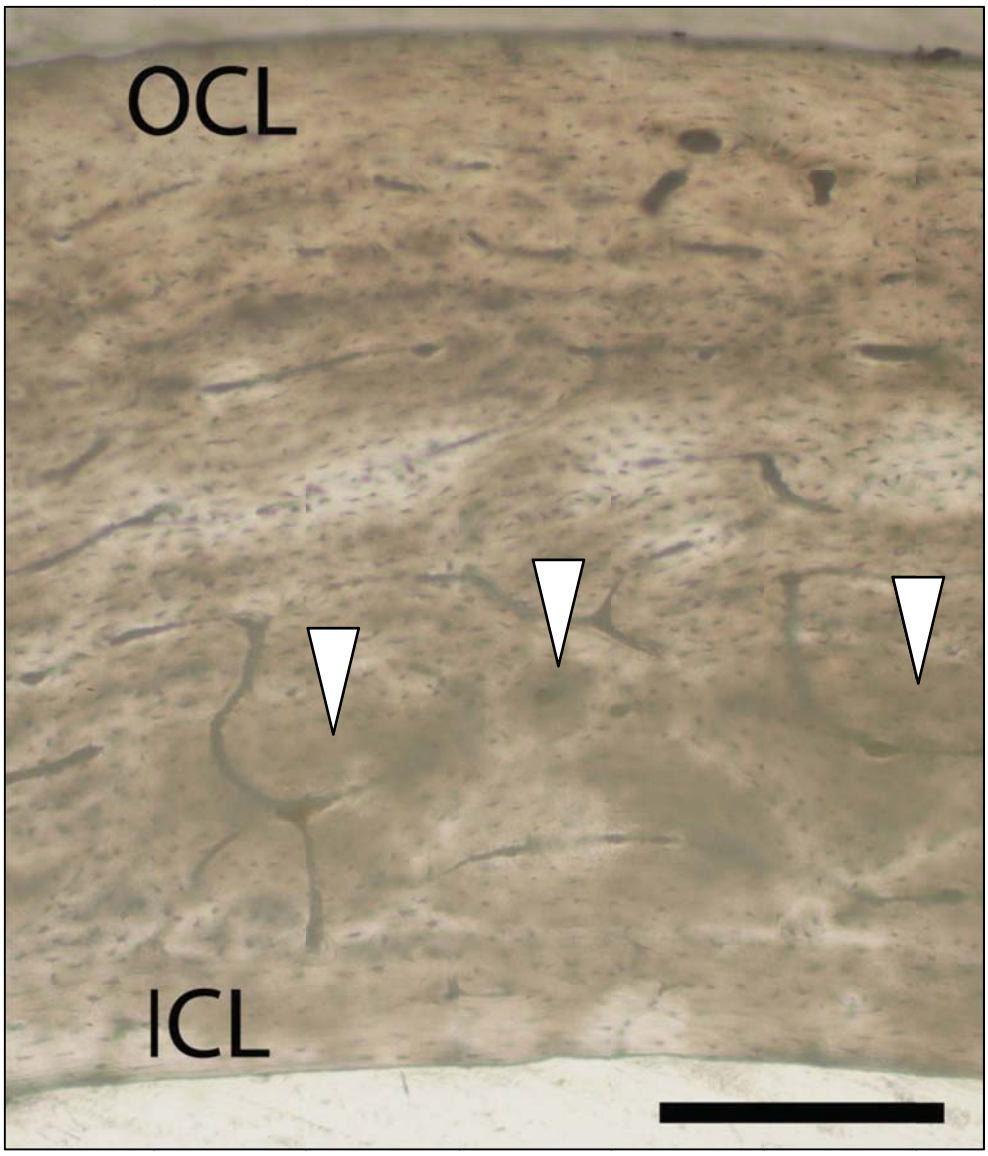

Figure 2.105 Cortical histology of the mid-diaphyseal humerus of *Buteo jamaicensis* (UWBM 82968) in regular transmitted light. The position of this cortical transect is indicated by the yellow box in Figure 2.104. No LAGs are present in this section. The inner circumferential layer (ICL) and outer circumferential layer (OCL) are both composed of parallel-fibered bone. The ICL is crossed in a few places by short radial simple primary canals, and the OCL is avascular. Within the middle layer, secondary osteons (white arrows) are present regionally. These anastomose with each other and with primary canals. In the inner half of the middle cortical layer, anastomoses may form small reticulations (as in this region of the bone), or connect more extensively to form a subplexiform pattern. In the outer half of the middle layer, vascular density and connectivity decrease periosteally, and reticulation is less common. Periosteum to the top of this image. Scale = 250 μm.

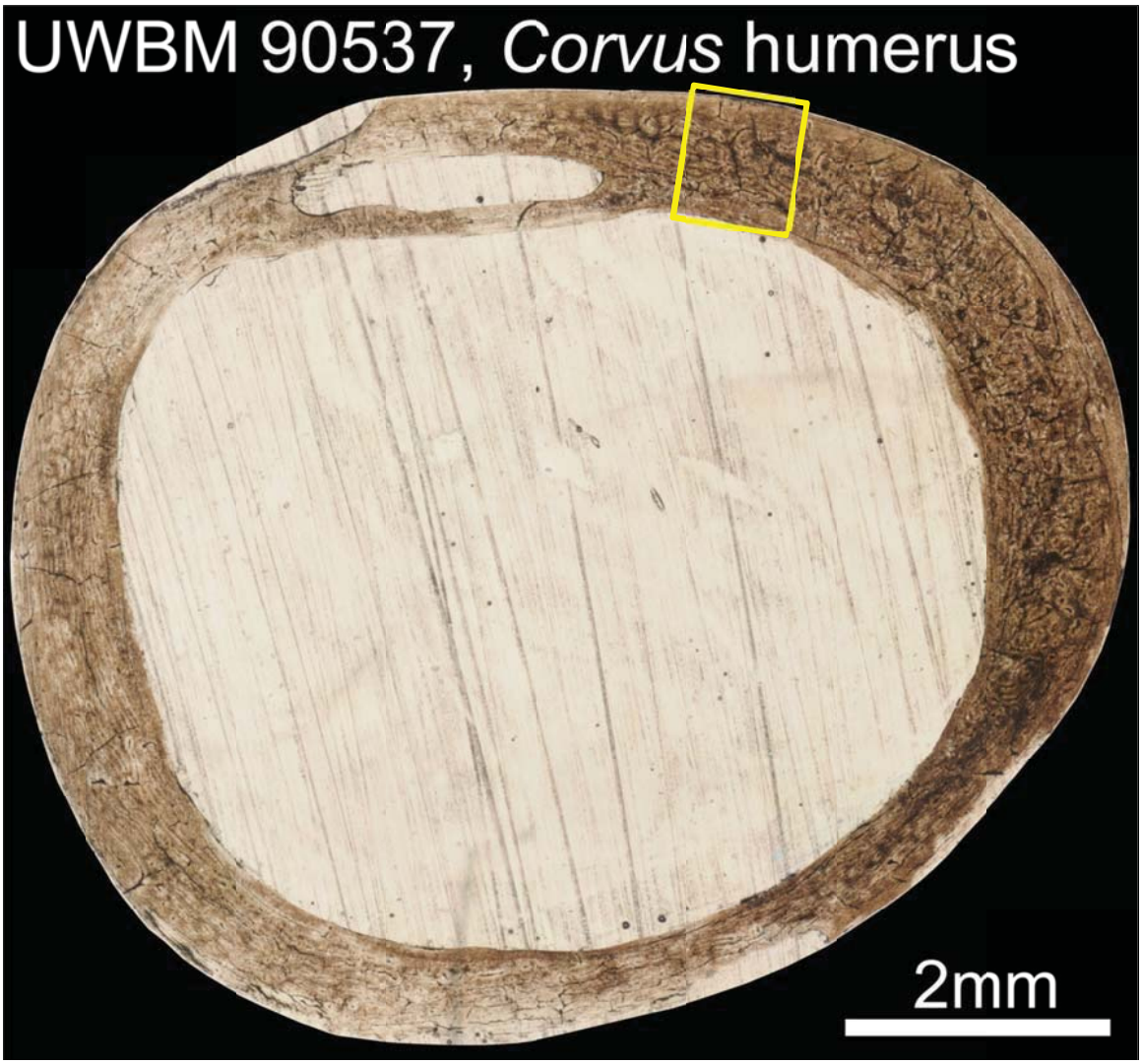

Figure 2.106 Cortical histology of the mid-diaphyseal humerus of *Corvus corax* (UWBM 90537) in regular transmitted light. The yellow box indicates the position of Figure 2.107. The humerus of this specimen is roughly circular in cross section, with a thin cortex as in *Buteo* (see Figure 2.104). The cortex is slightly thicker posteriorly (right side of image). Small secondary osteons are found throughout the cortex, but do not cluster in one region of the bone. In the medial quadrant of this bone, a large resorption room is visible (2.3 mm long). The inner margin of this room is a trabecular strut that forms a chord across the medullary cavity. Scale = 2 mm.

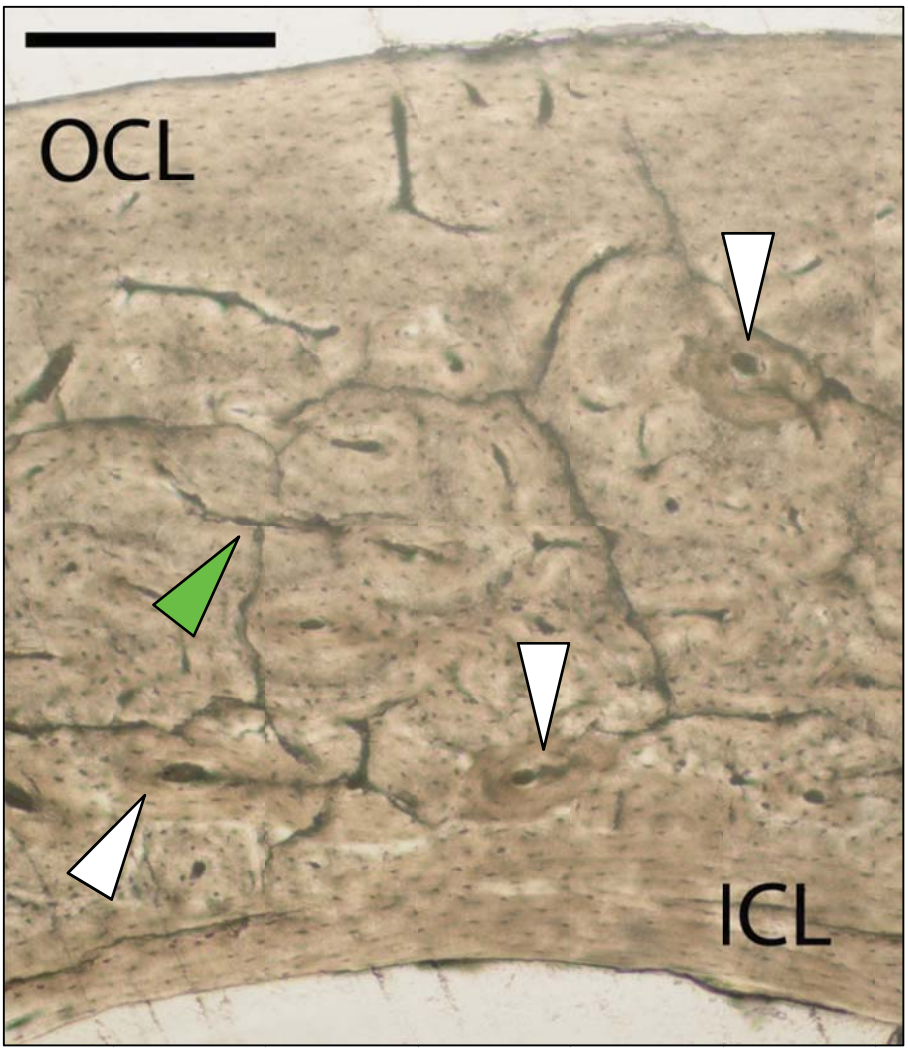

Figure 2.107 Cortical histology of the mid-diaphyseal humerus of *Corvus corax* (UWBM 90537) in regular transmitted light. The position of this cortical transect is indicated by the yellow box in Figure 2.106. Cracks (green triangle) are common in this section and resemble vascular canals, which they often intersect. They can be distinguished from canals by jagged edges and angular splits. The inner circumferential layer (ICL) is composed of lamellar bone, and is separated from the middle cortical layer by a distinct and uneven reversal line. The middle layer grades from woven-fibered bone in the inner cortex to parallel-fibered bone in the outer cortex. The transition between the middle layer and the outer circumferential layer (OCL) is indistinct. The middle layer is vascularized by both primary and secondary osteons (white triangles). Vascular density, connectivity, and patterning all vary dramatically around the section. This region is moderately to poorly vascularized by longitudinal primary osteons that may anastomose with one or two other osteons. Other regions in the cortex of this specimen show reticular or subplexiform patterns, or are nearly avascular. Periosteum to top of this image. Scale = 250 μm.

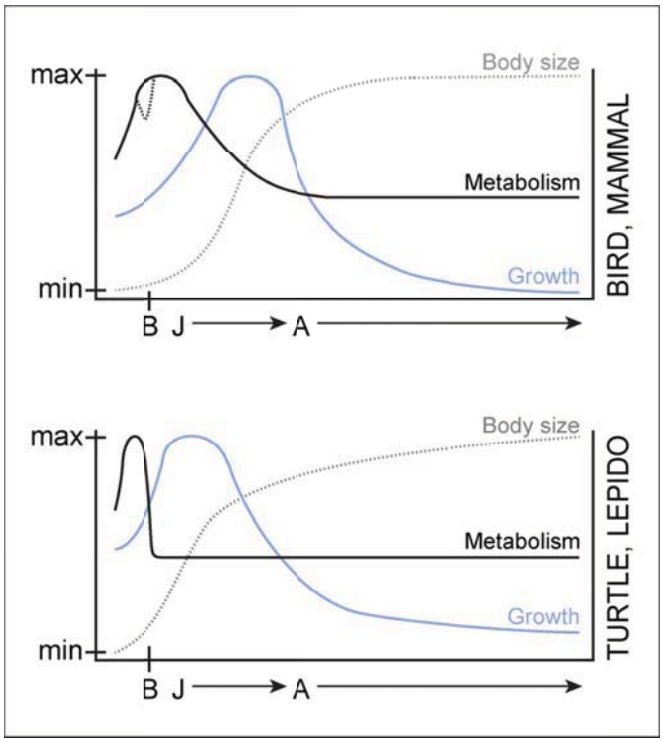

Figure 2.108 Ontogenetic changes in growth, metabolism, and body size in birds and mammals (top) and turtles and lepidosaurs (bottom). In both graphs, the x-axes represent age [labeled points represent birth/hatching (B), juvenile period (J) and adulthood (A); senescence and death not shown]. The y-axes are arbitrary scales (minima to maxima) for each of the three curves. Curves are representative of general trends only.

In mammals, basal metabolic rate (BMR) and mass-specific BMR (top graph, solid black line) increase throughout the embryonic phase. Birds follow a similar embryonic trajectory at first, but close to the time of hatching show a temporary decrease (top graph, downward excursion from metabolism line). In both clades, BMR and mass-specific BMR are much higher in juveniles than in adults. Approaching adulthood, BMR and mass-specific BMR decrease to adult levels and then remain fairly stable until senescence. In turtles and lepidosaurs, mass-specific standard metabolic rate (SMR) is higher in embryos and decreases after hatching (bottom graph, solid black line). Mass-specific SMR is the same for juveniles and adults in these taxa. Growth rates (blue lines) in both groups peak early in life, but this peak occurs relatively earlier in nonavian reptiles than in mammals and birds, and growth often continues (albeit at lower rates) through much of adulthood.

Histological indicators of metabolism (e.g., osteocyte density) should track the metabolism curves through ontogeny. In mammals, birds, and other animals with similar physiology, indicators should suggest much higher metabolic rates in juveniles than in adults (e.g., osteocyte density should be significantly higher in juveniles). In animals with physiologies more similar to those of turtles and lepidosaurs, these indicators should be stable throughout life. Histological indicators of growth will follow a similar trajectory to the blue curves, first showing signs of increasing growth rate, and then decreasing growth rate.

Table 2.1 Specimens sampled for this study. Specimens sampled for the first time as part of this study are indicated “this study”; specimens sampled as part of previous studies list the relevant reference. For many specimens, only certain microstructural features were described in previous works. For exam specimen the MorphoBank (MB) Project number is listed, as well as the MorphoBank accession numbers for high resolution digital images of cross sections (xs), radial transects, representative images, and osteocyte morphology. These images either are already available (for images associated with published papers) or will be made available on MorphoBank upon publication.

Taxon	Specimen	Element	Slides sectioned by?
Eureptilia			
Captorhinus aguti	UCMP 223509	humerus	Peabody 1961
Diapsida			
Lepidosauria			
Sphenodon punctatus	CMC 047	femur	Foote 1916
	JC A	femur	Castanet et al. 1990
	JC 57	femur	Castanet et al. 1990
	JC 58	femur	Castanet et al. 1990
	JC 807	femur	Castanet et al. 1990
	JC 833	femur	Castanet et al. 1990
Squamata			
Iguana iguana	UCMP 68286	humerus	Samuel Welles (unpublished)
	UCMP 68288	tibia	Samuel Welles (unpublished)
Varanus niloticus	UCMP 223456	femur	Peabody 1961
	VdB uncatalogued	femur	de Buffrénil & Castanet 2000
		tibia	de Buffrénil & Castanet 2000
Archosauromorpha			
Trilophosaurus buettneri	TMM 31025-849	humerus	this study
	TMM 31025-928	ulna	this study
	TMM 31025-787	femur	this study
	TMM 31025-1064	femur	this study
	TMM 31025-1063	femur	this study
	TMM 31025-862	femur	this study
	TMM 31025-885	femur	this study
	TMM 31025-786	femur	this study
	TMM 31025-788	tibia	this study
	TMM 31025-747	tibia	this study
	TMM 31025-887	tibia	this study
	TMM 31025-741	tibia	this study
Archosauriformes			
Vancleavea campi	UCMP 152662	femur	Nesbitt et al. 2009
	GR 250	femur	this study
Proterochampsia	MCZ 4038	femur	this study
Euparkeria capensis	AMNH FARB 2238	femur	this study
Phytosauria	UCMP 25921	femur	de Ricqlès et al. 2003b
Archosauria			
Pseudosuchia			
Revueltosaurus callenderi	PEFO 33843	femur	this study
Aetosauria	UCMP 32178	humerus	de Ricqlès et al. 2003b
	UCMP 25914	femur	de Ricqlès et al. 2003b
	GR 252	tibia	this study
Effigia okeeffeae	AMNH FARB 30587	femur	Nesbitt 2007
Loricata, cf. *Postosuchus*	UCMP 28353	humerus	de Ricqlès et al. 2003
	UCMP 25906	femur	de Ricqlès et al. 2003
Alligator mississippiensis	UCMP 68331	femur	Samuel Welles (unpublished)
	UCMP 68314	tibia	Samuel Welles (unpublished)

Taxon	Specimen	Element	Slides sectioned by?
Alligator mississippiensis	UF FWC 40723	humerus	Tumarkin-Deratzian 2007
		femur	Tumarkin-Deratzian 2007
		tibia	Tumarkin-Deratzian 2007
	UF FWC 40583	humerus	Tumarkin-Deratzian 2007
		femur	Tumarkin-Deratzian 2007
		tibia	Tumarkin-Deratzian 2007
	UF FWC LGS1	femur	Tumarkin-Deratzian 2007
Ornithodira			
Pterosauria			
Eudimorphodon cromptonellis	MGUH VP 3393	femur	Jenkins et al. 2001
Dimorphodon macronyx	YPM 350B	tibia-fibula	de Ricqlès et al. 2000
	YPM 9182E	tibia-fibula	de Ricqlès et al. 2000
Pterodactylus	CM 11430	femur	Padian et al. 2004
		tibia	Padian et al. 2004
Dinosauromorpha			
Dromomeron romeri	GR 221	femur	this study
	GR 253	tibia	this study
	GR 254	tibia	this study
Silesauridae			
Asilisaurus kongwe	NMT RB45	femur	this study
	NMT RB46	femur	this study
	NMT RB47	femur	this study
Silesauridae (GR)	GR 255	humerus	this study
	GR 190	tibia	this study
Dinosauriformes			
Nyasasaurus parringtoni	NHMUK R6586	humerus	Nesbitt et al. 2012
Dinosauria			
Ornithischia			
Fruitadens haagororum	LACM 120478	femur	Butler et al. 2010
	LACM 115727	femur	Butler et al. 2010
Neornithischia, cf. *Lesothosaurus* or *Stormbergia*	NM QR 3076	femur	Knoll et al. 2010
Scutellosaurus lawleri	UCMP 130580	humerus	Padian et al. 2004 (unpublished)

Taxon	Specimen	Element	Slides sectioned by?
Scutellosaurus lawleri	UCMP 170829	femur	Padian et al. 2004
	UCMP 130580	tibia	Padian et al. 2004
Psittacosaurus mongoliensis	PIN 1369/1-11/1948	humerus	Erickson & Tumanova 2000
	PIN 698/4-22/1946	femur	Erickson & Tumanova 2000
		tibia	Erickson & Tumanova 2000
	PIN 698/5-9/2/1946	tibia	Erickson & Tumanova 2000
Saurischia			
Sauropodomorpha			
Plateosaurus engelhardti	SMNS F48-1	femur	Klein 2004
	SMNS F14A	femur	Klein 2004
		tibia	Klein 2004
Massospondylus carinatus	BPI/1/5253a	femur	Chinsamy 1993a
	BPI/1/5241a	femur	Chinsamy 1993a
	BPI/1/4777a	femur	Chinsamy 1993a
Theropoda			
Herrerasaurus ischigualastensis	MCZ 7064	humerus	Padian et al. 2001
		tibia	Padian et al. 2001
Tawa hallae	GR 155	femur	this study
	GR 257	tibia	this study
Coelophysis bauri	AMNH FARB uncat.	tibia	this study
Megapnosaurus rhodesiensis	NMZB QG 715	femur	Chinsamy 1990
	NMZB QG 726	femur	Chinsamy 1990
Coelophysoidea [GR]	GR 256	femur	this study
Coelophysoidea [PEFO]	UCMP 129618	femur	de Ricqlès et al. 2003b
Aves			
Confuciusornis sanctus	NGMC 98-8-2 / MOR 1063	humerus	de Ricqlès et al. 2003a
		femur	de Ricqlès et al. 2003a
		tibia	de Ricqlès et al. 2003a
Hesperornis	YPM PU 22443	tibiotarsus	Houde 1987
Lithornis celetius	USNM 290554	tibiotarsus	Houde 1986
Paracathartes howardae	USNM 361407	tibiotarsus	Houde 1986
Rhynchotus rufescens	PU 728	tibiotarsus	Houde 1986
Crax rubra	USNM 19918	tibiotarsus	Houde 1987
Buteo jamaicensis	UWBM 82968	humerus	Rensberger & Watabe 2000
Corvus corax	UWBM 90537	humerus	Rensberger & Watabe 2000

Taxon	MB Project	MB numbers (xs)	MB numbers (transects with scale bar and other representative images)
Eureptilia			
Captorhinus aguti	p323	M287176, M287188	M287181, M287182, M287183
Diapsida			
Lepidosauria			
Sphenodon punctatus	p859	M152146, M152147	M153610, M153611, M153612, M153613
	p859	M152125, M152126	M153602, M153603, M153604, M153605
	p859	M152116, M152117	M153580, M153581, M153582, M153583
	p859	M152127, M152128	M153588, M153589, M153590
	p859	M152129, M152130	M153591
	p859	M152114, M152115	M153596, M153597, M153598, M153599
Squamata			
Iguana iguana	p323	M286706, M286706	-
	p323	M152658, M152659	M153615, M153616, M153621, M153622
Varanus niloticus	p323	M287203	M287199, M287200, M287201
	p323	M193353	-
	p323	M287192	-
Archosauromorpha			
Trilophosaurus buettneri	p455	M193354	M193362, M193363
	p455	M56153	M193359, M193360, M193361
	p455	M56074	M287222
	p455	M56073	-
	p455	M56077	-
	p455	M153269	-
	p455	M56078	-
	p455	M56076	-
	p455	M153272	-
	p455	M153271	-
	p455	M153274	-
	p455	M153270	-
Archosauriformes			
Vancleavea campi	p323	M57474	-
	p323	M151725, M151726	-
Proterochampsia	p323	M284709	M287219, M287220, M287221
Euparkeria capensis	p323	M151727, M287216	M287217, M287218
Phytosauria	p323	M68235	M287235, M287236
Archosauria			
Pseudosuchia			
Revueltosaurus callenderi	p620	M94275, M94276, M94279, M95080	M94282, M94728, M94729, M94731, M94733, M94734, M94735, M94736, M94737, M94738
Aetosauria	p323	-	M151728
	p323	M94117	-
	p323	M67646, M101796	M303944
Effigia okeeffeae	p323	M283536	M286131, M286132
Loricata, cf. *Postosuchus*	p323	M151729	M287382, M287383, M287384
	p323	M151730	M287391, M287392, M287393
Alligator mississippiensis	p323	M57491	M286197, M286199, M286200
	p323	M102233, M102233	-

Taxon	MB Project	MB numbers (xs)	MB numbers (transects with scale bar and other representative images)
Alligator mississippiensis	p323	M286220	-
	p323	M286213, M286219, M287445	-
	p323	M286221	M287465, M287466
	p323	M286223	-
	p323	M286222	-
	p323	M286224	-
	p323	-	M287480, M287481, M287482, M287483, M287484, M287485
Ornithodira			
Pterosauria			
Eudimorphodon cromptonellis	p323	M57541, M286090, M286091	-
Dimorphodon macronyx	p323	M102229, M287629	-
	p323	M102230, M287628	M287630
Pterodactylus	p323	M151737, M287631	M287677, M287678, M287679, M287680, M287681
	p323	M67564, M67565	M286277
Dinosauromorpha			
Dromomeron romeri	p323	M57537, M287669	M286283, M286284, M286285, M286286, M286287, M286289
	p323	M151735, M287670	M286295, M286296
	p323	M151736, M287627	M286297, M286298, M286299, M286300, M287671, M287672, M287673, M287674, M287675, M287676
Silesauridae			
Asilisaurus kongwe	p323	M151731	M286306, M286307
	p323	M67566, M67567	-
	p323	M151732, M286305	-
Silesauridae (GR)	p323	M151733	M286327, M286328, M287682, M287683
	p323	M286319	M287684, M287685
Dinosauriformes			
Nyasasaurus parringtoni	p485, p323	M67962	M68003, M68021, M68022, M68023, M68024, M68025
Dinosauria			
Ornithischia			
Fruitadens haagororum	p323	M68002	M286600, M286601, M286602, M286603, M286604, M286605
	p323	M68001	M286606, M286607, M286608
Neornithischia, cf. *Lesothosaurus* or *Stormbergia*	p323	M102232	M287910, M287911, M287912
Scutellosaurus lawleri	p323	M57488, M151723, M286579	M286637, M286638, M286639

Taxon	MB Project	MB numbers (xs)	MB numbers (transects with scale bar and other representative images)
Scutellosaurus lawleri	p323	M57519, M57521, M286578	M286640, M286641, M286642
	p323	M151724, M286585	M286643, M286644, M586645
Psittacosaurus mongoliensis	p323	M286576	-
	p323	M286572, M286573	M286646, M286647, M286648
	p323	M286574	-
	p323	M286575	M286649, M286650
Saurischia			
Sauropodomorpha			
Plateosaurus engelhardti	p323	M286582	-
	p323	M286581	-
	p323	M286580	-
Massospondylus carinatus	p323	M102234	M304044, M304045, M304210
	p323	M102235	M287186, M287187, M304046, M304047
	p323	M102236	-
Theropoda			
Herrerasaurus ischigualastensis	p323	M102231	-
	p323	M67905	-
Tawa hallae	p323	M57525, M286704	M304037, M304038, M304039
	p323	M151738, M286705	M304040, M304041, M304042, M304043
Coelophysis bauri	p323	M102237	M286674, M286675
Megapnosaurus rhodesiensis	p323	M151739	-
	p323	M151740	-
Coelophysoidea [GR]	p323	M286583	M286696, M286697, M286698, M286699
Coelophysoidea [PEFO]	p323	M286584	-
Aves			
Confuciusornis sanctus	p323	M304007, M304008	M304013, M304014, M304015
	p323	M304009, M304010	M304021, M304022, M304023
	p323	M304011, M304012	M304029, M304030, M304031
Hesperornis	p323	M287644	M287645, M303966
Lithornis celetius	p323	M287648, M287649	M303967, M303973, M303974, M303975, M303976, M303977, M303978
Paracathartes howardae	p323	M287740, M287741	M303980, M303981, M303982, M303983, M303984, M303985
Rhynchotus rufescens	p323	M287742, M287743	M303989
Crax rubra	p323	M287744, M287745	M303993, M304625
Buteo jamaicensis	p323	M287746	M303996
Corvus corax	p323	M287747	M304001

Taxon	MB numbers (transects with osteocyte squares)	Osteocytes
Eureptilia		
Captorhinus aguti	M287177, M287178, M287179, M287180	M287184
Diapsida		
Lepidosauria		
Sphenodon punctatus	-	M153614
	M153606, M153607, M153608, M153609	-
	M153584, M153585, M153586, M153587	-
	-	-
	M153592, M153593, M153594, M153595	-
	M153600, M153601	-
Squamata		
Iguana iguana	-	-
	M153617, M153618	M153619, M153620
Varanus niloticus	M287195, M287196, M287197	M287198
	M166304, M166305, M166306	M284684, M284685
	M166300, M166301, M166302, M166303	M284686, M284687
Archosauromorpha		
Trilophosaurus buettneri	M56151, M56152	-
	M56150	-
	M56089, M56090, M56091, M56092	M193364
	M56079, M56080, M56081	M286204, M286205
	M56082, M56083, M56084	M286206
	M56099, M56100	M286207
	M56102, M56104	M286208
	M56085, M56806	-
	M56142, M56143	M286709
	M56145, M56146	M286210, M286211
	M56147, M56148, M56149	M286212
	M56144	-
Archosauriformes		
Vancleavea campi	M284688, M284689, M284690, M284691	M298694, M294695
	M284696, M284697, M284698, M284699	M284700, M284701
Proterochampsia	M284702, M284703, M284704, M284705	M284706, M284707
Euparkeria capensis	M286092, M286093, M286094, M286095	M286097, M286098
Phytosauria	M286099, M286100	M286101, M286102
Archosauria		
Pseudosuchia		
Revueltosaurus callenderi	M286103, M286104, M286105, M286106	M94739, M94740
Aetosauria	-	-
	M286122, M286123, M286124	M286127
	M286120, M286121	M286119
Effigia okeeffeae	M286133, M286134, M286135, M286136	M286130
Loricata, cf. *Postosuchus*	M287387, M287388, M287389, M287390	M287385, M287386
	M286188, M286189, M286190, M286191	M286186, M286187
Alligator mississippiensis	M286194, M286195, M286196	M286192, M286193
	-	-

Taxon	MB numbers (transects with osteocyte squares)	Osteocytes
Alligator mississippiensis	-	-
	M286256, M286257	M286253
	M286258, M286259	M286254, M286255
	-	-
	M286260	M286251
	M286261	M286252
	-	-
Ornithodira		
Pterosauria		
Eudimorphodon cromptonellis	M284710	M284711, M284712, M284713, M284714, M284715, M284716
Dimorphodon macronyx	M286264, M286265, M286266	M286262, M286263
	M286268, M286269	M286267
Pterodactylus	M286271, M286272	M286270
	M286273, M286274, M286275	M286276
Dinosauromorpha		
Dromomeron romeri	M286278, M286279, M286280, M286281	M286282
	M286290, M286291, M286292, M286293	M286294
	M286301, M286302, M286303	M286304
Silesauridae		
Asilisaurus kongwe	M286308	M286309
	M286311, M286312	M286310
	M286313, M286314, M286315	M286316, M286317, M286318
Silesauridae (GR)	M286325, M286326, M286331	M286324
	M286332, M286333, M286334	M286329, M286330
Dinosauriformes		
Nyasasaurus parringtoni	M286182, M286183, M286184, M286185	M68007, M68008
Dinosauria		
Ornithischia		
Fruitadens haagororum	M286288, M286609, M286610, M286611	M286598, M286599
	M286612, M286613, M286614, M286615	M286597
Neornithischia, cf. *Lesothosaurus* or *Stormbergia*	M286616, M286617, M286618	M286619, M286620, M286621
Scutellosaurus lawleri	M286622, M286623, M286624, M286625	M286632

Taxon	MB numbers (transects with osteocyte squares)	Osteocytes
Scutellosaurus lawleri	M286626, M286627, M286628	M286633, M286634
	M286629, M286630, M286631	M286635, M286636
Psittacosaurus mongoliensis	-	-
	-	-
	M286651	-
	M286652	-
Saurischia		
Sauropodomorpha		
Plateosaurus engelhardti	M287400, M287401, M287402	-
	M287394, M287395	M286593
	M287396, M287397, M287398, M287399	M286594, M286595, M286596
Massospondylus carinatus	M286656, M286657, M286658	-
	M286654, M286655	M286653, M278185
	-	-
Theropoda		
Herrerasaurus ischigualastensis	M286659, M286660	M286663
	M286661, M286662	M286664
Tawa hallae	M286667, M286668, M286669	M286665
	M286670, M286671, M286672, M286673	M286666
Coelophysis bauri	M286676, M286677, M286678, M286679	M286680
Megapnosaurus rhodesiensis	M286688, M286689, M286690	M286681, M286682
	M286685, M286686, M286687	M286683, M286684
Coelophysoidea [GR]	M286691, M286692, M286693	M286694, M286695
Coelophysoidea [PEFO]	M286701, M286702, M286703	M286700
Aves		
Confuciusornis sanctus	M304016, M304017, M304018, M304019	M304020
	M304024, M304025, M304026, M304027	M304028
	M304032, M304033, M304034, M304035	M304036
Hesperornis	M287646, M287647	-
Lithornis celetius	M303968, M303969, M303970, M303971	M303972
Paracathartes howardae	M303986, M303987, M303988	M303979
Rhynchotus rufescens	M303990, M303991, M303992	-
Crax rubra	M303994, M303995	-
Buteo jamaicensis	M303997, M303998, M303999	M304000
Corvus corax	M304002, M304003, M304004, M304005	M304006

Table 2.2 Histological measurements for specimens examined in this study. For each sample, the following measurements are given: mid-diaphyseal circumference (MSC); mid-diaphyseal diameters (MDD) along the major axis (MA) and minor axis (ma); medullary cavity diameter (MCD) along the major and minor axes; average cortical thickness (ACT); relative bone wall thickness (RBT); osteocyte density (OD); and number of lines of arrested growth (LAGs) preserved.

Taxon	Specimen	Element	MSC (mm)	MSD (mm; MA x ma)
Eureptilia				
Captorhinus aguti	UCMP 223509	humerus	11.36	4.08 x 2.69
Diapsida				
Lepidosauria				
Sphenodon punctatus	CMC 047	femur	9.80	3.19 x 2.61
	JC A	femur	11.31	3.71 x 2.99
	JC 57	femur	11.83	3.76 x 3.19
	JC 58	femur	13.64	4.23 x 3.58
	JC 807	femur	12.98	3.75 x 3.37
	JC 833	femur	12.11	3.77 x 3.39
Squamata				
Iguana iguana	UCMP 68286	humerus	12.81 (est.)	4.5 (est.) x 3.20
	UCMP 68288	tibia	11.98 (est.)	4.06 x 3.55
Varanus niloticus	UCMP 223456	femur	NE	4.73 x 4.32
	VdB uncatalogued	femur	12.83	4.00 x 3.68
	VdB uncatalogued	tibia	10.22	3.48 x 2.62
Archosauromorpha				
Trilophosaurus buettneri	TMM 31025-849	humerus	NE	19.47 x 18.61
	TMM 31025-928	ulna	NE	16.8 (est.) x 7.92
	TMM 31025-787	femur	22.41	7.13 x 6.04
	TMM 31025-1064	femur	28.18	8.80 x 7.80
	TMM 31025-1063	femur	38.10	12.5 x 10.4
	TMM 31025-885	femur	52.9 (est.)	17.93 x 15.66
	TMM 31025-862	femur	NE	22.9 (est.) x 18.58
	TMM 31025-786	femur	81.5 (est.)	22.96 x 21.55
	TMM 31025-788	tibia	NE	6.82 x 5.82
	TMM 31025-747	tibia	NE	8.74 x 6.3 (est.)
	TMM 31025-887	tibia	NE	13.35 x 9.97
	TMM 31025-741	tibia	NE	14.49 x 10.6 (est.)
Archosauriformes				
Vancleavea campi	UCMP 152662	femur	27.36	8.49 x 7.86
	GR 250	femur	27.66	8.66 x 8.31
Proterochampsia, cf. *Chanaresuchus*	MCZ 4038	femur	32.2 (est.)	11.0 (est.) x 9.45
Euparkeria capensis	AMNH FARB 2238	femur	13.9 (est.)	5.13 x 3.55
Phytosauria	UCMP 25921	femur	NE	NE (inc.)
Archosauria				
Pseudosuchia				
Revueltosaurus callenderi	PEFO 33843	femur	41.23	15.07 x 9.44
Aetosauria	UCMP 25914	femur	NE	NE (inc.)
	GR 252	tibia	23.23	7.87 x 5.50
Effigia okeeffeae	AMNH FARB 30587	femur	NE	NE (inc.)
Loricata, cf. *Postosuchus*	UCMP 28353	humerus	NE	29 x 16 (est.)
	UCMP 25906	femur	NE	NE
Alligator mississippiensis	UCMP 68331	femur	NE	NE
	UCMP 68314	tibia	NE	9.57 x ?
	UF FWC 40723	humerus	37.7 (est.)	12 x 12
	UF FWC 40723	femur	48.9 (est.)	16.2 x 13 (est.)

Taxon	Specimen	Element	MSC (mm)	MSD (mm; MA x ma)
Alligator mississippiensis	UF FWC 40723	tibia	34.6 (est.)	11 x 11
	UF FWC 40583	humerus	34.6 (est.)	11 x 11
	UF FWC 40583	femur	NE	14.5 x 11
	UF FWC 40583	tibia	31.5 (est.)	10.5 x 9.5
	UF FWC LGS1	femur	NE	22 x 18.5
Ornithodira				
Pterosauria				
Eudimorphodon cromptonellis	MGUH VP 3393	femur	4.00	1.42 x 0.90
Dimorphodon macronyx	YPM 350B	tibia-fibula	NE	NE
	YPM 9182E	tibia-fibula	NE	NE
Pterodactylus	CM 11430	femur	14.28	4.44 x 3.96
	CM 11430	tibia	12.60	4.17 x 3.27
Dinosauromorpha				
Dromomeron romeri	GR 221	femur	28.19	9.17 x 7.57
	GR 253	tibia	28.86	9.43 x 7.63
	GR 254	tibia	21.83	6.39 x 6.30
Silesauridae				
Asilisaurus kongwe	NMT RB45	femur	NE	NE
	NMT RB46	femur	NE	NE
	NMT RB47	femur	NE	NE
Silesauridae (GR)	GR 255	humerus	27.94	9.27 x 7.44
	GR 190	tibia	NE	NE
Dinosauriformes				
Nyasasaurus parringtoni	NHMUK R6586	humerus	60.10	20.3 x 15.4
Dinosauria				
Ornithischia				
Fruitadens haagororum	LACM 120478	femur	14.1 (est.)	4.25 x 3.90
	LACM 115727	femur	20.9 (est.)	7.10 x 5.40
Neornithischia, cf. *Lesothosaurus* or *Stormbergia*	NM QR 3076	femur	NE	27.5 x 25.1
Scutellosaurus lawleri	UCMP 130580	humerus	17.58	6.04 x 4.51
	UCMP 170829	femur	NE	? x 9.69
	UCMP 130580	tibia	NE	NE
Psittacosaurus mongoliensis	PIN 1369/1-11/1948	humerus	NE	9.4 x 9.0
	PIN 698/4-22/1946	femur	NE	9.48 x ?
	PIN 698/4-22/1946	tibia	NE	10.00 x ?
	PIN 698/5-9/2/1946	tibia	78.27	25.82 x 16.89
Saurischia				
Sauropodomorpha				
Plateosaurus engelhardti	SMNS F48-1	femur	NE	NE
	SMNS F14A	femur	NE	NE
	SMNS F14A	tibia	NE	NE
Massospondylus carinatus	BPI 5253a	femur	NE	14.3 x 13.0
	BPI 5241a	femur	148 (est.)	47.74 x 36.21
	BPI 4777a	femur	NE	30.74 x 29.32
Theropoda				
Herrerasaurus ischigualastensis	MCZ 7064	humerus	NE	NE

Taxon	Specimen	Element	MSC (mm)	MSD (mm; MA x ma)
Herrerasaurus ischigualastensis	MCZ 7064	tibia	NE	NE
Tawa hallae	GR 155	femur	36.84	10.99 x 10.89
	GR 257	tibia	21.88	6.55 x 6.30
Coelophysis bauri	AMNH FARB uncat.	tibia	47 (est.)	15 x 13 (est.)
Megapnosaurus rhodesiensis	NMZB QG 715	femur	44.45	14.40 x 12.51
	NMZB QG 726	femur	NE	21.41 x 20.72
Coelophysoidea [GR]	GR 256	femur	66.37	20.81 x 17.78
Coelophysoidea [PEFO]	UCMP 129618	femur	NE	NE
Aves				
Confuciusornis sanctus	NGMC 98-8-2 / MOR 1063	humerus	NE	NE
	NGMC 98-8-2 / MOR 1063	femur	NE	NE
	NGMC 98-8-2 / MOR 1063	tibia	NE	NE
Hesperornis	YPM PU 22443	tibiotarsus	54.46	19.01 x 13.78
Lithornis celetius	USNM 290554	tibiotarsus	20.11	6.99 x 5.18
Paracathartes howardae	USNM 361407	tibiotarsus	30.8 (est.)	10.24 x 7.65
Rhynchotus rufescens	PU 728	tibiotarsus	17.4 (est.)	6 x 5
Crax rubra	USNM 19918	tibiotarsus	NE	NE
Buteo jamaicensis	UWBM 82968	humerus	28.93	9.45 x 8.24
Corvus corax	UWBM 90537	humerus	26.5 (est.)	8.51 x 7.12

Taxon	MCD (mm; MA x ma)	ACT (mm; # measures)	RBT	OD (cells/mm2)	GMs preserved
Eureptilia					
Captorhinus aguti	1.77 x 1.27	0.80; 4	23.7%	1,475	3
Diapsida					
Lepidosauria					
Sphenodon punctatus	1.36 x 0.91	0.82; 4	28.3%	NE	19
	1.61 x 0.67	1.00; 4	29.6%	437	20
	1.15 x 0.66	1.19; 4	34.2%	449	22
	1.84 x 1.61	0.96; 4	24.6%	NE	28
	1.06 x 0.81	0.96; 4	27.0%	465	31
	1.51 x 1.07	1.04; 4	29.1%	382	26
Squamata					
Iguana iguana	2.76 x 1.80	0.73;3	19.0%	NE	3 or 4
	2.31 x 1.82	0.78; 3	20.5%	1,224	4
Varanus niloticus	1.79 x 1.63	1.35; 4	29.8%	1,146	4
	1.50 x 1.41	1.14; 4	29.7%	1,637	NE
	1.54 x 1.12	0.87; 4	28.5%	1,578	NE
Archosauromorpha					
Trilophosaurus buettneri	13.13 x 11.89	3.18; 4	16.7%	816	15+
	9.08 x 4.29	2.17; 3	17.6%	1,169	14+
	4.55 x 3.73	1.20; 4	18.2%	1,245	3 or 4
	5.91 x 5.22	1.34; 4	16.1%	1,415	4 or 5
	8.51 x 7.51	1.72; 4	15.0%	1,053	8+
	12.32 x 11.36	2.51; 4	14.9%	1,102	8
	16.02 x 13.53	2.81; 3	13.5%	1,047	12 or 13
	15.83 x 14.87	3.52; 4	15.8%	924	8+
	3.73 x 2.84	1.48; 4	23.4%	1,775	5
	5.07 x 3.52	1.62; 4	21.5%	1,397	7+
	9.49 x 6.17	1.92; 4	16.5%	1,144	10+
	8.17 x 5.06	2.77; 3	22.1%	1,441	21
Archosauriformes					
Vancleavea campi	5.23 x 4.23	1.72; 4	21.0%	1,672	3
	2.60 x 2.34	3.01;4	35.4%	1,808	2 annuli
Proterochampsia, cf. *Chanaresuchus*	6.86 x 6.82	1.60; 4	15.6%	1,582	0
Euparkeria capensis	1.34 x 1.33	1.40;4	32.3%	2,157	5
Phytosauria	20.9 (est.) x 12.64	5.10; 2	NE	1,855	8+
Archosauria					
Pseudosuchia					
Revueltosaurus callenderi	6.50 x 4.10	2.48; 4	20.2%	1,287	5
Aetosauria	NE	6.91; 4	NE	971	18+
	5.36 x 3.12	1.08; 4	16.2%	1,742	0
Effigia okeeffeae	NE	6.81; 3	NE	1,869	6
Loricata, cf. *Postosuchus*	NE	4.34; 4	NE	992	20+
	NE	7.02; 4	NE	1,857	10+
Alligator mississippiensis	NE	2.10; 3	NE	974	4 annuli
	NE	3.37; 3	NE	NE	5 annuli
	NE	4.81; 3	40.1%	NE	4 annuli
	4.2 x 4.0 (est.)	5.09; 4	34.9%	638	4 annuli

Taxon	MCD (mm; MA x ma)	ACT (mm; # measures)	RBT	OD (cells/mm2)	GMs preserved
Alligator mississippiensis	NE	3.50; 3	31.9%	399	4 annuli
	NE	4.30; 3	39.1%	NE	14 annuli
	NE	4.61; 3	36.2%	554	15 annuli
	NE	3.69; 3	36.9%	528	13 annuli
	NE	7.1; 4	35.2%	571	8 annuli
Ornithodira					
Pterosauria					
Eudimorphodon cromptonellis	1.14 x 0.70	0.12; 4	10.3%	1,600.	0
Dimorphodon macronyx	NE	0.61; 3	NE	1,634	0
	NE	0.51; 3	NE	2,518	0
Pterodactylus	2.91 x 2.60	0.71; 4	16.9%	2,817	0
	2.56 x 1.91	0.73; 4	19.6%	2,511	0
Dinosauromorpha					
Dromomeron romeri	6.45 x 5.20	1.25; 4	14.9%	1,756	3
	6.04 x 4.77	1.56; 4	18.3%	1,978	1
	3.95 x 3.83	1.23; 4	19.4%	2,080.	2 (1 annulus)
Silesauridae					
Asilisaurus kongwe	NE	1.62; 3	NE	1,969	0
	NE	1.60; 3	NE	2,604	0
	NE	1.99; 3	NE	2,247	0
Silesauridae (GR)	5.55 x 3.87	1.83; 4	21.9%	1,995	1
	NE	3.05; 4	NE	3,005	3
Dinosauriformes					
Nyasasaurus parringtoni	10.2 x 7.5	4.2; 8	23.5%	1,777	1 annulus
Dinosauria					
Ornithischia					
Fruitadens haagororum	2.82 x 2.16	0.76; 4	18.7%	3,409	1
	4.76 x 3.81	0.96; 4	15.4%	3,265	4 (2 annuli)
Neornithischia, cf. *Lesothosaurus* or *Stormbergia*	17.9 x 15.9	4.2; 3	15.9%	2,273	4+
Scutellosaurus lawleri	3.16 x 1.83	1.39; 4	26.3%	2,732	5 (3 annuli)
	7.79 x 4.12	2.87; 3	NE	1,408	6 annuli
	NE	1.63; 4	NE	3,200.	5 (2 annuli)
Psittacosaurus mongoliensis	3.49 x 3.01	2.92; 4	31.7%	NE	3
	5.23 x 4.61	2.00; 3	NE	NE	3
	5.46 x ?	2.30; 2	NE	1,844	2 or 3
	12.39 x 6.11	5.92; 4	27.7%	2,167	6
Saurischia					
Sauropodomorpha					
Plateosaurus engelhardti	NE	14.4; 1	NE	1,313	5
	NE	NE	NE	1,117	2
	NE	>16; 1	NE	1,269	7
Massospondylus carinatus	8.4 x 7.2	2.9; 4	21.2%	2,692	0
	30.57 x 18.54	8.02; 2	19.1%	1,191	13 or 14
	18.78 x 16.52	5.40; 4	17.9%	NE	10
Theropoda					
Herrerasaurus ischigualastensis	NE	5.25; 2	NE	1,709	1

Taxon	MCD (mm; MA x ma)	ACT (mm; # measures)	RBT	OD (cells/mm2)	GMs preserved
Herrerasaurus ischigualastensis	NE	7.09; 2	NE	1,972	4 or 5 (1 annulus)
Tawa hallae	8.10 x 7.87	1.46; 4	13.3%	1,487	3 (2 annuli)
	4.25 x 3.33	1.29; 4	20.1%	1,708	3
Coelophysis bauri	10 x 7.5 (est.)	2.86; 4	20.4%	1,849	2 (1 annulus)
Megapnosaurus rhodesiensis	8.99 x 7.91	2.44; 4	18.1%	2,473	0 (3 bands)
	12.31 x 11.64	4.59; 3	23.4%	2,492	2
Coelophysoidea [GR]	12.73 x 9.95	3.98; 4	20.6%	3,364	2 (1 annulus)
Coelophysoidea [PEFO]	NE	4.43; 3	NE	2,001	0
Aves					
Confuciusornis sanctus	NE	0.91; 4	NE	1,878.	2
	NE	0.57; 4	NE	2,056.	2
	NE	0.55; 4	NE	2,341.	2
Hesperornis	9.90 x 8.00	3.57; 4	21.8%	2,778	1
Lithornis celetius	5.11 x 3.57	0.86; 4	14.1%	2,198	0
Paracathartes howardae	7.52 x 5.21	1.27; 4	14.2%	1,924	1 or 2
Rhynchotus rufescens	5 x 4	0.87; 3	15.8%	2,524	2 (1 annulus)
Crax rubra	NE	0.80; 3	NE	2,540.	2
Buteo jamaicensis	7.34 x 3.68	0.98; 4	11.1%	2,285	0
Corvus corax	6.55 x 5.44	0.87; 4	11.1%	1,706	0

Table 2.3 Summary of histological conditions for each taxon examined in this study. Character states are described in Chapter 1. Abbreviations: FLB, fibrolamellar bone; GMs, growth marks

Taxon	Fiber Type, Most Disorganized	Fiber Type, Dominant	Canal Type, Most Developed	Canal Type, Dominant
Eureptilia				
Captorhinus aguti	parallel-fibered	parallel-fibered	primary osteon	simple primary canal
Diapsida				
Lepidosauria				
Sphenodon punctatus	parallel-fibered	parallel-fibered	avascular/NA	avascular/NA
Squamata				
Iguana iguana	parallel-fibered	lamellar	simple primary canal	avascular/NA
Varanus niloticus	parallel-fibered	parallel-fibered	primary osteon	primary osteon
Archosauromorpha				
Trilophosaurus buettneri	lamellar	lamellar	simple primary canal	simple primary canal
Archosauriformes				
Vancleavea campi (PEFO)	weakly woven-fibered	parallel-fibered	primary osteon	primary osteon
Vancleavea campi (GR)	woven-fibered	woven-fibered	primary osteon	primary osteon
Proterochampsia, cf. *Chanaresuchus*	weakly woven-fibered	parallel-fibered	simple primary canals	simple primary canals
Euparkeria capensis	parallel-fibered	parallel-fibered	primary osteon	primary osteon
Phytosauria	woven-fibered	parallel-fibered	primary osteon	primary osteon
Archosauria				
Pseudosuchia				
Revueltosaurus callenderi	parallel-fibered	parallel-fibered	simple primary canal	simple primary canal
Aetosauria	woven-fibered	woven/parallel	primary osteon	primary osteon
Effigia okeeffeae	woven-fibered	woven-fibered	primary osteon	primary osteon
Loricata, cf. P*ostosuchus*	weakly woven-fibered	parallel-fibered	primary osteon	primary osteon
Alligator mississippiensis	woven-fibered	weakly woven-fibered	primary osteon	primary osteon
Ornithodira				
Pterosauria				
Eudimorphodon cromptonellis	parallel-fibered	parallel-fibered	primary osteon	primary osteon
Dimorphodon macronyx	woven-fibered	parallel-fibered	primary osteon	primary osteon
Pterodactylus	woven-fibered	woven-fibered	PFB primary osteon	PFB primary osteon
Dinosauromorpha				
Dromomeron romeri	woven-fibered	woven/lamellar	primary osteon	primary osteon
Silesauridae				
Asilisaurus kongwe	woven-fibered	woven-fibered	PFB primary osteon	PFB primary osteon
Silesauridae (GR)	woven-fibered	woven-fibered	primary osteon	primary osteon
Dinosauriformes				
Nyasasaurus parringtoni	woven-fibered	woven-fibered	primary osteon	primary osteon

Taxon	Fiber Type, Most Disorganized	Fiber Type, Dominant	Canal Type, Most Developed	Canal Type, Dominant
Dinosauria				
Ornithischia				
Fruitadens haagororum	woven-fibered	parallel-fibered	primary osteon	primary osteon
Neornithischia, cf. *Lesothosaurus* or *Stormbergia*	parallel-fibered	parallel-fibered	primary osteon	primary osteon
Scutellosaurus lawleri	woven-fibered	parallel-fibered	primary osteon	primary osteon
Psittacosaurus mongoliensis	woven-fibered	woven-fibered	primary osteon	primary osteon
Saurischia				
Sauropodomorpha				
Plateosaurus engelhardti	woven-fibered	woven-fibered	primary osteon	primary osteon
Massospondylus carinatus	woven-fibered	parallel-fibered	primary osteon	simple primary canal
Theropoda				
Herrerasaurus ischigualastensis	woven-fibered	woven-fibered	primary osteon	primary osteon
Tawa hallae	woven-fibered	woven/parallel	primary osteon	primary osteon
Coelophysis bauri	woven-fibered	woven-fibered	primary osteon	primary osteon
Megapnosaurus rhodesiensis	woven-fibered	woven-fibered	primary osteon	primary osteon
Coelophysoidea [GR]	woven-fibered	woven-fibered	primary osteon	primary osteon
Coelophysoidea [PEFO]	woven-fibered	woven-fibered	primary osteon	primary osteon
Aves				
Confuciusornis sanctus	woven-fibered	woven-fibered	primary osteon	primary osteon
Hesperornis	woven-fibered	woven-fibered	PFB primary osteon	PFB primary osteon
Lithornis celetius	woven-fibered	woven-fibered	primary osteon	primary osteon
Paracathartes howardae	woven-fibered	woven/parallel	primary osteon	primary osteon/ PFB primary osteon
Rhynchotus rufescens	woven-fibered	woven-fibered	PFB primary osteon	PFB primary osteon
Crax rubra	woven-fibered	woven/parallel	primary osteon	primary osteon
Buteo jamaicensis	woven-fibered	woven-fibered	primary osteon	primary osteon
Corvus corax	woven-fibered	woven/parallel	primary osteon	PFB primary osteon

Taxon	True FLB?	Vascular Density, Maximum	Vascular Density, Dominant	Extent of Anastomoses	Vascular Pattern, Maximum
Eureptilia					
Captorhinus aguti	absent	moderate	moderate	few	circumferential
Diapsida					
Lepidosauria					
Sphenodon punctatus	absent	avascular	avascular	none	avascular/NA
Squamata					
Iguana iguana	absent	poor	avascular	none	longitudinal
Varanus niloticus	absent	moderate	moderate	none	radial
Archosauromorpha					
Trilophosaurus buettneri	absent	moderate	poor	none	longitudinal, radial rows
Archosauriformes					
Vancleavea campi (PEFO)	possibly?	moderate	poor	rare, short	longitudinal, circumferential rows
Vancleavea campi (GR)	present	well	well	common, short	longitudinal, random
Proterochampsia, cf. *Chanaresuchus*	absent	well	moderate	common, short to moderate	small reticulations
Euparkeria capensis	absent	moderate	moderate	common, short	short anastomoses in all directions
Phytosauria	present	well	well	common, long	plexiform
Archosauria					
Pseudosuchia					
Revueltosaurus callenderi	absent	poor	poor	rare, short	short radial anastomoses
Aetosauria	present	well	well/moderate	common, moderate	small reticulations
Effigia okeeffeae	present	well	well	common, moderate	plexiform
Loricata, cf. P*ostosuchus*	present	well	moderate	common, moderate	short anastomoses in all directions
Alligator mississippiensis	present	well	moderate	common, moderate	radial, oblique anastomoses
Ornithodira					
Pterosauria					
Eudimorphodon cromptonellis	absent	moderate	moderate	rare, short	short radial anastomoses
Dimorphodon macronyx	present	moderate	moderate	variable, short	short radial anastomoses
Pterodactylus	absent (PFB PO)	well	well	common, moderate	small reticulations
Dinosauromorpha					
Dromomeron romeri	present	well	well/moderate	rare, short	isolated longitudinal in radial rows
Silesauridae					
Asilisaurus kongwe	absent (PFB PO)	well	well/moderate	common, moderate	small reticulations
Silesauridae (GR)	present	well	well	common, moderate	small reticulations
Dinosauriformes					
Nyasasaurus parringtoni	present	well	well	common, short	short radial

Taxon	True FLB?	Vascular Density, Maximum	Vascular Density, Dominant	Extent of Anastomoses	Vascular Pattern, Maximum
Dinosauria					
Ornithischia					
Fruitadens haagororum	present (uncommon)	well	moderate	common, short	radial
Neornithischia, cf. *Lesothosaurus* or *Stormbergia*	absent	very well	well	common, long	circumferential
Scutellosaurus lawleri	present	well	moderate	rare, short	short radial anastomoses
Psittacosaurus mongoliensis	present	well	well	common, moderate	radial or small reticulations
Saurischia					
Sauropodomorpha					
Plateosaurus engelhardti	present	well	well	common, long	circumferential
Massospondylus carinatus	(uncommon)	well	well	common, long	plexiform
Theropoda					
Herrerasaurus ischigualastensis	present	well	well	common, long	plexiform
Tawa hallae	present	well	well/moderate	rare, short	small reticulations
Coelophysis bauri	present	well	well	rare, short	short circumferential anastomoses
Megapnosaurus rhodesiensis	present	well	well	common, short	circumferential or short radial anastomoses
Coelophysoidea [GR]	present	well	well	common, short	short anastomoses in all directions
Coelophysoidea [PEFO]	present	very well	well	common, moderate	subplexiform
Aves					
Confuciusornis sanctus	present	moderate	moderate	common, short	small reticulations
Hesperornis	absent (PFB PO)	well	moderate	common, short or moderate	reticulations
Lithornis celetius	present	well	moderate	common, short	short circumferential or oblique anastomoses
Paracathartes howardae	present	well	well/moderate	common, long	circumferential
Rhynchotus rufescens	absent (PFB PO)	well	well/moderate	rare, short	short oblique anastomoses
Crax rubra	present	well	moderate	rare, short	circumferential or oblique anastomoses
Buteo jamaicensis	present	well	well/moderate	variable, variable	subplexiform or small reticulations
Corvus corax	present (uncommon)	well	variable: poor to well	variable, variable	subplexiform or small reticulations

Taxon	Vascular Pattern, Dominant	Osteocyte Orientation	Osteocyte Density	Cortical GMs?
Eureptilia				
Captorhinus aguti	isolated longitudinal in radial rows	perpendicular	1475	several
Diapsida				
Lepidosauria				
Sphenodon punctatus	avascular	perpendicular	440.	many
Squamata				
Iguana iguana	avascular	perpendicular	1224	several
Varanus niloticus	radial	perpendicular	1472	several
Archosauromorpha				
Trilophosaurus buettneri	isolated longitudinal	perpendicular	1199	many
Archosauriformes				
Vancleavea campi (PEFO)	isolated longitudinal in circumferential rows	mostly perpendicular	1671	several
Vancleavea campi (GR)	isolated longitudinal	random	1808	few
Proterochampsia, cf. *Chanaresuchus*	reticular	perpendicular to random	1582	none
Euparkeria capensis	isolated longitudinal in radial rows	mostly perpendicular	2157	several
Phytosauria	circumferential	random	1855	many
Archosauria				
Pseudosuchia				
Revueltosaurus callenderi	isolated longitudinal	parallel or oblique	1287	several
Aetosauria	small reticulations	random or parallel	1214	many
Effigia okeeffeae	small reticulations	random	1869	several
Loricata, cf. P*ostosuchus*	circumferential anastomoses	random	1518	many
Alligator mississippiensis	radial anastomoses	random	608	many
Ornithodira				
Pterosauria				
Eudimorphodon cromptonellis	isolated longitudinal	mostly perpendicular	1600.	none
Dimorphodon macronyx	isolated longitudinal in radial rows	random	2040.	none
Pterodactylus	small reticulations	random	2629	none
Dinosauromorpha				
Dromomeron romeri	isolated longitudinal in radial rows	random	1951	few
Silesauridae				
Asilisaurus kongwe	small reticulations	random	2320.	none
Silesauridae (GR)	small reticulations	random	2661	few
Dinosauriformes				
Nyasasaurus parringtoni	directions	random	1777	few

Taxon	Vascular Pattern, Dominant	Osteocyte Orientation	Osteocyte Density	Cortical GMs?
Dinosauria				
Ornithischia				
Fruitadens haagororum	isolated longitudinal	mostly perpendicular	3348	several
Neornithischia, cf. *Lesothosaurus* or *Stormbergia*	circumferential	perpendicular	2273	several
Scutellosaurus lawleri	isolated longitudinal in radial rows	perpendicular	2344	several
Psittacosaurus mongoliensis	isolated longitudinal in radial rows	random	1982	several
Saurischia				
Sauropodomorpha				
Plateosaurus engelhardti	circumferential	random	1256	several
Massospondylus carinatus	anastomoses	perpendicular	1735	many
Theropoda				
Herrerasaurus ischigualastensis	plexiform, reticular	random	1857	several
Tawa hallae	islolated longitudinal in circumferential rows	random	1604	few
Coelophysis bauri	isolated longitudinal canals	random	1849	few
Megapnosaurus rhodesiensis	short anastomoses in all directions	random	2485	several
Coelophysoidea [GR]	short circumferential or radial anastomoses	random	3364	few
Coelophysoidea [PEFO]	small reticulations	random	2001	none
Aves				
Confuciusornis sanctus	short anastomoses in all directions	random	2053	none
Hesperornis	small reticulations	random	2778	none
Lithornis celetius	short oblique or isolated longitudinal	random	2198	none
Paracathartes howardae	circumferential/ short circumferential anastomoses	random or perpendicular	1924	one
Rhynchotus rufescens	isolated longitudinal	random	2524	one
Crax rubra	isolated longitudinal	random	2540	none
Buteo jamaicensis	small reticulations	random	2285	none
Corvus corax	variable	random	1706	none

CHAPTER THREE

The femoral microstructure of Recent and extinct marsupials

ABSTRACT

Bone microstructure is influenced by many factors, including body size, growth rate, and phylogeny. Among extant mammals, the bone tissue of placentals has been fairly well characterized (especially that of xenarthrans, some laurasiatheres, and euarchontoglirans), and is known to vary with size and ecology. The bones of small placentals are composed of poorly vascularized lamellar or parallel-fibered tissue, though woven-fibered bone may be present in juveniles. The primary bone tissue of larger taxa is woven-fibered and well vascularized during the active phase of growth; the end of growth is signified by a thin layer of lamellar or parallel-fibered bone in the outermost cortex. The literature acknowledges no great differences between marsupial and placental bone histology, and so a common histological signature for therian mammals might be inferred. Comparative data on marsupials, however, are lacking, and without these data, larger questions regarding the relationship between marsupial growth strategies and bone microstructure and the plesiomorphic conditions of therian osteohistology and growth strategy cannot be addressed.

I sampled the mid-diaphyseal femora of more than 50 extant and extinct marsupial species, as well as some afrotherian, xenarthran, and laurasiatherian placentals. My marsupial sample encompasses all extant orders, spans a 10 g-2500 kg size range, and comprises mainly wild-caught animals. Small marsupials are histologically similar to placentals of similar size; woven-fibered bone, when present, is restricted to the innermost cortex, and most of the cortex is composed of nearly avascular parallel-fibered or lamellar bone. Lines of arrested growth (LAGs) are present in species that hibernate or experience extended bouts of daily torpor. Marsupials > ~50 g typically produce moderately to well vascularized woven bone early in life, but after 1-2 years, they only deposit poorly vascularized parallel-fibered lamellar bone. This pattern continues for several years, based on the presence of LAGs, which are often preserved in the inner, middle, and outer cortex. Remodeling is rare in marsupials except among the Vombatiformes. The histological pattern of larger marsupials differs from those of the large-bodied ungulates (exclusively well-vascularized woven bone) and primates (often, heavily remodeled bone) that dominate the literature, but interestingly, a similar pattern occurs in some afrotheres and xenarthrans. However, this pattern is far from universal among placental mammals.

The main factors influencing marsupial bone microstructure are life history and body size. The histological differences resulting from body size are subtle, occur gradually, and hold across six of the seven extant orders. The uniformity of marsupial bone histology reflects uniformity of their life history, especially related to the ontogeny of growth rates. Across all body sizes, marsupials share a common ontogeny: they are extremely altricial, experience their time of fastest growth at or just prior to weaning, and then continue to grow at lower rates for an extended period relative to their lifespan. Among placental mammals, histological variability likely reflects greater diversity in the ontogeny of growth rates. It is likely that

sampling biases have obscured both size and phylogenetic signals in the distribution of mammalian bone growth patterns.

INTRODUCTION

Comparative life history studies require an understanding of at least the relative age and growth rate of the individuals involved, in order to speak to the timing of key life events (Morris 1972; Sánchez-Villagra 2010). For some extant taxa, age, growth rate, and longevity may be directly observed, but for rare taxa, animals in the wild, dead individuals, and extinct forms, this is not possible. In these cases, age must be estimated, and growth rates reconstructed from ontogenetic series of individuals.

In reconstructing mammalian life history, a number of methods are commonly used to estimate relative age and growth (for more detailed summaries, see Morris 1972, Klevezal 1996, and Sánchez-Villagra 2010). These include morphometric studies of allometry in the cranial and postcranial skeleton (e.g., Hersch 1934; Radinsky 1984; Lammers and German 2002); dental eruption sequences (e.g., Brown 1895; Spinage 1973; Asher and Olbricht 1999; Smith 2000; Billet and Martin 2011); epiphyseal fusion sequences (e.g., Washburn 1946; Morris 1971; Roth 1984; Geiger et al. 2013); tooth wear analyses (e.g., Severinghaus 1949; Spinage 1973); odontochronology (e.g., Scheffer 1950; Spinage 1973; Clout 1982; Burke 1993); extent of bone remodeling (e.g., Kerley 1965; Alquist and Damsten 1969; Stover et al. 1992, Mulhern and Ubelaker 2003); cortical or trabecular thickness (e.g., Thompson 1980; Streeter and Stout 2003); and skeletochronology of cranial elements (e.g., Laws 1960; Klevezal and Povalishina 1970; Frylestam and von Schantz 1977; de Buffrénil et al. 2004; de Buffrénil and Lambert 2011). One method less commonly used is the histological analysis and skeletochronology of long bones (e.g., Klevezal 1996; Castanet et al. 2004; Köhler and Moyà-Solà 2009; García-Martínez et al. 2011; Köhler et al. 2012).

Skeletochronological studies estimate age based on the annual growth marks (AGMs; annuli and lines of arrested growth, or LAGs) deposited in bony tissues. Annual growth marks are known to occur in all major vertebrate groups and are plesiomorphic for tetrapods (de Ricqlès 1975, 1976). They occur in fast and slow growers, in endotherms and ectotherms, and are visible in extant and fossil bone (de Ricqlès 1975, 1976; Castanet et al. 1993). Although similar lines can form during times of physiological stress (such as hibernation, birth, or weaning; Castanet et al. 2004; García-Martínez et al. 2011), experimental studies have shown that the annual lines reflect endogenous rhythms (Klevezal 1975, 1996; Castanet et al. 2004). Even in the absence of AGMs, the bone tissues can provide a qualitative assessment of growth rate over time: several microstructural characters are known to vary with bone deposition rate, whole body growth rate, and metabolic rate (see Chapters 1 and 2 for summaries and references).

There are several reasons why long bone skeletochronology is not often used in studies of mammalian growth. First, as stated above, the method relies on annual recording structures such as LAGs and annuli. Any mammal that finishes growing in less than a year would not be expected to record annual growth marks. In mammals whose growth lasts a year or more, bone tissue may be secondarily remodeled, obscuring the initial growth record (e.g.,

Amprino and Godina 1947; Enlow and Brown 1958; Hall 2005). Additionally, some taxa live for years after reaching their growth asymptote, and so even if growth marks were visible, they would underestimate the actual age (Castanet et al. 2004; Castanet 2006). Finally, because the method is not as commonly used, the comparative dataset might be considered relatively small, especially compared to that of reptiles or amphibians (Castanet 2006).

However, there are several advantages to using bone histological and skeletochronological analyses to study age, growth, and life history in mammals, especially in combination with other methods described above. First, many of the methods listed above require series of individuals to make any statements about ontogenetic change. For example, external measurements from a single skeletal element would not offer much insight into ontogenetic changes in limb allometry. Conversely, a histological assessment of a single bone always provides some ontogenetic information, because bone is deposited over time and the previous record is often retained. In taxa that do not produce LAGs or annuli, qualitative assessments of ontogenetic stage and changes in growth through time are possible, based on changes in bone microstructure through the cortex (Amprino and Godina 1947; Enlow and Brown 1958; de Ricqlès 1975, 1976; Castanet et al. 1993). In taxa that do produce LAGs, numerical estimates of minimum age can be given, in addition to qualitative observations.

Bone histological studies also allow comparisons between extinct and extant taxa; fossil bone often preserves bone microstructural details (Enlow and Brown 1958; de Ricqlès 1975, 1976; Hurum and Chinsamy 2012), allowing insight into the growth dynamics of extinct mammals. Many histological characters that can be observed and measured in samples of Recent bone (e.g., vascular density, collagen fiber orientation, osteocyte lacunar density) can also be observed and measured in fossil bone (Enlow and Brown 1958; de Ricqlès 1975, 1976; Chinsamy-Turan 2005; Hurum and Chinsamy 2012). Because sampling methods for undecalcified fossilized and Recent bone are similar (Enlow and Brown 1956; de Ricqlès 1975; Lamm 2013), direct comparisons between fossil and Recent bone can be made. A large histological dataset of non-mammaliaform synapsids (e.g., Ray et al. 2004, 2009; Green et al. 2010; Botha-Brink et al. 2012; Green 2012; Huttenlocker and Rega 2012) and mammaliaforms (Hurum and Chinsamy 2012) is already available for comparison.

However, these comparisons are to some extent difficult to make, not for a lack of fossil specimens, but for a lack of extant comparisons. All of the larger surveys of extant mammalian bone tissue (Quekett 1855; Foote 1916; Amprino and Godina 1947; Enlow and Brown 1958) relied heavily on zoo animals, whose lifespan, habits, biomechanics, physiology, and pathologies often differ from conditions in the wild (Howell 1925; Greer et al. 1977; O'Regan and Kitchener 2005). Except for these studies, the mammalian osteohistological dataset is biased towards animals of economic importance: taxa used for medicine, housepets, or agriculture (mainly primates, rodents, and bovids) are generally the best described. Thus, the mammalian histological literature carries inherent phylogenetic biases (and likely size and ecological biases as well).

One of the largest phylogenetic holes in our understanding of mammalian bone histology is that of marsupials, which have not received as much attention as placental mammals. Only a handful of studies have included marsupial taxa in large comparative datasets, and none has focused exclusively on them. I include a summary of the taxa previously examined in Table 3.1.

Previous Studies of Marsupial Histology

The most extensive sampling of marsupial bone microstructure was also the first. Quekett (1855) listed ten species in his catalog of histological materials in the collections of the Royal College of Surgeons of England (Hunterian Museum, London). From each taxon, several elements were examined, each sectioned in several planes. His discussions (Quekett 1855: pp. 154-160) were limited to the morphology of the canals and osteocyte lacunae, but based on these, he commented that the "minute structure of the bone of Mammalia is nearly uniform throughout the class" (Quekett 1855: p. 151): each vascular canal was surrounded by several concentric layers of bone separated by layers of lacunae. Unfortunately, although many sections were made, only a single partial cross section of a *Macropus* radius is illustrated (Plate XI, Figures 9 and 10; all illustrations were hand-drawn using a camera lucida). Although some of Quekett's original slides remain intact, most of the Hunterian Museum collections were destroyed in the bombings of London during World War II, and thus in many cases the slides cannot be compared with original materials for taxonomic verification (Steel 2003).

Foote (1916) described and illustrated the femoral microstructure of four taxa, three of which had been examined by Quekett (1855). He noted features of the whole section, but as Quekett did, he focused on the canals and appearance of osteocyte lacunae. Foote (1916) noted differences between the "lower mammals" (monotremes, marsupials, edentates, and bats) and that of "higher mammals and man" (p. 16), namely that the secondary osteons were rarer and less distinct among the former group. Foote's original slides are still available, but frustratingly, they bear only a vague resemblance to his illustrations. The microstructural features were not drawn proportional to each other; some (e.g., osteocytes) were exaggerated and enlarged, whereas others (e.g., LAGs) were not illustrated. This is the only study of marsupial histology to date in which specimen numbers were provided, from which the ontogenetic stage and wild or captive status could be determined after publication.

Amprino and Godina (1947) included five marsupials as part of their survey of vertebrate microstructure; only one of these species had been described previously. Although only *Didelphis aurita* (which they called *D. azarae*) was described separately, their discussion of marsupial histology was the most descriptive in terms of microstructural features and variation. Amprino and Godina (1947) commented that they found the bone tissues of marsupials difficult to classify, but that they appeared different from those of most other mammals (notably, they found the tissues to be similar to the hyrax *Procavia* and some insectivorans). In the five taxa they observed, a thick layer of organized bone tissue formed much if not all of the outer cortex. They also noted that the microstructure of *Macropus* (kangaroos) differed from that of the smaller taxa. Whereas *Macropus* had some disorganized tissue in the inner cortex, the other species only had parallel-fibered or lamellar bone. The smaller taxa had fewer canals in general, and only rarely exhibited secondary osteons, which were restricted to the inner cortex when present. Like Foote (1916), Amprino and Godina (1947) observed that both primary and secondary osteons were somewhat indistinct from the surrounding primary cortical tissues.

More recent studies have included only one or two taxa, and not many elements. Additionally, most of them described specimens that could not be identified to the species level. Ruth (1953) examined the vascular canals in the femora of an opossum and a kangaroo,

but did not describe or illustrate them. Enlow and Brown (1958) described the microstructure of the rib, humerus, zygomatic, and nasal from a single specimen of *Didelphis* (species unknown), which was similar in all three elements. In contrast to Amprino and Godina (1947), they did not observe a distinct periosteal region of organized bone tissue. However, they did observe the indistinct primary osteons and rare secondary osteons noted in earlier work. Singh et al. (1974) surveyed 44 elements across Mammalia, including *Didelphis virginiana*. The opossum they examined had parallel-fibered bone with longitudinal canals and some regions of avascular bone, and no evidence of secondary remodeling. The sections they made are illustrated at a very high magnification (Singh et al. 1974: Figure 2, p. 426); the appearance of the bone at anything higher than a cellular level is not clear. In a conference abstract, Leahy (1991) briefly described the microstructure of a large diprotodontid, but did not list the element or specimen number of the individual involved. Surprisingly, this abstract was the first to note the presence of LAGs in marsupial bone, even though LAGs were clearly visible in all the sections Foote (1916) made (personal observation) and nearly every marsupial Amprino and Godina (1947) and Enlow and Brown (1958) illustrated. Chinsamy-Turan (2005) illustrated a kangaroo bone (Fig 3.5C: p. 52); at the time, no genus or element was provided, but Hurum and Chinsamy-Turan (2012) later identified this section as the femur of *Macropus* sp. Chinsamy-Turan (2005) confirmed the presence of LAGs in that specimen, although she did not describe other microstructural features. Most recently, Hurum and Chinsamy (2012) described the femoral microstructure of a kangaroo femur (*Macropus* sp.) and a single element (not identified) of the Virginia opossum, *Didelphis virginiana*. Though the authors did not provide an especially detailed histological description, they did touch on points related to fibrillar organization, vascular density, vascular pattern, and LAG presence in both taxa. Notably, Hurum and Chinsamy (2012) were the first to relate histological changes to ontogeny and life history of marsupials, and also suggested that the LAG in the opossum bone resulted from extended time in the den during the harsh North American winters.

To date, the bone histology of only 15 marsupial species has been described. Of these, seven have been illustrated, but only three have been illustrated using photographs. None of these studies provided relevant natural history data (e.g., age, sex, locality, or wild/captive status), and most did not provide specimen numbers so that these data could be determined later. It is therefore difficult to determine how our limited understanding of marsupial bone microstructure is influenced by phylogenetic, ontogenetic, and ecological differences among the taxa that have been sampled.

Study Rationale and Goals

Bone histological methods are one way to combine the extant and fossil records of growth, allowing larger questions related to the evolution of mammalian growth dynamics to be addressed. This type of study already has been undertaken by several authors. For example, based on their study of the bone histology of several Mesozoic mammals, Chinsamy and Hurum (2006) concluded that early mammals are less developmentally plastic than nonmammalian ancestors, a characteristic retained by many crown mammals. Other studies show that the types of bone tissues associated with the higher growth rates of extant mammals (i.e., compared to nonavian reptiles) were also present in non-mammalian synapsids (Ray et

al. 2004, 2009; Botha-Brink et al. 2012; Green 2012). These findings inform our understanding of when various aspects of the mammalian growth condition evolved. However, comparative studies rely on data from extant mammals in order to calibrate and interpret the histological signals of the extinct taxa. Given that the extant mammalian osteohistological dataset is so heavily biased toward certain placental clades, these studies may actually be comparing the growth physiology, rates, and dynamics of non-mammalian synapsids with a derived condition shared by only some placentals, rather than the plesiomorphic condition for therians or crown mammals. Without data from marsupials, this possibility cannot be eliminated.

Given that marsupials and placentals are sister taxa, they might be expected to grow more similarly to each other than to non-mammalian synapsids. If so, known osteohistological differences between non-mammalian synapsids and placentals would be much greater than any between placentals and marsupials. However, major differences in life history and growth are known between the two major therian clades. First, the reproductive strategies are quite different; marsupials gestate for much shorter time periods compared to most placentals, and then lactate for an extended period (Weisbecker and Goswami 2010). Postnatally and postweaning, marsupials grow at slower rates than placental mammals of the same adult body size (Case 1978; de Magalhães et al. 2007), and several orders also have a shorter time to reproductive maturity (de Magalhães et al. 2007). Marsupials have a shorter life-span than placentals of similar body size and ecology (Calder 1985; Austad and Fischer 1991; de Magalhães et al. 2007), despite having lower metabolic rates (Dawson et al. 1979; Austad and Fischer 1991; de Magalhães et al. 2007; McNab 2008). Recently, Geiger et al. (2013) established that marsupial long bone epiphyses generally remain open (i.e., the growth plate does not fuse the epiphyses to the diaphysis) past sexual maturity and even to senescence. They observed that marsupials kept epiphyses unfused much longer than many placental mammals, suggesting that they may experience prolonged skeletal growth.

Taken together, the differences in skeletal growth and life history between marsupials and placentals could result in dramatic differences in osteohistology between the two therian clades. Furthermore, because few non-placental eutherians and no non-marsupial metatherians have been sampled, the plesiomorphic patterns for Theria remain unknown. These questions about the patterns and evolution of therian growth patterns cannot be addressed without first incorporating more marsupials into the dataset.

By sampling long bone histology across the phylogeny of extant marsupials, my study establishes basic data needed to address these questions, as well as others relating to growth in extinct marsupial mammals whose size or life habits is not reflected among extant forms.

MATERIALS AND METHODS

Materials

I sampled the mid-diaphyseal femora of 53 marsupial (Table 3.2) and 14 placental mammals (Table 3.3) for osteohistological analysis. The marsupials dataset includes representatives of at least 43 species, 17 of 21 Recent (i.e., alive within the last 100 years)

families, and all seven extant orders. These specimens span the known size range for extant marsupials (Table 3.4), and include several fossil taxa that are much larger than any extant species (†*Diprotodon*, †*Ngapakaldia*, and †*Thylacoleo*). The placental samples include two previously unsampled orders of Afrotheria, as well as several taxa not examined in a recent survey of xenarthran bone histology (Straehl et al. 2013). Among the marsupial and placental data are several specimens originally sampled by Foote (1916). I also visited the Foote collection at Creighton Medical Center (Omaha, NE) to examine some of his original mammal slides.

In contrast to most previous surveys of extant mammalian histology, nearly every sample in my dataset was wild caught and field sacrificed (a few were wild caught but transferred to zoos or held in captivity for the remainder of their lives; e.g., *Ailurops, Thylacinus*). Species identifications were verified using a combination of collection locality data, cranial osteology, and specimen skins (where possible). Specimens are nearly all adults; ontogenetic stage (juvenile, subadult, adult) was assessed using a combination of methods for each specimen. These included age data, body length/mass measurements, the presence of a fully erupted adult dentition, and evidence of reproductive maturity (e.g., young in pouch or adult sized testes). For specimens in which body mass or length data were not available from original field data, I compared the skull length or femoral dimensions (or both) to specimens of verifiable adult status in the MVZ and UCMP osteological collections. Sources for adult body size and dental formulae are listed in the captions for Tables 3.2 and 3.3. Epiphyseal fusion cannot be used as an ageing criterion for marsupials because they fuse very late in life (if at all; Geiger et al. 2013; personal observation), and are thus unreliable.

No living animals were sacrificed for this study. Nearly every specimen in this dataset is from an existing museum collection. Three rodent skeletons (SW1, SW2, SW3) were found dead and mummified, and salvaged for use in this study. These specimens will be reposited in the osteological collections of the UCMP in October 2013.

Measurements

All specimens had been previously skeletonized and did not require additional preparation prior to histological sampling. Whenever possible, size, mass and sex data were recorded from museum labels (Table 3.2). Before sampling, the skulls and femora were digitally photographed, and the tooth formulae were assessed and compared to published adult dental formulae (Flannery 1995; Nowak 2005; Canevari and Vaccaro 2007; Menkhorst and Knight 2010). Some femoral dimensions also were measured (e.g., total proximal-distal length; distance from proximal end to the mid-diaphysis; see Table 3.2) using 8-inch digital calipers (model MC0008, Avenger, North Plains, OR; accuracy: 0.0005” [0.0127 mm]. Measurements longer than 209 mm were taken using 12-inch calipers [Neiko Tools, China; accuracy: 0.02 mm] or a tailor’s soft measuring tape [Amico, Richmond Hill, ON]).

Body mass estimates

Where available, body mass ranges (for extant taxa) and estimates (for extinct taxa) were taken from the literature. This was feasible for all extant and most fossil species examined. However, there are no published mass estimates for the extinct macropodids

†*Dorcopsoides fossilis* or †*Prionotemnus palankarinnicus*, or for the extinct diprotodontid †*Ngapakaldia tedfordi*. I estimated these using published equations for the estimation of mass in kangaroos and quadrupedal mammals. Different equations must be used to estimate mass in bipedal and quadrupedal taxa, which differ in body shape, the distribution of mass, and the proportions of their weight-bearing limbs (Anderson et al. 1985). The bipedal equations given in Anderson et al. (1985) were intended for the estimation of mass in bipedal dinosaurs, and were derived using data from quadrupedal placental mammals and scale models of dinosaurs. A more appropriate equation for estimating mass in extinct kangaroos is that of Helgen et al. (2006), whose model is based on mass and femoral circumference measurements of extant macropodids. The Helgen et al. (2006) equation is:

$$M_{est} = 1.0146*10^{[2.5932 \log_{10}(c_f) - 3.2842]} \qquad [1]$$

where M_{est} is the estimated body mass in g, and c_f is the mid-diaphyseal femoral circumference in mm (Helgen et al. 2006). Resulting mass estimates carry the assumption that body posture and femoral cross sectional geometry were similar in the extinct taxa and the extant macropodids from which the relationship is derived. This is a reasonable assumption; both taxa are macropodine macropodids and share synapomorphies relating to the articulation of the pelvic and ankle elements (Prideaux and Warburton 2010). Furthermore, their femora are proportioned similar to other macropodines (personal observation). Finally, they fall within the size range of extant macropodids examined by Helgen et al. (2006).

For quadrupeds, I used an equation given Wroe et al. (2004) for estimating mass in marsupial quadrupeds:

$$M_{est} = 10^{[2.89 \log_{10}(C_{h+f}) - 1.42]} \qquad [2]$$

where M_{est} is the estimated body mass, and C_{h+f} is the sum of the humeral and femoral mid-diaphyseal circumferences (Wroe et al. 2004). This equation is a modification of that of Anderson et al. (1985), who did not include marsupials in their original dataset. Wroe et al. (2004) added data from 18 quadrupedal marsupials to the original dataset of Anderson et al. (1985). Although this equation better predicts marsupial body mass than the original Anderson et al. (1985) equations, Wroe et al. (2004) showed that the slopes of the resulting regression lines differ for marsupials and placentals of similar size, suggesting that even this modified equation may underestimate marsupial mass.

For *Dorcopsoides* and *Prionotemnus*, I used the femoral circumferences from the specimens I sectioned [UCMP uncatalogued (44 mm) and UCMP 44597 (84 mm), respectively]. For *Ngapakaldia tedfordi*, the femur I sectioned (UCMP 72130, 89 mm) did not have an associated humerus; none of the UCMP specimens of this taxon have both a humerus and femur. Therefore, I measured the humerus of a similar-sized individual from the same locality (UCMP 69814, 91 mm humeral circumference; size similarity based on the elements each skeleton had in common, e.g., pelvis, vertebrae). All estimates of body mass are included in Table 3.4 and indicated with an asterisk.

Estimates of longevity, age at maturity, and age at weaning

Estimates of longevity in the wild and in captivity, age at reproductive maturity, and age at weaning were compiled from an existing database (AnAge Build 12 [2013]; de Magalhães and Costa 2009). Estimates of these ages were available for most extant taxa in my dataset except paucituberculates (*Caenolestes, Lestoros*). These ages are listed, along with the number of observed growth marks (annuli, LAGs) for each specimen, in Table 2.6. It should be noted that most of the ages are based on data from captive animals. Among marsupials, pouch-phase growth rates and especially weaning age are similar among wild and captive conspecifics (Lyne 1964; Sharman et al. 1964; Jones et al. 2004), although captive individuals grow faster in some species (Serena and Soderquist 1988). Lifespan in captivity is usually longer than in the wild (AnAge 2013).

Histological sampling and imaging

All specimens had been previously skeletonized and did not require additional skeletal preparation prior to histological preparation. Before sampling, all femora over 2 cm in total length were molded and cast following the methods described in Chapter 2. After molding, the mid-diaphysis was estimated externally by determining the point of smallest circumference along the midshaft. This point corresponded to a point approximately 50% of the total proximal-distal length in nearly every specimen. This point was marked with an archival marker and the distance from the proximal end to this point recorded.

Fossil specimens were sampled using the methods described in Chapter 2. Undecalcified sections of Recent bone were prepared using a modified method of that described in Chapter 2. For most specimens with a femoral length of less than 2 cm, the entire femur was embedded. For all specimens with femoral lengths over 2 cm and *Notoryctes* (AMNH15015), a portion of the mid-diaphysis was removed using an Isomet low-speed lapidary saw (Buehler, Inc., Lake Bluff, IL) for embedding, rather than the entire element. For the *Notoryctes* specimen, the entire mid-diaphysis was removed. In the other specimens, a 1 cm portion surrounding the marked mid-diaphysis was removed. Prior to embedding, Recent bones were fixed and dehydrated by submergence in progressively higher concentrations of ethanol (50%, 75%, 90%). Initial submergence was done under vacuum to increase penetration. Specimens remained in sealed containers of each concentration for 24 hours; the 90% ethanol bath was changed after 12 hours. Once fixed, the specimens were allowed to dry completely before embedding. As with the fossils, Recent bones were embedded in Silmar-41 clear polyester casting resin (Interplastic Corporation, Saint Paul, MN) catalyzed with methyl ethyl ketone peroxide (Norac, Inc., Helena, AK) at 1% by mass and allowed to cure for at least 24 hours. Thick sections were cut and mounted as in Chapter 2, but the mounting side was generally ground with 1200/P4000 grit CarbiMet abrasive papers (Buehler, Inc.) rather than 600/P1200.

Imaging, photomontaging, and analytical methods were described using the same equipment and software described in Chapter 2. These specimens have not yet been uploaded to MorphoBank (O'Leary and Kaufman 2012), but they will eventually be reposited there under project P672 (http://morphobank.org/permalink/?P672).

Histological Descriptions

Histological descriptions are based on direct observation of each histological thin section made through an Optiphot2-Pol light transmission microscope (Nikon Inc., Melville, New York) under regular transmitted light, and using compensators to enhance birefringence [both crossed plane-polarizing filters and a red tint plate (full wave retarder), λ =530 nm)]. My histological terminology follows that of Francillon-Vieillot et al. (1990), with clarifications to diagnosis as described in Werning (2012). I describe each character in detail, as well as how I diagnosed them, in Chapter 1 of this dissertation.

Institutional Abbreviations

AMNH, American Museum of Natural History (Mammalogy Collection), New York City, NY, USA; **CMC**, Foote Collection, Creighton Medical Center, Omaha, NE, USA; **MSB**, Museum of Southwestern Biology, University of New Mexico, Albuquerque, NM, USA; **MVZ**, Museum of Vertebrate Zoology, University of California, Berkeley, CA, USA; **UCMP**, University of California Museum of Paleontology, Berkeley, CA, USA; **SW**, personal collection of Sarah Werning (these specimens will be permanently reposited in the UCMP in October 2013).

HISTOLOGICAL OBSERVATIONS

Marsupials

Marsupial osteohistology strongly correlates with body size. Below, I discuss two common histological profiles, which more or less correspond to two body size classes: under ~40-50 g adult body mass, and over ~50 g (~ 50 g to 100+ kg) mass. These histological profiles grade into each other; they should be seen as not as discrete categories, but rather as a continuum (like body size). A summary of the vascular canal types, fibrillar organization, and position of growth marks visible in each specimen is included in Table 3.4.

Within each size class, long bone microstructure varies little among marsupials. Most specimens have little to no primary woven-fibered bone; when present it is generally restricted to the inner cortex. In nearly every specimen, at least half of the cortex is composed of primary parallel-fibered or lamellar bone. None of the specimens examined are especially well vascularized. The vascular canals are most often radially oblique primary osteons, and complex vascular patterns almost entirely absent. Similar to some taxa discussed in Chapter 2, osteocytes rarely orbit primary osteons, and the tissue that finishes the canals is not usually distinct from the interstitial tissues. As reported by other studies (Foote 1916; Amprino and Godina 1947), secondary remodeling is uncommon. Finally, annuli or LAGs are present in most specimens. In smaller individuals, these may represent weaning lines or hibernation lines. In larger taxa, LAGs are ubiquitous; in general, most taxa have several preserved throughout the cortex.

Taxa under ~40-50 g adult body mass (n = 10 species)

Parallel-fibered bone is the dominant tissue type in the cortex of all specimens in this size category, but in several taxa (*Acrobates, Cercartetus, Caenolestes, Lestoros*), some woven bone can be seen in the innermost cortex (Figures 3.1 through 3.4; note areas internal to dotted yellow line). The woven-fibered bone in these taxa is very similar in appearance to the embryonic bone of iguanid lizards (Hugi and Sánchez-Villagra 2012) and other amniotes (Francillon-Vieillot et al. 1990), especially in the appearance of the osteocytes. In this region, osteocytes are round in cross section and have no preferred orientation relative to the long axis of the bone or to each other. They are not regularly spaced; sometimes, they form small clusters. These regions of woven-fibered bone may correspond to the phase of rapid growth while still in the pouch (termed pouch-phase growth; see Discussion). External to these zones of woven fibered bone, the remaining two-thirds or more of the cortex is composed of parallel-fibered bone, or occasionally lamellar bone. In parallel-fibered regions; the osteocytes are oriented more or less perpendicular to the long axis of the bone (some may be slightly oblique), whereas in lamellar bone, all osteocytes are oriented perpendicular to the long axis of the bone. Osteocytes appear much thinner and flatter in regions of lamellar bone; they also line up evenly spaced along lamellae (Figure 3.4, compare osteocytes in the regions of parallel-fibered bone just internal to the LAG with those in the lamellar bone just external to it). Osteocytes are slightly thicker in parallel-fibered tissue than in lamellar bone, and spacing between them is more irregular.

Most taxa in this size category are avascular (e.g., *Cercartetus*, Figures 3.1, 3.2; *Acrobates*, Figure 3.4). The only exceptions are *Thylamys* and *Lestoros* (Figure 3.3, note white triangles), which are poorly vascularized by simple primary canals. These canals occur only in one region of the cortex. They are short and angled radial-obliquely relative to the long axis of the bone, and do not anastomose with each other. If the slide were cut very thin, these canals might appear to be longitudinally oriented, but by focusing through the plane of section on the microscope, the radial-oblique orientation can be confirmed.

Growth marks are visible in half the taxa in this size category (Figures 3.1, 3.2, 3.4, note arrows; Figure 3.3, note green line). In some taxa, the internalmost line may be a weaning line; however, I think this is unlikely for most of the taxa. In marsupials, the growth rate inflection occurs at or just before weaning, rather than at sexual maturity (Russell 1982), and so one would expect a weaning line to occur at the boundary between the fast-growing tissue deposited during pouch-phase growth and the slower-growing tissue deposited during post-pouch growth. This is the case for the innermost growth mark in *Cercartetus* (MVZ 127329; Figure 3.1, 3.2), but in the other taxa with LAGs or annuli (e.g., *Thylamys*, *Lestoros*, Figure 3.3; or *Acrobates*, Figure 3.4), there is space between the histological transition and the growth mark(s). Additionally, the sectioned specimen of *Cercartetus* has two additional growth marks that lie external to the histological transition point/innermost growth mark (Figures 3.1, 3.2, note arrows). These growth marks may reflect an annual truncation in growth (as in larger marsupials, see below), or they may reflect a pause in growth during hibernation (see Discussion).

Taxa larger than 50 g adult body mass (n = 29 extant and extinct species)

Representative images for this size class are shown in Figures 3.5 through 3.14; the general trend for this size category is illustrated in Figure 3.5.

Woven-fibered bone is the dominant tissue comprising the inner femoral cortex in nearly all taxa in this size category (Table 3.4). All of the specimens that lack woven-fibered bone (*Monodelphis*, *Lagostrophus*, †*Prionotemnus*, †*Ngapakaldia*) have extremely narrow cortices relative to the mid-diaphyseal diameter (i.e., their femora are very hollow). When woven-fibered bone is present, it invariably grades to parallel-fibered bone, usually in the midcortex (see Figures 3.5, 3.6, note dotted lines). In this character, the bone histology of larger taxa follows a similar pattern to that of the smaller taxa.

Growth marks are found in every specimen of this size class (Figures 3.5-3.14, note arrows and triangles). In general, several LAGs or annuli are visible in the mid- and outer cortex; the innermost (at least) is usually an annulus. Often, annuli are difficult to detect in regular transmitted light, but appear as bright bands of lamellar bone in elliptically polarized or crossed plane polarized light (e.g., Figures 3.7, 3.8, 3.10, 3.11, bottom images). This highlights the importance of using multiple filters in the diagnosis of bone microstructure.

Vascular density and the complexity of vascular patterning increase somewhat with size. In at least part of the cortex, all taxa except the petaurids, *Notoryctes*, *Vombatus* and †*Diprotodon* have radial primary osteons or short radially oblique primary osteons arranged in radial rows (see Exceptions below for a discussion of vascularity in these taxa). As in the < 40-50 g size category, vascularity decreases external to the weaning transition, but may take several growth cycles to become avascular (e.g., *Phascolarctos*, Figure 3.8; †*Thylacinus*, Figure 3.11). Within this size category, canals never anastomose in smaller taxa (e.g., *Isoodon* and *Bettongia*, Figures 3.6, 3.7). In species over ~10 kg adult body mass, small, comma-shaped reticulations may connect two to four canals in the innermost cortex (Figure 3.12, note canals at top of both images). Secondary remodeling is also common among species this size, but is usually restricted to the inner cortex.

General Trend

Table 3.4 illustrates the histological conditions of all marsupials sampled in this project, with taxa arranged by body mass rather than by phylogenetic relationship. In most taxa under ~40-50 g adult body mass, woven-fibered bone is restricted to the innermost cortex and vascular canals are rare. When they are present, they are simple primary canals and are generally restricted to the inner cortex. Woven-fibered bone is first found in the mid-cortex in taxa of approximately 40 g adult body size. In animals just larger than this, a mix of simple primary canals and short radial primary osteons are observed in the inner cortex. Species ~1 kg in body size are the first to vascularize their entire cortex with long radial primary osteons, though vascular density is always much lower in the outer cortex. At this size, secondary osteons are observed more frequently in the inner cortex. In taxa larger than ~4-5 kg, woven-fibered bone is regularly observed in the midcortex, though the midcortex almost always has a strong parallel-fibered component as well. Taxa with adult body mass of more than 10 kg may show short, comma-shaped anastomoses between primary osteons in the inner cortex; the midcortex is usually vascularized by long radial primary osteons, or short radial primary

osteons arranged in radial rows. Extensive secondary remodeling that obscures the entire cortex is only observed among the largest diprodontians.

Exceptions

Vombatus, †Diprotodon – Extensive cortical remodeling is rare among marsupials. When present, it is generally restricted to one region of the bone (e.g., †*Thylacoleo*) or the inner cortex (e.g., †*Thylacinus*, Figure 3.11). However, in some vombatiforms, secondary remodeling obscures much of the primary cortex. In *Vombatus* (UCMP 84850; Figure 3.15) and †*Diprotodon* (UCMP 57350, UCMP 79745; Figures 3.16, 3.17, 3.18), secondary osteons are visible even in the outer cortex. In *Vombatus*, these osteons are somewhat widely spaced, at least in the mid- and outer cortex, and so some details of the primary tissues (e.g., fibrillar organization, osteocyte density, and LAGs) are visible (Figure 3.15). In †*Diprotodon*, however, the cortex is remodeled by many generations of secondary osteons, and hints of the original tissue remain only in the outer cortex. As such, a minimum estimate of the number of annuli or LAGs (Figure 3.16, note arrows) is possible, but given the amount of remodeling, this probably underestimates actual age by a considerable amount. In the larger specimen of †*Driprotodon* (UCMP 57350), remodeling is more extensive and fewer intracortical annuli are visible than in the smaller individual (UCMP 79745). UCMP 57350 has another uncommon feature among marsupials: an external fundamental system, or EFS (Figure 3.18). This band of 8-10 thin lines appears much different compared to the annuli (Figure 3.19), which are broad bands of parallel-fibered bone. Therefore, it is unlikely a multiple LAG.

Among large eutherian mammals, dense secondary remodeling is common (Amprino and Godina 1947; Klevezal 1996; Chinsamy-Turan 2005; Köhler and Moyà-Solà 2009), and reflects (at least in part) the additional biomechanical loading associated with larger mass (Frost 1987; Biewener 1990; Klevezal 1996; Lieberman et al. 2003). Within my marsupial sample, most taxa lack extensive remodeling around the circumference of the cortex, even among large-bodied taxa such as †*Thylacoleo* or †*Prionotemnus*. However, there is still a considerable gap in body size between these species and †*Diprotodon*. It is likely that taxa of intermediate size between †*Thylacoleo* and †*Diprotodon* would also have shown extensive cortical remodeling.

Body mass shows a very strong phylogenetic signal in marsupials (Withers et al. 2006). The largest taxa are restricted to two orders, Diprotodontia and Dasyuromorphia. It is therefore difficult to assess whether the presence of secondary osteons in *Vombatus* and †*Diprotodon* reflects size, phylogeny, or a combination of both. Secondary remodeling is not common in the other vombatiforms examined in this study, *Phascolarctos* and †*Ngapakaldia*. Of the three koalas sampled (UCMP 58800, UCMP 77316, and UCMP 134825), only UCMP 58800 has secondary osteons, which are limited to the internalmost cortex. †*Ngapakaldia*, a diprotodontid but a much smaller taxon than †*Diprotodon*, also lacks remodeling. However, this taxon has very hollow femora, and the early growth record is likely lost to medullary cavity expansion. Though it lacks secondary osteons, UCMP 134825 has an EFS, similar to †*Driprotodon*. It is possible that vombatiforms are more likely to reach histological senescence before death than other marsupials are (see Discussion).

Petaurus – The femoral cortices of the petaurids (*Petaurus breviceps*, MVZ 127338; *Petaurus australis*, UCMP 77307, and a Pleistocene *Petaurus*, UCMP uncatalogued) are poorly vascularized given their size. In all three specimens, there are a few short primary osteons close to the endosteal margin, but otherwise the tissue is completely avascular (Figure 3.19, note white triangle). Additionally, osteocyte density appears lower than in other taxa of similar body sizes. In the Pleistocene specimen and in *P. australis*, the cortex is composed entirely of primary parallel-fibered bone (Figures 3.19, 3.20); in *P. breviceps*, woven-fibered bone comprises the inner third of the cortex. All three specimens have a LAG in the outermost cortex, close to the surface (Figures 3.19, 3.20; note arrows); *P. australis* has a second LAG close to the endosteal margin (Figure 3.20, note arrows). The inner LAG in this specimen is not likely a weaning line; the tissue internal to this LAG appears identical to the tissue in the rest of the cortex. Most other taxa in this size category have woven-fibered bone in the inner cortex, and all other taxa have better vascularized cortices and higher osteocyte densities.

Gliding marsupials are long-lived relative to non-volant, non-gliding mammals of similar body size (both eutherians and marsupials) and show delayed senescence (Austad and Fischer 1991; Holmes and Austad 1994). Captive *P. breviceps* reared under natural temperatures and photoperiods do not reach their body mass asymptote until approximately one year (Holloway and Geiser 2000), although they may reach adult lengths earlier (Suckling 1984). Even among gliders, *P. australis* grows slowly and reaches reproductive maturity late in life. Joeys leave the pouch after 100 days, but remain in the nest unweaned for an additional two months (Craig 1985; Tyndale-Biscoe 2005). A growth curve for *P. australis* has not been produced, but one study of wild individuals observed an 18-month male that was not fully grown, by length or by mass criteria (Craig 1985). Young stay with their parents until they are two years old (Henry and Craig 1984; Craig 1985; Tyndale-Biscoe 2005), the age of sexual maturity (AnAge 2013). The available data on growth duration and age at maturity is consistent with the number of LAGs observed in both extant species (1 in *P. breviceps*, 2 in *P. australis*).

Notoryctes – The bone microstructure of the Southern Marsupial Mole, *Notoryctes typhlops* (AMNH 15015), is unlike that of any other marsupial examined in this study. The femur is triangular in cross section, rather than round or oval as it is in nearly all other taxa, although it is similarly thin-walled. The inner cortex is remodeled by large secondary osteons in some areas (Figure 3.21, top of image) and large oval resorption rooms in other areas (Figure 3.21, note white triangle). These resorption rooms are lined with several layers of lamellar or parallel-fibered bone and their outer borders sometimes overlap. In some areas, the resorption rooms are separated by small patches of primary woven-fibered bone tissue. The outer cortex is composed entirely of woven-fibered bone (Figure 3.21, note pattern of osteocytes). Some vascular canals are visible in the outer cortex, but in general it is poorly vascularized. Most of these are primary osteons, but a few simple primary canals are also present. These canals have no common pattern or orientation, and may travel in any direction. A few open to the surface.

Growth and life history are very poorly understood in both species of marsupial mole, which, because of their fossorial desert lifestyle, are not as well studied as other Australian taxa. For example, length of gestation, weaning age, age at reproductive maturity, and lifespan are unknown for both species. Specimens have never remained alive in captivity for

more than 2.5 months, weaned young have never been observed, and females with young in pouch are rare in museum collections (Johnson and Walton 1989). Thus, it would be extremely useful if some life history information could be inferred from their bone histology. Unfortunately, no LAGs, annuli, or weaning transition are visible in this specimen. That the primary bone tissue is woven-fibered and vascularized throughout the cortex with no growth marks may suggest that *Notoryctes* grows relatively quickly to adult size. It is also possible that the growth marks and a weaning transition were present earlier in life, but later lost to medullary cavity expansion or obscured by secondary remodeling in the inner cortex.

It is unfortunate that the normal indicators of marsupial growth are not present in *Notoryctes*; weaning lines or growth marks would have helped to constrain the age of adults and given the first estimates of marsupial mole longevity. However, the differences in bone histology may suggest a difference in growth strategy or growth duration compared to other marsupials. If this were the case, it would also be an important discovery. Unfortunately, the latter hypothesis would be hard to test. Because pouch-phase *Notoryctes* are extremely rare in museum collections and juvenile specimens are absent from them, it is unlikely that an ontogenetic series could be made available for sectioning.

Fossil vs. Recent Marsupials

For three genera, I sampled both fossil (Pleistocene) and Recent specimens (*Bettongia, Petaurus, Sarcophilus*). In each case, the fossil specimens were Pleistocene in age. Overall, the fossil and Recent specimens were very similar to each other histologically, suggesting consistencies in growth patterns within each genus from the Pleistocene to the Recent. In *Petaurus*, both specimens showed similar number of LAGs, and were nearly indistinguishable in terms of their fibrillar organization, osteocyte density, and poor vascularity (Figure 3.19). The inner cortex of the Recent *Bettongia* specimen (MVZ 127709) had numerous secondary osteons in the inner cortex (Figure 3.22, top image), which obscured the primary growth signal. The fossil (UCMP 53685) had no secondary remodeling. However, the outer cortices of the two were very similar histologically. Both had LAGs in the outermost cortex, and the primary parallel-fibered bone tissue was vascularized by very short radial primary osteons. The two specimens of *Sarcophilus* were similar in terms of fibrillar organization and especially in the appearance of the longitudinal and short radial primary osteons arranged in radial rows (Figure 3.23). The annuli were similarly spaced in these individuals, but had different appearances. For example, the Recent specimen (MVZ 127032) has three annuli/LAGs, but the inner two regionally become double or triple lines in some regions and are indistinct in others. In the fossil (UCMP 53021), only two growth cycles are preserved, but the outer surface of the bone is worn, so a third may have been lost. The two annuli show breaks in the tissue in only one area of the bone.

Overall, the histology of the primary cortical tissues are very similar between the Recent and fossil congeners. It is difficult to tell whether the observed differences in histology reflect differences in growth dynamics between the Pleistocene and the Recent, individual variation (including sex or ontogenetic differences), species differences in growth, or some other factor. In the case of *Sarcophilus*, climate and species differences are plausible; the Pleistocene fossil is from New South Wales (Australian mainland), whereas MVZ 127032 is from Tasmania. Debates about whether the two populations are different species are long-

running (e.g., Stephenson 1963) and have not yet been resolved (Jones et al. 2003). I propose, however, that especially in the absence of additional samples and ontogenetic series, the histological differences between these groups are small enough that similarities in growth pattern can be inferred, and that the fossil marsupials do not radically differ from extant taxa in their growth biology.

Placentals

Although the focus of this study is the histology of marsupial mammals, I provide brief comments on the bone histology of placental mammals, based on a small number of sections I made (Table 3.3) and a literature review of some of the major surveys of placental mammal histology (Table 3.5).

As in marsupials, small-bodied placentals tend to have relatively avascular bone, mostly composed of parallel-fibered bone tissue, although woven bone is sometimes present in the innermost cortex, and a layer of lamellar bone may line the endosteal or periosteal margin (Foote 1916; Enlow and Brown 1958; Singh et al. 1974; Francillon-Vieillot et al. 1990; Klevezal 1996; Hurum and Chinsamy 2006; García-Martínez et al. 2011; Hurum and Chinsamy 2012). Larger taxa within this size class may have vascular canals; these are usually primary osteons with distinct borders (Foote 1916; Enlow and Brown 1958). As observed in the marsupials, hibernating taxa often deposit LAGs (Morris 1970; Whalen et al. 1972; Klevezal 1996; Klevezal 2002; García-Martínez et al. 2011). Of the sampled placentals under ~100 g adult body size, the vast majority have been rodents or bats. Other taxa have been sectioned, but generally have been used for different types of studies; for example, Meier et al. (2013) studied bone compactness in talpids but did not describe their histology.

In addition to a small deermouse (*Peromyscus*; SW 3), I examined the femoral microstructure of a sengi (*Elephantulus myurus*, MVZ 177073; Figure 3.24) and a golden mole (*Amblysomus hottentotus*, MVZ 117053; Figure 3.25), two afrotheres of ~40-100 g adult body mass (AnAge 2013). The *Peromyscus* specimen showed the expected histology for an animal its size: avascular parallel-fibered bone, with no LAGs. However, the afrotheres each had distinct histological profiles that looked nothing like that of *Peromyscus* or the marsupials. In the sengi, the inner third of the cortex is composed of parallel-fibered bone, which in some regions is poorly to moderately vascularized by short radial primary osteons. In the midcortex, a layer of woven-fibered primary bone is visible, which varies in thickness around the circumference of the cortex (Figure 3.24; note white triangle). This region is bounded externally by a LAG (Figure 3.25; note arrow). External to the LAG, additional parallel-fibered bone is present. In the golden mole, most of the cortex is composed of poorly vascularized primary woven-fibered bone, with a thick layer of lamellar bone that lines most of the endosteal margin (Figure 3.26). That individual has no growth marks. The canals are short primary osteons; these may travel in any direction.

Outside crown Placentalia, small-bodied stem eutherians have other histological profiles. The bone tissue of †*Zalambdalestes* is somewhat similar to that of extant rodents and bats (Chinsamy and Hurum 2006); a transition from parallel-fibered to lamellar occurs moving periosteally, and the cortex is poorly vascularized by both simple primary canals and primary osteons. However, the bone tissue of †*Barunlestes* is much more like that of marsupials of 50-500 g adult body mass. A small region of woven-fibered bone is preserved

in the innermost cortex, with four or five LAGs external to it, separating zones of parallel-fibered bone. The bone is poorly vascularized, but the canals visible in the figures are radial (Chinsamy and Hurum 2006: Figure $9B_1$, $9B_2$). Taken together, these reports suggest that there is unappreciated histological diversity among this size class of placental mammals.

Among larger eutherians, many taxa are thought to lose most of their primary cortical bone tissues to remodeling, including LAGs or other annual growth marks (Foote 1916; Amprino and Godina 1947; Klevezal 1996). It has also been argued that non-hibernating mammals rarely produce intracortical LAGs (Klevezal 1996; Chinsamy-Turan 2005), but many exceptions have been shown (e.g., Sander and Andrássy 2006; Köhler et al. 2012; Straehl et al. 2013). My re-examination of original materials and images presented in three classic comparative studies (Foote 1916; Amprino and Godina 1947; Enlow and Brown 1958) shows that intracortical growth marks (LAGs or annuli) are quite common across the sampled eutherian lineages (Table 3.5). Additionally, although secondary remodeling is common, it generally does not obscure the entire cortex. This allows, at least in some cases, estimates of the proportion of woven-fibered to parallel-fibered bone within the cortex (Table 3.5). From these data, it is possible to reconstruct the histological signature of relative growth rates through ontogeny for at least some taxa.

I do not attempt a thorough description of large-bodied placental growth dynamics here, but note some common trends. First, the number of intracortical growth marks in the long bones is higher among certain clades than among others. They are common in Afrotheria and Xenarthra (Table 3.5; Figures 3.26, 3.27; Amprino and Godina 1947; Sander and Andrássy 2006; Straehl et al. 2013). Among Euarchontoglires, growth marks have been observed in every clade, but occur in high numbers only in dermopterans and primates. Within Laurasiatheria, these include the bovids, felids, herpestids, and cetaceans (Table 3.5, Amprino and Godina 1947; de Buffrénil et al. 1990; Klevezal 1996; Köhler and Moyà-Solà 2009; Köhler et al. 2012).

Second, the type of primary tissue that comprises the cortex is variable. It has been reported that the primary bone tissues in the cortices of large mammals consist exclusively of well vascularized woven-fibered bone during the active phase of skeletal growth. Poorly vascularized or avascular parallel-fibered and lamellar bone are restricted to the outer cortex; these are deposited only after sexual maturity has been reached and growth rates have declined (Klevezal 1996, Chinsamy-Turan 2005). However, three recent studies show this is not always the case. Straehl et al. (2013) found that poorly vascularized lamellar bone comprised much of the cortex of *Bradypus* sloths, and Köhler and Moyà-Solà (2009) described a fossil *Myotragus* (Bovidae) whose entire femoral cortex was composed of poorly vascularized lamellar bone. In a study of primates, Warshaw (2008) found that many taxa only deposited woven-fibered bone early in life, and that most of the cortex was composed of moderately or poorly vascularized parallel-fibered or lamellar bone.

Even among my small sample, I noted several "atypical" histological patterns in the cortices of larger-bodied placentals. A specimen of Rock Hyrax, *Procavia capensis* (Afrotheria; UCMP 58880), has moderately vascularized woven-fibered bone in the inner femoral cortex (Figure 3.26, note bottom of image). External to this is a thick band of nearly avascular parallel-fibered bone that is punctuated by a central LAG (Figure 3.26, note bottom arrow). External to the annulus is a thinner band of moderately vascularized woven-fibered bone, followed by another broad annulus of parallel-fibered bone that terminates in a double

LAG. The cycle repeats again, and external to that LAG, two more LAGs are visible in the parallel-fibered bone that forms the outer cortex. This is consistent with what I observed in Foote's (1916) section of the same species. In a specimen of *Bradypus* (CMC 310, Figure 3.27), parallel-fibered bone is the only primary tissue observed in the outer half of the bone (the inner cortex is remodeled by secondary osteons). However, this individual is better vascularized than the *Bradypus* observed by Straehl et al. (2013); numerous radial primary osteons traverse the cortical wall. Neither of these histological profiles conforms to standard expectations for growth in mammals of their size.

Size influences the bone histology of placental mammals as well, but the effects seem to vary from clade to clade. For example, Straehl et al. (2013) surveyed the bone microstructure of a large number of xenarthrans. Among Cingulata (armadillos) and Folivora (sloths), bone histology differed among taxa with adult body masses less than 20 kg, and taxa whose adult body mass exceeded 20 kg. The larger size class exhibited more complex vascular patterns, less fibrillar organization, and more secondary remodeling throughout the cortex compared to the smaller class. Among primates, Warshaw (2008) found that vascular density strongly correlated with body size. The amount of woven-fibered bone also was influenced by size, but this was only evident in species over 500 g. In contrast, Köhler et al. (2012) found LAGs in bovids across a wide range of body sizes, but their presence or absence seemed influenced by phylogeny more than size.

In general, the bone histology of large (> 100 g) eutherians has been compared among large groups of distantly related taxa. From these studies (Foote 1916; Amprino and Godina 1947; Enlow and Brown 1958), general conclusions about mammalian growth have been drawn. However, based on these works, the effects of phylogeny, body size, and the ontogeny of growth on histology are difficult to tease apart within Placentalia. Far less attention has been focused on histological variation within and among the major eutherian clades. Three recent studies (Warshaw 2008; Köhler et al. 2012; Straehl et al. 2013) focused on individual clades (Primates, Bovidae, and Xenarthra, respectively). Each clade showed a different "typical" histology, and within each clade, histology was influenced by body size to different extents. Among placentals, it seems inappropriate to refer to a common histological profile, as observed among marsupials.

DISCUSSION

My hypotheses about the relationship between certain histological indicators of growth and longevity (the histological transition at weaning, the annual nature of LAGs) have not yet been confirmed by bone labeling, but all of my hypotheses are testable using that method. However, the histological signal observed in the sampled marsupials is consistent with what is known about marsupial growth rates through ontogeny, their longevity, and their patterns of long bone epiphyseal fusion. I discuss the strong relationship between marsupial histology and life history using each of these lines of evidence, then comment on the relationship between bone histology and life history in placentals.

Marsupial growth rates through ontogeny

The histological signal of growth shown in marsupials is consistent with what is known about their ontogenetic shifts in growth rate. All marsupials are extremely altricial; gestation does not exceed 46 days and neonates do not weigh more than 1 gram (Russell 1981). After birth, the rate of growth while in the mother's pouch (pouch-phase growth) is high, especially compared to growth rates after weaning (post-pouch growth; e.g., Sharman et al. 1964; Maynes 1976; Cutts et al. 1978; Russell 1982; Jackson 2007; McMahon et al. 2011). Weaning occurs when the joey leaves its mother's pouch permanently (in some taxa, joeys may leave temporarily, but return regularly to feed), and corresponds to major transitions in both diet and growth rates (Russell 1982). In general, weaning occurs before the end of the first year (Russell 1982; AnAge 2013), although it may occur later in larger-bodied taxa (dasyurids, macropodids, phascolarctids, and vombatids; Russell 1982). Different studies recover the growth rate inflection point either during late pouch-phase (Maynes 1976; McMahon et al. 2011) growth or at weaning (e.g., Pahl 1987; Ward 1990); this may reflect biological differences among taxa or statistical difficulties in describing the transition between such radically different growth phases (McMahon et al. 2011). This is notable because the growth rate inflection point has been proposed to correspond to sexual maturity in placental mammals, rather than weaning (Zullinger et al. 1984; Klevezal 1996; Chinsamy-Turan 2005).

After weaning, marsupial growth rates decline as they approach their body size asymptote. Reproductive maturity generally occurs earlier in marsupials than in placentals of similar body mass (de Magalhães et al. 2007); the length of time from birth to reproductive maturity is usually two or three times longer than from birth to weaning, and often longer in males than in females (AnAge 2013). Among eutherians, altricial taxa tend to reach the body mass asymptote (i.e., maximum adult size) relatively late and at slower rates than in precocial species (Gaillard et al. 1997). This is similar to what has been described for marsupials, which experience extended growth durations at fairly low growth rates (Case 1978; de Magalhães et al. 2007).

Osteohistological indicators of relatively fast growth (e.g., woven-fibered bone, higher vascular density, greater vascular connectivity, more complex vascular patterns) are expected to track the patterns of growth rate through ontogeny (Chapters 1, 2). However, as described above, some of the histological indicators of fast growth (vascular connectivity and complex vascular patterns) are not observed in any marsupial taxon. Small-bodied taxa are avascular (Table 3.4). In the taxa that have vascular canals, they are sometimes present only in the inner cortex (e.g., *Monodelphis, Petaurus, Philander*). More commonly, canals are present throughout the cortex but the outer cortex has fewer canals than the inner cortex (e.g., *Bettongia, Echymipera, Isoodon, Sarcophilus, Thylacinus, Thylacoleo*). Woven-fibered bone is present in most individuals observed in this study, but generally, it is restricted to the innermost cortex. In taxa that have LAGs, woven-fibered bone is present past the first LAG/annulus only in a few relatively large-bodied taxa (*Macropus, Sarcophilus, Thylacinus, Thylacoleo*).

Marsupial growth rates undergo a dramatic shift at weaning. Because of this, a histological change that reflects a rapid transition from faster growth to slower growth is expected to coincide with weaning and the start of the post-pouch growth phase. I hypothesize that the abrupt histological transition from woven-fibered to parallel-fibered bone visible in

the inner cortex of most taxa corresponds to weaning. In larger taxa, this transition in fibrillar organization occurs at the same point in the cortex as a decrease in vascular density and may be accompanied by a rest line or annulus (e.g., in *Dendrolagus*, Figure 3.10). Similar histological transitions are known in other mammals. For example, an indistinct rest line attributed to weaning marked a transition in vascularity in the Grey Mouse Lemur, *Microcebus murinus* (Castanet et al. 2004).

In taxa that both have LAGs and are weaned before the end of their first season of growth, the histological transition should occur internal to the first LAG (e.g., *Potorous*, Figure 3.5; *Isoodon*, Figure 3.6). This is the most common histological condition observed. In taxa that are weaned early in their first year, the histological transition always occurs well inside the first LAG, and is separated from it by a thick band of parallel fibered bone. In *Dendrolagus*, which weans just before the end of the first year, the histological transition coincides with the first LAG (Figure 3.10).

Altricial mammal species reach their body mass asymptote late relative compared to both the age at maturity and typical lifespan, and exhibit slower growth rates compared to precocial species (Gaillard et al. 1997). This is observed in many marsupials, especially larger-bodied taxa. For example, wild female Eastern Grey Kangaroos (*Macropus giganteus*) reach reproductive maturity in their second year, but continue to increase in weight until at least their eighth year. This gain in mass is not negligible; females nearly double in mass during this time period (Pearse 1981). However, average lifespan for this taxon in the wild is only twelve years (Pearse 1981). Such extended growth durations should also carry a histological signature; one of slower-growing bone tissue (compared to pouch-phase growth) and lasting a long time period (many years). This is exactly what is observed in most marsupials over ~50g. In general, after the transition from woven-fibered bone to parallel-fibered bone at weaning, parallel-fibered bone is deposited for the rest of the growth duration. Unlike what has been reported for many eutherians (Klevezal 1996; Chinsamy-Turan 2005), parallel-fibered bone comprises much of the marsupial femoral cortex. This region is usually punctuated by several LAGs or annuli, some of which are intracortical.

The annual nature of LAGs

The assumption that the LAGs are annual is reasonable, at least for the large-bodied taxa in my dataset. Two specimens of known age are included in this study. In both cases, the number of growth marks is similar to the animal's known age. One koala (*Phascolarctos cinereus*, UCMP 134825) was captive bred and died in the San Francisco Zoo at age seven. This individual exhibits the weaning transition in the inner cortex, has a double annulus in the midcortex, and has five lines that form an EFS in the outer cortex (Figures 3.8, 3.9). The number of growth marks underestimates known age only by one year, and the spacing between them is consistent with patterns of growth in koalas. As noted above, koalas wean at the end of their first year. In the wild, female koalas approach their body mass asymptotes in 2-4 years, and may live for several years after reaching adult size (Jackson 2007). This is generally consistent with the number and spacing of growth lines in UCMP 134825. The weaning transition is observed in the inner cortex (Figure 3.8, bottom image; note dotted line), but no annulus or LAG occurs with it. After weaning, growth rate decreases (as evidenced by changes in fibrillar organization and vascular density). External to the annulus,

vascular density decreases again (Figure 3.8, bottom image; note fewer canals external to white triangle). A similar decrease in vascular density happens external to the innermost line of the EFS (Figure 3.8, bottom image; note fewer canals external to yellow arrows). The histology suggests a pattern of a year of relatively fast growth, two years of moderate growth, and then several years of appositional (slow) growth.

The thylacine (†*Thylacinus cynocephalus*, AMNH 35244) died in its eighth year (Stephen Sleightholme, Project Director, International Thylacine Specimen Database Project, personal communication). This specimen has two intracortical annuli (Figure 3.11, bottom image) and three LAGs in the outer cortex (Figure 3.12); the number of preserved growth lines underestimates age by two years. The LAGs are more closely spaced than the annuli, and the outermost LAG is very close to the periosteal surface. The spacing of these growth lines suggests that the animal grew relatively faster for at least the first two years of life, then slowed its growth and was probably nearing its size asymptote. That there is no histological transition at or internal to the first LAG; it is possible that earlier growth marks were lost to medullary cavity expansion or remodeling of the inner cortex. Unfortunately, not enough data on thylacine growth and longevity are available to determine whether the microstructure reflects known growth patterns, as in the koala. Thylacines are not known to have bred in captivity, and were not observed breeding in the wild (Guiler 1985). Weaning likely occurred after three to five months and lifespan in captivity ranged from ~8.5-12 years, but growth rates and age at reproductive maturity for this species are not known (Dixon 1989).

The assumption that the LAGs observed in larger-bodied taxa are annual is also reasonable based on the lifespans of marsupials. Among the sampled species for which longevity is known, only *Echymipera kalubu* (MVZ 138478) has more growth marks than would be expected for its reported lifespan. However, the longevity of this species is known only from one report of a captive animal (AnAge 2013), and may not reflect growth in the wild (or typical growth in captivity).

Because juveniles and subadults were not sampled for most taxa, it is not known whether any growth marks were lost to medullary cavity expansion, but this is a reasonable assumption given that many taxa show evidence of endosteal resorption (e.g., Figures 3.10, 3.14, 3.15). I predict that underestimation of LAGs is most likely to occur in taxa whose femora are relatively thin-walled (e.g., macropodids), or taxa that remodel the internal cortex (e.g., *Vombatus*, †*Thylacinus*, †*Diprotodon*). This may explain, in part, why the kangaroos in my study exhibit many fewer LAGs than might be expected, given that many macropodid species take six years or longer to reach their body mass asymptotes (e.g., Catt 1981, Poole et al. 1982). It is also consistent with the higher number of observed annuli in the smaller, less remodeled individual of †*Diprotodon*.

In the small-bodied taxa, the LAGs may not be annual, but instead correspond to hibernation or extended periods of daily torpor. Hibernation lines have been observed in the long bones of two species of dormice (García-Martínez et al. 2011). In that study, a LAG was deposited during each hibernation event, even in animals that had not reached reproductive maturity. Such lines are common in other rodents that hibernate (Klevezal 1996, Klevezal 2002), and have also been observed in other hibernating taxa, including bats (Whalen et al. 1972) and hedgehogs (Morris 1970).

Among the small-bodied taxa, I observed LAGs or annuli in *Acrobates*, *Sminthopsis*, *Lestoros*, *Cercartetus*, *Dromiciops*, *Pseudantechinus*, and *Thylamys*. Among marsupials, true

hibernation occurs in *Dromiciops*, Burramyidae (including *Cercartetus*, which may hibernate for up to a year), *Acrobates*, and possibly *Thylamys* (Bruch 1917; Bozinovic et al. 2004; Geiser 2007; Geiser et al. 2008). *Sminthopsis crassicaudata* enters torpor daily during winter (Warnecke et al. 2008), and *Pseudantechinus macdonnellensis* does so on most days (Geiser and Pavey 2007; Geiser et al. 2008). Although torpor and hibernation have not been reported for *Thylamys venustus*, its close relatives do experience it: *T. elegans* experiences extended periods of daily torpor when temperatures are low and food is scarce (Bozinovic et al. 2005), and *T. pallidior* experiences months of daily torpor or possibly true hibernation at low temperatures (Bruch 1917). Hibernation and torpor have not yet been observed in Paucituberculata, but have been proposed for this clade based on the phylogenetic distribution of these traits (Geiser et al. 2008). If the single LAG/annulus visible in the other small-bodied marsupials does in fact correspond to hibernation, the presence of a single LAG in *Lestoros* suggests that it also likely hibernates or undergoes extended times of daily torpor. However, *Caenolestes*, another paucituberculate, does not have a LAG.

Some small-bodied taxa have more than one growth line. For example, *Cercartetus nanus* (MVZ 127329) has three. In this specimen, the innermost line is visible at the same point as the weaning transition from woven-fibered to parallel-fibered bone, and two more lines are visible in the mid- and outer cortex (Figures 3.1, 3.2, note arrows). In this taxon, it is reasonable that the subsequent lines result from later hibernation events. Because it is a small species, one might assume that growth would finish rapidly. However, hibernation bouts in *C. nanus* are the longest reported for any mammal (~310 days, and even up to 367 days in one individual; Geiser 2007). Weaning age in this species is 62 days, and reproductive maturity occurs at 190 days (AnAge 2013); it is quite possible that growth may extend two seasons or more.

Epiphyseal fusion

The histological signal of prolonged growth in marsupials is consistent with evidence from growth curves (above), but also with osteological evidence from unfused epiphyses. The fusion of the epiphyses to the diaphysis by bony replacement of the cartilaginous growth plate is the final stage in the growth plate (Nilsson and Baron 2004). Once the epiphyses are fused, the animal cannot elongate that element; hence, the linear growth of that element is completed. As long as the growth plate is active, the epiphyses remain unfused. The pattern of which epiphyses are fused and which remain open can be used to assess relative age (Morris 1971). Linear measurements of long bones or limb segments also may be used to estimate age as long as individuals follow similar size trajectory. In studies of marsupial growth, for example, pes length is often used to estimate age during pouch-phase growth (e.g., Catt 1981; McMahon et al. 2011). However, the accuracy of this method decreases as the animal ages; this is likely because the podial and ankle elements fuse early in marsupials, especially compared to the long bones of the hindlimb (Washburn 1964; personal observation).

Although most of the individuals sampled could be identified as adults based on their dentition, body size, or state of reproduction, few specimens had fused any of the femoral epiphyses, and none had fused all of their long bone epiphyses (Figure 3.28, note arrows). The one potential exception is that of *Notoryctes* (AMNH 15015), whose femoral epiphyses were fused, but the rest of the skeleton was unavailable for examination. Often, the distal humeral

epiphysis was the only one fused among all the major long bones in the individuals. Interestingly, the only two specimens that did show femoral epiphyseal fusion were UCMP 134825 (*Phascolarctos*; Figure 3.29, note arrows) and UCMP 57350 (†*Diprotodon*), which both had an EFS in the outermost femoral cortex.

This is consistent with previous studies that have found long bone epiphyseal fusion to occur relatively late in life in marsupials, if at all. Washburn (1946) examined epiphyseal closure in three didelphid opossums (*Didelphis virginiana*, *Metachirus*, and *Philander*) and found that most of the hindlimb epiphyses remained open at the end of life. Kingsmill (1962) found similar results when examining the phalangerid *Trichosurus* and the peramelid *Perameles*. A recent study (Geiger et al. 2013) found that marsupials fuse their epiphyses relatively earlier than some eutherians, although their study did not include xenarthrans or afrotherians, some of which are also known to fuse epiphyses late in life (Roth 1984; Ciancio 2012).

Histology and growth in placental mammals

The bone histology of placental mammals is much more variable than that of marsupials. Placentalia is taxonomically more diverse than Marsupialia (Nowak 2005), and this could account for some of the diversity in histological appearance. However, because most microstructural characters of bone tissue reflect growth rates, greater variation in placental growth strategies is likely the main driver of histological differences. Zullinger et al. (1984) suggested that most mammals follow a similar growth curve throughout life, because a single descriptive model (the Gompertz model) was always the model of best fit when asymptotic mass was held constant (a reasonable assumption for animals of determinate growth to known size). However, a more recent study found that growth among mammals is quite variable, at least among placentals, and that different growth models are more common at different ends of the altricial-precocial spectrum (Gaillard et al. 1997).

Four types of asymptotic models have been used to describe the ontogeny of postnatal growth rates in placental mammals: monomolecular, Gompertz, logistic, and von Bertalanffy (Zullinger et al. 1984, Gaillard et al. 1997). Differences in the shape of these curves carry different implications for how growth rates are distributed through ontogeny. For example, the monomolecular model describes taxa in which the highest growth rates occur before birth, and growth rates decline gradually through ontogeny as the animal approaches asymptotic body size. Among eutherians, this mode of growth is most common among highly precocial taxa (Gaillard et al. 1997). In taxa whose growth follows a von Bertalanffy or Gompertz model, the period of most rapid growth happens after birth but still early in life, and growth rates begin to decline at approximately 29% or 37% of asymptotic body mass, respectively (Zullinger et al. 1984; Gaillard et al. 1997; Lee et al. 2013). In taxa whose growth follows a logistic model, growth rates begin to decline relatively later in life, at 50% of asymptotic body mass (Zullinger et al. 1984; Gaillard et al. 1997; Lee et al. 2013). These models are common among progressively more altricial placentals. Interesting, this relationship holds among major clades (i.e., when phylogeny is controlled at the ordinal level), but not at the generic level (Gaillard et al. 1997).

Because bone microstructure tracks growth rates, we should expect to see differences in histology with each type of growth curve. For example, highly precocial placentals would

be expected to show histological indicators of fastest growth in fetal bone, and after birth, the histology should suggest progressively slowing growth. In these taxa, an abrupt transition from fast-growing to slow-growing tissue would not be expected in postnatal tissues, because the growth inflection occurs before birth. This is the histological pattern observed in the postnatal tissues of bovids and cervids (Köhler et al. 2012). Not only do zonal widths decline periosteally (indicating that less and less bone is deposited each successive year), but vascular patterning becomes less complex, and the proportion of non-anastomosing canals increases. Conversely, highly altricial species would be expected to show the time of fastest growth after birth, with histological indications of an increase and then decrease in bone deposition rates.

Although this seems relatively simple, such comparisons would be difficult in placentals without knowledge of life history and the shape of the growth curve, as well as quantification of microstructural characters through ontogeny. For example, in small, short-lived taxa with hollow bones, the histological differences may be subtle, occur over a narrow region of the cortex, or be lost to medullary cavity expansion. If the earliest record of growth was missing, a pattern of growth decline might be inferred incorrectly. Also, histological indicators of different life events may leave different signals in different taxa; for example, a LAG may reflect birth, weaning, or annual rhythms in growth. Or, a similar event may occur at different ontogenetic stages in different taxa. For example, the presence and timing of a growth inflection point, key to understanding how life history relates to histology in marsupials, happens at different times among placentals. The inflection in growth rates is often assumed to occur at reproductive maturity in mammals (Klevezal 1996; Chinsamy-Turan 2005). However, this is not the case in highly precocial eutherians, whose growth inflection occurs before birth (Gaillard et al. 1997). In animals of determinate growth, it is often claimed that growth either rapidly declines or is nonexistent after maturity (Charnov 1993; West 2001), but many large-bodied and slow-growing taxa reach maturity well before asymptotic size (Brody 1964; Promislow and Harvey 1990).

Placentals are much more variable in their life history and growth rates through ontogeny compared to marsupials, which share a common pattern of altriciality, fastest growth at weaning, and extended slow post-pouch growth. As shown for marsupials, many characters of bone microstructure make sense when interpreted in light of a growth curve. However, because placentals are so variable in their life histories, caution should be used when attempting to infer growth patterns from bone histology; similar features may result from different events in life history, and some trends may not be distinguished without quantification.

CONCLUSIONS

The main factors influencing marsupial bone microstructure are life history and body size. The histological differences resulting from body size are subtle, occur gradually, and hold across six of the seven extant orders. From a histological standpoint, a 50 kg kangaroo is very similar to a 10 kg dasyurid, a 1 kg peramelemorph, and a 25 g possum. This is because the types of bone deposited and the sequence of their deposition is uniform across most taxa; all that really differs is the length of time each tissue type is deposited. The uniformity of

marsupial bone histology reflects uniformity of their life history, especially related to the ontogeny of growth rates. All marsupials are extremely altricial, experience their time of fastest growth at or just prior to weaning, and then continue to grow for an extended period relative to their lifespan. In other words, the shape of the marsupial growth curve is the same across taxa; what differs is the body size to which it is scaled.

That *Notoryctes* shows a different histological pattern might suggest that its growth pattern fundamentally differs from that of other marsupials. However, like other marsupials, *Notoryctes* is born altricial; at least the beginning of its growth trajectory must resemble that of other marsupials, and indeed, its primary cortical tissues resemble the general histological condition in the joeys of other taxa. Based on its histology, I predict that *Notoryctes* differs in the second phase of growth; that the time of slow growth after weaning is truncated, or that the time of fastest growth is extended slightly. Similarly, histological indicators of senescence (the EFS) in some vombatiforms suggest that they too have altered the typical marsupial pattern, by truncating growth relatively earlier than most other taxa. What is important is that both of these patterns of growth and histology can be achieved merely by truncating the end phase of the typical marsupial growth pattern (albeit at different points).

Among placental mammals, histological variability likely reflects greater diversity in the ontogeny of growth rates and the timing of the period of fastest growth. In other words, the shape and slope of the growth curves, as well as the timing of the inflection point differ among taxa; not only the scale. However, phylogenetic signal may exist as well. As noted above, extensive studies of the bone histology of primates, bovids, and xenarthrans show that some microstructural features are shared within each clade, but the larger groups are quite different from each other. Therefore, the idea of a common pattern of growth and histology across Placentalia or Mammalia does not make sense in light of observed variation in the growth curves and bone histology among living taxa.

ACKNOWLEDGMENTS

I thank the following people and institutions for their assistance in accessing and destructively sampling specimens: Neil Duncan and Eileen Westwig (AMNH); Jim Bothmer, David Crawford, and Robert Heaney (CMC); Jon Dunnam (MSB); Chris Conroy, Eileen Lacey, and Jim Patton (MVZ); and Pat Holroyd and Mark Goodwin at the UCMP. I thank the UCMP, April Carr, and Kevin Padian for access to preparation and imaging facilities. I am extremely grateful to Bill Clemens, Pat Holroyd, Meike Köhler, Ralph Molnar, Jim Patton, and Marcelo Sánchez-Villagra for very helpful discussions about mammalian growth, ontogeny, and biology. The UCMP VP Lunch seminar group was a supportive and helpful sounding board at all stages of this project. Finally, I thank the following institutions for funding and financial support during this project: Paleontological Society (N. Gary Lane Award), University of California, Berkeley (Graduate Division Summer Fellowship), and UCMP (Peabody Fellowship). This chapter is dedicated to Bill Clemens, Pat Holroyd, and Rich Cifelli, whose work on fossil mammals continues to provide inspiration. That I should find myself working on marsupials is probably equally surprising to all of us.

Figure 3.1 Mid-diaphyseal femur of *Cercartetus nanus* **(**MVZ 127329) in regular transmitted light. A shows a histological overview, B highlights microstructural features such as LAGs (arrows) and the border between woven-fibered and parallel-fibered bone in the inner cortex (dotted yellow line). Along most of this border, a LAG is present. As in most marsupials under 40-50 g adult body mass, the mid-diaphyseal femur of *Cercartetus* is avascular. Scale = 250 µm.

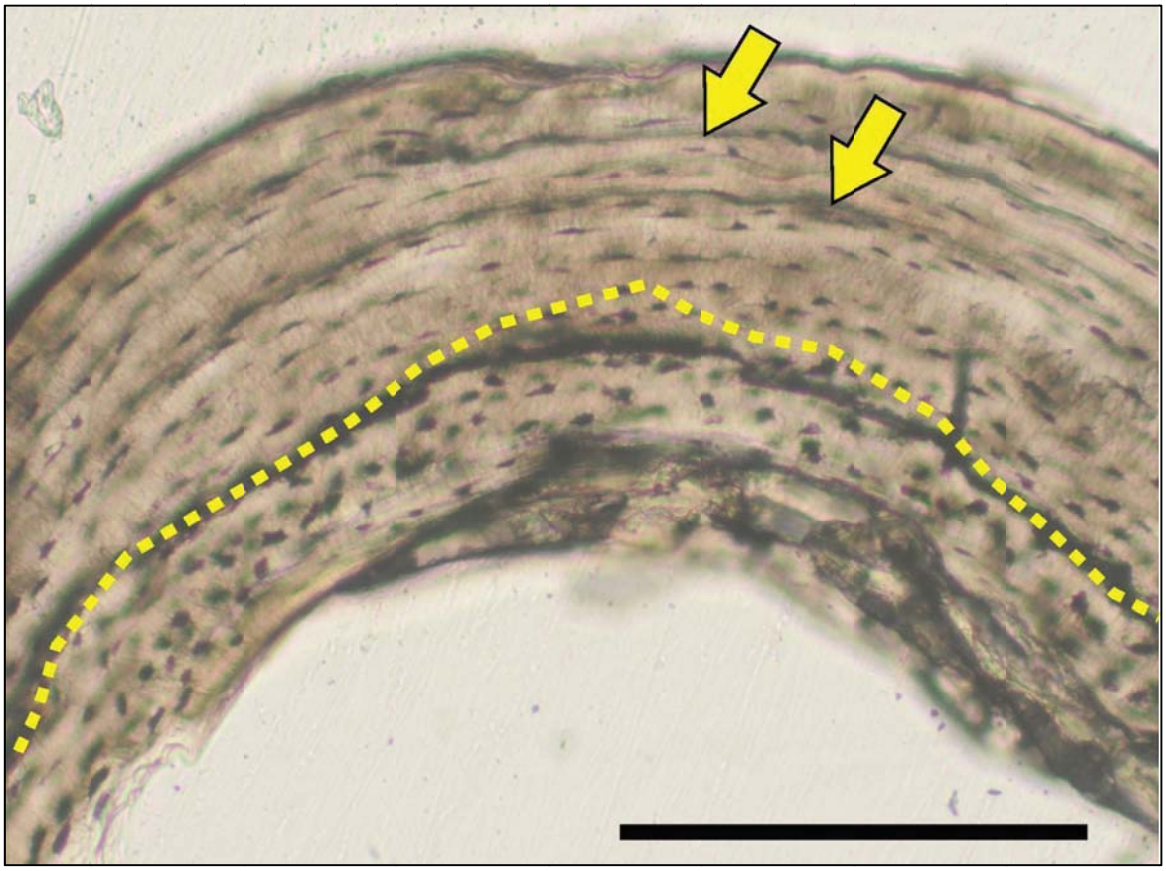

Figure 3.2 Mid-diaphyseal femur of *Cercartetus nanus* **(**MVZ 127329) in regular transmitted light. A shows a histological overview, B highlights microstructural features such as vascular canals (white triangles) and the border between woven-fibered and parallel-fibered bone tissue in the inner cortex (dotted yellow line). Along most of this border, a LAG is present. Periosteum to top of image. Scale = 250 µm.

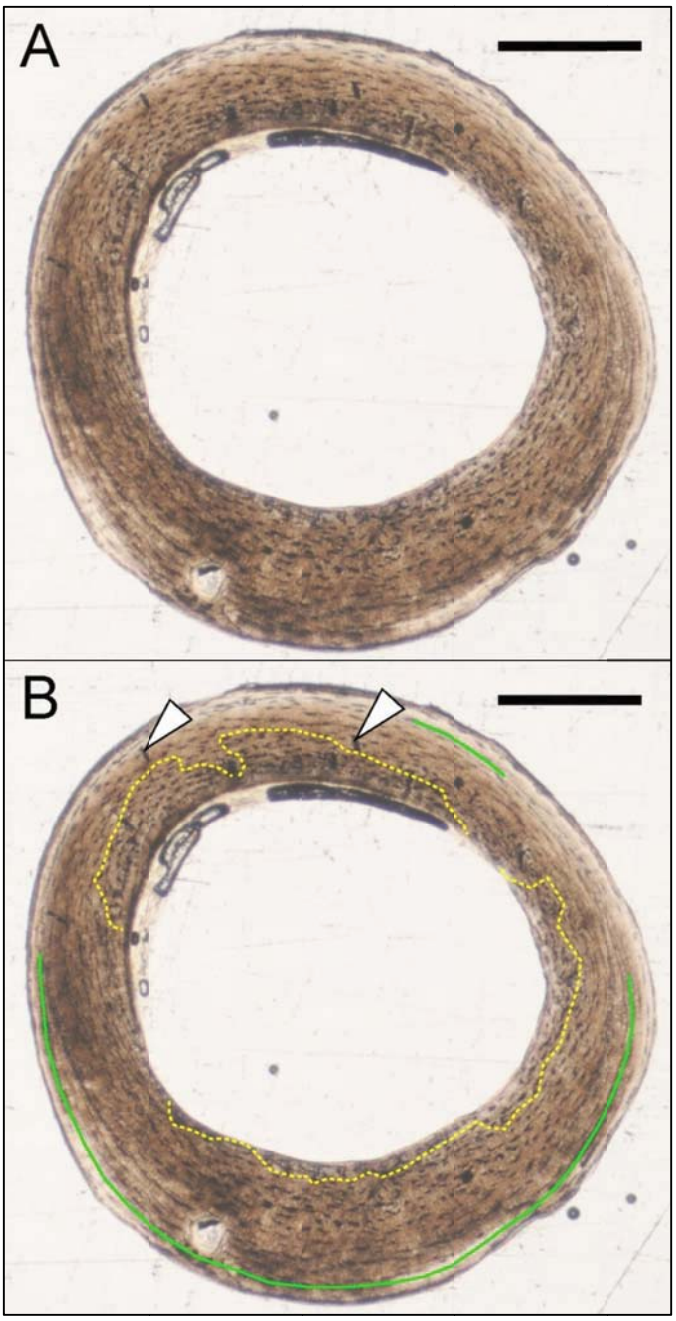

Figure 3.3 Mid-diaphyseal femur of *Lestoros inca* (MVZ 166511) in regular transmitted light. A shows a histological overview, B highlights microstructural features such as vascular canals (white triangles), the location of woven-fibered bone (internal to dotted yellow line), and a LAG (solid green line). External to the woven-fibered region, all tissue is parallel-fibered bone. This specimen poorly vascularized by simple primary canals that occur in only one region. As in most marsupials under 40-50 g adult body mass, the mid-diaphyseal femur of *Cercartetus* is avascular. No lamellae line the endosteal margin, suggesting that this animal was actively expanding the medullary cavity at the time of death. Scale = 250 μm.

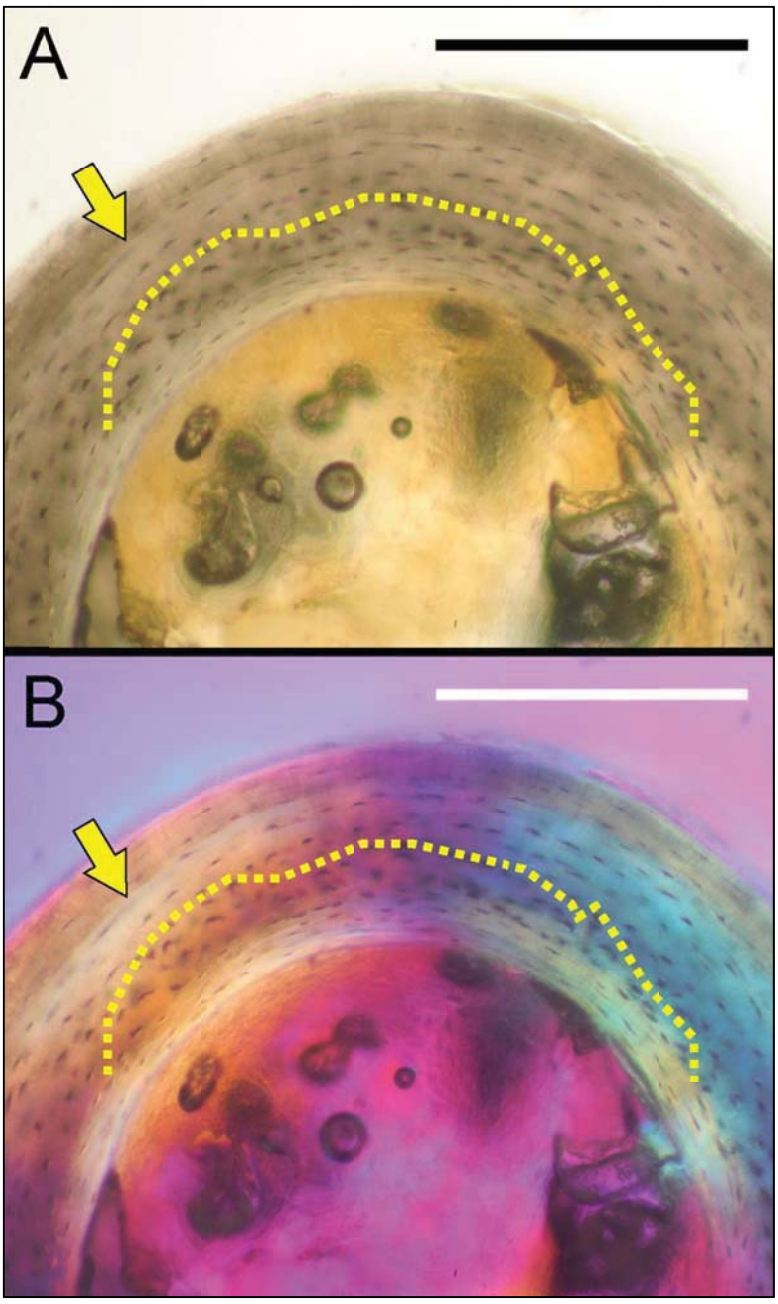

Figure 3.4 Mid-diaphyseal femur of *Acrobates pygmaeus* (MVZ 134404) in regular transmitted light (A) and elliptically polarized light (B). In both images, osteocyte orientation and shape in the woven-fibered region (internal to dotted yellow line) are distinctly different from regions of parallel-fibered bone (between dotted yellow line and LAG at arrow). External to the LAG, the tissue is lamellar. A band of lamellar bone lines the endosteal margin, suggesting that this animal was not actively expanding the medullary cavity at the time of death. Periosteum to top of both images. Scale = 250 μm.

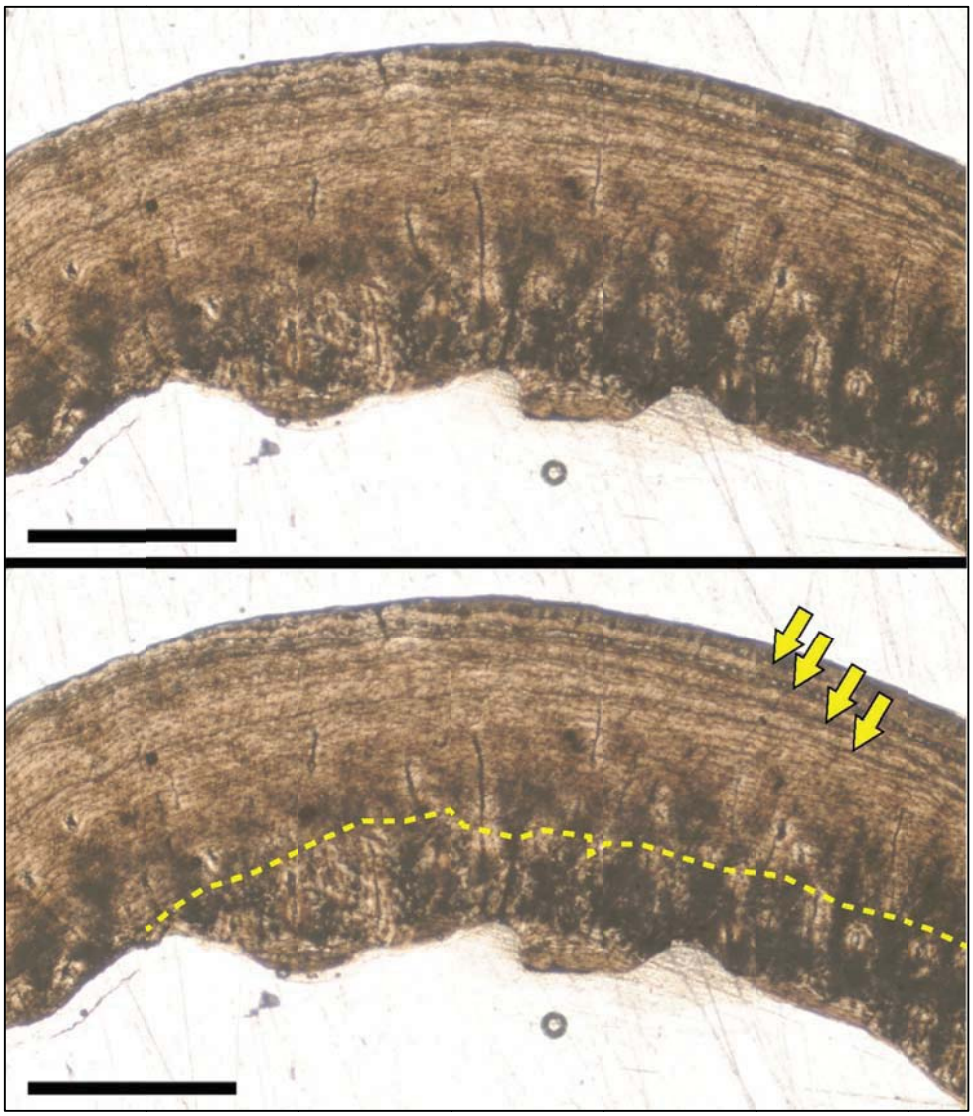

Figure 3.5 Mid-diaphyseal femur of *Potorous tridactylus* (MVZ 127712) in regular transmitted light. Top image shows a histological overview, bottom image highlights LAGs (arrows) and the border between woven-fibered and parallel-fibered bone in the inner cortex (dotted yellow line). In this specimen, the transition is separated from the first LAG by a thick band of parallel-fibered bone. All canals in this specimen are radial or radially oblique primary osteons (thin black lines). Vascular density begins to decrease external to the border between woven-fibered and parallel-fibered bone. Beyond the first LAG, the bone is nearly avascular. No lamellae line most the endosteal margin, suggesting that this animal was actively expanding the medullary cavity at the time of death. Periosteum to top of image. Scale = 500 μm.

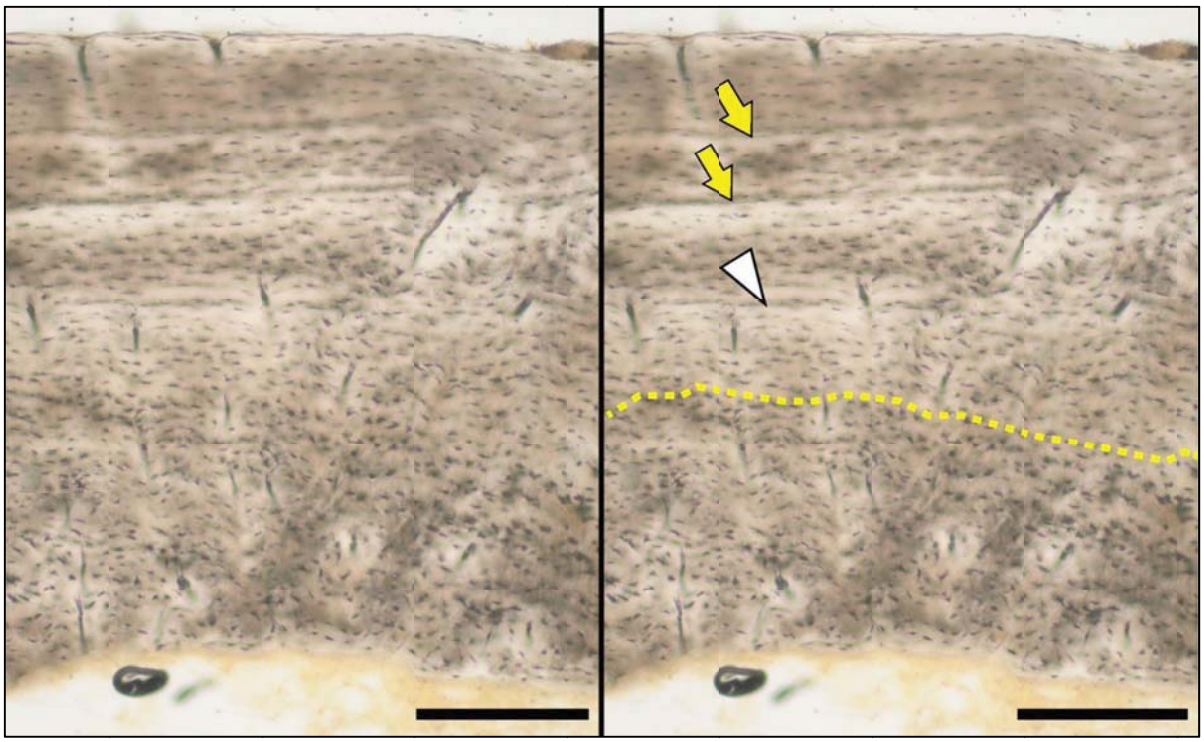

Figure 3.6 Radial transect through the mid-diaphyseal femur of *Isoodon macrourus* (UCMP 77305) in regular transmitted light. Left image shows a histological overview, right image highlights LAGs (arrows), an annulus (white triangle), and the border between woven-fibered and parallel-fibered bone in the inner cortex (dotted yellow line). All canals in this specimen are short radial or radially oblique primary osteons (thin vertical black lines). Vascular density begins to decrease external to the border between woven-fibered and parallel-fibered bone. Beyond the first LAG, the bone is only poorly vascularized. No lamellae line the endosteal margin, suggesting that this animal was actively expanding the medullary cavity at the time of death. Periosteum to top of image. Scale = 250 μm.

Figure 3.7 Mid-diaphyseal femur of *Bettongia* (UCMP 53685, Pleistocene) in regular transmitted light (top) and elliptically polarized light (bottom). Annuli (white triangles) are visible in the mid- and outer cortex, and three closely-spaced LAGs (arrows) lie close to the surface. The annuli are more distinct in polarized light. The bone tissue is woven-fibered on both sides of the inner annulus, but quickly grades to parallel-fibered bone approaching the second annulus. Vascular density also decreases approaching the second annulus. Most canals in this section are short radial or radially oblique primary osteons, but a few canals in the inner and midcortex form small reticulations connecting three or four longitudinal primary osteons. Periosteum to upper left of image. Scale = 1 mm.

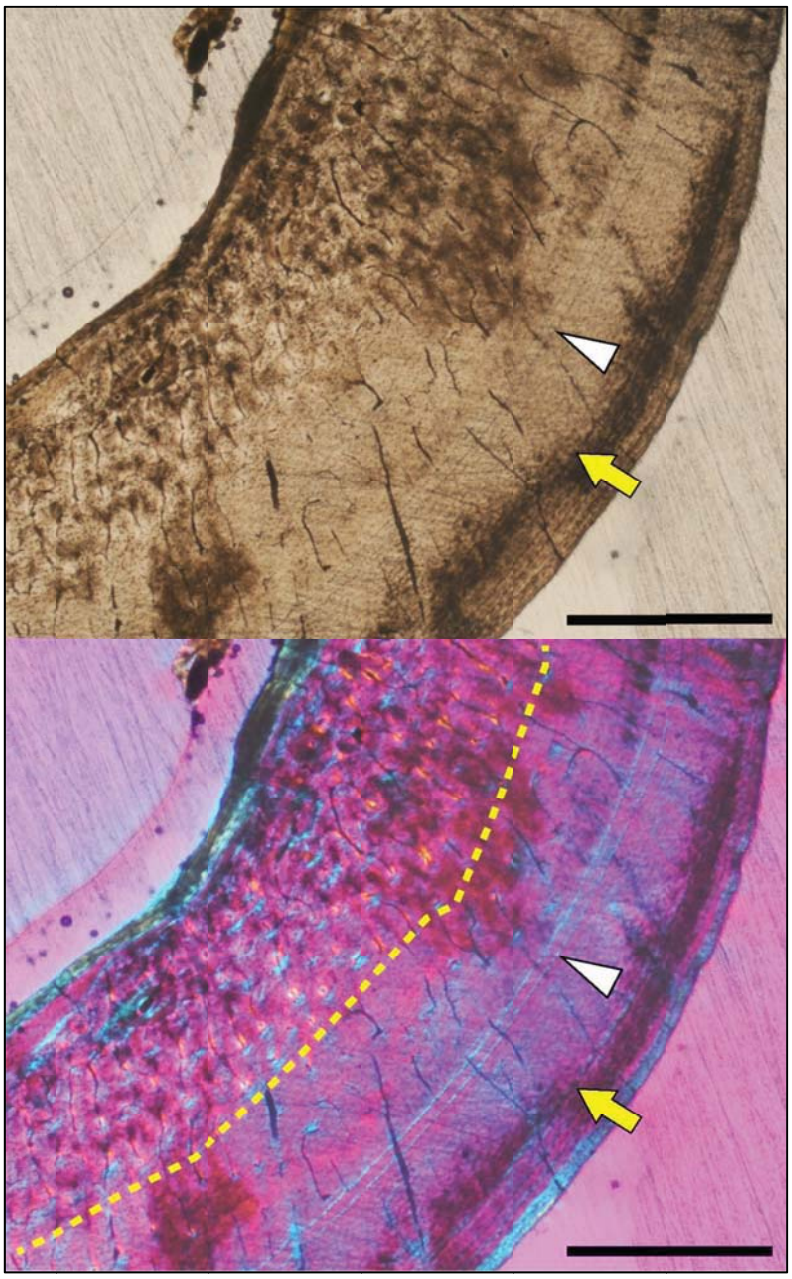

Figure 3.8 Mid-diaphyseal femur of *Phascolarctos cinereus* (UCMP 134825; captive reared) of known age (7 years) in regular transmitted light (top) and elliptically polarized light (bottom). The dotted yellow line indicates the border between woven-fibered and parallel-fibered bone in the inner cortex (weaning transition). The white triangle indicates a double annulus at the end of the second year of growth, and the yellow arrow indicates the innermost line of the EFS. Vascular density is highest in the inner cortex, and decreases external to the weaning transition and again external to the annulus. Five lines form an EFS in the outer cortex, but these are hard to distinguish at this magnification (see Figure 3.9). Periosteum to lower right of image. Scale = 1 mm.

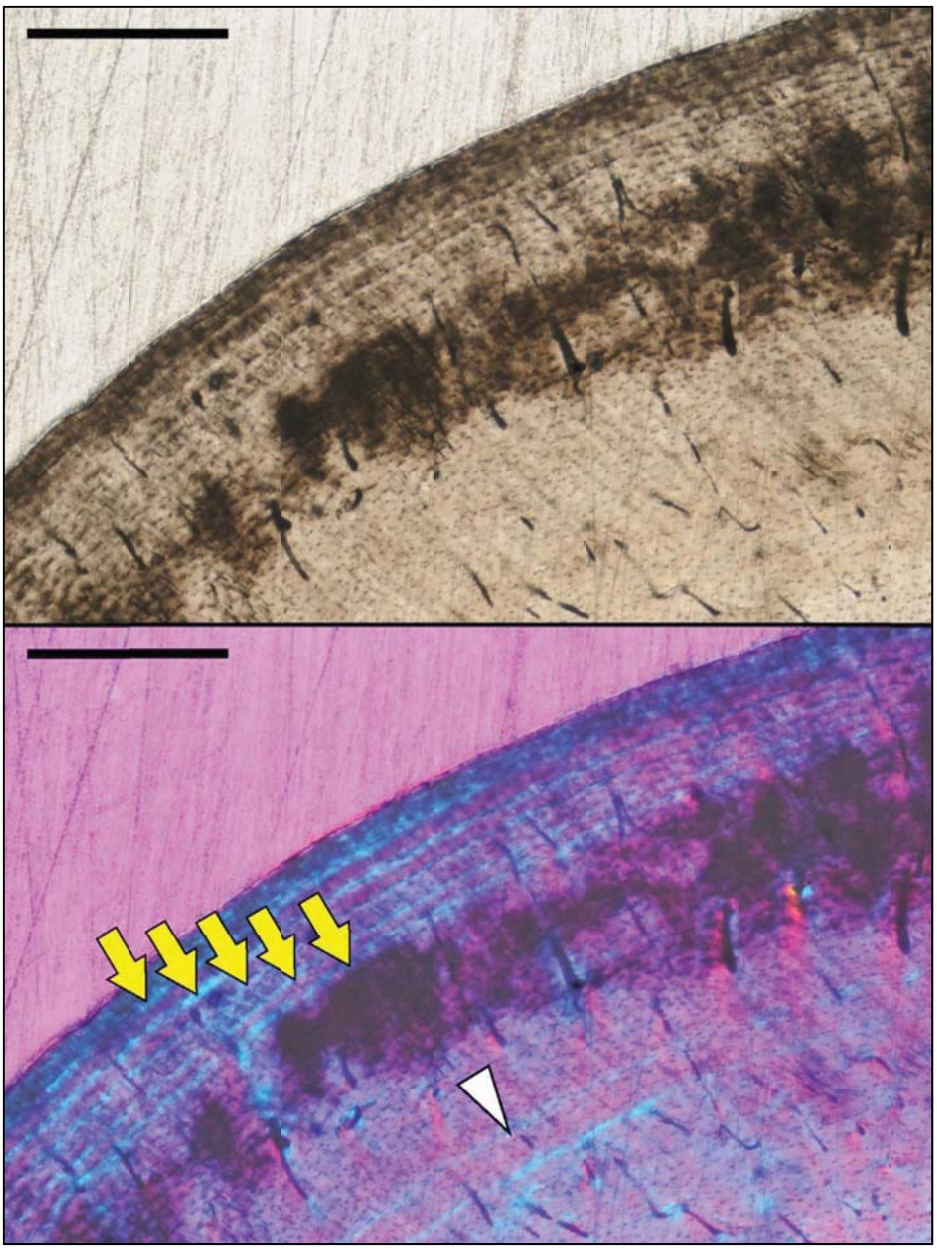

Figure 3.9 Mid-diaphyseal femur of *Phascolarctos cinereus* (UCMP 134825; captive reared) of known age (7 years) in regular transmitted light (top) and elliptically polarized light (bottom). The white triangle indicates the double annulus, and yellow arrows indicate the five lines that form the EFS. The total number of LAGs and annuli underestimates age in this specimen by one year, but in koalas, weaning is known to occur at the end of the first year. The number of growth marks plus the weaning transition provides an accurate assessment of age for this individual. Periosteum to upper left of image. Scale = 500 μm.

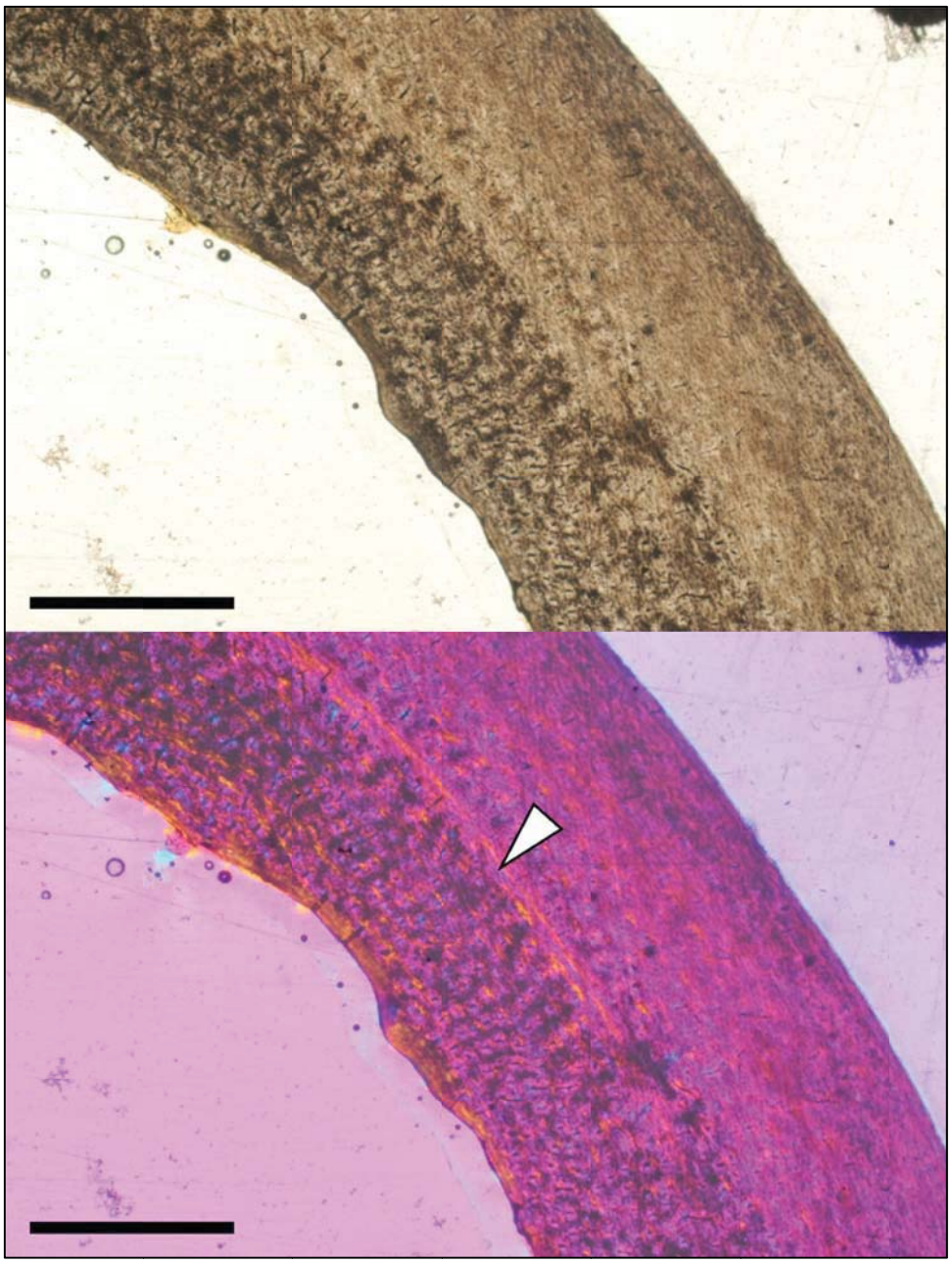

Figure 3.10 Mid-diaphyseal femur of *Dendrolagus goodfellowi* (UCMP 129785) in regular transmitted light (top) and elliptically polarized light (bottom). A single annulus (triangle) is visible in this section. Vascular density decreases dramatically external to the annulus. A transition from woven-fibered bone to parallel-fibered bone also occurs at the annulus. Juvenile *Dendrolagus* are weaned almost exactly at one year of age, and this annulus may reflect weaning or annual rhythms (or both). Periosteum to upper right of both images. Scale = 1 mm.

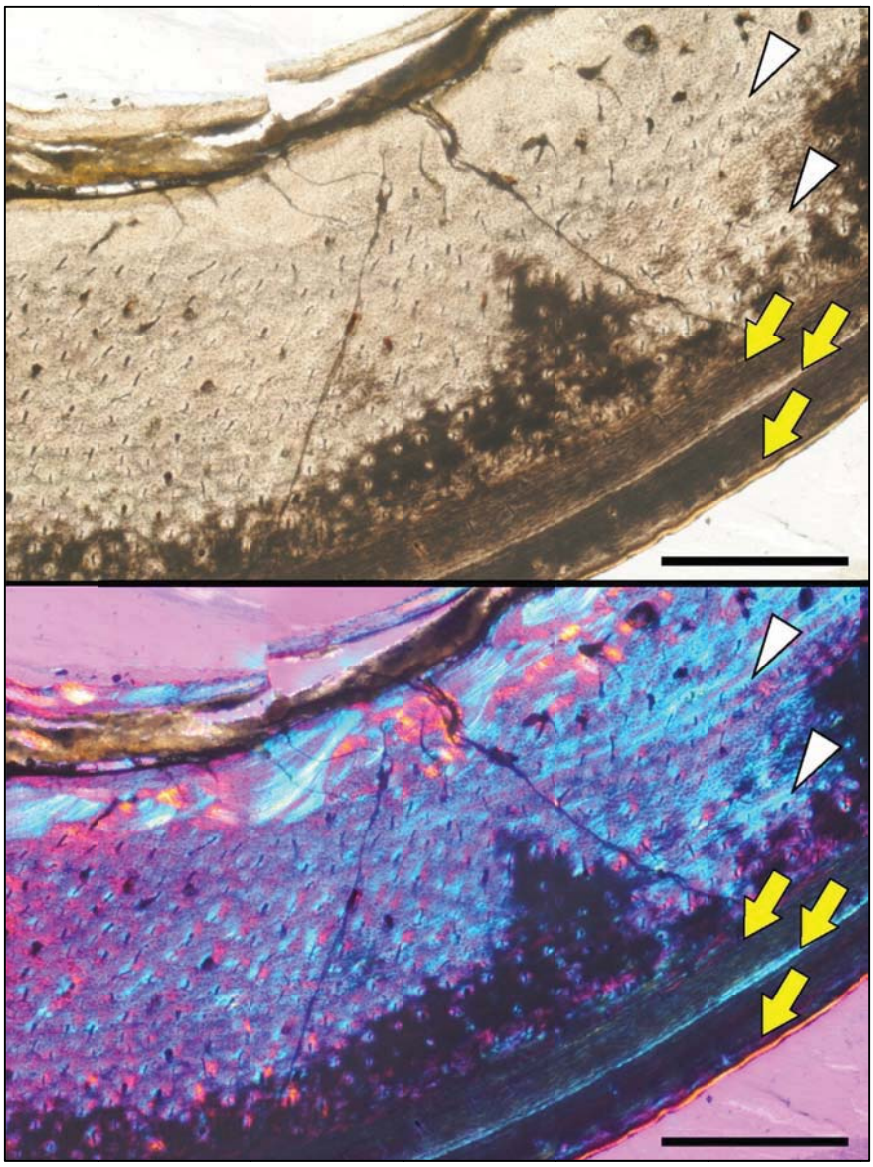

Figure 3.11 Mid-diaphyseal femur of a †*Thylacinus cynocephalus* (AMNH 35244, recently extinct) of known age (7.5 years) in regular transmitted light (top) and elliptically polarized light (bottom). In this region of the bone, annuli (white arrows) are visible in the inner and midcortex, and LAGs (arrows) are present in the outer cortex. The annuli are far more distinct in polarized light than in regular transmitted light. Only five growth marks are visible, and thus the growth marks underestimate known age by two years. Previous growth marks may have been lost to medullary expansion or remodeling, which is visible near the endosteal border (top of both images; multicolored in lower image). Most of the cortex is composed of woven-fibered primary tissue and is moderately to well vascularized by short radial-oblique primary osteons arranged in radial rows. The transition to avascular parallel-fibered bone is abrupt and occurs at the first LAG. Periosteum to lower right of both images. Scale = 1 mm.

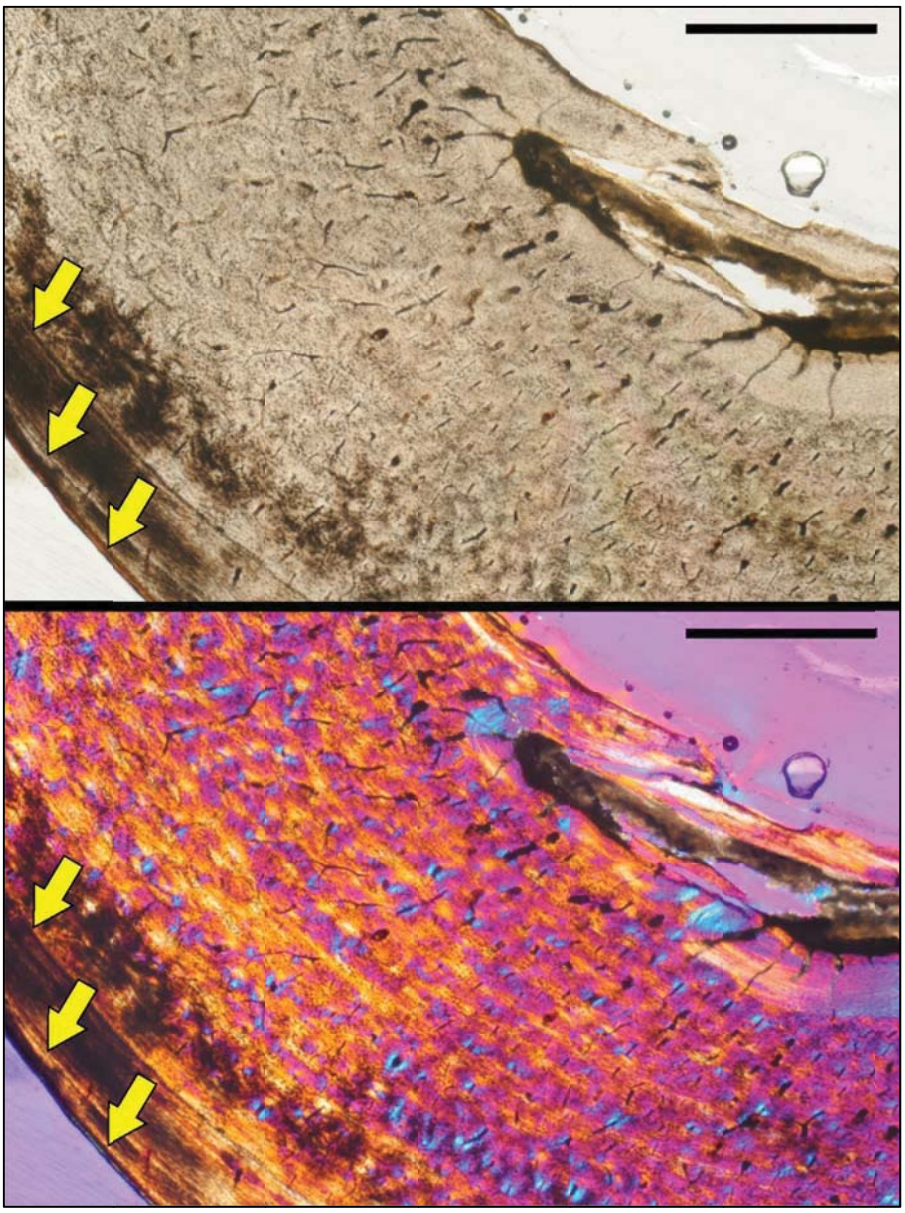

Figure 3.12 Mid-diaphyseal femur of †*Thylacinus cynocephalus* (AMNH 35244; recently extinct) in regular transmitted light (top) and elliptically polarized light (bottom). In this region of the bone (same bone and slide as Figure 3.11), annuli are not visible, although LAGs (arrows) are visible in the outer cortex. Most of the cortex is composed of woven-fibered primary tissue and is moderately to well vascularized. Compared to the region observed in Figure 3.11, fewer primary osteons are arranged radially, and small reticulations connect up to five canals. Nearly avascular lamellar bone is visible near the endosteal margin (top right). In this region of the bone, the transition to avascular parallel-fibered bone occurs just internal to the first LAG, rather than at the first LAG (compare to Figure 3.11). Periosteum to lower left of both images. Scale = 1 mm.

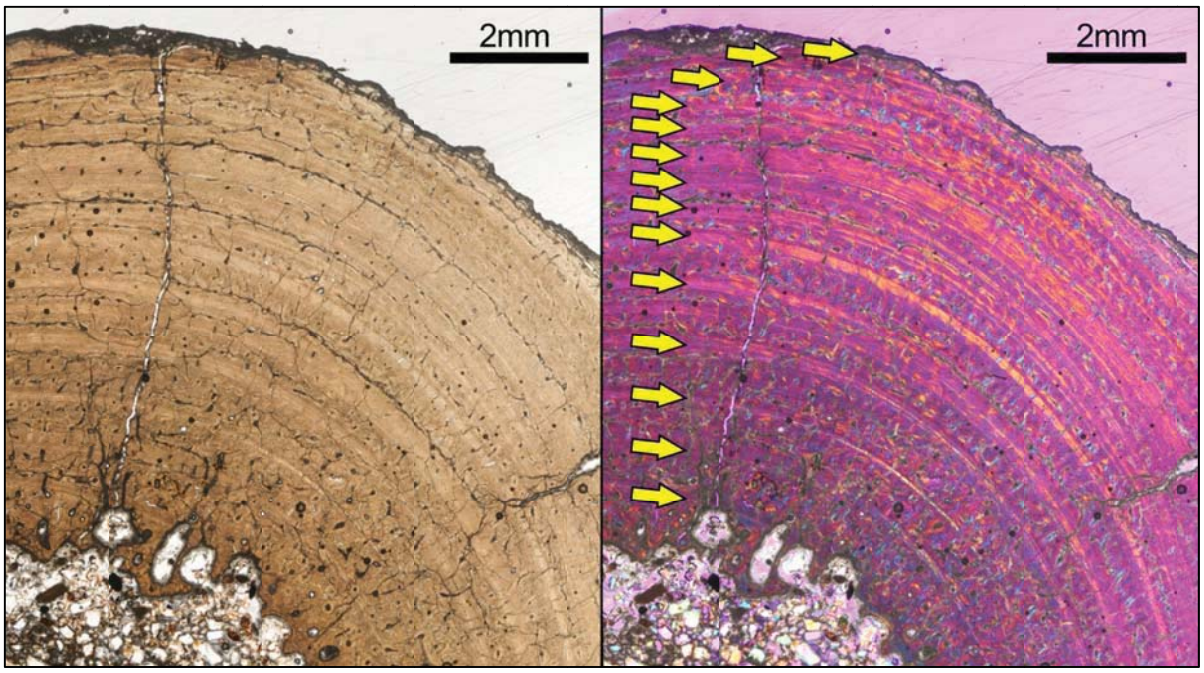

Figure 3.13 Mid-diaphyseal femur of †*Thylacoleo carnifex* (UCMP 56000; Pleistocene) in regular transmitted light (left) and elliptically polarized light (right). Fourteen growth cycles are visible around most of the circumference of this specimen, but in one region, secondary remodeling obscures the primary tissues (not pictured). In most cycles annuli (arrows) of parallel-fibered bone separate zones of woven-fibered bone, rather than LAGs. However, in three instances the annulus terminates in a LAG. The first six annuli (lower six arrows) are evenly spaced. The outer eight are also evenly spaced, but the distance between them is narrower. Moving periosteally (to top and upper right of image), the parallel-fibered annuli become proportionately broader. Most of the canals in this specimen are longitudinal primary osteons; these occasionally form small reticulations in the inner cortex. Scale = 2 mm.

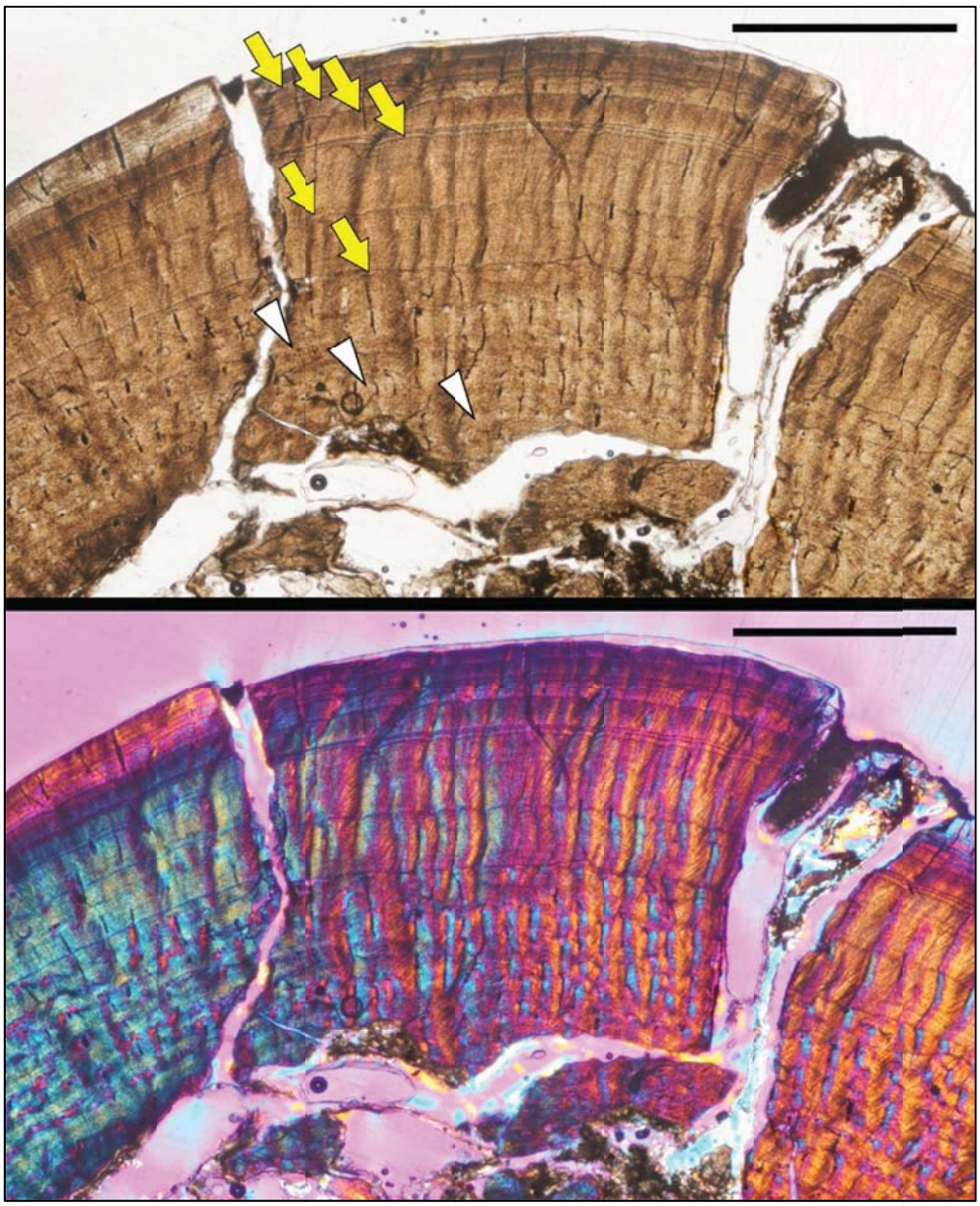

Figure 3.14 Mid-diaphyseal femur of †*Prionotemnus palankarinna* (UCMP 44597; Pleistocene) in regular transmitted light (top) and elliptically polarized light (bottom). This species is similar in size to the largest extant macropodid, *Macropus rufus* (Red Kangaroo). The entire cortex is composed of parallel-fibered bone. It is vascularized by long radial primary osteons, some of which weave in and out of the plane of section as they cross the width of the cortex. Three annuli (white triangles) and six LAGs (arrows) are preserved in this section. This likely underestimates the actual age of this individual; the femora of this this species are very hollow, and no traces of woven-fibered bone (common early in marsupial ontogeny) are visible. The early growth record was likely lost to expansion of the medullary cavity. Periosteum to top of image. Scale = 2 mm.

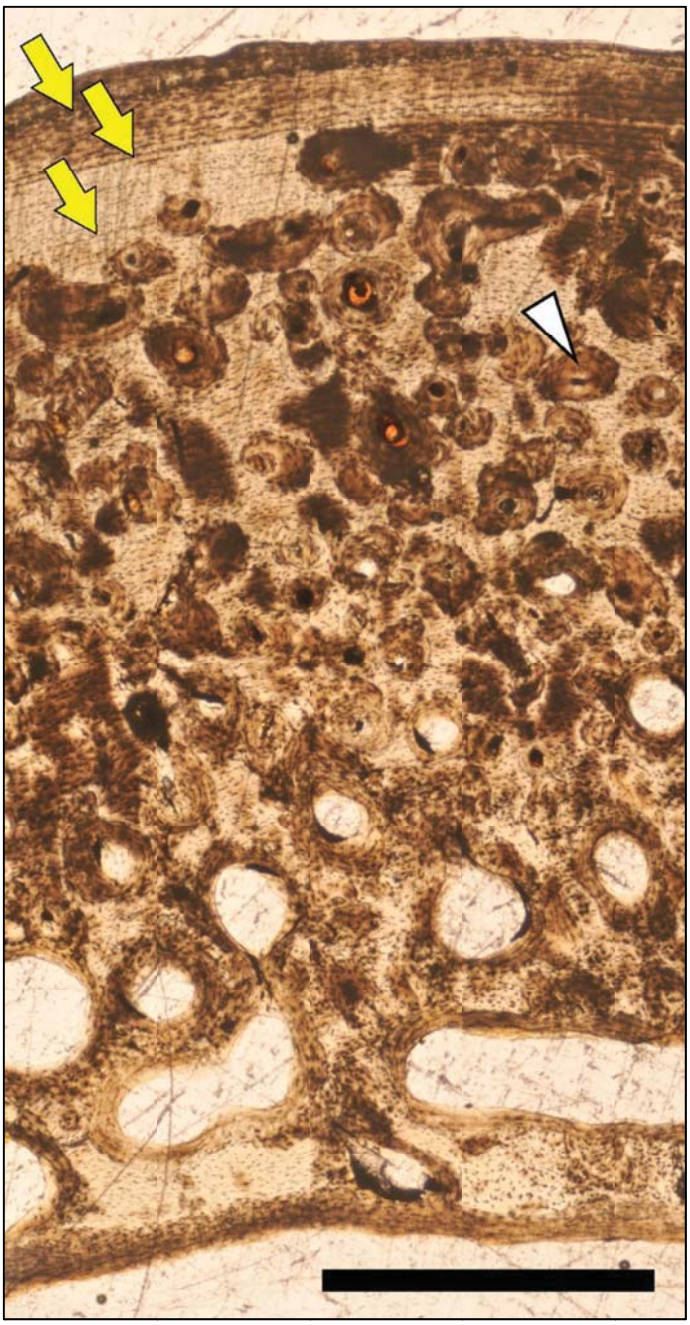

Figure 3.15 Mid-diaphyseal femur of *Vombatus ursinus* (UCMP 84850) in regular transmitted light. Unlike most marsupials, much of the inner cortex of this individual is obscured by secondary osteons (white triangle) or resorption of the inner cortex. Secondary osteons are irregular in shape and size; they often are thicker on one side of the osteon. Some primary tissue is visible between the secondary osteons; most of this is parallel-fibered bone tissue. Three LAGs are visible in the outer cortex. Periosteum to top of image. Scale = 1 mm.

Figure 3.16 Mid-diaphyseal femur of †*Diprotodon optatum* (UCMP 57350; Pleistocene) in regular transmitted light. The yellow box indicates the position of Figure 3.17. *Diprotodon* is atypical among marsupials in that most of the primary cortex is obscured by extensive secondary remodeling. Most of the original primary tissue is completely obscured by several generations of secondary osteons. However, in areas where only one generation of secondary osteons is present, hints of the original primary tissue can be seen. For example, two annuli (arrows) are visible in this section. An EFS is also visible in the outermost cortex (Figure 3.18). Periosteum to top of image. Scale = 5 mm.

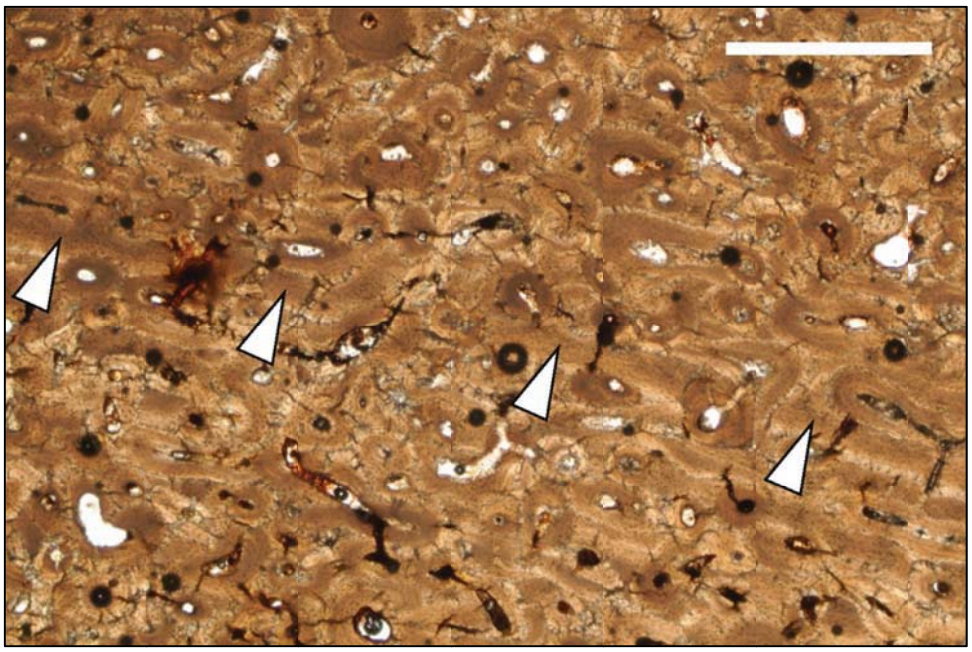

Figure 3.17 Mid-diaphyseal femur of †*Diprotodon optatum* (UCMP 57350; Pleistocene) in regular transmitted light. This specimen of †*Diprotodon* is atypical among marsupials in that most of the primary cortex is obscured by secondary remodeling. However, in areas where only one generation of secondary osteons occurs, hints of the original primary tissue can be seen. For example, traces of a thick annulus of parallel-fibered bone runs through the middle of this image at a slight angle (white triangles). The position of this image is represented by a yellow box in Figure 3.x. Periosteum to top of image. Scale = 1 mm.

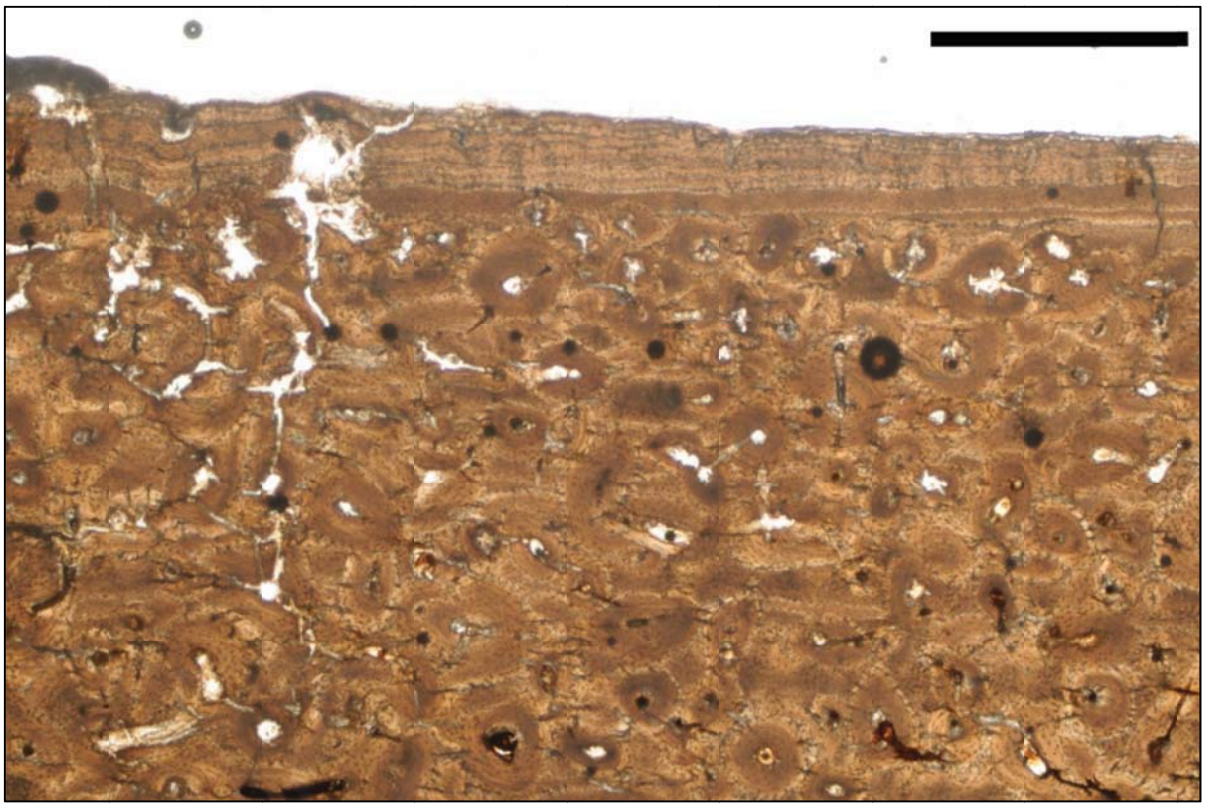

Figure 3.18 Mid-diaphyseal femur of †*Diprotodon optatum* (UCMP 57350; Pleistocene) in regular transmitted light. This specimen of †*Diprotodon* is atypical among marsupials in that most of the primary cortex is obscured by secondary remodeling, and that it preserves an EFS in the outermost cortex (thin black lines at surface). This image is taken from the same slide as Figure 3.16 and 3.17, but from a slightly different region of the cortex. Periosteum to top of image. Scale = 1 mm.

Figure 3.19 Mid-diaphyseal femora of Recent *Petaurus australis* (UCMP 77307, top) and Pleistocene *Petaurus* (UCMP uncatalogued, bottom) in regular transmitted light. The two specimens are nearly identical in size, osteocyte arrangement and density, fibrillar organization (entirely parallel-fibered), and near avascularity. Only a few short radial primary osteons are visible (white triangle); these are restricted to one region of the inner cortex in each specimen. Each of three petaurids sampled shows at least one LAG in the outermost cortex (arrow, bottom image); *P. australis* shows an additional LAG in the deep cortex (arrow, top image; see also Figure 3.20). Periosteum to left of top image, and to right of bottom image. Scale = 500 μm.

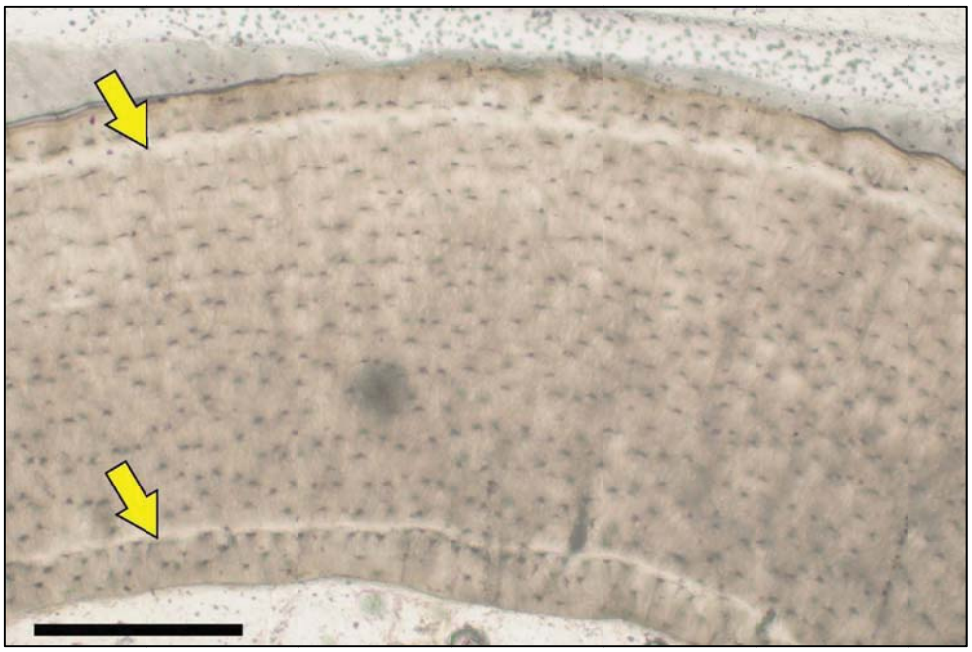

Figure 3.20 Mid-diaphyseal femur of *Petaurus australis* (UCMP 77307) in regular transmitted light. Most of the cortex is composed of avascular parallel-fibered bone, atypical of taxa in this size class. Two LAGs (arrows) are visible in this section. The similarly bright line at the bottom of this image may represent a weaning line or endosteal deposition of bone; this region is neither lamellar nor woven. Periosteum to top of image. Scale = 500 μm.

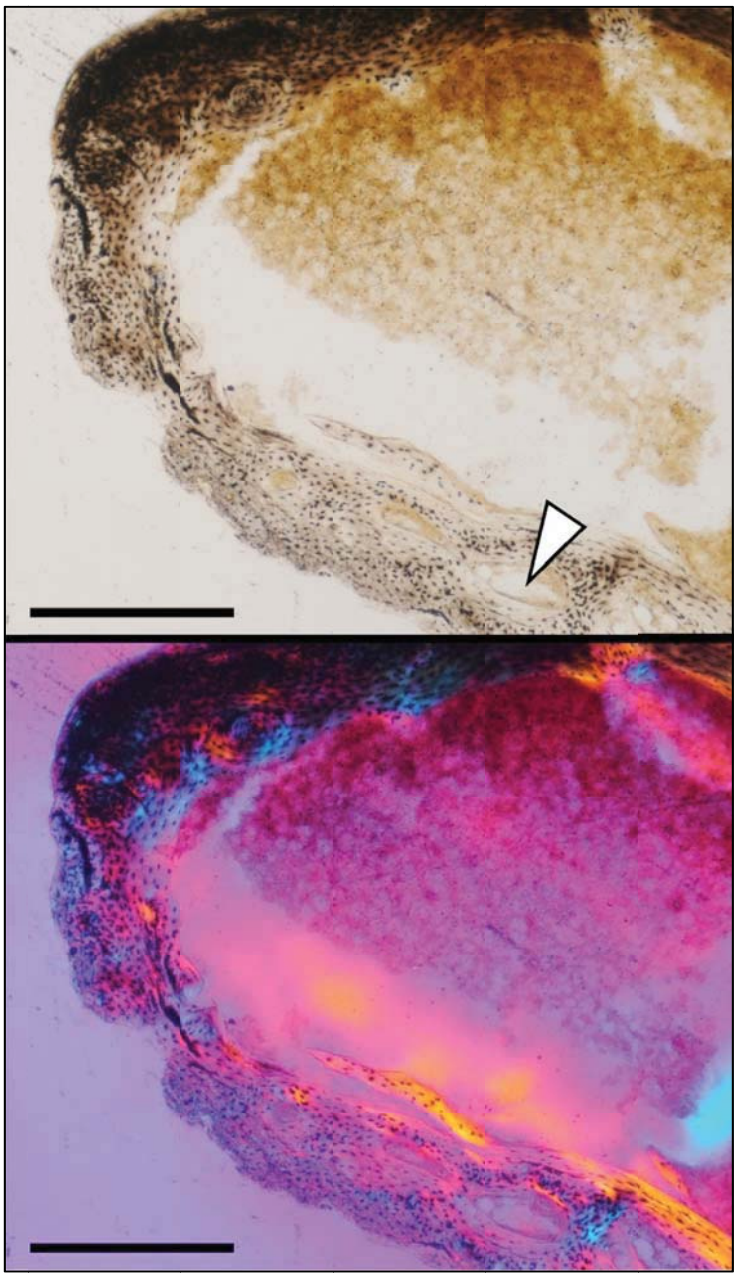

Figure 3.21 Mid-diaphyseal femur of *Notoryctes typhlops* (AMNH 15015) in regular transmitted light (top) and elliptically polarized light (bottom). This species is the only one that has woven-fibered bone throughout the entire cortex. Most of the inner cortex shows secondary resorption in the form of secondary osteons or resorption rooms (arrows). Growth and life history of *Notoryctes* are very poorly understood; unfortunately, there are no LAGs, annuli, or weaning lines present that might help to constrain age or shed light on the relative timing of weaning. Periosteum to lower left of both images. Scale = 500 μm.

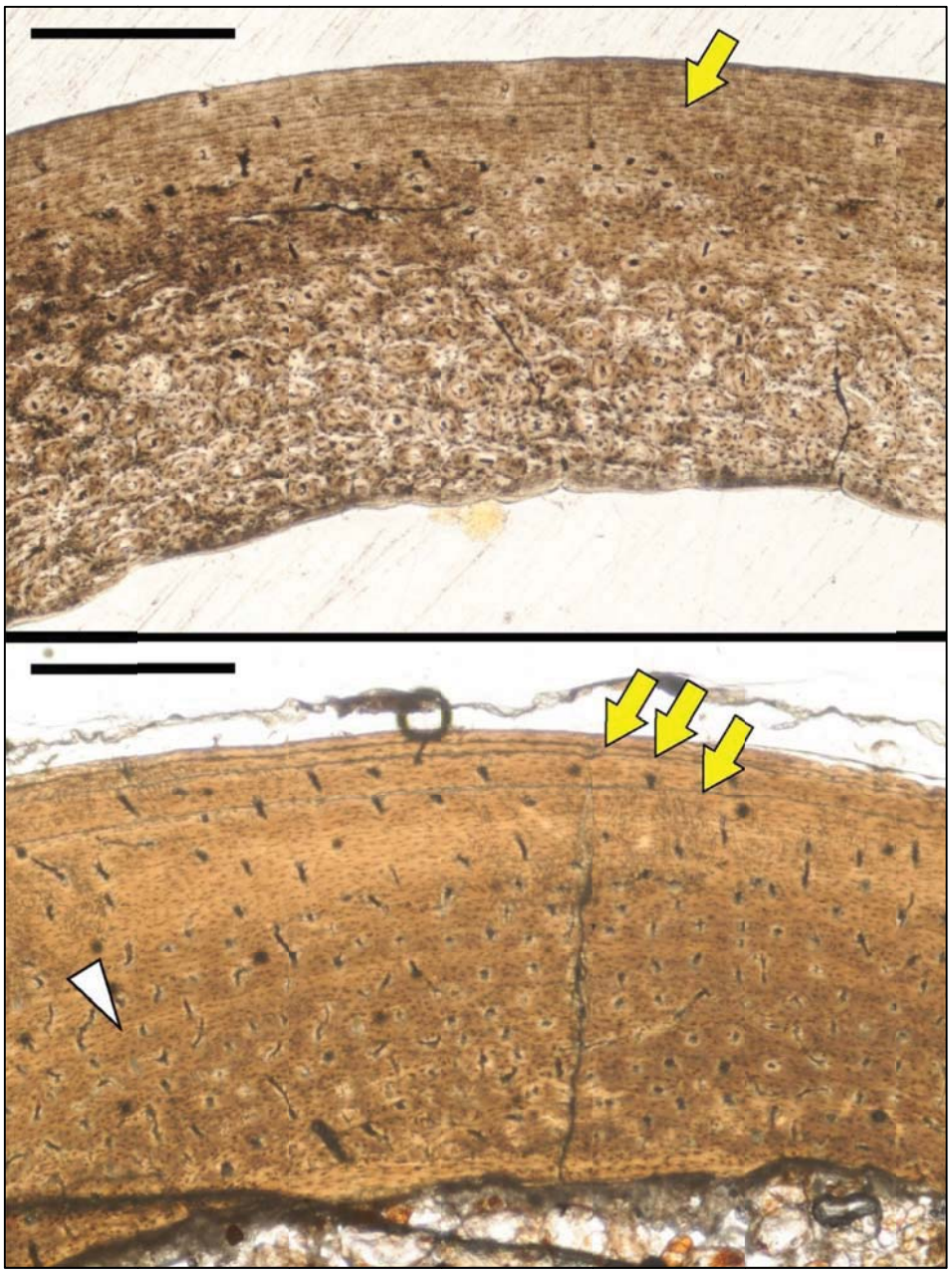

Figure 3.22 Mid-diaphyseal femora of Recent (MVZ 127709, top) and Pleistocene (UCMP 53685, bottom) *Bettongia* specimens in regular transmitted light. The two specimens are similar in size and have vascular patterns, but the Recent specimen appears ontogenetically older, despite having fewer LAGs (arrows) and annuli (white triangle) than the Pleistocene specimen. With only two specimens sectioned, it is difficult to determine whether these reflect individual variation, or differences in climate or biology between the Pleistocene and today. Periosteum to top of both images. Scale = 500 μm.

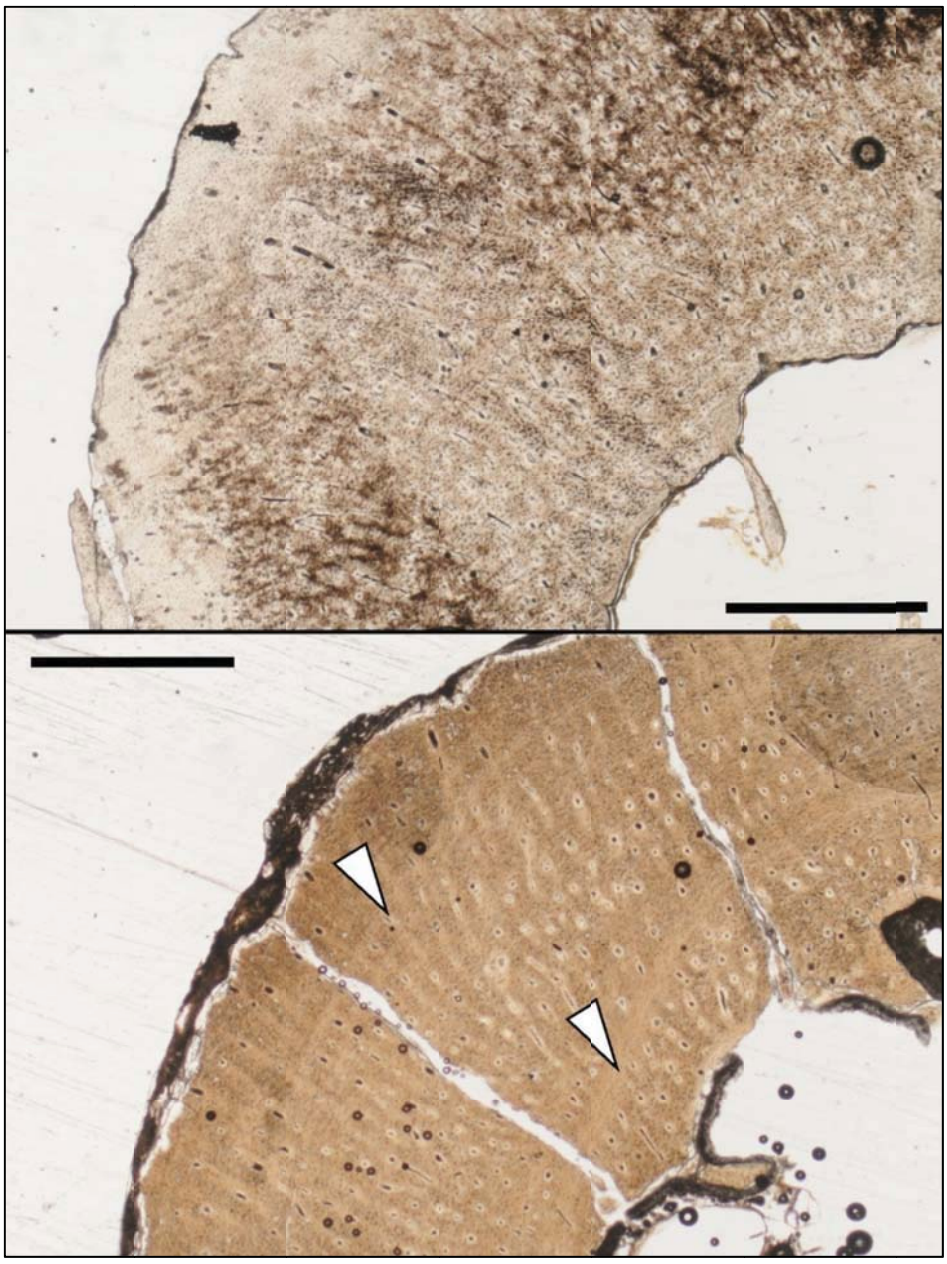

Figure 3.23 Mid-diaphyseal femora of Recent *Sarcophilus harrissii* from Tasmania (MVZ 127032, top) and Pleistocene *Sarcophilus* from the Australian mainland (UCMP 53021, bottom) in regular transmitted light. Both specimens have nearly identical vascular densities and patterns; however, the annuli are easier to see in the Pleistocene specimen. This results in part from difficulties in preparing the Recent slide; however, the annuli of MVZ 127032 are double annuli in other regions of the section. Periosteum to left of both images. Scale = 1 mm.

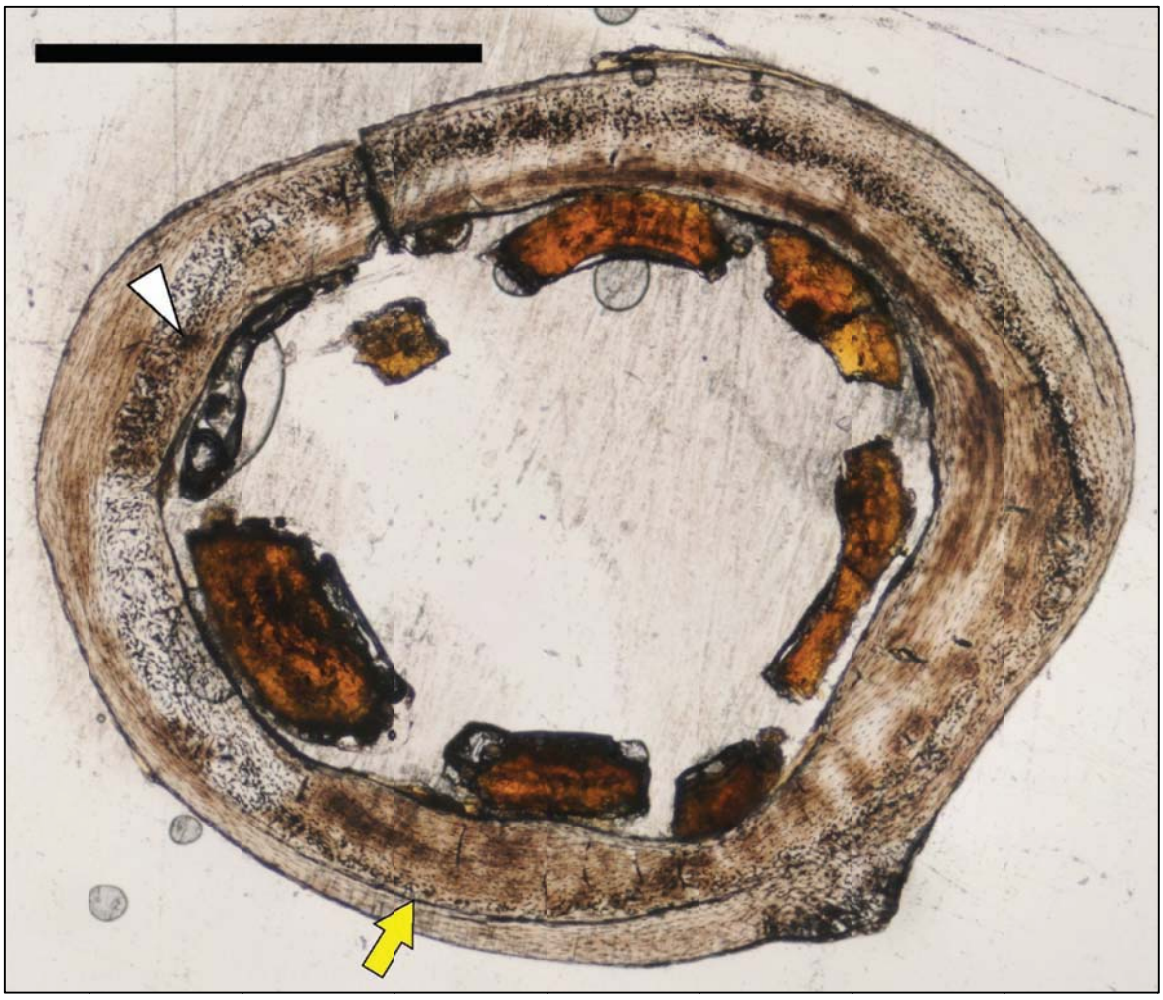

Figure 3.24 Mid-diaphyseal femur of *Elephantulus myurus* (Afrotheria; MVZ 177073) in regular transmitted light. The inner cortex is composed mostly of parallel-fibered bone, which in some regions is vascularized by short radial primary osteons. In the midcortex, a layer of woven-fibered primary bone (white triangle) is visible, bounded externally by a LAG (yellow arrow). Additional parallel-fibered bone is deposited external to the LAG. Scale = 1 mm.

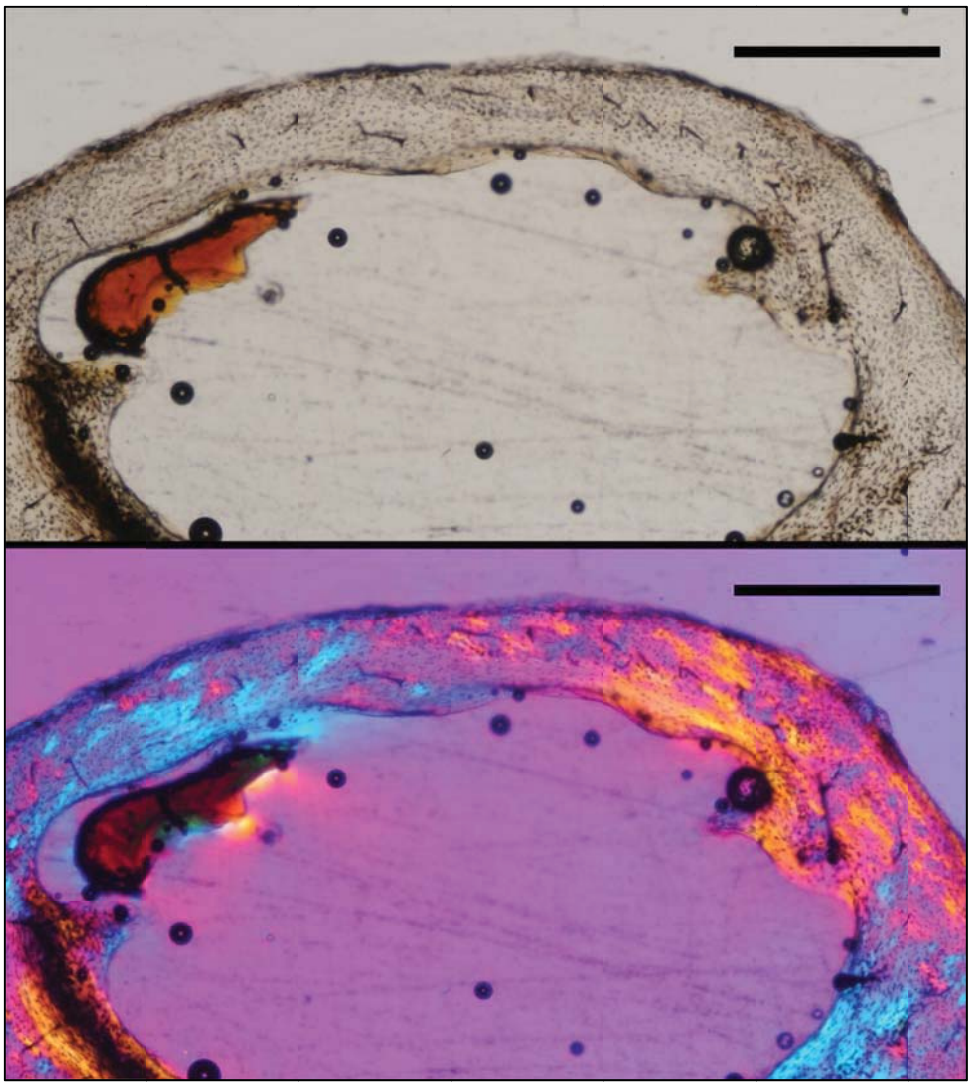

Figure 3.25 Mid-diaphyseal femur of *Amblysomus hottentotus* (Afrotheria; MVZ 117053) in regular transmitted light (top) and elliptically polarized light (bottom). This species has woven-fibered bone throughout the entire cortex. Primary osteons occur in the inner and midcortex and form small reticulations. This vascular pattern is not observed in marsupials except in taxa of much larger body size. Periosteum to top of image. Scale = 500 μm.

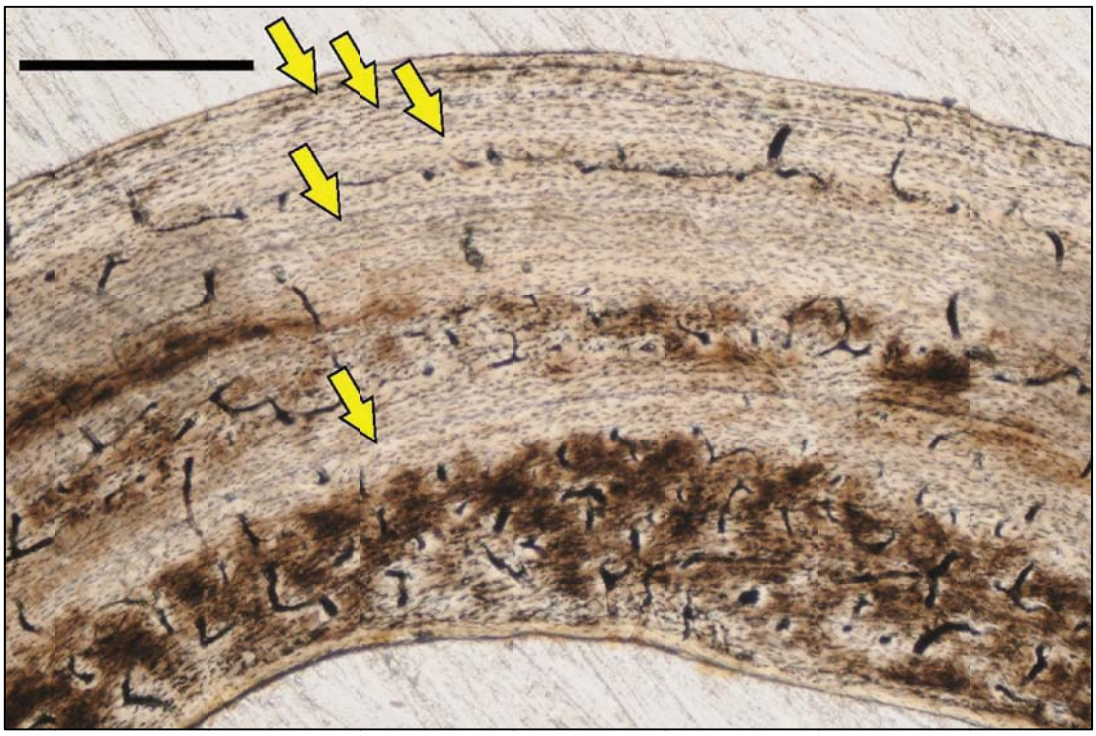

Figure 3.26 Mid-diaphyseal femur of *Procavia capensis* (Afrotheria; UCMP 58880) in regular transmitted light. The inner cortex (bottom of image) is composed of moderately vascularized woven-fibered bone. The primary osteons in this region anastomose to form small reticulations. Moving externally, this region is followed by a broad annulus of nearly avascular parallel-fibered bone. This annulus is punctuated by a central LAG (bottom arrow). External to the innermost annulus, the cycle repeats twice more, although each time the proportion of vascularized woven-fibered bone decreases. The outermost cortex is composed only of parallel-fibered bone, and two additional LAGs (top two arrows) are found in this region. Periosteum to top of image. Scale = 1 mm.

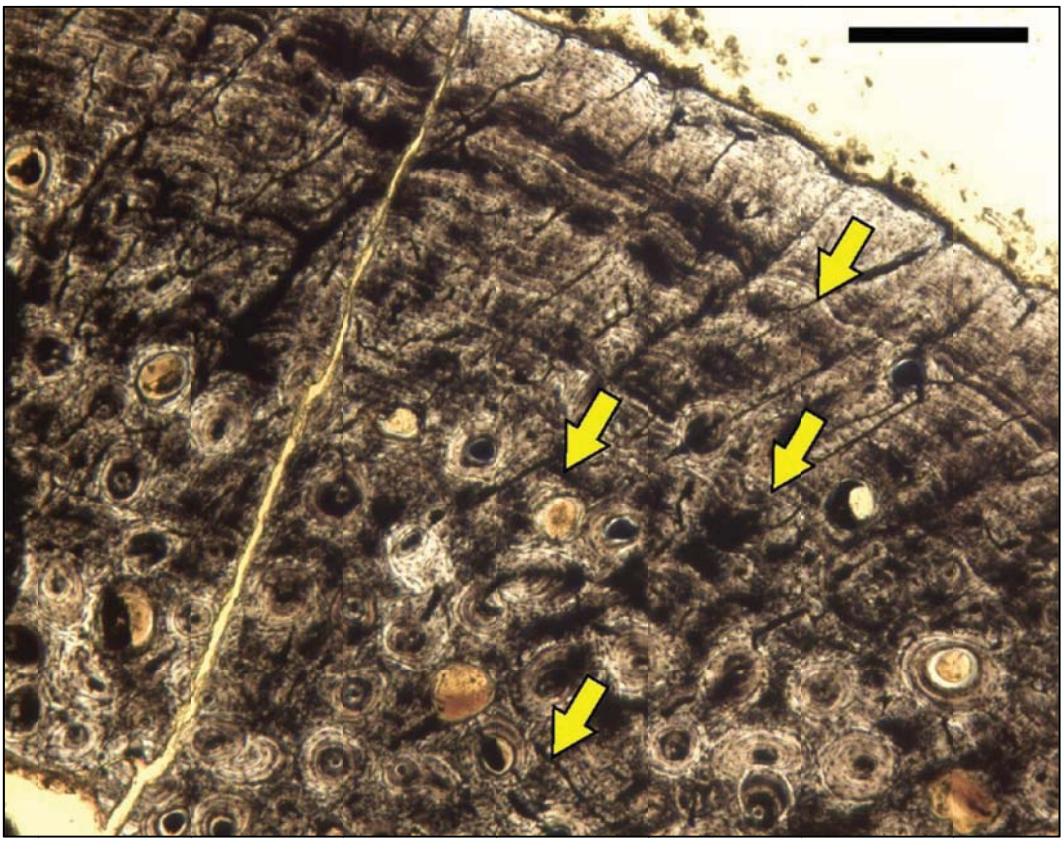

Figure 3.27 Mid-diaphyseal femur of *Bradypus tridactylus* (Xenarthra; CMC 310) in regular transmitted light. In this specimen, the inner cortex is remodeled by secondary osteons. Parallel-fibered bone is the only primary tissue observed in the outer half of the cortex. The outer cortex is moderately vascularized by radial primary osteons. Four LAGs are visible in this section (arrows). Periosteum to top right of image. Scale = 500 μm.

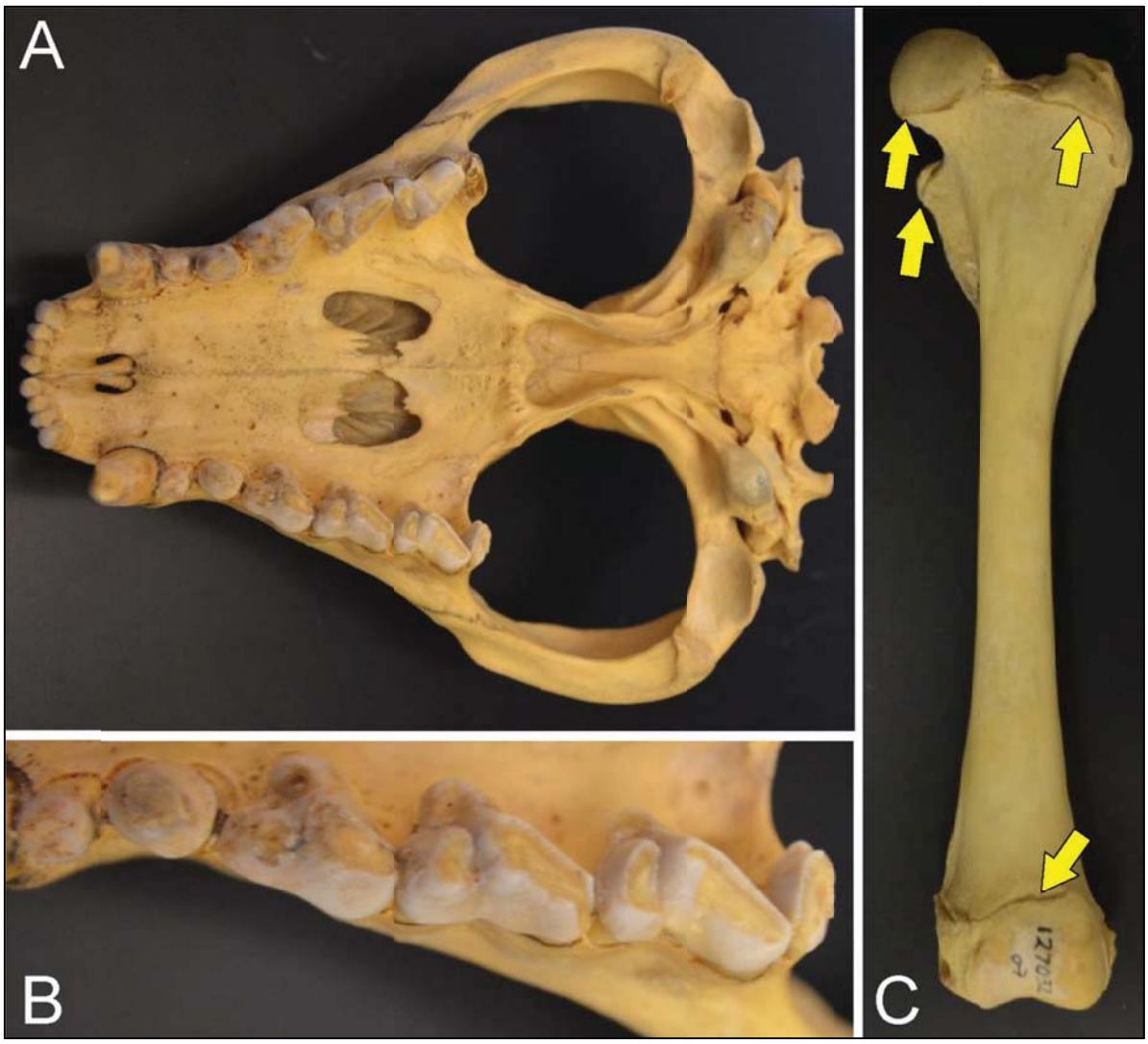

Figure 3.28 Osteological indicators of growth in a large adult individual of *Sarcophilus harissii* (MVZ 127032; wild-caught) showing A) the skull in ventral view, B) tooth wear in the upper right tooth row, and C) state of epiphyseal sutures in the left femur. This individual is above average in mass and body length for its species (Menkhorst and Knight 2011), skull sutures have begun to close, and the adult dentition is fully erupted (A). Additionally, all teeth are quite worn (B). However, every femoral epiphysis remains unfused (C). Of the six major long bones, only the humeral distal epiphysis is fused in this individual. This was the trend observed in most specimens examined for this study. A recent study (Geiger et al. 2013) has found that marsupial epiphyseal fusion occurs late in life relative to placental mammals, and that most long bone epiphyses remain open in wild individuals at the time of their death.

Figure 3.29 Epiphyseal fusion in the femora of *Phascolarctos cinereus*. The individual on the left (UCMP 134825) has fused its proximal femoral epiphysis to the diaphysis (arrow), whereas the same epiphysis remains open in the individual on the right (UCMP 58800). Once epiphyses are fused, longitudinal growth cannot occur, although appositional growth can occur at the mid-diaphysis. Histological examination of UCMP 134825 revealed an EFS in the outermost cortex (Figure 3.9), signifying the end of the active phase of skeletal growth. In contrast, UCMP 58800 does not have an EFS. The presence of an EFS is rare among marsupials. Both femora are shown pre-sectioning. Scale bars = 2 mm.

Table 3.1 Marsupial taxa sampled in previous comparative studies of osteohistology. Figure numbers and pagination are for the original references, and do not refer to images in this study.

Study	Species Examined	Species name used	Illustrated?
Quekett (1855)			
	Dasyurus viverrinus	(same)	No
	Didelphis virginiana	(same)	No
	†*Diprotodon optatum*	†*Diprotodon australis*	No
	Macropus giganteus	*Macropus major*	Yes: Plate XI, Figs. 9,10
	Petaurus norfolcensis	*Petaurus sciurœus*	No
	Phascolarctos cinereus	*Phascolarctos fuscus*	No
	Potorous gilbertii	*Hypsiprimnus murinus*	No
	Thylacinus cynocephalus	(same)	No
	Trichosurus vulpeca	*Phalangista vulpina*	No
	Vombatus ursinus	*Phascolomys vombatus*	No
Foote (1916)			
	Macropus rufogriseus	*Macropus* sp. - Wallaby	Yes: Plate 9, Fig. 174
	Thylacinus cynocephalus	(same)	Yes: Plate 14, Fig. 237
	Trichosurus vulpeca	(same)	Yes: Plate 9, Fig. 184
	Vombatus ursinus	*Phascolomys ursinus*	Yes: Plate 9, Fig. 185
Amprino and Godina (1947)			
	Didelphis aurita	*Didelphis azarae*	Yes: Plate , Figs. 48,49
	Macropus giganteus	(same)	Yes: Plate , Fig. 61
	Macropus sp.	(same)	Yes: Figs. 50-60,62,63
	Onychogalea lunata	(same)	No
	Pseudocheirus peregrinus	(same)	No
Enlow and Brown (1958)			
	Didelphis sp.	(same)	Plate XXVIII, Figs. 4-7
Leahy (1991)			
	Euryzygoma or *Zygomaturus*	(same)	No
Chinsamy-Turan (2005)			
	Macropus sp.	kangaroo	Yes (Figure 3.5C)
Hurum and Chinsamy-Turan (2012)			
	Didelphis virginiana	(same)	Yes (Figure 10.5)
	Macropus sp.	(same)	Yes (Figure 10.5)

Table 3.2 Marsupial specimens sectioned for this study, relevant natural history data, and histological sampling information.

Abbreviations: Sex: F, female; M, male; U, unknown. **Mass**: NR, not recorded; U, unknown. Lengths: NR, not recorded; U, unknown; numbers indicate the standard measurements of head-body length—tail length—pes length—ear length, all in millimeters. **Age**: A, adult; SA, subadult; numbers indicate age in years for animals of known age. **Basis** [for assessing age]: A, known age; BL, body lengths; D, dental formula; E, femoral epiphyses fused; FL, femoral length compared to specimens of known adult status; M, body mass; R, reproductive maturity based on young in pouch or lactation (females) or testes size (males); SkL skull length compared to specimens of known adult status. When different indicators suggested different ages, the subadult indicators precede the adult indicators. **Birth, Death**: U, unknown; **Locality**: ARG, Argentina; AUS, Australia; BOL, Bolivia; ECUA Ecuador; PNG, Papua New Guinea; USA, United States of America. **Side** [of femur sampled]: L, left; R, right. **TL**: TL, total proximal-distal length of femur sampled. **MDD**: distance from the proximal end of the femur to the mid-diaphysis. **LAGs** (numbers of lines of arrested growth): A, annulus; EFS, external fundamental system; L, LAG. Codes are sampling codes for slide labels.

Adult dental formulae, size, and body mass from: Kirsch and Waller (1979); Flannery (1995); Nowak (2005), Canevari and Vaccaro (2007); Menkhorst and Knight (2010).

Order	Family	Genus	species	Specimen	Sex
Dasyuromorphia	Dasyuridae	*Antechinus*	*flavipes*	UCMP 77310	U
		Dasyurus	*maculatus*	MVZ 127002	M
		Pseudantechinus	*macdonnellensis*	MVZ 133173	M
		Sarcophilus	-	UCMP 53021	U
		Sarcophilus	*harrisii*	MVZ 127032	M
		Sminthopsis	*crassicaudata*	UCMP 77311	U
	†Thylacinidae	†*Thylacinus*	*cynocephalus*	AMNH 35244*	M
Didelphimorphia	Didelphidae	*Didelphis*	*virginiana*	UCMP 122745	U
		Didelphis	*virginiana*	UCMP 131817	U
		Didelphis	*virginiana*	UCMP 77304	U
		Monodelphis	*domestica*	MSB 55847	M
		Philander	*opossum*	MSB 55074	M
		Thylamys	*venustus*	MSB 140325	M
Diprotodontia	Acrobatidae	*Acrobates*	*pygmaeus*	MVZ 134404	F
	Burramyidae	*Cercartetus*	*nanus*	MVZ 127329	F
	†Diprotodontidae	†*Diprotodon*	*optatum*	UCMP 57350	U
		†*Diprotodon*	*optatum*	UCMP 79745	U
		†*Ngapakaldia*	*tedfordi*	UCMP 72130	U
	Macropodidae	†*Dorcopsoides*	*fossilis*	UCMP uncat	U
		Dendrolagus	*goodfellowi*	MVZ 129785	F
		Lagorchestes	*hirsutus*	UCMP 81096	F
		Lagostrophus	*fasciatus*	UCMP 81095	U
		Macropus	*rufogriseus*	AMNH 22810*	U
		†*Prionotemnus*	*palankarinna*	UCMP 44597	U
		Setonix	*brachyurus*	UCMP 122729	U
		Wallabia	*bicolor*	UCMP 122734	U
	Petauridae	cf. *Petaurus*	-	UCMP uncat	U
		Petaurus	*australis*	UCMP 77307	U
		Petaurus	*breviceps*	MVZ 127338	M
	Phalangeridae	*Ailurops*	*ursinus*	MVZ 125528	F
		Phalanger	*gymnotis*	MVZ 129776	M
		Trichosurus	*vulpeca*	AMNH 22807*	F
		Trichosurus	*vulpeca*	UCMP 83004	F
	Phascolarctidae	*Phascolarctos*	*cinereus*	UCMP 58800	U
		Phascolarctos	*cinereus*	UCMP 77316	U
		Phascolarctos	*cinereus*	UCMP 134825	F
	Potoroidae	*Bettongia*	-	UCMP 53685	U
		Bettongia	*gaimardi*	MVZ 127709	M
		Potorous	*tridactylus*	MVZ 127712	F
	Pseudocheiridae	*Pseudocheirus*	*peregrinus*	UCMP 77306	U

Mass	Lengths	Age	Basis	Birth	Death
NR	NR	A	D,SkL	wild	wild
1.928 kg	449-450-90-46	SA/A	BL,M/D	wild	wild
NR	96-71-15.5-18	A	BL,D	wild	wild
U	U	A	FL	wild	wild
11.34 kg	659-248-103-70	A	BL,D,M	wild	wild
NR	NR	A	D,SkL	wild	wild
NR	NR	A, 7.5	A,FL	wild	zoo
NR	NR	J/SA	SkL	wild	wild
NR	NR	A	D,SkL	wild	wild
4.422 kg	858-317-75-28	A	BL,D,M	wild	wild
82 g	NR	A	M	wild	wild
300 g	NR	A	M	wild	wild
18 g	NR	A	M	wild	wild
NR	64-74-12-8*	A	BL,D,R	wild	wild
NR	NR	A	D	wild	capt
U	U	A	FL	wild	wild
U	U	A	FL	wild	wild
U	U	A	FL	wild	wild
U	U	A	FL	wild	wild
7.7 kg	600-757-140-66	A	BL,D,M,R	wild	wild
NR	NR	A	D,SkL	wild	wild
NR	NR	A	D,SkL	wild	wild
NR	NR	A	FL	U	zoo
U	U	A	FL	wild	wild
NR	NR	A	D,SkL	wild	wild
NR	NR	A	FL	wild	wild
U	U	A	FL	wild	wild
NR	NR	A	D,SkL	wild	wild
132.8 g	165-196-30-33	A	BL,D,M	wild	wild
NR	NR	A	BL,D	wild	zoo
4 kg	517-395-73-33	A	BL,D,M,R	wild	wild
NR	NR	A	FL	U	zoo
NR	NR	A	D,SkL	wild	wild
NR	NR	A	D,SkL	U	U
NR	NR	A	D,SkL	U	U
NR	NR	A, 7	A,D,SkL	U	zoo
U	U	A	FL	wild	wild
1.672 kg	380-333-133-51	A	BL,D,M	wild	wild
NR	316-255-85-45	A	BL,D	wild	wild
NR	NR	A	D,SkL	wild	wild

Locality	Side	TL (mm)	MDD (mm)
AUS	R	17.39	8
19 mi N Launceston, Tasmania, AUS	L	83.83	43
Palm Valley, 8 mi S and 4.5 mi W Hermannsburg Mission, Northern Territory, AUS	L	15.61	9
V5371, New South Wales, AUS (Pleistocene)	R	102.24	48
15.5 mi N Gladstone, Tasmania, AUS	R	117.57	61
AUS	R	14.25	7
(Bronx Zoo)	R	-	97
California, USA	R	102.6	50
Alameda County, California, USA	R	73.45	37
2 mi W Danville, Contra Costa County, California, USA	R	91.95	44
Porvenir, Chuquisaca, BOL	L	24.72	13
San Miguel Rincon, Santa Cruz, BOL	L	50.71	25
Tapecua, Tarija, BOL	R	16.22	9
AUS	R	15.38	8
Port Davey, Tasmania, AUS	L	15.59	8
V5374, South Australia, AUS (Pleistocene)	L	690	375
V5374, South Australia, AUS (Pleistocene)	R	610	350
V5858, South Australia, AUS (Miocene, Etadunna Formation)	R	235	115
V6345, Northern Territory, AUS (Teriary: Cheltenhamian)	L	166.28	85
W side of Mt. Missim, Morobe Prov., PNG	R	131.16	68
AUS	L	92.23	45
Bernier Island, Western Australia, AUS	L	88.16	47
(NY Zoological Society)	R	-	79 (D)
V5367, South Australia, AUS (Pleistocene)	L	-	152
coastal SW of Western Australia, AUS	R	102.83	58
Nepean River, New South Wales, AUS	R	190 +	108
V5545, New South Wales, AUS (Pleistocene)	R	38 +	21
11 mi NE Clifton, Darling Downs, Queensland, AUS	R	49.96	24
2 mi W Westbury, Tasmania, AUS	R	41.61	22
Tasmania, AUS/(San Diego Zoo)	R	112.85	59
1 mi SW Wau, Morobe Prov., PNG	R	92.33	48
(NY Zoological Society)	L	-	52
South Australia, AUS	R	86.23	45
U, possibly AUS	R	138.43	69
U, possibly AUS	R	145.98	75
(SF Zoo)	L	138.12	70
V67185, New South Wales, AUS (Pleistocene)	L	-	50
E Bay, 19 mi N Launceston, Tasmania, AUS	L	93.26	49
Hobart (Dynnyrne), Tasmania, AUS	L	76.11	39
AUS	L	20.93	35

LAGs	Code	Notes on LAGs
0	M1	
3-4A	M35	can't tell whether last two bracket one thick annulus or are two
1A, 1L	M39	annulus in midcortex, LAG close to surface
3L/A	MF3	inner two sidely spaced, outer may be EFS
2 3xA, 1L	M21	bright lamellar under xpol, 2 sets of triple annuli/LAGs, then 1 single LAG at the edge. Probably three growth cycles.
?1A	M2	at midcortex, but indistinct halfway around cortex
2A, 3L	M17	two annuli in woven-fibered bone
?1A, ?1L	M12	in one region there is an annulus at midcortex - same region, LAG in outer cortex
1A, 1A/L	M24	inner annulus at 2/3 cortex, A/L close to surface
1L	M27	close to surface, also texture change mid cortex
?1A	M32	possible annulus at midcortex
1A, 2L/A	M31	inner A only preserved in one region, middle in stutter, outer close to surface
1A/L	M34	close to surface, annulus portion goes around half the circumference
1A	M41	annulus at 2/3 cortex
3L	M40	innermost is thick but not even, generally encloses very woven tissue
4A, 1L +6EFS	MF9	much more remodeled than MF8, hard to see anything.
10A	MF8	8th is a LAG. Inner cortex very remodeled, LAGs as bands of PF/LB peeking through
5 mxL	MF5	5 growth cycles, last may be EFS
2-3A, 3 3xL	MF2	
3A, 1L	M22	LAG close to surface
1A, 1A/L, 1L	M8	
3L	M9	one in deep cortex, 2 close in outer cortex
4L	M16	decreasing zones, 4th LAG right at surface
2A, 5-6 mxL	MF4	inner A only under xpol light, outer A clearer under xpol, most LAGs 2x or 3x
3A, 2L	M3	
2A, 3L +?EFS	M14	burnt around half of the circumference
?1A/L	MF7	close to the surface on one side only
1L/A	M6	close to outer surface
?1A, 1L	M37	inner A hard to see in britefield, regionally bright in xpol light, L close to surface
3A +3EFS	M19	bright lamellar under xpol light
1A, 3L	M25	annulus shows small breaks, inner 2 LAGs show small lack of breaks, outer L close to surface
1A, 2L	M15	annulus very broad, inside maybe regionally L, L at midcortex, 2L just at surface
2A/L	M7	possibly a third annulus of lamellar bone in outer cortex?
1 2xA, 1A, 1L	M11	second A is close to L
1L +2EFS	M20	at 2/3 cortex
1 2xA +5EFS	M23	double A at midcortex
1L +2EFS	MF1	
1L	M26	about 4/5 of the way to the surface
2A, 1L +3EFS	M28	2 annuli visible under xpol light only as bright bands
2A, 1L	M5	slide thick, middle annulus hard to see

Order	Family	Genus	species	Specimen	Sex
Diprotodontia (continued)	Pseudocheiridae	*Pseudocheirus*	*peregrinus*	UCMP 82862	U
		Pseudochirops	*cupreus*	MVZ 140157	F
	Tarsipedidae	*Tarsipes*	*rostratus*	MVZ 134405	M
	†Thylacoleonidae	†*Thylacoleo*	*carnifex*	UCMP 56000	U
	Vombatidae	*Vombatus*	*ursinus*	UCMP 84580	U
Microbiotheria	Microbiotheriidae	*Dromiciops*	*gliroides*	MVZ 163430	F
		Dromiciops	*gliroides*	MVZ 184914	F
Notoryctemorphia	Notoryctidae	*Notoryctes*	*typhlops*	AMNH 15015	U
Paucituberculata	Caenolestidae	*Caenolestes*	*fulginosus*	MSB 70587	F
		Lestoros	*inca*	MVZ 166511	M
Peramelemorphia	Peramelidae	*Echymipera*	*kalubu*	MVZ 138478	M
		Isoodon	*macrourus*	UCMP 77305	F
		Perameles	*gunnii*	MVZ 132246	F

*sampled by Foote (1916)

Mass	Lengths	Age	Basis	Birth	Death
NR	NR	A	D,SkL	wild	wild
1.3632 kg	400-285-61-25	A	BL,D,M,R	wild	wild
NR	74-93-13-11*	A	BL,D	wild	wild
U	U		FL	wild	wild
NR	NR	A	D,SkL	U	U
41 g	115-103-19-19	A	BL,D,M	wild	wild
37 g	113-123-21-16	A	BL,D,M,R	wild	wild
NR	NR	U	-	wild	wild
23 g	NR	A	M	wild	wild
22 g	217-119-75-14	A	BL,D,M	wild	wild
385 g	320-62-54-26	SA/A	BL,M/D	wild	wild
1.035 kg	384-73-74-26	A	BL,D,M	wild	wild
769.1 g	415-77-87.6-51	A	BL,D,M	wild	wild

*measured on ethanol-preserved specimen

Locality	Side	TL (mm)	MDD (mm)
AUS	R	58.26	32
Tambul, Western Highlands Prov., PNG	R	72.58	37
Bornholm, Western Australia, AUS	R	13.49	7
V5371, New South Wales, AUS (Pleistocene)	L	270 +	155
U, possibly AUS	R	154.11	79
woods at NE end of Lago Quillen, 1km E and 1.3km S Cerro Quillen, Depto. Alumine, Neuquen Prov., ARG	L	18 (est.)	9
Refugio 3.5km N and 1.5 km E Estancia Paso Coihue, Depto. Los Lagos, Neuquen Prov, ARG	R	20.13	11
Charlotte Waters, Northern Territory, AUS	L	15.01	8
Rio Tatahuazo, 4km E of Cruz de Lizo, Bolivar, ECUA	L	14.15	7
32 km NE Paucartambo, Depto. Cuzco, PERU	R	15.22	8
Bayer River, Trauna Valley, Western Highlands Prov., PNG	R	68.47	35
Burleigh Heads, Queensland, AUS	R	64.03	34
1 mi NE Smithton, Tasmania, AUS	R	58.94	30

LAGs	Code	Notes on LAGs
2A/L	M10	one in deep cortex, one mid-outer cortex
0	M29	
0	M42	
12-13A/L	MF6	annuli mostly but some have LAGs within
2L +3EFS	M13	inner cortex remodeled, hard to see
1L	M44	very very close to surface, preserved only around half cortex
2L	M38	inner at MC, grades to A; outer distinct, close to surface
0	M18	
0	M33	
1L	M43	L close to periosteum
5L	M30	locally grade into annuli
3-4L	M4	hard to tell if periosteal surface would be LAG or not; similar change to lamellar bone right ther
1A, 2L +1-2 EFS	M36	inner annulus is in deep cortex, inner LAG fades to annulus

Table 3.3 Placental specimens sectioned for this study, relevant natural history data, and histological sampling information.

Abbreviations: Sex: F, female; M, male; NR, not recorded. Mass: NR, not recorded; U, unknown. Lengths: NR, not recorded; U, unknown; numbers indicate the standard measurements of head-body length—tail length—pes length—ear length, all in millimeters. Age: A, adult; SA, subadult; numbers indicate age in years for animals of known age. Basis [for assessing age]: A, known age; BL, body lengths; D, dental formula; E, femoral epiphyses fused; FL, femoral length compared to specimens of known adult status; M, body mass; R, reproductive maturity based on young in pouch or lactation (females) or testes size (males); SkL skull length compared to specimens of known adult status. When different indicators suggested different ages, the subadult indicators precede the adult indicators. Birth, Death: U, unknown; Locality: USA, United States of America. Side [of femur sampled]: L, left; R, right. TL: TL, total proximal-distal length of femur sampled. MDD: distance from the proximal end of the femur to the mid-diaphysis. LAGs (numbers of lines of arrested growth): A, annulus; EFS, external fundamental system; L, LAG. Codes are sampling codes for slide labels.

Superorder	Order	Genus	species	Specimen	Sex	Mass	Lengths
Afrotheria	Afrosoricida	*Amblysomus*	*hottentotus*	MVZ 117053	M	NR	113-0-16-0
Afrotheria	Hyracoidea	*Procavia*	*capensis*	UCMP 58884	F	U	NR
Afrotheria	Macroscelidea	*Elephantulus*	*myurus*	MVZ 117073	M	NR	272-137-38-x
Xenarthra	Cingulata	*Dasypus*	*novemcinctus*	UCMP 128147	NR	NR	NR
Xenarthra	Cingulata	*Dasypus*	*novemcinctus*	UCMP 128148	NR	NR	NR
Xenarthra	Pilosa	*Bradypus*	*variegatus*	MVZ 155186	M	5.1 kg	600-60-122-12
Xenarthra	Pilosa	*Tamandua*	*mexicana*	AMNH 14866*	NR	NR	NR
Xenarthra	Pilosa	*Tamandua*	*tetradactyla*	UCMP 117518	NR	NR	NR
Euarchontoglires	Rodentia	*Neotoma*	-	SW 1	NR	NR	NR
Euarchontoglires	Rodentia	*Ondatra*	*zibethicus*	SW 2	NR	NR	NR
Euarchontoglires	Rodentia	*Peromyscus*	-	SW 3	NR	NR	NR
Euarchontoglires	Rodentia	*Ratufa*	*indica*	AMNH 22837*	F	NR	787.4-482.6-63.5-x
Laurasiatheria	Artiodactyla	*Tragulus*	*javanicus*	AMNH 14128*	F	NR	NR
Laurasiatheria	Soricomorpha	*Solenodon*	*paradoxus*	AMNH 28271*	F	NR	NR

*sectioned by Foote (1916)

Age	Basis	Birth	Death	Locality	Side	TL (mm)	MDD (mm)	LAGs	Code
A	BL,D	wild	wild	Nico Smith Farm, 10 mi W Port Elizabeth, Cape Province, South Africa	R	15.88 +	10	1A	P10
A	D,FL,SkL	wild	wild	V4740, Little Witkrans, Cape Province, South Africa	R	74.83	38	3	P9
A	BL,M,D	wild	wild	Bolt Farm, 7 mi NW Krugersdorp, Guatend Province, South Africa	R	28.65	16	1L	P5
A	FL,SkL	wild	wild	NE Florida, USA	R	92.18	44	2A	P7
J	FL,SkL	wild	wild	Avon Park, Florida, USA	R	59.11 +	26	0	P8
A	BL,D,M	wild	wild	Rio Cenepa, vicinity of Aguaruna Villae, Departamento Amazonas, Peru	R	94.53	51	0	P6
A	FL,SkL	wild	wild	near Bonda, Colombia	R	-	48	3-4A	P1
J	FL,SkL	U	U	(purchased)	R	67.32	34	CND	P14
A	D	wild	wild	central USA	R	31.96	18	1A	P11
A	D	wild	wild	central USA	R	48.34	29	1+?EFS	P12
A	D	wild	wild	central USA	R	17.36	9	1A	P13
A	FL	U	zoo	"NY Zoo"	R	-	45	1A	P4
A	FL	U	zoo	"Central Park Menagerie"	R	-	45	1A	P2
A	FL	wild	wild	Haiti	R	-	32	1L	P3

Table 3.4 Adult body masses of the marsupial species examined in this study. Taxa highlighted in blue are extinct. Body masses for †*Dorcopsoides*, †*Ngapakaldia*, and †*Prionotemnus* were estimated using the equations of Wroe et al. (2004) and Helgen et al. (2006). Adult body masses are taken from these sources: Kirsch and Waller (1979); Flannery (1995); Nowak (2005), Wroe et al. (1999; 2004); Canevari and Vaccaro (2007); Menkhorst and Knight (2010).

Adult Mass	Species	Family	Order	VIC	VMC	VOC	FIC	FMC	FOC	GMP
5-10 g	*Tarsipes rostratus*	Tarsipedidae	Diprotodontia	-	-	-	P	P	P	-
10-14 g	*Acrobates pygmaeus*	Acrobatidae	Diprotodontia	-	-	-	W	P	P	M/O
10-20 g	*Sminthopsis crassicaudata*	Dasyuridae	Dasyuromorphia	-	-	-	P	P	P, L	?M
13.6-31.3 g	*Lestoros inca*	Caenolestidae	Paucituberculata	S	-	-	W	P	P, L	O
15-38 g	*Cercartetus nanus*	Burramyidae	Diprotodontia	-	-	-	W	P	L	M,O
16-42 g	*Dromiciops gliroides*	Microbiotheriidae	Microbiotheria	-	-	-	P	L	L	M,O
18-33 g	*Pseudantechinus macdonnellensis*	Dasyuridae	Dasyuromorphia	-	-	-	P	P	L	M,O
18-55 g	*Thylamys venustus*	Didelphidae	Didelphimorphia	S	-	-	P	P, L	L	O
20-75 g	*Antechinus flavipes*	Dasyuridae	Dasyuromorphia	-	-	-	P	P	P	-
34-39 g	*Caenolestes fulginosus*	Caenolestidae	Paucituberculata	-	-	-	W, P	W, P	P	-
40-70 g	*Notoryctes typhlops*	Notoryctidae	Notoryctemorphia	R, 1	-	-	W	W	W	-
58-98 g	*Monodelphis domestica*	Didelphidae	Didelphimorphia	S, 1	S, 1	-	P	P	P, L	M
90-150 g	*Petaurus breviceps*	Petauridae	Diprotodontia	S, 1	-	-	W, P	P	P, L	O
200-670 g	*Philander opossum*	Didelphidae	Didelphimorphia	1	S	-	W	P	L	M,O
450-700 g	*Petaurus australis*	Petauridae	Diprotodontia	S, R	-	-	W, P	P	P	O
0.45-1.5 kg	*Echymipera kalubu*	Peramelidae	Peramelemorphia	1, 2	1	1	W, P	P, L	P, L	I,M,O
0.5-1.1 kg	*Perameles gunnii*	Peramelidae	Peramelemorphia	1	1	1	W, P	P	P	I,M,O
0.5-3 kg	*Isoodon macrourus*	Peramelidae	Peramelemorphia	1	1	1	W, P	P	P	M,O
0.5-5.5 kg	*Didelphis virginiana*	Didelphidae	Didelphimorphia	1, 2	1	1	W	P	P	O
660-900 g	*Pseudocheirus peregrinus*	Pseudocheiridae	Diprotodontia	1	1	1	W, P	P	P	I,M,O
0.66-1.6 kg	*Potorous tridactylus*	Potoroidae	Diprotodontia	1	1	-	W, P	P	P	M,O
0.8-1.6 kg	*Lagorchestes hirsutus*	Macropodidae	Diprotodontia	1	1	1	W	P	P, L	I,M,O
1.0-2.3 kg	*Bettongia gaimardi*	Potoroidae	Diprotodontia	1, 2	1	-	W, P	P	P, L	M,O
1.3-2.25 kg	*Pseudochirops cupreus*	Pseudocheiridae	Diprotodontia	1, 2	1	1	W	W, P	P	-
1.5-3 kg	*Lagostrophus fasciatus*	Macropodidae	Diprotodontia	1	1	1	P	P	P, L	I,M,O
1.5-4 kg	*Trichosurus vulpeca*	Phalangeridae	Diprotodontia	1, 2, R	1	1	W, P	P	P, L	M,O
1.5-4.85 kg	*Phalanger gymnotis*	Phalangeridae	Diprotodontia	1	1	1	W	P	P, L	M,O
1.5-7 kg	*Dasyurus maculatus*	Dasyuridae	Dasyuromorphia	1	1	1	W, P	W, P	P	M,O
2.5-4.2 kg	*Setonix brachyurus*	Macropodidae	Diprotodontia	1	1, 2	1	W, P	W, P	P	M
6.7-9.1 kg	*Dendrolagus goodfellowi*	Macropodidae	Diprotodontia	1, 2	1	1	W, P	P	P	M,O
7-9 kg	*Sarcophilus harrisii*	Dasyuridae	Dasyuromorphia	1	1	1	W, P	W, P	P	M,O

Adult Mass	Species	Family	Order	VIC	VMC	VOC	FIC	FMC	FOC	GMP
7-10 kg	*Ailurops ursinus*	Phalangeridae	Diprotodontia	1, 2	1	1	W, P	W, P	P	M,O
7-14 kg	*Phascolarctos cinereus*	Vombatidae	Diprotodontia	1, 2	1	1	W, P	P	P	M,O
9.64 kg*	†*Dorcopsoides fossilis*	Macropodidae	Diprotodontia	1, 2	1	1	W, P	P	P	I,M,O
15-20 kg	*Wallabia bicolor*	Macropodidae	Diprotodontia	1	1	1	W	P	P, L	I,M,O
16-27 kg	*Macropus rufogriseus*	Macropodidae	Diprotodontia	1	1	1	W	W, P	P, L	M,O
20-35 kg	*Vombatus ursinus*	Vombatidae	Diprotodontia	1, 2, R	1, 2	1, 2	W	W, P	P	M,O
35 kg	†*Thylacinus cynocephalus*	†Thylacinidae	Dasyuromorphia	1, 2, R	1	1	W	W, P	P	M,O
52 kg*	†*Prionotemnus palankarinnicus*	Macropodidae	Diprotodontia	1	1	1	P	P	P	I,M,O
101-143 kg	†*Thylacoleo carnifex*	†Thylacoleonidae	Diprotodontia	1, 2	1, 2	1, 2	W, P	W, P	P	I,M,O
125 kg*	†*Ngapakaldia tedfordi*	†Diprotodontidae	Diprotodontia	1	1	1	P	P	P, L	I,M,O
2786 kg	†*Diprotodon optatum*	†Diprotodontidae	Diprotodontia	2	2	2	-	-	P, L	M,O

*mass estimated for this study

Table 3.5 Osteohistological assessments of marsupial and placental mammals, based on previously published images and personal observations of sections used in previous studies.

Abbreviations: AGMs, annual growth marks; CNBD, could not be determined; NWPB, nonwoven primary bone; Pl, plate; PO, personal observation; R completely remodeled.

Clade	Order	Family	Genus	species	Element	AGMs?
	Monotremata	Ornithorhynchidae	*Ornithorhychus*	*anatinus*	femur	1
	Monotremata	Tachyglossidae	*Tachyglossus*	*aureatus*	femur	2-3
	Monotremata	Tachyglossidae	*Tachyglossus*	*aureatus*	femur	?1
	Monotremata	Tachyglossidae	*Tachyglossus*	*aureatus*	tibia	R
Marsupialia	Didelphimorphia	Didelphidae	*Didelphis*	*aurita*	tibia	2
Marsupialia	Didelphimorphia	Didelphidae	*Didelphis*	-	humerus	1
Marsupialia	Diprotodontia	Macropodidae	*Macropus*	*giganteus*	tibia	3 ann
Marsupialia	Diprotodontia	Macropodidae	*Macropus*	-	femur	1+
Marsupialia	Diprotodontia	Macropodidae	*Macropus*	-	femur	4
Marsupialia	Diprotodontia	Macropodidae	*Macropus*	-	humerus	?ann
Marsupialia	Diprotodontia	Macropodidae	*Macropus*	-	humerus	?1
Marsupialia	Diprotodontia	Macropodidae	*Macropus*	-	humerus	1
Marsupialia	Diprotodontia	Macropodidae	*Macropus*	-	tibia	12-13
Marsupialia	Diprotodontia	Phalangeridae	*Trichosurus*	*vulpeca*	femur	2
Afrotheria	Hyracoidea	Procaviidae	*Procavia*	*capensis*	femur	3
Afrotheria	Hyracoidea	Procaviidae	*Procavia*	*capensis*	femur	10+
Afrotheria	Proboscidea	Elephantidae	*Elephas*	*maximus*	fibula	6
Xenarthra	Pilosa	Bradypodidae	*Bradypus*	*tridactylus*	femur	R
Xenarthra	Pilosa	Bradypodidae	*Bradypus*	*tridactylus*	femur	7+
Xenarthra	Pilosa	Bradypodidae	*Bradypus*	-	tibia	1
Euarchontoglires	Primates	Callitrichidae	*Callithrix*	*jacchus*	femur	3
Euarchontoglires	Primates	Callitrichidae	*Callithrix*	*jacchus*	tibia	3
Euarchontoglires	Primates	Callitrichidae	*Callithrix*	-	femur	6
Euarchontoglires	Primates	Callitrichidae	*Callithrix*	-	tibia	7
Euarchontoglires	Primates	Callitrichidae	*Leontopithecus*	*rosalia*	femur	0
Euarchontoglires	Primates	Callitrichidae	*Leontopithecus*	*rosalia*	humerus	1
Euarchontoglires	Primates	Callitrichidae	*Leontopithecus*	*rosalia*	tibia	4
Euarchontoglires	Primates	Cercopithecidae	*Cercopithecus*	-	femur	0
Euarchontoglires	Primates	Cercopithecidae	*Cercopithecus*	-	tibia	1-2
Euarchontoglires	Primates	Cercopithecidae	*Cercopithecus*	-	tibia	2
Euarchontoglires	Primates	Cercopithecidae	*Chlorocebus*	*sabaeus*	femur	?2 ann
Euarchontoglires	Primates	Cercopithecidae	*Macacus*	*nemestrinus*	tibia	1-3
Euarchontoglires	Primates	Cercopithecidae	*Macacus*	*nemestrinus*	tibia	2
Euarchontoglires	Primates	Hominidae	*Gorilla*	*gorilla*	femur	5
Euarchontoglires	Primates	Hominidae	*Gorilla*	*gorilla*	humerus	R
Euarchontoglires	Primates	Hominidae	*Pan*	*troglodytes*	femur	5
Euarchontoglires	Primates	Hominidae	*Pongo*	*pygmaeus*	femur	0
Euarchontoglires	Primates	Lemuridae	*Lemur*	-	femur	1-2
Euarchontoglires	Lagomorpha	Leporidae	*Lepus*	-	humerus	0
Euarchontoglires	Rodentia	Erethizontidae	*Coendou*	*prehensilis*	femur	1-2
Euarchontoglires	Rodentia	Erethizontidae	*Coendou*	*prehensilis*	tibia	1-2
Euarchontoglires	Rodentia	Hystricidae	*Hystrix*	*cristata*	femur	1-2

Genus	species	% Cortical NWPB	2° Osteons	Source	Figure
Ornithorhychus	*anatinus*	0 (woven)	None	Foote (1916)	PO
Tachyglossus	*aureatus*	0 (woven)	Isolated	Foote (1916)	PO
Tachyglossus	*aureatus*	CNBD	95%	Amprino & Godina (1947)	46
Tachyglossus	*aureatus*	CNBD	66%	Amprino & Godina (1947)	47
Didelphis	*aurita*	25%	None	Amprino & Godina (1947)	48
Didelphis	-	33-50%	None	Enlow & Brown (1958)	Pl 28: 5
Macropus	*giganteus*	CNBD	Throughout	Amprino & Godina (1947)	61
Macropus	-	CNBD	None	Amprino & Godina (1947)	50
Macropus	-	75%	None	Amprino & Godina (1947)	62
Macropus	-	CNBD	Throughout	Amprino & Godina (1947)	54
Macropus	-	25%	Inner cortex	Amprino & Godina (1947)	60
Macropus	-	CNBD	Isolated	Amprino & Godina (1947)	63
Macropus	-	75%	None	Amprino & Godina (1947)	51
Trichosurus	*vulpeca*	66%	Isolated	Foote (1916)	PO
Procavia	*capensis*	40%	Isolated	Foote (1916)	PO
Procavia	*capensis*	90%	None	Amprino & Godina (1947)	113
Elephas	*maximus*	CNBD	Isolated	Amprino & Godina (1947)	115
Bradypus	*tridactylus*	CNBD	100%	Amprino & Godina (1947)	64
Bradypus	*tridactylus*	40% +	50%	Foote (1916)	PO
Bradypus	-	CNBD	80%	Amprino & Godina (1947)	66
Callithrix	*jacchus*	CNBD	None	Amprino & Godina (1947)	120
Callithrix	*jacchus*	25%	75%	Amprino & Godina (1947)	121
Callithrix	-	CNBD	20	Amprino & Godina (1947)	118
Callithrix	-	25-50%	25-75%	Amprino & Godina (1947)	119
Leontopithecus	*rosalia*	CNBD	None	Amprino & Godina (1947)	122
Leontopithecus	*rosalia*	CNBD	Iso-75%	Amprino & Godina (1947)	125
Leontopithecus	*rosalia*	CNBD	Iso-100%	Amprino & Godina (1947)	123
Cercopithecus	-	CNBD	Isolated	Amprino & Godina (1947)	132
Cercopithecus	-	25%	75%	Amprino & Godina (1947)	131
Cercopithecus	-	33%	50%+	Amprino & Godina (1947)	133
Chlorocebus	*sabaeus*	CNBD	Isolated	Amprino & Godina (1947)	130
Macacus	*nemestrinus*	CNBD	75%	Amprino & Godina (1947)	128
Macacus	*nemestrinus*	20% +	75%	Amprino & Godina (1947)	129
Gorilla	*gorilla*	0 (woven, R)	Isolated	Amprino & Godina (1947)	142
Gorilla	*gorilla*	CNBD	80%	Amprino & Godina (1947)	143
Pan	*troglodytes*	CNBD	75%	Amprino & Godina (1947)	136
Pongo	*pygmaeus*	CNBD	50%	Amprino & Godina (1947)	138
Lemur	-	0 (woven)	5-25%	Amprino & Godina (1947)	116
Lepus	-	CNBD	None	Enlow & Brown (1958)	Pl 40: 3,4
Coendou	*prehensilis*	CNBD	90-95%	Amprino & Godina (1947)	73
Coendou	*prehensilis*	CNBD	90-95%	Amprino & Godina (1947)	74
Hystrix	*cristata*	33% +	50%	Amprino & Godina (1947)	67

Clade	Order	Family	Genus	species	Element	AGMs?
Euarchontoglires	Rodentia	Hystricidae	*Hystrix*	*cristata*	tibia	3
Euarchontoglires	Rodentia	Hystricidae	*Hystrix*	*indica*	femur	8-10
Euarchontoglires	Rodentia	Muridae	*Rattus*	-	femur	0
Euarchontoglires	Scandentia	Tupaiidae	*Tupaia*	-	femur	?1 ann
Euarchontoglires	Rodentia	Sciuridae	*Spermophilus*	-	femur	?1
Laurasiatheria	Artiodactyla	Bovidae	*Bos*	-	tibia	CNBD
Laurasiatheria	Artiodactyla	Bovidae	*Gazella*	*dorcas*	femur	0
Laurasiatheria	Artiodactyla	Bovidae	*Ovis*	-	humerus	CNBD
Laurasiatheria	Artiodactyla	Bovidae	*Taurotragus*	*oryx*	tibia	3+
Laurasiatheria	Artiodactyla	Camelidae	*Camelus*	*dromedarius*	femur	1-2+
Laurasiatheria	Artiodactyla	Camelidae	*Camelus*	*dromedarius*	humerus	R
Laurasiatheria	Artiodactyla	Camelidae	*Camelus*	*dromedarius*	tibia	R
Laurasiatheria	Artiodactyla	Camelidae	*Lama*	*glama*	femur	2?
Laurasiatheria	Artiodactyla	Camelidae	*Lama*	*glama*	tibia	R
Laurasiatheria	Artiodactyla	Tragulidae	*Moschiola*	*meminna*	femur	1-2
Laurasiatheria	Artiodactyla	Tragulidae	*Moschiola*	*meminna*	femur	2
Laurasiatheria	Carnivora	Canidae	*Canis*	-	humerus	CNBD
Laurasiatheria	Carnivora	Felidae	*Panthera*	*leo*	femur	4+
Laurasiatheria	Carnivora	Felidae	*Panthera*	*leo*	femur	2-3
Laurasiatheria	Carnivora	Felidae	*Panthera*	*tigris*	femur	3-4
Laurasiatheria	Carnivora	Herpestidae	*Herpestes*	-	femur	2-3
Laurasiatheria	Carnivora	Mephitidae	*Mephitis*	-	femur	0
Laurasiatheria	Carnivora	Mustelidae	*Martes*	*martes*	femur	1
Laurasiatheria	Carnivora	Mustelidae	*Martes*	*martes*	humerus	1
Laurasiatheria	Carnivora	Mustelidae	*Martes*	*martes*	tibia	1
Laurasiatheria	Carnivora	Mustelidae	*Mustela*	-	femur	0
Laurasiatheria	Carnivora	Mustelidae	*Mustela*	-	humerus	0
Laurasiatheria	Carnivora	Mustelidae	*Mustela*	-	tibia	1-2 ann
Laurasiatheria	Carnivora	Odobenidae	*Odobenus*	*rosmarus*	femur	5+
Laurasiatheria	Carnivora	Procyonidae	*Bassariscus*	-	femur	1-2
Laurasiatheria	Carnivora	Procyonidae	*Potos*	*flavus*	femur	CNBD
Laurasiatheria	Chiroptera	Pteropodidae	*Pteropus*	*poliocephalus*	femur	1-2
Laurasiatheria	Chiroptera	-	-	-	humerus	0
Laurasiatheria	Perissodactyla	Equidae	*Equus*	-	humerus	CNBD
Laurasiatheria	Perissodactyla	Tapiridae	*Tapirus*	*terrestris*	humerus	R
Laurasiatheria	Perissodactyla	Tapiridae	*Tapirus*	*terrestris*	humerus	R
Laurasiatheria	Soricomorpha	Solenodontidae	*Solenodon*	*paradoxicus*	femur	1
Laurasiatheria	Soricomorpha	Talpidae	*Talpa*	*europaea*	humerus	0
Laurasiatheria	Soricomorpha	Talpidae	*Talpa*	*europaea*	tibia	0

Genus	species	% Cortical NWPB	2° Osteons	Source	Figure
Hystrix	*cristata*	CNBD	66-100%	Amprino & Godina (1947)	68
Hystrix	*indica*	33%	None	Amprino & Godina (1947)	71
Rattus	-	CNBD	None	Enlow & Brown (1958)	Pl 40: 2
Tupaia	-	100%	None	Foote (1916)	PO
Spermophilus	-	66%	None	Enlow & Brown (1958)	Pl 39: 9
Bos	-	0 (woven)	Isolated	Enlow & Brown (1958)	Pl 37: 6-7
Gazella	*dorcas*	5%	Isolated	Amprino & Godina (1947)	97
Ovis	-	0 (woven)	Isolated	Enlow & Brown (1958)	Pl 37: 1
Taurotragus	*oryx*	0 (woven)	Isolated	Amprino & Godina (1947)	95
Camelus	*dromedarius*	laminar WFB	Isolated	Amprino & Godina (1947)	104
Camelus	*dromedarius*	CNBD	100%	Amprino & Godina (1947)	106
Camelus	*dromedarius*	CNBD	100%	Amprino & Godina (1947)	105
Lama	*glama*	laminar WFB	Isolated	Amprino & Godina (1947)	109
Lama	*glama*	CNBD	100%	Amprino & Godina (1947)	110
Moschiola	*meminna*	CNBD	Isolated	Amprino & Godina (1947)	98
Moschiola	*meminna*	25%	10-15%	Amprino & Godina (1947)	99
Canis	-	CNBD	CNBD	Enlow & Brown (1958)	Pl 33: 5
Panthera	*leo*	CNBD	90-95%	Foote (1916)	PO
Panthera	*leo*	CNBD	CNBD	Enlow & Brown (1958)	Pl 31: 9
Panthera	*tigris*	20% +	75%	Foote (1916)	PO
Herpestes	-	CNBD	None	Enlow & Brown (1958)	Pl 32: 8
Mephitis	-	50% +	None	Enlow & Brown (1958)	Pl 31: 7
Martes	*martes*	25%	None	Amprino & Godina (1947)	76
Martes	*martes*	50%	50%	Amprino & Godina (1947)	78
Martes	*martes*	CNBD	Throughout	Amprino & Godina (1947)	77
Mustela	-	0 (woven)	None	Enlow & Brown (1958)	Pl 31: 3
Mustela	-	0 (woven)	None	Enlow & Brown (1958)	Pl 31: 4
Mustela	-	CNBD	None	Enlow & Brown (1958)	Pl 31: 6
Odobenus	*rosmarus*	CNBD	Throughout	Amprino & Godina (1947)	81
Bassariscus	-	0 (woven)	None	Enlow & Brown (1958)	Pl 32: 3
Potos	*flavus*	CNBD	90%	Foote (1916)	PO
Pteropus	*poliocephalus*	50%	None	Foote (1916)	PO
(bat)	-	100%	None	Enlow & Brown (1958)	Pl 29: 3
Equus	-	CNBD	Isolated	Enlow & Brown (1958)	Pl 35: 1,4
Tapirus	*terrestris*	CNBD	Throughout	Amprino & Godina (1947)	88
Tapirus	*terrestris*	CNBD	100%	Amprino & Godina (1947)	89
Solenodon	*paradoxicus*	20%	None	Foote (1916)	PO
Talpa	*europaea*	CNBD	None	Enlow & Brown (1958)	Pl 29: 1
Talpa	*europaea*	100%	None	Enlow & Brown (1958)	Pl 28: 9

Table 3.6 Life history information for marsupials sampled in this study. Abbreviations for Sex, Age, and LAGs are the same as in Table 3.2. Max Age is the maximum recorded age in years in captivity (C) or the wild (W). The age at reproductive maturity (RM) for the species is given for females (F) and males (M) in days. Wean indicated the age at weaning in days.

Maximum recorded age, age at weaning, and age at reproductive maturity are taken from AnAge (Build 12; 2013).

Order	Family	Species	Specimen	Sex	Age
Dasyuromorphia	Dasyuridae	*Antechinus flavipes*	UCMP 77310	U	A
		Dasyurus maculatus	MVZ 127002	M	SA/A
		Pseudantechinus macdonnellensis	MVZ 133173	M	A
		Sarcophilus harrisii	MVZ 127032	M	A
		Sminthopsis crassicaudata	UCMP 77311	U	A
Didelphimorphia	Didelphidae	*Didelphis virginiana*	UCMP 122745	U	J/SA
		Didelphis virginiana	UCMP 131817	U	A
		Didelphis virginiana	UCMP 77304	U	A
		Monodelphis domestica	MSB 55847	M	A
		Philander opossum	MSB 55074	M	A
Diprotodontia	Acrobatidae	*Acrobates pygmaeus*	MVZ 134404	F	A
	Burramyidae	*Cercartetus nanus*	MVZ 127329	F	A
	Macropodidae	*Dendrolagus goodfellowi*	MVZ 129785	F	A
		Lagorchestes hirsutus	UCMP 81096	F	A
		Lagostrophus fasciatus	UCMP 81095	U	A
		Macropus rufogriseus	AMNH 22810	U	A
		Setonix brachyurus	UCMP 122729	U	A?
		Wallabia bicolor	UCMP 122734	U	A
	Petauridae	*Petaurus australis*	UCMP 77307	U	A
		Petaurus breviceps	MVZ 127338	M	A
	Phalangeridae	*Ailurops ursinus*	MVZ 125528	F	A
		Phalanger gymnotis	MVZ 129776	M	A
		Trichosurus vulpeca	AMNH 22807	F	A
		Trichosurus vulpeca	UCMP 83004	F	A
	Potoroidae	*Bettongia gaimardi*	MVZ 127709	M	A
		Potorous tridactylus	MVZ 127712	F	A
	Pseudocheiridae	*Pseudocheirus peregrinus*	UCMP 77306	U	A
		P. peregrinus	UCMP 82862	U	A
	Tarsipedidae	*Tarsipes rostratus*	MVZ 134405	M	A
	Vombatidae	*Phascolarctos cinereus*	UCMP 134825	F	A, 7
		Phascolarctos cinereus	UCMP 58800	U	A
		Phascolarctos cinereus	UCMP 77316	U	A
		Vombatus ursinus	UCMP 84580	U	A
Microbiotheria	Microbiotheriidae	*Dromiciops gliroides*	MVZ 163430	F	A
		Dromiciops gliroides	MVZ 184914	F	A
Peramelemorphia	Peramelidae	*Echymipera kalubu*	MVZ 138478	M	SA/A
		Isoodon macrourus	UCMP 77305	F	A
		Perameles gunnii	MVZ 132246	F	A

LAGs	Max Age (yr)	RM F (d)	RM M (d)	Wean (d)
0	M: 1W, F:3.9C	345	-	90
3-4A	~3W, 6.8C	340	340	135
1A, 1L	7C	350	350	106
2-3A	13C	730	730	243
?1A	1.5W, 5C	115	159	69
?1A, ?1L	2-3W, 6.6C	184	243	102
1A 1A/L	2-3W, 6.6C	184	243	102
1L	2-3W, 6.6C	184	243	102
?1A	5.1C	122	122	53
1A, 2L/A	2W, 4.4C	450	-	82
1A	8.8C	240	365	99
3L	10.3C	190	190	62
3A, 1L	23.6C	-	-	360
1A, 1A/L, 1L	13.2C	330	-	150
3L	4+W, 6.7C	365	365	270
4L	15.2+C	395	608	187
3A, 2L	10+W, 13.8C	252	389	190
2A, 3L, +?EFS	16.8C	426	426	256
1L/A	15C	725	-	152
?1A, 1L	17.8C	236	456	122
3A, +3EFS	5.9C	-	-	-
1A, 3L	18.9C	-	-	270
1A, 2L	1-2W, 15.9C	315	730	204
2A/L	1-2W, 15.9C	315	730	204
1L	8.3+C	252	272	161
2A, 1L, +3EFS	14.5C	400		154
2A, 1L	10.1C	365	365	180
2A/L	10.1C	365	365	180
0	2+W	167	167	90
1 2xA, 5EFS	22.1C	646	1095	342
1 2xA, 1A, 1L	22.1C	646	1095	342
1L +2EFS	22.1C	646	1095	342
2L +3EFS	30C	730	730	350
1L	3+	730	730	365
2L	3+	730	730	365
5L	2.7+C	-	-	-
3-4L	6.8C	122	200	60
1A,2L, 1-2EFS	6.1C	91	152	60

CHAPTER FOUR

A brief synthesis

Amprino (1947) was the first to propose that the appearance of bone microstructure primarily reflects the rate of bone growth. Since then, many studies have further described and quantified this relationship (e.g., de Ricqlès 1975; Castanet et al. 1996, 2000; de Margerie et al. 2002, 2004). This basic signal is modified and modulated by ontogeny; because the rate of bone growth is not constant through life, the appearance of bone microstructure is not constant through life (e.g., Horner et al. 1999, 2000, 2001; de Buffrénil et al. 2008). Additionally, bone histology is influenced by evolution. Growth rates vary among species and clades, reflecting differences in life history, body size, and metabolism; here too there are histological differences (e.g., de Buffrénil et al. 2008; Montes et al. 2010; Cubo et al. 2012; Bromage et al. 2009, 2012). At each level, bone microstructure can serve as a record of the rates of development: development of the tissue and organ, of the individual, and of growth strategies across larger phylogenetic groups.

To tease apart these influences, one must first be able to understand the scale at which bone acts as a recording structure. In Chapter 1, I review the literature that links bone growth rate to various aspects of bone microstructure. For this reason, Chapter 1 is relatively narrow in focus, both temporally and phylogenetically; in it, I examine the relationship between microstructure and growth, as established in the tissues of extant amniotes. Several aspects of bone microstructure do show a clear, positive correlation with bone growth rate; these include bone deposition rate, collagen fiber organization, vascular density, and vascular porosity. Some of these characteristics are more sensitive than others; for example, fibrillar organization as typically measured (categorically: woven-fibered, parallel-fibered, lamellar) correlates with growth rate, but is probably not as sensitive an indicator as the continuous characters, porosity and vascular density.

It is important to remember, however, that bone microstructural characters have been linked directly only to bone deposition rate (indeed, this was Amprino's [1947] main hypothesis). Bone microstructural characters represent tissue growth rates, but only at the time the bone was being deposited, in a specific region of a particular skeletal element. Different elements grow at different rates, and bone deposition may also vary in different regions within a single bone (Amprino 1947; Amprino and Godina 1947; de Ricqlès 1975; Horner et al. 1990). This is why observed bone deposition rates vary by element, even in tissues of similar appearance within the same individual (Castanet et al. 1996, Castanet et al. 2000; de Margerie et al. 2004).

Thus, it is only by comparison and integration with other data that inferences about relative growth rate at larger levels can be made from bone microstructure. To avoid conflating signals, comparisons should be made among tissues that are as similar as possible, and in consideration of what else is already known about the biology of bone. For example, previous studies have established that bone can expand rapidly under the periosteum when woven-fibered bone forms an initial scaffold that is then compacted toward the canals (de Ricqlès 1975; Francillon-Vieillot et al. 1990; Ferretti et al. 2002; Palumbo et al. 2004; Marotti et al. 2010; Stein and Prondvai 2013). It is only by comparing observations that a

microstructural approach can confirm this. This signal is assessed by looking at differences in bone tissues in the same small area of the bone, but moving in two directions from the woven scaffold: toward the periosteum and toward the canals.

In Chapter 2, I discuss the development of tissue in the long bone cortices of archosaurs and their ancestors, and confirm that the rates of radial deposition (the formation of the initial woven-fibered scaffold) often exceed those of canal compaction. Moving periosteally, woven-fibered bone is present in the interstices among canals. Commonly, the compacting tissues are parallel-fibered or lamellar, and must have formed more slowly than the scaffold. A more interesting inference can be made when data from different regions of the cortex, different bones in the skeleton, different stages of ontogeny, and different species are incorporated: not only do the absolute rates of bone deposition vary at all of these levels, but the relative rates vary as well. By varying the rates of bone deposition during these two phases of tissue formation, the same process can yield tissues that look quite different in appearance. For example, in many bones, the inner cortex often has a greater proportion of woven-fibered bone to parallel-fibered bone than in the outer cortex. This can result purely from a decrease in the rate of compaction, even if the rate of expansion remains constant.

This same concept can be used to examine differences in bone histology at other scales, but again, the integration of other data is required to understand the biological implications. In Chapter 2, I describe differences in the femoral histology between male and female American alligators. When the same region of the femur is compared in male and female animals of the same age, bone microstructure suggests that males experience much higher rates of bone deposition than females do, and for longer durations. Yet, these animals are conspecifics; they share many aspects of development, anatomy, and ecology. The different distributions of bone microstructure only make sense once information about alligator life history is integrated; there are sex differences in the growth curves because the timing of maturity and the duration of growth differ between the sexes (Chabreck and Joanen 1979; Joanen and McNease 1989; Elsey et al. 1992). These in turn reflect different reproductive pressures: once reproductively mature, larger males mate more often (Joanen and McNease 1975, 1980), but this is not the case for females. Differences in histology and growth between male and female alligators are even more interesting in that a single factor (incubation temperature) determines sex, and therefore growth pattern (Ferguson and Joanen 1982).

Inferences about the evolutionary history of growth can be made using bone histological methods, but these are most sound when microstructural data are integrated with ontogenetic, natural history, and phylogenetic data. In Chapter 3, I show that marsupials are remarkably uniform in their bone histology across a wide range of body sizes and ecologies, much more so than placental mammals are. Again, this makes sense only when information on the distribution of growth rates through ontogeny from each clade is integrated; marsupials are much more uniform in their life history.

The integration of paleontological information adds both temporal and evolutionary perspective to our understanding of bone in extant taxa. For example, in Chapter 2, I describe the bone histology of several living and fossil birds, all of which show several microstructural indicators of relatively rapid growth. Compared to other living reptiles, birds may seem unique in their growth syndrome. However, when their microstructure and growth are examined in context of a 250 million year record of archosaur bone histology, it is clear that

birds retain the characteristics of their dinosaurian, ornithodiran, and archosauriform ancestors.

The fossil record is also illuminated in light of the extant record. Not only are the basic relationships between bone tissue and bone growth rate established in living taxa, but the living forms are richer in available (or potential) natural history and life history data. In Chapter 3, I describe the femoral microstructure of several fossil marsupials, including the extinct taxa †*Ngapakaldia*, †*Prionotemnus*, and †*Diprotodon*. The first two taxa are similar to each other and to nearly all marsupials examined in this study in their bone microstructure. The bone tissue of †*Diprotodon*, however, was heavily remodeled and showed signs of growth senescence. It is the modern record that informs us that †*Ngapakaldia* and †*Prionotemnus* share a common marsupial pattern of growth, and thus we are able to infer various aspects of life history, such as the relative size at the timing of weaning. However, in light of the patterns observed across nearly every group of extant marsupials, †*Diprotodon* is atypical in its life history and, to some extent, its bone biology.

My dissertation research supports Amprino's (1947) hypothesis: variation in bone microstructure reflects variation in the rate of bone growth. However, the novelty of this work lies not in its discovery of differences in microstructure or the inferences of differences in rates. Rather, my approach is different in that it integrates many lines of evidence in order to understand the genesis of those differences in rates. My results in Chapters 2 and 3 show that by incorporating natural history and life history, the fossil record and the modern record, the study of bone microstructure can facilitate a much richer understanding of growth at the organismal level, and the evolution of growth strategies at higher levels.

REFERENCES

(listed by chapter)

REFERENCES: CHAPTER ONE

Alquist J and O Damsten. 1969. A modification of Kerley's method for the microscopic determination of age in human bones. *Journal of Forensic Sciences* 14: 205-212.

Amprino R. 1947. La structure du tissu osseux envisagée comme expression de différences dans la vitesse de l'accroissement. *Archives de Biologie* 58: 315-330. [In French]

Amprino R and G Godina. 1947. La struttura delle ossa nei vertebrati. Recerche comparative negli anfibi e negli amnioti. Pontificia Academia Scientiarum Commentationes 11: 329-464. [In Italian]

Anderson JF, A Hall-Martin, and DA Russell. 1985. Long-bone circumference and weight in mammals, birds and dinosaurs. *Journal of Zoology, London* 207: 53-61.

Bocherens H, J Michaux, D Billiou, J Castanet, and F Garcìa-Talavera. 2003. Contribution of collagen stable isotope biogeochemistry to the paleobiology of extinct endemic vertebrates from Tenerife (Canary Islands, Spain). *Isotopes in Environmental and Health Studies* 39: 197-210.

Botha-Brink J and RMH Smith. 2011. Osteohistology of the Triassic archosauromorphs *Prolacerta*, *Proterosuchus*, *Erythrosuchus* and *Euparkeria* from the Karoo Basin of South Africa. *Journal of Vertebrate Paleontology* 31: 1238-1254.

Bourdon E, J Castanet, A de Ricqlès, P Scofield, A Tennyson, H Lamrous, and J Cubo. 2009. Bone growth marks reveal protracted from in New Zealand kiwi (Aves, Apterygidae). *Biology Letters* 5: 639-642.

Bromage TG, HM Goldman, SC McFarlin, J Warshaw, A Boyde, and CM Riggs. 2003. Circularly polarized light standards for investigations of collagen fiber orientation in bone. *The Anatomical Record Part B: The New Anatomist* 274B: 157-168.

Bromage TG,RS Lacruz, R Hogg, HM Goldman, SC McFarlin, J Warshaw, W Dirks, A Perez- Ochoa, I Smolyar, DH Enlow, and AD Boyde. 2009. Lamellar bone is an incremental tissue reconciling enamel rhythms, body size, and organismal life history. *Calcified Tissue International* 84: 388-404.

Bromage TG, RT Hogg, RS Lacrus, and C Hou. 2012. Primate enamel evinces long period biological timing and regulation of life history. *Journal of Theoretical Biology* 305: 131-144.

Brusatte SL, MJ Benton, JB Desojo, and MC Langer. 2010a. The higher-level phylogeny of Archosauria (Tetrapoda: Dinosauria). *Journal of Systematic Paleontology* 8: 3-47.

Brusatte SL, SJ NEsbitt, RB Irmis, RJ Butler, MJ Benton, and MA Norell. 2010b. The origin and early radiation of dinosaurs. *Earth-Science Reviews* 101: 68-100.

Caetano MH and J Castanet. 1993. Variability and microevolutionary patterns in *Triturus marmoratus* from Portugal: Age, size, longevity and individual growth. *Amphibia-Reptilia* 14: 117-129.

Caetano MH, J Castanet, and H Francillon. 1985. Caetano et al 1985 Détermination de l'âge de *Triturus marmoratus marmoratus* (Latreille 1800) du Parc National de Peneda Gerês (Portugal) par squelettochronologie. *Amphibia-Reptilia* 6: 117-132.

Cameron GR. 1930. The staining of calcium. *Journal of Pathology and Bacteriology* 33: 929-955.

Case TJ. 1978a. On the evolution and adaptive significance of postnatal growth rates in the terrestrial vertebrates. *The Quarterly Review of Biology* 53: 243-282.

Case TJ. 1978b. Speculations on the growth rate and reproduction of some dinosaurs. *Paleobiology* 4: 320-328.

Castanet J. 1985. La squelettochronologie chez les Reptiles I. Résultats expérimentaux sur la signification des marques de croissance squelettiques chez les Lézards et les Tortues. *Annales des Sciences Naturelles, Zoologie, Paris* 7: 23-40. [In French with English Summary]

Castanet J. 1986-1987. La squelettochronologie chez les Reptiles III. Application. *Annales des Sciences Naturelles, Zoologie, Paris* 8: 157-172. [In French with English Summary]

Castanet J and G Naulleau. 1985. La squelettochronologie chez les Reptiles II. Résultats expérimentaux sur la signification des marques de croissance squelettiques chez les Serpents. Remaerques sur la croissance et la longévité de la Vipère Aspic. *Annales des Sciences Naturelles, Zoologie, Paris* 7: 41-62. [In French with English Summary]

Castanet J, DG Newman, and H Saint-Girons. 1988. Skeletochronological data on the growth, age, and population structure of the tuatara, *Sphenodon punctatus*, on Stephens and Lady Alice Islands, New Zealand. *Herpetologica* 44: 25-37.

Castanet J, H. Francillon-Vieillot, FJ Meunier, and A de Ricqlès. 1993. Bone and individual aging. pp.245-283 in: *Bone Volume 7: Bone Growth-—B*. BK Hall, Ed. CRC Press: Boca Raton.

Castanet JA, A Grandin, A Abourachid, and A. de Ricqlès. 1996. Expression de la dynamique de croissance dans la structure de l'os périostique chez *Anas platyrhynchos*. *Comptes Rendus de l'Académie des Sciences de Paris, Série III* 319: 301-308. [In French with English summary]

Castanet J, KC Rogers, J Cubo, and J Jacques-Boisard. 2000. Periosteal bone growth rates in extant ratites (ostriche and emu). Implications for assessing growth in dinosaurs. *Comptes Rendus de l'Académie des Sciences - Series III - Sciences de la Vie* 323: 543-550.

Castanet J, S Croci, M Perret, J Cubo, and E de Margerie. 2004. Lines of arrested growth in bone and age estimation in a small primate: *Microcebus murinus*. *Journal of Zoology* 263: 31-39.

Chidlow JA, CA Simpfendorfer, and GR Russ. 2007. Variable growth band deposition leads to age and growth uncertainty in the western wobbegong shark, *Orectolobus hutchinsi*. *Marine and Freshwater Research* 58: 856-865.

Chinsamy A. 1993. Image analysis and the physiological implications of the vascularisation of femora in archosaurs. *Modern Geology* 19: 101-108.

Chinsamy A. 2002. Bone microstructure of early birds. pp. 421-431 (Chapter 18) in: *Mesozoic Birds: Above the Heads of Dinosaurs*. LM Chiappe and LM Witmer, Eds. University of California Press: Berkeley, CA. 520pp.

Chinsamy-Turan A. 2005. *The Microstructure of Dinosaur Bone: Deciphering Biology with Fine-Scale Techniques*. The Johns Hopkins University Press: Baltimore. 195 pp.

Chinsamy-Turan A. 2011. The microstructure of bones and teeth of nonmammalian therapsids. pp. 65-88(Ch. 3) in: *Forerunners of Mammals: Radiation, Histology and Biology*. A Chinsamy-Turan, Ed. Indiana University Press: Bloomington, IN. 352 pp.

Cooper LN, AH Lee, ML Taper, and JR Horner. 2008. Relative growth rates of predator and prey dinosaurs reflect effects of predation. *Proceedings of the Royal Society of London B* 275: 2609-2615.

Cormack D. 1987. *Ham's Histology*. Lippincott: New York. 732pp.

Cubo J, F Ponton, M Laurin, E de Margerie, and J Castanet. 2005. Phylogenetic signal in the bone microstructure of sauropsids. *Systematic Biology* 54: 562-574.

Cubo J, P Legendre, A de Ricqlès, L Montes, E de Margerie, J Castanet and Y Desdevises. 2008. Phylogenetic, functional, and structural components of variation in bone growth rate of amniotes. *Evolution & Development* 10: 217-227.

Cubo J, N Le Roy, C Martinez-Maza, and L Montes. 2012. Paleohistological estimation of bone growth rate in extinct archosaurs. *Paleobiology* 38: 335-349.

de Buffrénil V and M Pascal. 1984. Croissance et morphogénèse postnatales de la mandibule du vison (Mustela vison Schreiber): données sur la dynamique et l'interprétation fonctionnelle de dépots osseux mandibulaires. *Canadian Journal of Zoology* 62: 2026-2037.

de Buffrénil V, A Houssaye, and W Böhme. 2008. Bone vascular supply in monitor lizards (Squamata: Varanidae): Influence of size, growth, and phylogeny. *Journal of Morphology* 269: 533-543.

de Margerie E. 2002. Laminar bone as an adaptation to torsional loads in flapping flight. *Journal of Anatomy* 201: 521-526.

de Margerie E. 2006. Fonction biomécanique des microstructures osseuses chez les oiseaux. *Comptes Rendus Palevol* 5: 619-628.

de Margerie E, J Cubo and J Castanet. 2002. Bone typology and growth rate: testing and quantifying 'Amprino's rule' in the mallard (*Anas platyrhynchos*). *Comptes Rendus Biologies* 325: 221-230.

de Margerie E, J-P Robin, D Verrier, J Cubo, R Groscolas, and J Castanet. 2004. Assessing a relationship between bone microstructure and growth rate: a fluorescent labelling study in the king penguin chick (*Aptenodytes patagonicus*). *The Journal of Experimental Biology* 207: 869-879.

de Ricqlès A. 1968. Recherches paléohistologiques sur les os longs des tétrapodes I. – Origine du tissu osseux plexiforme des dinosauriens sauropodes. *Annales de Paléontologie* 54: 133-145.

de Ricqlès A. 1969. Recherches paléohistologiques sur les os longs des tétrapodes II. – Quelques observations sur la structure des os longs des thériodontes. *Annales de Paléontologie* 55: 3-52.

de Ricqlès A. 1972. Recherches paléohistologiques sur les os longs des tétrapodes III. – Titanosuchiens, dinocéphales et dicynodontes. *Annales de Paléontologie* 58: 17-60.

de Ricqlès A. 1974a. Recherches paléohistologiques sur les os longs des tétrapodes IV. – Eothériodontes et pélycosaures. *Annales de Paléontologie* 60: 1-39.

de Ricqlès A. 1974b. Recherches paléohistologiques sur les os longs des tétrapodes V. – Cotylosaures et mésosaures. *Annales de Paléontologie* 60: 171-216.

de Ricqlès A. 1975. Recherches paléohistologiques sur les os longs des tétrapodes VII. – Sur la classification, la signification fonctionnelle et l'histoire des tissus oseux des tétrapodes. Première partie, structures. *Annales de Paléontologie* 61: 51-129.

de Ricqlès A. 1976. Recherches paléohistologiques sur les os longs des tétrapodes VII. — Sur la classification, la signification fonctionnelle et l'histoire des tissus osseux des tétrapodes. Deuxième partie, fonctions. *Annales de Paléontologie* 62: 71-126.

de Ricqlès A. 1977a. Recherches paléohistologiques sur les os longs des tétrapodes VII. – Sur la classification, la signification fonctionnelle et l'histoire des tissus osseux des tétrapodes. : Deuxième partie, fonctions, suite. *Annales de Paléontologie* 63: 33-56.

de Ricqlès A. 1977b. Recherches paléohistologiques sur les os longs des tétrapodes VII. – Sur la classification, la signification fonctionnelle et l'histoire des tissus osseux des tétrapodes. Deuxième partie, fonctions, fin. *Annales de Paléontologie* 63: 133–160.

de Ricqlès A. 1978a. Recherches paléohistologiques sur les os longs des tétrapodes VII. – Sur la classification, la signification fonctionnelle et l'histoire des tissus osseux des tétrapodes. Troisième partie, évolution. *Annales de Paléontologie* 64: 85–111.

de Ricqlès A. 1978b. Recherches paléohistologiques sur les os longs des tétrapodes VII. – Sur la classification, la signification fonctionnelle et l'histoire des tissus osseux des tétrapodes. Troisième partie, évolution, fin. *Annales de Paléontologie* 64: 153–184.

de Ricqlès A. 1981. Recherches paléohistologiques sur les os longs des tétrapodes. VI.– Stégocéphales. *Annales de Paléontologie* 67: 141–160.

de Ricqlès A. 2004. An introduction to biomineralization: diversity and unity. *Comptes Rendus Palevol* 3: 435-441.

de Ricqlès A, FJ Meunier, J Castanet, and H Francillon-Vieillot. 1991. Comparative microstructure of bone. pp. 1-78 in: Hall BK, Ed. *Bone*. CRC Press, Boca Raton, FL.

de Ricqlès AJ, K Padian, and JR Horner. 2003b. On the bone histology of some Triassic pseudosuchian archosaurs and related taxa. *Annales de Paléontologie* 89: 67-101.

de Ricqlès A, J Castanet, and H Francillon-Vieillot. 2004. 'The 'message' of bone tissue in paleoherpetology. *Italian Journal of Zoology* 71: 3-12.

Duhamel HL. 1739. Sur une racine qui a la faculté de teindre en rouge les os des animaux vivants. *Mémoires de l'Académie Royale des Sciences* 52: 1-13.

Duhamel HL. 1742. Sur le développement et la crue des os des animaux. *Mémoires de l'Académie Royale des Sciences* 55: 354-370.

Enlow DH. 1963. Principles of Bone Remodeling. Charles C. Thomas: Springfield, IL. 131pp.

Enlow DH. 1969. The bone of reptiles. pp.45-80 in *Biology of the Reptilia. Volume 1, Morphology*. A. C Gans, Ed. Academic Press: New York.

Enlow DH and SO Brown. 1956. A comparative histological study of fossil and recent bone tissues Part I. *Texas Journal of Science* 8: 405-443.

Enlow DH and SO Brown. 1957. A comparative histological study of fossil and recent bone tissues Part II. *Texas Journal of Science* 9: 186-214.

Enlow DH and SO Brown. 1958. A comparative histological study of fossil and recent bone tissues Part III. *Texas Journal of Science* 10: 187-230.

Epker BN and HM Frost. 1965. A histological study of remodeling at the periosteal, Haversian canal, cortical endosteal, and trabecular endosteal surfaces in human rib with aging. 41: 198-203. *The Anatomical Record* 152: 129-136.

Erickson GM. 2005. Assessing dinosaur growth patterns: a microscopic revolution. *TRENDS in Ecology and Evolution* 20: 677-684.

Erickson GM and TA Tumanova. 2000. Growth curve of *Psittacosaurus mongoliensis* Osborn (Ceratopsia: Psittacosauridae) inferred from long bone histology. *Zoological Journal of the Linnean Society* 130: 551-566.

Erickson GM, KC Rogers, and SA Yerby. 2001. Dinosaurian growth patterns and rapid avian growth rates. *Nature* 412: 429-433.

Erickson GM, PJ Makovicky, PJ Currie, MA Norell, SA Yerby, and CA Brochu. 2004. Gigantism and comparative life-history parameters of tyrannosaurid dinosaurs. *Nature* 430: 772-775.

Erickson GM, OWM Rauhut, Z Zhou, AH Turner, BD Inouye, D Hu, and MA Norell. 2009. Was dinosaurian physiology inherited by birds? Reconciling slow growth in *Archaeopteryx*. *PLoS ONE* 4(10): e7390.

Ferretti M, MA Muglia, F Remaggi, V Canè, and C Palumbo. 1999. Histomorphometric study on the osteocyte lacuno-canalicular network in animals of different species. II. Parallel-fibered and lamellar bones. *Italian Journal of Anatomy and Embryology* 104: 121-131.

Ferretti M, C Palumbo, M Contri, and G Marotti. 2002. Static and dynamic osteogenesis: Two different types of bone formation. *Anatomy and Embryology* 206: 21-29.

Foote JS. 1916. A contribution to the comparative histology of the femur. *Smithsonian Contributions to Knowledge* 35: 1-241.

Francillon-Vieillot H, V de Buffrénil, J Castanet, J Géraudie, FJ Meunier, JY Sire, L Zylberberg, and A de Ricqlès. 1990. Microstructure and mineralization of vertebrate skeletal tissues. pp. 471–530 in: *Skeletal biomineralization: patterns, processes and evolutionary trends, Volume 1*. JG Carter, Ed. Van Nostrand Reinhold: New York.

Frost HM. 1987. Bone "mass" and the "mechanostat": A proposal. *The Anatomical Record* 219: 1-9.

García-Martínez R, N Marín-Moratalla, X Jordana, and M Köhler. 2011. The ontogeny of bone growth in two species of dormice: Reconstructing life history traits. *Comptes Rendus Palevol* 10: 489-498.

Griebeler EM, N Klein, and PM Sander. 2013. Aging, maturation and growth of sauropodomorph dinosaurs as deduced from growth curves using long bone histological data: An assessment of methodological constraints and solutions. *PLoS ONE* 8(6): e67012. doi:10.1371/journal.pone.0067012

Gross W. 1934. Die Typen des mikroskopischen Knochenbaues bei fossilen Stegocepahlen und Reptilien. *Zeitschrift der Anatomie und Entwicklungsgeschichte* 203: 731-764. [In German]

Hall BK. 2005. *Bones and Cartilage: Developmental and Evolutionary Skeletal Biology.* Elsevier Academic Press: San Francisco. 760pp.

Hirose S, M Li, T Kojima, P Henrique, L de Freitas, S Ubaidus, K Oda, C Saito, and N Amizuka. 2007. A histological assessment on the distribution of the osteocytic lacunar canalicular system using silver staining. *Journal of Bone and Mineral Metabolism* 25: 374-382.

Horner JR and K Padian. 2004. Age and growth dynamics of *Tyrannosaurus rex*. *Proceedings of the Royal Society of London B* 271: 1875-1880.

Horner JR, A de Ricqlès, and K Padian. 1999. Variation in dinosaur skeletochronology indicators: Implications for age assessment and physiology. *Paleobiology* 25: 295-304.

Horner JR, A de Ricqlès, and K Padian. 2000. Long bone histology of the hadrosaurid dinosaur *Maiasaura peeblesorum*: Growth dynamics and physiology based on an ontogenetic series of skeletal elements. *Journal of Vertebrate Paleontology* 20: 115-129.

Horner JR, K Padian, and A de Ricqlès. 2001. Comparative osteohistology of some embryonic and perinatal archosaurs: Developmental and behavioral implications for dinosaurs. *Paleobiology* 27: 39-58.

Hunter J. 1798. Experiments and observations on the growth of bones. Republished in: Palmer JF, Ed. 1835. *The works of John Hunter, F.R.S., with Notes*. Longman, Rees, Orme, Brown, Green, and Longman, London.

Huttenlocker AK, H Woodward, and BK Hall. 2013. The biology of bone. pp.13-34 (Ch. 3) in: *Bone Histology of Fossil Tetrapods: Advancing Methods, Analysis, and Interpretation*. K Padian and E-T Lamm, Eds. University of California Press: Berkeley, CA. 298 pp.

Iwaniec UT, TD Crenshaw, MJ SChoeninger, SD Stout, and MF Ericksen. 1998. Methods for improving the efficiency of estimating total osteon density in the human anterior mid-diaphyseal femur. *American Journal of Physical Anthropology* 107: 13-24.

Kerley ER. 1965. The microscopic determination of age in human bone. *American Journal of Physical Anthropology* 23: 149-163.

Kerschnitzki M, W Wagermaier, P Roschger, J Seto, R Shahar, GN Duda, S Mundlos and P Fratzl. 2011. The organization of the osteocyte network mirrors the extracellular matrix orientation in bone. *Journal of Structural Biology* 173: 303-311.

Klein N and M Sander. 2008. Ontogenetic stages in the long bone histology of sauropod dinosaurs. *Paleobiology* 34: 247-263.

Klevezal GA. 1996. *Recording Structures of Mammals: Determination of Age and Reconstruction of Life History*. A.A. Balkema: Rotterdam, Netherlands. 274 pp.

Köhler M, N Marín-Moratalla, X Jordan, and R Aanes. 2012. Seasonal bone growth and physiology in endotherms shed light on dinosaur physiology. *Nature* 487: 358-361.

Lamm E-T. 2013. Preparation and sectioning of specimens. pp 55-160 in: *Bone Histology of Fossil Tetrapods: Advancing Methods, Analysis, and Interpretation*. K Padian and E-T Lamm, Eds. University of California Press: Berkeley, CA. 298 pp.

Langer MC, MD Ezcurra, JS Bittencourt, and FE Novas. 2009. The origin and early evolution of dinosaurs. *Biological Reviews* 84: 1-56.

LeClair Jr. R. 1990. Relationships between relative mass of the skeleton, endosteal resorption, habitat and precision of age determination in ranid amphibians. *Annales des Sciences Naturelles, Zoologie, Paris* 11: 205-208.

Lee AH and PM O'Connor. 2013. Bone histology confirms determinate growth and small body size in the noasaurid theropod *Masiakasaurus knopfleri*. *Journal of Vertebrate Paleontology* 4: 865-876.

Legendre LJ, L Segalen, and J Cubo. In press. Evidence for high bone growth rate in *Euparkeria* obtained using a new paleohistological inference model for the humerus. *Journal of Vertebrate Paleontology*.

Marangoni F, E Schaefer, R Cajade, and M Tejedo. 2009. Growth-mark formation and chronology of two Neotropical anuran species. *Journal of Herpetology* 43: 546-550.

Marotti G. 2010. Static and dynamic osteogenesis. *Italian Journal of Anatomy and Embryology* 115: 123-126.

Mattox NT. 1935. Annular rings in the long bones of turtles and their correlation with size. *Transactions of the Illinois State Academy of Science* 28: 255-256.

Mayr E. 1982. *The Growth of Biological Thought: Diversity, Evolution, and Inheritance*. Belknap Press: Cambridge, MA. 974pp.

McFarlin SC, CJ Terranova, AL Zihlman, DH Enlow, and TG Bromage. 2008. Regional variability in secondary remodeling within long bone cortices of catarrhine primates: The influence of bone growth history. *Journal of Anatomy* 213: 308-324.

Milch RA, DP Rall, and JE Tobie. 1958. Fluorescence of tetracycline antibiotics in bone. *The Journal of Bone and Joint Surgery* 40: 897-910.

Montes L, N Le Roy, M Perret, V de Buffrenil, J Castanet, and J Cubo. 2007. Relationships between bone growth rate, body mass and resting metabolic rate in growing amniotes: A phylogenetic approach. *Biological Journal of the Linnean Society* 92: 63-76.

Montes L, J Castanet, and J Cubo. 2010. Relationship between bone growth rate and bone tissue organization in amniotes: First test of Amprino's rule in a phylogenetic context. *Animal Biology* 60: 25-41.

Mulhern DM and DH Ubelaker. 2003. Histological examination of bone development in juvenile chimpanzees. *American Journal of Physical Anthropology* 122: 127-133.

Mullender MG, R Huiskes, H Versleyen, and P Buma. 1996. Osteocyte density and histomorphometric parameters in cancellous bone of the proximal femur in five mammalian species. *Journal of Orthopaedic Research* 14: 972-979.

Nesbitt SJ, ND Smith, RB Irmis, AH Turner, A Downs, and MA Norell. 2009. A complete skeleton of a Late triassic Saurischian and the early evolution of dinosaurs. *Science* 326: 1530-1533.

Nesbitt SJ, CA Sidor, RB Irmis, KD Angielczyk, RM Smith, and LA Tsuji. 2010. Ecologically distinct dinosaurian sister group shows early diversification of Ornithodira. *Nature* 464: 95-98.

Nesbitt SJ. 2011. The early evolution of archosaurs: Relationships and the origin of major clades. *Bulletin of the American Museum of Natural History* 352: 1–292.

Newell-Morris L and JE Sirianni. 1982. Parameters of bone growth in the fetal and infant macaque (*Macaca nemestrina)* humerus as documented by trichromatic bone labels. pp. 243–258 in: *Factors and Mechanisms Influencing Bone Growth*. AD Dixon and BG Sarnat, Eds. Alan R. Liss: New York. 657pp.

Pacheco MA, SR Beissinger, and C Bosque. 2010. Why grow slowly in a dangerous place? Postnatal growth, thermoregulation, and energetics of nestling Green-Rumped Parrotlets (*Forpus passerinus*). *The Auk* 127: 558-570.

Paine RR and LR Godfrey. 1997. The scaling of skeletal microanatomy in non-human primates. *Journal of Zoology,* London 241: 803-821.

Palumbo C, M Ferretti, and G Marotti. 2004. Osteocyte dendrogenesis in static and dynamic bone formation: An ultrastructural study. *The Anatomical Record* 278A: 474-480.

Pawlicki R, A Korbel, and H Kubiak. 1966. Cells, collagen fibrils, and vessels in dinosaur bone. *Nature* 211:655-657.

Peabody FE. 1961. Annual growth zones in vertebrates (living and fossil). *Journal of Morphology* 108: 11-62.

Petersen H. 1930. Die Organe des Skelettsystems.pp. 521-676 in: *Handbuch der mikroskopische Anatomie des Menschen, Vol. 2*. W von Möllendorff, Ed. Springer: Berlin. [In German]

Pritchard J. 1956. General anatomy and histology of bone. pp. 1-25 in: *The Biochemistry and Histology of Bone*. GH Bourne, Ed. Academic Press: New York.

Puchtler H, SN Meloan, and MS Terry. 1969. On the history and mechanism of alizarin and alizarin red S stains for calcium. *Journal of Histochemistry and Cytochemistry* 17: 110-124.

Quekett JT. 1849a. On the intimate structure of bone, as composing the skeleton in the four great classes of animals, viz., mammals, birds, reptiles and fishes, with some remarks on the great value of the knowledge of such structure in determining the affinities of minute fragments of organic remains. *Transactions of the Microscopical Society of London* 2: 46-58.

Quekett JT. 1849b. Additional observations on the intimate structure of bone. *Transactions of the Microscopical Society of London* 2: 59-64.

Quekett JT. 1855. Descriptive and Illustrated Catalogue of the Histological Series Contained in *The Museum of the Royal College of Surgeons of England, Prepared for the Microscope. Volume II. Structure of the Skeleton of Vertebrate Animals*. Taylor and Francis: London. 248 pp.

Rahn BA and SM Perren. 1971. Xylenol orange, a fluorochrome useful in polychrome sequential labeling of calcifying tissues. *Stain Technology* 46: 125-129.

Reid REH. 1981. Lamellar-zonal bone with zones and annuli in the pelvis of a sauropod dinosaur. *Nature* 292: 49-51.

Reid REH. 1984. The histology of dinosaurian bone, and its possible bearing on dinosaurian physiology. In: *The Structure, Development and Evolution of Reptiles*, MWJ Ferguson, Ed. *Symposium of the Zoological Society of London* 52: 629-663.

Reid REH. 1985. On supposed Haversian bone from the hadrosaur Anatosaurus, and the nature of compact bone in dinosaurs. *Journal of Paleontology* 59: 140-148.

Reid REH. 1987. Bone and dinosaurian "endothermy". *Modern Geology* 11: 133-154.

Reid REH. 1990. Zonal "growth rings" in dinosaurs. *Modern Geology* 15: 19-48.

Remaggi F, V Canè, C Palumbo, and M Ferretti. 1998. Histomorphometric study on the osteocyte lacuno-canalicular network in animals of different species. I. Woven-fibered and parallel-fibered bones. *Italian Journal of Anatomy and Embryology* 103: 145-155.

Ruben JA, TD Jones, and NR Geist. 2003. Respiratory and reproductive paleophysiology of dinosaurs and early birds. *Physiological and Biochemical Zoology* 76: 141-164.

Schaffler MB and DB Burr. 1984. Primate cortical bone microstructure: Relationship to locomotion. *American Journal of Physical Anthropology* 65: 191–197.

Skedros JG, TR Grunander, and MW Hamrick. 2005. Spatial distribution of osteocyte lacunae in equine radii and third metacarpals: Considerations for cellular communication, microdamage detection, and metabolism. *Cells, Tissues, Organs* 180: 215-236.

Seitz AL. 1907. Vergleichende Studien über den makroskopischen Knochenbau fossiler und rezenter Reptilien. *Nova Acta Academiae Caesareae Leopoldino-Carolinae Germanicae Naturae Curiosorum* 87: 230-370. [In German]

Seymour RS, SL Smith, CR White, DM Henderson, and D Schwarz-Wings. 2012. Blood flow to long bones indicates activity metabolism in mammals, reptiles and dinosaurs. *Proceedings of the Royal Society of London B* 279: 451-456.

Simons ELR and PM O'Connor. 2012. Bone laminarity in the avian forelimb skeleton and its relationship to flight mode: Testing functional interpretations. *The Anatomical Record* 295: 386-396.

Singh IJ, A Tonna, and CP Gandel. 1974. A comparative histological study of mammalian bone. *Journal of Morphology* 144: 421-438.

Starck JM and A Chinsamy. 2002. Bone microstructure and developmental plasticity in birds and other dinosaurs. Journal of Morphology 254: 232-246.

Stein KH. 2010. Long bone histology of basalmost and derived Sauropodomorpha: The convergence of fibrolamellar bone and the evolution of giantism and nanism. Unpublished PhD Dissertation, University of Bonn. 213pp.

Stein K and E Prondvai. 2013. Rethinking the nature of fibrolamellar bone: An integrative biological revision of sauropod plexiform bone formation. *Biological Reviews*: 24 pp. Available online in advance of print. doi: 10.1111/brv.12041

Stover SM, RR Pool, RB Martin, and JP Morgan. 1992. Histological features of the dorsal cortex of the third metacarpal bone mid-diaphysis during postnatal growth in thoroughbred horses. *Journal of Anatomy* 181: 455-469.

Suzuki HK and A Mathews. 1966. Two color labeling of mineralizing tissues with tetracycline and 2,4-bis[N,N'-di-(carbomethyl)aminomethyl] fluorescein. *Stain Technology* 41:57-60.

Turvey ST, OR Green, and RN Holdaway. 2005. Cortical growth marks reveal extended juvenile development in New Zealand moa. *Nature* 435: 940-943.

Warshaw J. 2008. Comparative primate bone microstructure: Records of life history, function, and phylogeny. pp.385-425 (Ch. 18) in: *Mammalian Evolutionary Morphology: A Tribute to Frederick S. Szalay*. EJ Sargis and M Dagosto, Eds. Springer: Dordrecht, Netherlands. 440pp.

Wells JW. 1963. Coral growth and geochronometry. *Nature* 197: 948-950.

Werning S. 2012. The ontogenetic osteohistology of *Tenontosaurus tilletti*. *PLoS ONE* 7(3): e33539.

Werning S, P Spector, and A Lee. 2008. How does sampling method influence our interpretation of bone growth? *Journal of Vertebrate Paleontology* 28(3): 159A.

Woodward HN and JR Horner. 2013. Combating skepticism of paleohistological techniques and interpretations by reducing subjectivity in initial processing and analysis. The Second International Symposium on Paleohistology (Bozeman, MT, 18-20 July 2013). Abstracts volume, p. 36.

Woodward HN, JR Horner, and JO Farlow. 2011. Osteohistological evidence for determinate growth in the American alligator. *Journal of Herpetology* 45: 339-342.

Woodward HN, K Padian, and AH Lee. 2013. Skeletochronology. pp. 195-215 in: *Bone Histology of Fossil Tetrapods: Advancing Methods, Analysis, and Interpretation*. K Padian and E-T Lamm, Eds. University of California Press: Berkeley, CA. 298 pp.

Wyckoff RWG, E Wagner, P Matter III, and AR Doberenz. 1963. Collagen in fossil bone. *Proceedings of the National Academy of the United States of America* 50: 215-218.

Zedda M, G Lepore, P Manca, V Chisu, and V Farina. 2008. Comparative bone histology of adult horses (*Equus caballus*) and cows (*Bos taurus*). *Anatomia, Histologia, Embryologia* 37: 442-445.

REFERENCES: CHAPTER TWO

Adolph EF. 1983. Uptakes and uses of oxygen, from gametes to maturity: An overview. *Respiration Physiology* 53:135–60.

Amprino R and G Godina. 1947. La struttura delle ossa nei vertebrati. Recerche comparative negli anfibi e negli amnioti. *Pontificia Academia Scientiarum Commentationes* 11: 329-464. [In Italian]

Andres B. 2012. The early evolutionary history and adaptive radiation of the Pterosauria. *Acta Geologica Sinica (English Edition)* 86: 1356-1365.

Arendt JD. 1997. Adaptive intrinsic growth rates: An integration across taxa. *The Quarterly Review of Biology* 72: 149-177.

Barreto C. 1997. Dinosaur growth plates and dinosaur bone growth. pp. 95–100 in: *DINOfest international: Proceedings of a symposium held at Arizona State University*. DL Wolberg, E Stump, and G Rosenberg, Eds. Philadelphia: The Academy of Natural Sciences. 587 pp.

Bell DJ and JG Campbell. 1961. Pathological and biochemical observations on virus-induced *Osteopetrosis gallinarum*. *Journal of Comparative Pathology* 71: 85-93.

Bennett AF and WR Dawson. 1976. Metabolism. pp. 127-223 in: *Biology of the Reptilia, Volume 5: Physiology A*. C Gans and WR Dawson, Eds. Academic Press: London. 571pp.

Benton MJ. 1999. S*cleromochlus taylori* and the origin of dinosaurs and pterosaurs. *Philosophical Transactions of the Royal Society of London B: Biological Sciences* 354: 1423-1446.

Blaxter KL. 1989. *Energy Metabolism in Animals and Man*. Cambridge University Press: Cambridge. 352pp.

Botha J and A Chinsamy. 2004. Growth and lifestyle adaptations of the Triassic non-mammalian cynodont *Trirachodon*. *Acta Palaeontologica Polonica* 49: 619-627.

Botha-Brink J and RMH Smith. 2011. Osteohistology of the Triassic archosauromorphs *Prolacerta*, *Proterosuchus*, *Erythrosuchus* and *Euparkeria* from the Karoo Basin of South Africa. *Journal of Vertebrate Paleontology* 31: 1238-1254.

Bourdon E, J Castanet, A de Ricqlès, P Scofield, A Tennyson, H Lamrous, and J Cubo. 2009. Bone growth marks reveal protracted from in New Zealand kiwi (Aves, Apterygidae). *Biology Letters* 5: 639-642.

Brochu CA. 2001. Crocodylian snouts in space and time: Phylogenetic approaches toward adaptive radiation. *American Zoologist* 41: 564-585.

Brochu CA. 2003. Phylogenetic approaches toward crocodylian history. *Annual Review of Earth and Planetary Sciences* 31: 357-397.

Bronowicz R. 2009. Osteohistology of the basal phytosaur *Paleorhinus* from the Late Triassic of southern Poland - a preliminary result: *Journal of Vertebrate Paleontology* 29: 70A.

Brown TK, KA Nagy, and DL Morafka. 2005. Costs of growth in tortoises. *Journal of Herpetology* 39: 19-23.

Brusatte SL, MJ Benton, JB Desojo, and MC Langer. 2010a. The higher-level phylogeny of Archosauria (Tetrapoda: Dinosauria). *Journal of Systematic Paleontology* 8: 3-47.

Brusatte SL, SJ Nesbitt, RB Irmis, RJ Butler, MJ Benton, and MA Norell. 2010b. The origin and early radiation of dinosaurs. *Earth-Science Reviews* 101: 68-100.

Butler RJ. 2005. The 'fabrosaurid' ornithischian dinosaurs of the Upper Elliot Formation (Lower Jurassic) of South Africa and Lesotho. *Zoological Journal of the Linnean Society* 145: 175-218.

Butler RJ, RMH Smith, and DB Norman. 2007. A primitive ornithischian dinosaur from the Late Triassic of South Africa, and the early evolution and diversification of Ornithischia. *Proceedings of the the Royal Society of London B: Biological Sciences* 274: 2041-2046.

Butler RJ, P Upchurch, and DB Norman. 2008. The phylogeny of the ornithischian dinosaurs. *Journal of Systematic Palaeontology* 6: 1-40.

Butler RJ, PM Galton, LB Porro, LM Chiappe, DM Henderson, and GM Erickson. 2010. Lower limits of ornithischian dinosaur body size inferred from a new Upper Jurassic heterodontosaurid from North America. *Proceedings of the the Royal Society of London B: Biological Sciences* 277: 375-381.

Caetano MH, J Castanet, and H. Francillon. 1985. Détermination de l'âge de *Triturus marmoratus marmoratus* (Latreille 1800) du Parc National de Penedae Gerês (Portugal) par squelettochronologie. *Amphibia-Reptilia* 6: 117-132.

Caetano MH and J Castanet. 1993. Variability and microevolutionary patterns in *Triturus marmoratus* from Portugal: Age, size, longevity and individual growth. *Amphibia-Reptilia* 14: 117-129.

Cambra-Moo O, ÁD Buscalioni, J Cubo, J Castanet, MM Loth, ED Margerie, A de Ricqlès. 2006. Histological observations of enantiornithine bone (Saurischia, Aves) from the Lower Cretaceous of Las Hoyas (Spain). *Comptes Rendus Palevol* 5: 685-691.

Campbell JG. 1966. A dinosaur bone lesion resembling avian osteopetrosis and some remarks on the mode of development of the lesions. *Journal of the Royal Microscopical Society* 85: 163-174.

Case TJ. 1978a. On the evolution and adaptive significance of postnatal growth rates in the terrestrial vertebrates. *The Quarterly Review of Biology* 53: 243-282.

Case TJ. 1978b. Speculations on the growth rate and reproduction of some dinosaurs. *Paleobiology* 4: 320-328.

Castanet J and A de Ricqlès. 1986-1987. Sur la relativité de la notion d'ostéones primaires et secondaires et de tissus osseaux primaire et secondaire en général. *Annales des Sciences Naturelles, Zoologie, Paris* 8: 103-109.

Castanet J, DG Newman, and H Saint-Girons. 1988. Skeletochronological data on the growth, age, and population structure of the tuatara, *Sphenodon punctatus*, on Stephens and Lady Alice Islands, New Zealand. *Herpetologica* 44: 25-37.

Castanet J, H Francillon-Vieillot, FJ Meunier, and A de Ricqlès. 1993. Bone and individual aging. pp.245-283 in: *Bone Volume 7: Bone Growth—B*. BK Hall, Ed. CRC Press: Boca Raton.

Castanet JA, A Grandin, A Abourachid, and A. de Ricqlès. 1996. Expression de la dynamique de croissance dans la structure de l'os périostique chez *Anas platyrhynchos*. *Comptes Rendus de l'Académie des Sciences de Paris, Série III* 319: 301-308. [In French with English summary]

Castanet J, KC Rogers, J Cubo, and J Jacques-Boisard. 2000. Periosteal bone growth rates in extant ratites (ostriche and emu). Implications for assessing growth in dinosaurs. *Comptes Rendus de l'Académie des Sciences - Series III - Sciences de la Vie* 323: 543-550.

Cerda IA and JB Desojo. 2011. Dermal armour histology of aetosaurs (Archosauria: Pseudosuchia), from the Upper Triassic of Argentina and Brazil. *Lethaia* 44: 417-428.

Cerda IA, JB Desojo, TM Scheyer, and CL Schultz. [In press]. Osteoderm microstructure of "rauisuchian" archosaurs from South America. *Geobios*. http://dx.doi.org/10.1016/j.geobios.2013.01.004

Chabreck RH and T Joanen. 1979. Growth rates of American alligators in Louisiana. *Herpetologica* 35: 51-57.

Chinsamy A. 1990. Physiological implications of the bone histology of *Syntarsus rhodesiensis* (Saurischia: Theropoda). *Palaeontologica Africana* 27: 77-82.

Chinsamy A. 1993a. Bone histology and growth trajectory of the prosauropod dinosaur *Massospondylus carinatus* Owen. *Modern Geology* 18: 319-329.

Chinsamy A. 1993b. Image analysis and the physiological implications of the vascularisation of femora in archosaurs. *Modern Geology* 19: 101-108.

Chinsamy A. 1994. Dinosaur bone histology: Implications and inferences. pp 213-227 in: *DINOfest international: Proceedings of a symposium held at Arizona State University*. DL Wolberg, E Stump, and G Rosenberg, Eds. Philadelphia: The Academy of Natural Sciences. 587 pp.

Chinsamy A. 2002. Bone microstructure of early birds. pp. 421-431 (Chapter 18) in: *Mesozoic Birds: Above the Heads of Dinosaurs*. LM Chiappe and LM Witmer, Eds. University of California Press: Berkeley, CA. 520pp.

Chinsamy-Turan A. 2005. *The Microstructure of Dinosaur Bone: Deciphering Biology with Fine-Scale Techniques*. The Johns Hopkins University Press: Baltimore. 195 pp.

Chinsamy A and A Elzanowski. 2001. Bone histology: Evolution of growth pattern in birds. *Nature* 412: 402-403.

Chinsamy A and WJ Hillenius. 2004. Physiology of nonavian dinosaurs. pp. 643-659 (Ch. 28) in: *The Dinosauria, Second Edition*. DB Weishampel, P Dodson, and H Osmólska, Eds. University of California Press: Berkeley. 861 pp.

Chinsamy A and MA Raath. 1992. Preparation of fossil bone for histological examination. *Palaeontologia Africana* 29: 39-44.

Chinsamy A and A Tumarkin-Deratzian. 2009. Pathologic bone tissues in a Turkey Vulture and a nonavian dinosaur: Implications for interpreting endosteal bone and radial fibrolamellar bone in fossil dinosaurs. *The Anatomical Record* 292: 1478-1484.

Chinsamy A, LM Chiappe, and P Dodson. 1995a. Mesozoic avian bone microstructure: Physiological implications. *Paleobiology* 21: 561-574.

Chinsamy A, LM Chiappe, and P Dodson. 1995b. Growth rings in Mesozoic birds. *Nature* 368: 196-197.

Chinsamy A, LD Martin, and P Dodson. 1998. Bone microstructure of the diving *Hesperornis* and the volant *Ichthyornis* from the Niobrara Chalk of western Kansas. *Cretaceous Research* 19: 225-235.

Chinsamy A, L Codorniú, and L Chiappe. 2008. Developmental growth patterns of the filter-feeder pterosaur, *Pterodaustro guiñazui*. *Biology Letters* 4: 282-285.

Chinsamy A, L Codorniú, and L Chiappe. 2009. Palaeobiological implications of the bone histology of *Pterodaustro guinazui*. *The Anatomical Record* 292: 1462-1477.

Chinsamy A, LM Chiappe, J Marugán-Lobón, C Gao, and F Zhang. 2013. Gender identification in the Mesozoic bird *Confuciusornis sanctus*. *Nature Communications* 4, article 1381: 1-5.

Clemmensen LB, DV Kent, and FA Jenkins, Jr. 1998. A Late Triassic lake system in East Greenland: Facies, depositional cycles and palaeoclimate. *Palaeogeography, Palaeoclimatology, Palaeoecology* 140: 135-159.

Colbert EH. 1995. *The Little Dinosaurs of Ghost Ranch*. Columbia University Press: New York. 250 pp.

Coulson TD, RA Coulson, and T Hernandez. 1973. Some observations on the growth of captive alligators. *Zoologica* 58: 47-52.

Cox RM, MA Butler, and HB John-Alder. 2007. The evolution of sexual size dimorphism in reptiles. pp. 38-49 (Ch 4) in: *Sex, Size and Gender Roles: Evolutionary studies of sexual size dimorphism*. DJ Fairbairn, WU Blanckenhorn, and T Székely, Eds. Oxford University Press: Oxford. 280 pp.

Cubo J, F Ponton, M Laurin, E de Margerie, and J Castanet. 2005. Phylogenetic signal in the bone microstructure of sauropsids. *Systematic Biology* 54: 562-574.

Cubo J, P Legendre, A de Ricqlès, L Montes, E de Margerie, J Castanet and Y Desdevises. 2008. Phylogenetic, functional, and structural components of variation in bone growth rate of amniotes. *Evolution & Development* 10: 217-227.

Cubo J, N Le Roy, C Martinez-Maza, and L Montes. 2012. Paleohistological estimation of bone growth rate in extinct archosaurs. *Paleobiology* 38: 335-349.

Currey JD. 1962. The histology of the bone of a prosauropod dinosaur. *Palaeontology* 5: 238-246.

Dalrymple, G. 1996. Growth of American alligators in the Shark Valley region of Everglades National Park. *Copeia* 1996: 212-216.

de Buffrénil V. 1980. Mise en évidence de l'incidence des conditions de milieu sur la croissance de *Crocodylus siamensis* (Schneider 1801(et valeur des marques de croissance squelletiques pour l'évaluation de l'âge individuel. *Archives de Zoologie Experimentales et Générales* 121: 63-76. [in French]

de Buffrénil V and J Castanet. 2000. Age estimation by skeletochronology in the Nile monitor (Varanus niloticus), a highly exploited species. *Journal of Herpetology* 34: 414-424.

de Buffrénil and Francillon-Vieillot. 2001. Ontogenetic changes in bone compactness in male and female Nile monitors (*Varanus niloticus*). *Journal of Zoology* 254: 539-546.

de Buffrénil V, A Houssaye, and W Böhme. 2008. Bone vascular supply in monitor lizards (Squamata: Varanidae): Influence of size, growth, and phylogeny. *Journal of Morphology* 269: 533-543.

de Margerie E. 2002. Laminar bone as an adaptation to torsional loads in flapping flight. *Journal of Anatomy* 201: 521-526.

de Margerie E, J Cubo, and J Castanet. 2002. Bone typology and growth rate: testing and quantifying 'Amprino's rule' in the mallard (*Anas platyrhynchos*). *Comptes Rendus Biologies* 325: 221-230.

de Margerie E, J-P Robin, D Verrier, J Cubo, R Groscolas, and J Castanet. 2004. Assessing a relationship between bone microstructure and growth rate: A fluorescent labelling study in the king penguin chick (*Aptenodytes patagonicus*). *The Journal of Experimental Biology* 207: 869-879.

de Ricqlès A. 1974. Recherches paléohistologiques sur les os longs des tétrapodes V. — Cotylosaures et mésosaures. *Annales de Paléontologie* 60: 171-216. [in French]

de Ricqlès A. 1975. Recherches paléohistologiques sur les os longs des Tétrapodes. VII: Sur la signification fonctionnelle et l'histoire des tissus osseux des Tétrapodes. Première partie: structures. *Annales de Paléontologie (Vertébrés)* 61: 51-129. [in French]

de Ricqlès A. 1976. On bone histology of fossil and living reptiles, with comments on its functional and evolutionary significance. pp. 123-150 in: *Morphology and Biology of Reptiles, Linnean Society Symposium Series 3*. Ad'A Bellairs and CB Cox, Eds. Academic Press Inc.: London. 290pp.

de Ricqlès AJ. 1980. Tissue structures of dinosaur Bone: Functional significance and possible relation to dinosaur physiology. pp. 103-139 in: *A Cold Look at the Warm Blooded Dinosaurs*. RDK Thomas and EC Olson, Eds. American Association for the Advancement of Science Symposium Series 28. Westview Press: Boulder. 514 pp.

de Ricqlès A. 2000. L'origine dinosaurienne des oiseaux et de l'endothermie avienne: Les arguments histologiques. *L'Année Biologique* 39: 69-100. [in French]

de Ricqlès A and JR Bolt. 1983. Jaw growth and tooth replacement in *Captorhinus aguti* (Reptilia: Captorhinomorpha): A morphological and histological analysis. *Journal of Vertebrate Paleontology* 3: 7-24.

de Ricqlès A, FJ Meunier, J Castanet, H Francillon-Vieillot. 1991. Comparative microstructure of bone. pp.1-78 in: *Bone Volume 3: Bone Matrix and Bone Specific Products*. BK Hall, Ed. CRC Press: Boca Raton.

de Ricqlès A, K Padian, JR Horner, H Francillon-Vieillot. 2000. Palaeohistology of the bones of pterosaurs (Reptilia: Archosauria): Anatomy, ontogeny, and biomechanical implications. *Zoological Journal of Linnean Society* 129: 349-385.

de Ricqlès A, K Padian, and JR Horner. 2001. The bone histology of basal birds in phylogenetic and ontogenetic perspectives. pp. 411-426 in: *New Perspectives on the Origin and Early Evolution of Birds: Proceedings of the International Symposium in Honor of John H. Ostrom*. J Gauthier and LF Gall, Eds. Yale Peabody Museum of Natural History: New Haven, CT. 613pp.

de Ricqlès AJ, K Padian, JR Horner, ET Lamm, and N Myhrvold. 2003a. Osteohistology of *Confuciusornis sanctus* (Theropoda: Aves). *Journal of Vertebrate Paleontology* 23: 373-386.

de Ricqlès AJ, K Padian, and JR Horner. 2003b. On the bone histology of some Triassic pseudosuchian archosaurs and related taxa. *Annales de Paléontologie* 89: 67-101.

de Ricqlès A, J Castanet, and H Francillon-Vieillot. 2004. 'The 'message' of bone tissue in paleoherpetology. *Italian Journal of Zoology* 71: 3-12.

de Ricqlès A, K Padian, F Knoll, and JR Horner. 2008. On the origin of high growth rates in archosaurs and their ancient relatives: Complementary histological studies on Triassic archosauriforms and the problem of a “phylogenetic signal” in bone histology. *Annales de Paléontologie* 94: 57-76

Dyke GJ and M van Tuinen. 2004. The evolutionary radiation of modern birds (Neornithes): reconciling molecules, morphology and the fossil record. *Zoological Journal of the Linnean Society* 141: 153-177.

Elsey RM, T Joanen, L McNease, and N Kinler. 1992. Growth rates and body condition factors of *Alligator mississippiensis* in coastal Louisiana wetlands: A comparison of wild and farm-released juveniles. *Comparative Biochemistry and Physiology Part A: Physiology* 103: 667-672.

Enlow DH. 1963. *Principles of Bone Remodeling*. Charles C. Thomas: Springfield, IL. 131pp.

Enlow DH. 1969. The bone of reptiles. pp.45-80 in *Biology of the Reptilia. Volume 1, Morphology A*. C Gans, Ed. Academic Press: New York.

Enlow DH and SO Brown. 1957. A comparative histological study of fossil and recent bone tissues Part II. *Texas Journal of Science* 9: 186-214.

Enlow DH and SO Brown. 1958. A comparative histological study of fossil and recent bone tissues Part III. *Texas Journal of Science* 10: 187-230.

Erickson GM and CA Brochu. 1999. How the 'terror crocodile' grew so big. *Nature* 398: 205-206.

Erickson GM and TA Tumanova. 2000. Growth curve of *Psittacosaurus mongoliensis* Osborn (Ceratopsia: Psittacosauridae) inferred from long bone histology. *Zoological Journal of the Linnean Society* 130: 551-566.

Erickson GM, K Curry Rogers, and SA Yerby. 2001. Dinosaurian growth patterns and rapid avian growth rates. *Nature* 412: 429-433.

Erickson GM, PJ Makovicky, PJ Currie, MA Norell, SA Yerby, and CA Brochu. 2004. Gigantism and comparative life-history parameters of tyrannosaurid dinosaurs. *Nature* 430: 772-775.

Erickson GM, K Curry Rogers, DJ Varricchio, MA Norell, and X Xu. 2007. Growth patterns in brooding dinosaurs reveals the timing of sexual maturity in non-avian dinosaurs and genesis of the avian condition. *Biology Letters* 3: 558-561.

Erickson GM, OWM Rauhut, Z Zhou, AH Turner, BD Inouye, D Hu, and MA Norell. 2009a. Was dinosaurian physiology inherited by birds? Reconciling slow growth in *Archaeopteryx*. *PLoS ONE* 4(10): e7390.

Erickson GM, PJ Makovicky, BD Inouye, C-F Zhou, and K-Q Gao. 2009b. A life table for *Psittacosaurus lujiatunensis*: Initial insights into ornithischian dinosaur population biology. *The Anatomical Record* 292: 1514-1521.

Erickson GM, PM Gignac, SJ Steppan, AK Lappin, KA Vliet, JD Brueggen, BD Inouye, D Kledzik, and GJW Webb. 2012. Insights into the ecology and evolutionary success of crocodilians revealed through bite-force and tooth-pressure experimentation. *PLoS ONE* 7: e31781. doi:10.1371/journal.pone.0031781

Evans DC, CM Brown, MJ Ryan, and K Tsogtbaatar K. 2011. Cranial ornamentation and ontogenetic status of *Homalocephale calathocercos* (Ornithischia: Pachycephalosauria) from the Nemegt Formation, Mongolia. *Journal of Vertebrate Paleontology* 31: 84-92.

Ferguson MWJ. 1984. Craniofacial development in *Alligator mississippiensis*. pp. 223-273 in: *The Structure, Development and Evolution of Reptiles. Zoological Society of London Symposium 52*. MWJ Ferguson, Ed. Academic Press: London. 697 pp.

Ferguson MWJ and T Joanen. 1982. Temperature of egg incubation determines sex in *Alligator mississippiensis*. *Nature* 296: 850-853.

Ferguson MWJ, LS Honig, P Bringas Jr., and HC Slavkin. 1982. In vivo and in vitro development of first branchial arch derivatives in *Alligator mississippiensis*. *Progress in Clinical and Biological Research* 101: 275-286.

Ferretti M, C Palumbo, M Contri, and G Marotti. 2002. Static and dynamic osteogenesis: Two different types of bone formation. *Anatomy and Embryology* 206: 21-29.

Foelix R and H-J Fischer. 1999. Röntgen im Museum. *Aargauische Naturforschende Gesellschaft, Mitteilungen* 35: 147-160. [In German]

Fox RC and MC Bowman. 1966. Osteology and relationships of *Captorhinus aguti* (Cope) (Reptilia: Captorhinomorpha). *University of Kansas Paleontological Contributions, Vertebrata* 11: 1-79.

Foote JS. 1916. A contribution to the comparative histology of the femur. *Smithsonian Contributions to Knowledge* 35: 1-241.

Fostowicz-Frelik Ł and T Sulej. 2010. Bone histology of *Silesaurus opolensis* Dzik, 2003 from the Late Triassic of Poland. *Lethaia* 43: 137-148.

Fowler DW, HN Woodward, EA Freedman, PL Larson, and JR Horner. 2011. Reanalysis of "*Raptorex kriegsteini*": A juvenile tyrannosaurid dinosaur from Mongolia. *PLoS ONE* 6(6): e21376. doi:10.1371/journal.pone.0021376

Francillon-Vieillot H, V de Buffrénil, J Castanet, J Géraudie, FJ Meunier, JY Sire, L Zylberberg, and A de Ricqlès. 1990. Microstructure and mineralization of vertebrate skeletal tissues. pp. 471–530 in: *Skeletal biomineralization: patterns, processes and evolutionary trends, Volume 1*. JG Carter, Ed. Van Nostrand Reinhold: New York.

Gauthier JA. 1984. A cladistic analysis of the higher systematic categories of the Diapsida. PhD Dissertation, University of California, Berkeley. 564 pp.

Gauthier JA. 1986. Saurischian monophyly and the origin of birds. In: *The origin of birds and the evolution of flight*. K Padian, Ed. *Memoirs of the California Academy of Sciences* 8: 1-55.

Gauthier J and K Padian. 1985. Phylogenetic, functional, and aerodynamic analyses of the origin of birds and their flight. pp 185-197 in: *The Beginnings of Birds: Proceedings of the International* Archaeopteryx *Conference* Eichstätt, 1984. MK Hecht, JH Ostrom, G Viohl and P Wellnhofer, Eds. Freunde des Jura-Museum: Eichstätt. 382 pp.

Gauthier JA, SJ Nesbitt, ER Schachner, GS Bever, and WG Joyce. 2011. The bipedal stem crocodilian *Poposaurus gracilis*: Inferring function in fossils and innovation in archosaur

locomotion. *Bulletin of the Peabody Museum of Natural History* 52: 107-126.

Germain D and M Laurin. 2005. Microanatomy of the radius and lifestyle in amniotes (Vertebrata, Tetrapoda). *Zoologica Scripta* 34: 335-350.

Gill JR and WA Cobban. 1966. Regional unconformity in Late Cretaceous, Wyoming. *U.S. Geological Survey Professional Paper* 550-B: B20-B27.

Gingerich PD, P Houde, and DW Krause. 1983. A new earliest Tiffanian (Late Paleocene) mammalian fauna from Bangtail Plateau, Western Crazy Mountain Basin, Montana. *Journal of Paleontology* 57: 957-970.

Gross W. 1934. Die Typen des mikroskopischen Knochenbaues bei fossilen Stegocepahlen und Reptilien. *Zeitschrift der Anatomie und Entwicklungsgeschichte* 203: 731-764. [In German]

Hall BK. 2005. *Bones and Cartilage: Developmental and Evolutionary Skeletal Biology*. Elsevier Academic Press: San Francisco. 760pp.

Hallam A. 1960. A sedimentary and faunal study of the Blue Lias of Dorset and Glamorgan. *Philosophical Transactions of the Royal Society of London B* 243: 1-44.

Hekkala ER, G Amato, R DeSalle, and MJ Blum. 2010. Molecular assessment of population differentiation and individual assignment potential of Nile crocodile (*Crocodylus niloticus*) populations. *Conservation Genetics* 11: 1435-1443.

Hekkala E, MH Shirley, G Amato, JD Austin, S Charter, J Thorbjarnarson, KA Vliet, ML Houck, R Desalle, and MJ Blum. 2011. An ancient icon reveals new mysteries: Mummy DNA resurrects a cryptic species within the Nile crocodile. *Molecular Ecology* 20: 4199-4215.

Hernandez CJ, RJ Majeska, and MB Schaffler. 2004. Osteocyte density in woven bone. *Bone* 35: 1095-1099.

Hicks JF, DL Brinkman, DJ Nichols, and M Watabe. 1999. Paleomagnetic and palynologic analyses of Albian to Santonian strata at Bayn Shireh, Burkhant, and Khuren Dukh, eastern Gobi Desert, Mongolia. *Cretaceous Research* 20: 829-850.

Hill JR and KA Rahimtulla. 1965. Heat balance and the metabolic rate of new-born babies in relation to environmental temperature; and the effect of age and weight on basal metabolic rate. *The Journal of Physiology* 180: 239-265.

Hirose S, M Li, T Kojima, P Henrique, L de Freitas, S Ubaidus, K Oda, C Saito, and N Amizuka. 2007. A histological assessment on the distribution of the osteocytic lacunar

canalicular system using silver staining. *Journal of Bone and Mineral Metabolism* 25: 374-382.

Holliday CM, RC Ridgley, JC Sedlmayr, and LM Witmer. 2010. Cartilaginous epiphyses in extant archosaurs and their implications for reconstructing limb function in dinosaurs. *PLoS ONE* 5(9): e13120. doi:10.1371/journal.pone.0013120

Horner JR and K Padian. 2004. Age and growth dynamics of *Tyrannosaurus rex*. *Proceedings of the Royal Society of London B* 271: 1875-1880.

Horner JR, A de Ricqlès, and K Padian. 1999. Variation in dinosaur skeletochronology indicators: Implications for age assessment and physiology. *Paleobiology* 25: 295-304.

Horner JR, A de Ricqlès, and K Padian. 2000. Long bone histology of the hadrosaurid dinosaur *Maiasaura peeblesorum*: Growth dynamics and physiology based on an ontogenetic series of skeletal elements. *Journal of Vertebrate Paleontology* 20: 115-129.

Horner JR, K Padian, and A de Ricqlès. 2001. Comparative osteohistology of some embryonic and perinatal archosaurs: Developmental and behavioral implications for dinosaurs. *Paleobiology* 27: 39-58.

Horner JR, A de Ricqlès, K Padian, and RD Scheetz. 2009. Comparative long bone histology and growth of the "hypsilophodontid" dinosaurs *Orodromeus makelai*, *Dryosaurus altus*, and *Tenontosaurus tillettii* [sic] (Ornithischia: Euornithopoda). *Journal of Vertebrate Paleontology* 29: 734-747.

Houde P. 1986. Ostrich ancestors found in the Northern Hemisphere suggest new hypothesis of ratite origins. *Nature* 324: 563-565.

Houde P. 1987. Histological evidence for the systematic position of *Hesperornis* (Odontornithes: Hesperornithiformes). *The Auk* 104: 125-129.

Houde PW. 1988. Paleognathous birds from the Early Tertiary of the Northern Hemisphere. *Publication of the Nuttall Ornithological Club* 22: 1-148.

Hua S and V de Buffrenil. 1996. Bone histology as a clue in the interpretation of functional adaptations in the Thalattosuchia. *Journal of Vertebrate Paleontology* 16: 703-717.

Hübner TR. 2012. Bone histology in *Dysalotosaurus lettowvorbecki* (Ornithischia: Iguanodontia) - Variation, growth, and implications. *PLoS ONE* 7(1): e29958. doi:10.1371/journal.pone.0029958

Hugi J and MR Sánchez-Villagra. 2012. Life history and skeletal adaptations in the Galapagos Marine Iguana (*Amblyrhynchus cristatus*) as reconstructed with bone histological data - A comparative study of iguanines. *Journal of Herpetology* 46: 312-324.

Hulbert AJ and PL Else. 2000. Mechanisms underlying the cost of living in animals. *Annual Review of Physiology* 62: 207-235.

Hutchison JH. 1982. Turtle, crocodilian, and champsosaur diversity changes in the Cenozoic of the north-central region of western United States. *Palaeogeography, Palaeoclimatology, Palaeoecology* 37: 149-164.

Huttenlocker AK and E Rega. 2011. The paleobiology and bone microstructure of pelycosaurian-grade synapsids. pp. 90-119 (Ch. 4) in: *Forerunners of Mammals: Radiation, Histology and Biology*. A Chinsamy-Turan, Ed. Indiana University Press: Bloomington, IN. 352 pp.

Hutton JM. 1986. Age determination of living Nile crocodiles from the cortical stratification of bone. *Copeia* 1986: 332-341.

Irmis RB, SJ Nesbitt, K Padian, ND Smith, AH Turner, D Woody, and A Downs. 2007. A Late Triassic dinosauromorph assemblage from New Mexico and the rise of dinosaurs. *Science* 317: 358-361.

Irmis RB, R Mundil, JW Martz, and WG Parker. 2011. High-resolution U-Pb ages from the Upper Triassic Chinle Formation (New Mexico, USA) support a diachronous rise of dinosaurs. *Earth and Planetary Science Letters* 309: 258-267.

Jenkins FA, Jr., SM Gatesy, NH Shubin, and K Padian. 2001. A diminutive pterosaur (Pterosauria: Eudimorphodontidae) from the Greenlandic Triassic. *Bulletin of the Museum of Comparative Zoology, Harvard University* 155: 487-506.

Joanen T and L McNease. 1975. Notes on the reproductive biology and captive propagation of the American alligator. *Proceedings of the Annual Conference of the Southeastern Association of Game and Fish Commissioners* 29: 407-415.

Joanen T and L McNease. 1980. Reproductive biology of the American alligator in southwest Louisiana. pp 153-160 in: *Reproductive Biology and Diseases of Captive Reptiles*. JB Murphy and JT Collins, Eds. Contributions to Herpetology No. 1, Society for the Study of the Amphibians and Reptiles: Lawrence, KS. 277 pp.

Joanen T and LL McNease. 1989. Ecology and physiology of nestling and early development of the American alligator. *American Zoologist* 29: 987-998.

Kirkland JI. 2006. Fruita Paleontological Area (Upper Jurassic, Morrison formation), Western Colorado: An example of terrestrial taphofacies analysis. *New Mexico Museum of Natural History and Science Bulletin* 36: 67–95.

Kerschnitzki M, W Wagermaier, P Roschger, J Seto, R Shahar, GN Duda, S Mundlos and P Fratzl. 2011. The organization of the osteocyte network mirrors the extracellular matrix orientation in bone. *Journal of Structural Biology* 173: 303-311.

Klein N. 2004. Bone histology and growth of the prosauropod dinosaur *Plateosaurus engelhardti* Meyer, 1837 from the Norian bonebeds of Trossingen (Germany) and Frick (Switzerland). Unpublished PhD Dissertation. Rheinischen Friedrich-Wilhelms-Universität Bonn. 128 pp.

Klein N and PM Sander. 2007. Bone histology and growth of the prosauropod dinosaur *Plateosaurus engelhardti* Meyer, 1837 from the Norian bonebeds of Trossingen (Germany) and Frick (Switzerland). *Special Papers in Palaeontology* 77: 169-206.

Klein N, T Scheyer, T Tütken. 2009. Skeletochronology and isotopic analysis of a captive individual of *Alligator mississippiensis* Daudin, 1802. *Fossil Record* 12: 121-131.

Knoll F, K Padian and A de Ricqlès. 2010. Ontogenetic change and adult body size of the early ornithischian dinosaur *Lesothosaurus diagnosticus*: Implications for basal ornithischian taxonomy. *Gondwana Research* 17: 171-179.

Kriloff A, D Germain, A Canoville, P Vincent, M Sache, and M Laurin. 2008. Evolution of bone microanatomy of the tetrapod tibia and its use in palaeobiological inference. *Journal of Evolutionary Biology* 21: 807-826.

Köhler M, N Marín-Moratalla, X Jordan, and R Aanes. 2012. Seasonal bone growth and physiology in endotherms shed light on dinosaur physiology. *Nature* 487: 358-361.

Kurochkin EN and N Barsbold 2000. The Russian-Mongolian expeditions and research in vertebrate paleontology. pp 235-255 (Ch. 13) in: MJ Benton, MA Shishkin, DM Unwin, and EN Kurochkin, Eds. *The Age of Dinosaurs in Russia and Mongolia*. Cambridge University Press: Cambridge, UK. 696pp.

Langer MC, MD Ezcurra, JS Bittencourt, and FE Novas. 2009. The origin and early evolution of dinosaurs. *Biological Reviews* 84: 1-56.

Lamm E-T. 2013. Preparation and sectioning of specimens. pp 55-160 in: *Bone Histology of Fossil Tetrapods: Advancing Methods, Analysis, and Interpretation*. K Padian and E-T Lamm, Eds. University of California Press: Berkeley, CA. 298 pp.

Lee AH. 2004. Histological organization and its relationship to function in the femur of *Alligator mississippiensis*. *Journal of Anatomy* 204: 197-207.

Lee AH. 2007. Interplay between growth and mechanics in the evolution of bone microstructure in dinosaurs. Unpublished PhD Dissertation, University of California,

Berkeley. 210 pp.

Lee AH and S Werning. 2008. Sexual maturity in growing dinosaurs does not fit reptilian growth models. *Proceedings of the National Academy of Sciences of the United States of America* 105: 582-587.

Lee AH and PM O'Connor. 2013. Bone histology confirms determinate growth and small body size in the noasaurid theropod *Masiakasaurus knopfleri*. *Journal of Vertebrate Paleontology* 33: 865-876.

Legendre LJ, L Segalen, and J Cubo. In press. Evidence for high bone growth rate in *Euparkeria* obtained using a new paleohistological inference model for the humerus. *Journal of Vertebrate Paleontology*.

Long RA and PA Murry. 1995. Late Triassic (Carnian and Norian) tetrapods from the southwestern United States. *New Mexico Museum of Natural History and Science Bulletin* 4: 1-254.

Magnusson WE, KA Vliet, AC Pooley, and R Whitaker. 1989. Reproduction. pp. 118-135 in: *Crocodiles and Alligators*. CA Ross, Ed. Facts on File, Inc.: New York. 240 pp.

Marotti G. 2010. Static and dynamic osteogenesis. *Italian Journal of Anatomy and Embryology* 115: 123-126.

Martin JE and A Cordes-Person. 2007. A new species of the diving bird Baptornis (Ornithurae: Hesperornithiformes) from the lower Pierre Shale Group (Upper Cretaceous) of southwestern South Dakota. pp 227-237 in: *The Geology and Paleontology of the Late Cretaceous Marine Deposits of the Dakotas*. JE Martin and DC Parris, Eds. *Geological Society of America Special Paper* 427.

Martinez RN, PC Sereno, OA Alcober, CA Colombi, PR Renne, IP Montañez, BS Currie. 2011. A basal dinosaur from the dawn of the dinosaur era in southwestern Pangaea. *Science* 331: 206-210.

Meister W. 1962. Histological structure of the long bones of penguins. *The Anatomical Record* 143: 377-387.

Montes L, N Le Roy, M Perret, V de Buffrenil, J Castanet, and J Cubo. 2007. Relationships between bone growth rate, body mass and resting metabolic rate in growing amniotes: A phylogenetic approach. *Biological Journal of the Linnean Society* 92: 63-76.

Montes L, J Castanet, and J Cubo. 2010. Relationship between bone growth rate and bone tissue organization in amniotes: First test of Amprino's rule in a phylogenetic context. *Animal Biology* 60: 25-41.

Nagy KA. 2000. Energy costs of growth in neonate reptiles. *Herpetological Monographs* 14: 378-387.

Nesbitt S. 2007. The anatomy of *Effigia okeeffeae* (Archosauria, Suchia), theropod-like convergence, and the distribution of related taxa. *Bulletin of the American Museum of Natural History* 302: 1-84.

Nesbitt SJ. 2011. The early evolution of archosaurs: Relationships and the origin of major clades. *Bulletin of the American Museum of Natural History* 352: 1–292.

Nesbitt SJ and MA Norell. 2006. Extreme convergence in the body plans of an early suchian (Archosauria) and ornithomimid dinosaurs (Theropoda). *Proceedings of the Royal Society of London B* 273: 1045-1048.

Nesbitt SJ, RB Irmis, and WG Parker. 2007. A critical re-evaluation of the Late Triassic dinosaur taxa of North America. *Journal of Systematic Palaeontology* 5: 209-243.

Nesbitt SJ, ND Smith, RB Irmis, AH Turner, A Downs, and MA Norell. 2009a. A complete skeleton of a Late triassic Saurischian and the early evolution of dinosaurs. *Science* 326: 1530-1533.

Nesbitt SJ, MR Stocker, BJ Small, and A Downs. 2009b. The osteology and relationships of *Vancleavea campi* (Reptilia: Archosauriformes). *Zoological Journal of the Linnean Society* 157: 814-864.

Nesbitt SJ, CA Sidor, RB Irmis, KD Angielczyk, RM Smith, and LA Tsuji. 2010. Ecologically distinct dinosaurian sister group shows early diversification of Ornithodira. *Nature* 464: 95-98.

Nesbitt SJ, PM Barrett, S Werning, CA Sidor, and AJ Charig. 2013. The oldest dinosaur? A Middle Triassic dinosauriform from Tanzania. *Biology Letters* 9: 20120949. http://dx.doi.org/10.1098/rsbl.2012.0949

Nitsch E. 2005. Der Keuper in der in der Stratigraphischen Tabelle von Deutschland 2002: Formationen und Folgen. *Newsletters on Stratigraphy* 41: 159-171. [in German]

Olsen PE and PM Galton. 1984. A review of the reptile and amphibian assemblages from the Stormberg of southern Africa, with special emphasis on the footprints and the age of the Stormberg. *Palaeontologia Africana* 25: 87-110.

Padian K. 1983. Osteology and functional morphology of *Dimorphodon macronyx* (Buckland) (Pterosauria: Rhamphorhynchoidea) based on new material in the Yale Peabody Museum. *Postilla* 189: 1-44.

Padian K. 1984. The origin of pterosaurs. pp 163-168 in: *Third Symposium on Mesozoic Terrestrial Ecosystems: Short Papers*. W-E Reif and F Westphal, Eds. Atempto: Tübingen, Germany.

Padian K. 1986. On the type material of Coelophysis Cope (Saurischia:Theropoda), and a new specimen from the Petrified Forest of Arizona (Late Triassic: Chinle Formation). pp. 45-60 (Chapter 5) in: *The Beginning of the Age of Dinosaurs: Faunal Change Across the Triassic-Jurassic Boundary*. K Padian, Ed. Cambridge University Press: Cambridge. 378 pp.

Padian K, A de Ricqlès, and JR Horner. 2001. Dinosaurian growth rates and bird origins. *Nature* 412: 405-408.

Padian K, JR Horner, and A de Ricqlès. 2004. Growth in small dinosaurs and pterosaurs: The evolution of archosaurian growth strategies. *Journal of Vertebrate Paleontology* 24: 555-571.

Palumbo C, M Ferretti, and G Marotti. 2004. Osteocyte dendrogenesis in static and dynamic bone formation: An ultrastructural study. *The Anatomical Record* 278A: 474-480.

Parker WG. 2008. Description of new material of the aetosaur *Desmatosuchus spurensis* (Archosauria: Suchia) from the Chinle Formation of Arizona and a revision of the genus *Desmatosuchus*. *PaleoBios* 28: 1-40.

Parker WG, RB Irmis, SJ Nesbitt, JM Martz, and LS Browne. 2005. The Late Triassic pseudosuchian *Revueltosaurus callenderi* and its implications for the diversity of early Ornithischian dinosaurs. *Proceedings of the Royal Society of London B* 272: 963-969.

Parker WG, MR Stocker, and RB Irmis. 2008. A new desmatosuchine aetosaur (Archosauria: Pseudosuchia) from the Upper Triassic Tecovas Formation (Dockum Group) of Texas. *Journal of Vertebrate Paleontology* 28: 692-701.

Pawlicki R. 1975. Studies of the fossil dinosaur bone in the scanning electron microscope. *Zeitschrift für mikroskopisch-anatomische Forschung* 89: 393-398.

Peabody FE. 1961. Annual growth zones in vertebrates (living and fossil). *Journal of Morphology* 108: 11-62.

Peterson F and GN Pipiringos. 1979. Stratigraphic relations of the Navajo Sandstone to Middle Jurassic formations, southern Utah and northern Arizona. *U.S. Geological Survey Professional Paper* 1035-B: 1–43.

Prondvai E, K Stein, A Ősi, MP Sander [sic]. 2012. Life history of *Rhamphorhynchus* inferred from bone histology and the diversity of pterosaurian growth strategies. *PLoS ONE* 7(2): e31392. doi:10.1371/journal.pone.0031392

Quekett JT. 1849a. On the intimate structure of bone, as composing the skeleton in the four great classes of animals, viz., mammals, birds, reptiles and fishes, with some remarks on the great value of the knowledge of such structure in determining the affinities of minute fragments of organic remains. *Transactions of the Microscopical Society of London* 2: 46-58.

Quekett JT. 1849b. Additional observations on the intimate structure of bone. *Transactions of the Microscopical Society of London* 2: 59-64.

Quekett JT. 1855. *Descriptive and Illustrated Catalogue of the Histological Series Contained in The Museum of the Royal College of Surgeons of England, Prepared for the Microscope. Volume II. Structure of the Skeleton of Vertebrate Animals*. Taylor and Francis: London. 248 pp.

Raath MA. 1977. The anatomy of the Triassic theropod Syntarsus rhodesiensis (Saurischia: Podokesauridae) and a consideration of its biology. Unpublished PhD Dissertation, Rhodes University. 358 pp.

Reid REH. 1981. Lamellar-zonal bone with zones and annuli in the pelvis of a sauropod dinosaur. *Nature* 292: 49-51.

Reid REH. 1984. The histology of dinosaurian bone, and its possible bearing on dinosaurian physiology. In: *The Structure, Development and Evolution of Reptiles*, MWJ Ferguson, Ed. Symposium of the Zoological Society of London 52: 629-663.

Reid REH. 1985. On supposed Haversian bone from the hadrosaur *Anatosaurus*, and the nature of compact bone in dinosaurs. *Journal of Paleontology* 59: 140-148.

Reid REH. 1987. Bone and dinosaurian “endothermy”. *Modern Geology* 11: 133-154.

Reid REH. 1990. Zonal “growth rings” in dinosaurs. *Modern Geology* 15: 19-48.

Reid REH. 1996. Bone histology of the Cleveland-Lloyd dinosaurs and of dinosaurs in general, Part I: Introduction: Introduction to bone tissues. *Brigham Young University Geology Studies* 41: 25-71.

Reid REH. 2012. How dinosaurs grew. pp. 621-635 in: *The Complete Dinosaur, 2nd Edition*. MK Brett-Surman, TR Holtz Jr., and JO Farlow, Eds. Indiana University Press: Bloomington, IN. 1128 pp.

Reisz RR, TD Huang, EM Roberts, S Peng, C Sullivan, K Stein, ARH LeBlanc, D Shieh, R Chang, C Chiang, C Yang, and S Zhong. 2013. Embryology of Early Jurassic dinosaur from China with evidence of presenrved organic remains. *Nature* 496: 210-214.

Ricklefs RE. 1973. Patterns of growth in birds. II. Growth rate and mode of development. *Ibis* 115: 177-201.

Riggs NR, TH Lehman, GE Gehrels, and WR Dickinson. 1996. Detrital zircon link between headwaters and terminus of the Upper Triassic Chinle-Dockum paleoriver system. *Science* 273: 97-100.

Riggs NR, SR Ash, AP Barth, GE Gehrels, and JL Wooden. 2003. Isotopic age of the Black Forest Bed, Petrified Forest Member, Chinle Formation, Arizona: An example of dating a continental sandstone. *Geological Society of America Bulletin* 115: 1315-1323.

Rensberger JM and M Watabe. 2000. Fine structure of bone in dinosaurs, birds, and mammals. *Nature* 406: 619-622.

Rogers RR, AB Arcucci, F Abdala, PC Sereno, CA Forster, and CL May. 2001. Paleoenvironment and taphonomy of the Chañares Formation tetrapod assemblage (Middle Triassic), Northwestern Argentina: Spectacular preservation in volcanogenic concretions. *Palaios* 16: 461-481.

Rootes WL, RH Chabreck, VL Wright, BW Brown, and TJ Hess. 1991. Growth rates of American alligators in estuarine and palustrine wetlands in Louisiana. *Estuaries* 14: 489-494.

Rosenbaum JN and K Padian. 2000. New material of the basal thyreophoran *Scutellosaurus lawleri* from the Kayenta Formation (Lower Jurassic) of Arizona. *PaleoBios* 20: 13-23.

Ross JP, D Carbonneau, S Terrell, T Schoeb, D Honeyfield, J Hinterkopf, A Finger, and R Owen. 2002. Continuing studies of mortality of alligators on central Florida lakes: Pathology and nutrition. Final Report to St. Johns River Water Management District, Contract #SE122A. Special Publication SJ2002-SP6: 36 pp. and 8 appendices. Available online at: http://www.sjrwmd.com/technicalreports/pdfs/SP/SJ2002-SP6.pdf. Accessed 1 July 2013.

Rubidge BS. 2005. Re-uniting lost continents: Fossil reptiles from the ancient Karoo and their wanderlust. *South African Journal of Geology* 108: 135-172.

Sanchez S and RR Schoch. 2013. Bone histology reveals a high environmental and metabolic plasticity as a successful evolutionary strategy in a long-lived homeostatic Triassic temnospondyl. *Evolutionary Biology*: 21 pp. Available online in advance of print. doi:10.1007/s11692-013-9238-3

Sander PM. 1992. The Norian *Plateosaurus* bonebeds of central Europe and their taphonomy. *Palaeogeography, Palaeoclimatology, Palaeoecology* 93: 255-299.

Sander PM. 1999. Life history of Tendaguru sauropods as inferred from long bone histology. *Mitteilungen aus dem Museum für Naturkunde der Humboldt-Universität Berlin, Geowissenschaftliche Reihe* 2: 103–112

Sander PM. 2000. Longbone histology of the Tendaguru sauropods: Implications for growth and biology. *Paleobiology* 26: 466-488.

Sander PM and M Clauss. 2008. Sauropod gigantism. *Science* 322: 200-201.

Sander PM and N Klein. 2005. Developmental plasticity in the life history of a prosauropod dinosaur. *Science* 310: 1800-1802.

Sander PM, O Mateus, T Laven, and N Knötschke. 2006. Bone histology indicates insular dwarfism in a new Late Jurassic sauropod dinosaur. *Nature* 441: 739-741.

Sayão JM. 2003. Histovariability in bones of two pterodactyloid pterosaurs from the Santana Formation, Araripe Basin, Brazil: preliminary results. In: *Evolution and Palaeobiology of Pterosaurs*. E Buffetaut and J-M Mazin, Eds. *Geological Society, London, Special Publications* 217: 335-342.

Scheyer TM and PM Sander. 2007. Shell bone histology indicates terrestrial palaeoecology of basal turtles. *Proceedings of the Royal Society of London B* 274: 1885-1893.

Scheyer TM and JB Desojo. 2011. Palaeohistology and external microanatomy of rauisuchian osteoderms (Archosauria: Pseudosuchia). *Palaeontology* 54: 1289–1302.

Schmitz A, P Mausfeld, E Hekkala, T Shine, H Nickel, G Amato, and W Böhme. 2003. Molecular evidence for species level divergence in African Nile crocodiles *Crocodylus niloticus* (Laurenti, 1786). *Comptes Rendus Palevol* 2: 703-12.

Schweitzer MH, JL Wittmeyer, and JR Horner. 2005. Gender-specific reproductive tissue in ratites and *Tyrannosaurus rex*. *Science* 308: 1456-1460.

Schweitzer MH, RM Elsey, CG Dacke, JR Horner, and E-T Lamm. 2007. Do egg-laying crocodilian (*Alligator mississippiensis*) archosaurs form medullary bone? *Bone* 40: 1152-1158.

Sereno PC. 1991. Basal archosaurs: Phylogenetic relationships and functional implications. *Society of Vertebrate Paleontology Memoir* 2: 1-53.

Seitz AL. 1907. Vergleichende Studien über den makroskopischen Knochenbau fossiler und rezenter Reptilien. *Nova Acta Academiae Caesareae Leopoldino-Carolinae Germanicae Naturae Curiosorum* 87: 230-370. [In German]

Simkiss K. 1967. *Calcium in Reproductive Physiology: A Comparative Study of Vertebrates*. Chapman and Hall: London. 264 pp.

Simons ELR and PM O'Connor. 2012. Bone laminarity in the avian forelimb skeleton and its relationship to flight mode: Testing functional interpretations. *The Anatomical Record* 295:

386-396.

Starck JM and A Chinsamy. 2002. Bone microstructure and developmental plasticity in birds and other dinosaurs. *Journal of Morphology* 254: 232-246.

Starck JM and RE Ricklefs. 1998a. Variation, constraint, and phylogeny. Comparative analysis of variation in growth. pp. 247-265 (Ch. 10) in: *Avian Growth and Development: Evolution within the altricial-precocial spectrum*. JM Starck and RE Ricklefs, Eds. Oxford University Press, New York City. 456pp.

Starck JM and RE Ricklefs. 1998b. Avian growth rate data set. pp. 381-423 (Ch. 17) in: *Avian Growth and Development: Evolution within the altricial-precocial spectrum*. JM Starck and RE Ricklefs, Eds. Oxford University Press, New York City. 456pp.

Steel L. 2003. The John Quekett sections and the earliest pterosaur histological studies. In: *Evolution and Palaeobiology of Pterosaurs*. E Buffetaut and J-M Mazin, Eds. *Geological Society, London, Special Publications* 217: 325-334.

Stein KH. 2010. Long bone histology of basalmost and derived Sauropodomorpha: The convergence of fibrolamellar bone and the evolution of giantism and nanism. Unpublished PhD Dissertation, University of Bonn. 213pp.

Stein K and PM Sander. 2009. Histological core drilling: A less destructive method for studying bone histology. pp. 69-80 in: *Methods In Fossil Preparation: Proceedings of the First Annual Fossil Preparation and Collections Symposium*. MA Brown, JF Kane, and WG Parker, Eds. [ebook]: Petrified Forest National Park. 142 pp.

Stein K and E Prondvai. 2013. Rethinking the nature of fibrolamellar bone: An integrative biological revision of sauropod plexiform bone formation. *Biological Reviews*: 24 pp. Available online in advance of print. doi: 10.1111/brv.12041

Stocker MR and RJ Butler. [In press]. Phytosauria. *Geological Society, London, Special Publications* 379: 27 printed pages. http://dx.doi.org/10.1144/SP379.5

Tsuihiji T, M Watabe, K Togtbaatar, T Tsubamoto, R Barsbold, S Suzuki, AH Lee, RC Ridgely, Y Kawahara, and LM Witmer. 2011. Cranial osteology of juvenile specimens of *Tarbosaurus bataar* (Theropoda, Tyrannosauridae) from the Nemegt Formation (Upper Cretaceous of Bugin Tzav, Mongolia). *Journal of Vertebrate Paleontology* 31: 497-517.

Tucker AD. 1997. Validation of skeletochronology to determine age of freshwater crocodiles (*Crocodylus johnstoni*). *Marine and Freshwater Research* 48: 343-351.

Tumarkin-Deratzian AR. 2007. Fibrolamellar bone in wild adult *Alligator mississippiensis*. *Journal of Herpetology* 41: 341-345.

Turvey ST, OR Green, and RN Holdaway. 2005. Cortical growth marks reveal extended juvenile development in New Zealand moa. *Nature* 435: 940-943.

Vleck CM and D Vleck. 1996. Embryonic energetics. Pp. 417-460 in: *Avian Energetics and Nutritional Ecology*. C Carey, Ed. Chapman and Hall: New York. 464pp.

von Huene FRF. 1914. Beiträge zur Geschichte der Archosaurier. *Geologische und paläontologische Abhandlungen* 13: 1-53.

Warren JW. 1963. Growth zones in the skeleton of Recent and fossil vertebrates. PhD Dissertation, University of California, Los Angeles. 136 pp.

Werning S. 2012. The ontogenetic osteohistology of *Tenontosaurus tilletti*. *PLoS ONE* 7(3): e33539. doi:10.1371/journal.pone.0033539

Wieser W. 1994. Cost of growth in cells and organisms: General rules and comparative aspects. *Biological Reviews* 68: 1-33.

Wilkinson PM. 2008. American alligator growth: determinate or indeterminate? pp. 182-187 In: *Proceedings of the 19th Working Meeting of the IUCN-SSC Crocodile Specialist Group, Santa Cruz, Bolivia*. World Conservation Union, Gland, Switzerland and Cambridge, UK. 490 pp.

Wilkinson PM and WE Rhodes. 1997. Growth rates of American alligators in coastal South Carolina. *Journal of Wildlife Management* 61: 397-402.

Wilson LE. 2012. Paleobiology and paleoecology of hesperornithiforms (Aves) from the Late CretaceousWestern Interior Seaway of North America. Unpublished PhD Dissertation. University of Colorado at Boulder. 168 pp.

Wilson JW. 1994. Histological techniques. pp. 205-234 in: *Vertebrate paleontological techniques, Volume one*. P Leiggi and P May, Eds. Cambridge University Press: Cambridge. 368 pp.

Wink CS and RM Elsey. 1986. Changes in femoral morphology during egg-laying in *Alligator mississippiensis*. *Journal of Morphology* 189: 183-188.

Wink CS, RM Elsey, and EM Hill. 1987. Changes in femoral robusticity and porosity during the reproductive cycle of the female alligator (*Alligator mississippiensis*). *Journal of Morphology* 193: 317-321.

Winkler DA. 1983. Paleoecology of an early Eocene mammalian fauna from paleosols in the Clarks Fork Basin, northwestern Wyoming (U.S.A.). *Palaeogeography, Palaeoclimatology, Palaeoecology* 43: 261-298.

Woodward AR, JH White, and SB Linda. 1995. Maximum size of the alligator (*Alligator mississippiensis*). *Journal of Herpetology* 29: 507-513.

Woodward HN, JR Horner, and JO Farlow. 2011. Osteohistological evidence for determinate growth in the American alligator. *Journal of Herpetology* 45: 339-342.

Zavattari E and I Cellini. 1956. La minuta architettura della uccelli eil suo valore nella sistematica dei grandi gruppi. *Monitore Zoologico Italiano* 64: 189-200.

Zhang F, L Hou, and L Ouyang. 1998. Osteological microstructure of Confuciusornis: Preliminary report. *Vertebrata PalAsiatica* 36: 126-135. [In Chinese with English translation]

Zhang F-C, X Xu, J-C Lu, and L Ouyang. 1999. Some microstructure difference [sic] among Confuciusornis, Alligator, and a small theropod dinosaur, and its implication. *Palaeoworld* 11: 296-308. [In Chinese with English abstract]

Zhou Q, MJ Benton, C Sullivan, PM Sander, and X Xu. 2013. Histology and postural change during the growth of the ceratopsian dinosaur Psittacosaurus lujiatunensis. *Nature Communications* 4: 2079. doi: 10.1038/ncomms3079

Zhou Z. 2006. Evolutionary radiation of the Jehol Biota: Chronological and ecological perspectives. *Geological Journal* 41: 377-393.

REFERENCES: CHAPTER THREE

Alquist J and O Damsten. 1969. A modification of Kerley's method for the microscopic determination of age in human bones. *Journal of Forensic Sciences* 14: 205-212.

Amprino R and G Godina. 1947. La struttura delle ossa nei vertebrati. Recerche comparative negli anfibi e negli amnioti. *Pontificia Academia Scientiarum Commentationes* 11: 329-464. [In Italian].

AnAge: The Animal Ageing and Longevity Database. (Build 12; 17/09/2012). Accessed 6 August 2013. http://genomics.senescence.info/species/

Anderson JF, A Hall-Martin, and DA Russell. 1985. Long-bone circumference and weight in mammals, birds and dinosaurs. *Journal of Zoology, London* 207: 53-61.

Asher RJ and G Olbricht. 2009. Dental ontogeny in *Macroscelides proboscideus* (Afrotheria) and *Erinaceus europaeus* (Lipotyphla). *Journal of Mammalian Evolution* 16: 99-115.

Austad SN and KE Fischer. 1991. Mammalian aging, metabolism, and ecology: Evidence from the bats and marsupials. *The Journal of Gerontology* 46: B47-B53.

Biewener AA. 1990. Biomechanics of mammalian terrestrial locomotion. *Science* 250: 1097-1103.

Billet G and T Martin. 2011. No evidence for an afrotherian-like delayed dental eruption in South American notoungulates. *Naturwissenschaften* 98: 509-517.

Botha-Brink J, F Abdala, and A Chinsamy-Turan. 2012. The radiation and osteohistology of nonmammaliaform cynodonts. pp. 223-246 (Ch. 9) in: *Forerunners of Mammals: Radiation, Histology, Biology*. A Chinsamy-Turan, Ed. Indiana University Press: Bloomington, IN. 330pp.

Bozinovic F, G Ruiz, and M Rosenmann. 2004. Energetics and torpor of a South American "living fossil", the microbiotheriid *Dromiciops gliroides*. *Journal of Comparative Physiology B* 174: 293-297.

Brody S. 1964. *Bioenergetics and Growth, with Special Reference to the Efficiency Complex in Domestic Animals, Second edition*. Hafner Publishing: New York. 1023pp.

Brown GT. 1895. *Dentition as Indicative of the Age of the Animals of the Farm, Fourth Edition*. John Murray: London. 61pp.

Bruch C. 1917. La comadrejita *Marmosa elegans*. *Revista del Jardin Zoológico de Buenos Aires* 13: 208-212.

Burke A. 1993. Applied skeletochronology: The horse as human prey during the pleniglacial in southwestern France. *Archeological Papers of the American Anthropological Association* 4: 145-150.

Calder WA, III. 1985. The comparative biology of longevity and lifetime energetics. *Experimental Gerontology* 20: 161-170.

Canevari M and O Vaccaro. 2007. *Guía de Mamíferos del Sur de América del Sur*. L.O.L.A. Literature of Latin América: Buenos Aires. 413 pp.

Case TJ. 1978. On the evolution and adaptive significance of postnatal growth rates in the terrestrial vertebrates. *The Quarterly Review of Biology* 53: 243-282.

Castanet J. 1980. Quelques remarques sur la méthode squellettochronologie chez les vertébrés supérieurs (oiseaux et mammiféres). *Bulletin Société Zoologique de France* 105: 371-376.

Castanet J. 2006. Time recording in bone microstructures of endothermic animals; functional relationships. *Comptes Rendus Paleovol* 5: 629-636.

Castanet J, H Francillon-Vieillot, FJ Meunier, and A de Ricqlès. 1993. Bone and individual aging. pp.245-283 in: *Bone Volume 7: Bone Growth—B*. BK Hall, Ed. CRC Press: Boca Raton.

Castanet J, S Croci, M Perret, J Cubo, and E de Margerie. 2004. Lines of arrested growth in bone and age estimation in a small primate: *Microcebus murinus*. *Journal of Zoology* 263: 31-39.

Catt DC. 1981. Growth and condition of Bennett's wallaby (*Macropus rufogriseus fruticus*) in South Canterbury, New Zealand. *New Zealand Journal of Zoology* 8: 295-300.

Charnov EL. 1993. *Life History Invariants: Some Explorations of Symmetry in Evolutionary Ecology*. Oxford University Press: Oxford. 184pp.

Chinsamy A and J Hurum. 2006. Bone microstructure and growth patterns of early mammals. *Acta Palaeontologica Polonica* 51: 325-338.

Chinsamy-Turan A. 2005. *The Microstructure of Dinosaur Bone: Deciphering Biology with Fine-Scale Techniques.* The Johns Hopkins University Press: Baltimore. 195 pp.

Ciancio MR, MC Castro, FC Galliari, AA Carlini, and RJ Asher. 2012. Evolutionary implications of dental eruption in *Dasypus* (Xenarthra). *Journal of Mammalian Evolution* 19: 1-8.

Clout MN. 1982. Determination of age in the brushtail possum using sections from decalcified molar teeth. *New Zealand Journal of Zoology* 9: 405-408.

Criag SA. 1985. Social organization, reproduction and feeding behaviour of a population of Yellow-Bellied Gliders, *Petaurus australis* (Marsupialia : Petauridae). *Australian Wildlife Research* 12: 1-18.

Cutts JH, WJ Krause, and CR Leeson. 1978. General observations on the growth and development of the young pouch opossum, *Didelphis virginiana*. *Biology of the Neonate* 33: 264-272.

Dawson TJ, TR Grant, and D Fanning. 1979. Standard metabolism of monotremes and the evolution of homeothermy. *Australian Journal of Zoology* 27: 511-515.

de Buffrénil V and O Lambert. 2011. Histology and growth pattern of the pachy-osteosclerotic premaxillae of the fossil beaked whale *Aporotus recurvirostris* (Mammalia, Cetacea, Odontoceti). *Geobios* 44: 45-56.

de Buffrénil V, A de Ricqlès, CE Ray, and DP Dominic. 1990. Bone histology of the archaeocetes (Mammalia: Cetacea). *Journal of Vertebrate Paleontology* 10: 455-466.

de Buffrénil V, W Dabin, and L Zylerberg. 2004. Histology and growth of the cetacean petro-tympanic bone complex. *Journal of Zoology, London* 262: 371-381.

de Magalhães JP, J Costa, and GM Church. 2007. An analysis of the relationship between metabolism, developmental schedules, and longevity using phylogenetic independent contrasts. *The Journal of Gerontology: Biological Sciences* 62: 149-160.

de Magalhães JP and J Costa. 2009. A database of vertebrate longevity records and their relation to other life-history traits. *Journal of Evolutionary Biology* 22: 1770-1774.

de Ricqlès A. 1975. Recherches paléohistologiques sur les os longs des Tétrapodes. VII: Sur la signification fonctionnelle et l'histoire des tissus osseux des Tétrapodes. Première partie: structures. *Annales de Paléontologie (Vertébrés)* 61: 51-129. [in French]

de Ricqlès A. 1976. On bone histology of fossil and living reptiles, with comments on its functional and evolutionary significance. pp. 123-150 in: *Morphology and Biology of Reptiles, Linnean Society Symposium Series* 3. Ad'A Bellairs and CB Cox, Eds. Academic Press Inc.: London. 290pp.

Dixon JM. 1989. Thylacinidae. Ch. 20 in: *Fauna of Australia, Volume 1B. Mammalia*. DW Walton and BJ Richardson, Eds. CSIRO Publishing / Australian Biological Resources Study: Canberra. 827pp.

Enlow DH and SO Brown. 1956. A comparative histological study of fossil and recent bone tissues Part I. *Texas Journal of Science* 8: 405-443.

Enlow DH and SO Brown. 1958. A comparative histological study of fossil and recent bone tissues Part III. *Texas Journal of Science* 10: 187-230.

Flannery T. 1995. *Mammals of New Guinea, Revised and Updated Edition*. Cornell University Press: Ithaca, NY. 568pp.

Foote JS. 1916. A contribution to the comparative histology of the femur. *Smithsonian Contributions to Knowledge* 35: 1-241.

Francillon-Vieillot H, V de Buffrénil, J Castanet, J Géraudie, FJ Meunier, JY Sire, L Zylberberg, and A de Ricqlès. 1990. Microstructure and mineralization of vertebrate skeletal tissues. pp. 471–530 in: *Skeletal biomineralization: patterns, processes and evolutionary trends, Volume 1*. JG Carter, Ed. Van Nostrand Reinhold: New York.

Frost HM. 1987. Bone "mass" and the "mechanostate": A proposal. *The Anatomical Record* 219: 1-9.

Frylestam B and T von Schantz. 1977. Age determination of European hares based on periosteal growth lines. *Mammal Review* 7: 151-154.

Gaillard J-M, D Pontier, D Allaine, A Loison, J-C Herve, and A Heizmann. 1997. Variation in growth form and precocity at birth in eutherian mammals. *Proceedings of the Royal Society of London B* 264: 859-868.

García-Martínez R, N Marín-Moratalla, X Jordana, and M Köhler. 2011. The ontogeny of bone growth in two species of dormice: Reconstructing life history traits. *Comptes Rendus Palevol* 10: 489-498.

Geiger M, AM Forasiepi, D Koyabu, and MR Sánchez-Villagra. 2013. Heterochrony and postnatal growth in mammals – An examination of growth plates in limbs. Program and Abstracts of the 10th International Congress of Vertebrate Morphology, Barcelona 2013. *Anatomical Record* 296, special feature: 191-192.

Geiser F. 2007. Yearlong hibernation in a marsupial mammal. *Naturwissenschaften* 94: 941-944.

Geiser F and CR Pavey. 2007. Basking and torpor a in rock-dwelling desert marsupial: Survival strategies in a resource-poor environment. *Journal of Comparative Physiology B* 177: 885-892.

Geiser F, N Christian, CE Cooper, G Körtner, BM McAllan, CR Pavey, JM Turner, L Warnecke, CKR Willis, and RM Brigham. 2008. Torpor in marsupials: Recent advances. pp. 297-306 (Ch. 33) in: *Hypometabolism in Animals: Hibernation, Torpor and Cryobiology.* BG Lovegrove and AE McKechnie, Eds. Interpak Books: Pietermaritzburg, South Africa. 424 pp.

Gemmell RT and JK Hendrikz. 1993. Growth rates of the bandicoot *Isoodon macrourus* and the Brushtail Possum *Trichosurus vulpeca*. *Australian Journal of Zoology* 41: 141-149.

Green JL, MH Schweitzer, and E-T Lamm. 2010. Limb bone histology and growth in *Placerias hesternus* (Therapsida: Anomodontia) from the Upper Triassic of North America. *Palaeontology* 53: 347-364.

Green J. 2012. Bone and dental histology of Late Triassic dicynodonts from North America. pp.179-196 (Ch.7) in: *Forerunners of Mammals: Radiation, Histology, Biology*. A Chinsamy-Turan, Ed. Indiana University Press: Bloomington, IN. 330pp.

Greer M, JK Greer, and J Gillingham. 1977. Osteoarthritis in selected wild mammals. *Proceedings of the Oklahoma Academy of Science* 57: 39-43.

Guiler, E.R. (1985). *Thylacine: The Tragedy of the Tasmanian Tiger*. Oxford University Press : Melbourne 207 pp.

Hall BK. 2005. *Bones and Cartilage: Developmental and Evolutionary Skeletal Biology*. Elsevier Academic Press: San Francisco. 760pp.

Helgen KM, RT Wells, BP Kear, WR Geerdtz, and TM Flannery. 2006. Ecological and evolutionary significance of sizes of giant extinct kangaroos. *Australian Journal of Zoology* 54: 293-303.

Henry SR and SA Craig. 1984. Diet, ranging behavior and social organization of the Yello-bellied Glider (Petaurus australis Shaw) in Victoria. pp. 331-341 (Ch, 31) in: *Possums and Gliders*. AP Smith and ID Hume, Eds. Australian Mammal Society: Sydney. 598pp.

Herring SW. 1985. The ontogeny of mammalian mastication. *American Zoologist* 25: 339-349.

Holmes DJ and SN Austad. 1994. Fly now, die later: Life-history correlates of gliding and flying in mammals. *Journal of Mammalogy* 75: 224-226.

Howell AB. 1925. Pathologic skulls of captive lions. *Journal of Mammology* 6: 163-168.

Hugi J and MR Sánchez-Villagra. 2012. Life history and skeletal adaptations in the Galapagos Marine Iguana (*Amblyrhynchus cristatus*) as reconstructed with bone histological data - A comparative study of iguanines. *Journal of Herpetology* 46: 312-324.

Hurum JH and A Chinsamy-Turan. 2012. The radiation, bone histology, and biology of early mammals. pp. 249-270 (Ch. 10) in: *Forerunners of Mammals: Radiation, Histology, Biology*. A Chinsamy-Turan, Ed. Indiana University Press: Bloomington, IN. 330pp.

Huttenlocker A and E Rega. 2012. The paleobiology and bone microstructure of pelycosaurian-grade synapsids. pp. 91-119 (Ch. 4) in: *Forerunners of Mammals: Radiation, Histology, Biology*. A Chinsamy-Turan, Ed. Indiana University Press: Bloomington, IN. 330pp.

Jackson S. 2007. *Australian Mammals: Biology and Captive Management*. CSIRO Publishing: Collingwood, Victoria. 548 pp.

Jones M, C Dickman, and M Archer. 2003. Preface. pp. xii-xviii in: *Predators with Pouches: The Biology of Carnivorous Marsupials.* M Jones, C Dickman, and M Archer, Eds. CSIRO Publishing: Collingwood, Victoria. 486pp.

Jones M, D Taggart, and P Temple-Smith. 2004. Age determination and growth in wild *Petrogale lateralis pearsoni* and captive *Petrogale lateralis* 'MacDonnell Ranges race'. *Australian Journal of Zoology* 52: 447-461.

Kirsch JAW and PF Waller. 1979. Notes on the trapping and behavior of the Caenolestidae (Marsupialia). *Journal of Mammalogy* 60: 390-395.

Kerley ER. 1965. The microscopic determination of age in human bone. *American Journal of Physical Anthropology* 23: 149-163.

Kingsmill E. 1962. An investigation of criteria for estimating age in the marsupials *Trichosurus vulpeca* Kerr and *Perameles nasuta* Geoffroy. Australian Journal of Zoology 10: 597-617.

Klevezal GA. 1996. *Recording Structures of Mammals: Determination of Age and Reconstruction of Life History*. A.A. Balkema: Rotterdam, Netherlands. 274 pp.

Klevezal GA. 2002. Reconstruction of individual life histories of rodents from their teeth and bone. *Acta Theriologica* 47, Supplement 1: 127-138.

Klevezal GA and TP Povalishina 1970 Year rings in bone and teeth of the red-tailed Lybian jird in nature and in laboratory. *Zoologicheskiĭ Zhurnal* 49: 145-147. [In Russian with English abstract]

Köhler M and S Moyà-Solà. 2009. Physiological and life history strategies of a fossil large mammal in a resource-limited environment. *Proceedings of the National Academy of Sciences of the United States of America* 106: 20354-20358.

Köhler M, N Marín-Moratalla, X Jordan, and R Aanes. 2012. Seasonal bone growth and physiology in endotherms shed light on dinosaur physiology. *Nature* 487: 358-361.

Lamm E-T. 2013. Preparation and sectioning of specimens. pp 55-160 (Ch. 4) in: *Bone Histology of Fossil Tetrapods: Advancing Methods, Analysis, and Interpretation*. K Padian and E-T Lamm, Eds. University of California Press: Berkeley, CA. 298 pp.

Lammers AR and RZ German. 2002. Ontogenetic allometry in the locomotor skeleton of specialized half-bounding mammals. *Journal of Zoology* 258: 485-495.

Laws 1960. Laminated structure of bones from some marine mammals. *Nature* 187: 338-339.

Leahy GD. 1991. Lamellar-zonal bone in fossil mammals: Implications for dinosaur and therapsid paleophysiology. *Journal of Vertebrate Paleontology* 11: 42A.

Lee AH, AK Huttenlocker, K Padian, and HN Woodward. 2013. Analysis of growth rates. pp. 217-251 (Ch. 8) in: *Bone Histology of Fossil Tetrapods: Advancing Methods, Analysis, and Interpretation*. K Padian and E-T Lamm, Eds. University of California Press: Berkeley, CA. 298 pp.

Lieberman DE, OM Pearson, JD Polk, B Demes, and AW Crompton. 2003. Optimization of bone growth and remodeling in response to loading in tapered mammalian limbs. *The Journal of Experimental Biology* 206: 3125-3138.

Lyne AG. 1964. Observations on the breeding and growth of the marsupial *Perameles nasuta* Geoffroy, with notes on other bandicoots. *Australian Journal of Zoology* 12: 322-239.

Maynes GM. 1976. Growth of the Parma Wallaby, *Macropus parma* Waterhouse. *Australian Journal of* Zoology 24: 217-236.

McMahon CR, M-J Buscot, NL Wiggins, N Collier, JH Maindonald, HI McCallum, and DMJS Bowman. 2011. A two-phase model for smoothly joining disparate growth phases in the macropodid *Thylogale billardierii*. *PLoS ONE* 6(10): e24934. doi:10.1371/journal.pone.0024934

McNab BK. 1986. Food habits, energetics, and the reproduction of marsupials. *Journal of Zoology, London (A)* 208: 595-614.

McNab BK. 2008. An analysis of the factors that influence the level and scaling of mammalian BMR. *Comparative Biochemistry and Physiology, Part A* 151: 5-28.

Meier PS, C Bickelmann, TM Scheyer, D Koyabu, and MR Sánchez-Villagra. 2013. Evolution of bone compactness in extant and extinct moles (Talpidae): Exploring humeral microstructure in small fossorial mammals. *BMC Evolutionary Biology* 13:55 (10pp.)

Menkhorst P and F Knight. 2011. *A Field Guide to the Mammals of Australia, Third Edition.* Oxford University Press: South Melbourne. 274pp.

Morris PA. 1970. A method for determining absolute age in the hedgehog. *Journal of Zoology* 161: 277-281.

Morris PA. 1971. Epiphyseal fusion in the forefoot as a means of age determination in the hedgehog (*Erinaceus europaeus*). *Journal of Zoology, London* 164: 254-259.

Morris P. 1972. A review of mammalian age determination methods. *Mammal Review* 2: 69-104.

Mulhern DM and DH Ubelaker. 2003. Histological examination of bone development in juvenile chimpanzees. *American Journal of Physical Anthropology* 122: 127-133.

Nilsson O and J Baron. 2004. Fundamental limits on longitudinal bone growth: Growth plate senescence and epiphyseal fusion. *TRENDS in Endocrinology and Metabolism* 15: 370-375.

Nowak RM. 2005. *Walker's Marsupials of the World*. The Johns Hopkins University Press: Baltimore. 226pp.

O'Leary MA and SG Kaufman. 2012. MorphoBank 3.0: Web application for morphological phylogenetics and taxonomy. http://www.morphobank.org

Pahl LI. 1987. Survival, age determination and population age structure of the Common Ringtail Possum, *Pseudocheirus peregrinus*, in a *Eucalyptus* woodland and a *Leptospermum* thicket in southern Victoria. *Australian Journal of Zoology* 35: 625-639.

Pearse RJ. 1981. Notes on breeding, growth and longevity of the Forester or Eastern Grey Kangaroo, *Macropus giganteus* Shaw, in Tasmania. *Australian Wildlife Research* 8: 229-235.

Poole WE, SM Carpenter, and JT Wood. 1982. Growth of Grey Kangaroos and the reliability of age determination from body measurements. I. The Eastern Grey Kangaroo, *Macropus giganteus*. *Australian Wildlife Research* 9: 9-20.

Promislow DEL and PH Harvey. 1990. Living fast and dying young: A comparative analysis of life-history variation among mammals. *Journal of Zoology* 220: 417-437.

Quekett JT. 1855. *Descriptive and Illustrated Catalogue of the Histological Series Contained in The Museum of the Royal College of Surgeons of England, Prepared for the Microscope. Volume II. Structure of the Skeleton of Vertebrate Animals*. Taylor and Francis: London. 248 pp.

Radinsky L. 1984. Ontogeny and phylogeny in horse skull evolution. *Evolution* 38: 1-15.

Ray S, J Botha, and A Chinsamy. 2004. Bone histology and growth patterns of some nonmammalian therapsids. *Journal of Vertebrate Paleontology* 24: 634-648.

Ray S, S Bandyopadhyay, and D Bhawal. 2009. Growth patterns as deduced from bone microstructure of some selected neotherapsids with special emphasis on dicynodonts: Phylogenetic implications. *Palaeoworld* 18: 53-66.

Roth VL. 1984. How elephants grow: Heterochrony and the calibration of developmental stages in some living and fossil species. *Journal of Vertebrate Paleontology* 4: 126-145.

Russell EM. 1981. Patterns of parental care and parental investment in marsupials. *Biological Reviews* 57: 423-486.

Ruth EB. 1953. Bone studies. II. An experimental study of the haversian-type vascular channels. *American Journal of Anatomy* 93: 429-455.

Sánchez-Villagra MR. 2010. Developmental palaeontology in synapsids: the fossil record of ontogeny in mammals and their closest relatives. *Proceedings of the Royal Society of London B* 277: 1139-1147.

Sander PM and P Andrássy. 2006. Lines of arrested growth and long bone histology in Pleistocene large mammals from Germany: What do they tell us about dinosaur physiology? *Palaeontographica Abteilung A* 277: 143-159.

Scheffer VB. 1950. Growth layers on the teeth of Pinnipedia as an indicator of age. *Science* 112: 309-311.

Serena M and TR Soderquist. 1988. Growth and development of pouch young of wild and captive *Dasyurus geoffroii* (Marsupialia: Dasyuridae). *Australian Journal of Zoology* 36: 533-543.

Severinghaus CW. 1949. Tooth development and wear as criteria of age in white-tailed deer. *Journal of Wildlife Management* 13: 195-216.

Sharman GB, HJ Frith, and JH Calaby. 1964. Growth of the pouch young, tooth eruption, and age determination in the Red Kangaroo, *Megaleia rufa*. *CSIRO Wildlife Research* 9: 20-49.

Singh IJ, EA Tonna, and CP Gandel. 1974. A comparative histological study of mammalian bone. *Journal of Morphology* 144: 421-438.

Smith BH. 2000. 'Schultz's Rule' and the evolution of tooth emergence and replacement patterns in primates and ungulates. pp. 212-227 (Ch. 15) in: *Development, Function and Evolution of Teeth*. MF Teaford, MM Smith, and MWJ Ferguson, Eds. Cambridge University Press: Cambridge. 324pp.

Spinage CA. 1973. A review of the age determination of mammals by means of teeth, with special reference to Africa. *East African Wildlife Journal* 11: 165-187.

Steel L. 2003. The John Quekett sections and the earliest pterosaur histological studies. In: *Evolution and Palaeobiology of Pterosaurs*. E Buffetaut and J-M Mazin, Eds. *Geological Society, London, Special Publications* 217: 325-334.

Stephenson NG. 1963. Growth gradients among fossil monotremes and marsupials. *Palaeontology* 6: 215-214.

Stover SM, RR Pool, RB Martin, and JP Morgan. 1992. Histological features of the dorsal cortex of the third metacarpal bone mid-diaphysis during postnatal growth in thoroughbred horses. *Journal of Anatomy* 181: 455-469.

Straehl FR, TM Scheyer, AM Forasiepi, RD MacPhee, and MR Sánchez-Villagra. 2013. Evolutionary patterns of bone histology and bone compactness in xenarthran mammal long bones. *PLoS ONE* 8(7): e69275. doi:10.1371/journal.pone.0069275

Streeter M and SD Stout. 2003. The histomorphometry of the subadult rib: Age-associated changes in bone mass and the creation of peak bone mass. pp. 91-101 (Ch. 7) in: *Bone Loss and Osteoporosis: An Anthropological Perspective.* SC Agarwal and SD Stout, Eds. Kluwer Academic / Plenum Publishers: New York. 240pp.

Suckling GC. 1984. Population ecology of the Sugar Glider, *Petaurus breviceps*, in a system of fragmented habitats. *Australian Wildlife Research* 11: 49-75.

Thompson DD. 1980. Age changes in bone mineralization, cortical thickness, and Haversian canal area. *Calcified Tissue International* 31: 5-11.

Tyndale-Biscoe H. 2005. *Life of Marsupials*. CSIRO Publishing: Collingwood, Victoria. 442pp.

Warnecke L, JM Turner, and F Geiser. 2008. Torpor and basking in a small arid zone marsupial. *Naturwissenschaften* 95: 73-78.

Warshaw J. 2008. Comparative primate bone microstructure: Records of life history, function, and phylogeny. pp.385-425 (Ch. 18) in: *Mammalian Evolutionary Morphology: A Tribute to Frederick S. Szalay*. EJ Sargis and M Dagosto, Eds. Springer: Dordrecht, Netherlands. 440pp.

Washburn SL. 1946. The sequence of epiphyseal union in the opossum. *The Anatomical Record* 95: 353-363.

West GB, JH Brown, and BJ Enquist. 2001. A general model for ontogenetic growth. *Nature* 413: 628-631.

Whalen JP, L Krook, and EA Nunez. 1972. A radiographic and histologic study of bone in the active and hibernating bat (*Myotis lucifugus*). *The Anatomical Record* 172: 97-107.

Withers PC, CE Cooper, and AN Larcombe. 2006. Environmental correlates of physiological variables in marsupials. *Physiological and Biochemical Zoology* 79: 437-453.
Weisbecker V and A Goswami. 2010. Brain size, life history, and metabolism at the marsupial/placental dichotomy. *Proceedings of the National Academy of Sciences of the United States of America* 107: 16216-16221.

Wroe S, TJ Myers, RT Wells, and A Gillespie. 1999. Estimating the weight of the Pleistocene marsupial lion, *Thylacoleo carnifex* (Thylacoleonidae: Marsupialia): Implications for the ecomorphology of a marsupial super-predator and hypotheses of impoverishment of Australian marsupial carnivore fauna. *Australian Journal of Zoology* 47: 489-498.

Wroe S, M Crowther, J Dortch, and J Chong. 2004. The size of the largest marsupial and why it matters. *Biology Letters* 274: S34-S36.

Zullinger EM, RE Ricklefs, KH Redford, and GM Mace. 1984. Fitting sigmoidal equations to mammalian growth curves. *Journal of Mammalogy* 65: 607-636.

REFERENCES: CHAPTER FOUR

Amprino R. 1947. La structure du tissu osseux envisagée comme expression de différences dans la vitesse de l'accroissement. *Archives de Biologie* 58: 315-330. [In French]

Amprino R and G Godina. 1947. La struttura delle ossa nei vertebrati. Recerche comparative negli anfibi e negli amnioti. Pontificia Academia Scientiarum Commentationes 11: 329-464. [In Italian]

Bromage TG, RT Hogg, RS Lacrus, and C Hou. 2012. Primate enamel evinces long period biological timing and regulation of life history. *Journal of Theoretical Biology* 305: 131-144.

Bromage TG,RS Lacruz, R Hogg, HM Goldman, SC McFarlin, J Warshaw, W Dirks, A Perez- Ochoa, I Smolyar, DH Enlow, and AD Boyde. 2009. Lamellar bone is an incremental tissue reconciling enamel rhythms, body size, and organismal life history. *Calcified Tissue International* 84: 388-404.

Castanet JA, A Grandin, A Abourachid, and A. de Ricqlès. 1996. Expression de la dynamique de croissance dans la structure de l'os périostique chez *Anas platyrhynchos*. *Comptes Rendus de l'Académie des Sciences de Paris, Série III* 319: 301-308. [In French with English summary]

Castanet J, KC Rogers, J Cubo, and J Jacques-Boisard. 2000. Periosteal bone growth rates in extant ratites (ostriche and emu). Implications for assessing growth in dinosaurs. *Comptes Rendus de l'Académie des Sciences - Series III - Sciences de la Vie* 323: 543-550.

Chabreck RH and T Joanen. 1979. Growth rates of American alligators in Louisiana. *Herpetologica* 35: 51-57.

Cubo J, N Le Roy, C Martinez-Maza, and L Montes. 2012. Paleohistological estimation of bone growth rate in extinct archosaurs. *Paleobiology* 38: 335-349.

de Buffrénil V, A Houssaye, and W Böhme. 2008. Bone vascular supply in monitor lizards (Squamata: Varanidae): Influence of size, growth, and phylogeny. *Journal of Morphology* 269: 533-543.

de Margerie E, J Cubo and J Castanet. 2002. Bone typology and growth rate: testing and quantifying 'Amprino's rule' in the mallard (*Anas platyrhynchos*). *Comptes Rendus Biologies* 325: 221-230.

de Margerie E, J-P Robin, D Verrier, J Cubo, R Groscolas, and J Castanet. 2004. Assessing a relationship between bone microstructure and growth rate: a fluorescent labelling study in the king penguin chick (*Aptenodytes patagonicus*). *The Journal of Experimental Biology* 207: 869-879.

de Ricqlès A. 1975. Recherches paléohistologiques sur les os longs des tétrapodes VII. – Sur la classification, la signification fonctionnelle et l'histoire des tissus oseux des tétrapodes. Première partie, structures. *Annales de Paléontologie* 61: 51-129.

Elsey RM, T Joanen, L McNease, and N Kinler. 1992. Growth rates and body condition factors of *Alligator mississippiensis* in coastal Louisiana wetlands: A comparison of wild and farm-released juveniles. *Comparative Biochemistry and Physiology Part A: Physiology* 103: 667-672.

Ferguson MWJ and T Joanen. 1982. Temperature of egg incubation determines sex in *Alligator mississippiensis*. *Nature* 298: 850-853.

Horner JR, A de Ricqlès, and K Padian. 1999. Variation in dinosaur skeletochronology indicators: Implications for age assessment and physiology. *Paleobiology* 25: 295-304.

Horner JR, A de Ricqlès, and K Padian. 2000. Long bone histology of the hadrosaurid dinosaur *Maiasaura peeblesorum*: Growth dynamics and physiology based on an ontogenetic series of skeletal elements. *Journal of Vertebrate Paleontology* 20: 115-129.

Horner JR, K Padian, and A de Ricqlès. 2001. Comparative osteohistology of some embryonic and perinatal archosaurs: Developmental and behavioral implications for dinosaurs. *Paleobiology* 27: 39-58.

Joanen T and L McNease. 1975. Notes on the reproductive biology and captive propagation of the American alligator. *Proceedings of the Annual Conference of the Southeastern Association of Game and Fish Commissioners* 29: 407-415.

Joanen T and L McNease. 1980. Reproductive biology of the American alligator in southwest Louisiana. pp 153-160 in: *Reproductive Biology and Diseases of Captive Reptiles*. JB Murphy and JT Collins, Eds. Contributions to Herpetology No. 1, Society for the Study of the Amphibians and Reptiles: Lawrence, KS. 277 pp.

Joanen T and LL McNease. 1989. Ecology and physiology of nestling and early development of the American alligator. *American Zoologist* 29: 987-998.

Montes L, J Castanet, and J Cubo. 2010. Relationship between bone growth rate and bone tissue organization in amniotes: First test of Amprino's rule in a phylogenetic context. *Animal Biology* 60: 25-41.

Ferretti M, C Palumbo, M Contri, and G Marotti. 2002. Static and dynamic osteogenesis: Two different types of bone formation. *Anatomy and Embryology* 206: 21-29.

Marotti G. 2010. Static and dynamic osteogenesis. *Italian Journal of Anatomy and Embryology* 115: 123-126.

Palumbo C, M Ferretti, and G Marotti. 2004. Osteocyte dendrogenesis in static and dynamic bone formation: An ultrastructural study. *The Anatomical Record* 278A: 474-480.

Stein K and E Prondvai. 2013. Rethinking the nature of fibrolamellar bone: An integrative biological revision of sauropod plexiform bone formation. *Biological Reviews*: 24 pp. Available online in advance of print. doi: 10.1111/brv.12041

APPENDIX A

OSTEOCYTE COUNTS (DATA USED IN CHAPTER TWO)

Taxon	Specimen	Element	Tsct	1	2	3	4	5	6	7	8	9	10
Captorhinus	UCMP 223509	humerus	A	12	16	8	15						
			B	11	8	20	20	16					
			C	11	13	18	13						
			D	19	17	19							
		IndAve:	**1475.00**										
Taxon	**Specimen**	**Element**	**Tsct**	**1**	**2**	**3**	**4**	**5**	**6**	**7**	**8**	**9**	**10**
Sphenodon	JC 57	femur	A	13	27	32							
			B	24	25	28	31						
			C	27	30	26							
			D	39	28	29	34						
		IndAve:	**449.14**										
	JC A	femur	A	28	28								
			B	27	23	33							
			C	26	28	26							
			D	31	27	23							
		IndAve:	**437.33**										
	JC 807	femur	A	30	28	35							
			B	31	26	29							
			C	23	22	25							
			D	38	31	31							
		IndAve:	**465.33**										
	JC 833	femur	A	28	20	25							
			B	20	24	27	23						
		IndAve:	**381.71**										
		CombAve	**439.82**										
Taxon	**Specimen**	**Element**	**Tsct**	**1**	**2**	**3**	**4**	**5**	**6**	**7**	**8**	**9**	**10**
Iguana	UCMP 68288	tibia	A	77	75	88							
			B	71	66	82							
		IndAve:	**1224.00**										
Taxon	**Specimen**	**Element**	**Tsct**	**1**	**2**	**3**	**4**	**5**	**6**	**7**	**8**	**9**	**10**
Varanus	UCMP 223456	femur	A	58	82	77							
			B	65	57	71	102						
			C	66	71	67							
		IndAve:	**1145.60**										
	VdB uncat	femur	A	123	107	123	104						
			B	132	102	113	95						
			C	85	78	93	73						
		IndAve:	**1637.33**										
	VdB uncat	tibia	A	88	88	104							
			B	114	102	90							

Taxon	Specimen	Element	Tsct	1	2	3	4	5	6	7	8	9	10
Varanus	VdB uncat	tibia	C	67	84								
			D	120	107	100	120						
		IndAve:	**1578.67**										
		FemAve:	1413.82										
		CombAve	**1472.00**										

Taxon	Specimen	Element	Tsct	1	2	3	4	5	6	7	8	9	10
Trilophosaurus	TMM 31025-849	humerus	A	10	8	10	46	50	54	54	37	47	54
				11	**12**	**13**	**14**						
			A cont.	44	50	42	61						
		IndAve:	**816.00**	**1**	**2**	**3**	**4**	**5**	**6**	**7**	**8**	**9**	**10**
	TMM 31025-928	ulna	A	10	13	13	86	78	62	61	51	14	13
				11	**12**								
			A cont.	45	16								
		IndAve:	**1169.00**										
	TMM 31025-787	femur	A	65	65	73	12	13					
			B	96	97	74							
			C	13	99	76	84	90					
			D	62	62	66	73	13					
		IndAve:	**1245.11**										
	TMM 31025-1064	femur	A	72	91	85	77	18					
			B	53	74	83	15						
			C	10	13	14	15	18	14	20	18		
		IndAve:	**1415.29**										
	TMM 31025-1063	femur	A	4	7	80	71	69					
			B	75	84	65	65	81					
			C	53	65	X	X	61	12	74			
		IndAve:	**1052.53**										
	TMM 31025-862	femur	A	X	49	X	56	52	41	52	59		
			B	X	78	78	82	71	57	88	79	74	
		IndAve:	**1046.86**										
				1	**2**	**3**	**4**	**5**	**6**	**7**	**8**	**9**	**10**
	TMM 31025-885	femur	A	11	63	64	71	67	74	79	15	10	11
				11									
			A cont.	8									
				1	**2**	**3**	**4**	**5**	**6**	**7**	**8**	**9**	**10**
			B	9	8	10	73	72	70	74	78	80	
		IndAve:	**1102.00**										
	TMM 31025-786	femur	A	40	53	50	58	62	53	55	48	52	
			B	55	64	71	53	70	64	66	68		
		IndAve:	**924.24**										

Taxon	Specimen	Element	Tsct	1	2	3	4	5	6	7	8	9	10
Trilophosaurus	TMM 31025-788	tibia	A	16	17	18	14	##	20	86			
			B	14	23	18	20	22					
			IndAve:	**1775.33**									
	TMM 31025-747	tibia	A	93	80	85	##	##	##				
			B	8	16	11	65	95	14	87	94		
			IndAve:	**1396.86**	**1**	**2**	**3**	**4**	**5**	**6**	**7**	**8**	**9**	**10**
	TMM 31025-887	tibia	A	12	11	11	11	11	9	11	12	10	10
				11	**12**	**13**							
			A cont.	13	9	12							
				1	**2**	**3**	**4**	**5**	**6**	**7**	**8**	**9**	**10**
			B	12	8	14	11	12	8	17	13	14	13
				11	**12**	**13**	**14**						
			B cont.	13	13	11	11						
				1	**2**	**3**	**4**	**5**	**6**	**7**	**8**	**9**	
			C	13	11	13	15	12	7	14	8	7	
			IndAve:	**1144.44**									
	TMM 31025-741	tibia	A	**1**	**2**	**3**	**4**	**5**	**6**	**7**	**8**	**9**	**10**
				13	17	17	15	18	17	17	13	14	14
			A cont.	**11**	**12**	**13**	**14**	**15**	**16**	**17**			
				11	14	13	15	13	15	9			
			IndAve:	**1441.18**									
			FemAve:	1135.33									
			TibAve:	1348.86									
			CombAve	**1197.48**									

Taxon	Specimen	Element	Tsct	1	2	3	4	5	6	7	8	9	10
Vancleavea	UCMP 152662	femur	A	104	68	50	48	7					
				*A is numbered endosteal to periosteal									
			B	18	69	94	102	119	251				
			C	12	16	88	103	163	135	138			
			D	20	30	30	121	101	133	225	193		
			IndAve:	**1671.54**									
	GR 250	femur	A	91	98	104	105	134	140	164	169		
				1	**2**	**3**	**4**	**5**	**6**	**7**	**8**	**9**	**10**
			B	128	129	121	120	135	134	115	113	111	103
				11	**12**	**13**	**14**						
			B cont.	100	X	102	110						
				1	**2**	**3**	**4**	**5**	**6**	**7**	**8**	**9**	**10**
			C	81	74	90	89	87	106	121	114		
			D	105	94	106	118	130	112	105	124		
			IndAve:	**1808.43**									

Taxon	Specimen	Element	Tsct	1	2	3	4	5	6	7	8	9	10
Proterochampsia	MCZ 4038	femur	A	91	86	94	86	74	21	22	19	20	
cf.			B	94	106	90	87	82	X	80			
Chanaresuchus			C	54	13	85	82	81	97	25	24	27	
			D	83	89	104	80	75					
		IndAve:	**1582.76**										

Taxon	Specimen	Element	Tsct	1	2	3	4	5	6	7	8	9	10
Euparkeria	AMNH FARB	femur	A	X	X	X	X	146	36	26	22		
	2238		B	105	79	127	31	29	29	18			
			C	98	115	122	121	137	96	15	18		
				1	**2**	**3**	**4**	**5**	**6**	**7**	**8**	**9**	**10**
			D	102	26	26	20	18	25	20	29	168	112
				11									
			D cont.	91									
		IndAve:	**2156.80**										

Taxon	Specimen	Element	Tsct	1	2	3	4	5	6	7	8	9	10
Phytosauria	UCMP 25921	femur	A	92	88	92	104	99	98	14	13	22	21
				1	**2**	**3**	**4**	**5**	**6**	**7**	**8**	**9**	**10**
			B	100	121	23	115	99	29	22	113	110	97
				11	**12**	**13**	**14**	**15**					
			B cont.	118	30	24	109	17					
		IndAve:	**1855.20**										

Taxon	Specimen	Element	Tsct	1	2	3	4	5	6	7	8	9	10
Revueltosaurus	PEFO 33843	femur	A	12	14	16	91	63	50	56	11	65	77
				11									
			A cont.	91	22	103							
				1	**2**	**3**	**4**	**5**	**6**	**7**	**8**	**9**	**10**
			B	109	83	76	78	86	91	79	73	69	X
				11									
			B cont.	83									
				1	**2**	**3**	**4**	**5**	**6**	**7**	**8**	**9**	**10**
			C	11	13	75	11	16	66	64	95	77	90
				11									
			C cont.	75									
				1	**2**	**3**	**4**	**5**	**6**	**7**	**8**	**9**	**10**
			D	72	82	80	86	69	X	85	72	X	
		IndAve:	**1287.22**										

Taxon	Specimen	Element	Tsct	1	2	3	4	5	6	7	8	9	10
Aetosauria	UCMP 25914	femur	A	159	147	122	152	30	35	33	30	153	126
				11	**12**	**13**							
			A cont.	21	29	35							
				1	**2**	**3**	**4**	**5**	**6**	**7**	**8**	**9**	**10**
			B	X	52	38	44	55	X	66	78	79	64
				11	**12**	**13**	**14**	**15**	**16**	**17**			
			B cont.	54	52	48	64	39	37	43			
				1	**2**	**3**	**4**	**5**	**6**	**7**	**8**	**9**	**10**
			C	100	105	149	130	122	134	134	140	136	111
				11									
			C cont.	143									
		IndAve:	**970.79**										
	GR 252	tibia	A	10	83	82	9	22	31	24	32	17	21
			B	96	87	88	86	16	16				
		IndAve:	**1741.78**										
		CombAve:	**1214.26**										

Taxon	Specimen	Element	Tsct	1	2	3	4	5	6	7	8	9	10
Effigia	AMNH FARB	femur	A	102	107	96	99	100	112	112	25		
	30587			**1**	**2**	**3**	**4**	**5**	**6**	**7**	**8**	**9**	**10**
			B	102	107	96	99	100	112	112	25	27	24
				11	**12**	**13**	**14**	**15**	**16**	**17**			
			B cont.	86	20	104							
				1	**2**	**3**	**4**	**5**	**6**	**7**	**8**	**9**	**10**
			C	87	111	107	146	104	113	103	115	96	94
				11	**12**	**13**	**14**	**15**	**16**	**17**	**18**	**19**	**20**
			C cont.	114	119	104	95	24	23	25	25	25	22
				1	**2**	**3**	**4**	**5**	**6**	**7**	**8**	**9**	**10**
			D	88	126	111	117	127	112	130	101	120	103
				11	**12**								
			D cont.	107	29								
		IndAve:	**1869.06**										

Taxon	Specimen	Element	Tsct	1	2	3	4	5	6	7	8	9	10
Loricata cf.	UCMP 28353	humerus	A	51	63	76	85	76	84	75	75	62	64
Postosuchus				**11**	**12**	**13**	**14**	**15**					
			A cont.	67	60	71	70	84					
				1	**2**	**3**	**4**	**5**	**6**	**7**	**8**	**9**	**10**
			B	54	65	64	63	68	56	53	49	85	
			C	52	51	58	54	48	51	42	58	71	72
			D	57	51	55	53	55	53	56	46		
		IndAve:	**991.62**										

Taxon	Specimen	Element	Tsct	1	2	3	4	5	6	7	8	9	10
Loricata cf.	UCMP 25906	femur	A	351	300	75	345	335	346	296	291	288	52
Postosuchus				**11**	**12**	**13**	**14**	**15**	**16**	**17**	**18**	**19**	**20**
			A cont.	298	316	294	328	330	309	339	61	54	68
				1	**2**	**3**	**4**	**5**	**6**	**7**	**8**	**9**	**10**
			B	259	252	297	229	296	280	304	58	61	324
				11	**12**	**13**							
			B cont.	62	73	64							
				1	**2**	**3**	**4**	**5**	**6**	**7**	**8**	**9**	**10**
			C	199	172	180	176	173	187	172	178	188	149
				11	**12**	**13**	**14**	**15**	**16**	**17**	**18**	**19**	**20**
			C cont.	31	30	158	175	207	175	195	38	41	39
				1	**2**	**3**	**4**	**5**	**6**	**7**	**8**	**9**	**10**
			D	276	242	290	265	275	316	61	338	70	59
				11	**12**								
			D cont.	62	74								
		IndAve:	**1857.38**										
		CombAve:	**1517.55**										

Taxon	Specimen	Element	Tsct	1	2	3	4	5	6	7	8	9	10
Alligator	UCMP 68331	femur	A	47	47	57	54	57	58	57	60		
			B	80	70	56	18						
			C	57	54	52	42	74					
		IndAve:	**973.65**										
	UF FWC 40583	femur	A	54	32	34	32	29	26	32	38		
		IndAve:	**554.00**										
		tibia	A	40	29	31	29	28	39	24	32	38	40
		IndAve:	**528.00**										
	UF FWC 40527	femur	A	36	39	39	44	45	34	38	43	X	56
			B	20	30	32	41	44	49	48			
		IndAve:	**638.00**	10	19	17	10	20	15	19	27	21	
		tibia	A	26	21	35	35	37	45	31	36		
		IndAve:	**399.06**	**1**	**2**	**3**	**4**	**5**	**6**	**7**	**8**	**9**	**10**
	UF FWC SG1	femur	A	26	32	42	29	40	40	33	37	45	33
				11	**12**	**13**	**14**	**15**	**16**	**17**	**18**	**19**	**20**
			A cont.	34	39	41	34	28	38	45	36	32	51
				21	**22**	**23**	**24**						
			A cont.	43	39	46	40						
				1	**2**	**3**	**4**	**5**	**6**	**7**	**8**	**9**	**10**
			B	26	16	28	38	25	24	41	28	31	29
				11									
			B cont.	24									
		IndAve:	**571.00**										
		FemAve:	707.51										

Taxon	Specimen	Element	Tsct	1	2	3	4	5	6	7	8	9	10
Alligator	(summaries)	TibAve:	446.81										
		CombAve:	**608.39**										
Taxon	**Specimen**	**Element**	**Tsct**	**1**	**2**	**3**	**4**	**5**	**6**	**7**	**8**	**9**	**10**
Eudimorphodon	MGUH VP 3393	femur	A	X	13	17	14	14	12	16	23	X	12
				11	**12**	**13**							
			A cont.	16	23	16							
		CombAve:	**1600.00**	* Trsct A encircles the entire circumference									
Taxon	**Specimen**	**Element**	**Tsct**	**1**	**2**	**3**	**4**	**5**	**6**	**7**	**8**	**9**	**10**
Dimorphodon	YPM 9182E	tib-fib	A	12	13	15	17						
			B	20	21	26	30	41	41	41			
		IndAve:	**2518.18**										
	YPM 350B	tib-fib	A	77	102	124							
			B	12	17	19	20	17					
			C	16	14	9	21	19					
		IndAve:	**1634.46**										
		CombAve:	**2039.50**										
Taxon	**Specimen**	**Element**	**Tsct**	**1**	**2**	**3**	**4**	**5**	**6**	**7**	**8**	**9**	**10**
Pterodactylus	CM 11430	femur	A	22	26	25	27	26	26				
			B	24	31	34	32	32	33				
		IndAve:	**2816.67**										
		tibia	A	18	18	24	33	27					
			B	27	26	29	19	31	26	22	28		
			C	30	21	22	26	27	23				
		IndAve:	**2510.53**										
		CombAve:	**2629.03**										
Taxon	**Specimen**	**Element**	**Tsct**	**1**	**2**	**3**	**4**	**5**	**6**	**7**	**8**	**9**	**10**
Dromomeron	GR 221	femur	A	121	111	116	109	25					
			B	113	113	106	96						
			C	104	107	113	136	124					
			D	13	89	91	89						
		IndAve:	**1756.00**										
	GR 254	tibia	A	133	148	144	141	141					
			B	92	136	127	120	131					
			C	92	102	114	110						
		IndAve:	**1978.29**										
	GR 253	tibia	A	128	101	106	82	123	30				
			B	127	132	111	124	131	123				
			C	96	210	114	125	148					
			D	124	136	122	142	162	131	135			

Taxon	Specimen	Element	Tsct	1	2	3	4	5	6	7	8	9	10
Dromomeron	GR 253	**IndAve:**	**2080.33**										
		TibAve:	2042.74										
		CombAve:	**1950.57**										

Taxon	Specimen	Element	Tsct	1	2	3	4	5	6	7	8	9	10
Asilisaurus	NMT RB45	femur	A	22	23	102	125	142	88				
		IndAve:	**1968.67**										
	NMT RB46	femur	A	139	130	153	135	19	28				
			B	29	130	152	151	52					
		IndAve:	**2603.64**										
	NMT RB47	femur	A	142	153	164	163	170					
			B	120	139	134	140	133					
			C	134	127	114	133						
		IndAve:	**2246.86**										
		CombAve:	**2319.61**										

Taxon	Specimen	Element	Tsct	1	2	3	4	5	6	7	8	9	10
Silesauridae GR	GR 255	humerus	A	135	120	126	121	136					
			B	97	148	124	118	123	143				
			C	122	105	126	106	103	162				
		IndAve:	**1995.00**	**1**	**2**	**3**	**4**	**5**	**6**	**7**	**8**	**9**	**10**
	GR 190	tibia	A	23	162	167	177	184	186	198	214	207	191
				11									
			A cont.	203									
				1	**2**	**3**	**4**	**5**	**6**	**7**	**8**	**9**	**10**
			B	151	151	162	202	214	218	269	253	214	260
			C	154	165	154	116	160	163	183	200	175	36
		IndAve:	**3004.77**										
		CombAve:	**2661.02**										

Taxon	Specimen	Element	Tsct	1	2	3	4	5	6	7	8	9	10
Nyasasaurus	NHMUK R6586	humerus	A	96	126	142	136	125	139	137	X	X	
			B	85	105	100	78	96	88	123	112		
				1	**2**	**3**	**4**	**5**	**6**	**7**	**8**	**9**	**10**
			C	116	122	99	109	111	116	118	88	107	104
				11	**12**	**13**	**14**						
			C cont.	116	X	X	X						
		IndAve:	**1776.97**										

Taxon	Specimen	Element	Tsct	1	2	3	4	5	6	7	8	9	10
Fruitadens	LACM 120478	femur	A	33	37	40	48	51	36	37			
			B	48	52	47	55	29					
			C	13	12	22	33	31	29	28			

Taxon	Specimen	Element	Tsct	1	2	3	4	5	6	7	8	9	10
Fruitadens	LACM 120478	femur	D	27	33	22	21						
		IndAve:	**3408.70**										
	LACM 120478	femur	A	36	24	34	41						
			B	31	21	40							
			C	27	36								
			D	32	39	26	32	29	40	33	34		
		IndAve:	**3264.71**										
		CombAve:	**3347.50**										

Taxon	Specimen	Element	Tsct	1	2	3	4	5	6	7	8	9	10
Neornithischia,	NM QR 3076	femur	A	133	151	147	182	124	141	141			
cf. *Lesothosaurus*			B	160	137	141	159	136	144	147			
or *Stormbergia*			C	123	134	126	145	137	133				
		IndAve:	**2272.80**										

Taxon	Specimen	Element	Tsct	1	2	3	4	5	6	7	8	9	10
Scutellosaurus	UCMP 130580	humerus	A	28	22	23	28	32	31	30	23	31	41
			B	18	22	23	39	22	31	27			
			C	22	27	25							
			D	29	28	22	27	24	24	26	34	31	30
				11									
			D cont.	27									
		IndAve:	**2732.26**										
				1	**2**	**3**	**4**	**5**	**6**	**7**	**8**	**9**	**10**
		tibia	A	48	30	33							
			B	38									
			C	28	19	29	31	27	37				
		IndAve:	**3200.00**										
	UCMP 170829	femur	A	67	54	58	68	71	79	90	84	91	
			B	74	91	92	100	93	104	107			
			C	109	111	98	101	93	101				
		IndAve:	**1408.00**										
		CombAve:	**2344.06**										

Taxon	Specimen	Element	Tsct	1	2	3	4	5	6	7	8	9	10
Psittacosaurus	PIN 698/4-22/1946	tibia	A	120	117	126	98						
		IndAve:	**1844.00**										
	PIN 698/5-9/1946	tibia	A	22	23	20							
		IndAve:	**2166.67**										
		CombAve:	**1982.29**										

Taxon	Specimen	Element	Tsct	1	2	3	4	5	6	7	8	9	10
Plateosaurus	SMNS 48-1	femur	A	95	88	96							

Taxon	Specimen	Element	Tsct	1	2	3	4	5	6	7	8	9	10
Plateosaurus	SMNS 48-1	femur	B	87	68	89	99	80	79				
			C	56	66								
		IndAve:	**1313.45**										
	SMNS F14A	femur	A	85	69	83	66	66	50				
		IndAve:	**1117.33**										
		tibia	A	72	70	81	85	85	86	80	85	83	73
				11	**12**	**13**	**14**	**15**					
			A cont.	78	87	76	71	78					
		IndAve:	**1269.33**										
		FemAve:	1244.24										
		CombAve:	**1256.00**										

Taxon	Specimen	Element	Tsct	1	2	3	4	5	6	7	8	9	10
Massospondylus	BPI/1/5253a	femur	A	142	141	175	184	193	173	160			
			B	87	131	198	160	183	174				
			C	31	172	156	165	183	200	185	177		
		IndAve:	**2691.62**										
				1	**2**	**3**	**4**	**5**	**6**	**7**	**8**	**9**	**10**
	BPI/1/5241a	femur	A	199	170	137	195	147	181	178	178	186	180
				11	**12**	**13**	**14**	**15**	**16**	**17**	**18**	**19**	**20**
			A cont.	167	190	193	188	191	203	193	206	205	200
				21	**22**	**23**	**24**						
			A cont.	190	189	184	202						
				1	**2**	**3**	**4**	**5**	**6**	**7**	**8**	**9**	**10**
			B	309	285	278	304	214	320	393	387	344	39
				11	**12**	**13**							
			B cont.	380	52	45							
		IndAve:	**1191.38**										
		CombAve:	**1734.57**										

Taxon	Specimen	Element	Tsct	1	2	3	4	5	6	7	8	9	10
Herrerasaurus	MCZ 7064	humerus	A	X	70	92	106	106	118	145	162	124	123
				11	**12**	**13**							
			A cont.	109	109	124							
				1	**2**	**3**	**4**	**5**	**6**	**7**	**8**	**9**	**10**
			B	99	86	90	76	104	78	82	114	126	
		IndAve:	**1708.95**	**1**	**2**	**3**	**4**	**5**	**6**	**7**	**8**	**9**	**10**
		tibia	A	153	137	115	131	129	107	132	135	99	123
				11	**12**	**13**	**14**						
			A cont.	100	93	162	X						
				1	**2**	**3**	**4**	**5**	**6**	**7**	**8**	**9**	**10**
			B	415	444	515	433	459	478	413	412	510	477

Taxon	Specimen	Element	Tsct	11	12	13	14	15
Herrerasaurus	MCZ 7064	tibia	B cont.	539	97	99	84	X
		IndAve:	**1971.70**					
		CombAve:	**1856.75**					

Taxon	Specimen	Element	Tsct	1	2	3	4	5	6	7	8	9	10
Tawa	GR 155	femur	A	90	85	98	79	107					
			B	83	74	81	74	79					
			C	18	71	109	107	106	117	107			
		IndAve:	**1486.59**										
	GR 257	tibia	A	19	19	86	89						
			B	93	142	144	140	110	87				
			C	62	98	85	116						
			D	119	109	109	114	88					
		IndAve:	**1708.21**										
		CombAve:	**1603.53**										

Taxon	Specimen	Element	Tsct	1	2	3	4	5	6	7	8	9	10
Coelophysis	AMNH FARB	tibia	A	78	79	92	106	102	88	105	108	112	104
	uncatalogued			**11**	**12**								
			A cont.	104	110								
				1	**2**	**3**	**4**	**5**	**6**	**7**	**8**	**9**	**10**
			B	114	139	109	89	82	125	119	141	121	132
				11									
			B cont.	142									
				1	**2**	**3**	**4**	**5**	**6**	**7**	**8**	**9**	**10**
			C	21	114	112	116	113	119	98	116	143	125
				11	**12**								
			C cont.	130	157								
				1	**2**	**3**	**4**	**5**	**6**	**7**	**8**	**9**	**10**
			D	9	144	142	150	104	21	28	98	120	19
				11									
			D cont.	16									
		IndAve:	**1848.52**										

Taxon	Specimen	Element	Tsct	1	2	3	4	5	6	7	8	9	10
Megapnosaurus	NMZB QG 715	femur	A	129	158	178	178	168	185	181	190	199	
			B	123	111	157	176	146	159	172			
			C	136	29	123	132	119	126	132	24		
		IndAve:	**2472.83**	**1**	**2**	**3**	**4**	**5**	**6**	**7**	**8**	**9**	**10**
	NMZB QG 726	femur	A	111	107	103	111	101	134	114	110	113	34
				11									
			A cont.	33									

Taxon	Specimen	Element	Tsct	1	2	3	4	5	6	7	8	9	10
Megapnosaurus	NMZB QG 726	femur	B	210	37	32	38	40	34	36	27	159	147
				11	**12**	**13**	**14**	**15**	**16**	**17**	**18**	**19**	**20**
			B cont.	162	26	24	30	159	170	189	32	36	23
				1	**2**	**3**	**4**	**5**	**6**	**7**	**8**	**9**	**10**
			C	95	106	104	21	19	118	123	114	115	116
				11	**12**								
			C cont.	28	27								
		IndAve:	**2492.00**										
		CombAve:	**2485.13**										

Taxon	Specimen	Element	Tsct	1	2	3	4	5	6	7	8	9	10
Coelophysoidea (indeterminate)	GR 256	femur	A	154	162	193	192	177	215	187	164	199	229
				11	**12**	**13**	**14**	**15**	**16**				
			A cont.	243	276	279	278	43	26				
				1	**2**	**3**	**4**	**5**	**6**	**7**	**8**	**9**	**10**
			B	157	194	196	201	208	205	199	208	184	221
				11	**12**	**13**	**14**	**15**					
			B cont.	201	191	198	186	34					
				1	**2**	**3**	**4**	**5**	**6**	**7**	**8**	**9**	**10**
			C	193	202	231	232	219	197	199	217	214	244
				11	**12**	**13**	**14**	**15**	**16**	**17**			
			C cont.	229	221	229	212	228	233	40			
		IndAve:	**3363.58**										

Taxon	Specimen	Element	Tsct	1	2	3	4	5	6	7	8	9	10
Coelophysoidea (indeterminate)	UCMP 129618	femur	A	135	156	162	174	141	125	131	131	141	103
				11	**12**	**13**	**14**	**15**	**16**	**17**	**18**		
			A cont.	117	155	118	134	162	144	137	158		
				1	**2**	**3**	**4**	**5**	**6**	**7**	**8**	**9**	**10**
			B	24	21	19	119	93	94	79	121	128	134
				11	**12**	**13**	**14**	**15**	**16**				
			B cont.	112	109	106	94	101	13				
				1	**2**	**3**	**4**	**5**	**6**	**7**	**8**	**9**	**10**
			C	123	111	126	132	122	140	143	114	23	120
				11	**12**	**13**	**14**	**15**	**16**	**17**	**18**		
			C cont.	12	23	115	113	122	111	20	127		
		IndAve:	**2000.54**										

Taxon	Specimen	Element	Tsct	1	2	3	4	5	6	7	8	9	10
Confuciusornis	NGMC 98-8-2 (MOR 1063)	humerus	A	79	138								
			B	107	109	123							
			C	120	151								
			D	115	128	104							

Taxon	Specimen	Element	Tsct	1	2	3	4	5	6	7	8	9	10
Confuciusornis	NGMC 98-8-2	humerus	-										
	(MOR 1063)	**IndAve:**	**1878.40**										
		femur	A	114									
			B	129									
			C	132	118								
			D	132	146								
		IndAve:	**2056.00**										
		tibia	A	143	164								
			B	138	172								
			C	126									
			D	135									
		IndAve:	**2341.33**										
		IndAve:	**2053.09**										

Taxon	Specimen	Element	Tsct	1	2	3	4	5	6	7	8	9	10
Hesperornis	YPM PU 22443	tibiotarsus	A	X	138	178	165	209	178				
		IndAve:	**2777.60**										

Taxon	Specimen	Element	Tsct	1	2	3	4	5	6	7	8	9	10
Lithornis	USNM 290554	tibiotarsus	A	95	151								
			B	149	160								
			C	109	130								
			D	109	196								
		IndAve:	**2198.00**										

Taxon	Specimen	Element	Tsct	1	2	3	4	5	6	7	8	9	10
Paracathartes	USNM 361407	tibiotarsus	A	101	120	112	118						
			B	126	116	141							
			C	97	113	146	133						
		IndAve:	**1924.36**										

Taxon	Specimen	Element	Tsct	1	2	3	4	5	6	7	8	9	10
Rhynchotus	PU 728	tibiotarsus	A	116									
			B	198	181								
			C	136	X								
		IndAve:	**2524.00**										

Taxon	Specimen	Element	Tsct	1	2	3	4	5	6	7	8	9	10
Crax	USNM 19918	tibiotarsus	A	138	156								
			B	162	179								
		IndAve:	**2540.00**										

Taxon	Specimen	Element	Tsct	1	2	3	4	5	6	7	8	9	10
Buteo	UWBM 82968	humerus	A	144	157								
			B	138	144								
			C	131									
			IndAve:	**2284.80**									

Taxon	Specimen	Element	Tsct	1	2	3	4	5	6	7	8	9	10
Corvus	UWBM 90537	humerus	A	104	90								
			B	101	108	100							
			C	112									
			D	117	121								
			IndAve:	**1706.00**									

GUIDE TO COLOR CODING IN CELLS

The colors of numbered boxes reflect the size of the digital sample boxes used to estimate osteocyte density.

100 µm x 100 µm
200 µm x 200 µm
250 µm x 250 µm
400 µm x 400 µm
500 µm x 500 µm

In cells marked with an X, osteocytes could not be counted because focus was problematic within the digital sample box.